

THE DISTRIBUTION OF SEISMIC
VELOCITIES AND ATTENUATION IN THE EARTH

Thesis by
Robert Stuart Hart

In Partial Fulfillment of the Requirements
for the Degree of
Doctor of Philosophy

California Institute of Technology
Pasadena, California

1977
(Submitted May 18, 1977)

Acknowledgements

Throughout my stay at the Seismological Laboratory, I have greatly benefited from my association with Dr. Don L. Anderson. The work presented here is a direct result of that association and our close collaboration. I am indebted to him for his guidance and support. I would also particularly like to express my gratitude to Dr. Hiroo Kanamori. His knowledge and enthusiasm have been a major resource and inspiration for me. The interest and advice of Carl E. Johnson, Robert J. Geller, and Drs. T. H. Jordan and D. V. Helmberger is greatly appreciated.

Dr. Thomas H. Jordan provided me with the inversion programs used in many portions of the research. Dr. Freeman Gilbert kindly provided normal mode eigenfunction tapes to me which greatly facilitated the latter stages of this research.

I also wish to especially thank my wife, Beth, for putting up with me and providing much needed understanding and affection during the past four and a half years.

For their assistance in the preparation of the final draft of this thesis, I thank Mrs. Marla Turner who so ably typed the manuscript and Mr. Laszlo Lenches who drafted many of the figures.

During most of my tenure as a graduate student, I was supported by a Beno Gutenberg Graduate Fellowship and a National Science Foundation Graduate Fellowship. Portions of this research were supported by the National Aeronautics and Space Administration under Contract No. NGL05-002-069, by the Chevron Research Co., and by the Advanced

Research Projects Agency of the Department of Defense monitored by the
Air Force Office of Scientific Research under Contract No. F49620-77-
0022.

Abstract

Estimates of the radial distribution of seismic velocities and density and of seismic attenuation within the earth are obtained through inversion of body wave, surface wave, and normal mode data. The effect of attenuation related dispersion on gross earth structure, and on the reliability of eigenperiod identifications is discussed. The travel time baseline discrepancies between body waves and free oscillation models are examined and largely resolved.

As preliminary steps in this study, a technique is developed for determining S wave arrival times and applied to records from several large nuclear explosions. The resulting low-scatter travel times are combined with other high resolution body wave results to help define a gross earth model, designated C2, which fits 86% of the normal mode data to within their 95% confidence limits.

The second stage considers the effect of attenuation on seismic dispersion and shows the perturbation of phase velocity to be approximately an order of magnitude greater than the observational error. Inclusion of an attenuation correction in the normal mode data and subsequent inversion results in an elimination of the baseline discrepancies.

The final portion of this research covers the inversion of all available seismic Q data to obtain a better estimate of the radial distribution of seismic absorption in the earth. Prominent features of the resulting Q models, designated SL1 and SL2, are low Q zones in both the upper mantle and in the 150 kilometers of the mantle just

above the core-mantle boundary and finite compressional dissipation in the inner core. Model SL1 is used to compute the attenuation corrections for the normal mode data for a final inversion for seismic velocities and density. The resulting attenuation-corrected earth model, QM3, fits the corrected observations to the same precision as model C2 fits the raw data. Moreover, QM3 represents a better match to the travel time data than previous earth models. The reliability of existing eigenperiod identifications in light of excitation criteria and computed attenuation is examined. For completeness, an appendix is included in which the relative excitations of a large set of spheroidal modes ($T \geq 45$ sec, $\ell \leq 150$, $n \leq 30$) and toroidal modes ($T \geq 45$ sec, $\ell \leq 150$, $n \leq 7$) is presented for both the Alaska earthquake (1964) and the Columbia earthquake (1970) sources.

TABLE OF CONTENTS

	<u>Page</u>
Chapter 1	
Introduction	
1.1 Statement of the problem	1
1.2 Motivation	1
1.3 Approach	3
Chapter 2	
Low-scatter teleseismic shear wave travel times	
2.1 Introduction	6
2.2 Technique	7
2.3 The data	10
2.4 Results of inversion	17
Chapter 3	
An earth model based on free oscillations and body waves	
3.1 Introduction	25
3.2 The starting model	28
3.3 The data sets	29
3.4 Inversion	39
3.5 The resulting model	47
3.5 Resolution	57
3.7 Comparison with body wave observations	58

	<u>Page</u>
Chapter 4	
The effect of attenuation upon gross earth models	
4.1 Introduction	73
4.2 The effect of attenuation upon dispersion	74
4.3 Implications on the inferred structure of the earth	81
4.4 The presence of a low velocity zone	91
4.5 The effect of attenuation upon a gross earth model	93
Chapter 5	
The Q of the earth	
5.1 Introduction	111
5.2 The data	112
5.3 The Q models	126
5.4 Summary of the fits of the Q models	154
Chapter 6	
Implications of the Q distribution upon the inferred elastic properties of the earth and upon the observation of the earth's free oscillations	
6.1 Introduction	160
6.2 The starting model	161
6.3 Data and inversion	163
6.4 Comparison with body wave data	177
6.5 Discussion of the normal mode data	187
6.6 Summary.	195

	<u>Page</u>
Bibliography	197
Appendix 1	211
Appendix 2	213

Chapter 1

INTRODUCTION

1.1 Statement of the problem. This thesis addresses the problems of estimating the radial variation of seismic velocities and attenuation in the earth and of resolving the discrepancies between seismological results based upon body wave observations and those derived from normal mode studies.

1.2 Motivation. In recent years, great progress has been made in the area of determining the internal elastic properties of the earth. The development and installation of high quality long-period seismometers permitted the observation of the earth's free oscillations. Subsequently, the acquisition of this very important data set was complemented by the development of powerful inversion techniques (e.g. - Backus and Gilbert, 1970; Jordan, 1972) which have allowed seismologists to estimate the radial variations of velocity and density in the earth with some confidence. The models which have been proposed through the application of these inversion techniques (Dziewonski and Gilbert, 1973; Jordan and Anderson, 1974; Gilbert and Dziewonski, 1975) have, however, all been characterized by a persistent, somewhat disturbing feature. The theoretical body wave travel times predicted by these models are much slower than most body wave observations. This is particularly true for shear waves. Since substantial evidence has accumulated that there are significant regional variations in

upper mantle structure, extending to depths of at least a few hundred kilometers, it has been generally assumed that the travel time baseline shifts were simply manifestations of these regional differences. Under closer examination, this assumption proves inadequate. The free oscillation models predict travel times that are not merely slower than the Jeffreys-Bullen (1940) times but slower than more recently obtained travel times for continental paths (e.g. Helmberger and Engen, 1974). Since a gross earth model should represent an average of both oceanic and continental mantle, this in turn requires that oceanic travel times be even slower than the continental observations, and the Jeffreys-Bullen (1940) times must be completely biased (by 4-10 seconds for shear waves) toward some very anomalous mantle. These two requirements are inconsistent with observed travel-times (there are no observations of travel times that slow) and with the care with which the Jeffreys-Bullen tables were compiled.

In comparison to the effort expended in investigating the elastic velocities and travel times in the earth, the study of the distribution of anelastic properties has been very much neglected. This neglect was largely due to both the difficulty in obtaining accurate and consistent measurements of seismic Q and to the lesser motivation for obtaining these values. In the last year, however, the important theoretical developments on seismic absorption by Liu, Anderson, and Kanamori (1976) and Anderson, Kanamori, Hart, and Liu (1977) provided seismologists with a substantial motivation for increased study. Liu et al. (1976) and Anderson et al. (1977) demonstrated that a simple,

physically realistic model for attenuation in the earth could explain the near constancy of Q and would additionally produce first order perturbations in observed phase velocities. The implication of this model is that the free oscillation models referred to above, in which any attenuation effect was assumed to be second order and thus ignored, do not accurately model the seismic velocities in the earth. The constant Q requires that seismic velocities in the earth be frequency dependent. In order to account for this frequency dependence when inverting for seismic velocities, an adequate representation of the Q distribution is required.

1.3 Approach. In addition to possible regional biases in observed travel times, uncertainties in earthquake location and origin time limit travel time accuracy. In the case of shear waves these problems are further compounded by the second arrival status of S waves. The shear phase onset is usually obscured by various compressional wave precursors making an accurate estimate of onset time almost impossible by conventional visual techniques. In Chapter 2, these problems are overcome by the development of a new technique for determining shear wave arrivals and the application of that technique to seismograms of large nuclear explosions.

One shortcoming of existing gross earth models is the inability of the normal mode data to resolve many of the short wavelength features of the mantle determined by high resolution body wave studies. In Chapter 3 the results of such body wave studies are included in

the starting model for a free oscillation inversion.

In Chapter 3 no attempt is made to include the effects of attenuation in determining a gross earth structure. As mentioned in the previous section, these effects are potentially very important. The effect of Q on the observed periods of the earth's free oscillations is discussed in Chapter 4. The implication of including attenuation in the inversion process upon the existence of an upper mantle low velocity zone is also discussed. Lastly the effect of attenuation upon a given gross earth velocity structure and upon the resulting theoretical body wave travel times is considered.

Since no model of the Q structure of the earth has been available which is completely acceptable for the full range of seismic absorption data, we have attempted, in Chapter 5, to collect all available seismic Q measurements, at all frequencies within the seismic band, and to invert that data for a gross earth Q model. The uncertainties and trade-offs between the various Q measurements are discussed here and in Appendix 1.

The resulting Q models are used in Chapter 6 to correct the observed normal mode periods for the effect of attenuation. The corrected data are then inverted to obtain estimates of the radial distributions of seismic velocities and density in the earth which are consistent with the assumed Q model. The features of this model are compared to earlier, uncorrected earth models. In Chapter 6, we also discuss some of the problems and internal inconsistencies of the normal mode data set. The reliability of reported eigenfrequencies

is examined in light of excitation efficiency and predicted attenuation. The development of a smoothed standard normal mode data set is proposed in order to avoid model-dependent mode identifications.

Chapter 2

LOW-SCATTER TELESEISMIC SHEAR WAVE TRAVEL-TIMES

2.1 Introduction. The shear velocity structure in the mantle is significantly less well determined than the compressional velocity structure in the same region. This uncertainty occurs primarily because shear waves are not the first arrival phases on a seismogram, and, due to P-SV coupling, the actual onset of the shear wave arrival is usually obscured by various precursor arrivals. As a consequence, most S wave travel time data sets show large scatter. Moreover, the overall uncertainty in epicenter locations and origin time determinations, particularly for the events used by Jeffreys over 40 years ago, led us to suspect that perhaps the baseline discrepancy in shear wave travel times, referred to in Chapter 1, was merely an artifact of poor data. The above difficulties and uncertainties associated with using earthquakes as shear wave sources can be greatly minimized by instead using large, underground nuclear explosions as our sources. The origin time, depth, and epicenter of these explosions are generally known to high accuracy, especially for the tests conducted in the Aleutian Islands and at the Nevada Test Site. Even the Soviet blasts on Novaya Zemlya have, for present purposes, fairly well determined source parameters.

The problems due to P-SV coupling and to the late-arrival status of shear waves were overcome by the development of a new technique for arrival time determination. This technique, based on a suggestion by

Helmberger (personal communication), utilizes the theoretically determined waveform of the shear wave and its precursors to compute the true arrival time of the phase.

2.2 Technique. Other investigators (Kogan, 1960; Ibrahim and Nuttli, 1967; Nuttli, 1969) have previously used explosion data in attempting to improve shear wave travel times. Ibrahim and Nuttli also attempted to eliminate the obscuring effects of compressional precursors by employing two separate techniques; particle motion analysis and determination of the product of the vertical and horizontal components of motion; to their analysis. While these techniques represent an improvement over simple visual identification of arrival times, neither method is entirely satisfactory since both rely on the initial portions of the waveform which are generally distorted by the precursor arrivals, particularly by the Sp phase. The Sp phase is the major precursor to the shear wave and arises from SV-P conversion at the M-discontinuity below the observing station. In addition, any departure from radial layering in the earth introduces further errors into these analysis methods. Our technique, described in more detail below, is not sensitive to such symmetry deviations, and, since it relies more heavily on the later portions of the wave form, is essentially insensitive to precursor contamination.

Synthetic seismograms of the phase pS, the dominant teleseismic shear energy from a near-surface explosion, a theoretically pure compressional source, were generated using the source function proposed

by HelMBERGER and HARKRIDER (1972). This source function has a faster rise time than the HASKELL (1967) source and has proved to be very accurate in reproducing the P waves from nuclear explosions. This function, therefore, was considered to be the most appropriate source representation for this study. The resulting synthetics were then compared to actual long-period WSSN records of events in Nevada, in the Aleutians, and at the Soviet test site on Novaya Zemlya. Figure 2.1 shows this comparison for several records as well as the HelMBERGER-HARKRIDER source time function. The Sp precursor is included in the second synthetic waveform (2.1b) and is also obvious in the actual seismograms. The correlation between observed records and synthetics is very good.

Our technique, then, is straightforward. We can compute the delay time between the actual S wave onset time of the synthetic and the time of the first peak in the waveform for any distance. Indeed, for distances greater than 30° , the waveform and, in particular, the width of the first peak is essentially constant. Thus, in our observations, we need only measure the arrival time of this first peak on the actual seismogram, and apply a correction, 3.7 seconds, to compute the actual onset time of the pS phase. We ignore the initial portions of the pulse altogether and thus avoid the necessity of removing the precursor contamination. Since we are using an explosive source, the ground motion of the pS phase at the observer will be up and radially back toward the source. Hence, consideration of the required polarity of the waveform on each component permits an unambiguous identification

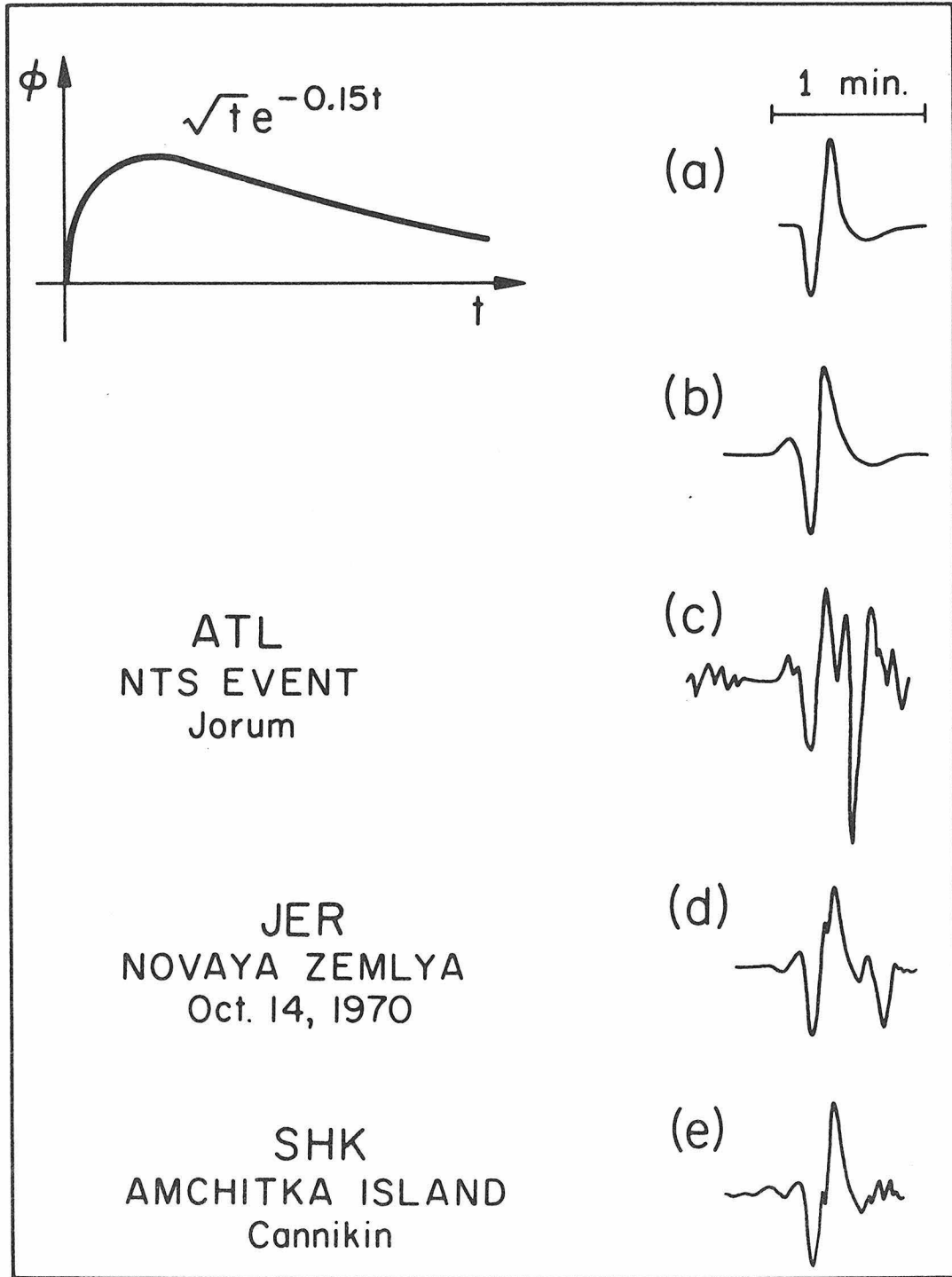


Figure 2.1 - The time function of the HelMBERGER and HARKRIDER (1972) explosion source (upper right) and synthetic seismograms for the shear wave (a) and shear wave with precursor (b). Also three typical observed records from the three source regions, (c), (d), and (e).

of the correct peak or trough. The arrival times are then corrected for ellipticity (Bullen, 1937) using a value of $1/298.26$ for the earth's flattening (Stacey, 1969), and for the elevation of the station and source. Lastly, a small time correction removes the initial compressional path contribution to the observed pS travel time and we obtain a surface focus S travel time. This last correction can be computed very accurately for the NTS events and for the Cannikin test in the Aleutians by using the near-field structures determined by aftershock studies (Hamilton and Healy, 1969; Stauder, 1971; Engdahl, 1970). For those explosions in Novaya Zemlya, this correction was estimated by assuming a reasonable mean velocity and depth of burial. Errors in these estimates do not cause significant errors in the overall travel times.

2.3 The Data. Five nuclear explosions were used in this study. Although records of about two dozen events were examined, only five underground tests were of sufficiently large yield to generate large teleseismic shear waves. These events are: two Nevada Test Site explosions, code-named Benham and Jorum; the Cannikin test on Amchitka in the Aleutians; and two Soviet tests on Novaya Zemlya, the first on October 27, 1966, the other on October 14, 1970. Seismograms from WWSSN and Canadian network stations were examined for clearly identifiable pS arrivals from all five events. Ninety-six travel times were obtained at distances ranging from 25.63° to 95.99° . Most of the data are for distances less than 75° .

In order to determine travel-times and then to invert to a velocity structure, it is necessary to obtain accurate locations and origin times. For the American tests, this is a simple matter, but for the Soviet blasts, no official announcement is released, and the available computed parameters were not completely trusted. The geographical location of the Novaya Zemlya test site is surrounded by stations at a wide range of distances and azimuths. As a result, and since the depth of an explosion is tightly constrained, the computed epicentral locations of the explosions will vary only by a few kilometers with any realistic travel-time model. Such small shifts will not produce resolvable differences in teleseismic travel-times. However, the computed origin time of an event depends critically upon the model employed. The two Soviet tests were relocated using four models: the Jeffreys-Bullen tables, the 1968 tables (Herrin et al., 1968), gross earth model B1 (Jordan and Anderson, 1974), and gross earth model UTD124B (Dziewonski and Gilbert, 1973). Since it was believed that the explosions were detonated on the minute or as close as possible to that time, that criterion was used to select the B1 solution. This solution also seemed most likely on the basis of the island terrain of the test site. The resulting source parameters and the corresponding I.S.C. determinations are as follows:

(1) October 27, 1966:

B1: 5:58:00.4; 73.38N, 54.62E

I.S.C.: 5:57:57.3; 73.40N, 54.57E

(2) October 14, 1970:

B1: 5:59:59.8; 73.35N, 54.94E

I.S.C.: 5:59:57.3; 73.31N, 54.89E

It should be pointed out that the adoption of the revised source parameters noticeably decreased the scatter between the two data sets.

Having determined the source parameters for the five explosions, the S arrival times are readily converted to absolute travel times by applying the corrections described earlier. Table 2.1 lists all of the corrected, absolute travel times used in this study as well as the residual of those observations with respect to the Jeffreys-Bullen Tables (1940). Since three different source regions were used, it was expected that the data would separate naturally into three sets, each with a different baseline. To examine this separation, the three data sets were plotted separately as residual times with respect to the computed J-B travel-times (Figure 2.2).

The most immediate difference among the data sets is the much greater scatter in the Cannikin data. This was not unexpected, however. The local tectonic setting of the test site has been shown to introduce large azimuthally and distance-dependent scatter into observed travel-times (Davies and McKenzie, 1969; Davies and Julian, 1972). Nevertheless, the basic trend of the residuals is consistent with the other data sets. However, because of this large scatter and a large baseline shift, these data were not used in the final inversion.

The NTS data and the Novaya Zemlya data both show very low scatter, less than ± 1.3 seconds. This is significantly less scatter than has

TABLE 2.1

Observed Travel Times

Station	Distance (deg)	Travel Time (sec)	J-B Residual (sec)
Benham (NTS); Dec. 19, 1968; 16:30:00.0; 37.23 N, 116.47 W			
AAM	25.63	603.5	4.1
BLA	28.60	650.0	2.1
SCP	30.04	672.2	1.4
CMC	30.66	680.9	0.3
OTT	31.41	693.7	1.3
RES	38.91	807.6	-0.5
FBC	39.00	808.3	-1.1
MBC	39.13	810.4	-0.9
BOG	50.53	979.4	3.5
CAR	51.79	995.7	2.4
NNA	61.50	1125.4	3.3
Jorum (NTS); Sept. 16. 1969; 14:30:00.0; 37.31 N, 116.46 W			
FCC	25.94	606.9	2.4
ATL	26.41	615.8	3.5
BLA	28.58	650.1	2.6
SCP	30.01	671.4	1.1
GWC	31.68	697.5	0.9
OGD	32.42	709.4	1.2
Novaya Zemlya; Oct. 27, 1966; 5:58:00.4; 73.38 N, 54.62 E			
MBC	30.53	680.3	2.2
RES	30.99	688.4	2.6
TRI	33.37	726.1	3.2
ATU	38.56	803.3	0.5
CMC	38.87	808.5	1.1
BLC	41.17	842.1	0.2
JER	42.86	866.8	0.0
LAH	43.12	870.2	-0.4
SCH	46.03	912.7	0.1
MAL	46.43	920.9	2.6
SHL	51.83	997.1	3.2
FSJ	52.48	1006.7	4.2
SES	56.12	1054.9	3.1
PNT	57.53	1074.2	3.8
VIC	58.39	1086.6	4.9
WES	58.80	1092.4	5.3
OGD	60.72	1117.2	5.4
BOZ	60.94	1119.2	4.6

TABLE 2.1 (cont'd)

Station	Distance (deg)	Travel Time (sec)	J-B Residual (sec)
BAG	67.58	1202.1	5.2
Novaya Zemlya; Oct. 14, 1970; 5:59:59.8; 73.35 N, 54.94 E			
MBC	30.57	682.0	3.1
RES	31.04	690.4	3.8
VAL	34.23	739.4	3.1
IST	34.68	744.1	0.9
TAB	35.61	758.7	1.0
FBC	38.11	795.5	-0.5
KBL	39.62	818.2	-0.6
COL	41.18	842.7	0.6
BLC	41.23	842.4	-0.4
JER	42.88	867.1	0.0
QUE	43.68	878.0	-0.8
SHI	43.80	881.0	0.5
YKC	44.25	888.1	1.1
EIL	45.10	901.3	2.0
HLW	45.26	902.9	1.3
SCH	46.12	915.2	1.3
NDI	46.24	916.5	0.9
FCC	46.49	919.6	0.4
MAL	46.51	919.6	0.1
GWC	47.67	938.3	2.4
FFC	51.24	989.2	3.5
SHL	51.75	997.6	4.9
FSJ	52.51	1008.1	5.0
EDM	53.47	1019.5	3.3
MAT	53.50	1019.9	3.3
HAL	55.11	1041.6	3.3
POO	55.86	1053.2	4.9
SES	56.16	1055.8	3.5
OTT	56.83	1065.1	3.9
PNT	57.57	1075.5	4.6
WES	58.89	1094.1	5.8
OGD	60.80	1118.3	5.9
AAM	61.21	1122.8	4.7
GOL	66.43	1188.5	5.5
DUG	66.43	1188.7	5.7
OXF	69.72	1226.4	4.1
SHA	73.28	1267.8	4.4
JCT	75.04	1288.1	5.1
CAR	88.63	1426.7	4.8
BOG	95.99	1492.9	6.2

TABLE 2.1 (cont'd)

Station	Distance (sec)	Travel Time (sec)	J-B Residual (sec)
Cannikin; Nov. 6, 1971; 22:00:00.1; 51.50 N, 179.10 E			
MAT	32.54	710.2	0.2
SHK	37.26	783.0	0.0
LON	38.02	792.7	-1.9
COR	38.22	798.3	0.7
BKS	42.70	863.4	-1.2
GSC	47.72	935.7	-0.9
ANP	50.69	979.2	1.1
GOL	51.87	996.5	2.0
TUC	53.45	1015.5	-0.4
ALQ	54.33	1028.4	0.6
HKC	57.36	1068.3	0.1
KEV	57.38	1069.8	1.3
BAG	57.85	1076.8	2.1
RAB	60.05	1103.0	-0.2
DAV	62.34	1132.7	0.3
BLA	67.70	1198.3	0.0
CHG	69.45	1218.1	-1.1
CTA	76.87	1303.1	0.0
MSH	77.83	1311.3	-2.2
QUE	79.29	1328.8	-0.3
SHI	86.63	1405.5	2.4
CAR	96.20	1491.4	3.0

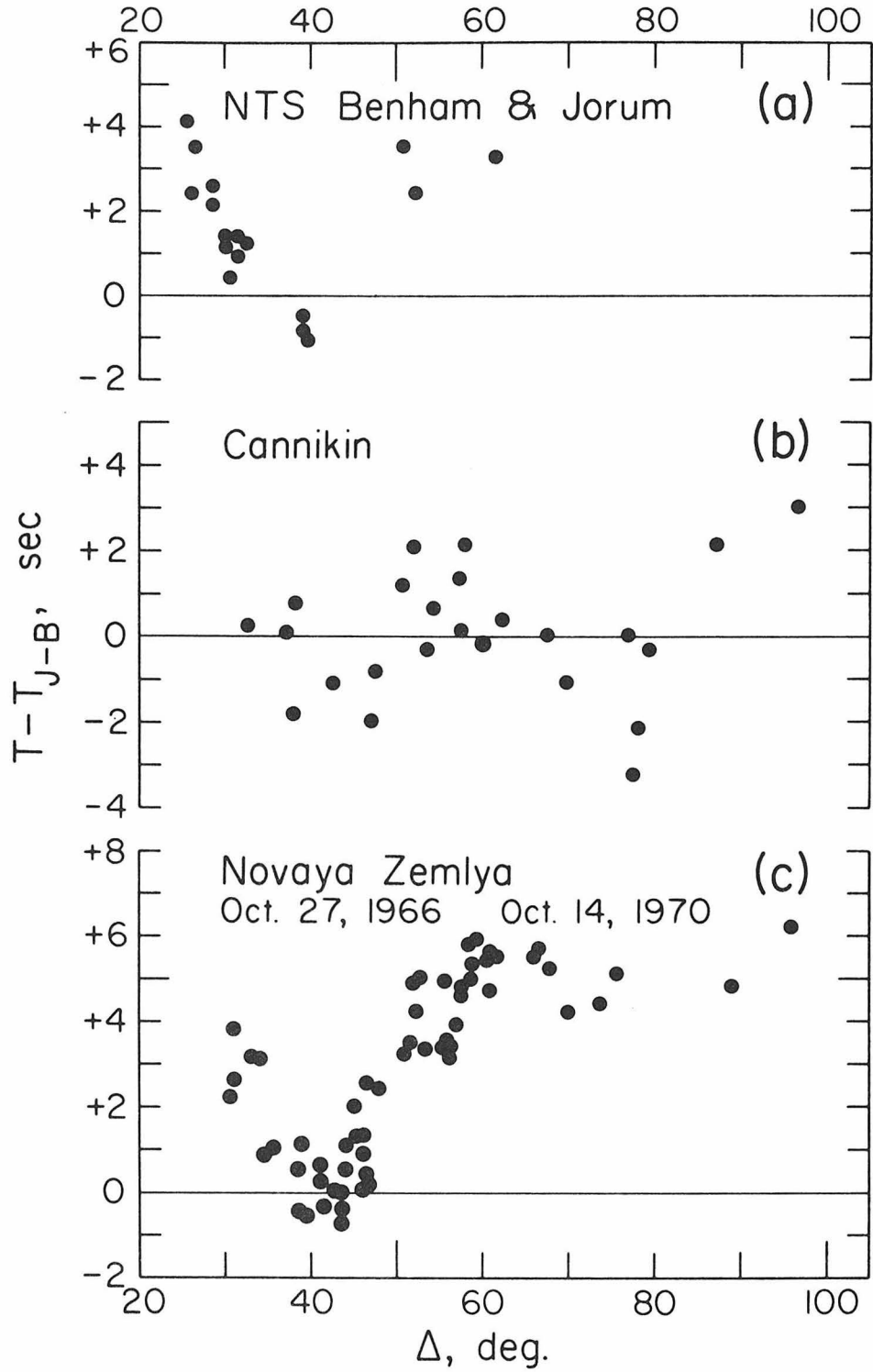


Figure 2.2 - Jeffreys-Bullen travel-time residual plots of the observed data from the Nevada Test Site (a), Cannikin (b), and Novaya Zemlya (c).

previously been reported in S wave studies (Kogan, 1960; Hales and Roberts, 1970; Robinson and Kovach, 1971). This low scatter is a result of the stability and accuracy of our technique. Additionally, we believe this low scatter indicates that shear wave station corrections, which were not included in this study, are not as large or as important as earlier investigators have proposed (Doyle and Hales, 1967).

The NTS data set is much smaller than the Novaya Zemlya data set and does not significantly extend the distance range covered by the latter. Additionally, the NTS data comprise only a small range of azimuths and distances. For these reasons, it was not judged worthwhile to attempt to apply the necessary baseline shift to the NTS data to make it compatible with the Novaya Zemlya data. Thus, only the 59 travel-times from the two Soviet blasts were used to determine a velocity structure. It was still necessary, however, to determine accurate origin times for these explosions since data from both events were combined. The Novaya Zemlya data also have the advantage of being a homogeneous data set from a non-tectonic source region, with a wide range of azimuths and distances included. This results in a more reliable average mantle sampling.

2.4 Results of the Inversion. These travel times were inverted for a lower mantle shear velocity distribution using the linear estimation method described by Jordan and Anderson (1974). This technique employs an iterative algorithm which finds the smallest smooth perturbation to

the starting model which satisfies the inversion data. A detailed description of the theory of the linear inverse problem is given in papers by Backus and Gilbert (1970), Jordan and Franklin (1971), Jordan and Minster (1972), Jordan (1972), and Jordan and Anderson (1974).

Unless specified otherwise, all inversions performed in the research covered by this thesis use this method. The discussions of uniqueness and resolution in Jordan and Anderson (1974), and reviewed in Section 3.6 of the following chapter of this thesis, also apply throughout. The starting model for this inversion was a modification of the Jordan and Anderson (1974) model B1. This model was modified to incorporate the upper mantle shear velocity structure, SHR14, determined by Helmberger and Engen (1974) for continental regions. Since the S wave data used in this study represent ray paths through generally continental upper mantle regions, this model was expected to be most appropriate, and indeed, no baseline shift was required in order to avoid any change in the SHR14 structure during the inversion. Since the ray paths involved have bottoming depths greater than 650 kilometers, the upper mantle serves primarily as a baseline adjustment, and although it will affect bottoming depths slightly, one is relatively free to select the most convenient realistic structure.

The resulting velocity model, S1, is shown in Figure 2.3 (see also Table 2.2) along with the Jordan and Anderson (1974) model B1. We are, as mentioned above, not concerned with differences in structure above a radius of 5700 km (see Figure 2.3 insert), but only with

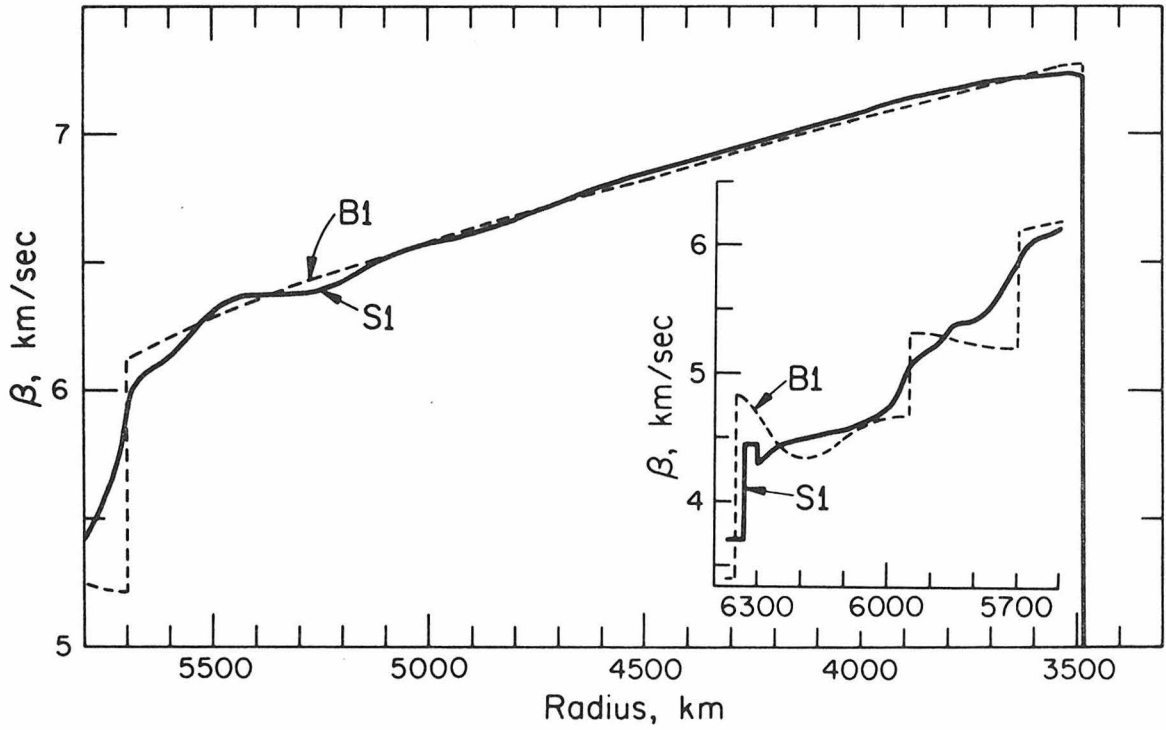


Figure 2.3 - The velocity structure for model S1, solid line, in the lower mantle and, in the insert, for the upper mantle. Also shown for comparison in both regions is model B1 (Jordan and Anderson, 1974), dashed line.

TABLE 2.2

Shear Wave Velocity Structure (Model S1)

Radius (km)	Velocity (km/sec)	Radius (km)	Velocity (km/sec)
6371	3.69	5350	6.38
6330	3.70	5275	6.39
6330	4.45	5200	6.45
6300	4.45	5125	6.51
6300	4.30	5050	6.55
6250	4.44	4975	6.58
6200	4.48	4900	6.61
6150	4.52	4825	6.65
6100	4.55	4750	6.70
6050	4.62	4675	6.75
6000	4.72	4600	6.79
5950	5.08	4525	6.83
5900	5.19	4450	6.87
5850	5.38	4375	6.91
5800	5.41	4300	6.94
5750	5.57	4225	6.98
5700	5.90	4150	7.01
5687	5.97	4075	7.04
5675	6.04	4000	7.08
5660	6.06	3925	7.12
5643	6.08	3850	7.15
5625	6.09	3775	7.18
5602	6.13	3700	7.21
5573	6.18	3625	7.22
5550	6.24	3550	7.23
5500	6.32	3510	7.24
5425	6.37	3485	7.23

the velocity structure below that depth. Model B1 has a very smooth shear wave gradient throughout the entire lower mantle. The newer model, S1, however, has substantial structure in this region, particularly between radii of 5100 km and 5700 km. Another prominent feature of this new model is a flattening of the velocity gradient in the bottom 200 kilometers of the mantle although this region is not well-constrained by the data set employed.

The shear wave travel-time curve is similarly more complex. Table 2.3 lists the surface focus travel-times for S1 but a better picture of the travel-times for this model can be obtained by considering the time residuals of S1 relative to the Jeffreys-Bullen times (Figure 2.4). The most prominent feature of the residual curve is the deep minimum at roughly 40° . This feature of the shear wave travel-time curve was also observed by Ibrahim and Nuttli (1967) and corresponds to a sharp velocity increase near a radius of 5500 km. However, beyond a distance of 60° , the S1 residual curve flattens out at roughly +5.0 seconds until, at 90° , the residuals sharply increase. This behavior is similar to the results of Hales and Roberts (1970) although with about a 4.5 second baseline shift. Both S1 and Ibrahim and Nuttli (1967) predict a definite change in $dt/d\Delta$ at about 50° . (See also Hales and Roberts, 1970).

By using only distances greater than 30° , all of the rays have nearly vertical paths through the upper mantle. Hence, since essentially all of the stations used are continental, the effects of major lateral inhomogeneities in the upper mantle should appear primarily as

TABLE 2.3

Surface Focus S Wave Travel Times

Delta (deg)	Time (sec)	Delta (deg)	Time (sec)
30	673.5	66	1183.3
32	704.3	68	1207.3
34	734.7	70	1230.8
36	764.9	72	1253.9
38	795.0	74	1276.5
40	824.7	76	1298.6
42	854.4	78	1320.3
44	884.0	80	1341.5
46	913.4	82	1362.2
48	942.8	84	1382.5
50	971.9	86	1402.2
52	999.9	88	1421.3
54	1027.3	90	1440.0
56	1054.4	92	1458.3
58	1081.1	94	1476.2
60	1107.5	96	1493.9
62	1133.4	98	1511.4
64	1158.8	100	1528.6

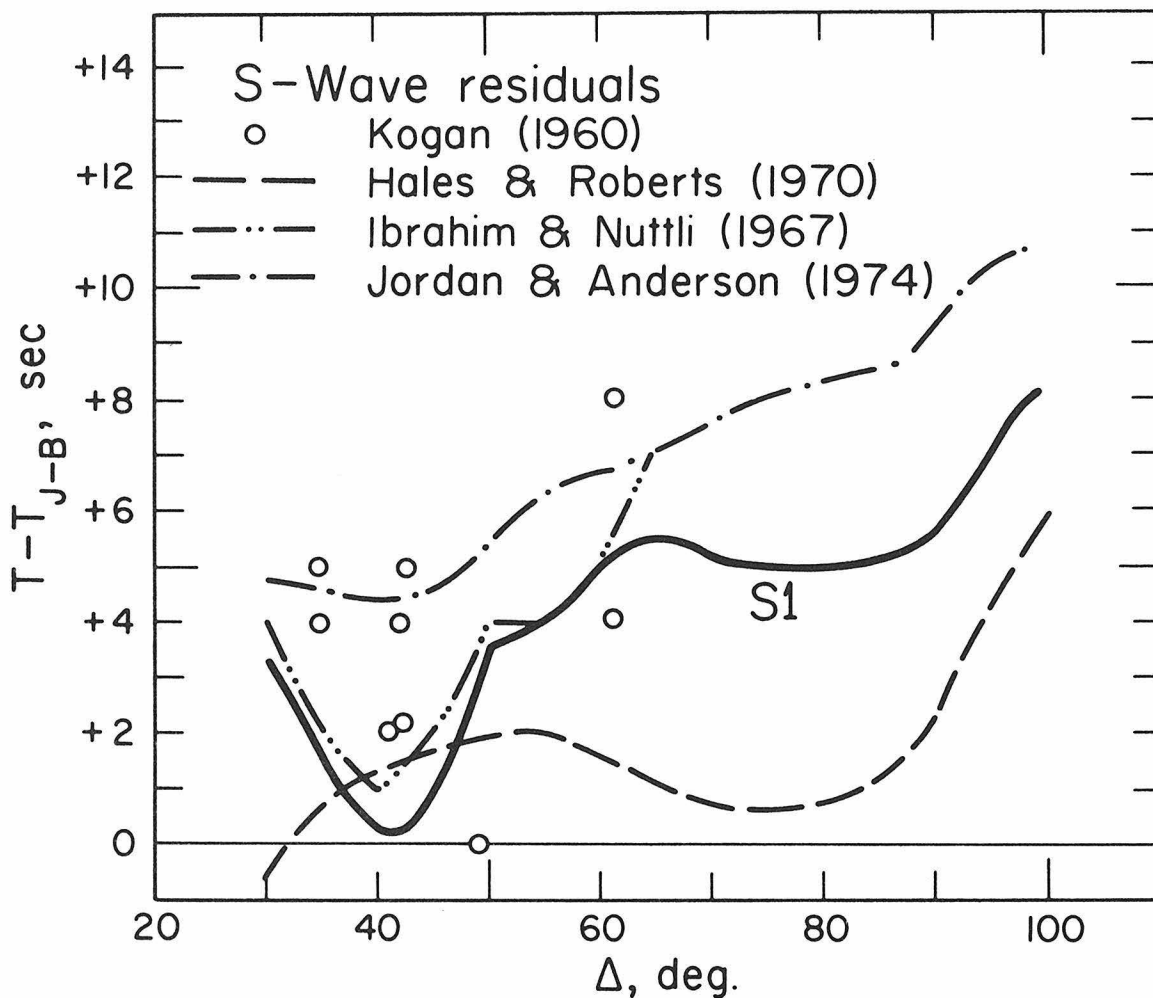


Figure 2.4 - Jeffreys-Bullen travel-time residual curves for model S1, B1 (Jordan and Anderson, 1974), Hales and Roberts (1970), Ibrahim and Nuttli (1967), and Kogan (1960).

baseline shifts between the three data sets. Indeed, there is a shift toward faster times from the Novaya Zemlya data to the Nevada Test Site data and especially to the Cannikin data. This correlates with the trend toward increasing tectonic activity among the three regions. Further, since the inversion data set covers a wide range of azimuths, the resultant model, S1, should represent a gross earth, lower mantle shear velocity structure.

Although we have thus obtained a highly reliable estimate for the shear velocity structure in the lower mantle, particularly for the region just below the 650 km discontinuity, we have not yet resolved the baseline problem in shear wave travel times. Indeed, at this point it would appear that substantial deep mantle differences do exist between continental regions and oceans. The preliminary studies of Sipkin and Jordan (1975) on ScS times also supported this conclusion.

As a final note on this study, it is possible that this technique could be extended to earthquake sources. In order to use an earthquake we require a very precise description of the spatial and temporal characteristics of the source. Possible candidates for such events would be the Borrego Mt. earthquake, studied by Burdick and Mellman (1976) or some of the North Atlantic events presently being studied now by David Blum and Donald Helmberger.

Chapter 3

AN EARTH MODEL BASED ON FREE OSCILLATIONS AND BODY WAVES

3.1 Introduction. The normal mode data set is now adequate to determine average velocities and densities in the upper and lower mantle and the core and to resolve a certain amount of structure in these regions. However, it is not adequate to resolve details having wavelengths of the order of 100-200 km. To resolve these features, which are particularly important in the upper mantle and the transition regions of the mantle and core, one must utilize higher resolving power body wave techniques, including travel times, apparent velocities, amplitudes and pulse shapes. These data, by their very nature, are much more path dependent than normal modes but it is reasonable to assume that fine structure determined by body wave techniques is largely characteristic of the Earth as a whole. The role of free oscillations, then, is to determine differences of the average Earth from the more path specific body wave structures and to determine compatible density structures. In this spirit we design a starting model based on high resolution body wave studies and perturb this model to fit the normal mode data set. The resulting model retains the features found by body wave studies but the average properties in the various regions are suitably adjusted to correspond to average Earth properties, as required by the normal mode data set. This model is appropriate for discussions of gross Earth chemistry and as a standard for discussing lateral variations.

Jordan and Anderson (1974) recently derived an Earth model consistent with a large body of free oscillation, surface wave and body wave data. These data tightly constrain the seismic velocities and densities in the lower mantle and outer core. However, the resolving power in the upper mantle and transition region, particularly for P waves, is very poor, and the resulting model, as in all studies of this sort, is to a large extent dependent on the starting model. Although model B1, derived by Jordan and Anderson (1974), fits the available gross Earth data, it has several unsatisfactory features. The upper mantle compressional velocity structure, because of the resolving power problem, appears to be inconsistent with the shear velocity profile which can be resolved to greater detail. In particular, the low P_n velocity, 7.91 km/sec, is inconsistent with both the high S_n velocity, 4.83 km/sec, and measurements of P_n in oceanic and most continental regions. Model B1 had no P-wave low-velocity layer in the upper mantle in contrast to a rather pronounced low-velocity zone for shear waves. Resolving power calculations indicate that an upper mantle P-wave LVZ can not be resolved by the normal mode data set even though detailed body wave studies demonstrate its existence in most parts of the Earth.

The low P_n velocity and the absence of a P-wave LVZ are related problems since only average properties of the upper mantle can be determined. If one accepts the P_n data, then inversion of the same data set would yield a P-wave LVZ. Model B1 also gives shear wave travel times that are not consistent with the travel times determined in the preceding chapter and other recent studies (e.g.-Hales and

Roberts, 1970).

Recent body wave studies of the upper mantle, using travel times, amplitudes and wave shapes (Helmberger and Wiggins, 1971; Helmberger and Engen, 1974), have yielded profiles having more structure than can probably ever be resolved from gross Earth data. These structures include LVZs for both P and S waves and discontinuities near 375, 500 and 600 km. Gradients between discontinuities, as well as average velocities, can also be resolved with these techniques. Although the above studies refer mostly to continental structure below North America, there is reason to believe that the major features also exist elsewhere. For example, evidence for the 375 and 600 km discontinuities appears in great circle, mainly oceanic, dispersion data (e.g., Anderson and Toksoz, 1963) and from upper mantle reflection studies (e.g., Engdahl and Flinn, 1974; Whitcomb and Anderson, 1970). Evidence for the 500 km discontinuity has also been discussed for oceanic regions (Whitcomb and Anderson, 1970) and for Australia (Simpson, 1973).

The interpretation of these discontinuities in terms of phase changes (Anderson, 1967 a,b; Burdick and Anderson, 1975) requires that they occur everywhere although their depths may vary slightly.

It seems appropriate, therefore, to adopt the high resolution body wave profiles as starting models in a gross Earth inversion, allowing them to be modified, as necessary, to satisfy the gross Earth data. We make no pretense that the fine structure in the starting and final models is required by the normal-mode data set.

3.2 The Starting Model. The basic starting model is a modification of the Helmberger and Wiggins (1971) and Helmberger and Engen (1974) structures for the upper mantle, B1 for the lower mantle and B1 and Whitcomb (1973) for the core. Whitcomb (1973) constructed his core model from observed $dt/d\Delta$'s relative amplitudes and arrival times of PKP, PKiKP, SKS and SKKS utilizing a recent mantle model (Jordan and Anderson, 1974) for the required stripping to the surface of the core. He discusses at length previous core studies. A crust and uppermost mantle model was derived which is an average of the tectonic subdivisions of the Earth. It includes a 3 km thick water layer in order to overcome the objections of Hales (1974). It has a 40 km thick "lid" (the mantle part of the lithosphere), a 58 km thick lithosphere, pronounced low-velocity zones for both P and S and discontinuities or rapid increases in velocity near 375, 500 and 670 km. The latter discontinuity was made sharp in order to satisfy P'P' precursor reflection data (Engdahl and Flinn, 1969; Whitcomb and Anderson, 1970).

Model B1 of Jordan and Anderson (1974) represented the "shortest smooth perturbation" from a simple initial model that incorporated the major seismic discontinuities (400 and 600 km) found from previous body wave and surface wave studies (Anderson and Toksoz, 1963; Niazi and Anderson, 1965, Julian and Anderson, 1968, Johnson, 1967) and which upon inversion, satisfied the normal mode data set of Dziewonski and Gilbert (1972) and a large body of supplementary data including travel times, apparent velocities and group velocities. The starting model had an adiabatic and homogeneous lower mantle and outer core.

The starting, or initial, model for the present study, incorporates fine structure of the upper mantle (HelMBERGER and Wiggins, 1971; HelMBERGER and Engen, 1974), uppermost lower mantle (see Chapter 2) and core (Whitcomb, 1973) which is unresolvable by the normal mode data set. In addition, we modified the starting V_p model to be consistent with the P_n data. The starting density model contains discontinuities in the upper mantle, at the depths of the seismic discontinuities.

It should be emphasized that, in linear inversion, the starting model is as important as the data set. Our starting model incorporates features found by techniques which have an intrinsic greater resolving power than the gross Earth data set itself. The inversion technique we used is identical to that described in Chapter 2. For the forward part of the calculations we used programs written by Martin Smith. The radius of the core was fixed at 3485 km, the value determined by Jordan and Anderson (1974) and verified by Engdahl and Johnson (1975). This core radius is also consistent with the solutions of Hales and Roberts (1970) and Gilbert and Dziewonski (1975). It is about 12 km larger than earlier determinations, such as Jeffreys and Bullen (1940).

3.3 The Datasets. For the initial inversion iterations, we used the same 177 normal mode periods used in the study of Jordan and Anderson (1974). This includes the first five radial modes, the fundamental spheroidal modes ${}_0^S_2 - {}_0^S_{63}$, the fundamental toroidal modes ${}_0^T_2 - {}_0^T_{46}$, 56 spheroidal overtones and 9 toroidal overtones. Most of these data

are from Dziewonski and Gilbert (1973), and Gilbert and Dziewonski (1975). Gilbert and Dziewonski (1975) have recently presented the results of a new analysis and have tabulated what they feel to be the "best" observation for each mode. However, their criterion for "best" is model dependent. In chapter 6 of this thesis, we discuss a more objective procedure for selecting the "best" eigenperiod observation and propose a method for smoothing these observations to obtain a standard normal mode data set.

In the final iterations we used 400 representative modes including 148 toroidal overtones up to ${}_7T_{49}$ and 136 spheroidal overtones up to ${}_5S_{35}$. Eight radial modes were used. The data are from Dziewonski and Gilbert (1973), Gilbert and Dziewonski (1975), Bolt and Currie (1975), Mendiguren (1973), Derr (1969), and Kanamori (unpublished results). Unfortunately, the techniques used by Mendiguren (1973) and Gilbert and Dziewonski (1975) do not yield reliable estimates of the errors. We follow the latter authors in assuming that 0.05% is a minimum error but otherwise adopt the published error estimates. In many cases the tabulated error is much less than one would infer by comparing the various data sets. The eigenperiods and estimates of their errors are tabulated in Table 3.1.

For the toroidal data set we have used essentially the same modes as Gilbert and Dziewonski (1975) except that we have deleted the data of Brune and Gilbert (1974) which have large uncertainties ($\sim 0.40\%$) are not fit well by the Gilbert-Dziewonski models, and represent properties only over a very short arc-length of the Earth's surface. The remaining

TABLE 3.1
Observed and Computed Eigenperiods

MODE	DATA (Sec)	ERROR (%)	C2	DIFF. (%)	MODE	DATA (Sec)	ERROR (%)	C2	DIFF. (%)
$0T_2$	2636.38	0.08	2630.18	0.24	$0T_{30}$	257.29	0.15	257.25	0.02
$0T_3$	1702.51	0.15	1702.30	0.01	$0T_{31}$	250.14	0.04	250.16	-0.01
$0T_4$	1303.60	0.07	1303.63	0.00	$0T_{32}$	243.43	0.07	243.46	0.01
$0T_5$	1075.20	0.09	1075.53	-0.03	$0T_{33}$	237.37	0.10	237.10	0.11
$0T_6$	925.36	0.09	925.55	-0.02	$0T_{34}$	231.29	0.10	231.07	0.09
$0T_7$	817.92	0.08	818.04	-0.01	$0T_{36}$	219.69	0.11	219.89	-0.09
$0T_8$	736.86	0.05	736.39	0.06	$0T_{37}$	213.89	0.10	214.69	-0.37
$0T_9$	671.80	0.06	671.76	0.01	$0T_{38}$	209.83	0.28	209.73	0.05
					$0T_{39}$	204.27	0.05	205.00	-0.36
$0T_{10}$	619.02	0.05	619.03	-0.00					
$0T_{11}$	574.62	0.08	574.99	-0.06	$0T_{40}$	199.96	0.19	200.48	-0.26
$0T_{12}$	536.93	0.05	537.52	-0.11	$0T_{41}$	195.88	0.22	196.15	-0.14
$0T_{13}$	504.94	0.08	505.16	-0.04	$0T_{42}$	191.26	0.13	192.00	-0.38
$0T_{14}$	476.64	0.08	476.86	-0.04	$0T_{43}$	187.40	0.26	188.02	-0.32
$0T_{15}$	451.83	0.06	451.83	-0.00	$0T_{44}$	183.78	0.15	184.21	-0.23
$0T_{16}$	429.50	0.07	429.52	0.00	$0T_{45}$	180.25	0.05	180.54	-0.16
$0T_{17}$	409.61	0.05	409.46	0.04	$0T_{46}$	176.85	0.05	177.02	-0.09
$0T_{18}$	391.16	0.10	391.32	-0.04					
$0T_{19}$	374.76	0.05	374.80	-0.01	$1T_2$	756.57	0.08	756.22	0.05
					$1T_3$	695.18	0.07	693.65	0.22
$0T_{20}$	359.59	0.08	359.68	-0.03	$1T_4$	629.98	0.10	629.61	0.06
$0T_{21}$	345.70	0.05	345.79	-0.03	$1T_6$	519.09	0.06	518.53	0.11
$0T_{22}$	333.15	0.13	332.97	0.05	$1T_7$	475.17	0.13	474.74	0.09
$0T_{23}$	321.21	0.09	321.10	0.04	$1T_8$	438.49	0.05	438.17	0.07
$0T_{24}$	310.18	0.08	310.06	0.04	$1T_9$	407.73	0.10	407.57	0.04
$0T_{25}$	299.51	0.10	299.78	-0.09					
$0T_{26}$	290.26	0.06	290.17	0.03	$1T_{10}$	381.65	0.10	381.68	-0.01
$0T_{27}$	281.21	0.16	281.16	0.02	$1T_{11}$	359.14	0.05	359.45	-0.09
$0T_{28}$	272.60	0.27	272.70	-0.04	$1T_{12}$	339.54	0.06	340.05	-0.15
$0T_{29}$	264.66	0.05	264.75	-0.03	$1T_{13}$	322.84	0.12	322.91	-0.02

TABLE 3.1(cont'd)

MODE	DATA (Sec)	ERROR (%)	C2	DIFF. (%)	MODE	DATA (Sec)	ERROR (%)	C2	DIFF. (%)
1 ^T ₁₆	280.59	0.06	281.35	-0.27	1 ^T ₅₁	124.13	0.43	124.03	0.08
					1 ^T ₅₂	122.26	0.14	122.28	-0.02
1 ^T ₂₀	240.98	0.09	241.29	-0.13	1 ^T ₅₄	118.96	0.13	118.94	0.02
1 ^T ₂₄	211.95	0.05	212.22	-0.13	1 ^T ₅₇	114.41	0.12	114.27	0.12
1 ^T ₂₅	205.85	0.05	206.16	-0.15	1 ^T ₅₈	112.92	0.12	112.81	0.10
1 ^T ₂₆	200.27	0.05	200.51	-0.12	1 ^T ₅₉	111.40	0.09	111.38	0.02
1 ^T ₂₉	185.34	0.05	185.57	-0.12					
					1 ^T ₆₀	110.24	0.13	109.98	0.23
1 ^T ₃₀	180.80	0.06	181.16	-0.20	1 ^T ₆₂	107.44	0.13	107.31	0.13
1 ^T ₃₁	176.85	0.07	177.00	-0.08	1 ^T ₆₄	104.94	0.13	104.76	0.17
1 ^T ₃₃	169.27	0.05	169.32	-0.03	1 ^T ₆₆	102.59	0.14	102.34	0.25
1 ^T ₃₄	165.72	0.05	165.78	-0.04					
1 ^T ₃₅	162.36	0.05	162.41	-0.03	2 ^T ₂	447.30	0.09	448.21	-0.20
1 ^T ₃₆	159.11	0.05	159.20	-0.06	2 ^T ₄	419.38	0.09	420.34	-0.23
1 ^T ₃₇	156.08	0.05	156.14	-0.04	2 ^T ₅	401.82	0.09	402.63	-0.20
1 ^T ₃₈	153.17	0.08	153.21	-0.02	2 ^T ₇	363.65	0.07	363.43	0.06
1 ^T ₃₉	150.28	0.07	150.41	-0.08	2 ^T ₈	343.34	0.06	343.43	-0.03
					2 ^T ₁₇	219.95	0.06	219.97	-0.01
1 ^T ₄₀	147.68	0.05	147.72	-0.03	2 ^T ₁₈	211.90	0.06	212.07	-0.08
1 ^T ₄₁	145.12	0.07	145.14	-0.02	2 ^T ₁₉	204.63	0.10	204.83	-0.10
1 ^T ₄₂	142.66	0.06	142.67	-0.01	2 ^T ₂₁	191.91	0.06	191.97	-0.03
1 ^T ₄₃	140.23	0.08	140.29	-0.04	2 ^T ₂₂	186.19	0.06	186.22	-0.02
1 ^T ₄₄	137.96	0.06	138.00	-0.03					
1 ^T ₄₅	135.64	0.24	135.79	-0.11	2 ^T ₂₅	171.12	0.12	171.14	-0.01
1 ^T ₄₆	133.63	0.07	133.66	-0.02	2 ^T ₂₆	166.50	0.07	166.72	-0.13
1 ^T ₄₇	131.59	0.17	131.60	-0.01	2 ^T ₂₇	162.58	0.09	162.54	0.02
1 ^T ₄₈	129.56	0.06	129.62	-0.04	2 ^T ₂₈	158.43	0.05	158.59	-0.10
					2 ^T ₂₉	154.70	0.06	154.85	-0.10
1 ^T ₅₀	125.92	0.08	125.83	0.07	2 ^T ₃₁	147.71	0.06	147.93	-0.15

TABLE 3.1 (cont'd)

MODE	DATA (Sec)	ERROR (%)	C2	DIFF. (%)	MODE	DATA (Sec)	ERROR (%)	C2	DIFF. (%)
2 ^T ₃₂	144.59	0.06	144.72	-0.09	3 ^T ₂₄	154.81	0.12	154.72	0.06
2 ^T ₃₄	138.62	0.06	138.74	-0.08	3 ^T ₂₅	150.66	0.05	150.87	-0.14
2 ^T ₃₅	135.73	0.06	135.94	-0.16	3 ^T ₂₉	137.24	0.07	137.35	-0.08
2 ^T ₃₆	133.14	0.06	133.28	-0.10	3 ^T ₃₃	126.16	0.06	126.21	-0.04
2 ^T ₃₇	130.51	0.06	130.72	-0.16	3 ^T ₃₄	123.75	0.06	123.72	0.02
2 ^T ₃₈	128.17	0.08	128.28	-0.09	3 ^T ₃₇	116.89	0.06	116.87	0.02
2 ^T ₃₉	125.71	0.06	125.93	-0.18	3 ^T ₄₁	108.87	0.06	108.94	-0.06
2 ^T ₄₀	123.56	0.06	123.68	-0.10	3 ^T ₄₇	99.08	0.06	99.08	0.00
2 ^T ₄₁	121.57	0.05	121.53	0.03	3 ^T ₅₁	93.67	0.09	93.56	0.12
2 ^T ₄₂	119.33	0.14	119.46	-0.11	3 ^T ₅₉	84.35	0.09	84.35	0.00
2 ^T ₄₄	115.49	0.06	115.55	-0.06	3 ^T ₆₅	78.69	0.10	78.70	-0.01
2 ^T ₄₅	113.57	0.06	113.72	-0.13	3 ^T ₇₂	73.16	0.10	73.16	0.00
2 ^T ₄₇	110.22	0.06	110.25	-0.02					
2 ^T ₄₉	106.98	0.06	107.03	-0.04	4 ^T ₇	216.81	0.18	217.27	-0.21
2 ^T ₅₁	104.01	0.06	104.03	-0.02	4 ^T ₁₁	199.74	0.19	200.99	-0.17
2 ^T ₅₂	102.60	0.06	102.62	-0.02	4 ^T ₁₄	184.86	0.19	185.44	-0.31
2 ^T ₅₄	99.93	0.06	99.92	0.01	4 ^T ₁₆	174.72	0.19	175.34	-0.35
2 ^T ₅₅	98.61	0.06	98.65	-0.04	4 ^T ₂₀	155.64	0.19	155.80	-0.10
2 ^T ₅₈	95.08	0.06	95.04	0.04	4 ^T ₂₂	147.47	0.19	147.17	0.20
2 ^T ₆₁	91.85	0.07	91.76	0.10	4 ^T ₂₃	143.67	0.19	143.24	0.30
					4 ^T ₂₅	136.30	0.20	136.11	0.14
3 ^T ₉	259.26	0.12	259.38	-0.05	4 ^T ₂₇	130.03	0.23	129.80	0.17
3 ^T ₁₁	240.50	0.10	240.80	-0.13	4 ^T ₄₀	101.27	0.30	101.32	-0.05
3 ^T ₁₇	189.97	0.13	190.77	-0.42					
3 ^T ₁₈	184.09	0.09	184.28	-0.10	4 ^T ₄₅	93.79	0.10	93.88	-0.09
3 ^T ₁₉	178.17	0.09	178.33	-0.09	4 ^T ₄₈	89.82	0.10	89.98	-0.17
3 ^T ₂₀	172.74	0.06	172.87	-0.07	4 ^T ₅₀	87.46	0.09	87.56	-0.12
3 ^T ₂₁	167.69	0.06	167.84	-0.09	4 ^T ₅₄	82.95	0.10	83.13	-0.22
3 ^T ₂₃	158.54	0.06	158.81	-0.17	4 ^T ₆₃	74.72	0.09	74.68	0.04

TABLE 3.1(cont'd)

MODE	DATA (Sec)	ERROR (%)	C2	DIFF. (%)	MODE	DATA (Sec)	ERROR (%)	C2	DIFF. (%)
4 ^T ₆₄	73.79	0.09	73.86	-0.10	7 ^T ₃₈	85.45	0.13	85.49	-0.05
4 ^T ₆₅	72.94	0.10	73.05	-0.15	7 ^T ₄₀	82.84	0.14	82.89	-0.06
4 ^T ₆₆	72.28	0.10	72.26	0.03	7 ^T ₄₆	76.18	0.13	76.19	-0.02
					7 ^T ₄₉	73.36	0.15	73.32	0.05
5 ^T ₉	174.33	0.10	174.67	-0.19					
5 ^T ₁₀	171.89	0.08	172.17	-0.16					
5 ^T ₁₅	157.57	0.10	157.65	-0.05	0 ^S ₀	1227.64	0.06	1228.47	-0.07
5 ^T ₃₈	97.11	0.09	97.11	0.00	1 ^S ₀	613.59	0.05	613.91	-0.05
5 ^T ₄₀	94.12	0.08	94.12	0.00	2 ^S ₀	398.55	0.05	398.58	-0.01
5 ^T ₄₄	88.64	0.09	88.69	-0.05	3 ^S ₀	305.84	0.05	306.01	-0.05
5 ^T ₄₅	87.47	0.09	87.43	0.05	4 ^S ₀	243.59	0.05	243.44	0.06
5 ^T ₅₀	81.60	0.10	81.65	-0.06	5 ^S ₀	204.61	0.05	204.70	-0.05
5 ^T ₅₅	76.52	0.09	76.61	-0.12	6 ^S ₀	174.25	0.09	174.10	0.09
5 ^T ₅₇	74.75	0.09	74.78	-0.04	8 ^S ₀	134.65	0.05	134.66	0.00
6 ^T ₃₄	97.13	0.10	97.06	0.07	0 ^S ₂	3233.26	0.06	3231.89	0.04
6 ^T ₃₅	95.46	0.09	95.42	0.04	0 ^S ₃	2133.58	0.11	2133.63	0.00
6 ^T ₄₁	86.70	0.09	86.77	-0.09	0 ^S ₄	1545.60	0.05	1545.43	0.01
6 ^T ₄₂	85.35	0.09	85.50	-0.17	0 ^S ₅	1190.12	0.05	1190.11	0.00
6 ^T ₄₅	81.85	0.10	81.90	-0.05	0 ^S ₆	963.17	0.05	963.46	-0.03
6 ^T ₄₉	77.65	0.09	77.59	0.08	0 ^S ₇	811.45	0.05	812.06	-0.08
6 ^T ₅₃	73.89	0.09	73.78	0.15	0 ^S ₈	707.64	0.05	707.68	0.00
					0 ^S ₉	633.95	0.05	633.73	0.03
7 ^T ₈	129.67	0.39	129.27	0.31	0 ^S ₁₀	580.06	0.05	579.32	0.13
7 ^T ₁₇	118.57	0.13	118.60	-0.03					
7 ^T ₁₉	115.58	0.14	115.69	-0.10	0 ^S ₁₁	536.98	0.05	537.04	-0.01
7 ^T ₂₈	101.15	0.13	101.42	-0.26	0 ^S ₁₂	502.33	0.06	502.45	-0.02
7 ^T ₂₉	99.53	0.13	99.74	-0.21	0 ^S ₁₃	473.17	0.06	473.27	-0.02
7 ^T ₃₀	97.93	0.13	98.05	-0.12	0 ^S ₁₄	448.20	0.05	448.11	0.02
7 ^T ₃₄	91.46	0.14	91.40	0.06	0 ^S ₁₅	426.06	0.05	426.11	-0.01

TABLE 3.1(cont'd)

MODE	DATA (Sec)	ERROR (%)	C2	DIFF. (%)	MODE	DATA (Sec)	ERROR (%)	C2	DIFF. (%)
0 ^S ₁₆	406.75	0.05	406.69	0.01	0 ^S ₄₄	197.19	0.05	197.19	0.00
0 ^S ₁₇	389.32	0.05	389.42	-0.03	0 ^S ₄₅	193.87	0.05	193.74	0.07
0 ^S ₁₈	374.02	0.05	373.93	0.02	0 ^S ₄₆	190.57	0.05	190.40	0.09
0 ^S ₁₉	360.11	0.05	359.96	0.04	0 ^S ₄₇	187.26	0.05	187.17	0.05
0 ^S ₂₀	347.50	0.05	347.27	0.07	0 ^S ₄₈	184.25	0.05	184.05	0.11
0 ^S ₂₁	335.81	0.05	335.68	0.04	0 ^S ₄₉	181.00	0.05	181.02	-0.01
0 ^S ₂₂	325.06	0.05	325.04	0.01	0 ^S ₅₀	178.31	0.05	178.08	0.13
0 ^S ₂₃	315.21	0.05	315.20	0.00	0 ^S ₅₁	175.27	0.05	175.23	0.02
0 ^S ₂₄	306.25	0.06	306.08	0.06	0 ^S ₅₂	172.54	0.05	172.47	0.04
0 ^S ₂₅	297.66	0.05	297.57	0.03	0 ^S ₅₃	169.97	0.05	169.79	0.11
0 ^S ₂₆	289.60	0.05	289.60	0.00	0 ^S ₅₄	167.38	0.05	167.19	0.12
0 ^S ₂₇	282.18	0.05	282.11	0.02	0 ^S ₅₆	162.41	0.09	162.20	0.13
0 ^S ₂₈	275.11	0.05	275.04	0.03	0 ^S ₅₇	160.01	0.05	159.81	0.12
0 ^S ₂₉	268.44	0.06	268.36	0.03	0 ^S ₅₈	157.70	0.09	157.49	0.13
0 ^S ₃₀	262.06	0.05	262.02	0.02	0 ^S ₅₉	155.01	0.05	155.23	0.14
0 ^S ₃₁	255.95	0.05	256.00	-0.02	0 ^S ₆₀	153.24	0.05	153.03	0.14
0 ^S ₃₂	250.31	0.05	250.26	0.02	0 ^S ₆₁	151.12	0.05	150.89	0.15
0 ^S ₃₃	244.92	0.05	244.78	0.06	0 ^S ₆₂	149.07	0.05	148.80	0.18
0 ^S ₃₄	239.59	0.05	239.53	0.03	0 ^S ₆₃	147.09	0.05	146.77	0.22
0 ^S ₃₅	234.58	0.05	234.52	0.03	0 ^S ₆₄	144.96	0.09	144.79	0.22
0 ^S ₃₆	229.74	0.05	229.70	0.02	0 ^S ₆₅	142.99	0.09	142.86	0.09
0 ^S ₃₇	225.16	0.05	225.08	0.04	0 ^S ₆₆	141.22	0.09	140.98	0.17
0 ^S ₃₈	220.62	0.05	220.64	0.01					
0 ^S ₃₉	216.43	0.05	216.37	0.03	1 ^S ₂	1470.85	0.08	1469.37	0.10
0 ^S ₄₀	212.31	0.05	212.25	0.03	1 ^S ₃	1063.96	0.11	1063.01	0.09
0 ^S ₄₁	208.35	0.05	208.28	0.03	1 ^S ₄	852.67	0.05	851.98	0.08
0 ^S ₄₂	204.57	0.06	204.46	0.06	1 ^S ₅	730.56	0.08	729.59	0.13
0 ^S ₄₃	200.93	0.05	200.76	0.08	1 ^S ₆	657.61	0.05	657.34	0.04

TABLE 3.1(cont'd)

MODE	DATA (Sec)	ERROR (%)	C2	DIFF. (%)	MODE	DATA (Sec)	ERROR (%)	C2	DIFF. (%)
1 ^S ₇	603.93	0.05	604.64	-0.12	1 ^S ₃₉	151.64	0.07	151.66	-0.01
1 ^S ₈	556.03	0.07	556.48	-0.08	1 ^S ₄₀	148.61	0.09	148.72	-0.08
1 ^S ₉	509.96	0.05	509.97	0.00	1 ^S ₄₁	145.83	0.05	145.93	-0.07
1 ^S ₁₀	465.45	0.06	466.18	-0.16	1 ^S ₄₂	143.17	0.09	143.25	-0.06
1 ^S ₁₄	337.01	0.05	336.48	0.16	1 ^S ₄₃	140.61	0.09	140.69	-0.06
1 ^S ₁₅	316.06	0.05	315.58	0.15	1 ^S ₄₄	138.25	0.09	138.25	0.00
1 ^S ₁₆	299.50	0.09	299.56	-0.02	1 ^S ₄₇	131.50	0.13	131.50	0.00
1 ^S ₁₇	286.22	0.07	286.27	-0.02	1 ^S ₄₈	129.18	0.13	129.43	-0.19
1 ^S ₁₈	274.75	0.10	274.45	0.11	1 ^S ₄₉	127.14	0.13	127.43	-0.23
1 ^S ₁₉	263.63	0.09	263.72	-0.03	1 ^S ₅₀	125.39	0.23	125.51	-0.09
1 ^S ₂₀	253.97	0.09	253.88	0.04	1 ^S ₅₂	121.96	0.05	121.87	0.07
1 ^S ₂₁	244.93	0.09	244.80	0.05	1 ^S ₅₃	120.07	0.05	120.14	-0.06
1 ^S ₂₂	236.21	0.09	236.38	-0.07	1 ^S ₅₄	118.50	0.13	118.47	0.03
1 ^S ₂₃	228.42	0.09	228.55	-0.06	1 ^S ₅₅	116.81	0.13	116.85	-0.04
1 ^S ₂₄	220.99	0.09	221.25	-0.12	1 ^S ₅₆	115.32	0.13	115.29	0.03
1 ^S ₂₅	214.44	0.09	214.43	0.07	1 ^S ₅₈	112.25	0.13	112.30	-0.05
1 ^S ₂₆	207.71	0.09	208.03	-0.16	1 ^S ₅₉	110.91	0.13	110.87	0.03
1 ^S ₂₇	201.70	0.09	202.04	-0.17	1 ^S ₆₁	108.06	0.13	108.14	-0.07
1 ^S ₂₈	196.31	0.09	196.40	-0.05	1 ^S ₆₃	105.69	0.13	105.55	0.13
1 ^S ₂₉	190.89	0.06	191.10	-0.11	1 ^S ₆₄	104.41	0.13	104.31	0.10
1 ^S ₃₀	185.94	0.09	186.10	-0.09	1 ^S ₆₈	99.71	0.13	99.64	0.07
1 ^S ₃₂	176.71	0.13	176.94	-0.13	1 ^S ₇₅	92.48	0.13	92.48	0.00
1 ^S ₃₃	172.34	0.13	172.73	-0.22					
1 ^S ₃₄	168.30	0.13	168.74	-0.26	2 ^S ₃	804.17	0.06	804.95	-0.10
1 ^S ₃₅	164.60	0.13	164.96	-0.22	2 ^S ₄	724.87	0.05	725.16	-0.04
1 ^S ₃₆	161.35	0.05	161.38	-0.02	2 ^S ₅	660.41	0.05	660.06	0.05
1 ^S ₃₇	157.67	0.13	157.98	-0.19	2 ^S ₆	594.71	0.05	594.64	0.01
1 ^S ₃₈	154.76	0.05	157.74	0.01					

TABLE 3.1(cont'd)

MODE	DATA (Sec)	ERROR (%)	C2	DIFF. (%)	MODE	DATA (Sec)	ERROR (%)	C2	DIFF. (%)
2 ^S ₇	535.70	0.08	535.80	-0.02	3 ^S ₉	338.90	0.08	338.53	0.11
2 ^S ₈	488.01	0.05	487.56	0.09	3 ^S ₁₀	323.94	0.06	323.92	0.01
2 ^S ₉	448.35	0.05	448.27	0.02	3 ^S ₁₁	310.27	0.08	310.19	0.02
2 ^S ₁₀	415.92	0.18	415.81	0.03	3 ^S ₁₂	297.41	0.08	297.22	0.06
2 ^S ₁₁	388.28	0.05	388.49	-0.05	3 ^S ₁₃	285.08	0.08	284.93	0.05
2 ^S ₁₂	365.13	0.05	365.09	0.01	3 ^S ₁₄	273.35	0.05	273.29	0.02
2 ^S ₁₃	344.72	0.06	344.71	0.00	3 ^S ₁₆	251.98	0.05	251.98	0.00
2 ^S ₁₄	326.59	0.09	326.45	0.04	3 ^S ₁₇	242.43	0.05	242.29	0.06
2 ^S ₁₅	309.20	0.05	308.88	0.10	3 ^S ₁₈	233.29	0.05	233.23	0.03
2 ^S ₂₇	174.03	0.06	173.90	0.08	3 ^S ₁₉	224.91	0.05	224.76	0.07
2 ^S ₂₈	169.25	0.05	169.14	0.06	3 ^S ₂₀	216.95	0.09	216.84	0.05
2 ^S ₃₀	160.51	0.05	160.43	0.05	3 ^S ₂₄	190.07	0.05	189.94	0.07
2 ^S ₃₂	152.68	0.24	152.65	0.02	3 ^S ₂₅	184.32	0.08	184.20	0.07
2 ^S ₃₅	142.61	0.05	142.42	0.13	3 ^S ₄₁	113.31	0.08	113.23	0.07
2 ^S ₄₀	128.54	0.05	128.41	0.10	3 ^S ₄₂	111.36	0.08	111.24	0.10
2 ^S ₄₅	117.34	0.06	117.20	0.12	3 ^S ₄₃	109.38	0.08	109.34	0.04
2 ^S ₄₆	115.33	0.06	115.22	0.09	3 ^S ₅₀	97.97	0.08	97.79	0.18
2 ^S ₄₉	108.37	0.26	108.04	0.31	3 ^S ₅₁	96.44	0.07	96.36	0.08
2 ^S ₅₇	98.04	0.26	97.71	0.33	3 ^S ₅₄	92.39	0.08	92.34	0.05
2 ^S ₆₀	94.14	0.26	93.99	0.16	3 ^S ₅₈	87.65	0.05	87.55	0.12
2 ^S ₆₅	88.65	0.26	88.53	0.14					
2 ^S ₇₁	82.97	0.26	82.97	0.00	3 ^S ₆₃	82.38	0.13	82.30	0.09
2 ^S ₇₆	78.89	0.26	78.99	-0.13	3 ^S ₇₀	76.11	0.13	76.05	0.08
					3 ^S ₇₃	73.78	0.13	73.68	0.14
3 ^S ₁	1058.09	0.08	1058.01	0.01					
3 ^S ₂	904.30	0.05	904.32	0.00	4 ^S ₂	580.81	0.10	580.67	0.02
3 ^S ₆	392.33	0.05	392.00	0.08	4 ^S ₃	489.05	0.07	488.23	0.17
3 ^S ₇	372.05	0.05	372.03	0.01	4 ^S ₄	439.17	0.11	438.48	0.16
3 ^S ₈	354.56	0.05	354.39	0.05	4 ^S ₅	414.62	0.06	414.50	0.03

TABLE 3.1(cont'd)

MODE	DATA (Sec)	ERROR (%)	C2	DIFF. (%)	MODE	DATA (Sec)	ERROR (%)	C2	DIFF. (%)
4 ^S ₉	269.59	0.06	269.86	-0.10	7 ^S ₂	397.37	0.05	397.07	0.08
4 ^S ₁₀	258.85	0.08	259.01	-0.06	7 ^S ₄	293.20	0.05	292.98	0.08
4 ^S ₁₁	249.60	0.08	249.59	0.00	7 ^S ₁₀	209.42	0.13	209.74	-0.15
4 ^S ₁₂	240.78	0.06	241.00	-0.09	7 ^S ₂₅	125.48	0.09	125.79	-0.19
4 ^S ₁₃	232.75	0.06	233.00	-0.11	7 ^S ₃₅	101.74	0.09	102.01	-0.26
4 ^S ₁₄	225.08	0.06	225.41	-0.15	8 ^S ₁	348.12	0.05	347.67	0.13
4 ^S ₁₅	218.17	0.05	218.17	0.00	8 ^S ₅	239.96	0.05	240.20	-0.10
4 ^S ₂₀	186.33	0.06	186.17	0.08	8 ^S ₃₀	106.04	0.09	105.97	0.07
4 ^S ₄₀	115.44	0.06	115.29	0.13	9 ^S ₂	310.04	0.09	309.27	0.25
					10 ^S ₂	247.74	0.05	246.80	0.38
5 ^S ₂	479.34	0.05	477.86	0.31	10 ^S ₁₆	134.95	0.05	134.88	0.05
5 ^S ₃	460.78	0.05	460.63	0.03	11 ^S ₁	271.36	0.09	271.47	-0.04
5 ^S ₄	420.36	0.05	420.42	-0.01	11 ^S ₂₄	104.43	0.05	104.63	-0.19
5 ^S ₅	370.10	0.05	370.06	0.01	12 ^S ₇	170.69	0.05	171.02	-0.19
5 ^S ₆	332.11	0.05	332.29	-0.05	13 ^S ₁	222.69	0.09	222.82	-0.06
5 ^S ₇	303.98	0.05	304.04	-0.02	13 ^S ₁₉	103.43	0.06	103.52	-0.09
5 ^S ₈	283.56	0.05	283.82	-0.09	14 ^S ₄	180.81	0.13	180.43	0.20
5 ^S ₁₀	237.81	0.05	238.02	-0.09	15 ^S ₃	165.83	0.05	165.63	0.12
5 ^S ₁₂	213.03	0.05	213.57	-0.25	15 ^S ₁₆	100.77	0.05	100.90	-0.13
5 ^S ₁₅	187.75	0.05	188.07	-0.17	16 ^S ₂	175.29	0.05	175.81	-0.30
					16 ^S ₁₀	118.62	0.09	118.58	0.03
5 ^S ₁₆	181.74	0.06	181.92	-0.10	17 ^S ₁₅	100.48	0.09	100.43	0.05
5 ^S ₂₀	162.45	0.06	162.51	-0.04	18 ^S ₃	145.28	0.05	145.27	0.00
5 ^S ₂₅	143.59	0.05	143.52	0.05	18 ^S ₈	115.62	0.05	116.04	-0.36
5 ^S ₃₀	128.51	0.06	128.52	-0.01	19 ^S ₉	110.55	0.05	110.41	0.13
5 ^S ₃₅	116.63	0.06	116.56	0.06	19 ^S ₁₁	103.63	0.09	103.49	0.14
6 ^S ₁	505.81	0.05	504.46	0.27	20 ^S ₄	123.18	0.05	123.15	0.02
6 ^S ₁₅	178.76	0.09	178.59	0.10	20 ^S ₉	102.09	0.06	101.98	0.11
					21 ^S ₆	112.96	0.05	112.93	0.03
6 ^S ₂₈	123.51	0.06	123.60	-0.07	21 ^S ₈	105.36	0.05	105.18	0.17

data include the fundamental and first seven toroidal overtones having periods greater than 73 seconds. This eliminates 156 modes from the Gilbert-Dziewonski toroidal data set.

Although not used in the inversion we have spot checked modes in each overtone group up to the 22nd spheroidal overtone. Agreement is satisfactory.

3.4 Inversion. As a first step, we inverted the toroidal mode data for shear velocity and density, thereby minimizing the coupling between V_p and V_s . We then inverted using a combination of toroidal modes and the spheroidal modes that are particularly sensitive to shear velocity, checking against ScS - S and the shape of the shear wave travel time curve at various stages. Once these data are satisfied we have an accurate shear velocity profile and a first approximation to the density perturbation. Modes that are sensitive to compressional velocity and density were then inverted for these parameters with checks being made at various stages of the iterative process against body wave data such as PcP-P, P-wave residuals and differential core times. The perturbations in density, at this stage, affected the fits of the toroidal modes since they are slightly dependent on density. They were consequently reinverted. Modes that are strongly affected by all three parameters were inverted at the end of each iteration cycle in order to decrease the coupling between parameters. More and more higher spheroidal overtones were incorporated into the data set as the number of iterations increased until it became clear that the fit to the more

accurate and complete lower order data were starting to degrade while the model itself was almost indistinguishable from earlier iterations. Satisfactory convergence was achieved after about 8 iteration cycles and a total of 32 iterations on various subsets of the data. All the modes and body wave parameters were then recomputed. This procedure, although cumbersome, seems preferable to inverting simultaneously for all parameters using all the normal mode data with equal weight.

The final model, designated C2, fits the toroidal data set, 192 modes, with an average error of 0.09% and the radial-spheroidal data set, 208 modes, with an average error of 0.07%. A summary of the fit is given in Table 3.2. The complete data set along with computed periods for model C2 is given in Table 3.1. The fits to the fundamental modes, ${}_0^S_2 - {}_0^S_{29}$ and ${}_0^T_2 - {}_0^T_{29}$, are 0.03 and 0.05%, respectively. These are, generally the best excited and most accurately determined modes and it is important that they be fit well. More determinations have also been made of these modes and they therefore represent a better gross Earth average than some of the higher modes for which, in many cases, only a single observation is available. Fifty-two of the modes, or 13%, are fit to better than 1 part in 10,000 and 282 modes, or 71%, are fit to 1 part in 1,000; 244 modes, or 61% are fit to 1σ and 343, or 86% are fit to 2σ . Although this represents a good overall fit it is not as good as it should be if all the data are independent and if the error estimates are reliable. In spite of the great increase in the normal mode data set there are still some modes whose identification or period assignment is questionable.

TABLE 3.2

Model C2: Summary of Fit

Modes	Error (%)	Modes	Error (%)
$0^S_2 - 0^S_{20}$	0.03	$0^T_2 - 0^T_{29}$	0.04
$0^S_{30} - 0^S_{66}$	0.08	$0^T_{30} - 0^T_{46}$	0.17
$1^S_2 - 1^S_{43}$	0.10	$0^T_{30} - 0^T_{46}$	0.08*
$1^S_{44} - 1^S_{75}$	0.07	$1^T_2 - 1^T_{29}$	0.11
$2^S_3 - 2^S_{49}$	0.07	$1^T_{30} - 1^T_{66}$	0.07
$2^S_{57} - 2^S_{76}$	0.15	$2^T_2 - 2^T_{61}$	0.08
$3^S_1 - 3^S_{54}$	0.05	$3^T_9 - 3^T_{72}$	0.08
$3^S_{58} - 3^S_{73}$	0.11	$4^T_7 - 4^T_{66}$	0.16
$4^S_2 - 4^S_{40}$	0.08	$5^T_9 - 7^T_{49}$	0.09
$5^S_2 - 5^S_{35}$	0.09	$0^S_0 - 8^S_0$	0.05

Radial and Spheroidal 0.07

Toroidal 0.09

*Includes travelling wave data sets

Of the present 400 mode data set there are 40 modes that are not fit well ($>0.15\%$ error) by, either model C2 or 1066B of Dziewonski and Gilbert (1973) and are inconsistent with adjacent modes. When these modes are deleted model C2 satisfies 68% of the data to one standard deviation and 95% of the data to two standard deviations. Model C2 is therefore a statistically satisfactory fit to the normal mode data set. The fit to the short period fundamental mode data, ${}_0^T_{37} - {}_0^T_{45}$, is improved when surface wave data are incorporated into the data set.

There is considerable spread in measured values for the shorter period fundamental toroidal oscillations. This probably represents real lateral variations in the structure of the upper mantle. Kanamori (1970) and Dziewonski et al. (1972) have measured the dispersion of Love waves over a considerable number of great circle paths. These data can be used to augment the data of Gilbert and Dziewonski (1975) in order to obtain a more representative gross Earth data set. Table 3.3 gives the values obtained for ${}_0^T_{21}$ to ${}_0^T_{46}$ by averaging the above data sets with equal weight. The error is the standard deviation of the data groups and does not include the errors associated with the individual groups. Table 3.1 also gives some spot checks of the very high spheroidal overtone data (37 modes). These additional modes were not used in the inversion but the fit is comparable to the models of Gilbert and Dziewonski (1975).

C2 group velocities are compared with the results of Dziewonski et al. (1972) in Table 3.4. The data set is not so large or representative in this case, but the agreement is good.

TABLE 3.3

	Short Period Toroidal Modes					
	Obs.* (sec)	Error (%)	C2 (sec)	Diff (%)	1066B (sec)	Diff (%)
0^T_{21}	345.60	0.15	345.79	-0.05	346.02	-0.12
0^T_{22}	332.75	0.13	332.97	-0.07	333.21	-0.14
0^T_{23}	320.92	0.12	321.10	-0.06	321.35	-0.14
0^T_{24}	310.00	0.14	310.06	-0.02	310.32	-0.10
0^T_{25}	299.81	0.16	299.78	+0.01	300.05	-0.08
0^T_{26}	290.12	0.15	290.17	-0.02	290.45	-0.11
0^T_{27}	281.16	0.15	281.16	0.00	281.45	-0.10
0^T_{28}	272.70	0.15	272.70	0.00	273.00	-0.11
0^T_{29}	264.72	0.14	264.75	-0.01	265.05	-0.12
0^T_{30}	257.19	0.14	257.25	-0.02	257.56	-0.14
0^T_{31}	250.13	0.14	250.16	-0.01	250.47	-0.14
0^T_{32}	243.65	0.23	243.46	+0.08	243.78	-0.05
0^T_{33}	237.11	0.16	237.10	0.00	237.43	-0.14
0^T_{34}	231.06	0.17	231.17	0.00	231.40	-0.15
0^T_{36}	220.07	0.26	219.89	+0.08	220.22	-0.07
0^T_{37}	214.33	0.22	214.69	-0.17	215.33	-0.33
0^T_{38}	209.68	0.17	209.73	-0.02	210.07	-0.19
0^T_{39}	204.65	0.17	205.00	-0.17	205.34	-0.38
0^T_{40}	200.19	0.17	200.48	-0.15	200.82	-0.32
0^T_{41}	195.94	0.14	196.15	-0.11	196.49	-0.28
0^T_{42}	191.65	0.19	192.00	-0.18	192.34	-0.36
0^T_{43}	187.73	0.19	188.02	-0.15	188.36	-0.34

TABLE 3.3 (cont'd)

	Obs.* (sec)	Error (%)	C2 (sec)	Diff (%)	1066B (sec)	Diff (%)
0^T_{44}	183.99	0.17	184.21	-0.12	184.55	-0.30
0^T_{45}	180.38	0.15	180.54	-0.09	180.88	-0.28
0^T_{46}	176.91	0.15	177.02	-0.06	177.36	-0.25

* Average of Kanamori(1970a), Dziewonski et al.(1972), and
Gilbert and Dziewonski(1975)

1066B is from Gilbert and Dziewonski(1975).

TABLE 3.4
Group Velocities

	T (sec)		U (km/sec)	
	Obs.*	C2	Obs.*	C2
0^S_{10}	579.40	579.32	5.67	5.66
0^S_{12}	502.43	502.45	5.01	5.01
0^S_{15}	426.12	426.11	4.54	4.55
0^S_{21}	335.93	335.68	3.93	3.94
0^S_{25}	297.78	297.57	3.73	3.72
0^S_{29}	268.48	268.36	3.62	3.62
0^S_{35}	234.58	234.52	3.57	3.58
0^S_{40}	212.34	212.25	3.58	3.59
0^S_{45}	193.88	193.74	3.60	3.62
0^T_{10}	617.47	619.03	5.07	5.01
0^T_{13}	503.38	505.16	4.76	4.74
0^T_{16}	428.14	429.52	4.58	4.58
0^T_{21}	344.90	345.79	4.46	4.46
0^T_{25}	299.12	299.78	4.43	4.43
0^T_{29}	264.19	264.75	4.42	4.41
0^T_{41}	195.68	196.15	4.42	4.41
0^T_{46}	176.62	177.02	4.42	4.41

*Dziewonski, Mills, and Bloch (1972)

Although the number of modes inverted is considerably fewer than the 1066 considered by Gilbert and Dziewonski (1975), they constitute a representative data set, particularly when one considers that the total data set includes only 57 significant Earth data (Backus and Gilbert 1968; Gilbert et al., 1973; Gilbert and Dziewonski, 1975). Many of the additional modes do not contain independent information from that contained in the differential travel times and the modes considered in this paper. The additional modes also do not contribute substantially to the resolving power required to distinguish between models of the upper mantle. For example, compare the upper mantles of models 1066A and 1066B in Gilbert and Dziewonski (1975). The former used a smooth upper mantle starting model and the latter used B1 as a starting model, a model with two upper mantle discontinuities. The smooth starting model remained smooth, showing that the additional modes cannot resolve the detail which is apparent from body wave studies. Additionally, when B1 was subjected to re-inversion using all 1066 modes, there were very few changes required, usually amounting to less than 0.05% and the changes introduced in the upper mantle were in the same direction and generally of the same nature as the differences between C2 and B1. We feel, therefore, that our procedure of using high resolution body wave structures as starting models in the inversion and checking the resulting model against both the very high overtone data and body wave data is at least equivalent to, and perhaps better than, relying exclusively on the short period higher mode data. The fact that the lower mantle and core of model C2 are very similar

to the Gilbert-Dziewonski models, which were based on all 1066 modes, justifies this approach.

3.5 The Resulting Model. The inverted model, designated C2, is shown in Figures 3.1 and 3.2. The model parameters are given in Table 3.5. In addition to V_p , V_s and density as a function of layer index, radius and depth, we also tabulate the seismic parameter $\Phi (=K/\rho = V_p^2 - (4/3) V_s^2)$, bulk modulus (K), rigidity (μ), Lamé constant (λ), Poisson's ratio (σ), pressure and gravity. Also shown in Figure 2, are the Helmberger-Wiggins-Engen profiles which can be considered models of the upper mantle under western North America. Except for the large differences in the structure of the low-velocity zone and the lithospheric lid, the main effect of the inversion was to decrease both P and S velocities between the 400 and 670 discontinuities by about 0.05 to 0.1 km/sec.

The average lithosphere velocities of model C2 are 8.38 and 4.71 km/sec, for V_p and V_s respectively. These can be compared with 8.28 ± 0.03 and 4.79 ± 0.04 km/sec recorded over long distances in the Pacific (Sutton and Walker, 1972) and 8.27 ± 0.01 and 4.75 ± 0.07 km/sec for P_n and S_n over the Australian shield (Simpson, 1973). Hart and Press (1973) determined a value of 4.71 km/sec for S_n for 50 m. y. to 150 m. y. old oceanic lithosphere. There is evidence from refraction studies that V_p may be as high as 8.6 km/sec in the lower lithosphere (e.g. Kosminskaya et al., 1972). These studies are consistent with the average velocities of the lithosphere found here. The depth to the top of the low-velocity zone is 61 km although this could be

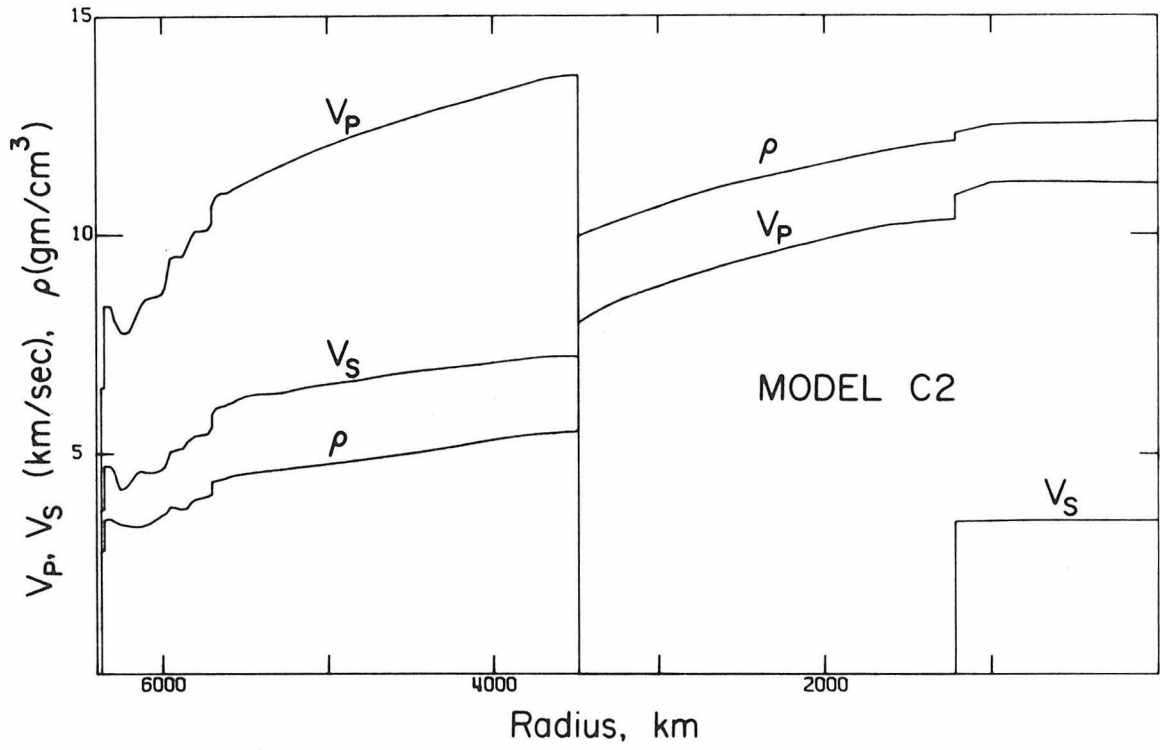


Figure 3.1 - Model C2; V_p (compressional velocity), V_s (shear velocity) and ρ (density) as a function of radius.

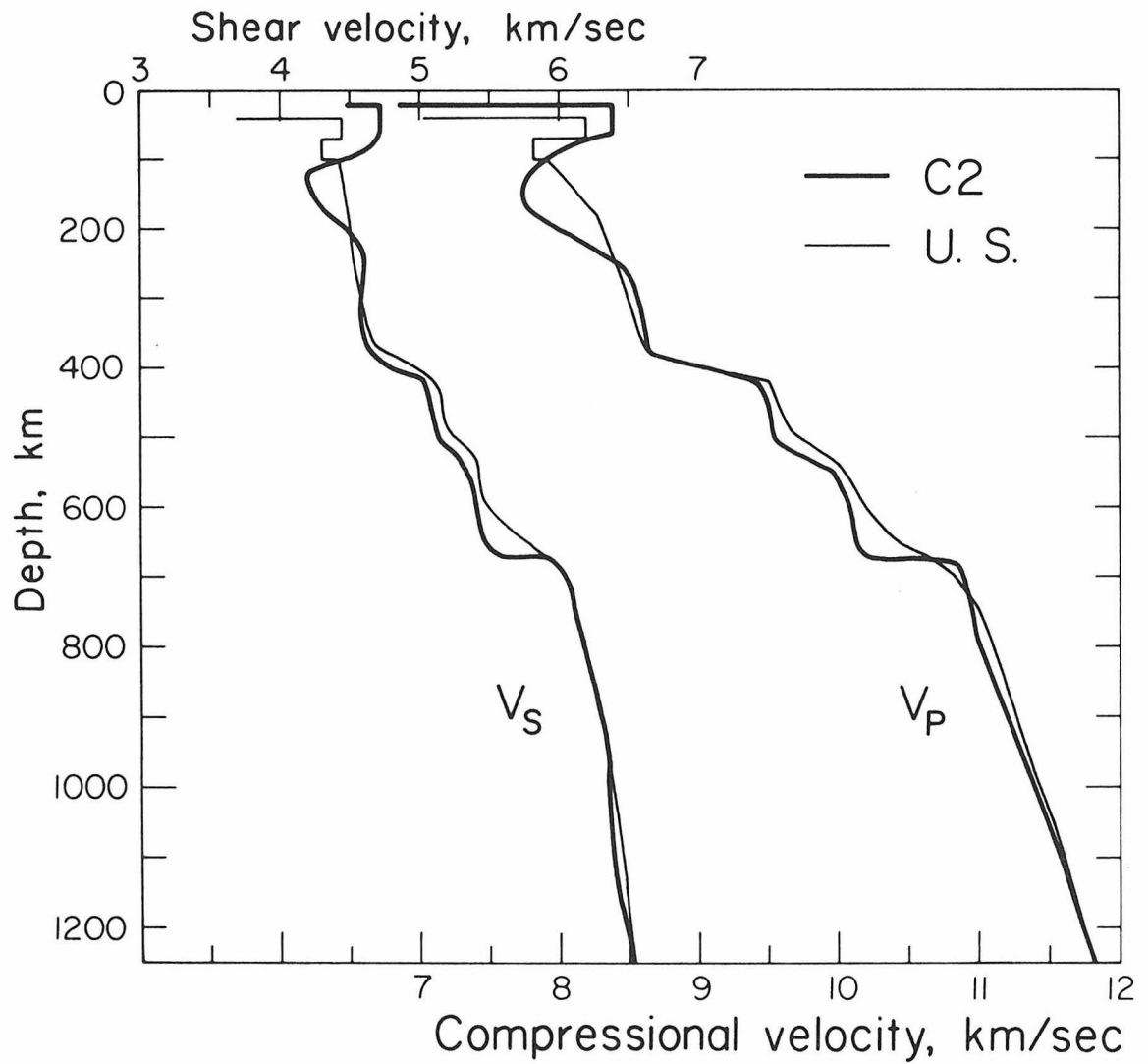


Figure 3.2 - Upper mantle structure of model C2 compared with results of HelMBERGER and Wiggins (1971) and HelMBERGER and Engen (1974), which are based on amplitude and wave-form studies in western U.S.

TABLE 3.5
MODEL C2

INDEX	RADIUS (KM)	DEPTH (KM)	VP (KM/S)	VS (KM/S)	RHC (G/CM**3)	PHI (KM/S)**2	K (KB)	MU (KB)	LAMBDA (KB)	SIGMA	PRESSURE (KB)	G (CM/S**2)
1	1	6370	11.17	3.50	12.58	108.43	13637	1541	12610	0.4456	3617	0
2	100	6271	11.18	3.50	12.57	108.56	13651	1541	12623	0.4456	3614	52
3	300	6071	11.19	3.50	12.53	108.84	13642	1536	12618	0.4457	3592	123
4	400	5971	11.20	3.50	12.53	109.00	13655	1534	12632	0.4458	3575	151
5	600	5771	11.20	3.50	12.52	109.10	13660	1530	12640	0.4460	3529	219
6	800	5571	11.20	3.48	12.52	109.26	13681	1520	12667	0.4464	3465	287
7	1000	5371	11.17	3.47	12.48	108.80	13580	1502	12579	0.4467	3385	355
8	1215	5156	10.89	3.46	12.30	102.60	12625	1471	11644	0.4439	3281	428
9	1215	5156	10.35	0.0	12.12	106.74	12940	0	12940	0.5000	5281	428
10	1300	5071	10.31	0.0	12.09	105.36	12867	0	12867	0.5000	3235	455
11	1400	4971	10.28	0.0	12.05	105.75	12742	0	12742	0.5000	3178	486
12	1500	4871	10.24	0.0	11.99	104.88	12577	0	12577	0.5000	3118	518
13	1600	4771	10.21	0.0	11.92	104.20	12425	0	12425	0.5000	3054	549
14	1700	4671	10.14	0.0	11.85	102.89	12192	0	12192	0.5000	2987	580
15	1800	4571	10.06	0.0	11.77	101.19	11909	0	11909	0.5000	2917	611
16	1900	4471	9.98	0.0	11.69	99.50	11629	0	11629	0.5000	2843	642
17	2100	4271	9.79	0.0	11.52	95.82	11041	0	11041	0.5000	2687	702
18	2200	4171	9.71	0.0	11.44	94.24	10782	0	10782	0.5000	2605	732
19	2300	4071	9.61	0.0	11.36	92.29	10485	0	10485	0.5000	2520	761
20	2400	3971	9.51	0.0	11.28	90.37	10194	0	10194	0.5000	2432	790
21	2500	3871	9.41	0.0	11.20	88.46	9904	0	9904	0.5000	2342	818
22	2600	3771	9.30	0.0	11.10	86.53	9608	0	9608	0.5000	2249	847
23	2700	3671	9.19	0.0	11.00	84.38	9283	0	9283	0.5000	2154	874
24	2800	3571	9.07	0.0	10.89	82.22	8953	0	8953	0.5000	2057	901
25	2900	3471	8.95	0.0	10.76	80.11	8624	0	8624	0.5000	1958	928
26	3000	3371	8.82	0.0	10.63	77.74	8267	0	8267	0.5000	1857	954
27	3200	3171	8.55	0.0	10.37	73.10	7578	0	7578	0.5000	1652	1004
28	3300	3071	8.39	0.0	10.23	70.40	7203	0	7203	0.5000	1547	1027
29	3400	2971	8.18	0.0	10.09	66.95	6757	0	6757	0.5000	1441	1051
30	3485	2886	7.98	0.0	9.96	63.74	6350	0	6350	0.5000	1351	1070
31	3485	2836	13.64	7.24	5.51	115.05	6389	2888	4464	0.3036	1351	1070
32	3510	2861	13.63	7.24	5.50	115.98	6383	2885	4460	0.3036	1336	1066
33	3550	2821	13.62	7.23	5.50	115.81	6367	2877	4450	0.3037	1313	1060
34	3625	2746	13.59	7.22	5.47	115.07	6299	2858	4394	0.3030	1270	1051
35	3700	2671	13.53	7.21	5.45	113.64	6209	2836	4318	0.3018	1227	1042

TABLE 3.5 (CONT'D)

INDEX	RADIUS (KM)	DEPTH (KM)	VP (KM/S)	VS (KM/S)	RHO (G/CM**3)	PHI (KM/S)**2	K (KB)	MU (KB)	LAMBDA (KB)	SIGMA	PRESSURE (KB)	G (CM/S**2)
36	3775	2596	13.45	7.18	5.43	112.27	6096	2799	4230	0.3009	1184	1035
37	3850	2521	13.37	7.14	5.40	110.64	5974	2756	4137	0.3001	1142	1028
38	3925	2446	13.28	7.11	5.36	109.00	5842	2712	4034	0.2990	1101	1022
39	4000	2371	13.20	7.07	5.31	107.56	5714	2659	3941	0.2986	1060	1017
40	4075	2296	13.12	7.04	5.27	106.09	5589	2612	3848	0.2979	1020	1013
41	4150	2221	13.04	7.01	5.22	104.62	5458	2562	3750	0.2971	980	1009
42	4225	2146	12.97	6.98	5.16	103.20	5330	2515	3653	0.2961	941	1005
43	4300	2071	12.89	6.95	5.12	101.72	5205	2471	3557	0.2950	902	1002
44	4375	1996	12.80	6.92	5.07	100.13	5079	2427	3461	0.2933	864	1000
45	4450	1921	12.71	6.89	5.03	98.42	4953	2386	3362	0.2924	826	998
46	4525	1846	12.63	6.85	4.99	96.86	4837	2344	3275	0.2914	789	996
47	4600	1771	12.54	6.81	4.96	95.27	4723	2302	3188	0.2904	752	994
48	4675	1696	12.44	6.77	4.92	93.76	4613	2253	3110	0.2899	715	993
49	4750	1621	12.35	6.72	4.88	92.50	4515	2203	3046	0.2902	678	993
50	4825	1546	12.26	6.67	4.84	91.12	4413	2153	2978	0.2902	642	992
51	4900	1471	12.16	6.63	4.81	89.33	4293	2113	2885	0.2886	606	992
52	4975	1396	12.06	6.59	4.77	87.41	4171	2075	2788	0.2866	571	992
53	5050	1321	11.95	6.56	4.74	85.42	4047	2039	2688	0.2844	535	992
54	5125	1246	11.83	6.52	4.71	83.35	3923	1998	2591	0.2823	500	992
55	5200	1171	11.71	6.45	4.67	81.52	3811	1945	2514	0.2819	465	993
56	5275	1096	11.58	6.38	4.64	79.66	3698	1891	2437	0.2816	430	994
57	5350	1021	11.45	6.37	4.61	76.98	3547	1867	2303	0.2761	396	995
58	5425	946	11.31	6.36	4.58	74.05	3390	1850	2157	0.2691	362	996
59	5500	871	11.17	6.31	4.54	71.78	3259	1805	2056	0.2662	328	997
60	5550	821	11.07	6.23	4.51	70.83	3195	1751	2028	0.2683	305	998
61	5573	798	11.03	6.17	4.50	70.85	3186	1711	2045	0.2723	295	999
62	5602	769	10.96	6.13	4.45	69.95	3120	1675	2003	0.2723	282	999
63	5625	746	10.95	6.09	4.43	70.40	3116	1640	2022	0.2761	272	999
64	5643	728	10.95	6.08	4.41	70.55	3111	1629	2025	0.2771	264	1000
65	5660	711	10.91	6.06	4.40	69.99	3079	1615	2003	0.2768	256	1000
66	5675	696	10.86	6.04	4.38	69.43	3041	1596	1976	0.2766	250	1000
67	5700	671	10.84	5.90	4.36	68.92	2917	1516	1906	0.2785	239	1001
68	5700	671	10.25	5.60	4.07	63.17	2572	1278	1720	0.2869	239	1001
69	5725	646	10.11	5.45	4.00	62.66	2522	1195	1725	0.2953	228	1000
70	5750	621	10.09	5.43	4.00	62.43	2500	1183	1712	0.2957	218	1000
71	5775	596	10.08	5.42	3.98	62.47	2486	1168	1707	0.2968	208	1000
72	5800	571	10.07	5.40	3.95	62.55	2474	1155	1704	0.2980	199	999

TABLE 3.5 (CONT'D)

INDEX	RADIUS (KM)	DEPTH (KM)	VP (KM/S)	VS (KM/S)	RHO (G/CM**3)	PHI (KM/S)**2	K (KB)	MU (KB)	LAMBDA (KB)	SIGMA	PRESSURE (KB)	G (CM/S**2)
73	5825	546	9.93	5.34	3.90	60.52	2360	1113	1618	0.2942	189	999
74	5850	521	9.70	5.26	3.76	57.10	2144	1040	1451	0.2912	179	998
75	5875	496	9.51	5.12	3.74	55.40	2072	981	1418	0.2956	170	998
76	5900	471	9.51	5.10	3.76	55.76	2097	979	1445	0.2981	160	997
77	5925	446	9.50	5.07	3.79	55.99	2124	977	1473	0.3006	151	997
78	5950	421	9.45	5.04	3.80	55.59	2111	965	1467	0.3016	142	996
79	5967	404	9.12	4.86	3.69	51.79	1910	870	1330	0.3022	135	996
80	5983	388	8.79	4.71	3.62	47.68	1728	802	1193	0.2989	129	995
81	6000	371	8.64	4.64	3.59	46.00	1654	773	1138	0.2977	123	995
82	6025	346	8.50	4.59	3.53	45.80	1613	745	1121	0.3004	114	994
83	6050	321	8.58	4.57	3.47	45.69	1585	725	1102	0.3015	106	993
84	6075	296	8.55	4.57	3.41	45.51	1545	712	1071	0.3002	97	992
85	6100	271	8.52	4.59	3.37	44.61	1504	709	1031	0.2962	89	991
86	6125	246	8.40	4.62	3.34	42.06	1407	713	931	0.2931	81	990
87	6150	221	8.19	4.57	3.34	39.30	1314	697	849	0.2746	72	989
88	6175	196	7.98	4.45	3.35	37.26	1250	663	808	0.2746	64	988
89	6200	171	7.78	4.30	3.37	35.89	1210	623	794	0.2801	56	987
90	6225	146	7.75	4.22	3.39	36.34	1230	603	828	0.2894	47	986
91	6250	121	7.79	4.18	3.40	37.29	1268	595	872	0.2971	39	986
92	6270	101	7.93	4.36	3.44	37.63	1293	652	958	0.2841	32	985
93	6290	81	8.08	4.62	3.48	36.83	1280	743	785	0.2569	25	984
94	6310	61	8.38	4.72	3.52	40.47	1425	784	902	0.2676	19	984
95	6330	41	8.38	4.73	3.51	40.31	1413	785	990	0.2656	12	984
96	6350	21	8.38	4.71	3.49	40.52	1419	775	902	0.2690	5	983
97	6350	21	6.50	3.72	2.80	23.79	665	387	407	0.2564	5	983
98	6368	3	6.50	3.72	2.80	23.76	665	387	407	0.2563	0.3	982
99	6368	3	1.45	0.0	1.02	2.09	22	0	22	0.4889	0.3	982
100	6371	0	1.45	0.0	1.02	2.09	22	0	22	0.4889	0	981

increased to about 80 km if the entry into the low-velocity zone is abrupt rather than gradual. The thickness of the LVZ is about 180 km. The density of the uppermost mantle is 3.50 gm/cm^3 , but see the later discussion on resolving power. A small amount of structure in the shear velocity is evident between about 670 and 1200 km depth. This results in a pronounced dip in the S-wave residual curve near 40° (see Figure 3.3). This feature of the model results from the inclusion of the model S1 structure from Chapter 2 in the starting model. The persistence of this feature through the inversion process indicates that it is compatible with the normal mode data and is indeed the gross earth structure we surmised it to be in Chapter 2. The shape of the S wave residual curve at distances beyond 60° is also more in line with body wave studies (i.e. Hales and Roberts, 1970) than is model B1.

The major effect of the inversion on core velocities is an increase of about 0.05 km/sec from the starting model. The other effects of the inversion are slight changes in the velocity gradient in the outer 400 km of the core, an increase in the velocity gradient in the outer part of the inner core and a decrease in the velocity jump across the outer core-inner core boundary. The density jump and compressional velocity jump at the boundary are, respectively, 0.02 g/cm^3 and 0.56 km/sec. The average density, compressional velocity and shear velocity of the inner core are 12.52 g/cm^3 , 11.19 km/sec and 3.50 km/sec. The shear velocity at the top of the inner core is 3.46 km/sec.

The small compressional velocity jump at the inner core-outer core

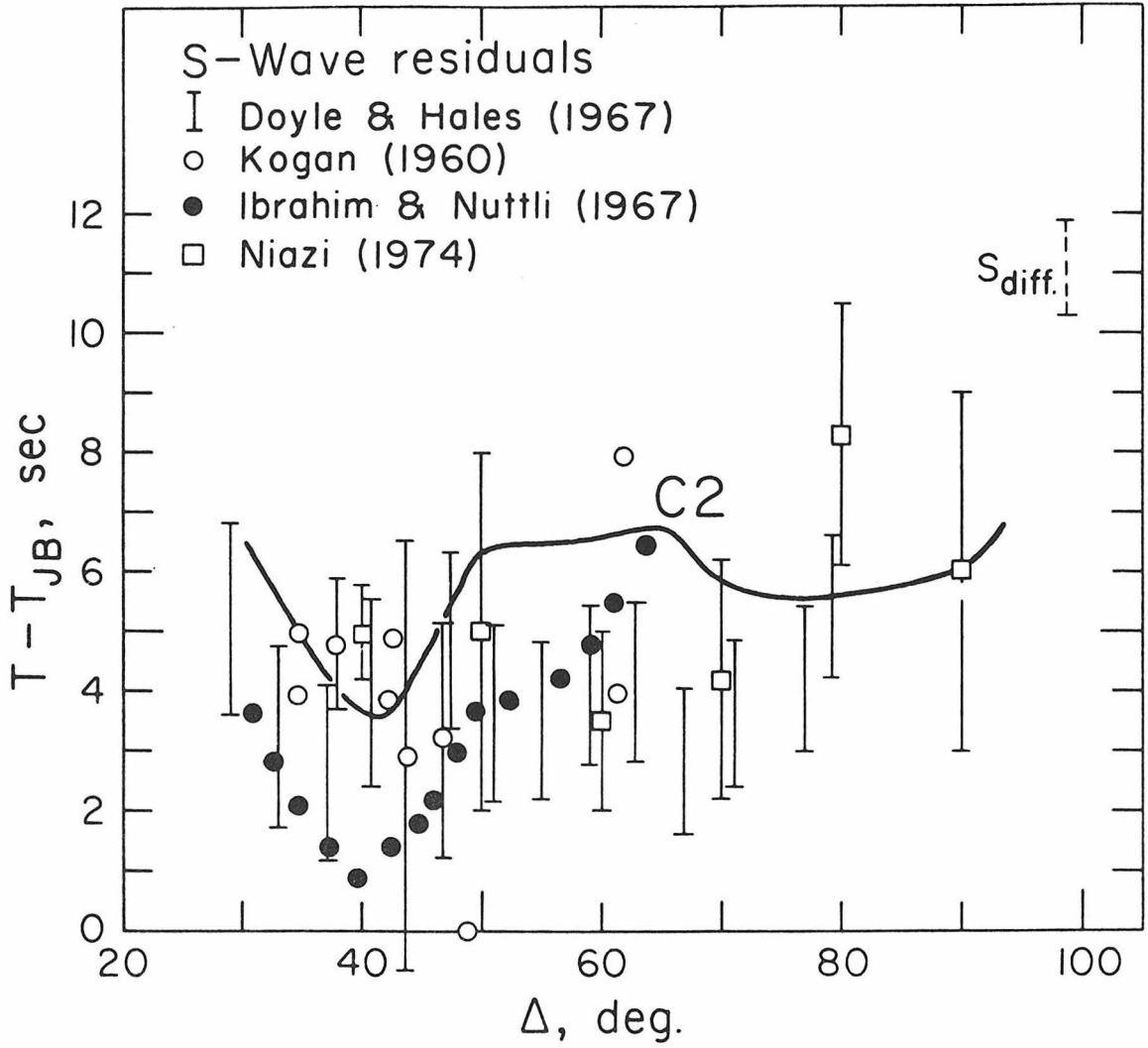


Figure 3.3 - Shear velocity residues, relative to the Jeffreys-Bullen Tables, of model C2 and other recent studies.

boundary (+0.56 km/sec) is in agreement with the evidence from amplitudes of long period core phases (Müller, 1973) which gives 0.58 km/sec. The high velocity gradient at the top of the inner core is also consistent with amplitude studies (Müller, 1973). The shear velocity at the top of the inner core, 3.46 km/sec, is in general agreement with the bounds, 3-4 km/sec, established by Müller (1973).

There is some evidence for inhomogeneity in the outer core, both at its upper and lower boundaries. The velocity gradient is about 0.24 km/sec per 100 km at the top of the core decreasing to 0.13 km/sec at a radius of 2800 km or about 700 km deep into the core. The gradient then decreases gradually to 0.08 km/sec per 100 km a radius of 1700 km. The velocity increases much more slowly, 0.03 km/sec per 100 km in the lowermost 500 km of the outer core. A similar effect occurs in the density profile, with a relatively high density gradient in the outer portion of the core compared with deeper levels.

It is of interest to compare the lower mantle and core of C2 with 1066A and 1066B (Gilbert and Dziewonski, 1975). The latter authors utilized the complete high overtone data set while we leaned more heavily on the nominally equivalent body waves and the more abundant fundamental and lower overtone data and only a sparse sampling of the high overtone data. Below a radius of 5600 km the mantle shear velocities and densities for these models are virtually identical. The P-velocities differ at most by 0.2 km/sec; the main difference is that the P velocity for the 1066 models have a long wavelength oscillation while C2 is much smoother. Dziewonski et al. (1975), using the

full mode data set also have a smooth lower mantle for V_p . The density and V_p in the core are also in very good agreement. There are small differences in the inner core for V_p and V_s . In model C2 the slight structure for V_p in the inner core, particularly the rapid increase in the outer portion, is inherited from the starting model of Whitcomb (1973) and is therefore a requirement of the core phases rather than the modes. The differences between C2, 1066A and 1066B in the inner core are probably unresolvable using the modes alone. The differences are slight. For example, V_p at the top of the inner core ranges from 10.97 km/sec (1066A), 11.04 km/sec (1066B) and 10.89 km/sec (C2), a spread of 1%. The central V_p is 11.34 km/sec (1066A), 11.28 km/sec (1066B) and 11.17 km/sec (C2), also a spread of 1%. The average V_s for the inner core is 3.57 km/sec (1066A), 3.50 km/sec (1066B) and 3.48 km/sec (C2). The major difference among the models is the density of the inner core. This is not unexpected since the resolving power for density is very poor in this region. This is unfortunate since the density is the main constraint on the composition of the inner core. If the density jump at the outer core-inner core boundary is small, as in C2, then the inner core can be the same material as the outer core since freezing at core pressures can be expected to increase the density only slightly. If the density jump is large then it is probable that inner core is lacking in the light elements that are required to satisfy the outer core densities. Average inner core densities are 13.12 g/cm^3 (1066A), 12.85 g/cm^3 (1066B) and 12.35 g/cm^3 (C2). The density of iron at inner core pressures is about $12.9 - 13.4 \text{ g/cm}^3$.

3.6 Resolution. The resolving power of gross earth data has been discussed by Backus and Gilbert (1970) and Jordan and Anderson (1974). Although the data set used in the present inversion is more extensive than that used by the latter authors, we use their estimates of averaging lengths as conservative guides. The trade-offs between parameters such as density and shear velocity are also discussed in Jordan and Anderson (1975) and Dziewonski (1970). These trade-offs make it particularly important to have independent estimates of the shear velocity structure and to first fit those modes that are sensitive to shear velocity.

Resolution is poor for density below 2400 km, shear velocity structure in the inner core and in the lower 500 km of the mantle and the compressional velocity in the vicinity of 2400 km radius. In these regions only very long wavelength perturbations from the starting model are justified by the data. The averaging lengths for shear velocity in the upper mantle and transition region are about 200 km and 400 km respectively. The averaging kernels for V_p in the outer core are about 1,000 km. As Jordan and Anderson (1974) point out the density of the lithosphere cannot be discussed with any useful precision because the averaging length for density in the upper mantle is about 400 km. However, the high average shear velocity in the lithosphere is resolvable and is consistent with body wave data. Structure in the lithosphere is not resolvable. The averaging lengths for density in the lower mantle are about 1,000 km.

Considering the above, the slight reversal in shear velocity below

246 (0.05 km/sec over 100 km) depth and in density below 421 km (0.06 g/cm³ over 25 km) are clearly not resolvable.

3.7 Comparison with Body Wave Observations. Most recent studies indicate that the J.B. tables for P-waves are slow by up to 3 seconds. Qualitatively, the present study indicates the same thing but the average discrepancy between 30° and 95° is only 1.2 sec with maximum deviations from J.B. times near 30° (1.6 sec) and between 55° and 75° (1.7 - 3.0 sec). Model C2 is 1.5 sec slow, on the average, over the range 30° - 95°, compared to the 1968 tables, with the residuals decreasing from 2.4 sec at 30° to 0.8 sec at 80° and increasing to 1.5 sec at 95°. A possible bias of this type in the 1968 tables was pointed out by Jordan and Anderson (1974). The travel times of Hales et al. (1968) agree with those predicted by model C2 to within 0.6 sec with maximum deviations of 1 sec at 45° and 90°. Model C2 averages 0.6 sec slower than Hales et al. (1968). The discrepancies between the various body wave studies confound efforts to determine differences between the "average" mantle (free oscillations) and tectonic to continental paths (most body wave studies) but the present study combined with the most recent body wave data suggests that the average Earth is about 0.6 sec slower than that portion of the Earth available to study by body wave techniques, i.e. continental sources and receivers. Alternatively, one could say that model C2 is consistent with P wave travel time studies since it falls between the J.B. and '68 solutions (Herrin et al. 1968) and is close to solutions of Cleary and Hales

(1966), Hales et al. (1968) and Carder et al. (1966). Throughout most of the distance range between 30° and 95° it is slightly slower than these three studies and is closest to Cleary and Hales (1966); see Figure 3.4 and Table 3.6.

Table 3.7 compares the apparent velocities, $(dt/d\Delta)$, of model C2 with 4 sets of published data. The fit is satisfactory in that predicted values fall within the scatter of the observations except near 85° but even there the difference is only 0.6%.

Model C2 averages 2 sec faster than J.B. times for PcP between 30° and 90° (Table 3.8). The difference in the size of the core accounts for about 1.8 sec of this difference. The remainder is accounted for by the 0.3 sec difference in travel times between J.B. and C2, at 95° . PcP times from Pacific events (Gogna, 1973) agree with model C2 to 0.3 sec, ranging from +2.2 sec at 50° to -2.0 sec at 80° (O-C). The modified PcP times (Engdahl and Johnson, 1975) consistent with the 1968 tables average 1.3 sec faster than model C2. Since these times were determined from differential PcP-P times and the B1, and C2, core radius, this difference must be accounted for in mantle velocities. In fact, the 1968 tables average 1.5 sec faster than C2 for P-waves between 30° and 95° . Within the uncertainty of the data no statement can be made, from PcP data regarding the differences between the average Earth and body wave solutions. The C2 PcP-P times (Table 3.9) average 0.5 sec fast between 30° and 60° and 0.3 slow beyond 65° but seem to be generally consistent with the data.

The core phase PKP averages 1.7 sec faster for C2 than J.B. This

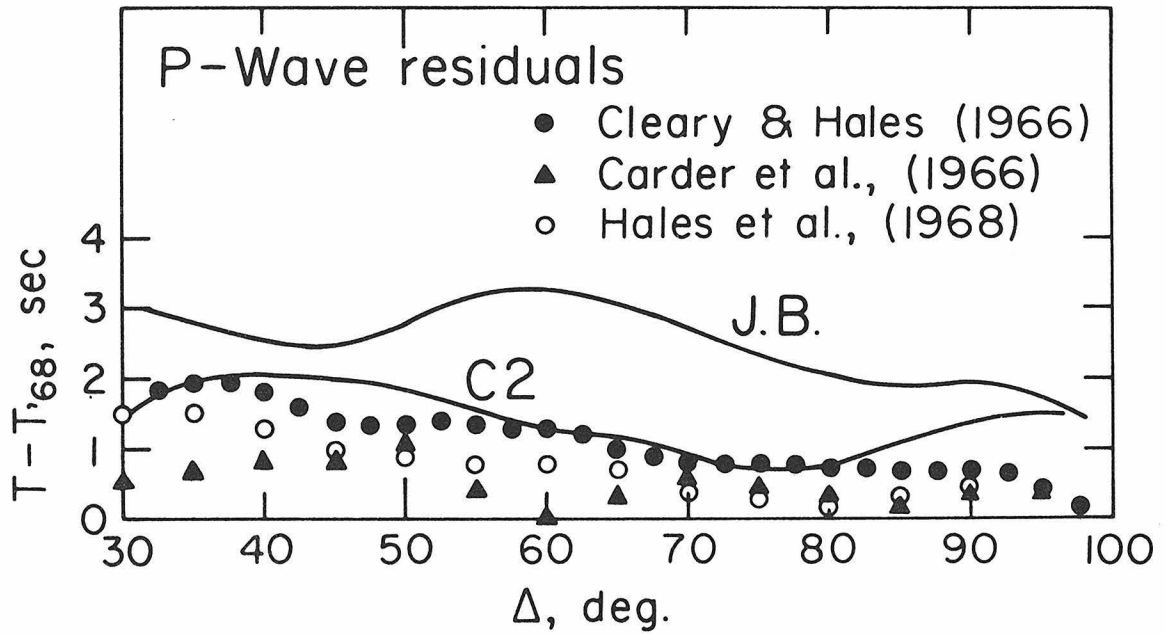


Figure 3.4 - Compressional velocity residuals, relative to the 1968 Tables (Herrin et al., 1968) of model C2 and other recent studies. Jeffreys-Bullen (J.B.) times are also shown.

TABLE 3.6

Compressional Wave Travel Times (sec)							
Δ (deg)	JB (1)	HCR (2)	1968 (3)	C2	δ_1	δ_2	δ_3
30	372.5	371.0	368.5	370.9	1.6	0.1	-2.4
35	416.1	414.8	413.3	415.3	0.8	-0.5	-2.0
40	458.1	457.0	455.7	457.8	0.3	-0.8	-2.1
45	498.9	497.4	496.4	498.4	0.5	-1.0	-2.0
50	538.0	536.1	535.2	537.7	1.0	-0.9	-1.8
55	575.4	573.0	572.2	573.7	1.7	-0.7	-1.5
60	610.7	608.2	607.4	608.7	2.0	-0.5	01.3
65	644.0	641.6	640.9	642.1	1.9	-0.5	-1.2
70	675.4	673.1	672.7	673.6	1.8	-0.5	-1.4
75	705.0	702.9	702.6	703.3	1.7	-0.4	-0.7
80	732.7	730.8	730.6	731.4	1.3	-0.6	-0.8
85	758.5	756.9	756.6	757.7	0.8	-0.8	-1.1
90	782.7	781.1	780.7	782.1	.6	-1.0	-1.4
95	805.7		803.9	805.4	0.3		-1.5
Average difference (sec)					+1.2	-0.6	-1.5

(1) Jeffreys and Bullen (1940)

(2) Hales et al. (1968)

(3) Herrin et al. (1968)

TABLE 3.7

dt/d Δ of P Waves (sec/deg)

Δ (deg)	HCR (1)	CGJ (2)	LJ (3)	DJC (4)	C2
30	8.94	8.88	8.92	9.13 \pm 0.05*	8.99
35	8.60	8.67	8.60	8.70 \pm 0.05	8.67
40	8.26	8.30	8.38	8.26 \pm 0.07	8.32
45	7.91	7.99	7.90	8.11 \pm 0.10	7.93
50	7.56	7.52	7.51	7.52 \pm 0.10	7.53
55	7.21	7.10	7.22	7.19 \pm 0.08	7.17
60	6.86	6.84	6.75	6.95 \pm 0.07	6.83
65	6.50	6.66	6.53	6.69 \pm 0.08	6.49
70	6.14	6.17	6.24	6.21 \pm 0.09	6.13
75	5.77	5.77	5.83	5.88 \pm 0.06	5.78
80	5.40	5.35	5.48	5.47 \pm 0.06	5.44
85	5.03	4.98	4.93	4.95 \pm 0.06	5.06
90	4.66	4.74	4.65	4.60 \pm 0.09	4.75
95	4.28	4.55	4.48	4.52 \pm 0.07	4.57

(1) Hales et al. (1968)

(2) Carder et al. (1966)

(3) Johnson (1969)

(4) Corbishley (1970)

* 95% C.I.

TABLE 3.8

Δ (deg)	PcP Times (sec)						
	JB (1)	Gogna (2)	68M (3)	C2	δ_1	δ_2	δ_3
30	554.9	553.0	551.1	552.2	2.7	0.8	-1.1
35	568.6	567.4	564.9	566.1	2.5	1.3	-1.2
40	583.9	583.2	580.3	581.4	2.5	1.8	-1.1
45	600.5	600.2	596.9	598.1	2.4	2.1	-1.2
50	618.3	618.2	614.8	616.0	2.3	2.2	-1.2
55	637.0	636.8	633.7	634.9	2.1	1.9	-1.2
60	656.6	656.0	653.3	654.6	2.0	1.4	-1.3
65	676.9	675.9	673.7	675.0	1.9	0.9	-1.3
70	697.8	695.6	694.7	696.0	1.8	-0.4	-1.3
75	719.9	716.0	716.1	717.4	1.7	-1.4	-1.3
80	740.6	737.1	737.8	739.1	1.5	-2.0	-1.3
85	762.3	759.2	759.7	761.1	1.2	-1.9	-1.4
90	784.2	781.6	781.8	783.3	0.9	-1.7	-1.5
Average difference (sec)					+2.0	+0.3	-1.3

(1) Jeffreys and Bullen (1940)

(2) Gogna (1973)

(3) Engdahl and Johnson (1974)

TABLE 3.9
PcP-P (surface focus)

Δ (deg)	(1)	(2)	C2	Error
30	181.9 <u>±</u> 0.4	181.6 <u>±</u> 0.6	181.3	0.3
35	151.4 <u>±</u> 0.3	151.6 <u>±</u> 0.6	150.8	0.8
40	125.1 <u>±</u> 0.5	124.6 <u>±</u> 0.6	123.6	1.0
45	100.7 <u>±</u> 0.4	100.5 <u>±</u> 0.6	99.7	0.8
50	79.9 <u>±</u> 0.4	79.6 <u>±</u> 0.6	79.0	0.6
55	62.3 <u>±</u> 1.0	61.5 <u>±</u> 0.6	61.2	0.3
60	46.1 <u>±</u> 1.0	45.9 <u>±</u> 0.6	45.9	0.0
65	33.0 <u>±</u> 1.0	32.8 <u>±</u> 0.6	32.9	-0.1
70	22.0 <u>±</u> 2.7	22.0 <u>±</u> 0.6	22.4	-0.4
75	13.4 <u>±</u> 2.1	13.5 <u>±</u> 0.6	14.1	-0.6
80		7.2 <u>±</u> 0.6	7.7	-0.5
85		3.1 <u>±</u> 0.6	3.4	-0.3
90		1.1 <u>±</u> 0.6	1.2	-0.1

(1) Jordan (1973)

(2) 68M

is in agreement, within 0.3 sec, of the differences in PcP times and therefore can be accounted for by differences in core radii and mantle velocities. The differential core times ($P'_{AB} - P'_{DF}$, $P'_{BC} - P'_{DF}$) agree with the recent study of Whitcomb (1973), with differences ranging from +0.4 to -0.9 sec. For comparison, other PKP data is tabulated in Table 3.10. The average difference between model C2 and the 68 tables is 0.3 sec. The PKP times for the AB and BC branches for model C2 are generally bracketed by the values given in the 1968 tables and the times given by Whitcomb (1973). However, the DF branch is generally 1 to 2 seconds fast. This could be corrected by, a) decreasing the velocity of the region surrounding the inner core, keeping the velocity jump at the inner core fixed or increasing it at most by 0.14 km/sec in order to satisfy the amplitude data, or b) by decreasing the radius of the inner core, or c) decreasing the average velocity in the inner core by 0.05 to 0.1 km/sec, again honoring the velocity jump at the boundary. Only the last alternative would be consistent with the PKiKP-PcP data which, as it stands, suggests the reverse of options a) and b).

The differential time PKiKP-PcP (Table 3.11) is a measure of the radius of the inner core. Model C2 averages 0.6 sec slower than the data of Engdahl et al. (1975). Assuming that core velocities in C2 are accurate this suggests that the inner core is 3 km larger than C2 or 1218 km. The scatter in the data, however, is such (-1.4 to +0.2 sec) that inner core radii from 1214 to 1222 km are acceptable. The uncertainty in PcP and PKP, i.e. average velocities in the mantle,

TABLE 3.10
PKP (surface focus)

Δ (deg)	JB (1)	68 (2)	JW (3)	C2	δ_1	δ_2	δ_3
170A	1286.3	1283.7		1284.7	1.6	-1.0	-
160	1242.7	1239.7	1241.8	1240.5	2.2	-0.8	1.3
150	1200.2	1196.9	1199.2	1197.7	2.5	-0.8	1.5
145B	1180.4	1178.0	1179.4	1177.7	2.7	+0.3	1.7
145B	1179.3	1174.4	1178.9	1176.7	2.6	-2.3	2.2
150	-	1188.1	1192.6	1190.1	-	-2.0	2.5
155C	-	1201.0	1204.1	1201.4	-	-0.4	2.7
122D			1136.8	1134.7			2.1
125			1142.7	1140.5			2.2
130	1152.0	1151.3	1152.5	1150.2	1.8	1.1	2.3
140	1170.5	1170.1	1171.2	1169.3	1.2	0.8	2.1
150	1187.4	1186.8	1188.0	1185.9	1.5	0.9	2.1
160	1200.8	1200.0	1201.5	1199.3	1.5	0.7	2.2
170	1209.2	1208.4	1210.4	1208.3	1.1	0.1	2.1
180F	1212.2	1211.0	1213.6	1211.8	0.4	-0.8	1.8
					+1.7	-0.3	+2.1
$P'_{AB} - P'_{DF}$							
170	77.1	75.3	-	76.4	0.7	-1.1	-
160	41.9	39.7	40.3	41.2	0.7	-1.5	-0.9
150	12.8	10.1	11.2	11.8	1.0	-1.7	-0.6
$P'_{BC} - P'_{DF}$							
150	-	1.3	4.6	4.2	-	-2.9	+0.4

(1) Jeffreys and Bullen (1940)

(2) Herrin et al. (1968)

(3) Whitcomb (1973)

TABLE 3.11

PKiKP-PcP Differential Times

Delta (deg)	Obs.*	C2	Error
10.90	477.5	478.3	-0.8
11.73	477.2	477.6	-0.4
21.34	464.9	466.3	-1.4
26.64	457.4	457.7	-0.3
27.71	454.8	455.7	-0.9
29.69	451.2	452.1	-0.9
30.50	450.4	450.5	-0.1
30.60	449.5	450.3	-0.8
31.08	448.2	449.3	-1.1
35.94	438.4	439.1	-0.7
36.04	438.8	438.9	-0.1
38.17	433.5	433.3	+0.2
47.18	411.9	412.1	-0.2
		Mean	-0.6

*Engdahl et. al. (1974)

core and outer core radius, are such that the value 1227.4 ± 0.6 km, preferred by Engdahl et al. (1974) is an acceptable solution although their error estimate appears to be optimistic. An uncertainty in outer core travel times of 1 sec immediately introduces an error of 5 km in the radius of the inner core.

Compared with published S wave travel times (Table 3.12) model C2 is 4.4 to 5.9 seconds slow, between 30° and 95° . Compared with unpublished data of Followill and Nuttli (1971), appropriate for paths to western U.S. (tectonic) the average discrepancy is 0.5 seconds. For other paths the discrepancy varies from about 5 sec at 35° to 3 sec at 95° . From about 30° to 40° C2 agrees with data of Kogan (1960) for Pacific surface explosions and falls between "continental" and "tectonic" solutions. Beyond 40° C2 is 2-4 sec slow compared to most shear wave travel times. Some of the data reported by Kogan (1960), Niazi (1973) and Bolt et al. (1970), are even slower than C2. However, when studying the data, one gets the impression that model C2 is slow by 2.4 seconds when compared to the majority of shear wave travel time studies. Since a gross earth model such as C2 should be heavily biased toward oceanic mantle, this time difference of 2-4 seconds should be close to the overall continent-ocean mantle differential. Indeed, the recent ScS data of Sipkin and Jordan (1975) does exhibit a travel time differential of about 4 seconds. Table 3.12 tabulates both observed and theoretical surface focus S wave travel times and $dt/d\Delta$'s. The calculated $dt/d\Delta$ for C2 is generally consistent with the observations except perhaps between 45° and 50° . This is the

TABLE 3.12
Shear Wave Times (surface focus)

Δ (deg)	t(sec)				dt/d Δ (sec/deg)		
	J.B. (1)	F.E.F. (2)	H.R. (3)	C2	H.R. (3)	F.E.F. (2)	C2
30	670.2	680.0	669.5	676.7	15.4	16.0	15.5
35	748.2	757.2	749.0	753.1	15.3	15.3	15.2
40	824.5	831.5	825.7	821.1	15.2	14.6	14.9
45	897.9	902.3	899.5	902.4	14.5	14.1	14.8
50	968.6	972.5	970.5	975.0	13.9	13.8	14.5
55	1036.8	1041.1	1038.7	1043.2	13.4	13.3	13.4
60	1102.6	1106.5	1104.1	1109.2	12.8	12.9	13.0
65	1165.5	1169.5	1166.7	1172.2	12.2	12.3	12.1
70	1225.6	1229.9	1226.4	1231.4	11.7	11.9	11.6
75	1282.6	1288.1	1283.2	1288.1	11.1	11.1	11.1
80	1336.5	1341.9	1337.3	1342.1	10.5	10.3	10.6
85	1387.3	1391.2	1388.5	1393.3	10.0	9.7	9.9
90	1435.5	1438.9	1436.9	1441.1	9.4	9.2	9.2
95	1478.2	1484.0	1482.4	1486.0	8.8	8.8	8.8

(1) Jeffreys and Bullen (1940)

(2) Followill and Nuttli (personal communication)

(3) Hales and Roberts (1970)

distance, however, where the shear wave data discussed in the last chapter indicate a revision of earlier solutions.

ScS times are even less studied than S times. Model C2 is 6.0 seconds slower than J.B. or Gogna times. This is consistent with C2 S times which are 4.5 to 5.9 slower than J.B. and Gogna times. The S and ScS data are therefore reasonably consistent with the view that average shear wave travel times in the mantle are about 4 seconds slower than standard body wave solutions. This can be compared with the earlier conclusions that the average Earth is 0.6 seconds slower for P-waves than obtained for that part of the Earth available for P-wave inspection.

The scatter in measured ScS-S times is 5 to 10 seconds (Hales and Roberts, 1970; Jordan, 1972; Jordan and Lynn, 1974). This has been attributed to lateral variations in mantle S times (Jordan and Lynn, 1974) deep in the mantle. The average residual $(ScS-S)_{C2} - (ScS-S)_{JB}$ over the distance range 30° to 80° is +0.7 sec, for deep focus events. The Jordan (1972) data set gives $+1.7 \pm 1.3$ sec (95% confidence interval). Between 40° and 70° model C2 has a J.B. residual of 0.4 sec compared with the Jordan (1972) value +0.5 sec. The ScS-S data are summarized in Table 3.12. We conclude that model C2 is an adequate fit to the ScS-S data.

At this point, we have developed an earth model which contains many short wavelength features compatible with high resolution body wave studies but which is as good or better a fit to the normal mode, travel time, and differential travel time data as any previous model.

TABLE 3.13

ScS-S Times (deep focus)

Δ (deg)	Observed time* (sec)	C2 time (sec)	Diff. (sec)
30	311.3+ <u>1.8</u>	306.8	-4.5
35	259.4+ <u>1.5</u>	258.3	-1.1
40	215.7+ <u>1.6</u>	213.3	-2.4
45	174.3+ <u>1.1</u>	172.2	-2.1
50	138.6+ <u>1.4</u>	137.9	-0.8
55	108.5+ <u>1.3</u>	107.2	-1.3
60	82.0+ <u>1.1</u>	80.7	-1.3
65	59.7+ <u>0.9</u>	59.2	-0.5
70	40.6+ <u>1.0</u>	41.2	-0.6
75	25.5+ <u>1.3</u>	26.6	1.1
80	14.0+ <u>0.8</u>	15.1	1.1

*Jordan and Anderson (1974); uncertainty
is 95% confidence interval

It is not completely satisfying, however, since the baseline problem with the shear waves is still present. It appeared that the only solution was that adopted by Dziewonski et al. (1975). That solution consisted of adopting two separate "gross earth" upper mantle structures for the earth, one for oceans and one for continents. By this means, the shear wave baseline could be circumvented but the meaning and derivation of the upper mantle structures is somewhat obscure. Moreover, it requires the concept that continental and oceanic mantle differ substantially to 600 km or 700 km in depth. While such a difference may exist, it is difficult to accept in light of conventional plate tectonics.

Chapter 4

THE EFFECT OF ATTENUATION UPON GROSS EARTH MODELS

4.1 Introduction. With the development of model C2 (see Chapter 3), the evolution of gross earth models seemed to have reached a turning point. We had gone as far as the data justified in constructing a radially symmetric earth model and the next step was to attempt laterally heterogeneous models. Dziewonski et al. (1975) had already made a preliminary venture in this direction and presumably the baseline problem with S travel times would be resolved in this manner. However, about one year ago, a major theoretical advance was made by Liu, Anderson, and Kanamori (1976) concerning the role of attenuation in seismic dispersion. In all previous surface wave and free oscillation studies, including that discussed in the preceding chapter, the effect of attenuation upon dispersion was assumed to be second order and thus ignored. Jeffreys (1965) and others had objected to this assumption, basing their arguments on the work of Lomnitz (1957), Futterman (1962), and Strick (1967), but due to the physical problems with those theories, these objections were discounted. Liu et al. (1976) showed that a physically realizable attenuation model would indeed predict first order perturbations in phase velocity across the seismic band. The inclusion of the Liu et al. (1976) model has produced a substantial revision in earth structure. As we shall see, one of the most important side effects of this revision has been the resolution of the shear wave travel time baseline.

4.2 The Effect of Attenuation Upon Dispersion. It has long been recognized that physical dispersion of elastic waves occurs in the presence of attenuation. While this dispersion has been included in some body wave studies (e.g. Carpenter, 1966, Helmberger, 1973) using Futterman's theory (Futterman, 1962) the effect has usually been ignored in surface wave and free oscillation investigations. The reason, possibly, is that there are arbitrary assumptions and physical shortcomings in most of the theories which had been put forward to explain the near constancy of Q over seismic frequencies. For example, Knopoff and MacDonald (1958) showed that the inclusion of infinitesimal attenuation in a linear system results in Q which is proportional to odd powers of frequency; therefore, a constant Q model (i.e. $Q \propto \omega^0$) is inconsistent with a linear system. This led Knopoff and MacDonald to introduce a non-linear model. No explicit dispersion relation has been obtained for such a non-linear system. Futterman's (1962) dispersion theory which is widely used in body-wave seismology predicts that inclusion of anelasticity increases the propagation velocity of a pulse in the medium. Because of this apparent paradox, Futterman's (1962) theory, which is widely used in phase equalization of body waves, has not been extensively used in surface wave and free oscillation studies. However, these problems do not directly apply to the situation in the earth's mantle.

In the earth, relaxation phenomena are most likely to be responsible for absorption (Anderson, 1967c). Relaxation mechanisms include grain boundary effects, partial melting, phase changes, atomic

reordering, and thermoelasticity. Absorption in a medium with a single characteristic relaxation time, τ , gives rise to the familiar bell-shaped Debye peak centered at a frequency $\omega = \tau^{-1}$. The specific dissipation function, Q^{-1} , and phase velocity satisfy the differential equation for the standard linear solid and can be written (7)

$$Q^{-1}(\omega) = 2Q_m^{-1} \omega\tau / (1 + \omega^2\tau^2) \quad (4.1)$$

$$C^2(\omega) = C_o^2 (1 + \omega^2\tau^2 C_\infty^2 / C_o^2) / \left[(1 + \omega^2\tau^2)^2 + 2\omega^2\tau^2 Q_m^{-1} \right]^{1/2} \quad (4.2)$$

The high frequency C_∞ , and low frequency, C_o , velocities are related by

$$\frac{C_\infty^2 - C_o^2}{C_o C_\infty} = 2Q_m^{-1}$$

In the above Q_m^{-1} is the peak value of the specific dissipation function at $\omega\tau = 1$. The low and high frequency limits of Q^{-1} are, respectively,

$$Q^{-1}(\omega) = 2Q_m^{-1} \omega\tau \quad (4.3)$$

and

$$Q^{-1}(\omega) = 2Q_m^{-1} (\omega\tau)^{-1} \quad (4.4)$$

Note that the magnitude of the peak dissipation depends on the total

range of velocities. The phase velocity is only constant at high or low frequencies; within those limits Q^{-1} varies as ω or ω^{-1} . In the earth, however, Q^{-1} within the seismic band is nearly constant (Knopoff, 1964). Moreover, laboratory data (Zener, 1948; Nowick and Berry, 1961) also indicate a much broader absorption peak than given by equation 4.1 above. In order to account for these observations, Liu et al. (1976) proposed a superposition of relaxation peaks which yields a broad absorption spectrum. The relaxation mechanisms that have been proposed for the earth (Anderson, 1967c; Jackson, 1969; Jackson and Anderson, 1970) have characteristic relaxation times spanning the seismic band (roughly 1 second to 1 hour). Even if a single mechanism were responsible for the absorption of seismic energy, the variation within the earth of temperature, pressure, grain size, activation energy and volume will serve to greatly broaden the absorption peak. A superposition of elementary Debye relaxation peaks, having a continuous distribution of relaxation times from τ_1 to τ_2 , distributed as τ^{-1} yields the following expressions for Q^{-1} and $C(\omega)$:

$$Q^{-1} = (2 Q_m^{-1} / \pi) \tan^{-1} \left[\omega(\tau_2 - \tau_1) / (1 + \omega^2 \tau_1 \tau_2) \right] \quad (4.5)$$

and

$$C(\omega) = C_o \left(1 + Q_m^{-1} / 2\pi \right) \ln \left[(1 + \omega^2 \tau_2^2) / (1 + \omega^2 \tau_1^2) \right] \quad (4.6)$$

These expressions were derived by Liu et al. (1976) where a fuller discussion may be found. Kanamori and Anderson (1977) also give a

complete and particularly clear review of the importance of attenuation in seismic dispersion. The above relations for $C(\omega)$ and $Q^{-1}(\omega)$ for the Liu et al. (1976) band-limited constant Q model are plotted in Figure 4.1. If we choose ω such that $\tau_1 \ll \omega^{-1} \ll \tau_2$, then we have

$$Q^{-1}(\omega) \sim Q_m^{-1} = \text{constant}$$

and

$$C(\omega) = C_o \left(1 + \frac{1}{\pi Q_m} \ln(\omega \tau_2) \right) \quad (4.7)$$

or

$$C(\omega) = C_\infty \left(1 - \frac{1}{\pi Q_m} \ln\left(\frac{1}{\omega \tau_1}\right) \right) \quad (4.8)$$

where

$$C_\infty = C_o \left(1 + \frac{1}{\pi Q_m} \ln\left(\frac{\tau_1}{\tau_2}\right) \right)$$

and $\frac{1}{\pi Q_m} \ln\left(\frac{\tau_1}{\tau_2}\right) \ll 1$ is assumed. These relations are fundamentally identical to those derived by various investigators (e.g. Kolsky, 1956; Lomnitz, 1957; Futterman, 1962; Savage, 1965; Strick, 1967; Liu et al., (1976) on the basis of a variety of assumptions, methods and approximations, and can be regarded as a universal dispersion relation for any linear models in the frequency range where Q is constant. They can also be derived from the equations given by Nowick and Berry (1961) for a log-normal distribution of relaxation times. We choose τ_1 and τ_2 in such a way that the period range of our interest, say 1 second to 1 hour, is completely bracketed by τ_1 and τ_2 . It is important to note that while the ratio $C_\infty/C_o = \left(1 + \frac{1}{\pi Q_m} \ln\left(\frac{\tau_1}{\tau_2}\right) \right)$ depends upon the ratio of the arbitrary upper and lower bounds of period, the ratio of

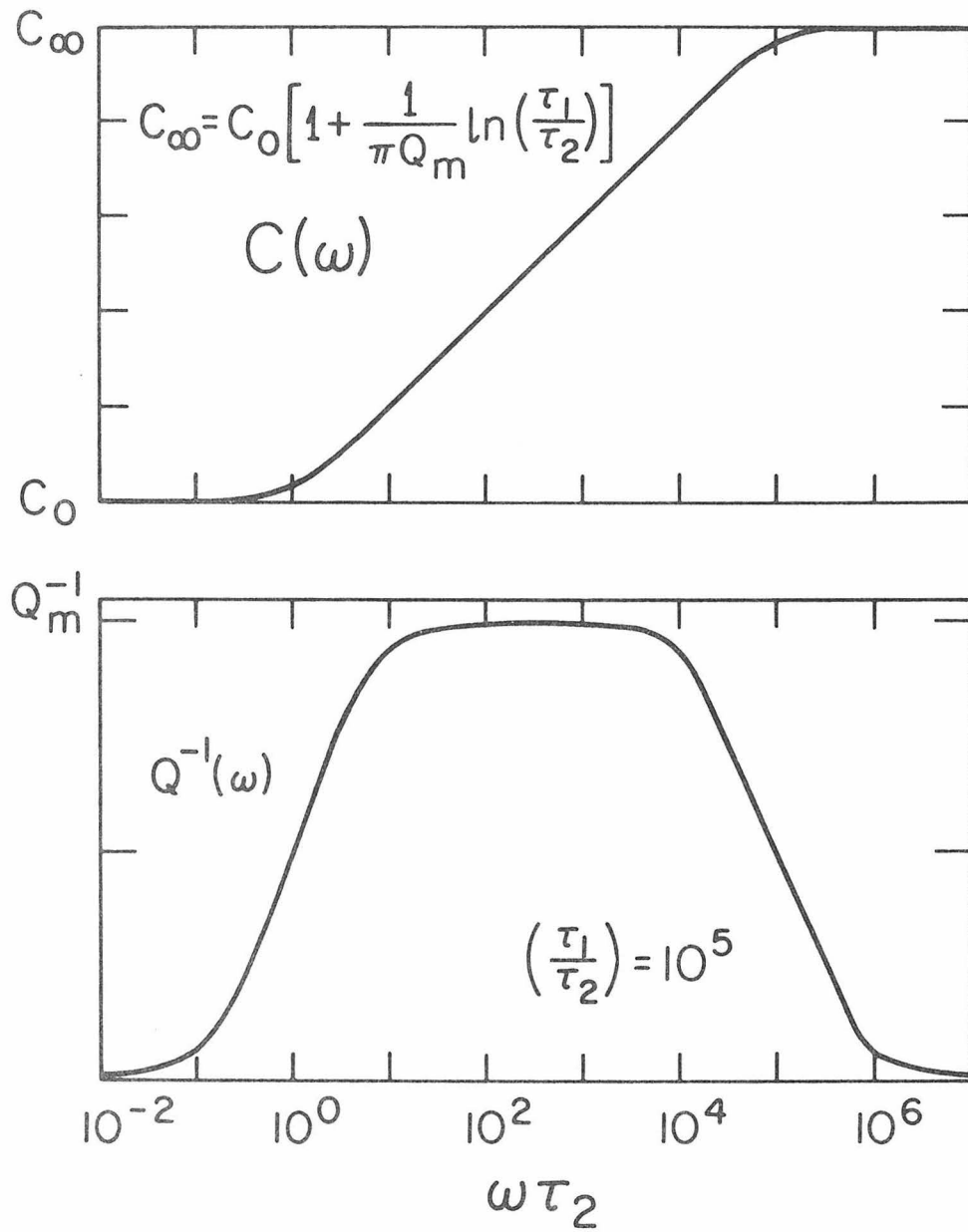


Figure 4.1 - Band-limited constant Q model derived from a linear visco-elastic model. τ_1 and τ_2 are long and short period cut-offs respectively.

of the phase velocities at angular frequencies ω_I and ω_{II} within the range of our interest ($\tau_2^{-1} \ll \omega_I < \omega_{II} \ll \tau_1^{-1}$)

$$\frac{C(\omega_{II})}{C(\omega_I)} \sim 1 + \frac{1}{\pi Q_m} \ln \left(\frac{\omega_{II}}{\omega_I} \right) \quad (4.9)$$

does not depend upon these arbitrary constants. Thus, in the frequency range where $Q = Q_m = \text{const}$, the relative dispersion can be determined unambiguously without knowledge of Q and the phase velocity outside the frequency band considered.

From equation 4.9 we can see that at high frequencies the elastic velocities are higher. Thus if this dispersion due to anelasticity is not taken into account, there will be systematic discrepancies among body wave, surface wave, and free oscillation results.

The discussion thus far has been confined to a simple homogeneous space, however the expressions derived generalize quite simply for an N -layered spherical model. In each layer, we have the following dispersion relations

$$\begin{aligned} \alpha_\ell(\omega) &= \alpha_\ell(\omega_R) \left[1 + \frac{1}{\pi Q_{\alpha_\ell}} \ln(\omega/\omega_R) \right] \\ \beta_\ell(\omega) &= \beta_\ell(\omega_R) \left[1 + \frac{1}{\pi Q_{\beta_\ell}} \ln(\omega/\omega_R) \right] \end{aligned} \quad (4.10)$$

where α , β , Q_β , Q_α are P velocity, S velocity, Q for shear waves, and Q for P waves respectively; ℓ is the layer index, and ω_R is the reference frequency (both ω and ω_R are assumed to lie within the

absorption band). We may use equations 4.10 to derive the phase velocity perturbations for Love and Rayleigh waves. From Anderson et al. (1965), the apparent Q_L^{-1} and Q_R^{-1} for Love and Rayleigh waves in a N-layered spherical earth are given by

$$Q_L^{-1} = \sum_{\ell=1}^N \frac{\beta_{\ell}}{C_L} \frac{\partial C_L}{\partial \beta_{\ell}} Q_{\beta_{\ell}}^{-1}$$

and

(4.11)

$$Q_R^{-1} = \sum_{\ell=1}^N \left[\frac{\beta_{\ell}}{C_R} \frac{\partial C_R}{\partial \beta_{\ell}} Q_{\beta_{\ell}}^{-1} + \frac{\alpha_{\ell}}{C_R} \frac{\partial C_R}{\partial \alpha_{\ell}} Q_{\alpha_{\ell}}^{-1} \right]$$

where C_L and C_R are the Love and Rayleigh phase velocities.

The phase velocity perturbations can be obtained by evaluating

$$\Delta C_L(\omega) = \sum_{\ell=1}^N \frac{\partial C_L(\omega)}{\partial \beta_{\ell}(\omega)} \Delta \beta_{\ell}(\omega)$$

and

(4.12)

$$\Delta C_R(\omega) = \sum_{\ell=1}^N \left[\frac{\partial C_R(\omega)}{\partial \beta_{\ell}(\omega)} \Delta \beta_{\ell}(\omega) + \frac{\partial C_R(\omega)}{\partial \alpha_{\ell}(\omega)} \Delta \alpha_{\ell}(\omega) \right]$$

Substituting equations 4.10 and 4.11 into 4.12 above

$$\Delta C_L(\omega) = C_L(\omega) (\pi Q_L)^{-1} \ell n(\omega/\omega_R)$$

(4.13)

$$\Delta C_R(\omega) = C_R(\omega) (\pi Q_R)^{-1} \ell n(\omega/\omega_R)$$

Equations 4.13 are the corrections which must be applied to the observed

phase velocities to obtain the phase velocity at the reference frequency. Since we will be most interested in comparing long period observations to body wave results, the choice of 1 hertz as the reference frequency will generally be most convenient. Moreover, the correction terms then take on the rather simple form

$$\frac{\Delta C_L(\omega)}{C_L(\omega)} = - \frac{\Delta T_L}{T_L} = (\pi Q_L(\omega))^{-1} \ln T$$

and (4.14)

$$\frac{\Delta C_R(\omega)}{C_R(\omega)} = - \frac{\Delta T_R}{T_R} = (\pi Q_R(\omega))^{-1} \ln T$$

where $T = 2\pi/\omega$.

Thus, if the dissipation function, Q^{-1} , is known for a particular surface wave period or a particular normal mode, we can simply determine the required correction term. Alternatively, given a model of the distribution of Q_β^{-1} and Q_α^{-1} with depth, we can compute theoretical values of Q_L^{-1} and Q_R^{-1} (equations 4.11) and use those values in equation 4.14.

4.3 Implications on the Inferred Structure of the Earth. Observed values of Q for most normal modes of the earth range from around 100 to about 500. If such values are substituted into equations 4.14 it is easy to see that the perturbation due to anelasticity, for either phase velocity or period, is on the order of 1%. When this value is contrasted with the value of 0.1%, the accuracy to within

which normal modes are generally modelled, the importance and magnitude of the attenuation effect is obvious.

From equation 4.10 we expect a fairly simple inverse tradeoff between Q in a layer and the velocity perturbation in that layer. Moreover, since Q_β is almost always substantially less than Q_α (see Chapter 5), the shear velocity perturbation should be equally larger than the compressional velocity change.

To obtain an initial indication of the details and consequences of the attenuation effect in the earth we corrected the observed toroidal eigenperiods of the earth and inverted for shear velocity in the mantle.

To obtain the necessary values of Q for the mode data, we adopted the Q model MM8 (Anderson et al., 1965) and computed theoretical Q values via equations 4.11. Model MM8, Table 4.1, was developed to match the observed attenuation of surface waves up to 300 seconds in period but does an excellent job of fitting all of the observed values of Q for the toroidal modes. Our data set consists of the 192 toroidal modes used in the C2 inversion (Chapter 3). In Figure 4.2, we have plotted the percent change in period for the fundamental modes and first five overtones of our toroidal data set. As our starting shear velocity profile, we used the C2 velocity structure. The inversion technique is the same as described in Chapter 2. In this case only a fairly simple, very smooth perturbation to the starting model was necessary. The resulting model, designated QM1, fits the corrected toroidal data with an average error of 0.07%; 77% of the modes are

TABLE 4.1

Q Model MM8

Layer Thickness (km)	Depth to Top of Layer (km)	Q_{β}
38	0	450
22	38	60
10	60	80
55	70	100
375	125	150
100	500	180
100	600	250
100	700	450
100	800	500
100	900	600
1886	1000	750
3485	2886	∞

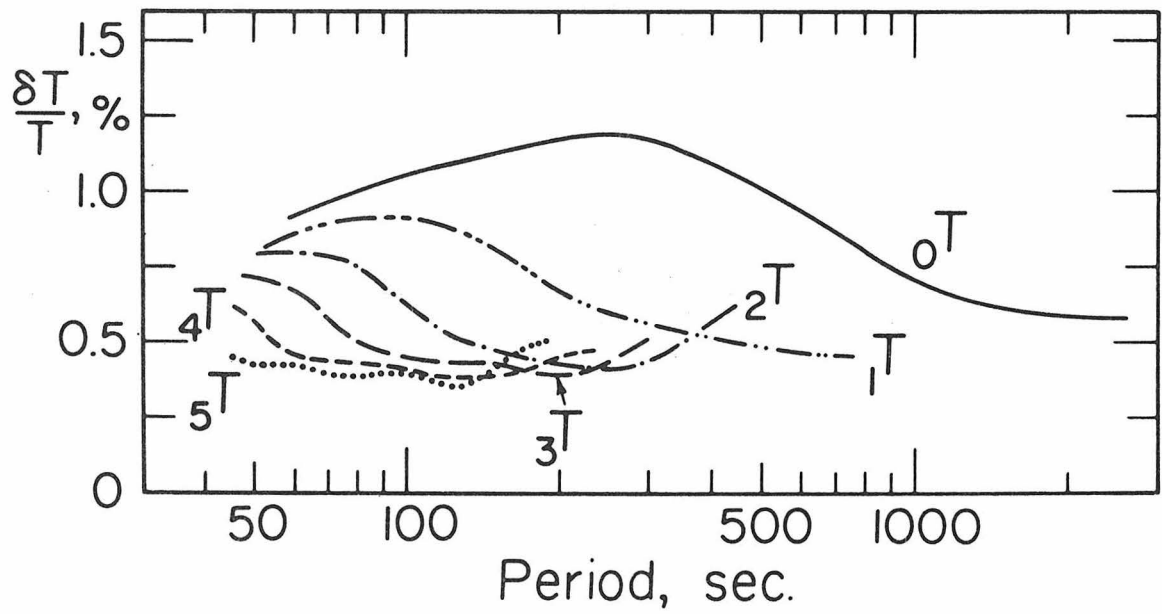


Figure 4.2 - Percentage change in period, as a function of period, for the fundamental toroidal modes and for the first five toroidal over-tones.

fit to within one standard deviation and 97% to within two standard deviations (the 95% confidence interval).

The errors assigned to the "observed" periods are based entirely on the uncertainties of the data and do not include uncertainties in the Q correction. The correction term is uncertain by about 20%, considering the scatter in the Q data, and the errors assigned to the corrected data should be increased by about this amount, i.e. data assigned an error of 0.05% should probably be assigned an error of 0.06%. This small difference is unimportant for present purposes.

The largest perturbation to the C2 structure occurs in the upper mantle, particularly in the region of the low velocity zone. Since these are the areas of lowest Q in model MM8, this result is exactly as we anticipated in the previous section. Figure 4.3 shows the upper mantle shear velocity structures for model QM1 and model C2. The change is almost a uniform increase throughout. Below about 800 km in depth, the change in velocity was essentially negligible. In Table 4.2, we have listed the upper mantle shear velocities of model QM1 along with those of model C2 and the Helmberger and Engen model SHR14 for comparison.

The most important, and, at the time, unanticipated consequence of this change in velocity was the magnitude of change in shear wave travel times. Table 4.3 lists the theoretical surface focus S travel times for model QM1 with the Jeffreys-Bullen (1940) travel-times. In Figure 4.4, we have plotted the J-B residuals for model QM1 along with those for models C2 and B1 (Jordan and Anderson, 1974) and for

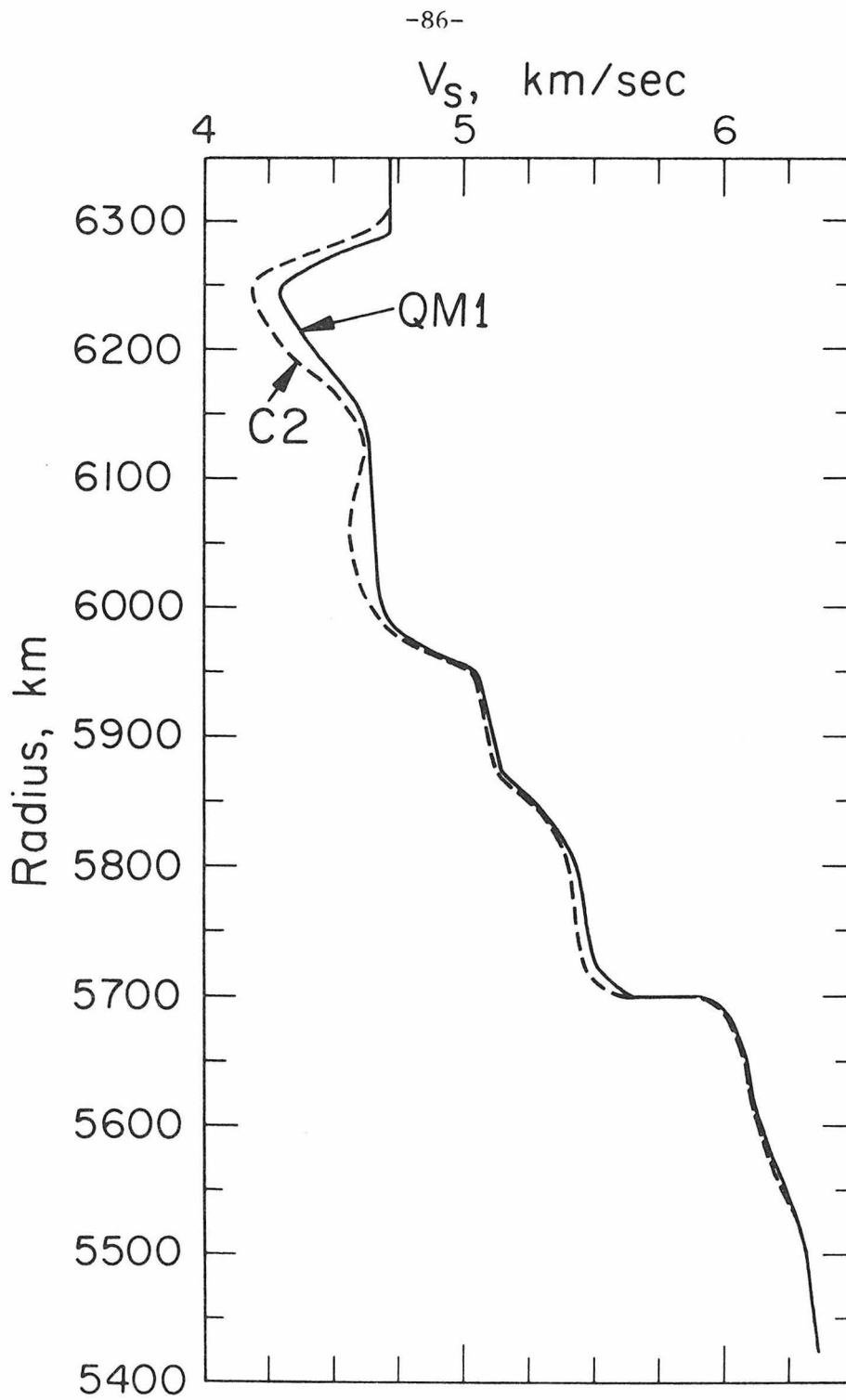


Figure 4.3 - Upper mantle shear velocity structure of model QM1 compared with that of model C2.

TABLE 4.2

Upper Mantle Shear Velocities

Radius (km)	SHR14 (km/sec)	C2 (km/sec)	QM1 (km/sec)
6371	3.69	0.0	0.0
6368	3.69	0.0	0.0
6368	3.69	3.72	3.72
6350	3.69	3.72	3.72
6350	4.45	4.71	4.71
6330	4.45	4.73	4.73
6310	4.39	4.72	4.72
6290	4.32	4.62	4.73
6270	4.43	4.36	4.46
6250	4.44	4.18	4.29
6225	4.46	4.22	4.33
6200	4.48	4.30	4.42
6175	4.50	4.45	4.52
6150	4.52	4.57	4.60
6125	4.54	4.62	4.63
6100	4.56	4.59	4.64
6075	4.58	4.57	4.65
6050	4.62	4.57	4.65
6025	4.65	4.59	4.66
6000	4.72	4.64	4.68
5983	4.85	4.71	4.72

TABLE 4.2 (cont'd)

Radius (km)	SHR14 (km/sec)	C2 (km/sec)	QM1 (km/sec)
5967	4.98	4.86	4.87
5950	5.10	5.04	5.05
5925	5.16	5.07	5.08
5900	5.18	5.10	5.11
5875	5.22	5.12	5.13
5850	5.39	5.26	5.27
5825	5.43	5.34	5.37
5800	5.43	5.40	5.43
5775	5.47	5.42	5.46
5750	5.57	5.43	5.48
5725	5.75	5.45	5.50
5700	5.90	5.60	5.57

TABLE 4.3

Shear Wave Travel Times

Δ (deg)	Time (sec)		QM1	dt/d Δ (sec/deg)	
	(1)	(2)		(2)	QM1
30	670.2	669.5	671.5	15.4	15.5
35	748.2	749.0	747.8	15.3	15.1
40	824.5	825.7	822.8	15.2	14.9
45	897.9	899.5	896.9	14.5	14.7
50	968.6	970.5	969.6	13.9	13.9
55	1036.8	1038.7	1037.8	13.4	13.4
60	1102.6	1104.1	1103.8	12.8	13.0
65	1165.5	1166.7	1166.8	12.2	12.1
70	1225.6	1226.4	1226.0	11.7	11.6
75	1282.6	1283.2	1282.6	11.1	11.1
80	1336.5	1337.3	1336.7	10.5	10.6
85	1387.3	1388.5	1388.0	10.0	9.9
90	1434.5	1436.9	1435.8	9.4	9.2
95	1478.2	1482.4	1480.6	8.8	8.8
100	1520.4		1523.6		8.4

(1) Jeffreys and Bullen (1940)

(2) Hales and Roberts (1970)

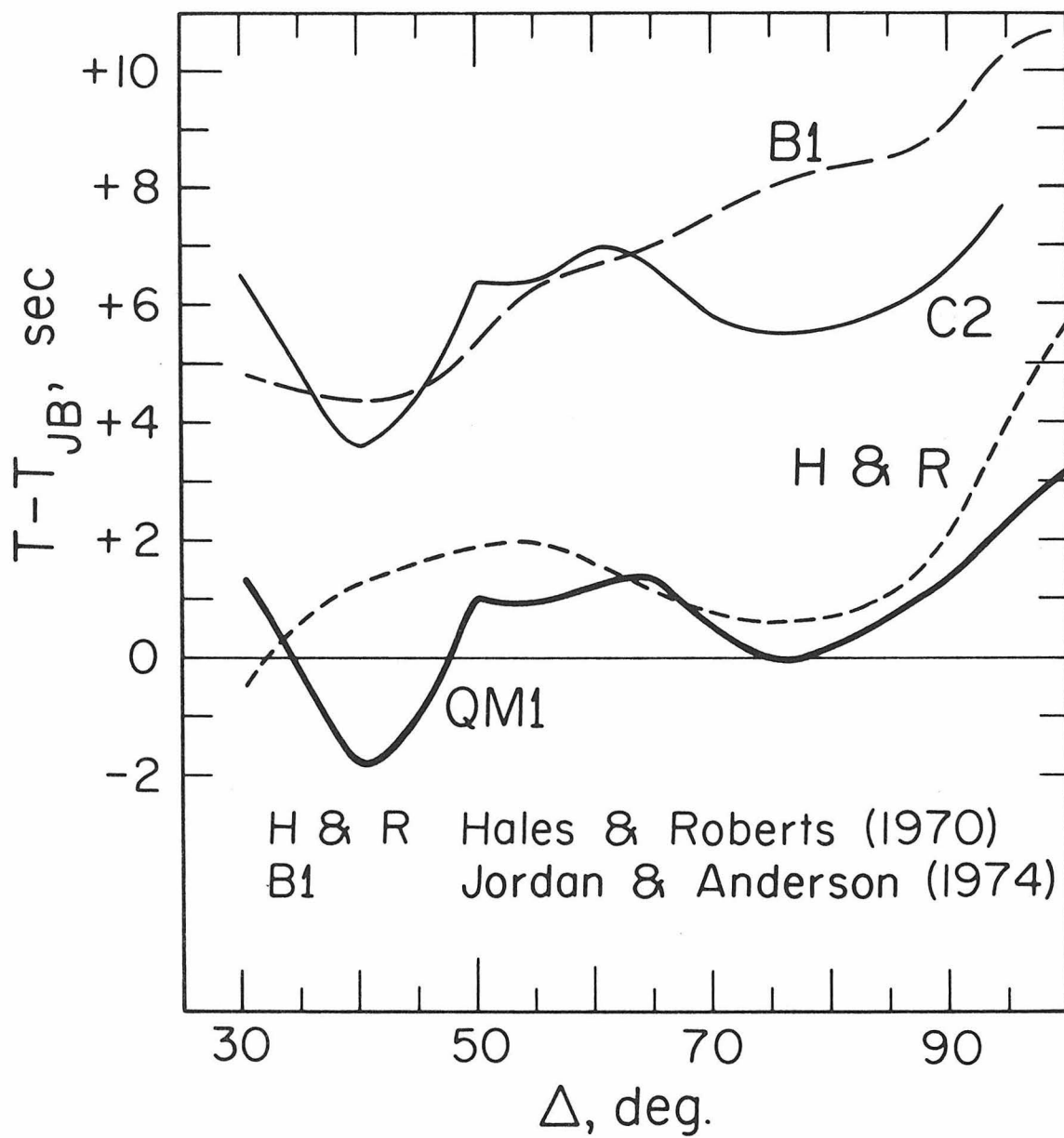


Figure 4.4 - Shear wave travel-time residuals, relative to the Jeffreys-Bullen Tables (1940), for model QM1, Hales and Roberts (1970), model B1 (Jordan and Anderson, 1974), and model C2.

the data of Hales and Roberts (1970). Since the velocity perturbation occurs primarily in the upper mantle, the shape of the residual curve is essentially identical with that of C2; however, what is significant is that the QM1 baseline shift is only +0.5 seconds. The inclusion of the attenuation effect in our normal mode data set almost exactly removes the baseline discrepancy in shear wave travel times. This is an immensely satisfying development as, indeed, the resolution of that discrepancy was the initial impetus for this research program. The next step is, obviously, the somewhat larger task of including the spheroidal and radial modes in an attenuation-corrected inversion.

4.4 The Presence of a Low Velocity Zone. Before undertaking the full inversion problem, it is interesting to examine what effect, if any, the inclusion of attenuation in the normal data has upon the requirement that an upper mantle low shear velocity zone exist. Jeffreys (1967) has maintained that this feature of the previous earth models (e.g.-Jordan and Anderson (1974) model B1; Gilbert and Dziewonski (1975) model 1066A; model C2) is an artifact arising from the neglect of the attenuation effect. Evidence for a low shear velocity zone is found in body wave studies such as the S_n studies of Molnar and Oliver (1969) and Hart and Press (1973) and in HelMBERGER's (1973) study of the western U.S. However, the S_n evidence is rather circumstantial and perhaps HelMBERGER's results are the result of a limited local structure. Thus much of the support for the existence of an upper mantle low-velocity zone has come from the inversion of normal mode

data that have been uncorrected for physical dispersion due to absorption. In light of these developments, we decided to re-examine the question of a shear wave low-velocity zone.

A starting model was constructed with monotonically increasing velocity and density in the upper 400 km of the mantle. The P and S velocities were chosen to satisfy the Jeffreys-Bullen (1940) travel time tables to 30° . A smooth, Bullen (1975) model A, density structure was used for this region. The model has a 3 km thick ocean layer, and an 18 km thick crustal layer. These are average values for the Earth (see Chapter 3). Below 400 km the parameters are the same as model C2.

We corrected the observed eigenperiods for absorption using a reference period of 1 second. The corrected data included 66 fundamental spheroidal modes, 46 fundamental toroidal modes, 10 spheroidal overtones and 80 toroidal overtones. The spheroidal modes were selected for their sensitivity to shear velocity. The Q model MM8 (Anderson et al., 1965) was again used to compute the correction. This data set was inverted using the technique described earlier.

The starting model does not provide a satisfactory fit to the normal mode data. The rms error is 0.7% while the rms error of the data is 0.09%. Only three modes are fit to within 1 standard deviation of the data and the errors for the shorter fundamental spheroidal modes (Rayleigh waves) are as large as 1.9%. The final model fits the data with an rms error of 0.07%; of the representative 78 modes used in the inversion, 62% fit the data to 1σ and 95% fit to 2σ .

The resulting upper mantle shear velocity (solid line) is shown

in Figure 4.5 along with the starting model. The new model has a pronounced low-velocity zone with shear velocity decreasing from 4.77 km/sec at the top of the mantle to a minimum of 4.42 km/sec at 170 km. The average J.B. shear wave travel time residual for the new model is +0.05 sec over the distance range 30° - 95° . We conclude that although some important revisions are required to earth models derived with uncorrected data, the low velocity is a required global feature.

4.5 The Effect of Attenuation upon a Gross Earth Model. There are two important limitations on gross earth models based upon the linear estimation inversion method we are employing here. The first is the dependence of the final model upon the starting model employed. We discussed this limitation briefly in Chapters 2 and 3. The second limit concerns the imposed emphasis of the data in the presence of errors. By this we mean whether goodness of fit to some subset or subsets of the data is valued more highly than the fit of other subsets of the data. This second limitation becomes more pronounced when the inversion procedure uses only relatively small subsets of the total dataset as we do here. Hence, if we were to correct the entire observed eigenperiod data set for attenuation and proceed with a C2-type inversion at this point, the net perturbation to the starting model would be some complex combination of the attenuation effect and the difference in data emphasis. It would be essentially impossible to avoid or separate out that latter effect. If by some means we could eliminate the errors (and consequent inconsistencies) from the

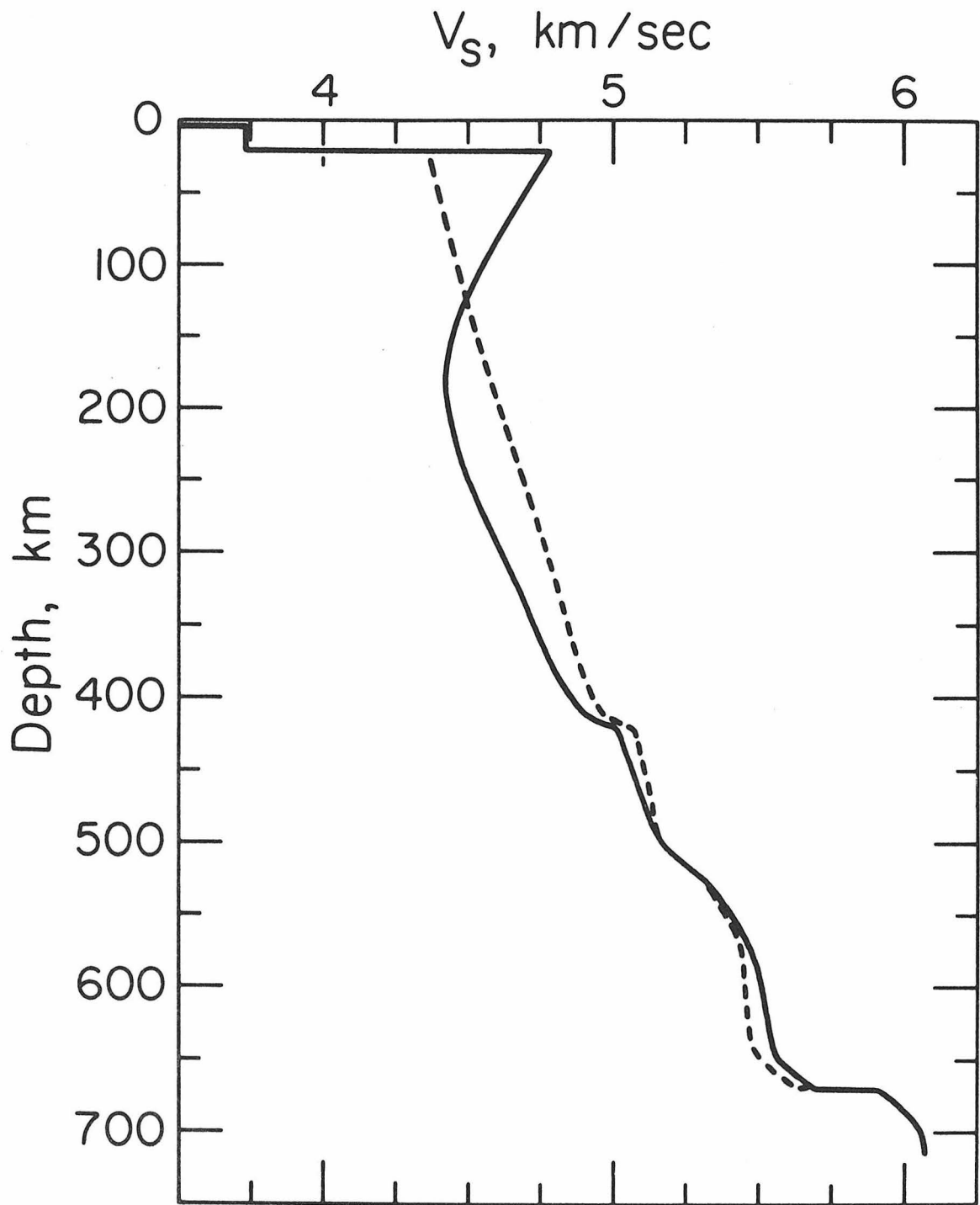


Figure 4.5 - Shear velocity (V_s) as a function of depth for the starting model (dashed) and final model (solid).

data, we could essentially eliminate the emphasis problem. We cannot, of course, eliminate the errors from the observed normal mode data. We can, however, do the next best thing. We can examine the perturbation to an existing gross earth model such as C2. For such a model we have a complete normal mode set whose frequencies we know exactly; no errors, no internal inconsistencies. By correcting the theoretical C2 eigenperiods using some Q model, such as MM8, and using C2 as the starting model, the model perturbation after inversion will be a reflection of the Q effect alone.

We have followed precisely that procedure with model C2 using Q model MM8 to obtain what we call a differential earth model. The inversion data set consists of some 400 radial, spheroidal, and toroidal modes, corrected for Q. In Figure 4.2, the period perturbation due to attenuation for Q model MM8 is plotted for the fundamental and first five overtones of the toroidal data. In Figure 4.6, we have plotted the equivalent perturbations for the spheroidal modes. In this figure, those modes which correspond to Stoneley waves at the inner core-outer core boundary and at the core-mantle boundary stand out very clearly. These modes have much higher apparent Q's than adjacent non-Stoneley modes of the same radial overtone number. Hence the percentage period change for such a mode is much smaller, and, in Figure 4.6, these modes show up as deep wells on the period change curves. At the same time, the cross over of energy between adjacent radial overtones is clearly illustrated as these modes alternate as Stoneley modes and ordinary mantle modes. Only two iterations were

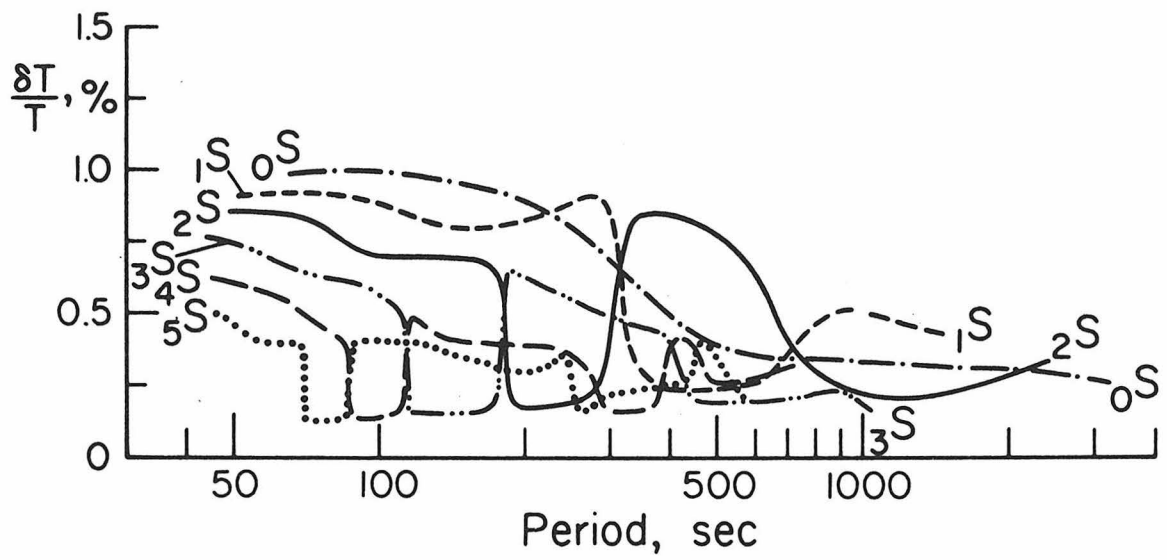


Figure 4.6 - The percentage change in period due to attenuation for the fundamental spheroidal modes and for the first five spheroidal overtones.

required to produce a differential model, designated QM2 (Table 4.4), which satisfies the corrected theoretical C2 periods to within the numerical accuracy of the computational algorithm. This very quick convergence results from the similarity between the Q perturbation kernels and the Frechet velocity kernels used in the inversion.

In Figure 4.7, we have plotted the perturbations in the seismic velocities and density as a function of depth for the change from C2 to QM2. The most dramatic effect is again an overall increase in shear velocity in the mantle.

In Figure 4.8, we have plotted the QM2 and C2 shear wave travel times as residuals with respect to the J-B Tables. As with model QM1, the QM2 travel times oscillate around the Jeffreys-Bullen predicted times. The mean residual is -0.2 seconds, at least an order of magnitude below the scatter in shear wave travel times. In Table 4.5, we have compiled the deep-focus ScS-S differential travel times for models QM2 and C2. The fits of QM2 and C2 are roughly the same although QM2 does slightly better. Since ScS-S is primarily lower mantle data and the Q for Q model MM8 is high in that region, this is the expected result. We have listed the surface focus ScS travel-times for model QM2 and for the Jeffreys-Bullen Tables in Table 4.6. The mean difference over the 30° - 95° distance range is less than -0.2 seconds.

The surface focus compressional travel-times, Table 4.7 (Table 4.8 contains the compressional $\partial t/\partial \Delta$'s), are slightly slower than those predicted by the 1968 Tables (Herrin et al., 1968) over the 30° - 95°

TABLE 4.4

RADIUS (KM)	MODEL QM2			MODEL C2		
	VP (KM/S)	VS (KM/S)	RHO (GM/CC)	VP (KM/S)	VS (KM/S)	RHO (GM/CC)
6371	1.45	0.0	1.02	1.45	0.0	1.02
6368	1.45	0.0	1.02	1.45	0.0	1.02
6368	6.50	3.72	2.80	6.50	3.72	2.80
6350	6.50	3.72	2.80	6.50	3.72	2.80
6350	8.38	4.73	3.49	8.38	4.71	3.49
6330	8.38	4.73	3.50	8.38	4.73	3.51
6310	8.38	4.74	3.52	8.38	4.72	3.52
6290	8.35	4.74	3.45	8.08	4.62	3.48
6270	7.82	4.58	3.39	7.93	4.36	3.44
6250	7.69	4.25	3.31	7.79	4.18	3.40
6225	7.68	4.17	3.29	7.75	4.22	3.39
6200	7.74	4.27	3.21	7.78	4.30	3.37
6175	7.46	4.50	3.33	7.98	4.45	3.35
6150	8.21	4.65	3.35	8.19	4.57	3.34
6125	8.45	4.76	3.36	8.40	4.62	3.34
6100	8.59	4.68	3.36	8.52	4.59	3.37
6075	8.63	4.60	3.38	8.55	4.57	3.41
6050	8.65	4.57	3.43	8.58	4.57	3.47
6025	8.67	4.59	3.51	8.60	4.59	3.53
6000	8.71	4.67	3.59	8.64	4.64	3.55
5983	8.85	4.77	3.65	8.79	4.71	3.62
5967	9.18	4.94	3.71	9.12	4.86	3.69
5950	9.51	5.14	3.82	9.46	5.04	3.80
5925	9.54	5.14	3.81	9.50	5.07	3.79
5900	9.53	5.12	3.76	9.51	5.10	3.76
5875	9.52	5.12	3.72	9.51	5.12	3.74
5850	9.70	5.25	3.73	9.70	5.26	3.76
5825	9.93	5.42	3.89	9.93	5.34	3.90
5800	10.07	5.50	3.95	10.07	5.40	3.95
5775	10.06	5.50	3.97	10.08	5.42	3.98
5750	10.06	5.47	3.99	10.09	5.43	4.00
5725	10.07	5.44	4.00	10.11	5.45	4.03
5700	10.21	5.58	4.04	10.25	5.60	4.07
5700	10.67	5.93	4.38	10.64	5.90	4.36
5675	10.89	6.07	4.40	10.86	6.04	4.38
5660	10.94	6.09	4.42	10.91	6.06	4.40
5643	10.98	6.11	4.43	10.95	6.08	4.41
5625	10.98	6.12	4.44	10.95	6.09	4.43
5602	10.99	6.15	4.47	10.96	6.13	4.46
5575	11.06	6.20	4.51	11.03	6.17	4.50
5550	11.10	6.26	4.52	11.07	6.23	4.51
5500	11.20	6.33	4.55	11.17	6.31	4.54
5425	11.34	6.38	4.58	11.31	6.36	4.58
5350	11.47	6.38	4.61	11.45	6.37	4.61
5275	11.60	6.40	4.64	11.58	6.38	4.64
5200	11.73	6.47	4.68	11.71	6.45	4.67
5125	11.85	6.53	4.71	11.83	6.52	4.71
5050	11.97	6.58	4.74	11.95	6.56	4.74
4975	12.08	6.61	4.77	12.06	6.59	4.77
4900	12.18	6.65	4.81	12.16	6.63	4.81

TABLE 4.4 (CONT'D)

RADIUS (KM)	MODEL QM2			MODEL C2		
	VP (KM/S)	VS (KM/S)	RHO (GM/CC)	VP (KM/S)	VS (KM/S)	RHO (GM/CC)
4825	12.27	6.69	4.85	12.26	6.67	4.84
4750	12.36	6.74	4.89	12.36	6.72	4.88
4675	12.45	6.79	4.94	12.44	6.77	4.92
4600	12.54	6.83	4.97	12.54	6.81	4.96
4525	12.62	6.87	5.01	12.63	6.85	4.99
4450	12.71	6.90	5.05	12.71	6.89	5.03
4375	12.80	6.93	5.09	12.80	6.92	5.07
4300	12.88	6.96	5.14	12.89	6.95	5.12
4225	12.96	6.99	5.19	12.97	6.98	5.16
4150	13.04	7.02	5.24	13.04	7.01	5.22
4075	13.12	7.06	5.29	13.12	7.04	5.27
4000	13.20	7.09	5.34	13.20	7.07	5.31
3925	13.28	7.13	5.38	13.28	7.11	5.36
3850	13.37	7.17	5.42	13.37	7.14	5.40
3775	13.46	7.21	5.45	13.45	7.18	5.42
3700	13.54	7.24	5.48	13.53	7.21	5.45
3625	13.60	7.26	5.49	13.59	7.22	5.47
3550	13.63	7.27	5.51	13.62	7.23	5.50
3510	13.64	7.27	5.52	13.63	7.24	5.50
3485	13.65	7.28	5.52	13.64	7.24	5.53
3485	7.98	0.0	9.97	7.98	0.0	9.96
3400	8.18	0.0	10.10	8.18	0.0	10.09
3300	8.39	0.0	10.24	8.39	0.0	10.23
3200	8.55	0.0	10.38	8.55	0.0	10.37
3000	8.82	0.0	10.65	8.82	0.0	10.63
2900	8.96	0.0	10.76	8.95	0.0	10.76
2800	9.08	0.0	10.91	9.07	0.0	10.89
2700	9.20	0.0	11.02	9.19	0.0	11.00
2600	9.31	0.0	11.12	9.30	0.0	11.10
2500	9.42	0.0	11.21	9.41	0.0	11.20
2400	9.52	0.0	11.29	9.51	0.0	11.28
2300	9.62	0.0	11.37	9.61	0.0	11.36
2200	9.72	0.0	11.45	9.71	0.0	11.44
2100	9.80	0.0	11.53	9.79	0.0	11.52
1900	9.99	0.0	11.69	9.98	0.0	11.69
1800	10.07	0.0	11.78	10.06	0.0	11.77
1700	10.15	0.0	11.85	10.14	0.0	11.85
1600	10.22	0.0	11.93	10.21	0.0	11.92
1500	10.25	0.0	11.99	10.24	0.0	11.99
1400	10.29	0.0	12.05	10.28	0.0	12.05
1300	10.32	0.0	12.09	10.31	0.0	12.09
1215	10.34	0.0	12.12	10.33	0.0	12.12
1215	10.89	3.46	12.30	10.89	3.46	12.30
1000	11.17	3.47	12.48	11.17	3.47	12.48
800	11.20	3.48	12.52	11.20	3.48	12.52
600	11.20	3.50	12.52	11.20	3.50	12.52
400	11.20	3.50	12.52	11.20	3.50	12.52
300	11.19	3.50	12.53	11.19	3.50	12.53
100	11.18	3.50	12.57	11.18	3.50	12.57
1	11.17	3.50	12.57	11.17	3.50	12.58

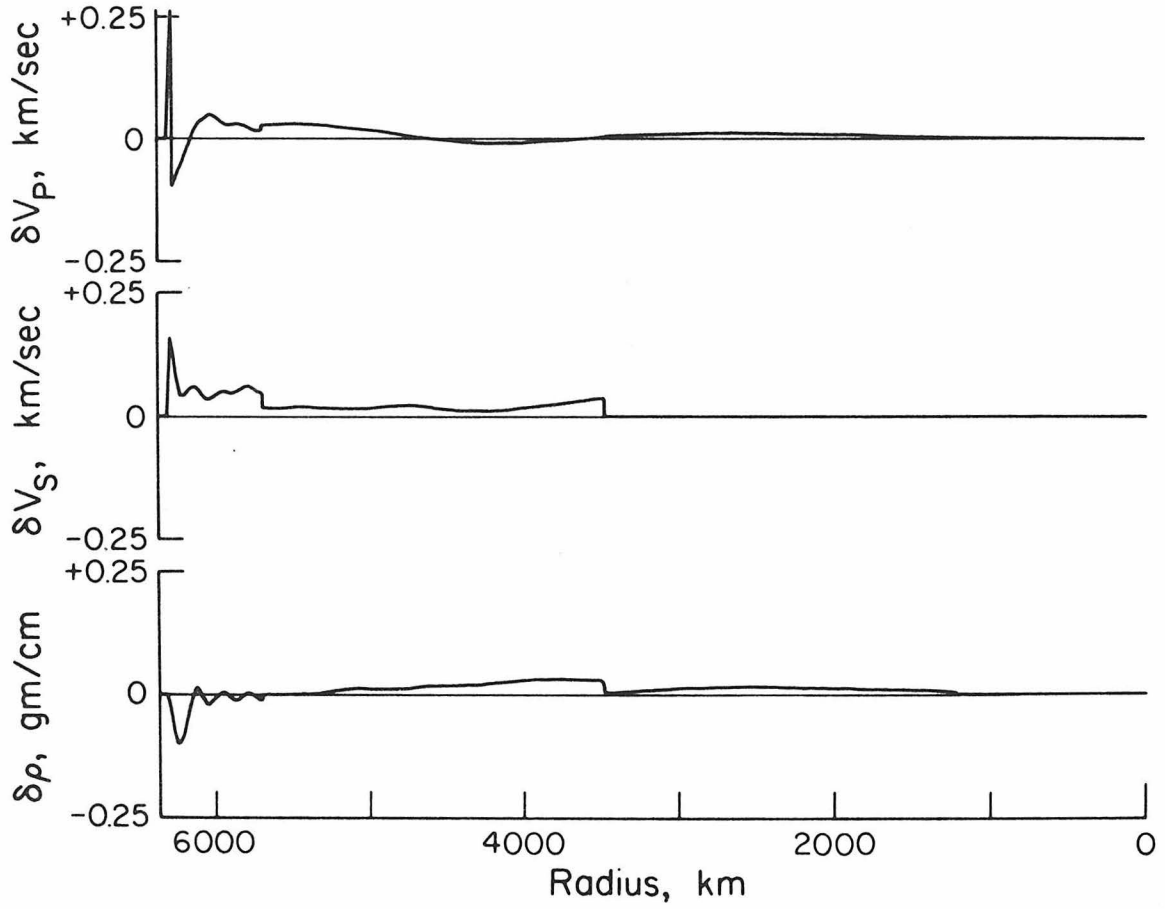


Figure 4.7 - The cumulative perturbation in the model parameters V_p , V_s , and ρ as a function of radius for the change between model C2 and P^s model QM2.

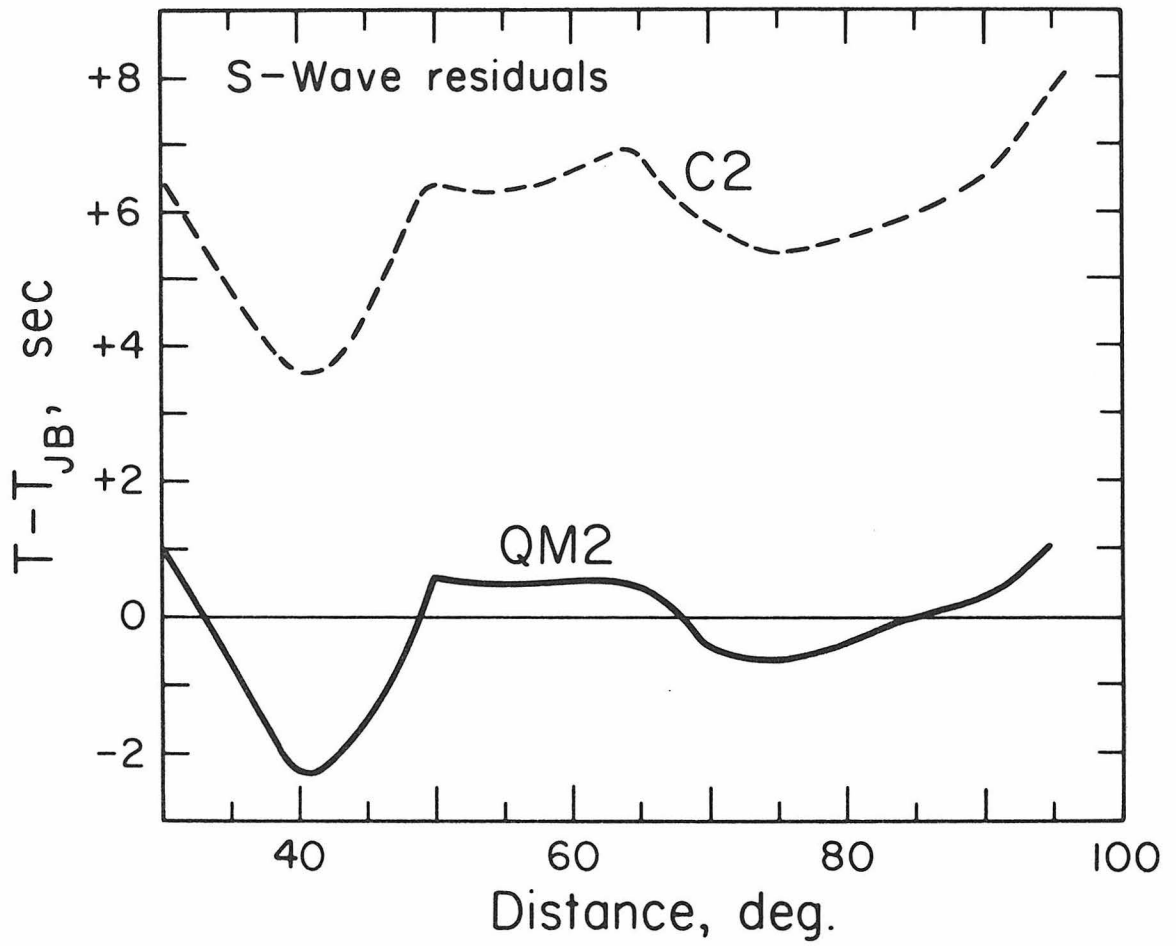


Figure 4.8 - Residual shear wave travel-times relative to the Jeffreys-Bullen Tables (1940) for models C2 and QM2.

TABLE 4.5

ScS-S Times (deep focus)

Δ (deg)	Observed [*] (sec)	C2 (sec)	QM2 (sec)	δ QM2 (sec)
30	311.3±1.8	306.8	307.0	-4.3
35	259.4±1.5	258.3	258.4	-1.0
40	215.7±1.6	213.3	213.6	-2.1
45	174.3±1.1	172.2	172.3	-2.0
50	138.6±1.4	137.9	137.9	-0.7
55	108.6±1.4	107.2	107.3	-1.3
60	82.0±1.1	80.7	80.8	-1.2
65	59.7±0.9	59.2	59.2	-0.5
70	40.6±1.0	41.2	41.0	+0.4
75	25.5±1.3	26.6	26.1	+0.6
80	14.0±0.8	15.1	14.4	+0.4

* Jordan and Anderson (1974); uncertainty is 95% C.I.

TABLE 4.6

Surface Focus PcP and ScS

Δ (deg)	PcP				ScS		
	J-B [*] (sec)	1968 ^{**} (sec)	QM2 (sec)	δ_{68}	J-B (sec)	QM2 (sec)	δ_{JB}
30	554.9	552.1	551.5	0.6	1011.0	1009.4	1.6
35	568.6	565.9	565.3	0.6	1036.4	1034.9	1.5
40	583.9	581.1	580.7	0.4	1064.6	1063.3	1.3
45	600.5	597.7	597.4	0.3	1095.1	1094.2	0.9
50	618.3	615.5	615.2	0.3	1127.8	1127.3	0.5
55	637.0	634.3	634.1	0.2	1162.5	1162.2	0.3
60	656.6	653.9	653.8	0.1	1198.8	1198.8	0.0
65	676.9	674.2	674.2	0.0	1236.4	1236.6	-0.2
70	697.8	695.1	695.2	-0.1	1275.2	1275.6	-0.4
75	719.1	716.5	716.6	-0.1	1315.0	1315.5	-0.5
80	740.6	738.0	738.3	-0.3	1355.5	1356.0	-0.5
85	762.3	759.9	760.3	-0.4	1396.5	1397.1	-0.6
90	784.2	781.9	792.5	-0.6	1437.8	1438.5	-0.7
95					1479.2	1480.2	-1.0

* Jeffreys and Bullen (1940)

** Herrin et al. (1968)

TABLE 4.7

Compressional Wave Travel Times (sec)

Δ (deg)	JB (1)	HCR (2)	1968 (3)	QM2	δ_{68}
30	372.5	371.0	369.5	369.9	0.4
35	416.1	414.8	413.3	414.2	0.9
40	458.1	457.0	455.7	456.6	0.9
45	498.9	497.4	496.4	497.2	0.8
50	538.0	536.1	535.2	535.7	0.5
55	575.4	573.0	572.2	572.5	0.3
60	610.7	608.2	607.4	607.5	0.1
65	644.0	641.6	640.9	641.0	0.1
70	675.5	673.1	672.7	672.7	0.0
75	705.0	702.9	702.6	702.6	0.0
80	732.7	730.8	730.6	730.7	0.1
85	758.5	756.9	756.6	757.0	0.4
90	782.7	781.1	780.7	781.3	0.6
95	805.7		803.9	804.5	0.6

Average Difference 0.4

(1) Jeffreys and Bullen (1940)

(2) Hales et al. (1968)

(3) Herrin et al. (1968)

TABLE 4.8

dt/d Δ of P Waves (sec/deg)

Δ (deg)	HCR (1)	CGJ (2)	LJ (3)	DJC (4)	QM2
30	8.94	8.88	8.92	9.13±0.05	8.96
35	8.60	8.67	8.60	8.70±0.05	8.65
40	8.26	8.30	8.38	8.26±0.07	8.30
45	7.91	7.99	7.90	8.11±0.10	7.92
50	7.56	7.52	7.51	7.52±0.10	7.52
55	7.21	7.20	7.22	7.19±0.08	7.18
60	6.86	6.84	6.75	6.95±0.07	6.85
65	6.50	6.66	6.53	6.69±0.08	6.52
70	6.14	6.17	6.24	6.21±0.09	6.16
75	5.77	5.77	5.83	5.88±0.06	5.80
80	5.40	5.35	5.48	5.47±0.06	5.45
85	5.03	4.98	4.93	4.95±0.06	5.05
90	4.66	4.74	4.65	4.60±0.09	4.74
95	4.28	4.55	4.48	4.52±0.07	4.56

(1) Hales et al. (1968)

(2) Carder et al. (1966)

(3) Johnson (1969)

(4) Corbishley (1970); uncertainty is the 95% C.I.

distance range. The mean residual is +0.5 seconds. These travel times are plotted as residual times relative to the 1968 Tables in Figure 4.9 along with those of model C2 and several body wave studies. The QM2 times are about a second faster than the C2 times and fit the observed data of Carder et al. (1966) and Hales et al. (1968) very well. The surface focus PcP travel-times for this model are in Table 4.6. The mean PcP residual, relative to the 1968 Tables, is less than 0.1 second. In Table 4.9, we compare the surface focus PcP-P differential travel-times of this model with observed values and with model C2. The agreement with the observations is about the same for both models.

In the above inversion, the reference frequency was chosen to correspond to a period of one second. This is roughly the characteristic period of body waves and allows the results of normal mode studies to be directly compared to those obtained from body waves. Although teleseismic shear waves have dominant periods in the 10-20 second period range, a period of one second is nevertheless an appropriate value for the characteristic period in the context of travel time studies. Most arrival time readings are performed by picking the first break of the S wave on a seismogram. This portion of the waveform on WWSSN instruments is dominated by much higher frequencies, probably 0.5 cps and less. If, however, a period of 5 seconds is taken as the reference period, the change from model C2 is about 30% less than in the case of QM2 and the reduction in travel time is similarly reduced. The mean S wave travel time residual with respect to the Jeffreys-Bullen Tables (1940) would then be approximately +1.0

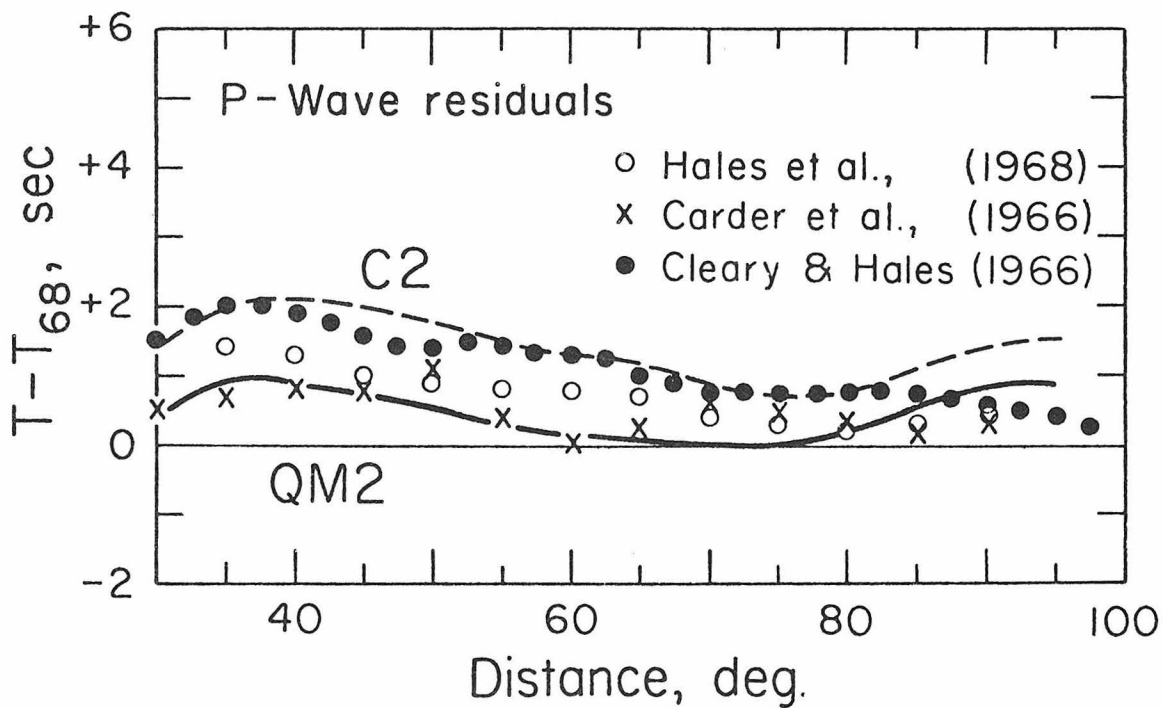


Figure 4.9 - Residual compressional wave travel-times relative to the 1968 Tables (Herrin et al., 1968) for models C2 and QM2. Also shown are the data of Carder et al. (1966) and Hales et al., (1968).

TABLE 4.9

PcP-P Times (surface focus)

Δ (deg)	THJ (1)	68M (2)	C2	QM2	δ_{68}
30	181.9±0.4	181.6±0.6	181.3	181.6	0.0
35	151.4±0.3	151.6±0.6	150.8	151.1	0.5
40	125.1±0.5	124.6±0.6	123.6	124.1	0.5
45	100.7±0.4	100.5±0.6	99.7	100.2	0.3
50	79.9±0.4	79.6±0.6	79.0	79.4	0.2
55	62.3±1.0	61.5±0.6	61.2	61.6	-0.1
60	46.1±1.0	45.9±0.6	45.9	46.3	-0.4
65	33.0±1.0	32.8±0.6	32.9	33.2	-0.4
70	22.0±2.7	22.0±0.6	22.4	22.5	-0.5
75	13.4±2.1	13.5±0.6	14.1	14.0	-0.5
80		7.2±0.6	7.7	7.6	-0.4
85		3.1±0.6	3.4	3.3	-0.2
90		1.1±0.6	1.2	1.2	-0.1

(1) Jordan (1973)

(2) Engdahl and Johnson (1974)

seconds.

Model QM2 is actually more than simply a differential earth model. Since it is essentially an exact fit to the corrected C2 eigenperiods, it fits the observed normal mode data, when corrected for Q, to within 0.08% (as does model C2 for the uncorrected data). Thus if we are satisfied with this level of goodness of fit and with the various model features of C2 (which may have been accentuated by the Q perturbation (see Figure 4.10)), then there is no need to do a complete inversion on the corrected data. The weakest link in this model is, obviously, the assumed Q distribution (Q model MM8 in this instance). As we discussed earlier in this chapter, Q trades-off inversely with velocity in the model. Thus inadequacies or errors in our Q model map directly into errors in the inferred earth model. Before we can continue to develop an acceptable gross earth model, we need to examine and refine our estimate of the radial distribution of seismic attenuation within the earth.

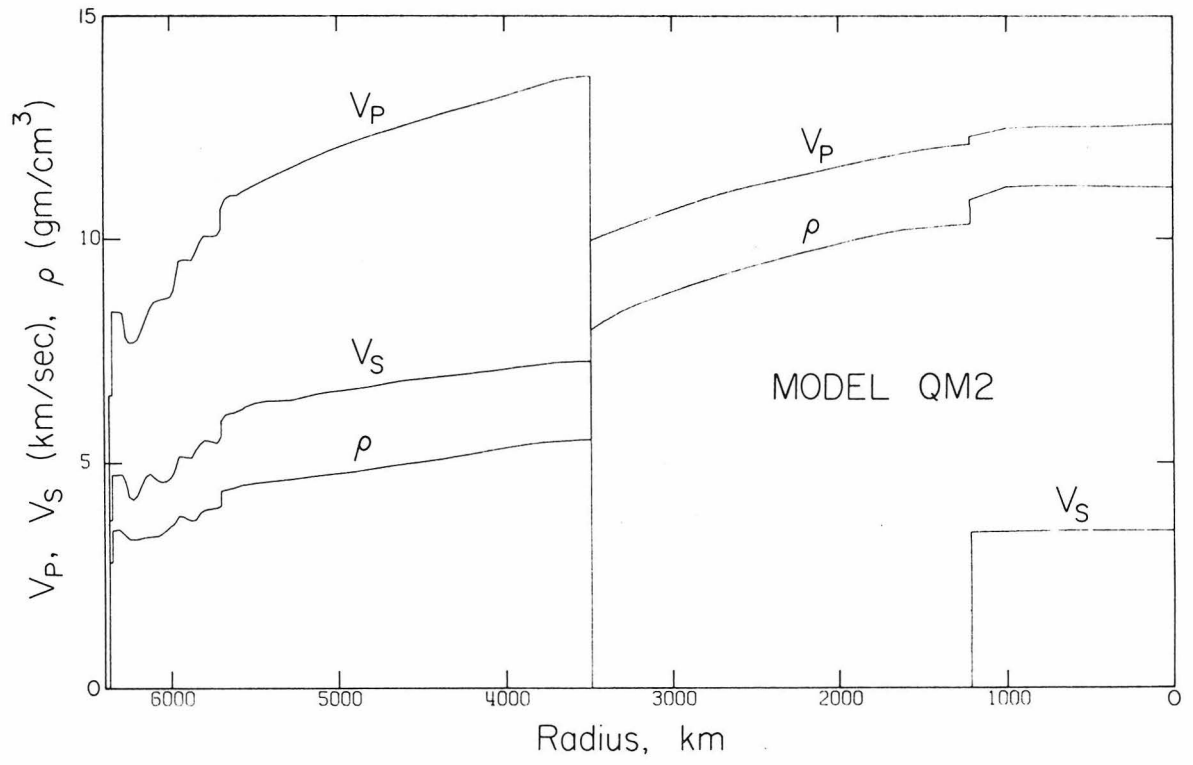


Figure 4.10 - V_p , V_s , and ρ as a function of depth for model QM2.

Chapter 5

THE Q OF THE EARTH

5.1 Introduction. In our investigation thus far into the role of attenuation in the earth we have adopted the Anderson et al. (1965) Q model MM8. But because of the great influence of the assumed Q distribution upon the final velocity structure, it is important to obtain the best possible Q model for the earth before proceeding. The Q model MM8 is a fairly simple model and it represents a reasonable fit to most of the fundamental mode Q data. It does not, however, fit the observed Q's for the low order ${}_0S_\ell$ ($\ell < 10$) spheroidal modes. These modes have apparent Q's on the order of 500 but MM8 predicts an almost monotonically increasing Q for these modes with a predicted value for ${}_0S_2$ of about 1000. The MM8 Q's for the low order radial modes and overtones are similarly too large. MM8 is also not an entirely adequate model for the available body wave data. We have attempted to improve upon model MM8 and to construct a Q model which not only satisfies the entire normal mode data set but which is also appropriate for teleseismic body wave observations. Although there are observational and theoretical reasons for believing Q may not be completely independent of frequency throughout the earth, we have attempted to find such a model that is consistent with as much of the data as possible. If the period range from about 1 second to 1 hour, most of the data can be satisfied by a frequency-independent Q versus depth model. Although Q is probably frequency dependent in the high Q regions of the Earth,

it is the low Q regions that dominate the absorption of teleseismic body waves and normal modes and these regions are likely to have a dissipation that is only weakly dependent on frequency. With this improved model for absorption, we can normalize the body wave, surface wave, and free oscillation data to a common base and derive a self consistent earth model (Jeffreys, 1965; Davies, 1967; Liu et al., 1976; Anderson et al., 1977; Kanamori and Anderson, 1977).

5.2 The Data. The intrinsic attenuation of seismic waves is difficult to measure because of the other factors which affect amplitudes such as scattering, geometric spreading, multipathing, source radiation effects, instrumental uncertainties, radial and lateral inhomogeneities, rotational and ellipticity effects, and mode interference. These uncertainties, plus the unknown influence of frequency, make the measurement and interpretation of Q difficult. The scatter and error bounds of Q measurements are thus very large. We have collected a large data set of Q measurements, at all frequencies within the seismic band, with which we hope to minimize as many of the above problems as possible.

Body Wave Data. The observed decay of near vertical multiple ScS phases provides a simple measure of the average shear wave attenuation in the mantle that is relatively uncontaminated by source, instrument, path, spreading, and local effects. The average mantle Q_{β} obtained by these observations is appropriate for the period range of about 10-50 seconds. These data provide a powerful integral constraint on

Q_{β} models of the mantle. With somewhat less certainty we can use ScS to obtain average Q_{β} values above and below a deep source (Anderson and Kovach, 1964; Kovach and Anderson, 1964). By using spectral ratios of P waves and P and PcP it is possible to provide constraints for Q_{α} for certain regions of the mantle (Kanamori, 1967a, b; Mikumo and Kurita, 1968; Berzon et al., 1974).

In Table 5.1 we tabulate the ScS observations. There is a suggestion of regional variations but different authors have used different techniques and assumptions. There is also slight suggestion of a frequency effect (Sato and Espinosa, 1967; Yoshida and Tsujiura, 1975). The South American events give the largest Q; this may be due to the thick lithosphere and absence of a pronounced low-velocity zone (James, 1971). The Hawaiian, Japanese, Pacific and S. W. United States observations have a lower average mantle Q; these are regions where the ScS phases pass through a pronounced low-velocity zone. The values presented in Table 5.1 do not indicate the difficulty and ambiguity involved in obtaining these numbers. For example, in some multiple ScS observations, the amplitude of a particular phase is occasionally larger than that of a phase with a lower multiplicity from the same event. Two-thirds of the observations lie between 230 and 380 and the mean value of the observations in this range is 285. We adopt this value as the average Q of the mantle for shear waves in the period range 10-50 seconds. This is admittedly a rather rough estimate. Moreover the recent study of multiple ScS in the southwestern Pacific by Jordan and Sipkin (1977) yielded an average Q_{β} of 156, or 178 when an

TABLE 5.1

Shear Wave Attenuation in the Mantle

<u>Region</u>	<u>Depth</u>	<u>Period</u> (sec)	<u>Q</u>	<u>Reference</u>
-	whole	12	700	(2)
-	whole	24	400	(2)
South America	whole	11	500	(1)
South America	whole	25	508	(5)
South America	whole	25	440	(5)
South America	whole	14-67	600	(7)
South America	whole	25	330	(12)
South America	whole	25	360	(12)
South America/ North America	whole	30	690	(8)
South America/ North America	whole	40	590	(8)
South America/ North America	whole	50	500	(8)
South America/ North America	whole	90	230	(8)
Southwestern U.S.	whole	1.5-5.0	230	(9)
Japan	whole	2-20	260	(3)
Japan	whole	2-20	280	(3)
Japan	whole	5	300	(4)
Sea of Japan	whole	1.25-66	290	(11)
Southwestern Pacific	whole	16-160	156-178	(15)
Hawaii	whole	-	300	(13)

TABLE 5.1 (cont'd)

<u>Region</u>	<u>Depth</u>	<u>Period</u> (sec)	<u>Q</u>	<u>Reference</u>
Tonga/Albuquerque	whole	25	380	(12)
Tonga/Hawaii	whole	25	230	(12)
Tonga/Guam	whole	25	365	(12)
Tonga/Solomon Is.	whole	25	300	(12)
Celebes Is./ Solomon Is.	whole	25	230	(12)
Kurile Is./Dugway	whole	25	270	(12)
Kurile Is./Manila	whole	25	270	(12)
Tasman Sea/ South Pole	whole	25	325	(12)
Tasman Sea/ South Pole	whole	10	380	(10)
South America	<600 km	-	160	(6)
South America	<600 km	25	151	(5)
South America	<600 km	25	185	(5)
South America	<600 km	14-67	200	(7)
Japan	<600 km	2-20	110	(3)
Sea of Japan	<600 km	28-67	150	(11)
Sea of Japan	<600 km	10-28	220	(11)
Sea of Japan	<600 km	1.25-3.3	260	(11)
Japan	<1000 km	2-20	260	(3)
Japan	<1000 km	5-50	180	(14)
Japan	<2000 km	5-50	200	(14)

TABLE 5.1 (cont'd)

<u>Region</u>	<u>Depth</u>	<u>Period</u> (sec)	<u>Q</u>	<u>Reference</u>
South America	>600	-	500	(6)
South America	>600	25	1430	(5)
South America	>600	14-67	2200	(7)
Japan	>1100	2-20	350	(3)

References :

- | | |
|-------------------------------|---------------------------------|
| 1) Press (1956) | 9) Kanamori (1967) |
| 2) Gutenberg (1958) | 10) Choudbury and Dorel (1973) |
| 3) Otsuka (1962) | 11) Yoshida and Tsujiura (1975) |
| 4) Otsuka (1963) | 12) Okal (unpublished data)* |
| 5) Anderson and Kovach (1964) | 13) Best et al. (1974) |
| 6) Steinhart et al. (1964) | 14) Sima (1965) |
| 7) Kovach and Anderson (1964) | 15) Jordan and Sipkin (1977) |
| 8) Sato and Espinosa (1967) | |

* These data have very large error bounds.

estimate of scattering from discontinuities is included. Jordan and Sipkin concluded that the harmonically averaged Q_β for the Pacific is probably less than 200. While this study is probably the most carefully conducted of existing work in this area and used very high quality SRO data, the authors do not argue convincingly that their low value is not simply a regional variation. Perhaps the most important result of the Jordan and Sipkin study is that they found no evidence for frequency dependence in their period range of about 15-150 seconds. An additional constraint can be placed on the distribution of shear attenuation in the mantle. Observations of multiple ScS phases from deep earthquakes have been used in a number of studies (Otsuka, 1962; Anderson and Kovach, 1964; Kovach and Anderson, 1964; Steinhart et al., 1964; Yoshida and Tsujiura, 1975) to estimate Q_β above 600-700 km depth. These measurements indicate that the mean Q_β in the upper mantle is about 165. Other integral body wave constraints on mantle Q's have been obtained from observations of PcP and spectral studies on direct P and S arrivals. These results are summarized in Tables 5.1 and 5.2.

The ratio of body wave travel-time (T) to apparent Q for both direct P and S waves (T/Q_α and T/Q_β) also serves as a useful constraint on possible Q models. Carpenter and Flinn (1965) suggested that, for short period P waves, the ratio of travel time to the path average of Q is almost constant, about 1 sec at teleseismic distances. In subsequent body wave studies (HelMBERGER and Wiggins, 1971; HelMBERGER, 1973; HelMBERGER and Engen, 1974), values of 1 sec for T/Q_α and 4 sec for

TABLE 5.2

Observed Average Mantle P-Wave Q's

Depth Interval (km)	(1)	Q_{α} (2)	(3)	(4)
0-100	220	100		
0-760	530 ± 150	150		166-272
0-900			180-240	
0-2900	+ 420 845 - 260	375	410-630	300-412
100-760	710 ± 150	165		
100-2900	+ 420 1080 - 285	420		
760-2900	+ 950 1260 - 365	1210		2050-3650
900-2900			1600-6000	

(1) Berzon et al. (1974) [0.6 - 5 sec]

(2) Kanamori (1967a) [1 sec]

(3) Kanamori (1967b) [1 sec]

(4) Mikumo and Kurita (1968) [33 - 8 sec]

T/Q_β have been adopted. For frequencies of about 1 Hz, most observed values of T/Q_α fall in the range of 0.4 to 1.3 (Carpenter, 1966; Mikumo and Kurita, 1968; Frasier and Filson, 1972; Helmberger, 1973) with some higher frequency observations as low as 0.2 (e.g. Douglas et al., 1974). Observed values of T/Q_β generally range from about 3.5 to 4.5 for the frequency range of 0.1 to 0.05 Hz (Carpenter and Flinn, 1965; Helmberger and Engen, 1974) although Burdick (personal communication) has found values as high as 5.2 for shear waves from the Borrego Mt. (California) earthquake. There is only a slight distance dependence for T/Q_α and T/Q_β over the distance range of 30° to 80° . Beyond 80° , Mikumo and Kurita (1968) reported a substantial increase in T/Q_α , indicating that there may be a low-Q zone at the base of the mantle.

Body wave observations were also employed to constrain the attenuation in the core and inner core. In all of our modelling efforts, we assumed that no appreciable dissipation occurred within the outer core (Buchbinder, 1971; Sacks, 1971a; Sacks, 1972; Adams, 1972; Müller, 1973; Qamar and Eisenberg, 1974). Most of these studies give a Q for the outer core of greater than 4000. Cormier and Richards (1976) conclude that Q_α in the outer core is at least 10^4 and probably much greater.

We are aware of five body wave measurements of the dissipation in the inner core. Buchbinder (1971), using PKP amplitude ratios, found an average inner core Q_α of about 400. Spectral ratios of inner core and outer core phases (Sacks, 1971b) indicate an average inner core Q_α of 600. Sacks' data suggest that Q_α is not constant through the inner core but ranges from 100-200 in the outer 300 km to 1000 in the

remainder of the inner core. Qamar and Eisenberg (1974) determined a value between 120 and 400 for Q_{α} in the outer 450 km of the inner core. Doornbos (1974) found that Q rises from a value of about 200 near the inner core-outer core boundary to about 600 at a depth of 400 km inside the inner core. Kuster (1972) found a value of 300 for Q_{α} from the spectral ratios of PKP and PKKP recorded at LASA. In our modelling efforts we examined both the case in which no dissipation occurs in either outer core or inner core and the case supported by the above studies in which the inner core contributes significant attenuation.

Surface Wave and Normal Mode Data. We have generally considered only surface wave attenuation data for periods longer than about 65 seconds. At shorter periods, the attenuation is strongly influenced by local upper mantle and crustal structure. However, shorter period observations were used to determine the average attenuation for the upper layers where the longer period data lack sufficient resolution. The usual technique in surface wave analyses is to measure the spectral amplitude decay with distance between two stations along the same great circle path or at one station using multiple surface waves (e.g. Anderson, Ben-Menahem and Archambeau, 1965). Free oscillation attenuation values are obtained from the temporal decay of spectral peaks (Smith, 1972) or the measurement of peak half-widths (Benioff et al., 1961; Ness et al., 1961). The relation between temporal and spatial decay was derived by Brune (1962), Anderson and Archambeau (1964) and Knopoff et al. (1964).

Free oscillation and surface wave observations are our primary

data base for determining the variation of Q with depth. These data are summarized in Figure 5.1 for fundamental toroidal modes and Love waves and in Figure 5.2 for fundamental spheroidal modes and Rayleigh waves.

In addition to the fundamental spheroidal and toroidal modes we have also used the radial modes (Table 5.3 and Figure 5.3) and the available data for overtones in the inversion. The observed Q 's for the radial modes are extremely high, suggesting that losses in compression are low, as proposed by Anderson et al. (1965). The overtone data are more difficult to interpret. The observations (Dratler et al., 1971; Smith, 1972; Nowroozi, 1974; Sailor and Dziewonski, 1976; Jobert and Roullet, 1976) exhibit considerable scatter and internal inconsistencies. Possible mode mis-identifications further complicate the interpretation of this data. Jobert and Roullet (1976) have presented the largest collection of overtone measurements but the scatter of their measurements is also very large. Rather than attempt to tabulate all of the observations we present our own model values, Table 5.7, for those modes which the above authors have analyzed together with the range of observations.

The values of Q for the low order spheroidal and toroidal modes are not accurately known. This is unfortunate since the low order spheroidal modes are particularly sensitive to the Q at the base of the mantle and represent a prime constraint on attenuation in that region. The primary difficulty with determining the Q 's of these modes arises from the large influence of splitting on the amplitudes

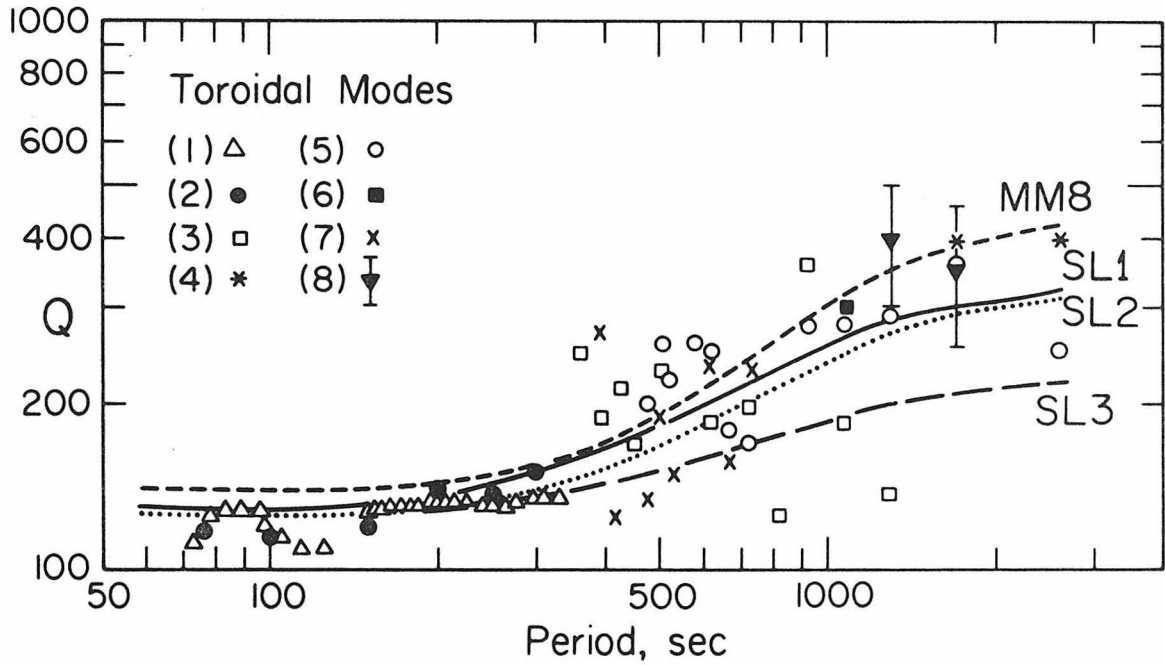


Figure 5.1 - Observed and theoretical apparent Q's for the fundamental toroidal modes. (1) Anderson et al. (1965); (2) Ben-Menahem (1965), smoothed curve; (3) Bolt and Brillinger (1975); (4) Smith (1961); (5) Smith (1972); (6) Alsop et al. (1961); (7) Nowroozi (1968); (8) Stein and Geller (1977). The data of Jobert and Roullet (1976) are not shown but are consistent with our model values.

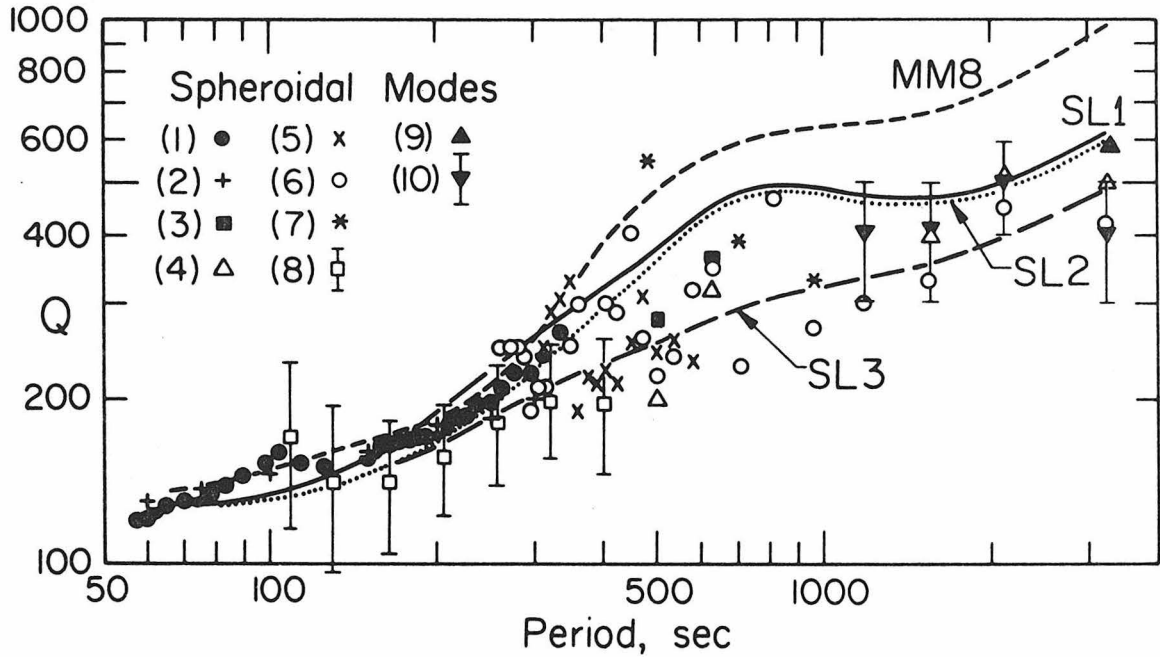


Figure 5.2 - Observed and theoretical apparent Q 's for the fundamental spheroidal modes. (1) Anderson et al. (1965); (2) Ben-Menahem (1965); (3) Ness et al. (1961); (4) Slichter (1967); (5) Nowroozi (1968); (6) Smith (1972); (7) Bolt and Brillinger (1975); (8) Mills and Hales (1977); (9) Dziewonski (personal communication); (10) Stein and Geller (1977). The data of Jobert & Roullet (1976) are not shown but are consistent with our model values.

TABLE 5.3
Radial Mode Q's

<u>Mode</u>	<u>Observed Q</u>	<u>Reference</u>
0^S_0	7500	Ness et al. (1961)
	900	Smith (1961)
	12000	Slichter (1967)
2^S_0	672	Dratler et al. (1971)
	704	Dratler et al. (1971)
4^S_0	1173	Dratler et al. (1971)
	1156	Dratler et al. (1971)
	790	Smith (1972)
	750	Smith (1972)
5^S_0	938	Dratler et al. (1971)
	927	Dratler et al. (1971)
	1570	Smith (1972)

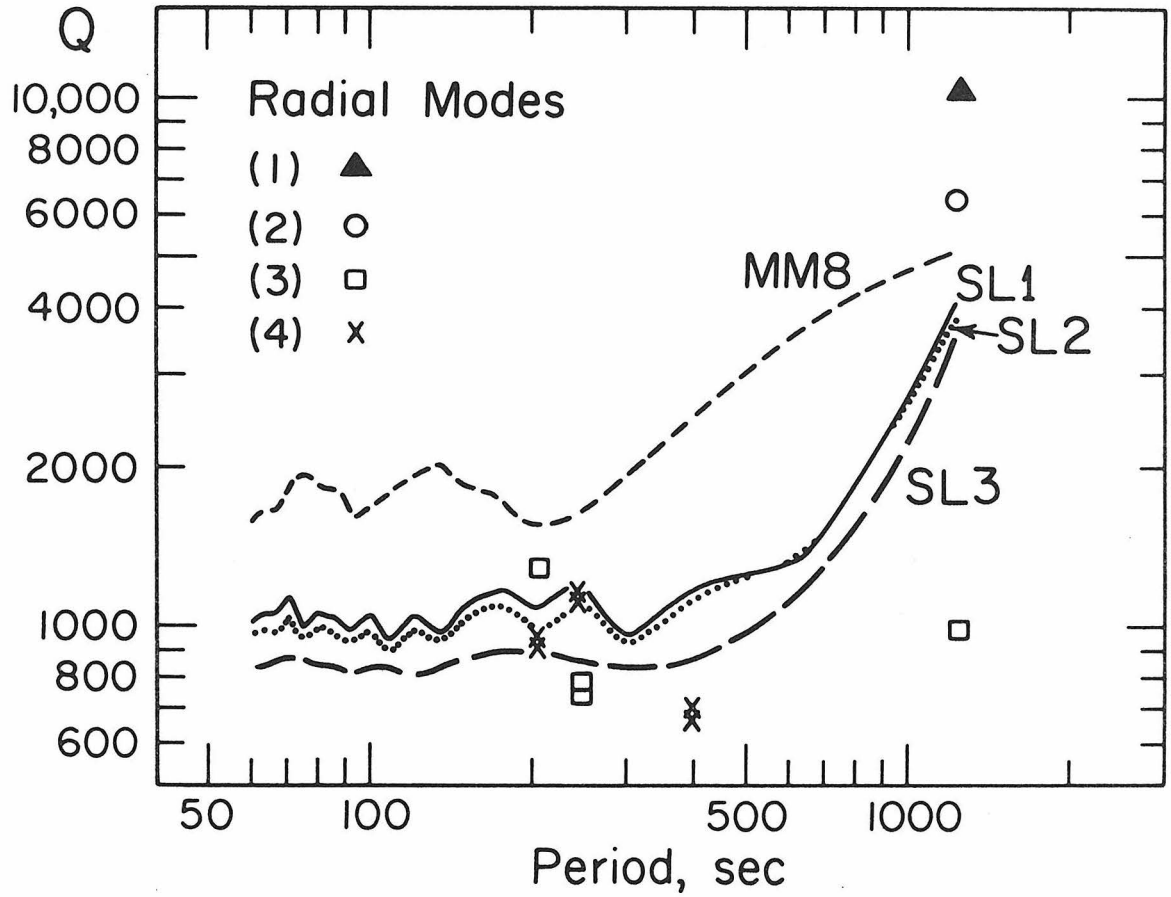


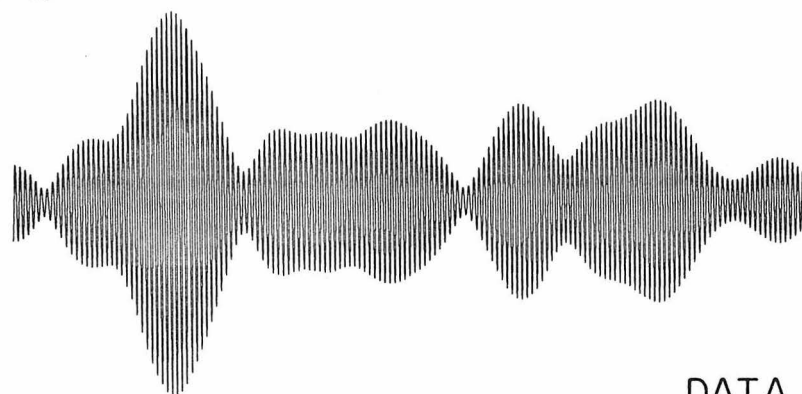
Figure 5.3 - Observed and theoretical apparent Q's for the radial modes. (1) Slichter (1961); (2) Ness et al. (1961); (3) Smith (1972); (4) Dratler et al. (1971).

at these oscillations. Because of the arbitrary phase assumptions involved it is essentially impossible to remove this effect in the common spectral amplitude analysis method for determining Q . Recently, Stein and Geller (1977) have developed a new technique of fitting time domain synthetic seismograms to narrow-band filtered data to obtain Q values for ${}_0S_2$ through ${}_0S_5$ and ${}_0T_3$ and ${}_0T_4$. This technique explicitly includes the amplitude and phase of each singlet of the split modes. The application of this technique promises to produce highly reliable estimates of these rather crucial Q values. In Figures 5.4 and 5.5 we show some examples of the application of the Stein and Geller (1977) technique, first for ${}_0S_2$, then for ${}_0S_3$. Clearly the middle trace (the synthetic with splitting) matches the data (top trace) extremely well. On the other hand, the bottom trace (the synthetic with no splitting) does not reproduce any of the essential features of the data. If the standard technique of using the decaying amplitudes of spectral peaks from successively windowed data were used for these modes, no reliable Q value could be obtained. For example, in Figure 5.6, we demonstrate the results of applying that method to ${}_0S_3$ with a Q of 500. Given the resulting scatter in amplitudes, for either 10 hour or 20 hour windows, it is unlikely that a correct estimate of Q would be obtained.

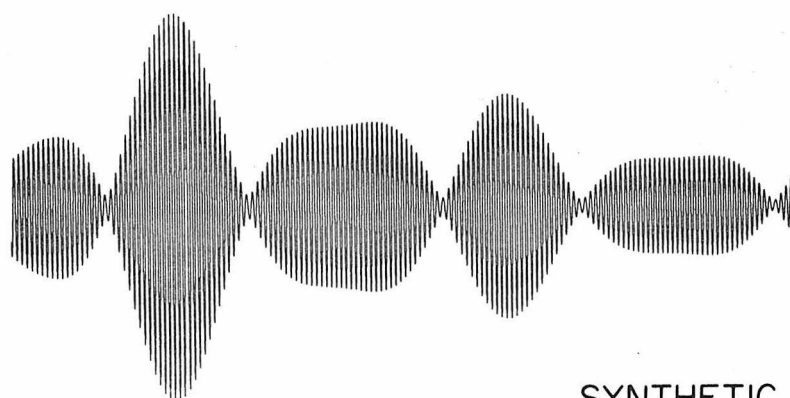
5.3 The Q Models. The Q models discussed below were obtained through trial and error computation. An interactive program on the NOVA computer system at the Seismological Laboratory allowed us to rapidly and

${}_0S_2$

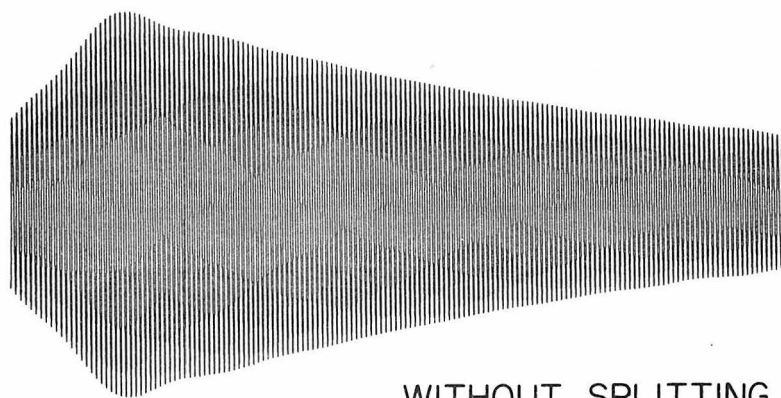
T=53.8 min, Q=400



DATA



SYNTHETIC



WITHOUT SPLITTING

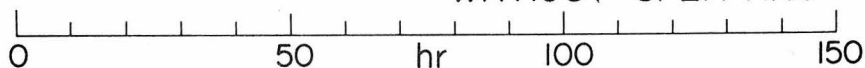


Figure 5.4 - Data and synthetics for ${}_0S_2$. The top trace is filtered data from the Isabella strain record of the Chilean earthquake. The middle trace is the synthetic seismogram, including the effects of splitting and the bottom trace is the synthetic without splitting. Q = 400 was used for both synthetics. The synthetics were tapered and filtered in the same way as the data. (Stein and Geller, 1977)

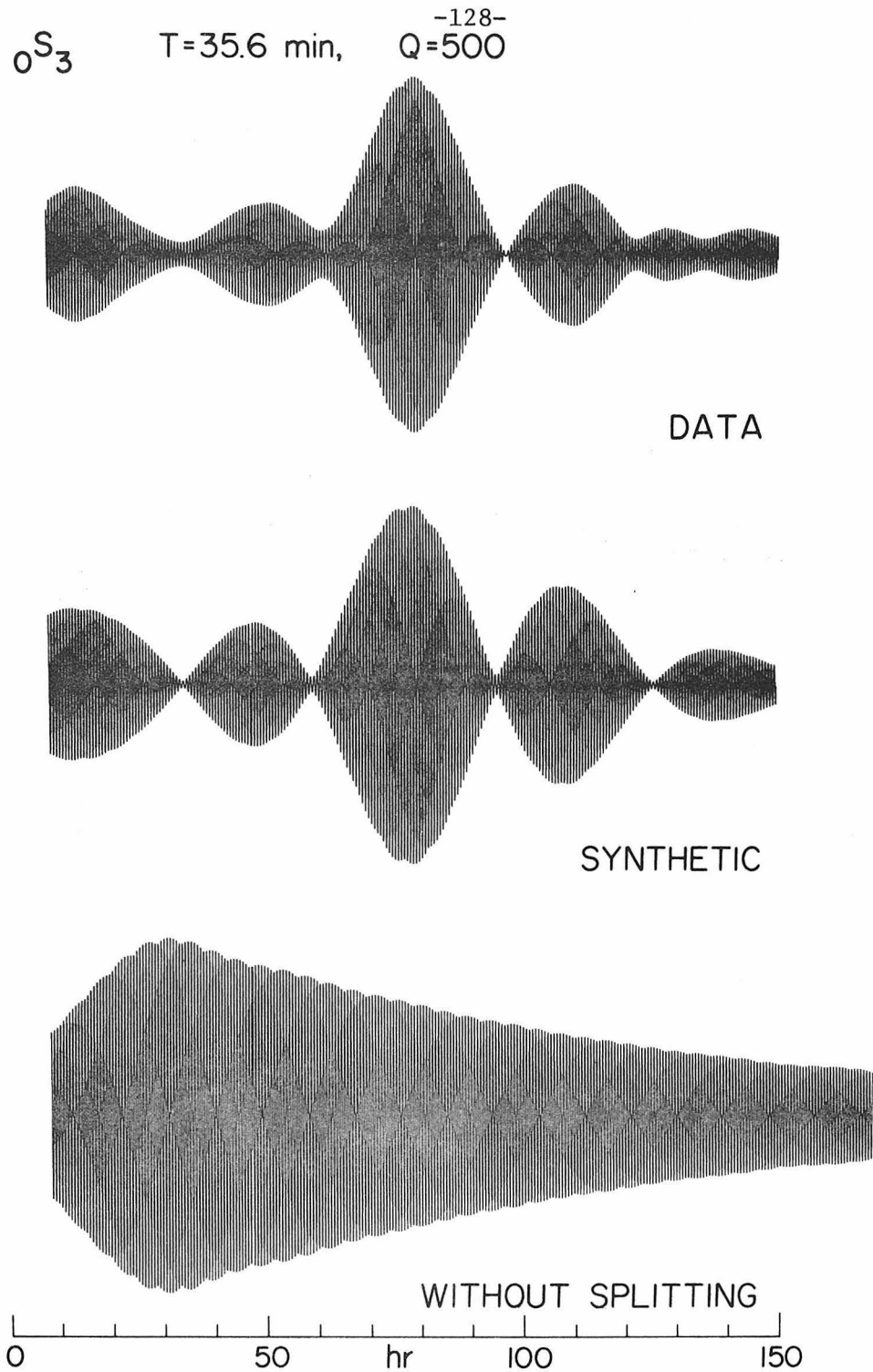


Figure 5.5 - Data and synthetics for $0S_3$. The top trace is filtered data from the Isabella strain record of the Chilean earthquake. The middle trace is the synthetic seismogram including the effects of splitting, and the bottom trace is the synthetic without splitting. $Q = 500$ was used for both synthetics. The synthetics were tapered and filtered in the same way as the data. (Stein and Geller, 1977)

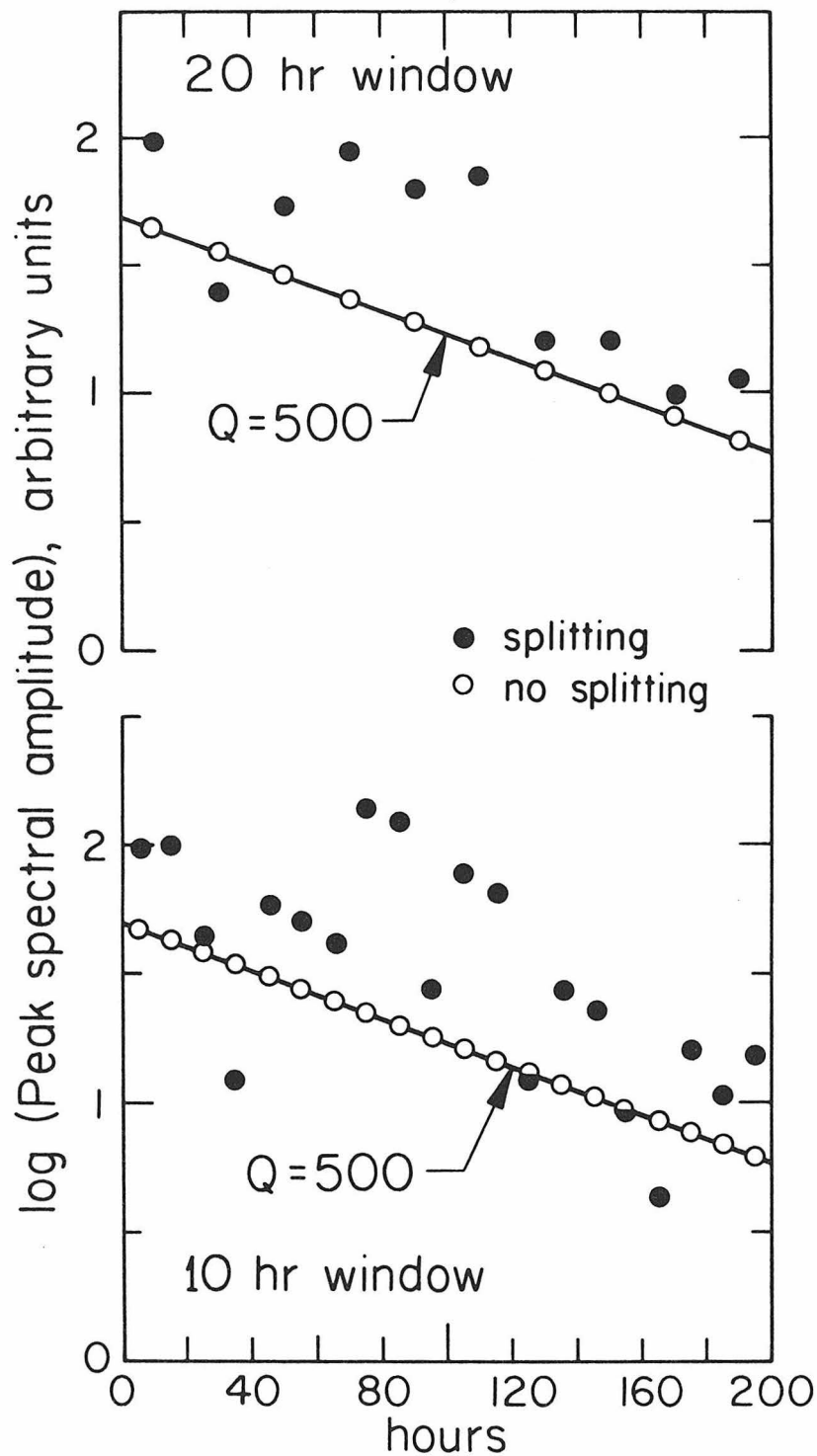


Figure 5.6 - Results of a numerical test of estimating Q of $0S_3$ from spectral peaks of successive windowed intervals, calculated using equation (2). In the top half of the figure it can be seen that when there is no splitting (open circles) good results are obtained, but when splitting is present (closed circles) extremely poor and scattered spectral peaks result. The bottom half of the figure is the same except that a window length of 10 hours was used. (Stein and Geller, 1977)

efficiently test and modify several hundred models.

The model consists of 50 concentric homogeneous spherical shells; the mantle contains 46 shells, the inner and outer core contain 2 shells each. Within each shell, we specify either Q_β and Q_α or Q_μ and Q_K . These quality factors are related by the following equations:

$$Q_\beta = Q_\mu \quad (5.1)$$

$$Q_\alpha^{-1} = LQ_\mu^{-1} + (1-L) Q_K^{-1} \quad (5.2)$$

$$Q_K = \frac{1-L}{(Q_\beta/Q_\alpha) - L} Q_\mu \quad (5.3)$$

where $L = (4/3) (\beta/\alpha)^2$ and α and β refer to the compressional and shear velocities respectively. Since Q_μ and Q_K must be positive, Q_α and Q_β must satisfy,

$$Q_\beta/Q_\alpha \geq L \quad (5.4)$$

Only when Q_K^{-1} is identically zero; i.e. all losses occur in shear, will the ratio of Q_β to Q_α be exactly equal to L . Larger ratios of Q_β to Q_α occur when finite dissipation occurs due to bulk modulus relaxation. Such losses occur, for example, if thermoelastic effects contribute significantly to attenuation. We have examined, and discuss below, the consequences of assuming finite Q_K^{-1} values in the earth.

For a given distribution of Q versus depth, the mode Q 's were computed using the expressions given by Anderson et al. (1965):

$$Q_T^{-1} = \sum_{\ell=1}^N \left\{ \left(\frac{\beta_{\ell}}{C_T} \frac{\partial C_T}{\partial \beta_{\ell}} \right)_{K, \rho, \alpha} Q_{\beta_{\ell}}^{-1} \right\} \quad (5.5)$$

for torsional oscillations, and

$$Q_S^{-1} = \sum_{\ell=1}^N \left\{ \left(\frac{\alpha_{\ell}}{C_S} \frac{\partial C_S}{\partial \alpha_{\ell}} \right)_{K, \rho, \beta} Q_{\alpha_{\ell}}^{-1} + \left(\frac{\beta_{\ell}}{C_S} \frac{\partial C_S}{\partial \beta_{\ell}} \right)_{K, \ell, \alpha} Q_{\beta_{\ell}}^{-1} \right\} \quad (5.6)$$

for spheroidal oscillations. In equations (5.5) and (5.6), C is the phase velocity, ρ is the density; the subscript ℓ is the layer index; the subscripts S , T , α , and β associated with Q refer to the mode or wave type. Other subscripts refer to quantities being held constant. The density, ρ , is real while α , β and μ are complex. These are the same equations we used in the last chapter (Equation 4.11). Eigenfunctions from the gross earth model 1066A (Gilbert and Dziewonski, 1975) were used to compute the required partial derivatives.

Since our objective is to determine an average Q model for the Earth, we concentrated on fitting the attenuation of the earth's normal modes, and average mantle values determined from ScS amplitudes and T/Q data. Previous models such as MM8 (Anderson et al., 1965) and LMS (Smith, 1972) were good fits to most of the observed toroidal modes and to the shorter period ($T < 400$ sec) spheroidal modes. At longer periods, however, these models predict rapidly increasing Q 's for spheroidal modes whereas the observations show a leveling out of apparent Q . This feature of the data led Zharkov, Dorofeyeva, Dorofeyeva, and Lyubinov (1974), to suggest a broad low Q zone in the lower mantle. We examined both this possibility and an alternative

possibility that Q_K^{-1} is non-zero in the lower mantle.

We considered a large number of Q_K distributions in the mantle. In no instance was the effect on the apparent spheroidal mode Q 's sufficient to match the observations. Moreover, the radial mode data, particularly ${}_0S_0$, were strongly, and adversely, affected. Even with a narrow zone of finite Q_K in the lower mantle, the theoretical radial mode Q 's approach values of a few hundred, unacceptably below the observational data. We therefore rejected the possibility of finite Q_K^{-1} as a mechanism for seismic absorption in the mantle. In subsequent calculations we assume no losses in pure compression, i.e. $Q_K = \infty$.

The other means to effect the fall-off in apparent Q for the low order spheroidal modes is the inclusion of a low Q zone immediately above the core-mantle boundary. A large number of body wave observations are consistent with this interpretation. Mikumo and Kurita (1968) observed an increase in T/Q_α at distances beyond 85° . Such an increase implies a corresponding decrease in Q_α in the lower mantle. The model adopted by Mikumo and Kurita has a lower mantle Q_α of approximately 10,000 which falls rapidly to a value of about 100 beginning some 300 km above the core. Teng (1968) determined the variation of Q_α with depth from the spectra of P phases from deep earthquakes. His data indicate the presence of a 200 km thick zone of low Q ($Q_\alpha \sim 200$) at the base of the mantle. The observed amplitude ratios of ScS/S of Mitchell and HelMBERGER (1973) require either a thin low Q zone (approximately 150 km thick with Q_β about 100) at the base of the mantle or finite rigidity in the outer core. The amplitudes of grazing PKP phases

(Sacks and Snoke, 1976) also indicate a low Q zone with parameters consistent with those obtained for the Mitchell and HelMBERGER data. Kuster (1972) proposed a low Q zone ($Q_\alpha = 300$, thickness = 150 km) on the basis of PKP and PKKP spectral amplitude ratios. In our models, we settled upon a low-Q zone ($Q_\beta \sim 100$; $Q_\alpha \sim 270$) in the bottom 150 km of the mantle. This feature is sufficient to reduce the low order spheroidal Q's but does not significantly affect the toroidal mode Q's.

In Tables 5.4 and 5.5 we tabulate two Q models, SL1 and SL2, which represent satisfactory fits to the observations. These models are plotted in Figure 5.7. Model SL1 is also plotted with model MM8 (Anderson et al., 1965) in Figure 5.8. In all three models, no significant dissipation occurs in the outer core. In the inner core, both Q_μ and Q_K contribute to the attenuation. These features are consistent with both the body wave data referred to earlier and are necessary to reproduce the observed Q's for the radial overtones.

The observed values of Q_α for the inner core imply extremely low values of Q_β if there are no losses in compression. From equation (5.2) values of Q_α from 100 to 600 imply Q_β of 13-81 for the β/α ratio appropriate for the inner core. This would probably make the inner core shear modes ($_{10}S_2$, $_{11}S_2$) unobservable. On the other hand, with no losses in compression $_{2}S_0$, and, probably, $_{4}S_0$ would have Q's much higher than observed.

Models with negligible loss in pure compression and high Q_β and Q_α in the inner core give very high values for Q of the low order radial modes $_{0}S_0$ through $_{3}S_0$. The observed Q for $_{2}S_0$ suggests that Q_K is

TABLE 5.4

Q Model SL1

TOP OF LAYER		THICKNESS (km)	Q_{β}	Q_{α}	Q_K^{-1}
RADIUS (km)	DEPTH (km)				
614.75	5756.25	614.75	600	900	0.0010
1229.50	5141.50	614.75	200	450	0.0017
2326.40	4044.60	1096.90	0	1000000	0.0000010
3484.30	2886.70	1157.90	0	1000000	0.0000010
3527.77	2843.23	43.47	100	268	0.0
3614.70	2756.30	86.93	100	269	0.0
3701.62	2669.38	86.92	250	674	0.0
3788.55	2582.45	86.93	2000	5373	0.0
3875.48	2495.52	86.93	2000	5330	0.0
3962.41	2408.59	86.93	2000	5273	0.0
4049.33	2321.67	86.92	2000	5213	0.0
4136.25	2234.75	86.92	2000	5163	0.0
4223.18	2147.82	86.93	2000	5129	0.0
4310.10	2060.90	86.92	2000	5116	0.0
4397.02	1987.98	86.92	2000	5117	0.0
4483.94	1887.06	86.92	2000	5124	0.0
4570.86	1800.14	86.92	2000	5123	0.0
4657.78	1713.22	86.92	800	2043	0.0
4744.70	1626.30	86.92	600	1525	0.0
4831.62	1539.38	86.92	500	1264	0.0
4918.54	1452.46	86.92	450	1130	0.0

TABLE 5.4 (cont'd)

TOP OF LAYER		THICKNESS (km)	Q_{β}	Q_{α}	Q_K^{-1}
RADIUS (km)	DEPTH (km)				
5005.47	1365.53	86.93	400	997	0.0
5092.39	1278.61	86.92	350	864	0.0
5179.31	1191.69	86.92	350	856	0.0
5266.23	1104.77	86.92	325	786	0.0
5353.15	1017.85	86.92	300	720	0.0
5440.08	930.92	86.93	275	660	0.0
5527.00	844.00	86.92	275	662	0.0
5613.93	757.07	86.93	250	607	0.0
5700.00	671.00	86.07	250	615	0.0
5741.65	629.35	41.65	250	624	0.0
5783.31	587.69	41.66	250	630	0.0
5824.97	546.03	41.66	250	634	0.0
5866.64	504.36	41.67	250	639	0.0
5908.30	462.70	41.66	250	644	0.0
5950.00	421.00	41.70	250	649	0.0
5984.15	386.85	34.15	250	655	0.0
6018.31	352.69	34.16	200	529	0.0
6052.47	318.53	34.16	150	400	0.0
6086.64	284.36	34.17	125	335	0.0
6120.80	250.20	34.16	125	335	0.0
6154.97	216.03	34.17	125	332	0.0
6189.13	181.87	34.16	110	286	0.0

TABLE 5.4 (cont'd)

TOP OF LAYER		THICKNESS (km)	Q_{β}	Q_{α}	Q_K^{-1}
RADIUS (km)	DEPTH (km)				
6223.29	147.71	34.16	110	278	0.0
6257.46	113.54	34.17	85	206	0.0
6291.62	79.38	34.16	85	195	0.0
6325.79	45.21	34.17	200	436	0.0
6360.00	11.00	34.19	1500	3141	0.0
6365.50	5.50	5.50	1500	3732	0.0
6371.00	0.00	5.50	1500	3726	0.0

TABLE 5.5

Q Model SL2*

Depth (km)	Q_{β}	Q_{α}
504	200	511-497
421	175	456-450
353	150	396-393
284	135	362-360
216	120	322-319
148	105	273-265
79	90	218-207
45	160	349
0	800	1987-1675

* Identical to Model SL1 below a depth of 671 km. $Q_k^{-1} = 0$ throughout the mantle. Layer depths and thicknesses are the same as for Model SL1. The depths given here are to the top of the layer, rounded to the nearest kilometer. Q_{α} varies for constant Q_{β} due to variation in the ratio of α/β (see equation 5.2).

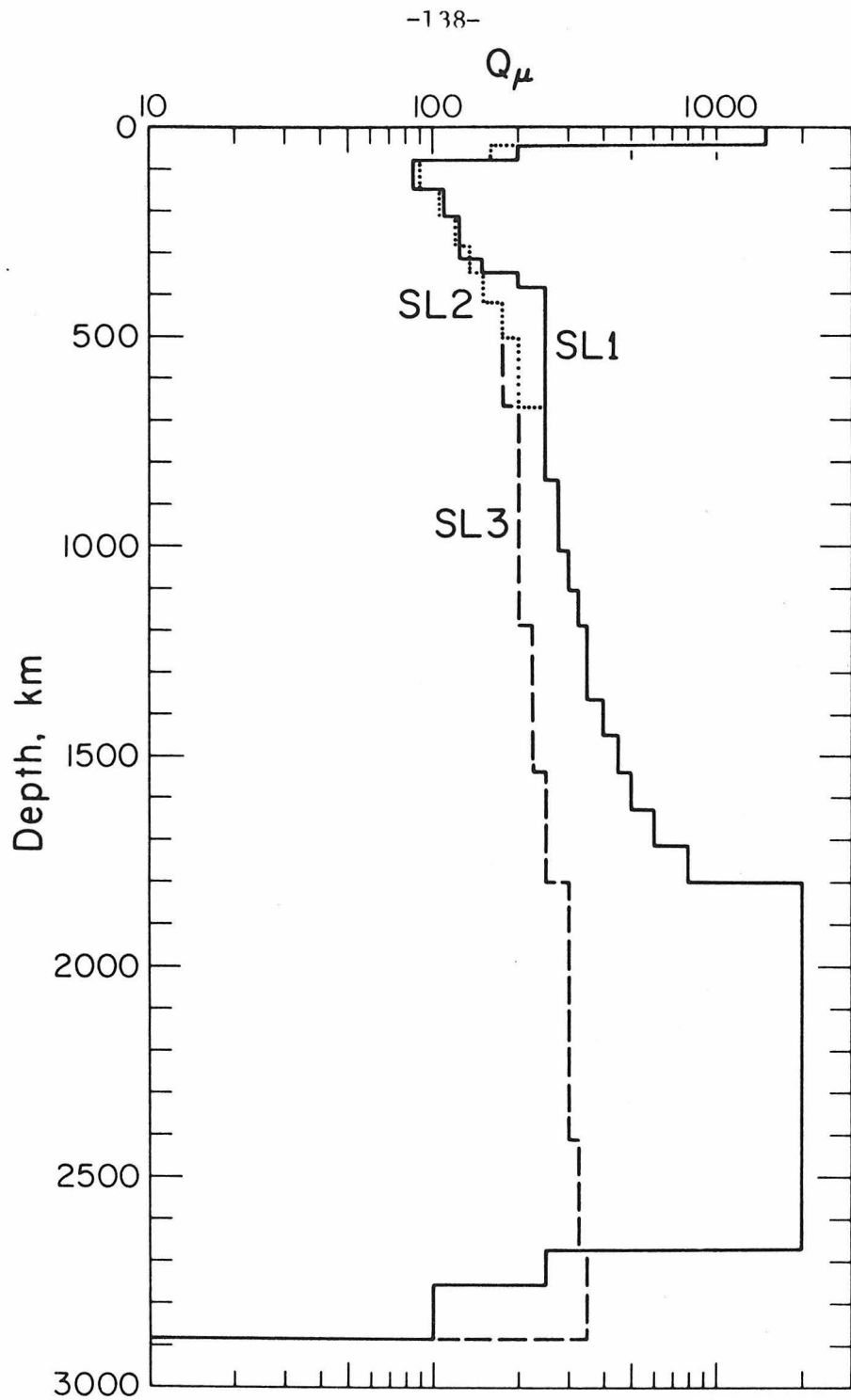


Figure 5.7 - Variation of $Q_\mu (= Q_\beta)$ with depth in the mantle for Q models SL1, SL2, and SL3.

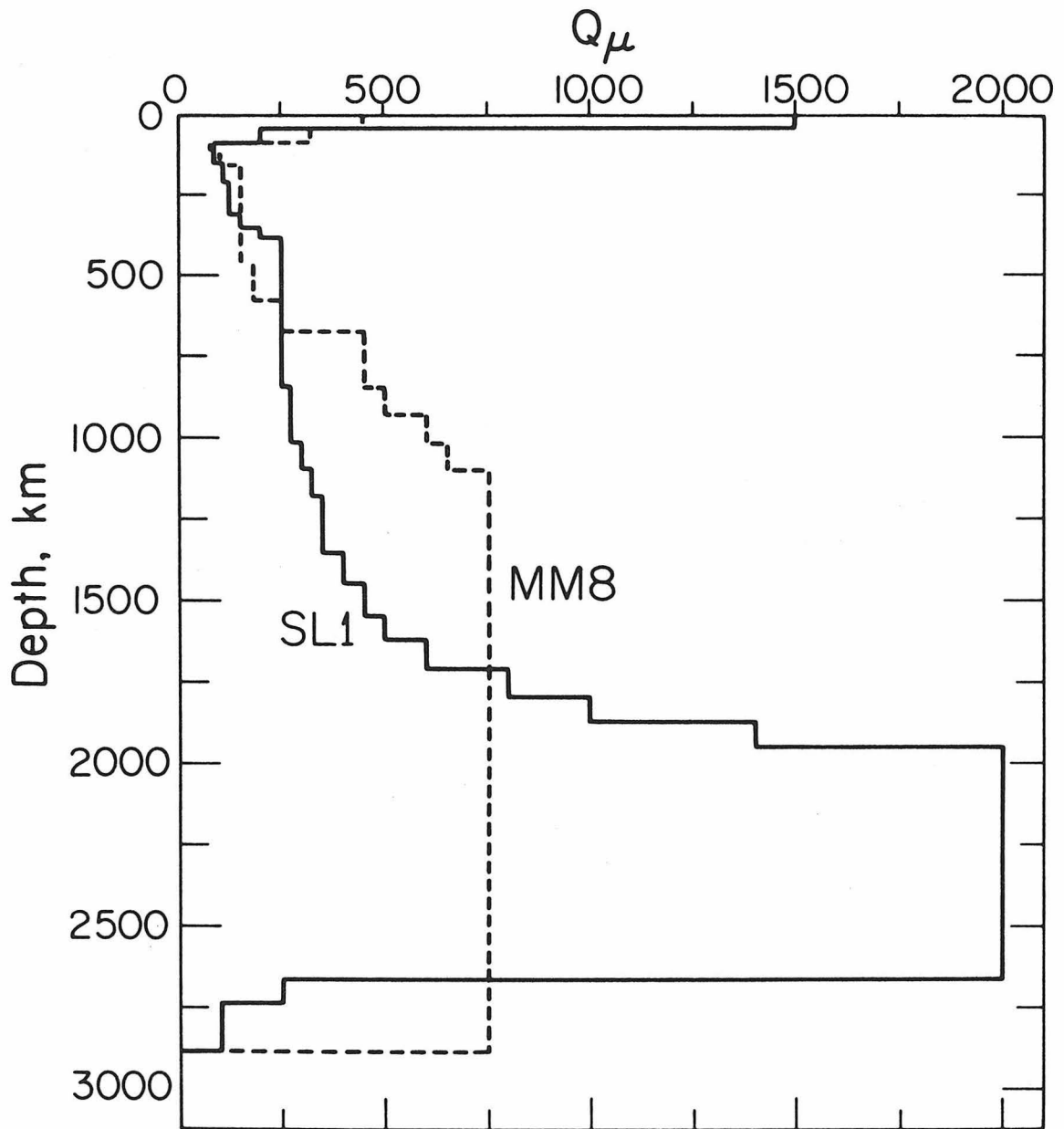


Figure 5.8 - Variation of Q_μ with depth in the mantle for Q models SL1 and MM8 (Anderson et al., 1965).

appreciable in the inner core since low Q_α and Q_β alone cannot substantially reduce the Q of this mode with $K^* = 0$. Dratler's values for Q of ${}_4S_0$ favor a model like SL1 or SL2, with finite K^* , or a model with Q_α in the inner core of 120 with Q_β of about 20. The latter, however, gives Q for ${}_2S_0$ about 3 times the observed value, and values for ${}_5S_0$ much less than observed. The observations for ${}_2S_0$ and ${}_6S_1$ suggest that Q_k may be even smaller than in the model. Lowering Q_α and Q_β with $Q_k^{-1} = 0$ does not help for ${}_2S_0$.

In Figures 5.1, 5.2, and 5.3, the theoretical Q values for the models are presented along with the observational data. In Table 5.6, we tabulate theoretical Q 's for the fundamental modes for models SL1 and SL2. Table 5.7 lists the theoretical Q 's for the overtones for which some observation exists. In some cases we give values for other overtones which are close in period to those which have been assigned. In fact, if Q is reliably determined, it can be used to help identify the mode (see Appendix 1). In many cases a reassignment of overtone number brings the theoretical value into accord with the observation. Alternate mode designations have not been given for the toroidal overtones but inspection of Figure 5.9 shows that many of the modes for which the observed Q is greater than the theoretical may be explained if the overtone number is higher than given by the experimenter. In particular this may explain the high Q 's observed for ${}_1^T_{16}$, ${}_1^T_{25}$, ${}_1^T_{27}$, ${}_1^T_{28}$, and ${}_1^T_{38}$. A complete excitation calculation must be performed before it is known if these reassignments are reasonable. Figures 5.9 and 5.10 show Q vs period for the fundamental

TABLE 5.6

Fundamental Mode Q Values

Mode	Period (sec)	SL1	SL2
0 SPHR 2	3231.72	623	606
0 SPHR 3	2134.00	505	489
0 SPHR 4	1545.60	477	461
0 SPHR 5	1190.18	484	469
0 SPHR 6	963.54	497	482
0 SPHR 7	812.19	501	486
0 SPHR 8	707.82	487	474
0 SPHR 9	633.95	461	447
0 SPHR 10	579.55	430	416
0 SPHR 11	537.26	403	388
0 SPHR 12	502.72	381	364
0 SPHR 13	473.55	363	344
0 SPHR 14	448.39	348	327
0 SPHR 15	426.40	336	312
0 SPHR 16	406.98	325	299
0 SPHR 17	389.69	316	288
0 SPHR 18	374.19	307	277
0 SPHR 19	360.20	299	268
0 SPHR 20	347.50	292	259
0 SPHR 25	297.75	261	224
0 SPHR 30	262.21	236	201
0 SPHR 35	234.73	215	185

TABLE 5.6 (cont'd)

Mode	Period (sec)	SL1	SL2
0 SPHR 40	212.48	198	173
0 SPHR 45	198.97	184	164
0 SPHR 50	178.29	174	157
0 SPHR 55	164.84	165	151
0 SPHR 60	153.18	158	146
0 SPHR 65	142.98	152	143
0 SPHR 70	133.99	148	139
0 SPHR 75	126.01	144	137
0 SPHR 80	118.89	141	135
0 SPHR 85	112.49	138	133
0 SPHR 90	106.72	136	131
0 SPHR 95	101.49	134	130
0 SPHR 100	96.73	132	129
0 SPHR 110	88.40	130	128
0 SPHR 120	81.36	129	127
0 SPHR 130	75.33	128	126
0 SPHR 140	70.12	128	126
0 SPHR 150	65.58	128	126
0 SPHR 0	1230.07	5375	5141
1 SPHR 0	613.70	1481	1475
2 SPHR 0	398.51	1258	1220
3 SPHR 0	305.74	991	947
4 SPHR 0	243.71	1270	1170

TABLE 5.6 (cont'd)

Mode		Period (sec)	SL1	SL2
5 SPHR	0	204.85	1126	1043
6 SPHR	0	174.25	1249	1173
7 SPHR	0	151.97	1160	1109
8 SPHR	0	134.57	1029	1004
9 SPHR	0	120.95	1098	1064
10 SPHR	0	110.37	969	947
0 TORO	2	2630.81	325	308
0 TORO	3	1702.54	307	289
0 TORO	4	1303.72	286	267
0 TORO	5	1075.55	265	246
0 TORO	6	925.53	247	228
0 TORO	7	818.04	232	213
0 TORO	8	736.41	220	201
0 TORO	9	671.81	209	191
0 TORO	10	619.11	201	183
0 TORO	11	575.08	194	176
0 TORO	12	537.63	187	170
0 TORO	13	505.28	182	165
0 TORO	14	476.99	173	161
0 TORO	15	451.98	174	157
0 TORO	16	429.67	170	154
0 TORO	17	409.63	167	151
0 TORO	18	391.49	164	149

TABLE 5.6 (cont'd)

Mode	Period (sec)	SL1	SL2
0 TORO 19	374.98	161	147
0 TORO 20	359.87	159	143
0 TORO 25	300.01	150	138
0 TORO 30	257.50	144	133
0 TORO 35	225.61	140	130
0 TORO 40	200.75	137	128
0 TORO 45	189.81	135	127
0 TORO 50	164.47	133	126
0 TORO 55	150.82	131	125
0 TORO 60	139.26	130	124
0 TORO 65	129.33	130	124
0 TORO 70	120.73	129	123
0 TORO 75	113.19	128	123
0 TORO 80	106.53	128	123
0 TORO 85	100.62	128	123
0 TORO 90	95.32	128	123
0 TORO 95	90.55	128	123
0 TORO 100	86.24	128	123
0 TORO 110	78.73	128	123
0 TORO 120	72.43	128	124
0 TORO 130	67.06	129	124
0 TORO 140	62.44	129	125
0 TORO 150	58.41	130	126

TABLE 5.7

Higher Mode Q Values

Mode	Period (sec)	SL1	SL2	Observed
1 SPHR 11	426.48	631	616	214
1 SPHR 18	274.23	197	175	143
1 SPHR 20	253.64	193	173	259
3 SPHR 16	252.12	289	271	
1 SPHR 21	244.56	192	172	130-166
1 SPHR 22	236.15	191	172	110-212
1 SPHR 23	228.33	190	172	102
1 SPHR 24	221.04	189	171	135-164
1 SPHR 25	214.22	188	171	256
5 SPHR 12	213.05	460	423	
1 SPHR 26	207.84	187	171	122-264
1 SPHR 28	196.23	185	170	231
1 SPHR 29	190.93	184	169	127-170
1 SPHR 30	185.95	183	168	84
1 SPHR 31	181.24	181	168	231
1 SPHR 33	172.58	179	166	156-289
1 SPHR 35	164.82	177	165	325-337
1 SPHR 36	161.24	176	164	207
1 SPHR 37	157.83	175	163	197
1 SPHR 38	154.60	174	162	346
5 SPHR 22	154.37	372	358	
1 SPHR 39	151.51	173	161	339

TABLE 5.7 (cont'd)

Mode	Period (sec)	SL1	SL2	Observed
1 SPHR 40	148.58	172	161	174-308
1 SPHR 41	145.78	171	159	234
3 SPHR 32	145.08	260	260	
1 SPHR 43	140.55	169	158	169
1 SPHR 47	131.35	166	155	254
1 SPHR 48	129.28	165	154	168
1 SPHR 49	127.29	164	153	163-216
1 SPHR 50	125.37	164	152	145
1 SPHR 52	121.73	163	152	137-154
1 SPHR 55	116.73	161	149	230
1 SPHR 56	115.16	161	149	237
1 SPHR 57	113.65	161	148	175-242
1 SPHR 59	110.76	160	147	216
1 SPHR 60	109.37	160	147	157
1 SPHR 64	104.21	159	145	200
1 SPHR 69	98.45	158	143	201
2 SPHR 15	308.92	324	298	244
2 SPHR 17	274.07	522	571	274
3 SPHR 14	273.43	310	291	
2 SPHR 26	179.21	227	216	275
2 SPHR 28	169.34	209	198	312
2 SPHR 36	139.47	192	182	324
5 SPHR 26	140.18	362	347	

TABLE 5.7 (cont'd)

Mode	Period (sec)	SL1	SL2	Observed
2 SPHR 38	133.73	190	180	332
5 SPHR 28	134.06	352	336	
2 SPHR 39	131.05	190	179	234
3 SPHR 12	297.35	328	307	80-358
3 SPHR 13	285.05	320	300	271
3 SPHR 14	273.41	310	291	417
2 SPHR 17	274.07	522	517	
7 SPHR 5	273.37	754	708	
3 SPHR 15	262.43	300	281	394
3 SPHR 16	252.11	289	271	285
3 SPHR 17	242.43	279	262	303-349
3 SPHR 18	233.38	269	253	232
3 SPHR 19	224.91	260	245	198-294
3 SPHR 30	154.76	280	280	306
3 SPHR 36	128.97	229	229	368
6 SPHR 26	128.86	406	371	
7 SPHR 24	128.52	329	310	
3 SPHR 41	113.41	239	229	398
3 SPHR 44	107.69	228	217	408
6 SPHR 35	107.88	410	372	
7 SPHR 32	107.67	387	349	
8 SPHR 29	108.06	334	322	
3 SPHR 45	105.92	224	212	342

TABLE 5.7 (cont'd)

Mode	Period (sec)	SL1	SL2	Observed
3 SPHR 48	100.98	215	205	460
7 SPHR 35	101.70	397	354	
3 SPHR 49	99.45	213	203	474
6 SPHR 40	98.92	388	350	
4 SPHR 9	269.53	431	407	286
4 SPHR 14	225.24	353	332	288
4 SPHR 25	161.21	340	325	260
4 SPHR 31	138.75	296	285	299
4 SPHR 40	115.46	244	233	391
5 SPHR 10	237.67	427	389	406
5 SPHR 13	203.15	452	419	514
5 SPHR 22	154.37	372	358	415
5 SPHR 23	150.57	371	357	477
5 SPHR 25	143.48	366	351	433
5 SPHR 32	123.47	331	312	626
5 SPHR 34	118.85	323	304	448
6 SPHR 1	505.47	1126	1051	613-700
1 SPHR 9	509.65	632	620	
11 SPHR 1	271.29	930	883	380-1341
2 SPHR 17	274.07	522	517	
7 SPHR 5	273.38	754	708	
13 SPHR 1	222.48	1043	968	574-1573
11 SPHR 3	224.05	672	631	

TABLE 5.7 (cont'd)

Mode	Period (sec)	SL1	SL2	Observed
11 SPHR 4	209.81	1200	1095	652
3 SPHR 21	209.61	244	230	
7 SPHR 10	209.83	340	323	
25 SPHR 5*	98.74	1020	938	791
1 TORO 16	280.82	251	233	361
1 TORO 19	249.62	234	217	203
1 TORO 21	232.80	226	209	107
1 TORO 23	218.38	219	202	139-182
1 TORO 24	211.92	216	199	124
1 TORO 25	205.89	213	196	286
1 TORO 27	194.98	207	190	275-300
1 TORO 28	190.02	205	188	284
1 TORO 29	185.36	203	185	172-175
1 TORO 30	180.97	201	183	174-207
1 TORO 32	172.89	198	179	173-191
1 TORO 34	165.63	194	175	172-181
1 TORO 35	162.27	193	173	215-255
1 TORO 36	159.07	192	172	145-249
1 TORO 37	156.01	191	170	147-239
1 TORO 38	153.10	190	169	310
1 TORO 39	150.30	189	168	134-245
1 TORO 40	147.63	188	166	163-180
1 TORO 41	145.06	187	165	145-179

TABLE 5.7 (cont'd)

Mode	Period (sec)	SL1	SL2	Observed
1 TORO 42	142.59	186	164	152-209
1 TORO 43	140.22	185	163	122-193
1 TORO 44	137.93	185	162	145-173
1 TORO 45	135.73	184	161	151-202
1 TORO 46	133.61	183	160	165
1 TORO 47	131.56	183	160	212-236
1 TORO 48	129.57	182	159	159
1 TORO 50	125.80	181	157	122-193
1 TORO 55	117.33	178	154	135
1 TORO 59	111.38	176	152	134
1 TORO 61	108.64	176	151	138
2 TORO 2	447.57	328	288	320

Periods Correspond to Model 1066A (Gilbert and Dziewonski, 1975).

*There are 17 spheroidal modes having periods within 0.5 seconds of 98.7 seconds having theoretical Q values ranging from 122 to 1080.

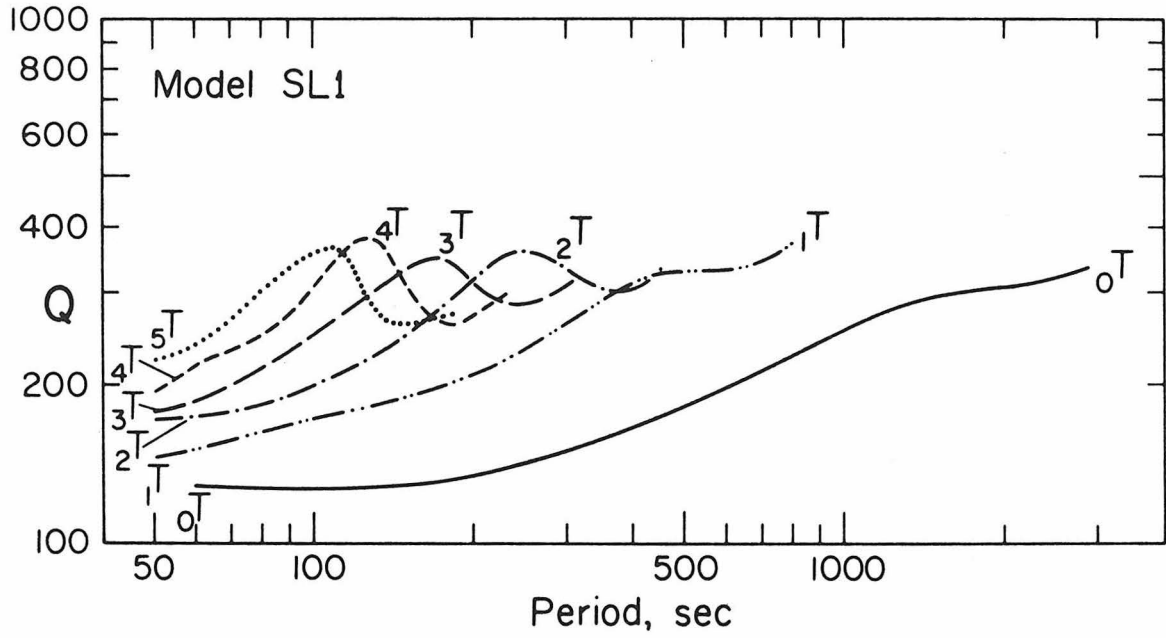


Figure 5.9 - Apparent Q vs. period for the fundamental toroidal ($0T$) and first five toroidal overtones for Q model SL1. The equivalent curves for model SL2 have slightly lowered Q values.

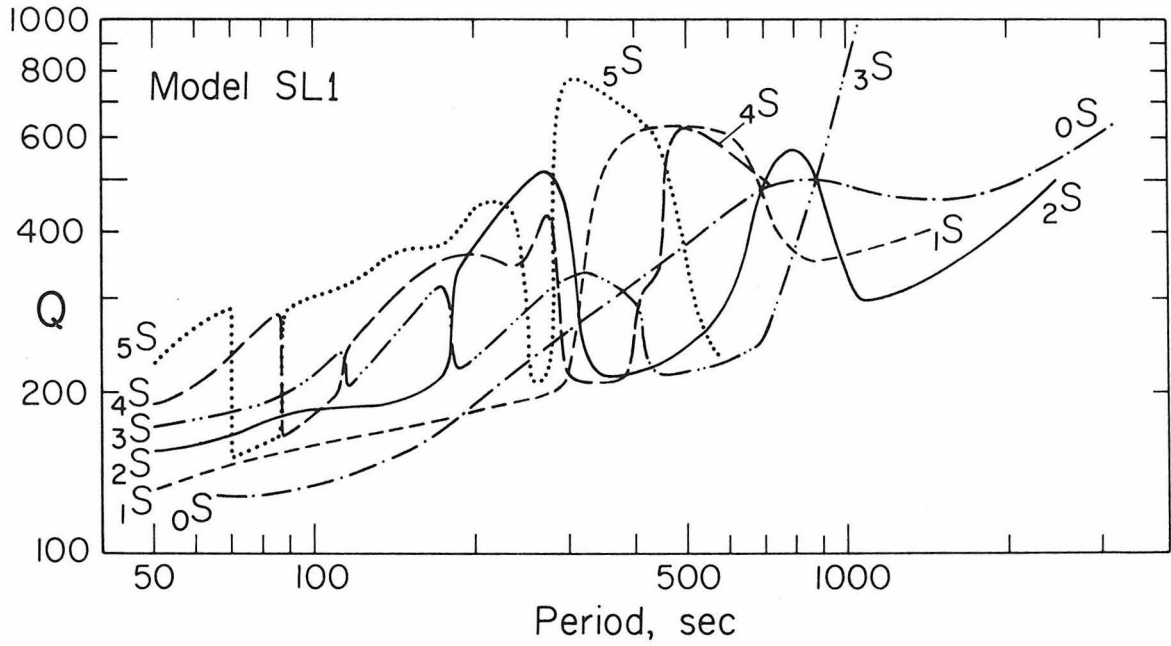


Figure 5.10 - Apparent Q vs. period for the fundamental spheroidal (${}_0S$) and first five spheroidal overtones (${}_1S, {}_2S \dots {}_5S$) for Q model SL1. The equivalent curves for model SL2 show a very slight overall shift to lower Q values. The sharp wells along the overtone curves correspond to the low Q Stoneley modes.

and first five overtone toroidal and spheroidal modes for model SL1. The equivalent SL2 curves are almost identical except for a slight shift to lower Q . The low Q troughs in the spheroidal overtone curves correspond to Stoneley waves at the core-mantle and inner core-outer core boundaries.

Figure 5.9 shows that the Q of fundamental mode toroidal modes, or Love waves, is significantly less than the overtones. In general, Q increases with overtone number. The fundamental mode has highest amplitudes in the upper mantle and therefore is rapidly attenuated, except for the short period lithosphere modes. The overtones have significant energy in the lower mantle and for certain period ranges, have Q 's as high as 400. Higher modes can therefore dominate the later portions of the seismogram, particularly for intermediate and deep focus earthquakes.

The Q structure of the spheroidal modes, Figure 5.10, is very complex. At short periods, less than 50 seconds, modal Q 's increase with overtone number, at least up to the 7th overtone. A given mode changes from high Q to low Q as the character of the mode on a particular overtone branch changes from a simple mantle oscillation to a Stoneley mode at the core-mantle boundary.

In models SL1 and SL2, Q_β has a peak value of 2000 in the lower mantle. This peak level is not well-constrained by the data. Since attenuation averages as Q^{-1} , the high Q regions of the Earth contribute little to the observed attenuation and there is therefore little control on the actual value. Specifically, if we replace the values of

2000 in our models by a value of 10,000, only the lowest order modes are affected. Even for those modes, the increase in apparent Q is less than 4%, far below the resolution of the data. In low Q regions, however, the opposite is true. These regions dominate the observed attenuation and the average values of the dissipation are fairly well constrained.

5.4 Summary of the Fits of the Q Models. In order to select the most reasonable Q model for our earth structure inversion program we need to compare models MM8, SL1, and SL2 to the full range of Q data discussed earlier in this chapter. For completeness we also include at this time a fourth model, SL3, which has the same upper mantle Q distribution as model SL2 but has a very low, around 200, Q_{β} throughout the lower mantle. Model SL3 is equivalent to the two layer Q model proposed by Sailor and Dziewonski (1976). Model SL3 is plotted in Figure 5.7 and is included in Figures 5.1, 5.2, and 5.3 which illustrate normal model Q 's. As a brief review of differences between the first three models, SL1 and SL2 differ from MM8 primarily by the inclusion of a low Q zone at the base of the mantle and by a lower Q in the mid-mantle region (depths between about 600 km and 1500 km). SL1 and SL2 are very similar, differing only in the upper mantle. The Q for model SL1 increases in that region in two stages, for model SL2 the increase occurs in a single stage (see Figure 5.7).

Studies of surface wave attenuation are fairly consistent up to about 300 seconds in period both for Love waves and for Rayleigh waves. In this period range as well, all four Q models predict pretty

much the same Q values. At periods greater than 300 or 400 seconds, the data begin to show greater scatter and the theoretical Q curves begin to diverge (Figures 5.1 and 5.2). On the basis of toroidal modes alone, model MM8 is satisfactory, but it predicts very much too high Q values for the low order spheroidal modes and radial modes and can be eliminated from further consideration. (Additionally, the average mantle Q_{β} for MM8 is 345, again too high to be acceptable.) Models SL1 and SL2 represent a compromise in fitting the mode data. These models go through the center of gravity of the longer period toroidal modes and represent a more-or-less upper bound to the longer period spheroidal mode data. They also satisfy the recent spheroidal mode data of Stein and Geller (1977). SL3 represents a minimum estimate that is consistent with the scatter of the spheroidal modes but is not a satisfactory fit to the toroidal or body wave data. All three models are satisfactory fits to the radial mode data (Figure 5.3).

Models SL1 and SL2 both satisfy the average Q_{β} of the mantle from ScS studies, Table 5.8. SL1 has an average mantle shear wave Q of 286 in agreement with the studies of Otsuka (1962, 1963), Yoshida and Tsujiura (1975), Best et al. (1974) and the mean value discussed earlier. Model SL3 has a much lower value. The Q of the upper 600 km of the models ranges from 166 (SL1) to 144 (SL3) which can be compared with the range 150-185 determined in the studies of Anderson and Kovach (1964), Steinhart et al. (1964), and Yoshida and Tsujiura (1975). Some other measurements fall outside this range, Table 5.1. The average Q_{β} of SL1 for depths less than 1000 km, 184, is also a good fit

TABLE 5.8

Average Model Q Values

<u>Depth Interval (km)</u>	<u>Q_β</u>		
	<u>SL1</u>	<u>SL2</u>	<u>SL3</u>
Whole Mantle	286	268	208
< 600	166	147	144
< 1000	184	167	156
< 2000	252	234	183
>600	415	415	258
>1100	528	528	280

<u>Depth Interval (km)</u>	<u>Q_α</u>		
	<u>SL1</u>	<u>SL2</u>	<u>SL3</u>
Whole Mantle	722	678	524
< 100	540	475	475
< 760	433	387	375
< 900	452	408	385
100 - 760	418	374	360
100 - 2886	737	695	525
760 - 2886	1085	1085	654
900 - 2886	1142	1142	673

to the data of Sima (1965). $(T/Q)_\beta$ for the models are given in Table 5.9. For models SL1 and SL2 this parameter ranges from 3.5 to 4.8 in the distance range 30° to 90° and therefore satisfies the limited amount of available data. Model SL3 has $(T/Q)_\beta$ monotonically increasing from 4.21 at 30° to 6.57 at 90° , which seems too high. $(T/Q)_\alpha$ of the three models is given in Table 5.9. Again, models SL1 and SL2 are superior to model SL3, although the data of Mikumo and Kurita (1968) does not permit the rejection of any of these models.

Average mantle values for Q_α are not as well determined as Q_β . The value from model SL1 (722) is consistent with estimates of Berzon et al. (1974) but is higher than estimates of Kanamori (1967a). Kanamori's results were obtained at the Tonto Forest Observatory in the Basin and Range Province of the Western United States. McGinley and Anderson (1969) showed that this region is underlain by anomalously low-Q mantle compared to stations in central and eastern U. S. Kanamori also comments that his values may be lower than appropriate for "normal" areas. Other average properties of the models are given in Table 5.8 which can be compared with the data in Tables 5.1 and 5.2. Regional variations in the thickness of the upper mantle low-Q zone may be responsible for the large spread of experimental values.

The effects of finite record length, scattering, multipathing, splitting, lateral heterogeneity and mode interference all serve to decrease the apparent Q and there is therefore reason to bias the fits toward the higher values of Q when attempting to satisfy the mode data.

TABLE 5.9

T/Q_{α} & T/Q_{β} as a function of distance *

Delta (deg)	Model SL1		Model SL2		Model SL3	
	T/Q_{α}	T/Q_{β}	T/Q_{α}	T/Q_{β}	T/Q_{α}	T/Q_{β}
30	0.76	3.45	0.83	3.79	0.91	4.13
40	0.88	3.96	0.95	4.28	1.08	4.88
50	0.93	4.27	0.99	4.57	1.21	5.57
60	0.92	4.30	0.97	4.58	1.28	5.95
70	0.85	4.16	0.90	4.42	1.33	6.27
80	0.78	3.72	0.83	3.97	1.35	6.33
90	0.87	3.58	0.92	3.82	1.33	6.45

* Surface focus values. T/Q_{α} for intermediate depth earthquakes (113 km) is 0.04 secs lower. For deep focus earthquakes (590 km) T/Q_{α} is 0.14 to 0.28 secs lower.

Model SL3 is a lower bound in the sense that it satisfies the lower bounds of the estimates of Q_S for ${}_0S_3$, ${}_0S_4$, and ${}_0S_5$ which have been obtained by time domain seismogram matching (Stein and Geller, 1977). It, however, predicts values of Q for the low-order toroidal modes which are much lower than observed. It is also not a very good model for the presently available ScS data.

From this comparison, it seems that models SL1 and SL2 represent the better fit to the overall Q data. There is no particular basis for choosing one over the other except perhaps that model SL2 is the simpler of the two. We will use both models in the final chapter in determining a Q -corrected earth model.

Chapter 6

IMPLICATIONS OF THE Q DISTRIBUTION UPON
THE INFERRED ELASTIC PROPERTIES OF THE EARTH
AND UPON THE OBSERVATION OF THE EARTH'S
FREE OSCILLATIONS

6.1 Introduction. The Q models developed in the preceding chapter provide a reliable and acceptable basis for determining the normal mode period corrections. The next step, logically, is to use these models and invert the normal mode observations for a velocity and density structure of the earth. We have adopted Q model SL1 for this purpose and the model derived below is compatible with that Q distribution. We shall also briefly consider what sort of differences would occur if Q model SL2 were adopted instead.

In Chapter 3, we have discussed the concept and rationale for the inclusion of fine structure determined by high resolution body wave studies in the starting model. We have retained this philosophy in designing the starting model for the present inversion. However, several features of the model have been changed to conform to more recent body wave studies. In particular, the 500 km discontinuity present in model C2 (and the C2 starting model) was removed. The justification for this change comes from the very high quality upper mantle P wave study by Burdick (Ph. D. Thesis, in preparation). Burdick's data indicate that the velocity gradient is smooth between depths of about 400 km and 670 km in the mantle. Average changes to

the C2 structure due to including attenuation (model QM2, Chapter 4) were also considered in the starting model design. As with model C2, the fine structure contained in the final model here is not required by the normal mode data themselves.

6.2 The starting model. If the density structure of the earth could be independently (from the normal mode data) constrained, it would be possible to simply derive a gross earth structure, compatible with the SL1 Q distribution, once we have model QM2 (the MM8 compatible differential earth model derived in Chapter 4). From Chapter 4, we have the dispersion relations for each layer for a given Q distribution

$$\begin{aligned}\Delta\alpha_{\ell}/\alpha_{\ell} &= (\pi Q_{\alpha_{\ell}}^{(i)})^{-1} \ln(\omega/\omega_R) \\ \Delta\beta_{\ell}/\beta_{\ell} &= (\pi Q_{\beta_{\ell}}^{(i)})^{-1} \ln(\omega/\omega_R)\end{aligned}\tag{6.1}$$

where α , β are the P velocity and S velocity; $Q_{\alpha}^{(i)}$ and $Q_{\beta}^{(i)}$ are the compressional wave Q and the shear wave Q respectively for Q model i; ℓ is the layer index; and ω_R is the reference frequency. Thus, if we change to a new Q model, j, the perturbation to α and β in each layer be related by the expressions

$$\begin{aligned}Q_{\alpha_{\ell}}^{(i)} \Delta\alpha_{\ell}^{(i)} &= Q_{\alpha_{\ell}}^{(j)} \Delta\alpha_{\ell}^{(j)} \\ Q_{\beta_{\ell}}^{(i)} \Delta\beta_{\ell}^{(i)} &= Q_{\beta_{\ell}}^{(j)} \Delta\beta_{\ell}^{(j)}\end{aligned}\tag{6.2}$$

where the superscripts (i) and (j) refer to the Q and velocity perturbation associated with Q models (i) and (j) respectively.

In Chapter 4, we obtained the velocity perturbations to model C2 when Q model MM8 was adopted. We could now use those perturbations and compute a new set of velocity perturbations compatible with model SL1 through equations 6.2. The resulting model would then fit the corrected C2 eigenperiods (using SL1 Q corrections) to the same accuracy (relative error less than 0.02%) as model QM2 fits the periods corrected with MM8 if the density perturbation in the QM2 inversion had been zero (see Figure 4.7). The model derived with equations 6.2 will not attain quite that accuracy. Indeed if we use the QM2 density change with velocity changes from equations 6.2, the resulting model fits the corrected C2 periods to an average error of 0.03% - 0.04%. If we had desired, of course, that model could have been iterated upon and would have rapidly approached a perfect fit to the corrected C2 eigenperiods. We did not follow that procedure for basically two reasons. First, we were not satisfied with many of the structural features of a model produced in this manner. The low Q zone at the base of the mantle results, with the application of equations 6.2, in a large step in velocity in that region. Further the upper mantle features of QM2 (see Figure 4.10) were accentuated. The second reason was the existence of the new upper mantle P wave velocities referred to in the previous section. Thus the velocity structures obtained through application of equations 6.2 were used only to help define average regional velocities in the starting model.

The basic starting model is a modification of model C2 (Chapter 3). The upper mantle was smoothed below a depth of about 400 km to conform to Burdick's (Ph. D. Thesis, in preparation) velocity model. The upper mantle starting density structure was also greatly simplified to be compatible with the general features of the velocity distributions. Below a depth of 1200 km the C2 P wave and S wave velocity structures were smoothed and an Adams-Williamson density structure was imposed. The radius of the core was decreased by 2 km to 3483 km in order to better satisfy the observed mass and moment of the earth. The justification for other model features remains the same as discussed in Section 2 of Chapter 3.

6.3 Data and Inversion. The inversion procedures discussed in Chapter 3 were again applied with the attenuation corrected data set. A total of 12 iterations on various subsets of the data were required to achieve a satisfactory fit to the observations. The final model, designated QM3, fits the total data set to within an average error of less than 0.08%. The fit of model QM3 to various subsets of the data is summarized in Table 6.1.

The normal mode data used for the inversion are the same 400 modes (208 spheroidal and radial modes and 192 toroidal modes) used to obtain model C2. The Q-corrected eigenperiods, observational errors, Q's, and Q corrections are tabulated in Table 6.2 along with the QM3 periods and differences. The errors listed in Table 6.2 are the observational uncertainties and do not include any estimate of

TABLE 6.1

Summary of Fit of QM3 to Normal Mode Data

Modes	Error, %
$0^S_2 - 0^S_{29}$	0.04
$0^S_{30} - 0^S_{66}$	0.05
$1^S_2 - 1^S_{43}$	0.10
$1^S_{44} - 1^S_{75}$	0.09
$2^S_3 - 2^S_{49}$	0.06
$2^S_{57} - 2^S_{76}$	0.23
$3^S_1 - 3^S_{54}$	0.05
$3^S_{58} - 3^S_{73}$	0.10
$4^S_2 - 4^S_{40}$	0.11
$5^S_2 - 5^S_{35}$	0.09
$0^T_2 - 0^T_{29}$	0.05
$0^T_{30} - 0^T_{46}$	0.16
$1^T_2 - 1^T_{29}$	0.12
$1^T_{30} - 1^T_{66}$	0.11
$2^T_2 - 2^T_{61}$	0.08
$3^T_9 - 3^T_{72}$	0.08
$4^T_7 - 4^T_{66}$	0.16
$5^T_9 - 7^T_{49}$	0.13
$0^S_0 - 8^S_0$	0.04

TABLE 6.2 (CCNT'D)

MODE	DATA (S)	C	DT# (S)	ERRCR (%)	QM3 (S)	DIFF (%)	MCDE	DATA (S)	C	DT# (S)	ERRCR (%)	QM3 (S)	DIFF (%)
1 T 59	110.46	177	-0.54	0.10	110.30	-0.14	3 T 11	239.04	286	-1.46	0.11	239.35	0.14
1 T 60	109.31	176	-0.93	0.14	108.92	-0.35	3 T 17	189.02	333	-0.95	0.14	189.67	0.35
1 T 62	106.53	175	-0.50	0.14	106.26	-0.25	3 T 18	183.20	342	-0.85	0.10	183.25	0.03
1 T 64	104.06	174	-0.88	0.14	103.74	-0.30	3 T 19	177.33	348	-0.84	0.10	177.38	0.03
2 T 2	444.66	328	-2.64	0.10	445.49	0.15	3 T 20	171.94	350	-0.80	0.07	171.97	0.03
2 T 4	416.82	313	-2.56	0.10	417.72	0.22	3 T 21	166.91	349	-0.78	0.07	166.58	0.05
2 T 5	399.33	307	-2.45	0.10	400.10	0.20	3 T 23	157.80	342	-0.74	0.07	158.02	0.14
2 T 7	361.41	303	-2.24	0.08	361.18	-0.04	3 T 24	154.08	337	-0.73	0.13	153.95	-0.08
2 T 8	341.27	307	-2.07	0.07	341.35	0.03	3 T 25	149.94	332	-0.72	0.06	150.11	0.12
2 T 17	218.86	344	-1.09	0.07	218.89	0.02	3 T 29	136.56	312	-0.68	0.08	136.64	0.07
2 T 18	210.83	334	-1.07	0.07	211.00	0.09	3 T 32	125.50	293	-0.65	0.07	125.54	0.03
2 T 19	203.57	324	-1.06	0.11	203.75	0.10	3 T 34	123.10	289	-0.65	0.07	123.06	-0.02
2 T 21	190.86	305	-1.05	0.07	190.50	-0.03	3 T 37	116.26	277	-0.63	0.07	116.24	-0.01
2 T 22	185.15	296	-1.04	0.07	185.16	0.01	3 T 41	108.26	263	-0.61	0.07	109.36	0.10
2 T 25	170.10	274	-1.02	0.13	170.11	0.01	3 T 47	98.50	246	-0.58	0.07	98.56	0.07
2 T 26	165.49	268	-1.00	0.08	165.70	0.13	3 T 51	93.11	237	-0.56	0.10	93.06	-0.05
2 T 27	161.58	262	-1.00	0.10	161.54	-0.02	3 T 59	83.83	223	-0.53	0.10	83.86	0.04
2 T 28	157.45	258	-0.98	0.06	157.60	0.11	3 T 65	78.19	214	-0.50	0.11	78.18	-0.01
2 T 29	153.73	253	-0.97	0.07	153.88	0.10	3 T 72	72.68	205	-0.48	0.11	72.59	-0.12
2 T 31	146.76	246	-0.95	0.13	146.98	0.16	4 T 7	215.52	285	-1.29	0.19	216.00	0.23
2 T 32	143.65	242	-0.94	0.07	143.79	0.10	4 T 11	198.50	270	-1.24	0.20	199.83	0.17
2 T 34	137.71	237	-0.91	0.07	137.83	0.09	4 T 14	183.69	261	-1.17	0.20	184.21	0.29
2 T 35	134.83	234	-0.90	0.07	135.05	0.17	4 T 16	173.63	262	-1.09	0.20	174.15	0.30
2 T 36	132.25	231	-0.89	0.07	132.39	0.11	4 T 20	154.81	258	-0.83	0.20	154.85	0.03
2 T 37	129.63	229	-0.88	0.07	129.84	0.17	4 T 22	146.77	331	-0.70	0.20	146.39	-0.25
2 T 38	127.30	227	-0.86	0.09	127.40	0.08	4 T 23	143.02	347	-0.65	0.20	142.54	-0.33
2 T 39	124.86	225	-0.85	0.07	125.06	0.17	4 T 25	135.73	371	-0.57	0.21	135.52	-0.15
2 T 40	122.72	223	-0.84	0.07	122.82	0.09	4 T 27	129.51	381	-0.52	0.24	129.29	-0.16
2 T 41	120.74	221	-0.83	0.06	120.67	-0.05	4 T 40	100.79	307	-0.48	0.31	100.79	0.01
2 T 42	118.51	219	-0.82	0.15	118.61	0.09	4 T 45	93.32	280	-0.48	0.11	93.37	0.07
2 T 44	114.68	215	-0.80	0.07	114.72	0.03	4 T 48	89.35	269	-0.47	0.11	89.50	0.17
2 T 45	112.77	213	-0.79	0.07	112.83	0.10	4 T 50	87.00	263	-0.47	0.10	87.10	0.13
2 T 47	109.44	210	-0.78	0.07	109.42	-0.01	4 T 54	82.50	254	-0.45	0.11	82.70	0.24
2 T 49	106.22	206	-0.76	0.07	106.22	0.01	4 T 63	74.30	240	-0.42	0.10	74.28	-0.03
2 T 51	103.26	203	-0.75	0.07	103.24	-0.01	4 T 64	73.38	239	-0.42	0.10	73.44	0.10
2 T 52	101.86	202	-0.74	0.07	101.83	-0.01	4 T 65	72.53	238	-0.41	0.11	72.63	0.15
2 T 54	99.20	199	-0.73	0.07	99.16	-0.04	4 T 66	71.87	237	-0.41	0.11	71.84	-0.04
2 T 55	97.89	198	-0.72	0.07	97.89	0.01	5 T 9	173.28	272	-1.04	0.11	173.73	0.26
2 T 58	94.38	194	-0.70	0.07	94.33	-0.05	5 T 10	170.35	271	-1.03	0.09	171.25	0.23
2 T 61	91.17	191	-0.68	0.08	91.08	-0.06	5 T 15	156.63	267	-0.94	0.11	156.82	0.13
3 T 5	257.68	289	-1.58	0.13	257.57	-0.12	5 T 38	96.71	348	-0.40	0.10	96.74	0.03

TABLE 6.2 (CONT'D)

MCDE	DATA (S)	Q	DT* (S)	ERROR (%)	QM3 (S)	DIFF (%)	MODE	DATA (S)	C	DT* (S)	ERRCR (%)	QM3 (S)	DIFF (%)
5 T 40	93.73	342	-0.39	0.09	53.77	0.04	0 S 9	631.13	461	-2.82	0.06	630.75	-0.06
5 T 44	88.27	330	-0.38	0.10	88.35	0.09	0 S 10	577.34	430	-2.72	0.06	576.52	-0.14
5 T 45	87.10	327	-0.37	0.10	87.08	-0.01	0 S 11	534.32	403	-2.66	0.06	534.33	0.01
5 T 50	81.24	309	-0.36	0.11	81.27	0.04	0 S 12	499.73	381	-2.60	0.07	499.86	0.03
5 T 55	76.17	290	-0.36	0.10	76.18	0.02	0 S 13	470.62	363	-2.55	0.07	470.74	0.03
5 T 57	74.40	285	-0.36	0.60	74.33	-0.08	0 S 14	445.71	348	-2.49	0.06	445.62	-0.01
6 T 34	96.73	347	-0.40	0.11	96.61	-0.12	0 S 15	423.62	336	-2.44	0.06	423.66	0.01
6 T 35	95.08	356	-0.38	0.10	95.00	-0.08	0 S 16	404.37	325	-2.38	0.06	404.27	-0.02
6 T 41	86.38	373	-0.32	0.10	86.47	0.11	0 S 17	385.99	316	-2.33	0.06	387.02	0.01
6 T 42	85.03	371	-0.32	0.10	85.20	0.19	0 S 18	371.73	307	-2.29	0.06	371.56	-0.04
6 T 45	81.54	364	-0.31	0.11	81.59	0.06	0 S 19	357.87	299	-2.24	0.06	357.61	-0.07
6 T 49	77.35	349	-0.30	0.10	77.24	-0.14	0 S 20	345.29	292	-2.21	0.06	344.95	-0.09
6 T 53	73.59	332	-0.30	0.10	73.38	-0.28	0 S 21	333.64	285	-2.17	0.06	333.39	-0.07
7 T 8	128.97	286	-0.70	0.40	128.56	-0.31	0 S 22	322.92	279	-2.14	0.06	322.77	-0.04
7 T 17	117.92	275	-0.65	0.14	117.89	-0.02	0 S 23	313.10	273	-2.11	0.06	312.96	-0.04
7 T 19	114.94	270	-0.64	0.15	114.59	-0.05	0 S 24	304.17	267	-2.08	0.07	303.66	-0.05
7 T 28	100.56	249	-0.59	0.14	100.83	0.27	0 S 25	295.60	261	-2.06	0.06	295.38	-0.07
7 T 29	98.95	249	-0.58	0.14	99.17	0.22	0 S 26	287.56	255	-2.04	0.06	287.45	-0.04
7 T 30	97.37	251	-0.56	0.14	97.49	0.13	0 S 27	280.16	250	-2.02	0.06	279.58	-0.06
7 T 34	91.01	285	-0.45	0.15	90.91	-0.10	0 S 28	273.11	245	-1.98	0.07	266.30	-0.05
7 T 38	85.11	345	-0.34	0.14	85.07	-0.05	0 S 29	266.46	240	-1.96	0.06	259.99	-0.04
7 T 40	82.53	365	-0.31	0.15	82.48	-0.06	0 S 30	260.10	236	-1.96	0.06	259.99	-0.04
7 T 46	75.90	369	-0.28	0.14	75.79	-0.15	0 S 31	254.00	231	-1.95	0.06	253.59	0.00
7 T 49	73.09	362	-0.27	0.16	72.92	-0.23	0 S 32	248.38	227	-1.93	0.06	248.28	-0.04
0 S 0	1227.12	5375	-0.51	0.07	1226.78	-0.02	0 S 33	243.00	223	-1.92	0.06	242.82	-0.07
0 S 0	612.75	1481	-0.84	0.06	612.44	-0.05	0 S 34	237.69	219	-1.90	0.06	237.61	-0.03
0 S 0	134.45	1030	-0.20	0.06	134.56	0.09	0 S 35	232.69	215	-1.89	0.06	232.61	-0.03
0 S 0	397.95	1258	-0.60	0.06	397.70	-0.06	0 S 36	227.67	211	-1.87	0.06	227.62	-0.01
0 S 0	305.28	991	-0.56	0.06	305.36	0.03	0 S 37	223.30	208	-1.86	0.06	223.23	-0.03
0 S 0	243.26	1270	-0.33	0.06	243.06	-0.08	0 S 38	218.77	204	-1.85	0.06	218.81	0.02
0 S 0	204.31	1126	-0.30	0.06	204.41	0.05	0 S 39	214.60	201	-1.83	0.06	214.55	-0.01
0 S 0	174.03	1249	-0.22	0.10	173.96	-0.03	0 S 40	210.49	198	-1.82	0.06	210.46	-0.01
0 S 2	3219.91	623	-13.34	0.07	3219.10	-0.02	0 S 41	206.54	195	-1.81	0.06	206.51	-0.01
0 S 3	2123.27	505	-10.30	0.12	2123.59	0.02	0 S 42	202.78	192	-1.79	0.07	202.70	-0.03
0 S 4	1538.03	477	-7.57	0.06	1537.66	-0.01	0 S 43	199.15	189	-1.78	0.06	199.03	-0.06
0 S 5	1184.59	484	-5.53	0.06	1184.38	-0.01	0 S 44	195.43	187	-1.76	0.06	195.48	0.03
0 S 6	958.94	497	-4.23	0.06	958.95	0.01	0 S 45	192.12	184	-1.75	0.06	192.05	-0.03
0 S 7	808.00	501	-3.45	0.06	808.31	0.04	0 S 46	188.83	182	-1.74	0.06	189.73	-0.05
0 S 8	704.62	488	-3.02	0.06	704.36	-0.03	0 S 47	185.54	180	-1.72	0.06	185.52	-0.01

TABLE 6.2 (CONT'D)

MODE	DATA (S)	Q	CT* (S)	ERRCR (%)	QM3 (S)	CIFF (%)	MCOE	DATA (S)	C	CT* (S)	ERRCR (%)	QM3 (S)	CIFF (%)
0 S 52	170.89	170	-1.65	0.06	170.90	0.01	1 S 34	166.76	178	-1.54	0.14	167.21	0.28
0 S 53	168.33	168	-1.64	0.06	168.23	-0.05	1 S 35	163.09	176	-1.51	0.14	163.46	0.23
0 S 54	165.75	167	-1.63	0.06	165.65	-0.06	1 S 36	159.87	175	-1.48	0.06	159.89	0.02
0 S 56	160.81	163	-1.60	0.10	160.69	-0.07	1 S 37	156.22	174	-1.45	0.14	156.50	0.19
0 S 57	158.42	162	-1.59	0.06	158.32	-0.06	1 S 38	153.33	173	-1.42	0.06	153.28	-0.03
0 S 58	156.13	161	-1.57	0.10	156.01	-0.07	1 S 39	150.24	172	-1.40	0.06	150.22	-0.01
0 S 59	153.46	159	-1.55	0.06	153.77	0.21	1 S 40	147.24	171	-1.37	0.10	147.30	0.05
0 S 60	151.70	158	-1.54	0.06	151.58	-0.07	1 S 41	144.48	170	-1.35	0.06	144.52	0.03
0 S 61	149.59	157	-1.53	0.06	149.45	-0.09	1 S 42	141.84	169	-1.33	0.10	141.86	0.02
0 S 62	147.55	156	-1.52	0.06	147.38	-0.11	1 S 43	139.30	168	-1.31	0.10	139.32	0.02
0 S 63	145.59	154	-1.50	0.06	145.37	-0.15	1 S 44	136.96	167	-1.29	0.10	136.89	-0.05
0 S 64	143.47	153	-1.49	0.10	143.40	-0.04	1 S 47	130.27	165	-1.23	0.14	130.19	-0.06
0 S 65	141.52	152	-1.47	0.10	141.49	-0.02	1 S 48	127.97	164	-1.21	0.14	128.13	0.13
0 S 66	139.76	151	-1.46	0.10	139.62	-0.10	1 S 49	125.95	164	-1.19	0.14	126.15	0.17
1 S 2	1462.55	411	-8.30	0.05	1461.27	-0.08	1 S 50	124.22	163	-1.17	0.24	124.25	0.03
1 S 3	1057.58	369	-6.37	0.12	1056.62	-0.05	1 S 52	120.82	162	-1.14	0.06	120.64	-0.14
1 S 4	847.54	356	-5.13	0.06	846.69	-0.10	1 S 53	118.95	162	-1.12	0.06	118.93	-0.01
1 S 5	726.83	410	-3.73	0.09	725.57	-0.17	1 S 54	117.39	161	-1.11	0.14	117.28	-0.09
1 S 6	655.13	546	-2.48	0.06	654.57	-0.08	1 S 55	115.72	161	-1.09	0.14	115.68	-0.03
1 S 7	601.92	610	-2.01	0.06	602.43	0.09	1 S 56	114.24	161	-1.08	0.14	114.13	-0.09
1 S 8	554.24	624	-1.79	0.08	554.55	0.06	1 S 58	111.20	160	-1.05	0.14	111.17	-0.02
1 S 9	508.36	631	-1.60	0.06	508.23	-0.02	1 S 59	109.88	160	-1.03	0.14	109.76	-0.10
1 S 10	464.03	636	-1.42	0.07	464.58	0.12	1 S 61	107.06	159	-1.00	0.14	107.05	0.00
1 S 14	335.62	447	-1.39	0.06	334.95	-0.20	1 S 63	104.71	159	-0.98	0.14	104.49	-0.20
1 S 15	314.02	283	-2.04	0.06	313.50	-0.16	1 S 64	103.44	159	-0.97	0.14	103.26	-0.17
1 S 16	296.97	214	-2.53	0.10	296.99	0.01	1 S 68	98.80	158	-0.92	0.14	98.65	-0.14
1 S 17	283.66	201	-2.56	0.08	283.69	0.02	1 S 75	91.64	156	-0.94	0.14	91.55	-0.09
1 S 18	272.26	197	-2.49	0.11	271.58	-0.10	2 S 3	801.21	577	-2.96	0.07	801.72	0.07
1 S 19	261.24	194	-2.39	0.10	261.36	0.05	2 S 4	722.05	538	-2.82	0.06	722.15	0.02
1 S 20	251.66	192	-2.31	0.10	251.63	-0.01	2 S 5	657.02	401	-3.39	0.06	656.75	-0.04
1 S 21	242.70	192	-2.23	0.10	242.65	-0.02	2 S 6	590.61	294	-4.09	0.06	590.69	0.02
1 S 22	234.06	191	-2.14	0.10	234.32	0.12	2 S 7	531.56	258	-4.14	0.09	531.76	0.04
1 S 23	226.35	189	-2.07	0.10	226.58	0.11	2 S 8	484.04	241	-3.97	0.06	483.66	-0.07
1 S 24	218.99	188	-2.00	0.10	219.35	0.17	2 S 9	444.58	231	-3.77	0.06	444.53	-0.01
1 S 25	212.49	187	-1.94	0.10	212.59	0.05	2 S 10	412.36	223	-3.56	0.14	412.21	-0.03
1 S 26	205.83	186	-1.88	0.10	206.25	0.21	2 S 11	384.92	218	-3.36	0.06	385.07	0.04
1 S 27	199.87	185	-1.83	0.10	200.30	0.22	2 S 12	361.97	216	-3.16	0.06	361.87	-0.02
1 S 28	194.53	184	-1.78	0.10	194.71	0.10	2 S 13	341.79	218	-2.93	0.07	341.70	-0.02
1 S 29	189.16	183	-1.73	0.07	189.44	0.16	2 S 14	324.03	234	-2.56	0.10	323.78	-0.07
1 S 30	184.25	182	-1.69	0.10	184.48	0.13	2 S 15	307.46	323	-1.74	0.06	306.56	-0.16
1 S 32	175.10	180	-1.61	0.14	175.37	0.16	2 S 27	172.69	212	-1.34	0.07	172.73	0.03
1 S 33	170.77	179	-1.57	0.14	171.18	0.25	2 S 28	167.93	208	-1.32	0.06	167.99	0.04

TABLE 6.2 (CONT'D)

MODE	DATA (S)	G	CT* (S)	ERRCF (%)	QM3 (S)	DIFF (%)	MODE	DATA (S)	G	CT* (S)	ERRCF (%)	QM3 (S)	DIFF (%)
2 S 30	159.24	202	-1.27	0.06	159.32	0.06	4 S 4	436.61	332	-2.55	0.12	436.03	-0.13
2 S 32	151.45	198	-1.23	0.25	151.57	0.08	4 S 5	412.08	312	-2.54	0.07	412.16	0.02
2 S 35	141.45	193	-1.16	0.06	141.39	-0.04	4 S 9	268.48	430	-1.11	0.07	268.77	0.11
2 S 40	127.49	188	-1.05	0.06	127.46	-0.02	4 S 10	257.63	372	-1.22	0.09	257.86	0.10
2 S 45	116.40	187	-0.94	0.07	116.31	-0.06	4 S 11	248.37	353	-1.23	0.09	248.48	0.05
2 S 46	114.41	187	-0.92	0.07	114.35	-0.04	4 S 12	239.58	349	-1.20	0.07	239.58	0.17
2 S 49	109.19	187	-0.88	0.27	108.88	-0.28	4 S 13	231.60	349	-1.15	0.07	232.05	0.20
2 S 57	97.28	186	-0.76	0.27	96.69	-0.39	4 S 14	224.12	352	-1.10	0.07	224.55	0.19
2 S 60	93.41	184	-0.73	0.27	93.17	-0.25	4 S 15	217.13	356	-1.04	0.06	217.37	0.12
2 S 65	87.96	182	-0.65	0.27	87.72	-0.27	4 S 20	185.48	363	-0.85	0.07	185.58	0.06
2 S 71	82.32	177	-0.65	0.27	82.19	-0.16	4 S 40	114.73	243	-0.71	0.07	114.57	-0.13
2 S 76	78.27	174	-0.62	0.27	78.24	-0.03							
3 S 1	1055.86	1051	-2.22	0.09	1054.91	-0.08	5 S 2	477.30	461	-2.04	0.06	475.66	-0.34
3 S 2	900.80	558	-3.50	0.06	900.83	0.01	5 S 3	458.32	364	-2.46	0.06	458.20	-0.02
3 S 6	389.93	310	-2.40	0.06	389.84	-0.02	5 S 4	419.11	643	-1.25	0.06	419.24	0.04
3 S 7	368.93	315	-2.22	0.06	370.04	0.06	5 S 5	369.11	701	-0.99	0.06	369.01	-0.02
3 S 8	352.52	323	-2.04	0.06	352.59	0.02	5 S 6	331.31	762	-0.80	0.06	331.34	0.02
3 S 9	337.00	330	-1.90	0.06	335.66	-0.04	5 S 7	303.28	786	-0.70	0.06	303.16	-0.03
3 S 10	322.16	333	-1.78	0.07	322.34	0.06	5 S 8	282.72	605	-0.84	0.06	282.88	0.06
3 S 11	308.57	332	-1.70	0.09	303.65	-0.04	5 S 10	236.84	426	-0.56	0.06	236.55	0.05
3 S 12	295.77	327	-1.64	0.09	295.77	0.00	5 S 12	212.25	460	-0.78	0.06	212.71	0.23
3 S 13	283.48	320	-1.60	0.09	283.51	0.01	5 S 15	186.98	404	-0.77	0.06	187.36	0.21
3 S 14	271.78	310	-1.57	0.06	271.89	0.05	5 S 16	180.96	385	-0.77	0.07	181.21	0.14
3 S 17	240.91	278	-1.51	0.06	240.55	-0.02	5 S 20	161.75	372	-0.70	0.07	161.81	0.04
3 S 18	231.79	268	-1.50	0.06	231.90	0.05	5 S 25	142.98	366	-0.61	0.06	142.89	-0.06
3 S 19	223.42	259	-1.49	0.06	223.45	0.02	5 S 30	127.93	341	-0.58	0.07	128.00	0.06
3 S 20	215.48	251	-1.47	0.10	215.54	0.04	5 S 35	116.08	320	-0.55	0.07	115.15	0.06
3 S 24	189.67	226	-1.40	0.06	188.72	-0.03							
3 S 25	182.96	223	-1.36	0.09	183.01	0.04							
3 S 41	112.60	235	-0.71	0.09	112.51	-0.07							
3 S 42	110.65	235	-0.70	0.09	110.53	-0.10							
3 S 43	108.68	231	-0.70	0.09	109.63	0.04							
3 S 50	97.30	210	-0.67	0.09	97.11	-0.04							
3 S 51	95.77	208	-0.67	0.08	95.69	-0.09							
3 S 54	91.74	202	-0.65	0.09	91.63	-0.06							
3 S 58	87.02	195	-0.63	0.06	86.92	-0.12							
3 S 63	81.78	190	-0.60	0.14	81.71	-0.08							
3 S 70	75.56	187	-0.56	0.14	75.51	-0.05							
3 S 73	73.25	186	-0.54	0.14	73.16	-0.11							
4 S 2	578.79	592	-2.02	0.11	579.93	0.03							
4 S 3	487.54	635	-1.51	0.06	485.89	-0.13							

* : PERIOD CHANGE DUE TO Q

uncertainty in Q (and hence Q correction). Inclusion of those uncertainties would increase the errors by about 20% (i.e.—an error of 0.05% would become 0.06%). In Figure 6.1, the percentage change in period, due to the SL1 Q model, is plotted for the fundamental toroidal modes and the first five toroidal overtones. The effect upon the toroidal periods of changing Q models from MM8 to SL1 is small as can be seen through a comparison of Figure 6.1 with Figure 4.2. In Figure 6.2, the percentage period change for the fundamental spheroidal modes and first five spheroidal overtones is shown, again for Q model SL1. The behavior of these curves is considerably more complex than the corresponding toroidal curves and is somewhat more complicated than the spheroidal period changes computed for Q model MM8 (Figure 4.6). Since the base of the mantle is a low Q region in model SL1, the Stoneley modes are now low Q modes and appear in Figure 6.2 as pedestals along the overtone curves rather than the high Q wells observed in Figure 4.2.

Forty-four of the 400 modes in our data set (11%) are fit to better than 0.01%, 61% are fit to within 1 standard deviation and 88% are fit to within 2 standard deviations. This is slightly better than model C2. In determining those percentages, the raw observation error was used. If, for example, these errors were increased by a 20% to estimate the Q uncertainties, 93% of the data would be fit to 2σ .

The resulting model, QM3, is shown in Figure 6.3. The model parameters are given in Table 6.3. In addition to V_p , V_s and density

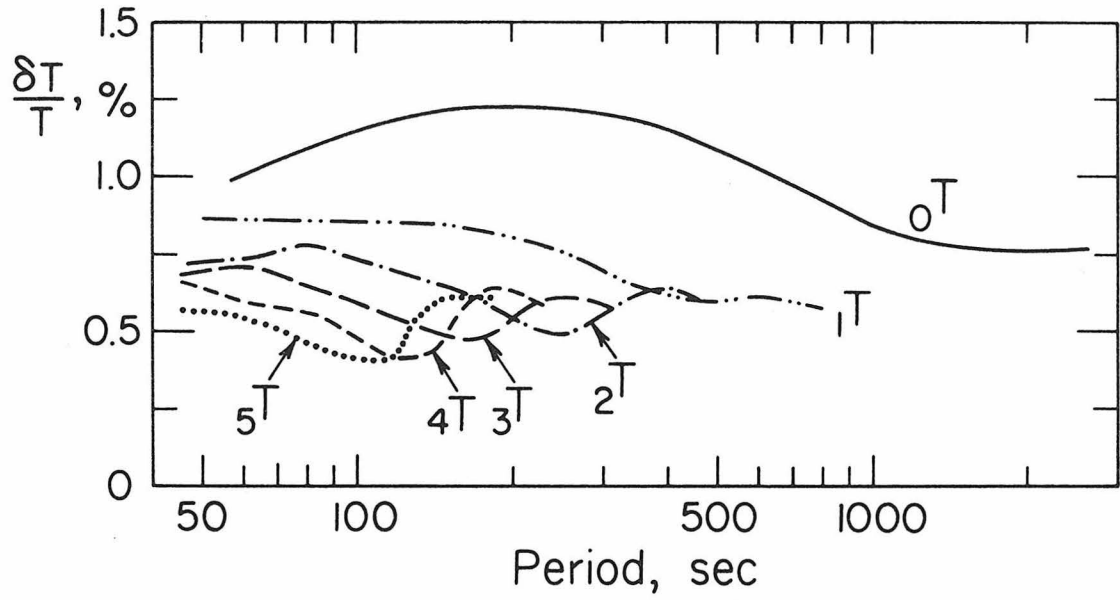


Figure 6.1 - Percentage change in period, as a function of period, due to attenuation for Q model SL1 for the fundamental toroidal modes and for the first five toroidal overtones.

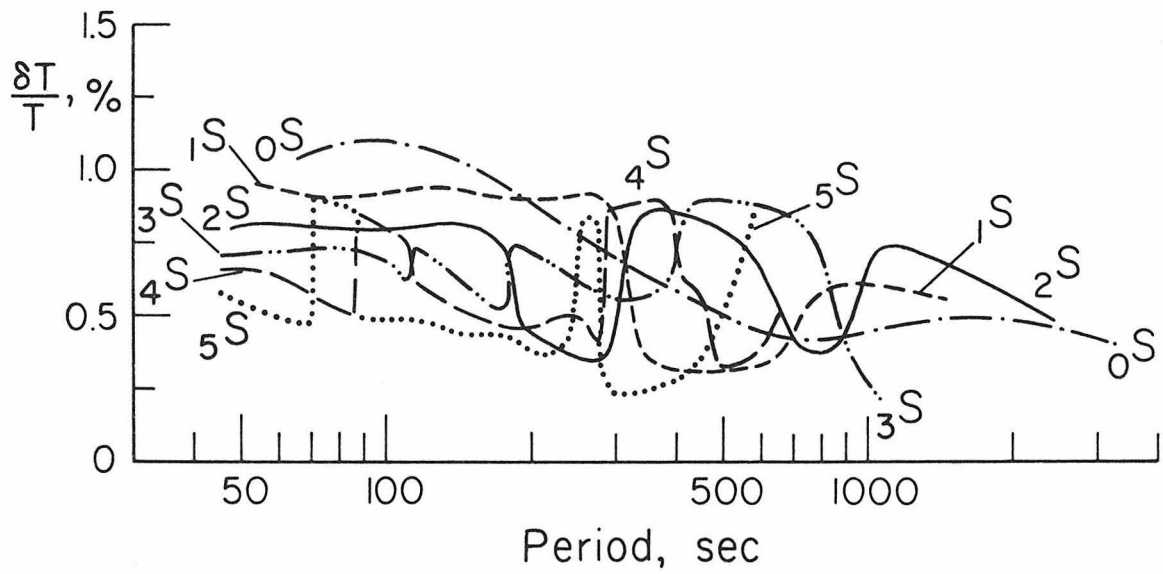


Figure 6.2 - Percentage change in period, as a function of period, due to attenuation for Q model SL1 for the fundamental spheroidal modes and for the first five spheroidal overtones.

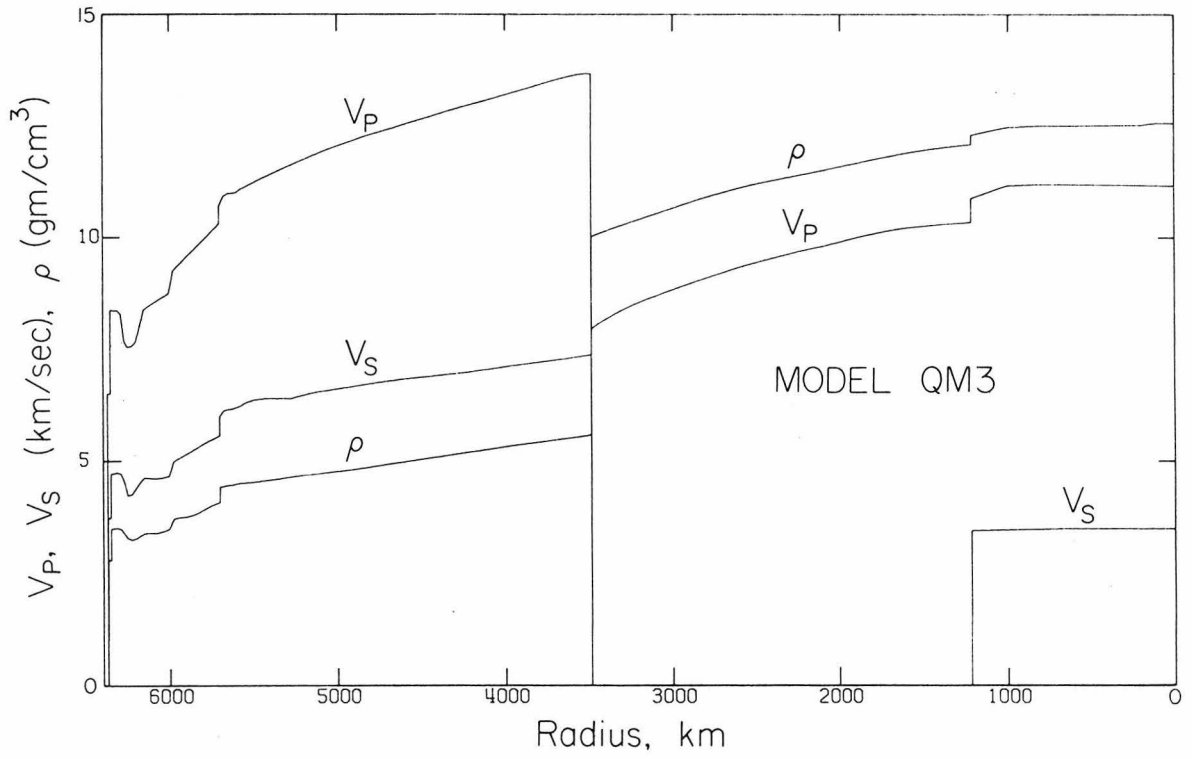


Figure 6.3 - Model QM3; V_p (compressional velocity), V_s (shear velocity), and ρ (density) as a function of radius.

TABLE 6.3
MODEL GM3

INDEX	RADIUS (KM)	DEPTH (KM)	VP (KM/S)	VS (KM/S)	RHC (G/CM**3)	PHI (KM/S)**2	K (KB)	MU (KB)	LAMBDA (KB)	SIGMA	PRESSURE (KB)	G (CM/S**2)
1	1	6370	11.17	3.50	12.56	108.43	13624	1539	12598	0.4456	3619	0
2	100	6271	11.18	3.50	12.56	108.56	13638	1540	12611	0.4456	3616	52
3	200	6171	11.19	3.50	12.52	108.84	13630	1535	12606	0.4457	3607	79
4	400	5971	11.20	3.50	12.52	109.00	13642	1533	12621	0.4458	3579	151
5	600	5771	11.20	3.50	12.51	109.10	13648	1529	12629	0.4460	3532	219
6	800	5571	11.20	3.48	12.51	109.26	13668	1519	12656	0.4464	3469	287
7	1000	5371	11.17	3.47	12.47	108.80	13568	1501	12567	0.4467	3389	355
8	1215	5156	10.89	3.46	12.29	102.60	12613	1469	11634	0.4439	3285	428
9	1215	5156	10.35	0.0	12.09	107.05	12938	0	12938	0.5000	3285	428
10	1300	5071	10.33	0.0	12.06	106.70	12867	0	12867	0.5000	3240	454
11	1400	4971	10.30	0.0	12.01	106.10	12747	0	12747	0.5000	3183	485
12	1500	4871	10.26	0.0	11.96	105.27	12589	0	12589	0.5000	3123	517
13	1600	4771	10.23	0.0	11.90	104.62	12446	0	12446	0.5000	3059	548
14	1700	4671	10.17	0.0	11.82	103.35	12221	0	12221	0.5000	2993	579
15	1800	4571	10.08	0.0	11.75	101.66	11943	0	11943	0.5000	2923	610
16	1900	4471	10.00	0.0	11.67	99.97	11664	0	11664	0.5000	2849	641
17	2000	4371	9.91	0.0	11.59	98.13	11371	0	11371	0.5000	2773	671
18	2100	4271	9.81	0.0	11.51	96.31	11084	0	11084	0.5000	2694	701
19	2200	4171	9.74	0.0	11.43	94.81	10840	0	10840	0.5000	2612	731
20	2300	4071	9.64	0.0	11.36	92.96	10562	0	10562	0.5000	2527	760
21	2400	3971	9.55	0.0	11.29	91.12	10286	0	10286	0.5000	2439	789
22	2500	3871	9.45	0.0	11.21	89.22	10001	0	10001	0.5000	2349	818
23	2600	3771	9.34	0.0	11.12	87.22	9699	0	9699	0.5000	2256	846
24	2700	3671	9.22	0.0	11.02	84.96	9360	0	9360	0.5000	2161	874
25	2800	3571	9.09	0.0	10.91	82.68	9017	0	9017	0.5000	2063	901
26	2900	3471	8.97	0.0	10.79	80.46	8678	0	8678	0.5000	1964	928
27	3000	3371	8.83	0.0	10.66	77.98	8313	0	8313	0.5000	1863	954
28	3100	3271	8.69	0.0	10.53	75.48	7951	0	7951	0.5000	1761	980
29	3200	3171	8.55	0.0	10.41	73.02	7599	0	7599	0.5000	1657	1004
30	3300	3071	8.38	0.0	10.28	70.15	7210	0	7210	0.5000	1552	1029
31	3400	2971	8.16	0.0	10.15	66.58	6756	0	6756	0.5000	1446	1052
32	3483	2888	7.96	0.0	10.02	63.34	6347	0	6347	0.5000	1357	1071
33	3483	2888	13.68	7.37	5.57	114.57	6397	3036	4373	0.2951	1357	1071
34	3510	2861	13.67	7.36	5.57	114.74	6389	3017	4378	0.2960	1341	1067
35	3550	2821	13.66	7.34	5.55	114.85	6372	2988	4380	0.2972	1317	1062

TABLE 6.3 (CCNT'D)

INDEX	RADIUS (KM)	DEPTH (KM)	VP (KM/S)	VS (KM/S)	RHC (G/CM**3)	PHI (KM/S)**2	K (KB)	MU (KB)	LAMBDA (KB)	SIGMA	PRESSURE (KB)	G (CM/S**2)
36	3625	2746	13.60	7.30	5.51	113.95	6279	2934	4323	0.2979	1273	1052
37	3700	2671	13.53	7.26	5.47	112.76	6171	2882	4250	0.2979	1230	1044
38	3775	2596	13.44	7.22	5.44	111.19	6044	2833	4155	0.2973	1187	1036
39	3850	2521	13.36	7.18	5.40	109.62	5917	2784	4061	0.2966	1145	1030
40	3925	2446	13.27	7.14	5.36	108.12	5793	2735	3970	0.2961	1104	1024
41	4000	2371	13.19	7.10	5.32	106.68	5673	2683	3884	0.2957	1063	1019
42	4075	2296	13.11	7.06	5.28	105.29	5556	2631	3802	0.2955	1023	1014
43	4150	2221	13.02	7.02	5.23	103.92	5439	2580	3720	0.2952	983	1011
44	4225	2146	12.95	6.98	5.19	102.64	5329	2530	3642	0.2950	943	1007
45	4300	2071	12.87	6.95	5.15	101.25	5213	2484	3557	0.2944	904	1004
46	4375	1996	12.78	6.92	5.11	99.88	5088	2442	3459	0.2931	866	1002
47	4450	1921	12.69	6.89	5.06	97.88	4958	2403	3356	0.2914	828	1000
48	4525	1846	12.61	6.86	5.02	96.21	4832	2363	3257	0.2897	790	998
49	4600	1771	12.52	6.83	4.98	94.58	4710	2323	3162	0.2882	752	997
50	4675	1696	12.43	6.75	4.94	92.98	4591	2279	3071	0.2870	715	996
51	4750	1621	12.35	6.75	4.89	91.71	4488	2232	3000	0.2867	679	995
52	4825	1546	12.26	6.71	4.85	90.37	4385	2184	2929	0.2864	642	994
53	4900	1471	12.17	6.66	4.81	88.90	4279	2137	2854	0.2859	606	994
54	4975	1396	12.07	6.62	4.78	87.33	4171	2093	2776	0.2851	571	994
55	5050	1321	11.97	6.58	4.74	85.69	4063	2051	2696	0.2840	535	995
56	5125	1246	11.86	6.54	4.71	83.75	3942	2010	2602	0.2821	500	995
57	5200	1171	11.74	6.47	4.68	82.13	3846	1958	2541	0.2824	465	995
58	5275	1096	11.62	6.40	4.65	80.48	3739	1902	2472	0.2826	430	996
59	5350	1021	11.49	6.39	4.60	77.66	3574	1880	2321	0.2762	395	997
60	5425	946	11.37	6.39	4.56	74.74	3411	1863	2168	0.2689	361	998
61	5500	871	11.22	6.35	4.53	72.13	3267	1829	2048	0.2642	327	999
62	5550	821	11.12	6.29	4.51	71.08	3208	1783	2019	0.2655	305	1000
63	5575	796	11.08	6.23	4.51	71.05	3203	1748	2038	0.2691	293	1001
64	5600	771	11.01	6.15	4.45	70.06	3143	1721	1996	0.2685	282	1001
65	5625	746	11.00	6.16	4.45	70.42	3143	1694	2014	0.2716	271	1001
66	5650	721	10.98	6.15	4.46	70.18	3127	1684	2004	0.2717	260	1002
67	5675	696	10.92	6.12	4.44	69.26	3073	1664	1964	0.2707	248	1002
68	5700	671	10.70	5.99	4.42	66.71	2949	1584	1893	0.2722	237	1003
69	5700	671	10.31	5.56	4.07	65.04	2646	1257	1808	0.2949	237	1003
70	5725	646	10.21	5.52	4.04	63.66	2572	1229	1753	0.2938	227	1003
71	5750	621	10.11	5.47	4.00	62.35	2496	1198	1697	0.2930	217	1002
72	5775	596	10.02	5.42	3.96	61.11	2418	1164	1642	0.2926	207	1002

TABLE 6.3 (CONT'D)

INDEX	RADIUS (KM)	DEPTH (KM)	VP (KM/S)	VS (KM/S)	RHO (G/CM**3)	PHI (KM/S)**2	K (KB)	MU (KB)	LAMBDA (KB)	SIGMA	PRESSURE (KB)	G (CM/S**2)
73	5800	571	9.92	5.37	3.90	59.96	2341	1126	1590	0.2926	157	1002
74	5825	546	9.83	5.32	3.85	58.89	2268	1088	1542	0.2932	188	1001
75	5850	521	9.73	5.26	3.81	57.83	2201	1053	1499	0.2937	178	1000
76	5875	496	9.64	5.20	3.77	56.77	2143	1023	1461	0.2941	165	1000
77	5900	471	9.54	5.15	3.76	55.67	2091	997	1427	0.2943	155	999
78	5925	446	9.45	5.10	3.75	54.55	2043	974	1394	0.2943	150	999
79	5950	421	9.35	5.05	3.73	53.44	1994	950	1361	0.2945	140	998
80	5975	396	9.25	4.99	3.71	52.37	1942	922	1327	0.2951	131	998
81	6000	371	8.74	4.66	3.48	47.42	1650	756	1147	0.3013	122	997
82	6025	346	8.69	4.64	3.45	46.79	1613	742	1119	0.3006	114	996
83	6050	321	8.64	4.62	3.41	46.09	1574	729	1088	0.2993	105	995
84	6075	296	8.58	4.62	3.40	45.19	1535	724	1053	0.2963	97	994
85	6100	271	8.52	4.62	3.39	44.13	1497	724	1015	0.2918	88	993
86	6125	246	8.46	4.63	3.35	42.97	1458	726	974	0.2864	80	992
87	6150	221	8.39	4.63	3.33	41.78	1414	727	930	0.2806	71	991
88	6175	196	8.02	4.52	3.34	37.05	1237	683	781	0.2668	63	990
89	6200	171	7.65	4.35	3.27	32.88	1077	630	657	0.2553	55	989
90	6225	146	7.56	4.25	3.24	33.13	1074	585	684	0.2694	47	987
91	6250	121	7.56	4.23	3.28	33.24	1090	588	659	0.2710	39	986
92	6270	101	7.70	4.54	3.38	31.88	1078	696	613	0.2341	32	986
93	6290	81	8.30	4.72	3.48	39.12	1383	776	846	0.2607	25	985
94	6310	61	8.38	4.75	3.51	40.12	1407	790	881	0.2636	15	985
95	6330	41	8.38	4.73	3.50	40.21	1412	784	889	0.2656	12	984
96	6350	21	8.38	4.72	3.49	40.54	1415	776	858	0.2681	5	984
97	6350	21	6.50	3.72	2.75	23.75	665	387	407	0.2564	5	984
98	6368	3	6.50	3.72	2.75	23.78	665	387	407	0.2563	0.3	983
99	6368	3	1.45	0.0	1.02	2.09	21	0	21	0.5000	0.3	983
100	6371	0	1.45	0.0	1.02	2.09	21	0	21	0.5000	0	982

as a function of layer index, radius, and depth, we also tabulate in Figure 6.3 the seismic parameter $\phi (= K/\rho = V_p^2 - \frac{4}{3} V_s^2)$, bulk modulus K , rigidity μ , the Lamé constant λ , Poisson's ratio σ , pressure, and gravity. In Figure 6.4, we have plotted the cumulative perturbations to V_p , V_s , and ρ between the starting model and the final model QM3. The maximum perturbation in any of the three parameters is about 0.05. In a visual inspection of the model (Figure 6.3) the only obvious feature added is a slight gradient change in density at a depth of about 500 km, no velocity effects are apparent at this depth however. In comparison with model C2, the density and velocity structures of model QM3 are substantially smoother and simpler. No troublesome features such as the large C2 velocity and density reversals at 300 km and 400 km depths occur. The general features of Burdick's (Ph. D. thesis, in preparation) velocity structure remain and are compatible with the normal mode data.

6.4 Comparison with body wave data. As noted above, model QM3 has, overall, faster body wave velocities than model C2 and these changes should be most clearly apparent in the theoretical body wave times of the two models.

In comparison with the 1968 P tables, model QM3 shows an almost insignificant deviation. The QM3 P times average 0.2 seconds fast over the range $30^\circ - 95^\circ$ with a maximum deviation of about 0.6 seconds occurring at the distance range of between 50° and 60° ; with respect to the JB tables, the QM3 P times average 2.8 seconds fast. The

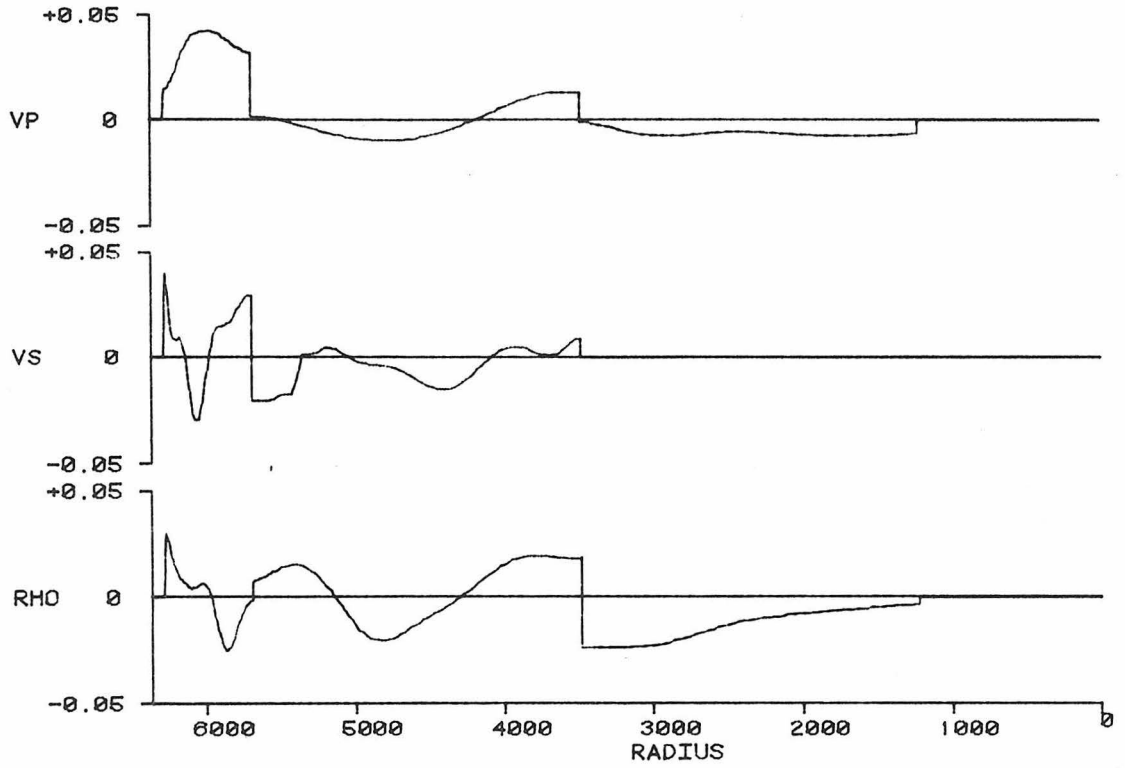


Figure 6.4 - The cumulative perturbation in the model parameters V_p , V_s , and ρ as a function of radius for model QM3 relative to the starting model.

QM3 P wave residuals with respect to the 1968 tables are plotted in Figure 6.5. In Table 6.4, we have listed the QM3 P times and $dt/d\Delta$'s. Both parameters are in better general agreement with the observations than all previous gross earth models.

Table 6.5 compares observed PcP (surface focus) times with the predicted QM3 travel times. The QM3 times are substantially faster than the JB times and Gogna's (1973) observations but fall essentially exactly on the times of Engdahl and Johnson (1974). The average difference across the range 30° - 95° is less than -0.05 seconds. Since the Engdahl and Johnson (1974) times are consistent with the 1968 tables, this agreement is not surprising in light of the QM3 direct P times. The QM3 PcP - P times (Table 6.6) average 0.3 seconds slower than the data for the range 30° - 95° . The PKP times calculated for model QM3 average almost 4 seconds faster than Whitcomb's (1973) model, however the differential core times ($P'_{AB} - P'_{DF}$, $P'_{BC} - P'_{DF}$) agree very closely to Whitcomb's values. The differential PKiKP - PcP times (Table 6.7) average 0.5 seconds faster than the data of Engdahl et al. (1974). If we accept the QM3 core velocities, this would imply a smaller inner core radius. However, since the PKP times for QM3 are significantly faster than observations, we cannot use this differential time to change our inner core radius.

The direct, surface focus S times and $dt/d\Delta$'s for model QM3 are contained in Table 6.8. In Figure 6.6 the S times are plotted as residuals relative to the Jeffreys-Bullen Tables. Model QM3 averages 2.8 seconds faster than the JB tables across the distance range of

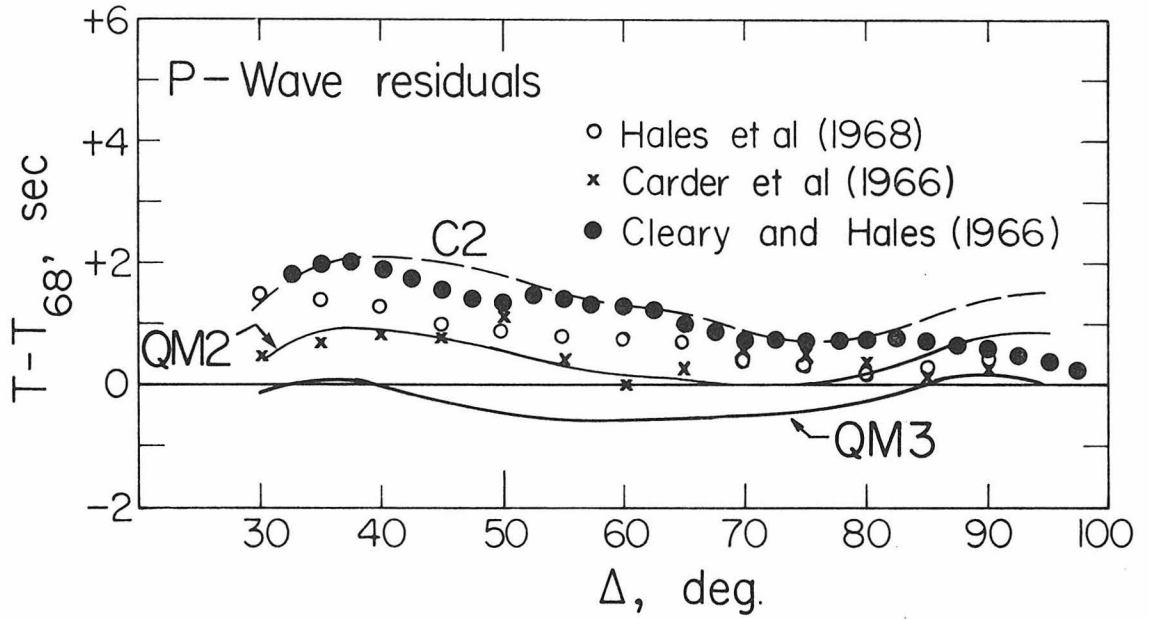


Figure 6.5 - Residual compressional wave travel times relative to the 1968 Tables (Herrin et al., 1968) for models C2, QM2, and QM3. Also shown are the data of Carder et al. (1966), Cleary and Hales (1966), and Hales et al. (1968).

TABLE 6.4

P Wave Travel Times and $dt/d\Delta$'s

Δ (deg)	Travel Time			δ_{68}	$dt/d\Delta$	
	J-B* (sec)	1968** (sec)	QM3 (sec)		Obs.*** (sec/deg)	QM3
30	372.5	369.5	369.4	0.1	8.97	8.94
35	416.1	413.3	413.4	0.0	8.64	8.62
40	458.1	455.7	455.6	0.1	8.30	8.28
45	498.9	496.4	496.1	0.3	7.98	7.91
50	538.0	535.2	534.8	0.4	7.53	7.53
55	575.4	572.2	571.6	0.6	7.21	7.21
60	610.7	607.4	606.8	0.6	6.85	6.87
65	644.0	640.9	640.5	0.5	6.60	6.56
70	675.5	672.7	672.2	0.5	6.19	6.18
75	705.0	702.6	702.1	0.5	5.81	5.81
80	732.7	730.6	730.3	0.3	5.43	5.45
85	758.5	756.6	756.6	0.0	4.97	5.07
90	782.7	780.7	781.0	-0.3	4.66	4.72
95	805.7	803.9	803.9	0.0	4.52	4.51

Average Difference 0.2

* Jeffreys and Bullen (1940)

** Herrin et al. (1968)

*** Average of Hales et al. (1968), Carder et al. (1966),
Johnson (1969), and Corbishley (1970).

TABLE 6.5

Surface Focus PcP and ScS

Δ (deg)	PcP				ScS		
	J-B [*] (sec)	68M ^{**} (sec)	QM3 (sec)	δ_{68}	J-B (sec)	QM3 (sec)	δ_{JB}
30	554.9	551.1	551.2	-0.1	1011.0	1007.4	3.6
35	568.6	564.9	565.0	-0.1	1036.4	1032.8	3.6
40	583.9	580.3	580.3	0.0	1064.6	1061.0	3.6
45	600.5	596.9	597.0	-0.1	1095.1	1091.8	3.3
50	618.3	614.8	614.8	0.0	1127.8	1124.8	3.0
55	637.0	633.7	633.7	0.0	1162.5	1159.6	2.9
60	656.6	653.3	653.4	-0.1	1198.8	1196.0	2.8
65	676.9	673.7	673.8	-0.1	1236.4	1233.7	2.7
70	697.8	694.7	694.7	0.0	1275.2	1272.5	2.7
75	719.1	716.1	716.1	0.0	1315.0	1312.2	2.8
80	740.6	737.8	737.8	0.0	1355.5	1352.4	3.1
85	762.3	759.7	759.8	-0.1	1396.5	1393.2	3.3
90	784.2	781.8	781.8	0.0	1437.8	1434.2	3.6
95					1479.2	1475.4	3.8

* Jeffreys and Bullen (1940)

** Engdahl and Johnson (1974)

TABLE 6.6

PcP-P Times (surface focus)

Δ (deg)	THJ (1)	68M (2)	C2	QM3	δ_{68}
30	181.9±0.4	181.6±0.6	181.3	181.8	-0.2
35	151.4±0.3	151.6±0.6	150.8	151.6	0.0
40	125.1±0.5	124.6±0.6	123.6	124.7	-0.1
45	100.7±0.4	100.5±0.6	99.7	100.9	-0.4
50	79.9±0.4	79.6±0.6	79.0	80.1	-0.5
55	62.3±1.0	61.5±0.6	61.2	62.1	-0.6
60	46.1±1.0	45.9±0.6	45.9	46.6	-0.7
65	33.0±1.0	32.8±0.6	32.9	33.4	-0.6
70	22.0±2.7	22.0±0.6	22.4	22.5	-0.5
75	13.4±2.1	13.5±0.6	14.1	14.0	-0.5
80		7.2±0.6	7.7	7.5	-0.3
85		3.1±0.6	3.4	3.2	-0.1
90		1.1±0.6	1.2	0.9	0.2

(1) Jordan (1972)

(2) Engdahl and Johnson (1974)

TABLE 6.7

PKiKP-PcP Times

Δ (deg)	EFM [*] (sec)	QM3 (sec)	δ (sec)
10.90	477.5	477.1	0.4
11.73	477.2	476.5	0.7
21.34	464.9	465.2	-0.3
26.64	457.4	456.6	0.8
27.71	454.8	454.7	0.1
29.69	451.2	450.4	0.8
30.50	450.4	449.4	1.0
30.60	449.5	449.1	0.4
31.08	448.2	448.3	-0.1
35.94	438.4	438.1	0.3
36.04	438.8	437.8	1.0
38.17	433.5	433.1	0.4
47.18	411.9	411.2	0.7

Average difference : 0.5

* : Engdahl et al. (1974)

TABLE 6.8

Shear Wave Travel Times

Δ (deg)	Time (sec)		QM3	dt/d Δ (sec/deg)	
	(1)	(2)		(2)	QM3
30	670.2	669.5	668.4	15.4	15.4
35	748.2	749.0	744.4	15.3	15.1
40	824.5	825.7	819.4	15.2	14.9
45	897.9	899.5	893.3	14.5	14.7
50	968.6	970.5	966.6	13.9	14.5
55	1036.8	1038.7	1034.9	13.4	13.4
60	1102.6	1104.1	1100.5	12.8	12.8
65	1165.5	1166.7	1162.9	12.2	12.2
70	1225.6	1226.4	1222.5	11.7	11.7
75	1282.6	1283.2	1279.8	11.1	11.2
80	1336.5	1337.3	1334.4	10.5	10.5
85	1387.3	1388.5	1384.9	10.0	9.7
90	1434.5	1436.9	1431.9	9.4	9.1
95	1478.2	1482.4	1475.4	8.8	8.3

(1) Jeffreys and Bullen (1940)

(2) Hales and Roberts (1970)

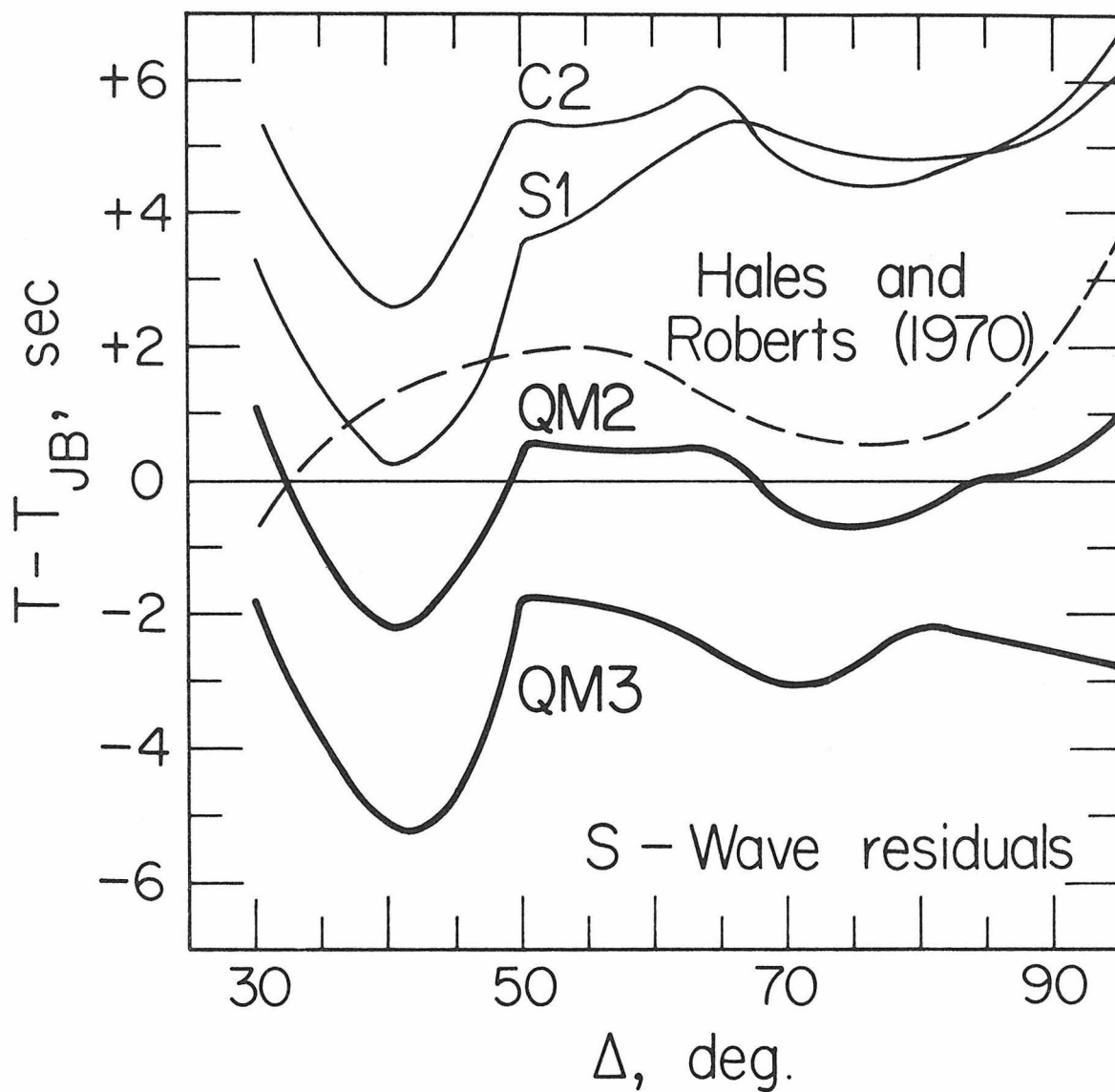


Figure 6.6 - Residual shear wave travel times relative to the Jeffreys-Bullen Tables (1940) for models S1, C2, QM2, and QM3. Also shown is the residual curve for the data of Hales and Roberts(1970).

30° - 90° . The general shape of the residual curve remains largely unchanged from the results reported in the earlier chapters except for distances beyond about 85° . At these longer distances, the residual curve begins to arc gently toward more negative values. This contrasts with the fairly sharp upward trend of previous studies. In light of the usual scatter in shear wave studies, a mean residual of less than 3 seconds is not inconsistent with the JB values. However this negative residual may result from a limitation of our attenuation correction. If the absorption band is not flat to periods at least as short as 1 second or if, as is almost unquestionably the case, the absorption band shifts in and out of the seismic band with changes in depth through the earth, our simple assumptions of Chapter 4 would lead to over-correction of the eigenperiods. A less likely possibility would be that the Q model used has average Q's which are too low.

The surface focus ScS times (Table 6.5) are 3.2 seconds faster than the JB values. This is consistent with the faster shear wave times mentioned above. The deep focus ScS - S times for QM3 are also fast compared with the Jordan and Anderson (1974) observed differential times. This is again consistent with the overall high shear velocity of model QM3.

6.5 Discussion of the normal mode data. An examination of Table 6.2 reveals some of the data problems associated with the inversion of free oscillations. Some of the observed eigenperiods seem clearly

to be in error. For example, ${}_0S_{10}$ has an observed (uncorrected) period of 580.06 seconds (Dziewonski and Gilbert, 1973), yet gross earth models which fit the adjacent fundamental spheroidal modes to almost zero error consistently fail to predict this period to within 2σ (0.12%).

A more serious difficulty arises in the simple choice of which individual observation of a particular mode to include in the data set. The normal mode data set currently being used was compiled by Gilbert and Dziewonski (1975). Those authors used as their data source their own study of the Columbian earthquake, their earlier study of the Alaskan earthquake (Dziewonski and Gilbert, 1973), Mendiguren's (1973) study of the Columbian earthquake, some data from Derr (1969) and effective toroidal overtone data from Brune and Gilbert (1974). But instead of at least combining all of these observations together and using a mean period, Gilbert and Dziewonski (1975) chose individual observations from different studies depending on which observation fit their model (1066A) best. Such a subjective, model-dependent data set should not come into general acceptance. The development of an objectively derived standard normal mode data set is currently in progress. The first step in this process is the collection of all reliable observations of the earth's free oscillations and combination, with appropriate weightings, of those observations to obtain mean observational periods. The second step involves smoothing those observations to eliminate obvious tears and inconsistent data points. For the toroidal modes, this smoothing

can be done along the standard overtone branches in the $w - \ell$ plane (Figure 6.7). The conventional spheroidal overtone branches in $w - \ell$ space (Figure 6.8) are badly distorted due to various mode interactions. The conventional branches are of little use for our present purpose. If the spheroidal modes are reorganized into physical overtone branches (i.e. - modes with similar physical properties are grouped together) as Okal (1977) has proposed, the correct branches for the smoothing operation can be determined. In Figures 6.9 and 6.10 we show two such reorganized mode branches, the vertical mode (almost purely compressional modes) branches and the Rayleigh-type mode branches respectively.

A third problem is related to the excitation of the various eigenperiods. It is important to consider the efficiency of excitation for many modes to determine which modes are actually observed when two or more theoretical peaks fall almost on top of one another and to avoid completely spurious identifications by picking random noise in the spectrum. In Appendix 2 we discuss the theoretical excitation of the normal mode data set by the Alaskan and Columbian earthquakes and show, in detail, the theoretical excitation spectra for the fundamental spheroidals and first thirty spheroidal overtones and for the fundamental toroidal modes and first seven toroidal overtones. The effect of Q on these spectra is shown as well. As an example of the third problem mentioned above, consider the identification in the Alaska earthquake spectra of the PKJKP-type mode ${}_{11}S_2$ (Dziewonski and Gilbert, 1973). Dziewonski and Gilbert "confirm" this identification

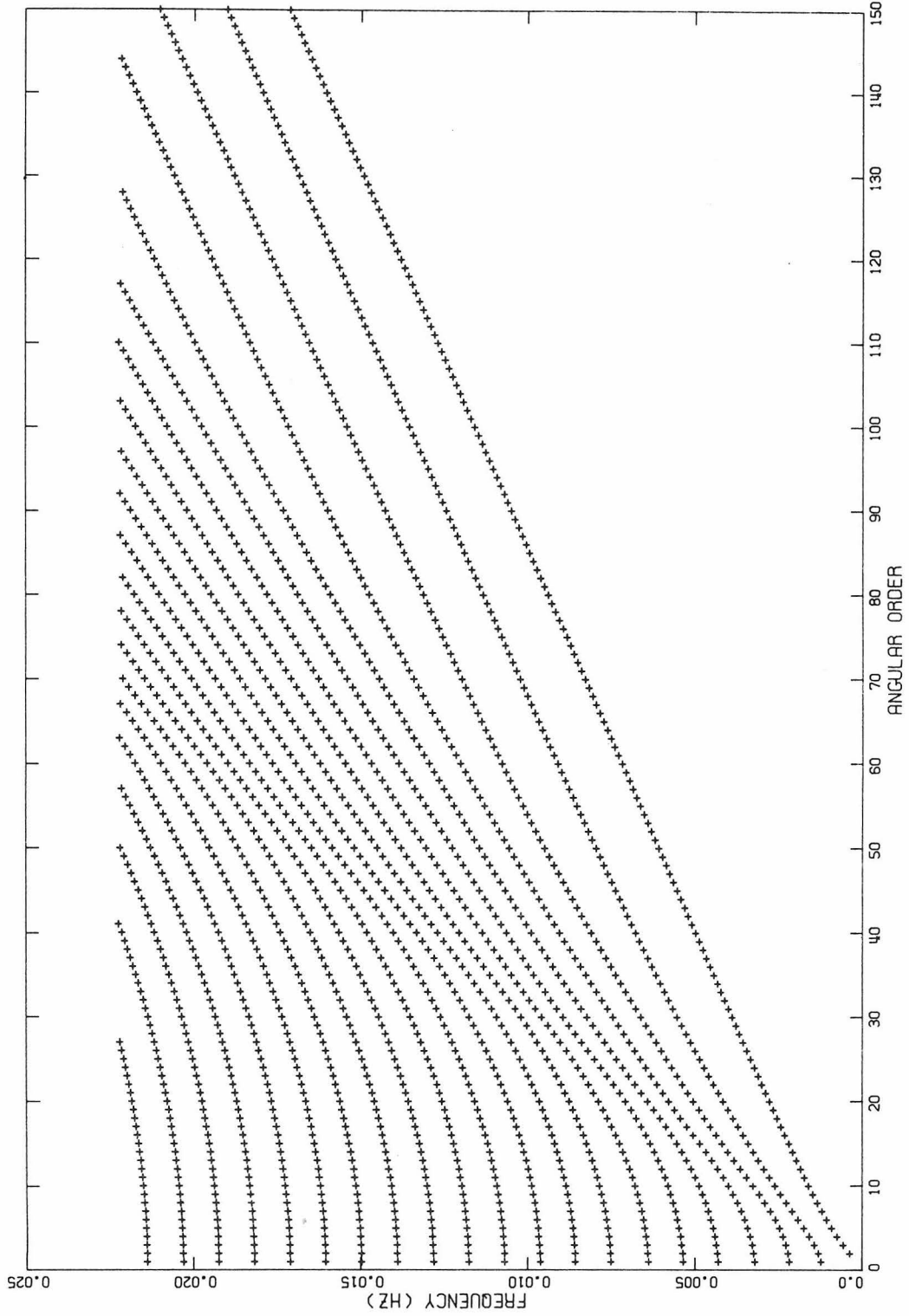


Figure 6.7 - The toroidal modes in (ω, l) space (frequencies correspond to model 1066A, Gilbert and Dziewonski, 1975).

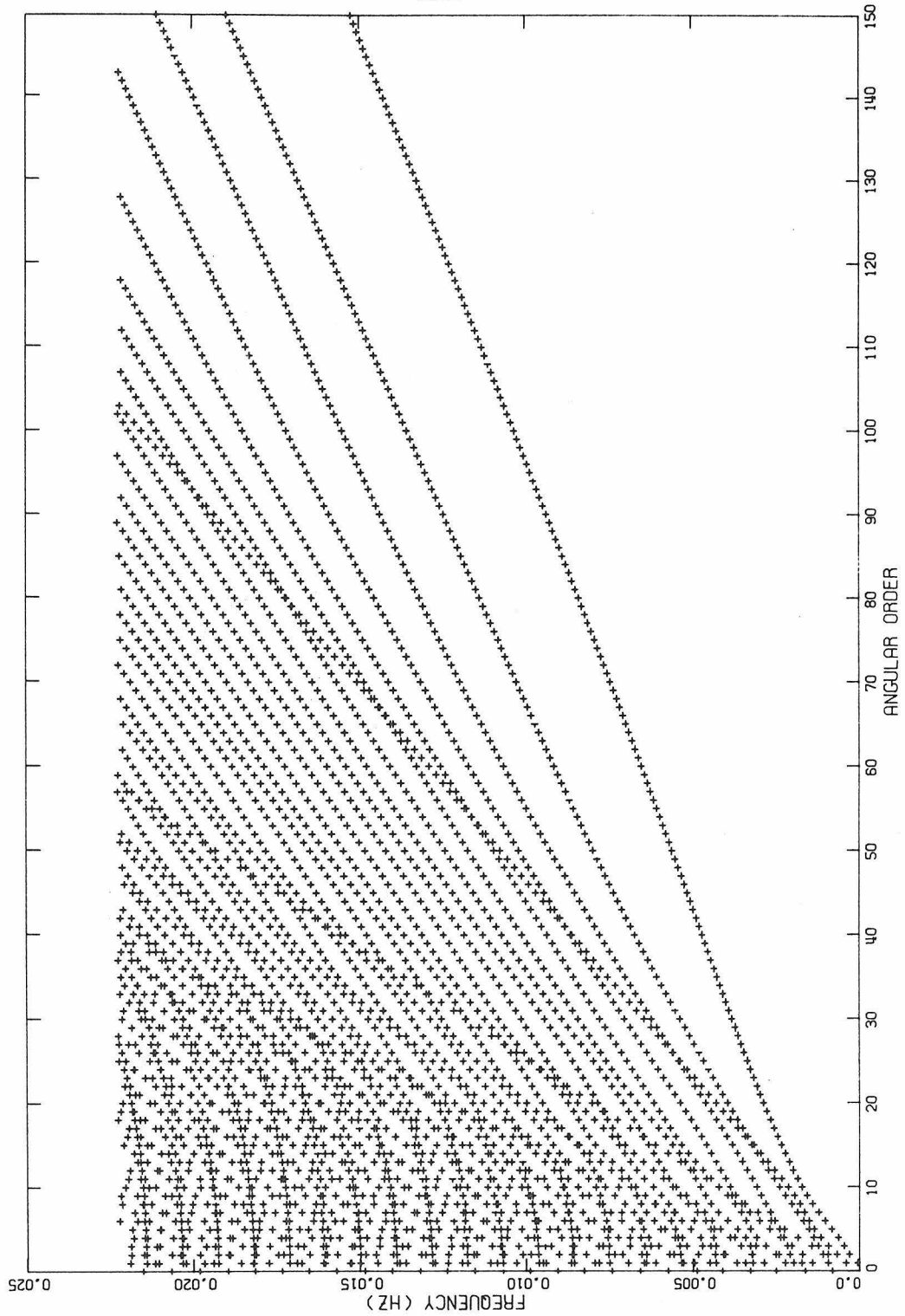


Figure 6.8 - The spheroidal modes in (ω, ℓ) space (frequencies correspond to model 1066A, Gilbert and Dziewonski, 1975).

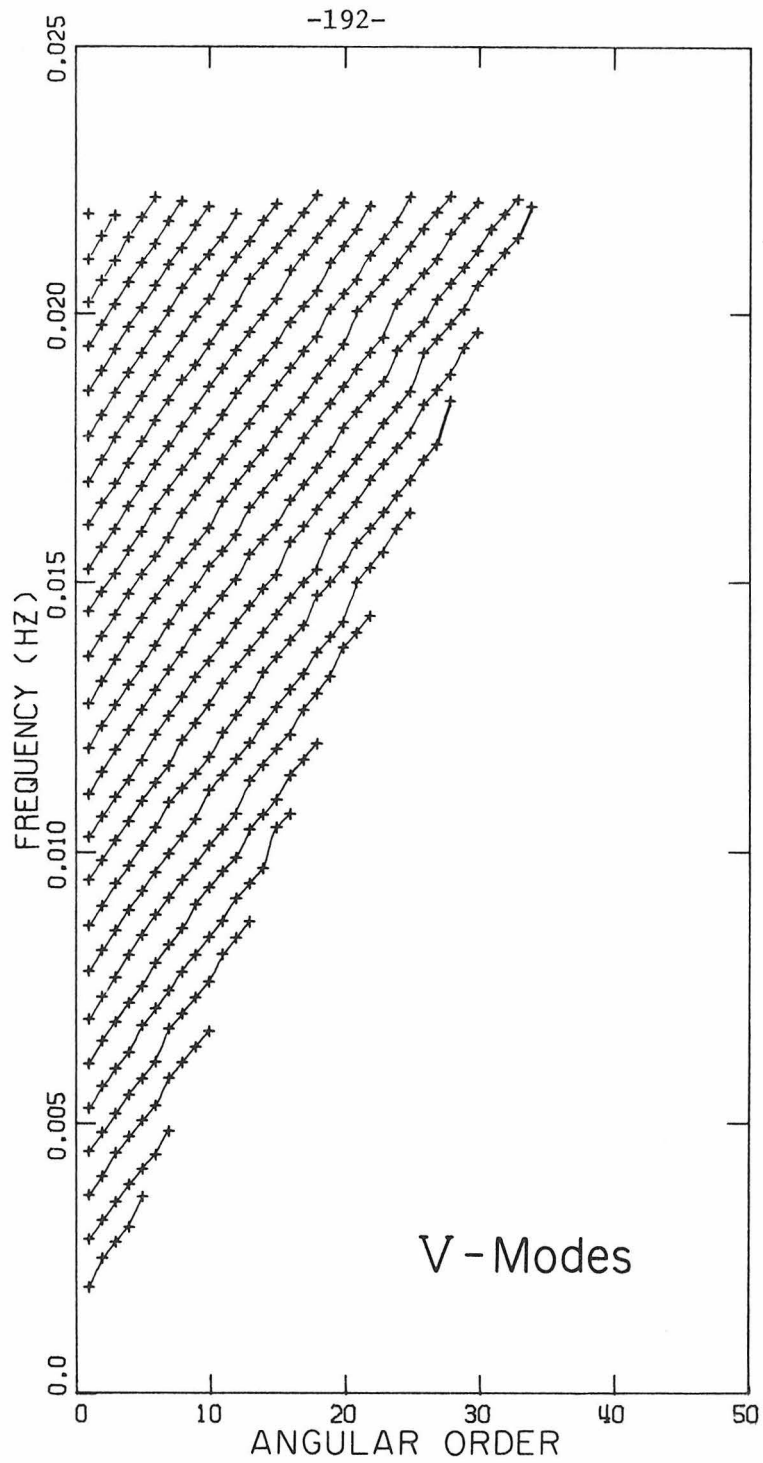


Figure 6.9 - The pure compressional spheroidal modes (V modes in the notation of Okal, 1977) in (ω, ℓ) space (frequencies correspond to model 1066A, Gilbert and Dziewonski, 1975).

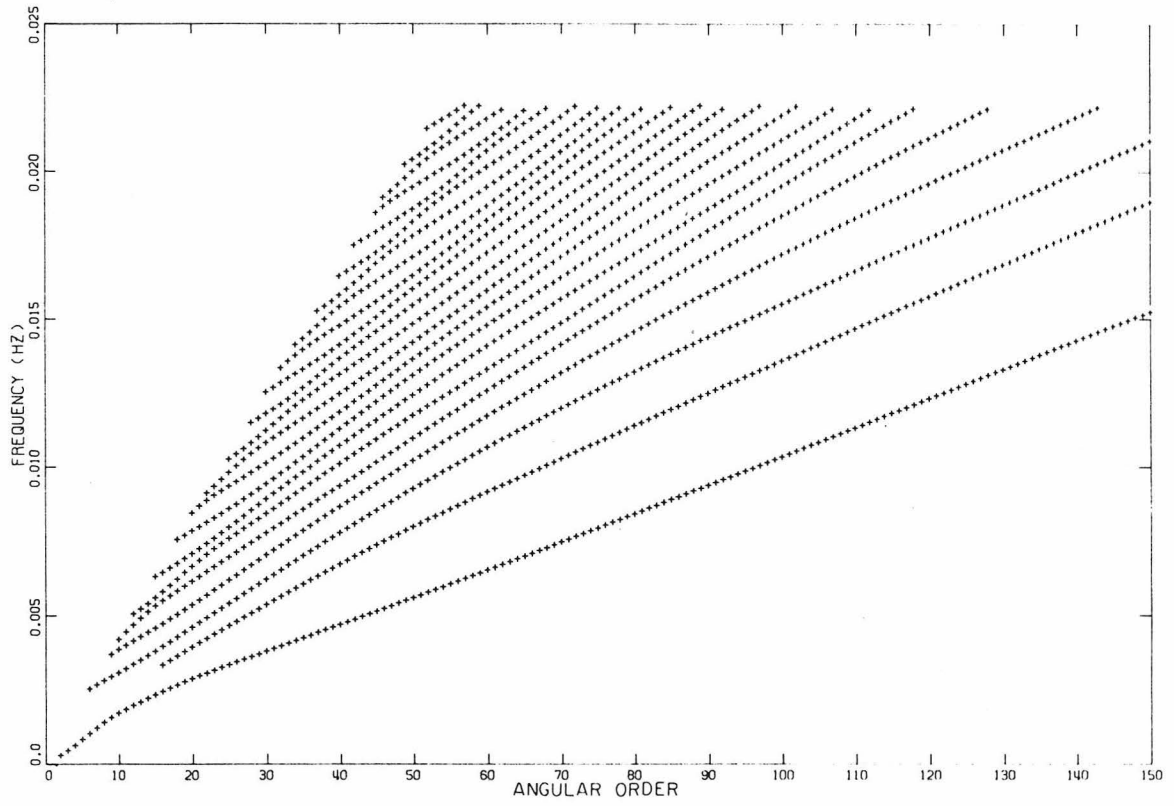


Figure 6.10 - The Rayleigh-type spheroidal modes (S modes in the notation of Okal, 1977) in (ω, ℓ) space (frequencies correspond to model 1066A, Gilbert and Dziewonski, 1975).

by claiming that "...the theoretical surface amplitude of $_{11}S_2$ is only 2.2 times less than that of $_{10}S_2$ (assuming that the total kinetic energies of these modes are equal)". The problem occurs because, as a trivial calculation shows, the kinetic energies are far from equal; indeed the amplitude of $_{11}S_2$ is actually at least 30 db less than $_{10}S_2$. More compelling evidence comes from consideration of the excitation of $_{0}S_{24}$. This mode, whose period is very close to that of $_{11}S_2$, was the best observed peak in the Dziewonski and Gilbert (1973) spectra having a signal to noise ratio of about 40 db. Relative to $_{0}S_{24}$, the excitation of $_{11}S_2$ is down by a factor of over 50 db. When the fact that the $_{0}S_{24}$ peak resulted from a stack of 44 spectra while only 11 spectra were used to obtain $_{11}S_2$, the theoretical amplitude of $_{11}S_2$ is an order of magnitude below the noise. A second example apparent in Appendix 2 is the mode identified in the Columbia spectra by Gilbert and Dziewonski (1975) as $_{26}S_1$. The theoretical amplitude for this mode is also far below the noise. The peak observed almost certainly is $_{27}S_1$ which has nearly the same period and is well excited.

In Appendix 1, it is concluded that assignment of an observed Q to the correct mode requires an excitation calculation. Using the line spectra in Appendix 2 we can quickly examine some of the alternate mode designations suggested in Appendix 1 and in Table 5.7. For example, in Table 5.7, we propose that $_{3}S_{16}$ be substituted for $_{1}S_{20}$ and $_{1}S_{25}$ be replaced by $_{5}S_{12}$. On the basis of excitation both substitutions would be acceptable alternatives. On the other hand

${}_3S_{32}$ is not excited and thus cannot be used in place of ${}_1S_{41}$. Of the 17 spheroidal modes named as possibly interfering with the observation of ${}_{25}S_5$, 15 have substantial excitation, indeed about a half are better excited than ${}_{25}S_5$, and only two, ${}_4S_{47}$ and ${}_{28}S_2$ are unobservable and thus can be excluded from contributing.

6.6 Summary. We have derived a model of the radial distribution of seismic Q in the earth and have constructed a gross earth velocity-density model QM3, which is compatible with that Q distribution as well as with a large set of high resolution body wave data. This earth model represents a more acceptable fit to the mode data and to the direct and differential travel time data than previous models. The QM3 upper mantle is also compatible with the most recent body wave studies. A most important result is the resolution of the travel time baseline problem and demonstration that the discrepancy was primary due to neglect of Q. Further, the entire model is smoother and simpler than model C2 and is a better overall fit to the data than C2. However, given the present status of our understanding of attenuation in the earth and the importance of attenuation on the earth model demonstrated here, it seems premature to undertake too detailed an analysis of the features of model QM3. The model, together with Q models SL1 and SL2, should serve as a useful basis for further investigations, both theoretical and observational, into seismic absorption in the earth. Only after the acquisition of large quantities of reliable Q data and the further development of an

understanding of the mechanisms of absorption throughout the varying thermodynamic conditions of the mantle will it be possible to substantially refine these models and to then examine the consequences of the physical parameters proposed.

BIBLIOGRAPHY

- Adams, R. D. Multiple inner core reflections from a Novaya Zemlya explosion, *Bull. Seism. Soc. Am.*, 62, 1063, 1972.
- Alsop, L. E., G. H. Sutton, and M. Ewing. Measurement of Q for very long period free oscillations, *J. Geophys. Res.*, 66, 2911, 1961.
- Anderson, D. L. Phase changes in the upper mantle, *Science*, 157, 1165, 1967a.
- Anderson, D. L. Latest information from seismic observations, in *The Earth's Mantle*, edited by T. F. Gaskell, Academic Press, N. Y., 1967b, p. 355.
- Anderson, D. L. The anelasticity of the mantle, *Geophys. J. R. astr. Soc.*, 14, 135, 1967c.
- Anderson, D. L., and C. B. Archambeau. The anelasticity of the earth, *J. Geophys. Res.*, 69, 2071, 1964.
- Anderson, D. L., A. Ben-Menahem, and C. B. Archambeau. Attenuation of seismic energy in the upper mantle, *J. Geophys. Res.*, 70, 505, 1965.
- Anderson, D. L., H. Kanamori, R. S. Hart, and H. P. Liu. The earth as a seismic absorption band, *Science*, (in press), 1977.
- Anderson, D. L. and R. L. Kovach. Attenuation in the mantle and rigidity of the core from multiple reflected core phases, *Proc. Nat. Acad. Sci.*, 51, 168, 1964.
- Anderson, D. L., and M. N. Toksoz. Surface waves on a spherical earth, 1, Upper mantle structure from Love waves, *J. Geophys. Res.*, 68, 3483, 1963.
- Backus, G., and F. Gilbert. Uniqueness in the inversion of inaccurate gross earth data, *Phil. Trans R. Soc. Lond. A.*, 266, 123, 1970.
- Benioff, H., F. Press, and S. Smith. Excitation of the free oscillations of the earth by earthquakes, *J. Geophys. Res.*, 66, 605, 1961.
- Ben-Menahem, A. Observed attenuation and Q values of seismic waves in the upper mantle, *J. Geophys. Res.*, 70, 4641, 1965.
- Ben-Menahem, A., M. Rosenman, and D. G. Harkrider. Fast evaluation of source parameters from isolated surface-wave signals, *Bull. Seism. Soc. Am.*, 60, 1337, 1970.

- Berzon, I. S., I. P. Passechnik, and A. M. Polikarpov. The determination of P-wave attenuation values in the Earth's mantle, *Geophys. J. R. astr. Soc.*, 39, 603, 1974.
- Best, W. J., L. R. Johnson, and T. V. McEvelly. ScS and the mantle beneath Hawaii, (abstract), *EOS, Trans. Amer. Geophys. Un.*, 56, 1147, 1974.
- Bolt, B. A., and D. R. Brillinger. Estimation of uncertainties in fundamental frequencies of decaying geophysical time series, (abstract), *EOS*, 56, 403, 1975.
- Bolt, B. A., and R. G. Currie. Maximum entropy estimates of earth torsional eigenperiods from 1960 Triote data, *Geophys. J. R. astr. Soc.*, 40, 107, 1975.
- Bolt, B. A., M. Niazi, and M. Sommerville. Diffracted ScS and the shear velocity at the core boundary, *Geophys. J. R. astr. Soc.*, 19, 299, 1970.
- Brune, J. N. Attenuation of dispersed wave trains, *Bull. Seism. Soc. Am.*, 52, 109, 1962.
- Brune, J. N., and F. Gilbert. Torsional overtone dispersion from correlations of S waves to SS waves, *Bull. Seism. Soc. Am.*, 64, 313, 1974.
- Buchbinder, G. G. A velocity structure of the earth's core, *Bull. Seism. Soc. Amer.*, 61, 429, 1971.
- Bullen, K. E. A suggested new "seismological" latitude, *Geophys. Suppl., Mon. Not. Roy. astron. Soc.*, 4, 158, 1937.
- Bullen, K. The Earth's Density, John Wiley and Sons, New York, 1975.
- Burdick, L. J., and D. L. Anderson. Interpretation of velocity profiles of the mantle, *J. Geophys. Res.*, 80, 1070, 1975.
- Burdick, L. J., and G. R. Mellman. Inversion of the body waves from the Borrego Mountain earthquake to the source mechanism, *Bull. Seism. Soc. Am.*, 66, 1485, 1976.
- Carder, D. S., D. W. Gordon, and J. N. Jordan. Analysis of surface foci travel times, *Bull. Seism. Soc. Am.*, 56, 815, 1966.
- Carpenter, E. W. Absorption of elastic waves—An operator for a constant Q mechanism, *AWRE Report No. 0-43/66*, 1966.
- Carpenter, E. W. A quantitative evaluation of teleseismic explosion records, *Proc. R. Soc. Lond. A.*, 290, 396, 1966.

- Carpenter, E. W. and D. Davies. Frequency dependent seismic phase velocities; an attempted reconciliation between the Jeffreys/Bullen and the Gutenberg models of the upper mantle, *Nature*, 212, 134, 1966.
- Carpenter, E. W. and E. A. Flinn. Attenuation of teleseismic body waves, *Nature*, 207, 745, 1965.
- Choudbury, M. A. and J. Dorel. Spectral ratio of short-period ScP and ScS phases in relation to the attenuation in the mantle beneath the Tasman Sea and Antarctic region, *J. Geophys. Res.*, 78, 462, 1973.
- Cleary, J. R., and A. L. Hales. An analysis of the travel times of P waves to North American stations in the distance range of 32° to 100° , *Bull. Seism. Soc. Am.*, 56, 467, 1966.
- Corbishley, D. J. Multiple array measurements of the P-wave travel-time derivative, *Geophys. J. R. astr. Soc.*, 19, 1, 1970.
- Davies, D. On the problem of compatibility of surface wave data, Q, and body wave travel times, *Geophys. J. R. astr. Soc.*, 13, 421, 1967.
- Davies, D., and B. R. Julian. A study of short period P-waves from Longshot, *Geophys. J. R. astr. Soc.*, 29, 185, 1972.
- Davies, D., and D. P. Mc Kenzie. Seismic travel times and plates, *Geophys. J. R. astr. Soc.*, 18, 51, 1969.
- Derr, J. S. Free oscillation observations through 1968, *Bull. Seism. Soc. Am.*, 59, 2079, 1969.
- Derr, J. S. Internal structure of the earth inferred from free oscillations, *J. Geophys. Res.*, 74, 5202, 1969.
- Doornbos, D. J. The anelasticity of the inner core, *Geophys. J. R. astr. Soc.*, 38, 397, 1974.
- Douglas, A., J. A. Hudson, P. D. Marshall, and J. B. Young. Earthquakes that look like explosions, *Geophys. J. R. astr. Soc.*, 36, 227, 1974.
- Doyle, H. A., and A. L. Hales. An analysis of the travel times of S waves to North American stations in the distance range 28° to 82° , *Bull. Seism. Soc. Am.*, 57, 761, 1967.
- Dratler, J., W. E. Farrell, B. Block, and F. Gilbert. High Q overtone modes of the earth, *Geophys. J. R. astr. Soc.*, 23, 399, 1971.

- Dziewonski, A. On regional differences in dispersion of mantle Rayleigh waves, *Geophys. J. R. astr. Soc.*, 22, 289, 1970.
- Dziewonski, A. and F. Gilbert. Observations of normal modes from 84 recordings of the Alaskan earthquake of 1964, March 28, *Geophys. J. R. astr. Soc.*, 27, 393, 1972.
- Dziewonski, A. and F. Gilbert. Observations of normal modes from 84 recordings of the Alaskan earthquake of 1964, March 28 -- II. Further remarks based on new spheroidal overtone data, *Geophys. J. R. astr. Soc.*, 35, 401, 1973.
- Dziewonski, A. M., and F. Gilbert. The effect of small, a spherical perturbations on travel-times and a re-examination of the corrections for ellipticity, *Geophys. J. R. astr. Soc.*, 44, 7, 1976.
- Dziewonski, A., A. L. Hales, and E. R. Lapwood. Parametrically simple earth models consistent with geophysical data, *Phys. Earth Planet. Int.*, 10, 12, 1975.
- Dziewonski, A., J. Mills, and S. Bloch. Residual dispersion measurement -- A new method of surface wave analysis, *Bull. Seism. Soc. Am.*, 62, 129, 1972.
- Engdahl, E. R. Seismic effects of the Milrow and Cannikin nuclear explosions, *Bull. Seism. Soc. Am.*, 60, 1427, 1970.
- Engdahl, E. R. and E. A. Flinn. Seismic waves reflected from discontinuities within the upper mantle, *Science*, 163, 177, 1974.
- Engdahl, E. R. and L. E. Johnson. Differential PcP travel-times and the radius of the core, *Geophys. J. R. astr. Soc.*, 39, 435, 1974.
- Engdahl, E. R., E. A. Flinn, and R. P. Masse. Differential PKiKP travel-times and the radius of the inner core, *Geophys. J. R. astr. Soc.*, 39, 457, 1974.
- Fairborn, J. W. Shear wave velocities in the lower mantle, *Bull. Seism. Soc. Am.*, 59, 1983, 1969.
- Frasier, C. W. and J. J. Filson. A direct measurement of the earth's short period attenuation along a teleseismic ray path, *J. Geophys. Res.*, 77, 3782, 1972.
- Futterman, W. I. Dispersive body waves, *J. Geophys. Res.*, 67, 5279, 1962.

- Gilbert, F. and A. Dziewonski. An application of normal mode theory to the retrieval of structural parameters and source mechanisms from seismic spectra, *Phil. Trans. R. Soc. Lond. A.*, 278, 187, 1975.
- Gogna, M. L. Travel times of S, PcP, and ScS from Pacific earthquakes, *Geophys. J. R. astr. Soc.*, 33, 103, 1973.
- Gutenberg, B. Attenuation of seismic waves in the earth's mantle, *Bull. Seism. Soc. Am.*, 48, 269, 1958.
- Hales, A. L. Eigenperiods of earth models and the determination of travel-time baselines, *J. Geophys. Res.*, 79, 422, 1974.
- Hales, A. L., J. R. Cleary, and J. L. Roberts. Velocity distributions in the lower mantle, *Bull. Seism. Soc. Am.*, 58, 1975, 1968.
- Hales, A. L. and J. L. Roberts. Shear velocities in the lower mantle and the radius of the core, *Bull. Seism. Soc. Am.*, 60, 1427, 1970.
- Hamilton, R. M. and J. H. Healy. Aftershocks of the Benham nuclear explosion, *Bull. Seism. Soc. Am.*, 59, 2271, 1969.
- Hart, R. S. and F. Press. S_n velocities and the composition of the lithosphere in the regionalized Atlantic, *J. Geophys. Res.*, 78, 407, 1973.
- Haskell, N. A. Analytic approximation for the elastic radiation from a contained underground explosion, *J. Geophys. Res.*, 72, 2582, 1967.
- HelMBERGER, D. V. On the structure of the low velocity zone, *Geophys. J. R. astr. Soc.*, 34, 251, 1973.
- HelMBERGER, D. V. and G. R. Engen. Upper mantle shear structure, *J. Geophys. Res.*, 79, 4017, 1974.
- HelMBERGER, D. V. and D. G. Harkrider. Seismic source descriptions of underground explosions and a depth discriminate, *Geophys. J. R. astr. Soc.*, 31, 45, 1972.
- HelMBERGER, D. V. and R. A. Wiggins. Upper mantle structure of middle-western United States, *J. Geophys. Res.*, 76, 3229, 1971.
- Herrin, E. (chairman). 1968 Seismological Tables for P phases, *Bull. Seism. Soc. Am.*, 58, 1193, 1968.
- Ibrahim, A. K., and O. Nuttli. Travel-time curves and upper mantle structure from long period S waves, *Bull. Seism. Soc. Am.*, 57, 1063, 1967.

- Jackson, D. D. Elastic relaxation model for seismic wave attenuation in the earth, *Phys. Earth Planet. Int.*, 2, 30, 1969.
- Jackson, D. D., and D. L. Anderson. Physical mechanisms of seismic-wave attenuation, *Rev. Geophys. Space Phys.*, 8, 1, 1970.
- James, D. E. Andean crustal and upper mantle structure, *J. Geophys. Res.*, 76, 3246, 1971.
- Jeffreys, H. The damping of S waves, *Nature*, 208, 675, 1965.
- Jeffreys, H., and Bullen, K. E. Seismological Tables, Brit. Assoc. Adv. of Sci., Gray-Milne Trust, London, 55pp, 1940.
- Jobert, N. and G. Rault. Periods and damping of free oscillations observed in France after sixteen earthquakes, *Geophys. J. R. astr. Soc.*, 45, 155, 1976.
- Johnson, L. R. Array measurements of P velocities in the upper mantle, *J. Geophys. Res.*, 72, 6309, 1967.
- Johnson, L. R. Array measurement of P velocities in the lower mantle, *Bull. Seism. Soc. Am.*, 59, 973, 1969.
- Jordan, T. H. Estimation of the radial variation of seismic velocities and density in the earth, Ph.D. thesis, Calif. Inst. of Tech., 1972.
- Jordan, T. H. Lateral heterogeneity and mantle dynamics, *Nature*, 257, 745, 1975.
- Jordan, T. H. and D. L. Anderson. Earth structure from free oscillations and travel-times, *Geophys. J. R. astr. Soc.*, 36, 411, 1974.
- Jordan, T. H. and J. Franklin. Optimal solutions to a linear inverse problem in geophysics, *Proc. Nat. Acad. Sci.*, 68, 291, 1971.
- Jordan, T. H. and W. S. Lynn. A velocity anomaly in the lower mantle, *J. Geophys. Res.*, 79, 2679, 1974.
- Jordan, T. H. and J. B. Minster. Applications of a stochastic inverse to the geophysical inverse problem, in The Mathematics of Profile Inversion, ed. L. Calin, Marcell Dekker Inc., New York, 1972.
- Jordan, T. H. and S. A. Sipkin. Estimation of the attenuation operator for multiple ScS waves, submitted to *Geophys. Res. Lett.*, 1977.

- Julian, B. R. and D. L. Anderson. Travel times, apparent velocities and amplitudes of body waves, Bull. Seism. Soc. Am., 58, 339, 1968.
- Kanamori, H. Attenuation of P waves in the upper and lower mantle, Bull. earthq. Res. Inst., 45, 299, 1967a.
- Kanamori, H. Spectrum of P and PcP in relation to the mantle-core boundary and attenuation in the mantle, J. Geophys. Res., 72, 559, 1967b.
- Kanamori, H. Spectrum of short-period core phases in relation to the attenuation in the mantle, J. Geophys. Res., 72, 2181, 1967c.
- Kanamori, H. Velocity and Q of mantle waves, Phys. Earth Planet. Int., 2, 259, 1970a.
- Kanamori, H. The Alaska earthquake of 1964: Radiation of long-period surface waves and source mechanism, J. Geophys. Res., 75, 5029, 1970b.
- Kanamori, H. and D. L. Anderson. Amplitude of the earth's free oscillations and long-period characteristics of the earthquake source, J. Geophys. Res., 80, 1075, 1975.
- Kanamori, H. and D. L. Anderson. Importance of physical dispersion in surface-wave and free-oscillation problems-Review, Rev. Geophys. Space Phys., 15, 105, 1977.
- Kanamori, H. and J. J. Cipar. Focal process of the great Chilean earthquake May 22, 1960, Phys. Earth Planet. Int., 9, 128, 1974.
- Knopoff, L. Q, Rev. Geophys., 2, 625, 1964.
- Knopoff, L., K. Aki, C. B. Archambeau, A. Ben-Menahem, and J. A. Hudson. Attenuation of dispersed waves, J. Geophys. Res., 69, 1655, 1964.
- Knopoff, L. and G. J. F. Mac Donald. Attenuation of small amplitude stress waves in solids, Rev. Mod. Phys., 30, 1178, 1958.
- Kogan, S. D. Travel times of longitudinal and transverse wave calculated from data on nuclear explosions made in the region of the Marshall Islands, Bull. Acad. Sci., USSR (Izvest.), Geophys. Series, 3, 246, 1960.
- Kolsky, H. The propagation of stress pulses in visco-elastic solids, Phil. Mag., 1, 693, 1956.

- Kosminskaya, I. P., N. N. Puzyrev, and A. S. Alekseyev. Explosion seismology: Its past, present, and future, *Tectonophysics*, 13, 309 1972.
- Kovach, R. L. and D. L. Anderson. Attenuation of shear waves in the upper and lower mantle, *Bull. Seism. Soc. Amer.*, 54, 1855, 1964.
- Kurita, T. Attenuation of short-period P waves and Q in the mantle, *J. Phys. Earth*, 16, 61, 1968.
- Kuster, G. T. Seismic wave propagation in two-phase media and its applications to the earth's interior, Ph.D. thesis, Massachusetts Institute of Technology, 1972.
- Liu, H.-P., D. L. Anderson, and H. Kanamori. Velocity dispersion due to anelasticity; Implications for seismology and mantle composition, *Geophys. J. R. astr. Soc.*, 47, 41, 1976.
- Liu, H.-P. and C. B. Archambeau. The effect of anelasticity on periods of the Earth's free oscillations (toroidal modes), *Geophys. J. R. astr. Soc.*, 43, 795, 1975.
- Liu, H.-P. and C. B. Archambeau. Correction to 'The effect of anelasticity on periods of the Earth's free oscillations (toroidal modes)', *Geophys. J. R. astr. Soc.*, 47, 1, 1976.
- Lomnitz, C. Linear dissipation in solids, *J. Appl. Phys.*, 28, 201, 1957.
- Mendiguren, J. A. Identification of the free oscillation spectra peaks for 1970 July 31, Columbian deep shock using the excitation criterion, *Geophys. J. R. astr. Soc.*, 33, 281, 1973.
- Mikumo, T. and T. Kurita. Q distribution for long-period P waves in the mantle, *J. Phys. Earth*, 16, 11, 1968.
- Mills, J. M. and A. L. Hales. Great circle Rayleigh wave attenuation and group velocity, Part I: Observations for periods between 150 and 600 seconds for 7 great circle paths, *Phys. Earth Planet Int.* (in press), 1977.
- Mitchell, B. J. and D. V. Helmberger. Shear velocities at the base of the mantle from observations of S and ScS, *J. Geophys. Res.*, 78, 6009, 1973.
- Molnar, P. and J. Oliver. Lateral variations of attenuation in the upper mantle and discontinuities in the lithosphere, *J. Geophys. Res.*, 74, 2648, 1969.

- Müller, G. Amplitude studies of core phases, *J. Geophys. Res.*, 78, 3469, 1973.
- McGinley, J. R. and D. L. Anderson. Relative amplitudes of P and S waves as a mantle reconnaissance tool, *Bull. Seism. Soc. Am.*, 59, 1189, 1969.
- Ness, N. F., J. C. Harrison, and L. B. Slichter. Observations of the free oscillations of the earth, *J. Geophys. Res.*, 66, 621, 1961.
- Niazi, M. SH travel times and lateral heterogeneities in the lower mantle, *Bull. Seism. Soc. Am.*, 63, 2035, 1973.
- Niazi, M. and D. L. Anderson. Upper mantle structure of western North America from apparent velocities of P waves, *J. Geophys. Res.*, 70, 4633, 1965.
- Nowick, A. S. and B. S. Berry. Lognormal distribution function for describing anelastic and toher relaxation processes, part 1 and part 2, *IBM Journal*, October, 1961, 297, 1961.
- Nowroozi, A. A. Measurement of Q values from the free oscillations of the earth, *J. Geophys. Res.*, 73, 1407, 1968.
- Nowroozi, A. A. Characteristic periods of fundamental and overtone oscillations of the Earth following a deep-focus earthquake, *Bull. Seism. Soc. Am.*, 62, 247, 1972.
- Nowroozi, A. A. Characteristic periods and Q for oscillations of the Earth following an intermediate-focus earthquake, *J. Phys. Earth*, 22, 1, 1974.
- Nuttli, O. W. Travel times and amplitudes of S waves from nuclear explosions in Nevada, *Bull. Seism. Soc. Am.*, 59, 385, 1969.
- Okal, E. A. A physical classification of the Earth's spheroidal modes, submitted to *Geophys. J. R. astr. Soc.*, 1977.
- Otsuka, M. On the forms of the S and ScS waves of some deep earthquakes (In Japanese), *Zisin*, (2)15, 169, 1962.
- Otsuka, M. Some considerations on the waveforms of ScS phases, *Spec. Contrib. Geophys. Inst., Kyoto Univ.*, 2, 415, 1963.
- Press, F. Rigidity of the earth's core, *Science*, 124, 1204, 1956.
- Qamar, A. and A. Eisenberg. The damping of core waves, *J. Geophys. Res.*, 79, 758, 1974.

- Randall, M. J. Attenuative dispersion and frequency shifts of the earth's free oscillations, *Phys. Earth Planet. Int.*, 12, 1, 1976.
- Robinson, R. and R. L. Kovach. Shear wave velocities in the earth's mantle, *Phys. Earth Planet. Int.*, 5, 30, 1971.
- Sacks, I. S. Anelasticity of the outer core, *Annu. Rep. Dir. Dep. Terr. Magn.*, 1969-1970, Carnegie Inst., Washington, D.C., 414, 1971a.
- Sacks, I. S. Anelasticity of the inner core, *Annu. Rep. Dir. Dep. Terr. Magn.*, 1969-1970, Carnegie Inst., Washington, D.C., 416, 1971b.
- Sacks, I. S. Q structure of the inner and outer core (abstract), *EOS Trans. AGU*, 53, 601, 1972.
- Sacks, I. S. and J. A. Snoke. Heterogeneous structure at the base of the mantle, 2: observations and interpretations (abstract), paper presented at the 11th International Symposium on Mathematical Geophysics, Seeheim, W. Germany, 1976.
- Sailor, R. V. and A. Dziewonski. Attenuation of shear energy in the mantle from normal mode analysis, *Lincoln Lab. Semi-Annual Technical Report on Seismic Discrimination*, 23, 1976.
- Saito, M. Excitation of free oscillations and surface waves by a point source in a vertically heterogeneous earth, *J. Geophys. Res.*, 72, 3689, 1967.
- Sato, R. and A. F. Espinosa. Dissipation in the earth's mantle and rigidity and viscosity in the earth's core determined from waves multiply reflected from the mantle core boundary, *Bull. Seism. Soc. Amer.*, 57, 829, 1967.
- Savage, J. C. Attenuation of elastic waves in granular mediums, *J. Geophys. Res.*, 70, 3935, 1965.
- Sima, H. On the attenuation of SS and SSS waves, (In Japanese), *Quart. Journ. Seism.*, 29, 109, 1965.
- Simpson, D. W. P wave velocity structure of the upper mantle in the Australian region, Ph.D. thesis, Aus. Nat. Univ., Canberra, 1973.
- Sipkin, S. A. and T. H. Jordan. Lateral heterogeneity of the upper mantle determined from the travel times of multiple ScS, *J. Geophys. Res.*, 80, 1474, 1975.

- Slichter, L. B. Spherical oscillations of the earth, *Geophys. J. R. astr. Soc.*, 14, 171, 1967.
- Smith, S. W. An investigation of the earth's free oscillations, Ph.D. thesis, Calif. Inst. Tech., Pasadena, Calif., 1961.
- Smith, S. W. Free oscillations excited by the Alaskan earthquakes, *J. Geophys. Res.*, 71, 1183, 1966.
- Smith, S. W. The anelasticity of the mantle, *Tectonophysics*, 13, 601, 1972.
- Solomon, S. C. and M. N. Töksoz. Lateral variation of attenuation of P and S waves beneath the United States, *Bull. Seism. Soc. Am.*, 60, 819, 1970.
- Stacey, F. D. *Physics of the Earth*, John Wiley and Sons, Inc., New York, p. 25, 1969.
- Stauder, W. Smaller aftershocks of the Benham nuclear explosion, *Bull. Seism. Soc. Am.*, 61, 417, 1971.
- Stein, S. and R. J. Geller. Time domain analysis and synthesis of rotationally split spheroidal and toroidal modes: Preliminary results, submitted to *Geophys. Res. Lett.*, 1977.
- Steinhart, J. S., T. J. Smith, I. S. Sacks, R. Sumner, Z. Suzuki, A. Rodriguez, C. Lomnitz, M. A. Tuve, and L. T. Aldrich. *Explosion seismology*, Year Book 62, Carnegie Institute of Washington, D. C., p. 286, 1964.
- Strick, E. The determination of Q, dynamic viscosity, and transient creep curves from wave propagation measurements, *Geophys. J. R. astr. Soc.*, 13, 197, 1967.
- Sutton, G. H. and D. A. Walker. Oceanic mantle phases recorded on seismographs in the Northwestern Pacific at distances between 7° and 40° , *Bull. Seism. Soc. Am.*, 62, 631, 1972.
- Teng, T. L. Attenuation of body waves and the Q structure of the mantle, *J. Geophys. Res.*, 73, 2195, 1968.
- Tsai, Y. B. and K. Aki. Simultaneous determination of the seismic moment and attenuation of seismic surface waves, *Bull. Seism. Soc. Am.*, 59, 275, 1969.
- Walker, D. A. High-frequency P_n and S_n phases recorded in the western Pacific, submitted to *J. Geophys. Res.*, 1976.

- Walker, D. A. and G. H. Sutton. Oceanic mantle phases recorded on hydrophones in the Northwestern Pacific at distances between 9° and 40° , Bull. Seism. Soc. Am., 61, 65, 1971.
- Whitcomb, J. H. A study of the velocity structure of the earth by the use of core phases, Part 1, Ph.D. thesis, Calif. Inst. of Tech., Pasadena, 1973.
- Whitcomb, J. H. and D. L. Anderson. Reflection of P'P'(PKPPKP) seismic waves from discontinuities in the mantle, J. Geophys. Res., 75, 5713, 1970.
- Yoshida, M. and M. Tsujiura. Spectrum and attenuation of multiply reflected core phases, J. Phys. Earth, 23, 31, 1975.
- Zener, C. Elasticity and Anelasticity of Metals, Univ. of Chicago Press, Chicago, 1948.
- Zharkov, V. N., L. N. Dorofeyeva, V. M. Dorofeyeva, and V. M. Lyubinov. Model distributions of the dissipation function $Q(\ell)$ in the mantle of the earth, Izv., Earth Phys., No. 12, 783, 1974.

APPENDICES

Appendix 1

A1.1 Discussion of Mode Q's. It is difficult to determine the Q in either the frequency or time domain if there are several or many modes with nearly the same period. For example, Dratler et al. (1971) determined a Q of about 400 for a mode having a period of 273.68 seconds which he designated ${}_3S_2$. Modes having similar periods are ${}_1S_{18}$, ${}_2S_{17}$, ${}_3S_{14}$, ${}_7S_5$, and ${}_{11}S_1$. The theoretical Q's of these modes range from 896 (${}_{11}S_1$) and 697 (${}_7S_5$) to 168 (${}_1S_{18}$) and 282 (${}_3S_{14}$). In general, the lower overtones are more efficiently excited by seismic sources but some of the higher overtones persist longer because of their higher Q. It is likely therefore that an intermediate Q will be determined by conventional techniques of determining Q.

Similarly the value for Q of 574-696 of the mode designated as ${}_{10}S_1$ (${}_{13}S_1$ in the system of Gilbert and Dziewonski, 1975) of a period of 222.80 sec is possibly contaminated by ${}_{10}S_5$, ${}_{11}S_3$ and ${}_{13}S_1$ which have similar periods and Q's ranging from 293 to 934.

Similarly, the Sailor and Dziewonski (1976) observation for a mode of period 209.6 sec, designated ${}_{11}S_4$, has competitors of nearby period (${}_3S_{21}$, ${}_4S_{16}$, ${}_7S_{10}$). The theoretical Q for ${}_{11}S_4$ is about 1100 and the other modes have theoretical Q's ranging from 220 to 320. The composite Q of the interfering modes should therefore lie between 220 and 1100, as observed.

An extreme example is represented by the mode designated ${}_{25}S_5$ by Sailor and Dziewonski (1976) with a period of 98.65 sec and a Q of 791.

There are 17 spheroidal modes within 0.5 seconds of this period with theoretical Q's ranging from 977 to 122. Virtually every overtone is represented [0^S_{98} , 1^S_{69} , 4^S_{47} , 5^S_{45} , 6^S_{40} , 7^S_{37} , 8^S_{34} , 9^S_{30} , 12^S_{24} , 16^S_{16} , 18^S_{13} , 20^S_{11} , 20^S_{12} , 21^S_{20} , 25^S_5 , and 28^S_2]. The more easily excited lower modes with Q's of 120-300 will quickly decay into the background but the lesser excited higher modes with Q's of 350-1100 will keep the level high at this period and intermediate to high Q levels will be reported for this period range.

It is clear, therefore, that detailed studies of Q must include an excitation calculation so that the observed decay of energy in a given frequency band can be assigned to the appropriate mode.

Appendix 2

Knowledge of the relative excitation of the free oscillations of the earth for a particular earthquake source can be an invaluable aid in the identification of spectral peaks and in the assignment of measured Q to the proper mode. The excitation of free oscillations may be computed using the expressions derived by Kanamori and Cipar (1974). These expressions, which we summarize below, are modifications of the formulation of Saito (1967) using the fault representation of Ben-Menahem et al. (1970). The source is assumed to be a point double-couple with a step time function.

The transverse component of displacement, in spherical coordinates (r, θ, ϕ) , for a toroidal oscillation of order ℓ can be given by

$$U_{\phi}(r, t) = y_1(r) \cos(\omega_{\ell} t) \left(-L_1 q_L \frac{dP_{\ell}^1}{d\theta} + L_2 p_L \frac{dP_{\ell}^2}{d\theta} \right) \quad (\text{A2.1})$$

where y_1 is the radial displacement factor; t is time measured from the source origin time; ω_{ℓ} is the angular frequency; P_{ℓ}^n is the associated Legendre function; L_1 and L_2 are the excitation functions of Kanamori and Cipar (1974); and q_L and p_L are the source geometry terms given by

$$\begin{aligned} q_L &= -\cos(\lambda) \cos(\delta) \sin(\phi) + \sin(\lambda) \cos(2\delta) \cos(\phi) \\ p_L &= \sin(\lambda) \sin(\delta) \cos(\delta) \sin(2\phi) + \cos(\lambda) \sin(\delta) \cos(2\phi) \end{aligned} \quad (\text{A2.2})$$

Here λ and δ are the slip angle and the dip angle of the fault and ϕ is the station azimuth.

For spheroidal oscillations, the vertical displacement for the ℓ^{th} mode can be given by

$$U_r(r,t) = y_1(r) \cos(\omega_\ell t) (K_0 s_R P_\ell^0 - K_1 q_R P_\ell^1 + K_2 p_R P_\ell^2) \quad (\text{A2.3})$$

where K_0 , K_1 , and K_2 are the spheroidal excitation functions (Kanamori and Cipar, 1974) and the source geometry terms, s_R , p_R , q_R , are given by

$$\begin{aligned} s_R &= \sin(\lambda)\sin(\delta)\cos(\delta) \\ q_R &= \sin(\lambda)\cos(2\delta)\sin(\phi) + \cos(\lambda)\cos(\delta)\cos(\phi) \\ p_R &= \cos(\lambda)\sin(\delta)\sin(2\phi) - \sin(\lambda)\cos(\delta)\sin(\delta)\cos(2\phi) \end{aligned} \quad (\text{A2.4})$$

Similarly, the radial displacement for spheroidal oscillations is given by

$$U_\theta(r,t) = y_3(r) \cos(\omega_\ell t) (K_0 s_R \frac{dP_\ell^0}{d\theta} - K_1 q_R \frac{dP_\ell^1}{d\theta} + K_2 p_R \frac{dP_\ell^2}{d\theta}) \quad (\text{A2.5})$$

where y_3 is the radial stress factor.

In order to examine the efficiency of excitation for a particular source over the entire suite of modes, without the influence of station location dependence, it is necessary to remove the θ and ϕ dependencies from equations A2.1, A2.3, and A2.5 through application of a suitable set of assumptions. The first such approximation is the replacement of the Legendre functions by their asymptotic expansions:

$$P_{\ell}^n \approx \exp(n\pi i) \ell^n \sqrt{\frac{2}{\ell \pi \sin(\theta)}} \cos\left[(\ell + 1/2)\theta + \frac{n\pi}{2} - \frac{\pi}{4}\right] \quad (\text{A2.6})$$

The station distance and azimuth terms may now be eliminated by arbitrarily setting all sine and cosine terms involving θ and ϕ to unity. While this is, strictly speaking, an impossibility, since we are only interested in order of magnitude comparisons, this procedure yields an adequate approximation to the maximum excitation. The Legendre functions can thus be replaced as follows

$$\begin{aligned} P_{\ell}^0 &\rightarrow 1/\sqrt{\ell} ; P_{\ell}^1 \rightarrow \sqrt{\ell} ; P_{\ell}^2 \rightarrow \ell\sqrt{\ell} \\ \frac{dP_{\ell}^0}{d\theta} &\rightarrow (\ell+1/2)/\sqrt{\ell} ; \frac{dP_{\ell}^1}{d\theta} \rightarrow (\ell+1/2)\sqrt{\ell} ; \frac{dP_{\ell}^2}{d\theta} \rightarrow (\ell+1/2)\sqrt{\ell} \end{aligned} \quad (\text{A2.7})$$

The effect of attenuation can be easily included for a window beginning at time t_0 (after the origin time) and continuing until $t_0 + \tau$ by multiplying the amplitudes by the factor

$$\frac{[1 - \exp(-\pi\tau/Q_i T_i)] \exp(-\pi t_0/Q_i T_i)}{\pi\tau/Q_i T_i} \quad (\text{A2.8})$$

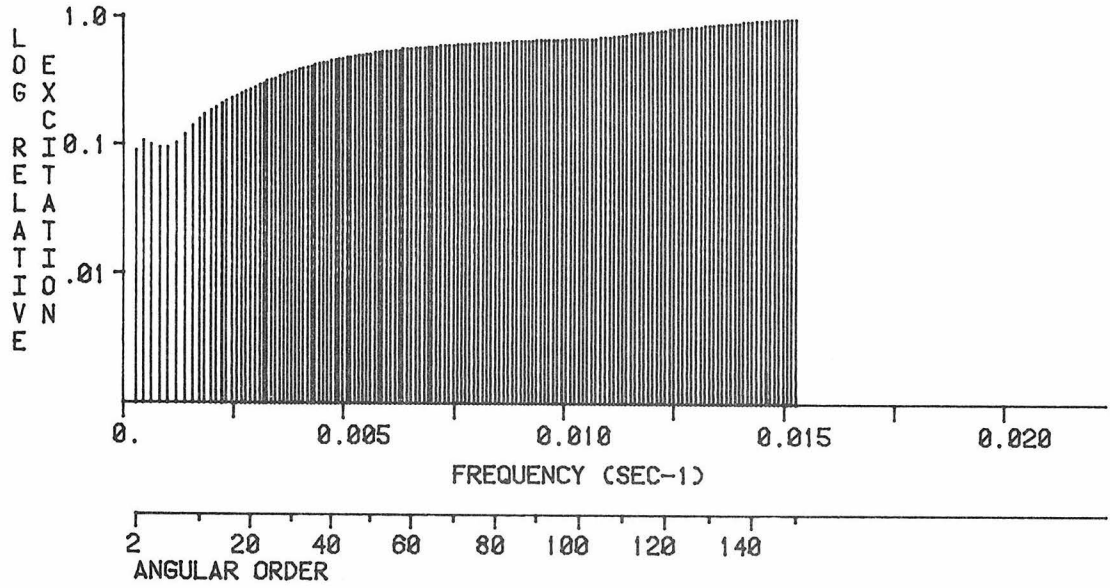
for each mode i .

We have used the above expressions to compute the relative excitation spectra for the 1964 Alaska earthquake (using the source function of Kanamori, 1970b) and the 1970 deep Columbia earthquake (using the source solution of Mendiguren, 1973). Most of the presently available normal mode data are derived from these two events.

In Figure A2.1 (31 pages), we present the raw excitation, without attenuation, for the Alaska earthquake. In Figure A2.2 (again 31 pages), the same spectra are plotted with attenuation (computed for model SL2) included. The toroidal modes, without attenuation, are shown in Figure A2.3 (4 pages). In Figures A2.4, A2.5, and A2.6, we show the corresponding excitation spectra for the Columbia earthquake. In all cases the excitations are normalized to the maximum excitation of the fundamental mode branch.

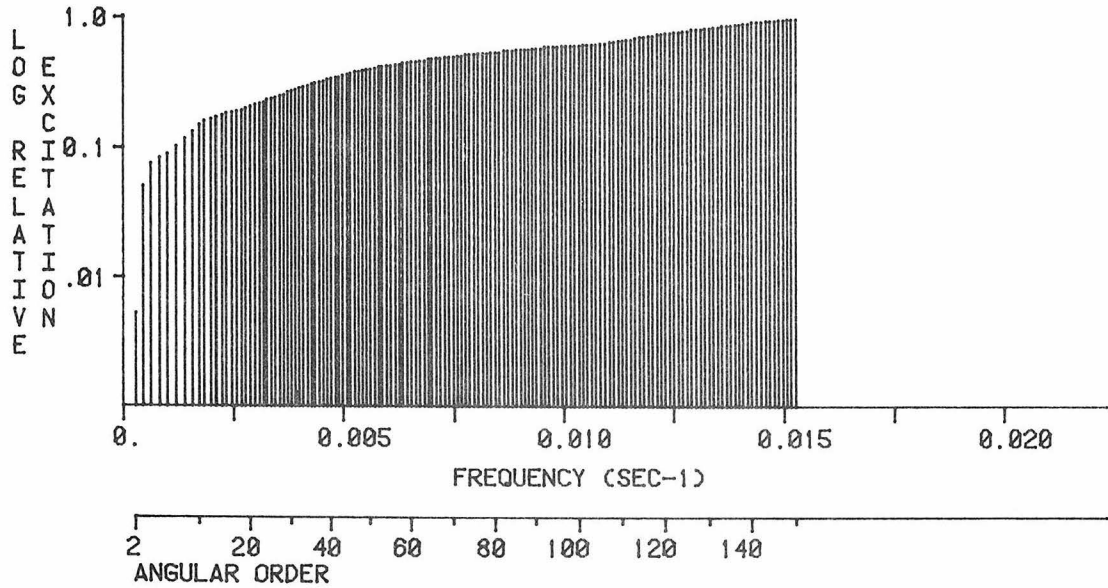
Figure A2.1 - The excitation spectra for the fundamental spheroidal branch and first thirty spheroidal overtone branches generated by the 1964 Alaska earthquake. Both the vertical and the radial components of displacement are shown. All excitations are normalized to the maximum fundamental mode excitation on the appropriate component. Modes with an excitation level more than 60 db below the maximum fundamental mode excitation are plotted as small negative tick marks along the horizontal axis. This figure extends over the following 31 pages.

VERTICAL COMPONENT; RADIAL ORDER 0



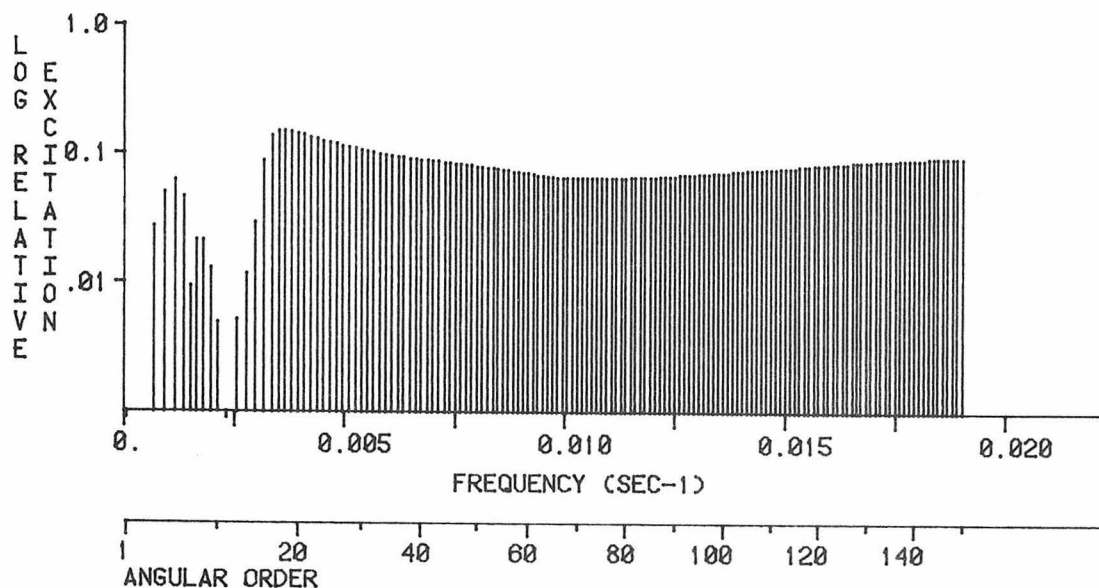
MAXIMUM EXCITATION = 0.160270E -2 CM-SEC ; (0 S 150; T= 65.58 SEC)

RADIAL COMPONENT; RADIAL ORDER 0



MAXIMUM EXCITATION = 0.147346E -2 CM-SEC ; (0 S 150; T= 65.58 SEC)

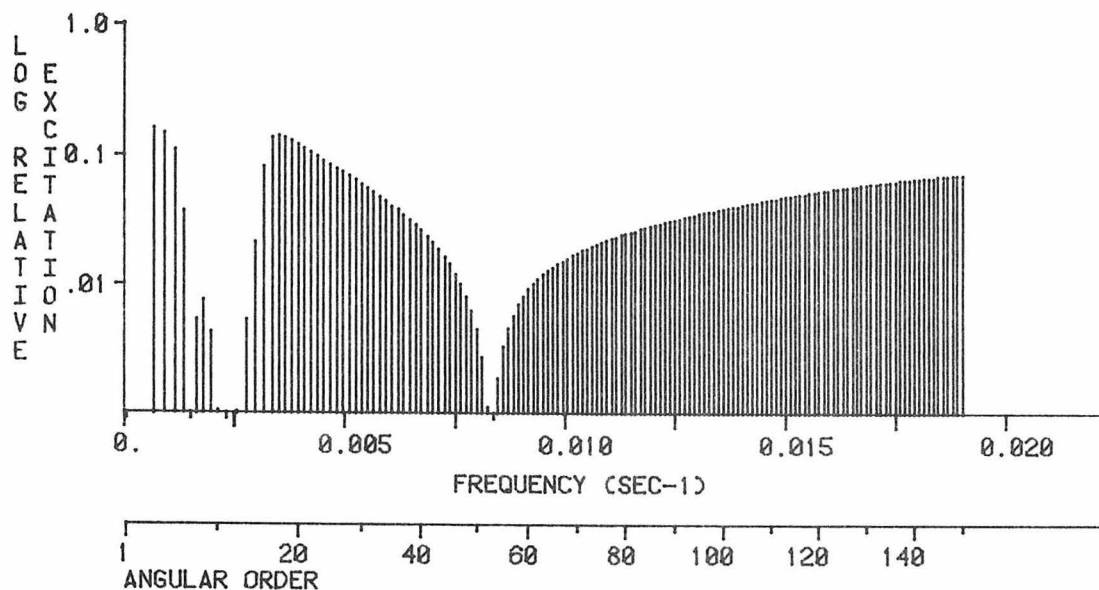
VERTICAL COMPONENT; RADIAL ORDER 1



MAXIMUM EXCITATION = 0.237874E -3 CM-SEC ; (I S 18; T= 274.23 SEC)

EXCITATION NORMALIZED TO 0 S 150 (VERT. COMP.) ; 0.16027000E -2

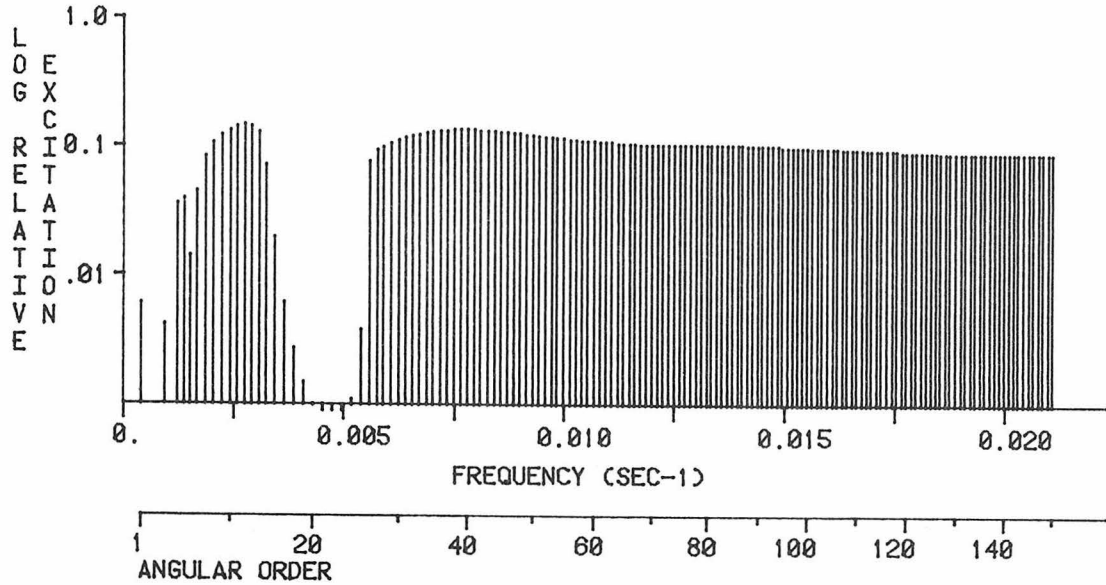
RADIAL COMPONENT; RADIAL ORDER 1



MAXIMUM EXCITATION = 0.235031E -3 CM-SEC ; (I S 2; T=1469.85 SEC)

EXCITATION NORMALIZED TO 0 S 150 (RAD. COMP.) ; 0.14734600E -2

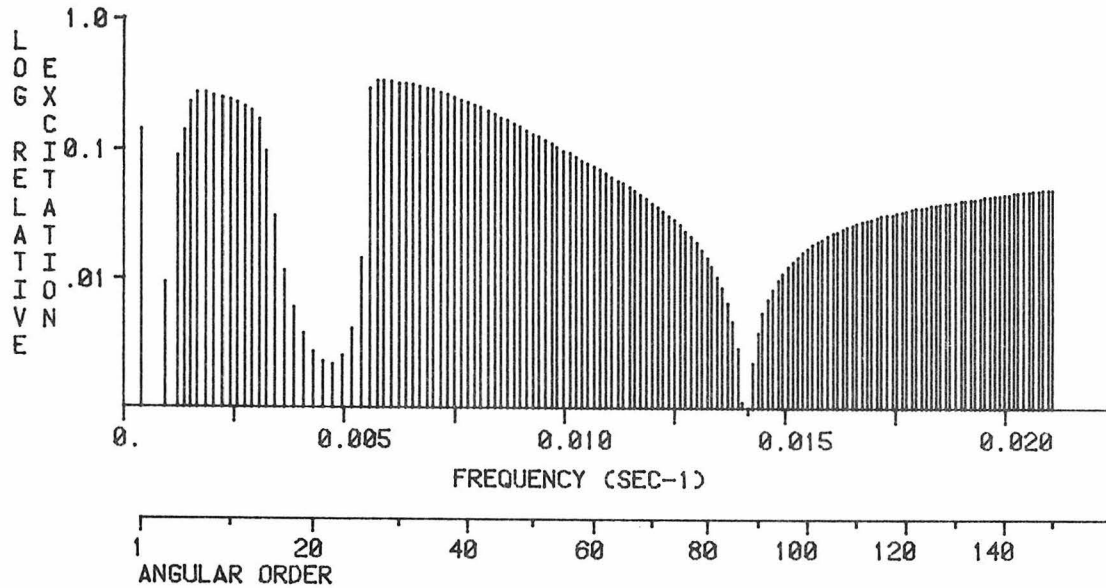
VERTICAL COMPONENT; RADIAL ORDER 2



MAXIMUM EXCITATION = 0.233500E -3 CM-SEC ; (2 S 12; T= 365.15 SEC)

EXCITATION NORMALIZED TO 0 S 150 (VERT. COMP.) ; 0.16027000E -2

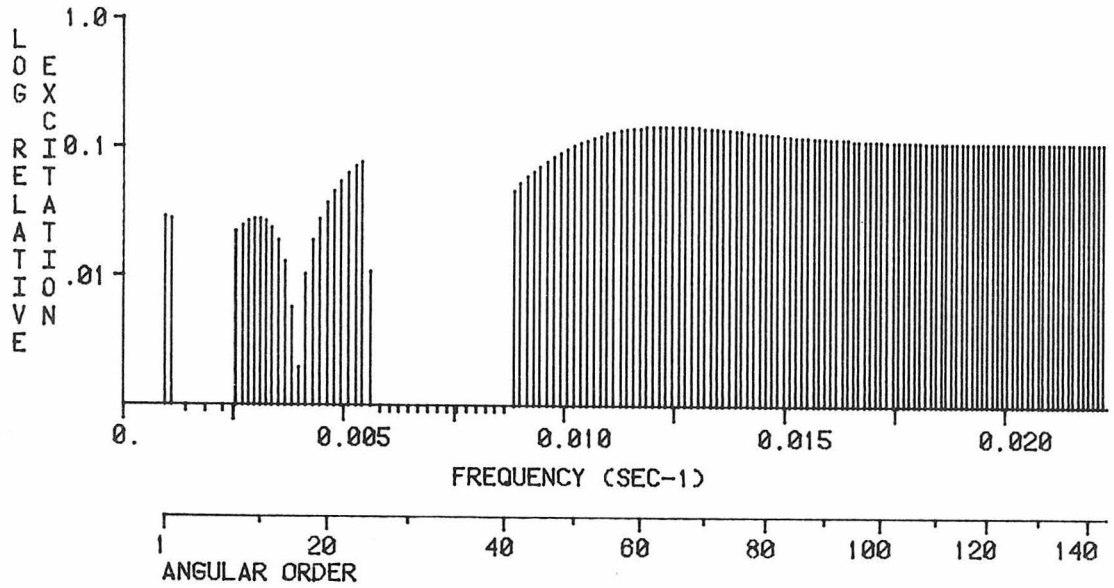
RADIAL COMPONENT; RADIAL ORDER 2



MAXIMUM EXCITATION = 0.498284E -3 CM-SEC ; (2 S 27; T= 174.10 SEC)

EXCITATION NORMALIZED TO 0 S 150 (RAD. COMP.) ; 0.14734600E -2

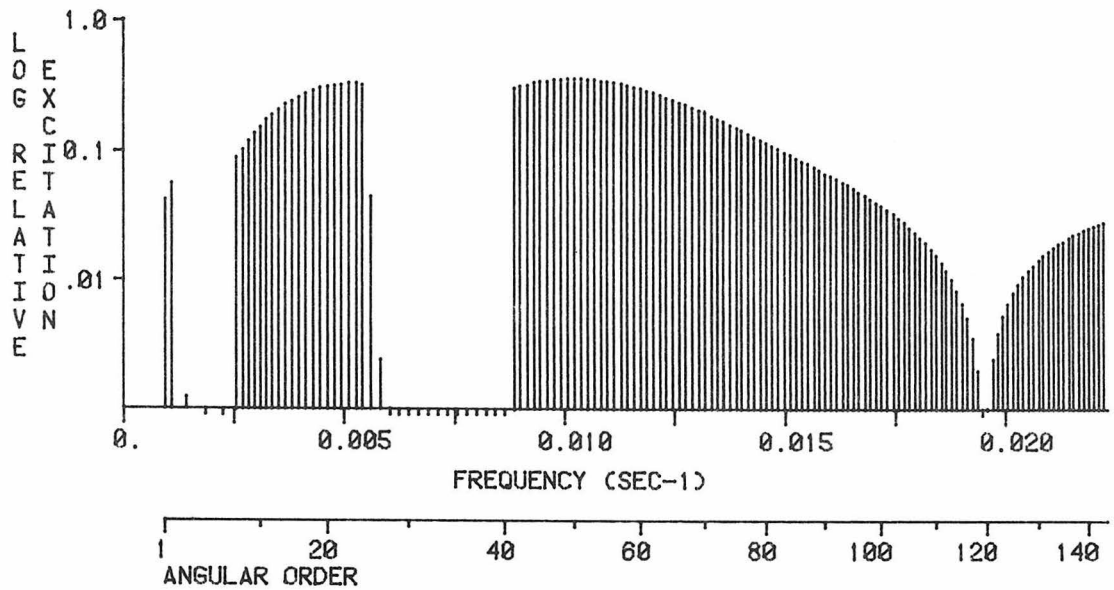
VERTICAL COMPONENT; RADIAL ORDER 3



MAXIMUM EXCITATION = 0.236448E -3 CM-SEC ; (3 S 65; T= 80.40 SEC)

EXCITATION NORMALIZED TO 0 S 150 (VERT. COMP.) ; 0.16027000E -2

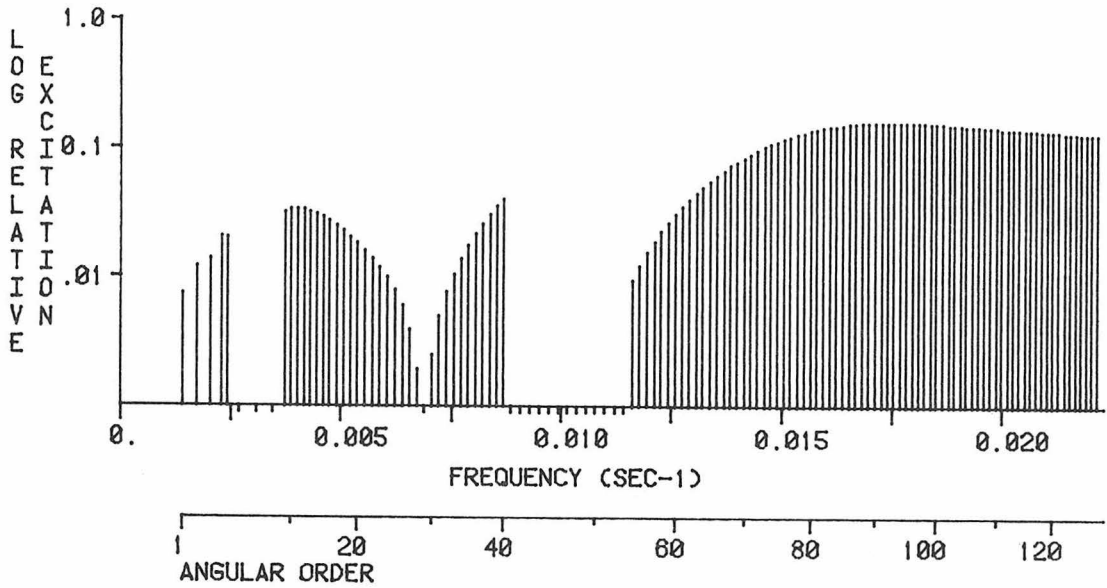
RADIAL COMPONENT; RADIAL ORDER 3



MAXIMUM EXCITATION = 0.534015E -3 CM-SEC ; (3 S 50; T= 97.96 SEC)

EXCITATION NORMALIZED TO 0 S 150 (RAD. COMP.) ; 0.14734600E -2

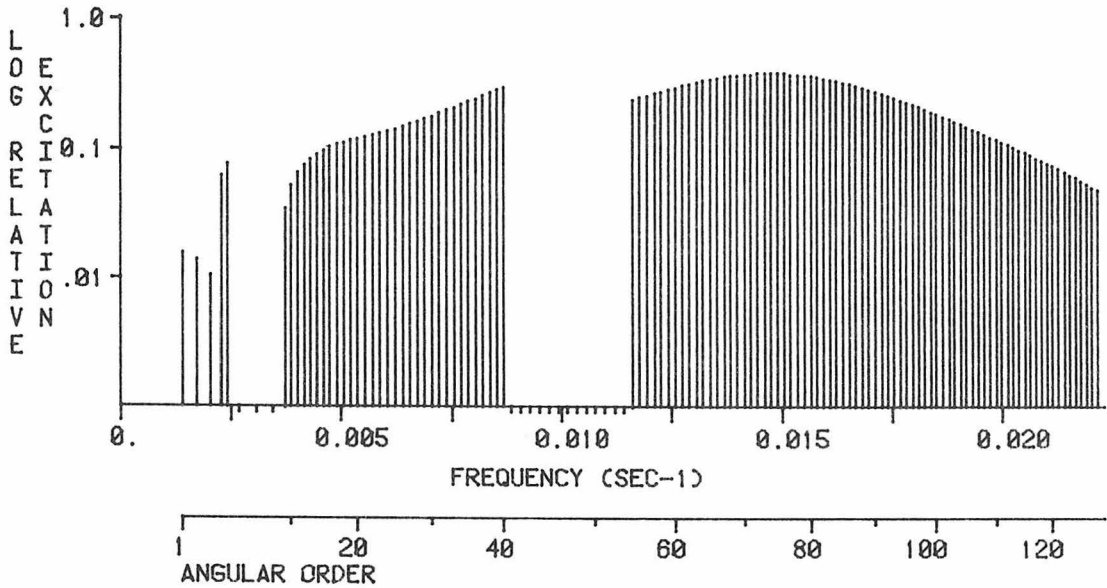
VERTICAL COMPONENT; RADIAL ORDER 4



MAXIMUM EXCITATION = 0.256868E -3 CM-SEC ; (4 S 93; T= 57.12 SEC)

EXCITATION NORMALIZED TO 0 S 150 (VERT. COMP.) ; 0.16027000E -2

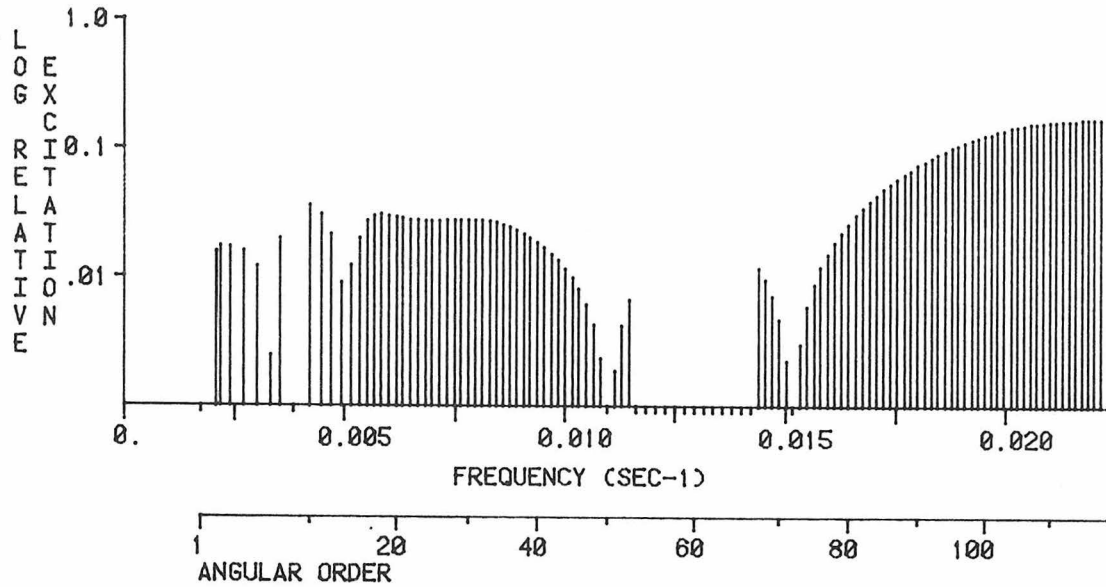
RADIAL COMPONENT; RADIAL ORDER 4



MAXIMUM EXCITATION = 0.559990E -3 CM-SEC ; (4 S 74; T= 67.88 SEC)

EXCITATION NORMALIZED TO 0 S 150 (RAD. COMP.) ; 0.14734600E -2

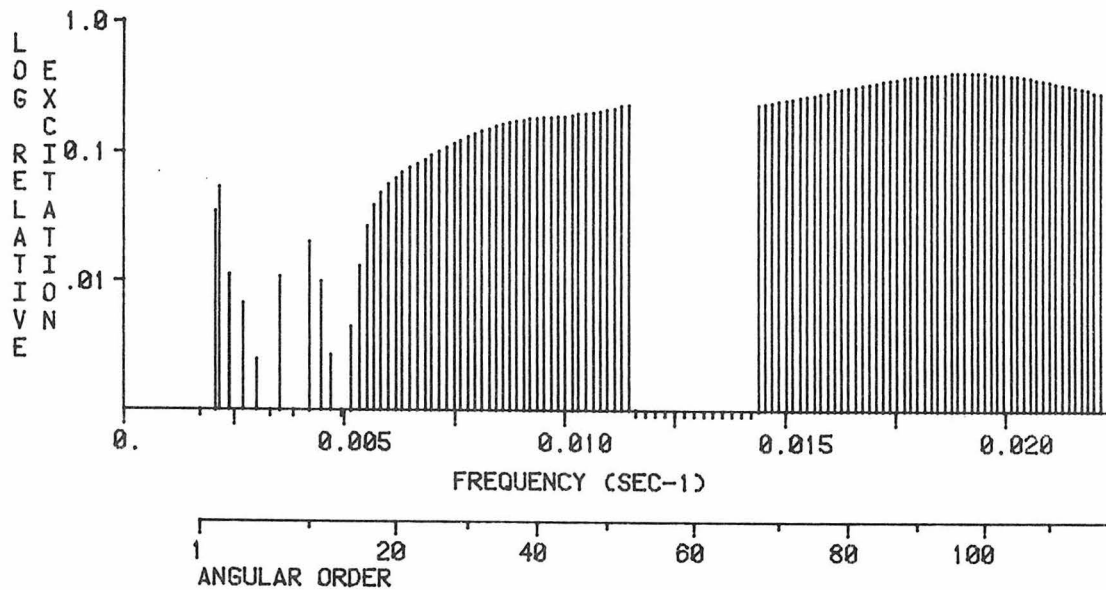
VERTICAL COMPONENT; RADIAL ORDER 5



MAXIMUM EXCITATION = 0.274352E -3 CM-SEC ; (5 S 118; T= 45.24 SEC)

EXCITATION NORMALIZED TO 0 S 150 (VERT. COMP.) ; 0.16027000E -2

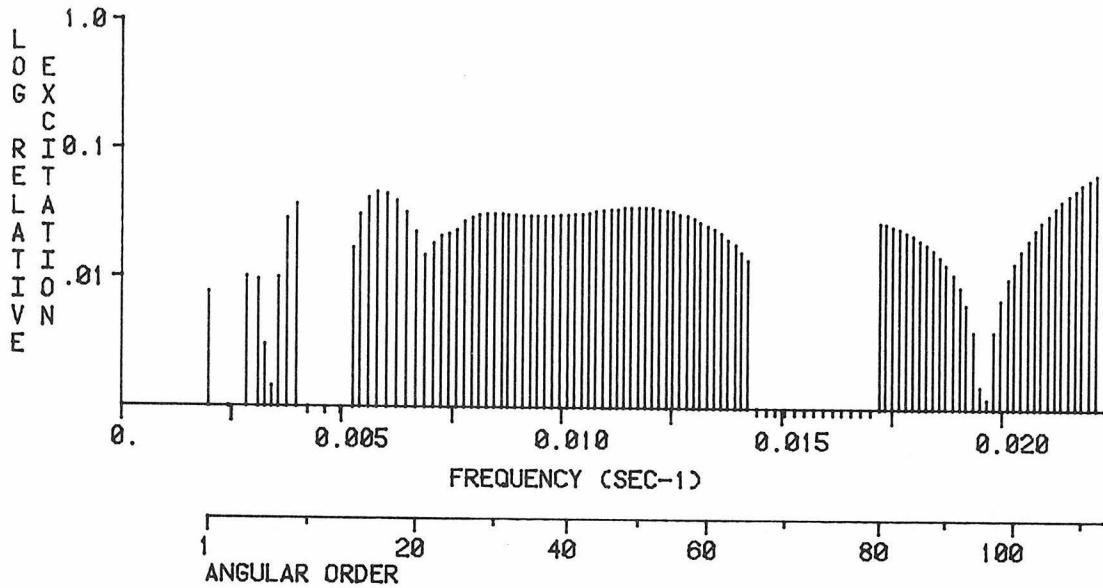
RADIAL COMPONENT; RADIAL ORDER 5



MAXIMUM EXCITATION = 0.612928E -3 CM-SEC ; (5 S 98; T= 52.13 SEC)

EXCITATION NORMALIZED TO 0 S 150 (RAD. COMP.) ; 0.14734600E -2

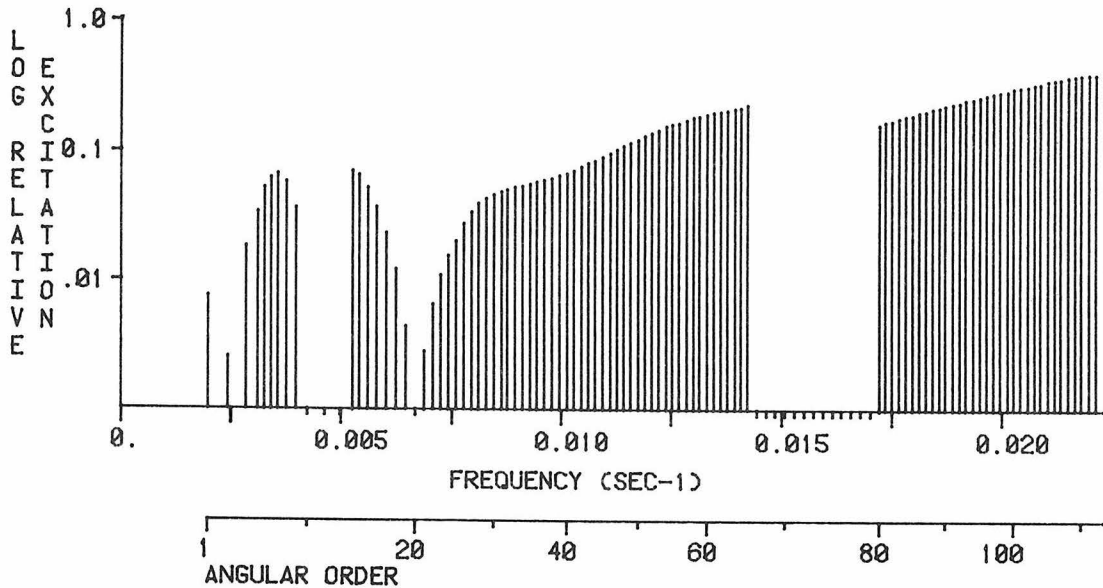
VERTICAL COMPONENT; RADIAL ORDER 6



MAXIMUM EXCITATION = 0.106342E -3 CM-SEC ; (6 S 112; T= 45.30 SEC)

EXCITATION NORMALIZED TO 0 S 150 (VERT. COMP.) ; 0.16027000E -2

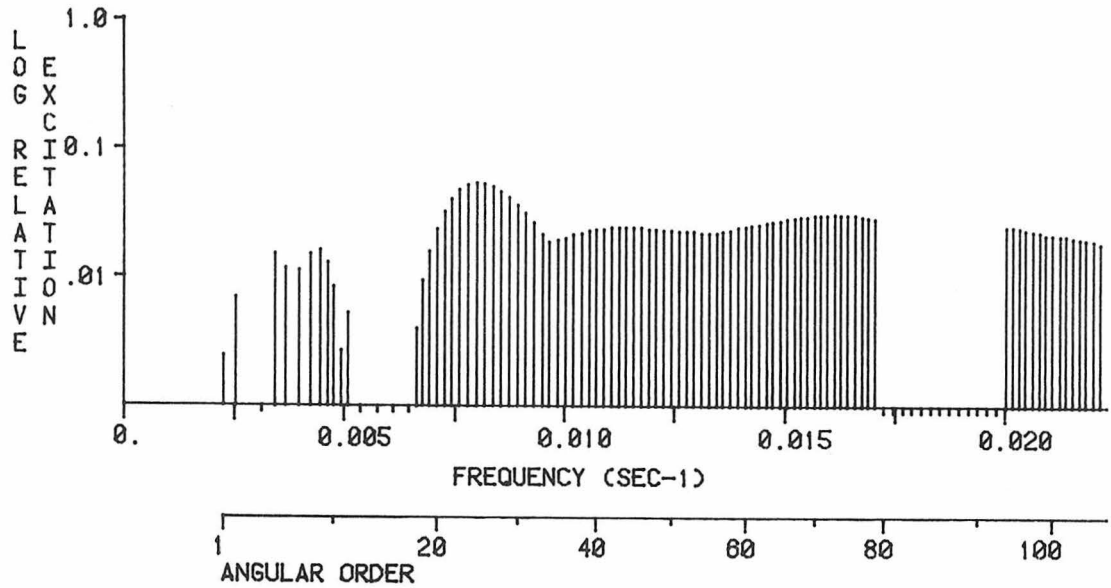
RADIAL COMPONENT; RADIAL ORDER 6



MAXIMUM EXCITATION = 0.604576E -3 CM-SEC ; (6 S 112; T= 45.30 SEC)

EXCITATION NORMALIZED TO 0 S 150 (RAD. COMP.) ; 0.14734600E -2

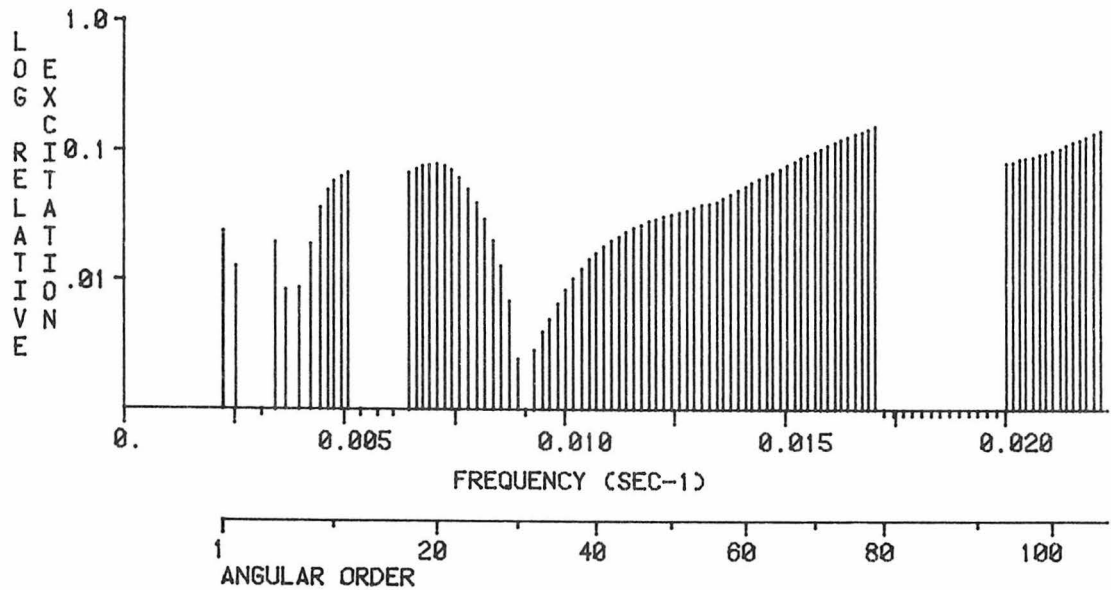
VERTICAL COMPONENT; RADIAL ORDER 7



MAXIMUM EXCITATION = 0.869810E -4 CM-SEC ; (7 S 25; T= 125.48 SEC)

EXCITATION NORMALIZED TO 0 S 150 (VERT. COMP.) ; 0.16027000E -2

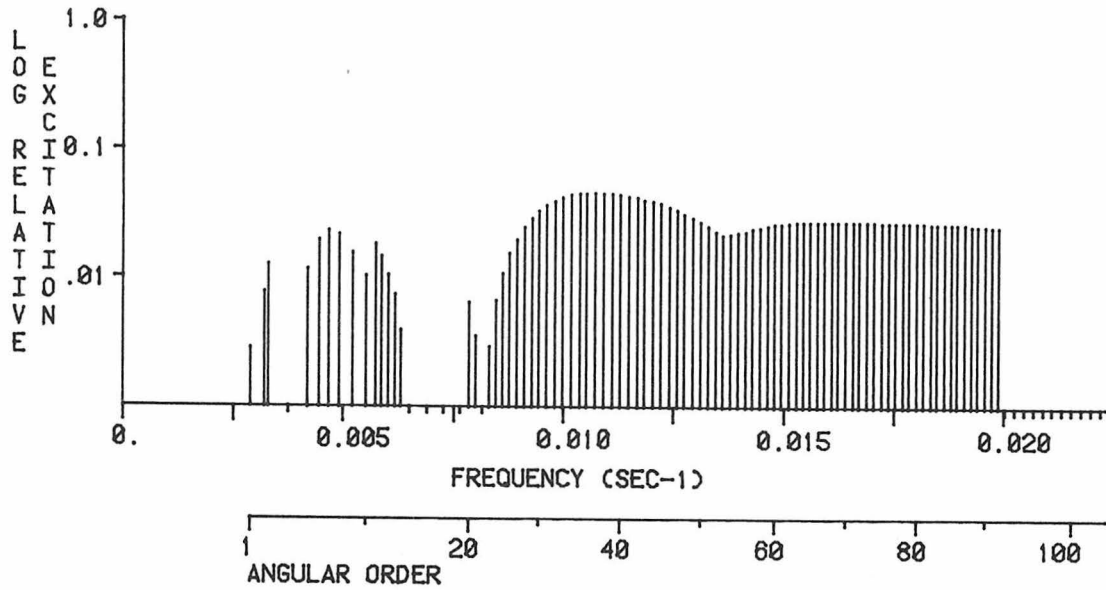
RADIAL COMPONENT; RADIAL ORDER 7



MAXIMUM EXCITATION = 0.229559E -3 CM-SEC ; (7 S 79; T= 58.75 SEC)

EXCITATION NORMALIZED TO 0 S 150 (RAD. COMP.) ; 0.14734600E -2

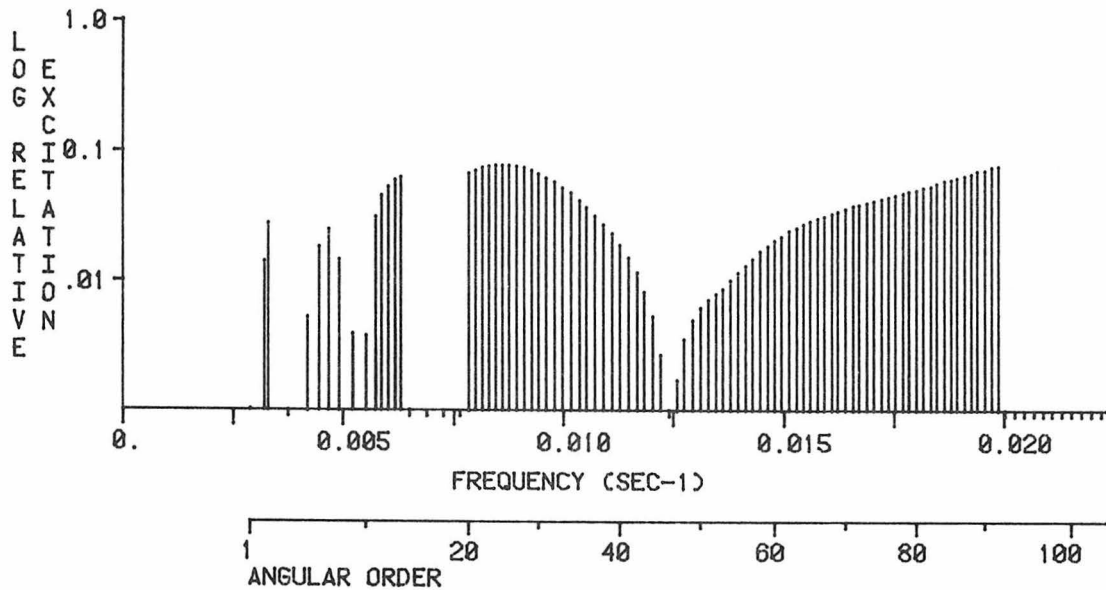
VERTICAL COMPONENT; RADIAL ORDER 8



MAXIMUM EXCITATION = 0.743290E -4 CM-SEC ; (8 S 37; T= 93.31 SEC)

EXCITATION NORMALIZED TO 0 S 150 (VERT. COMP.) ; 0.16027000E -2

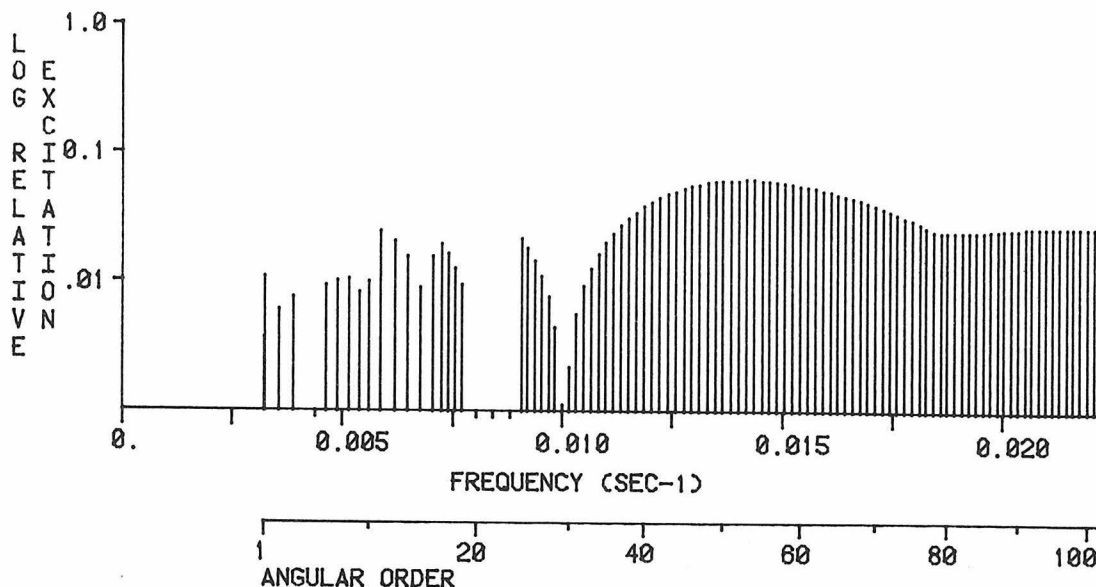
RADIAL COMPONENT; RADIAL ORDER 8



MAXIMUM EXCITATION = 0.115733E -3 CM-SEC ; (8 S 92; T= 50.42 SEC)

EXCITATION NORMALIZED TO 0 S 150 (RAD. COMP.) ; 0.14734600E -2

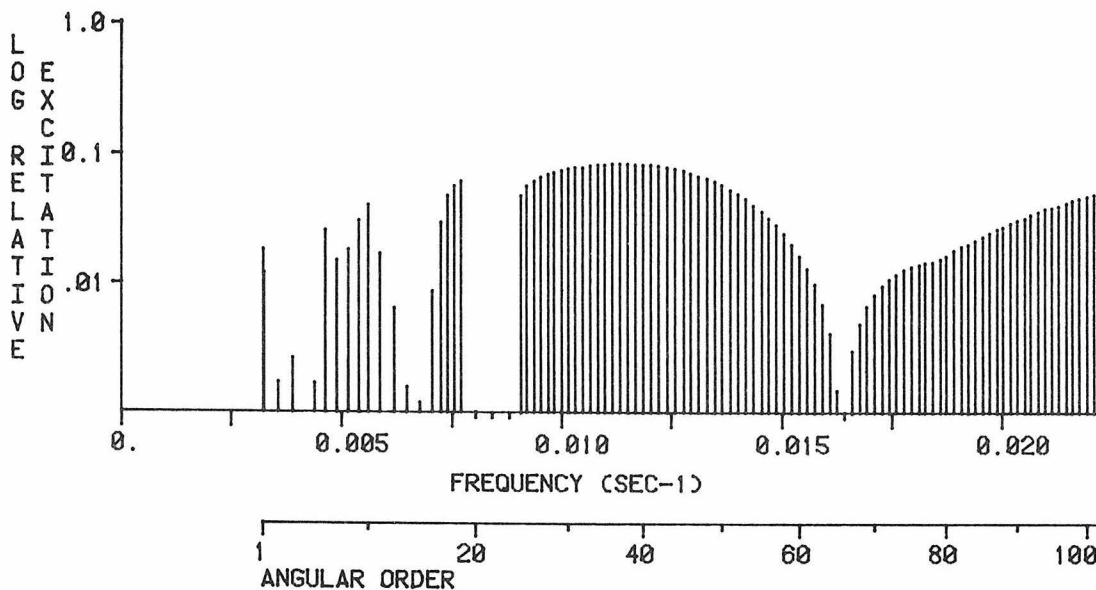
VERTICAL COMPONENT; RADIAL ORDER 9



MAXIMUM EXCITATION = 0.103835E -3 CM-SEC ; (9 S 53; T= 70.62 SEC)

EXCITATION NORMALIZED TO 0 S 150 (VERT. COMP.) ; 0.16027000E -2

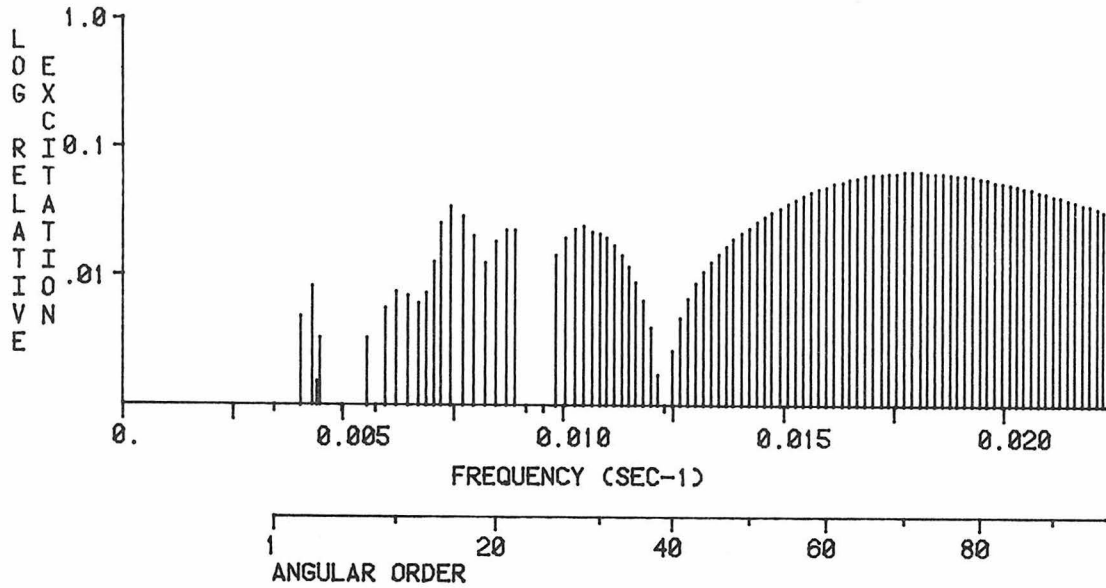
RADIAL COMPONENT; RADIAL ORDER 9



MAXIMUM EXCITATION = 0.125038E -3 CM-SEC ; (9 S 37; T= 88.36 SEC)

EXCITATION NORMALIZED TO 0 S 150 (RAD. COMP.) ; 0.14734600E -2

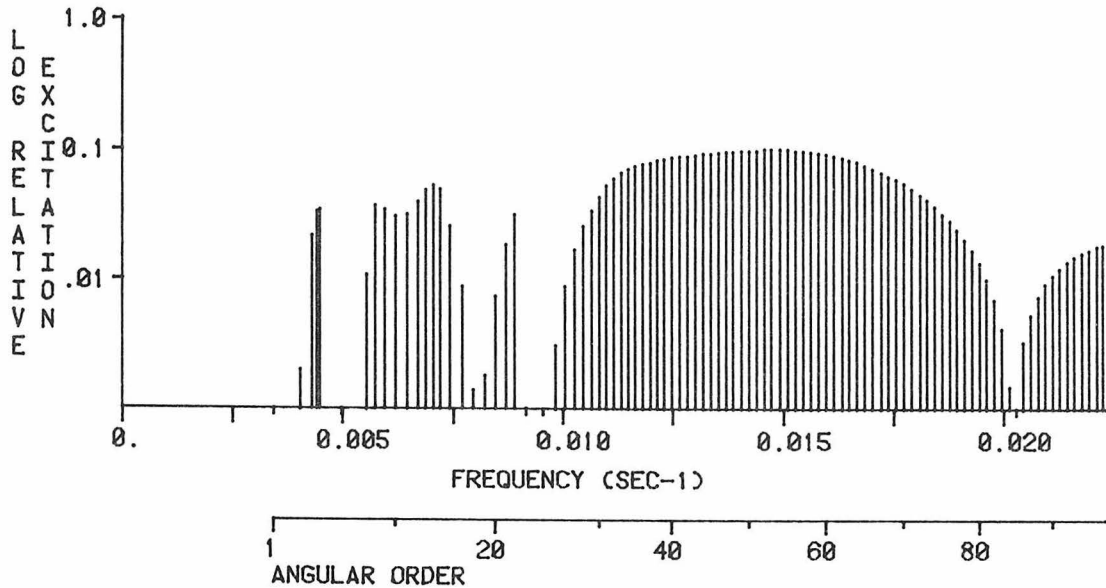
VERTICAL COMPONENT; RADIAL ORDER 10



MAXIMUM EXCITATION = 0.104157E -3 CM-SEC ; (10 S 71; T= 55.96 SEC)

EXCITATION NORMALIZED TO 0 S 150 (VERT. COMP.) ; 0.16027000E -2

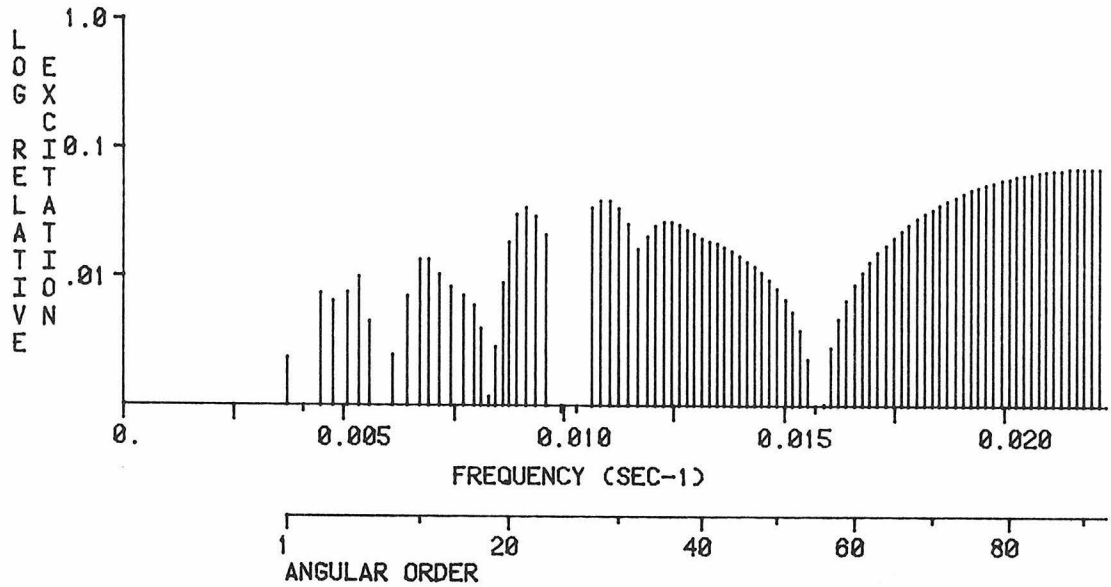
RADIAL COMPONENT; RADIAL ORDER 10



MAXIMUM EXCITATION = 0.149802E -3 CM-SEC ; (10 S 53; T= 67.92 SEC)

EXCITATION NORMALIZED TO 0 S 150 (RAD. COMP.) ; 0.14734600E -2

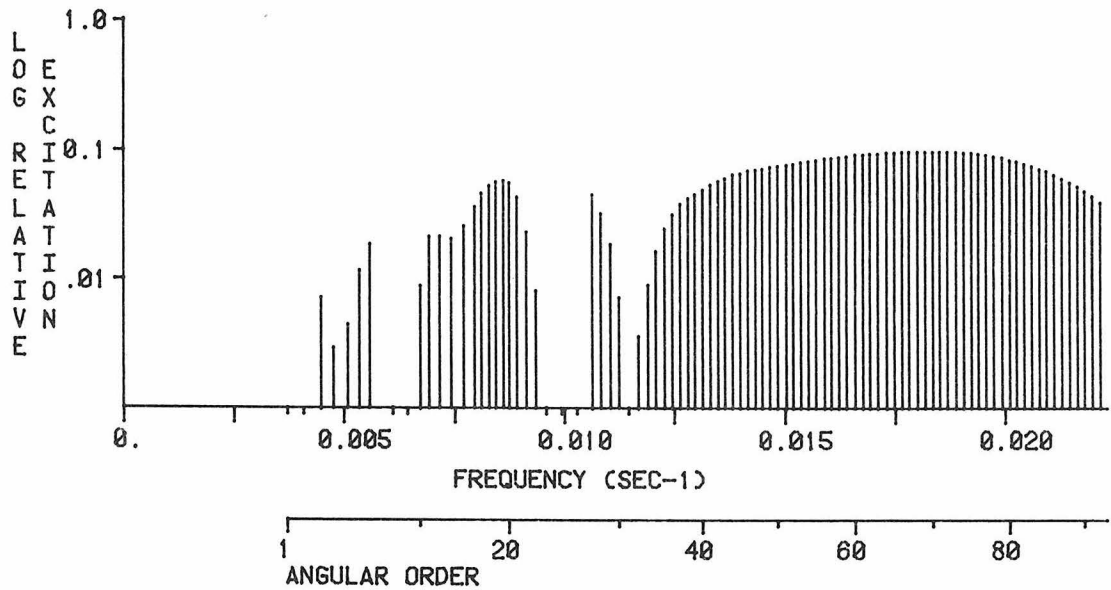
VERTICAL COMPONENT; RADIAL ORDER 11



MAXIMUM EXCITATION = 0.111677E -3 CM-SEC ; (11 S 91; T= 45.60 SEC)

EXCITATION NORMALIZED TO 0 S 150 (VERT. COMP.) ; 0.16027000E -2

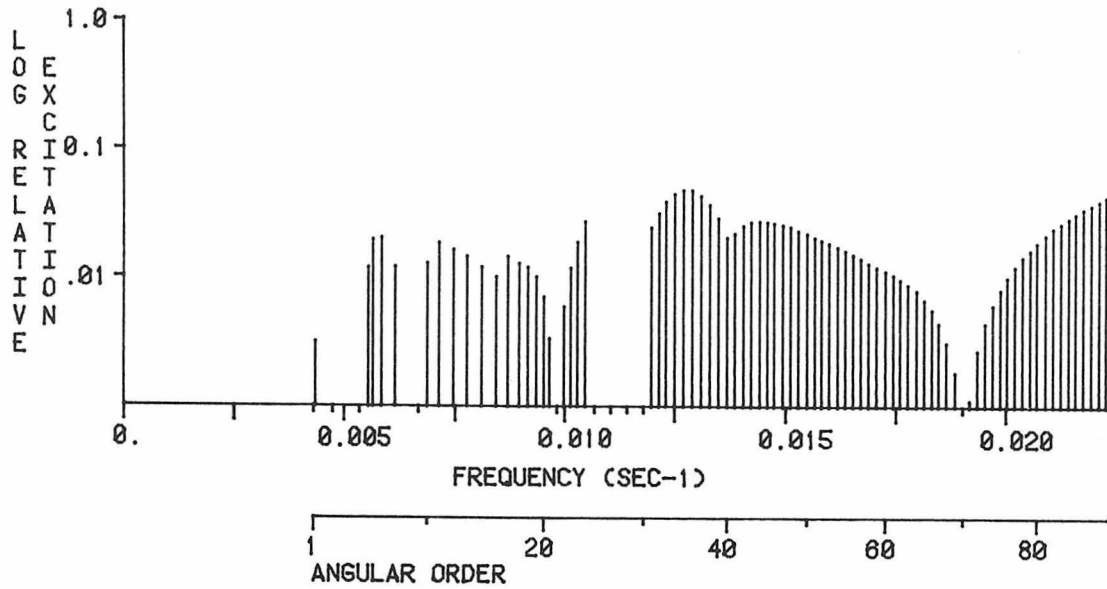
RADIAL COMPONENT; RADIAL ORDER 11



MAXIMUM EXCITATION = 0.148155E -3 CM-SEC ; (11 S 70; T= 54.57 SEC)

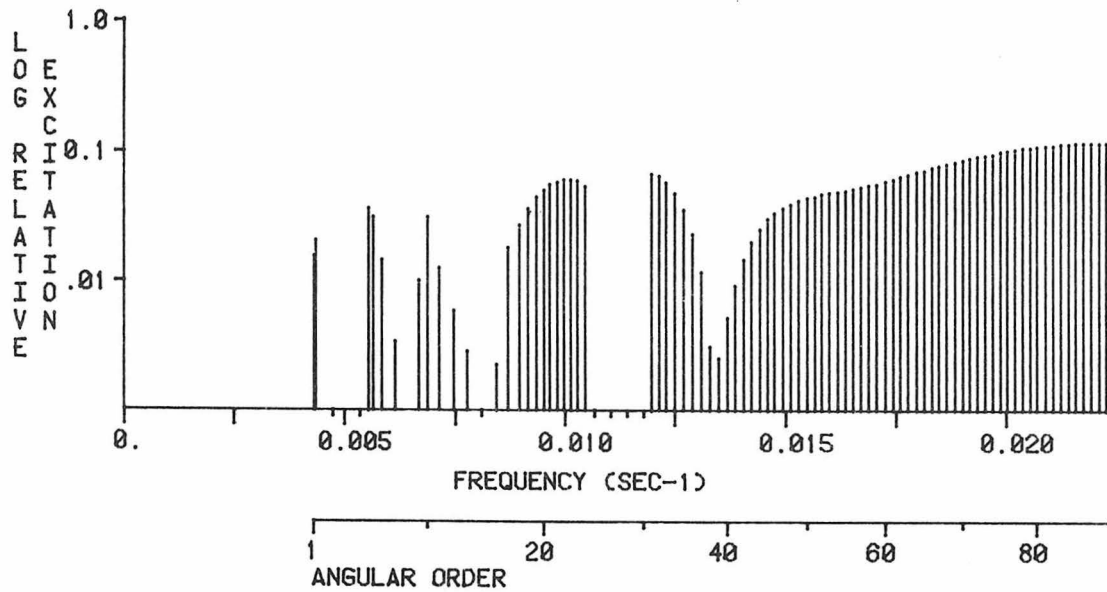
EXCITATION NORMALIZED TO 0 S 150 (RAD. COMP.) ; 0.14734600E -2

VERTICAL COMPONENT; RADIAL ORDER 12



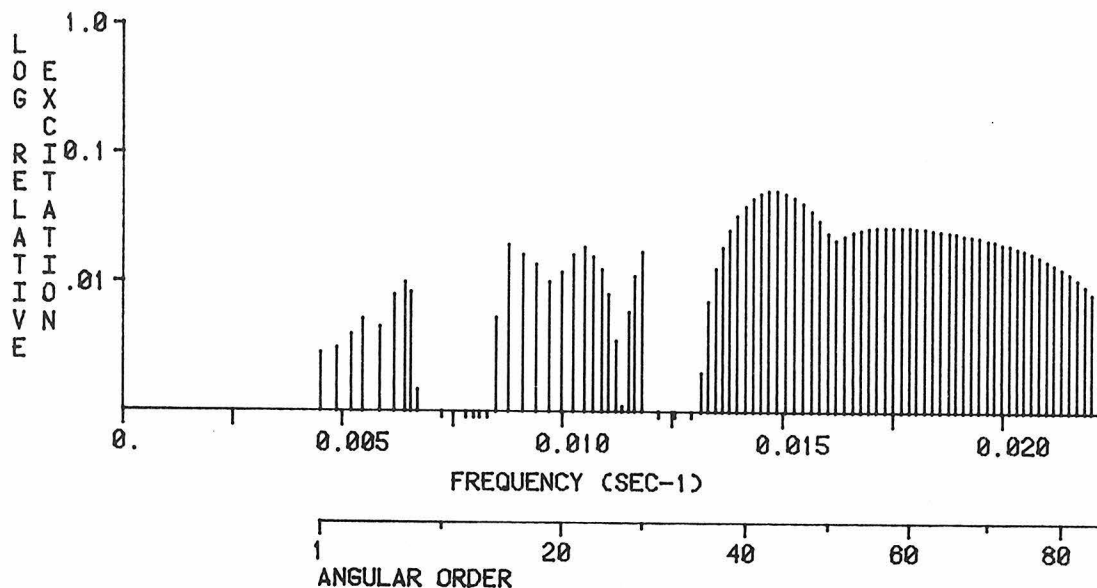
MAXIMUM EXCITATION = 0.766720E -4 CM-SEC ; (12 S 35; T= 78.95 SEC)
EXCITATION NORMALIZED TO 0 S 150 (VERT. COMP.) ; 0.16027000E -2

RADIAL COMPONENT; RADIAL ORDER 12



MAXIMUM EXCITATION = 0.175315E -3 CM-SEC ; (12 S 87; T= 45.71 SEC)
EXCITATION NORMALIZED TO 0 S 150 (RAD. COMP.) ; 0.14734600E -2

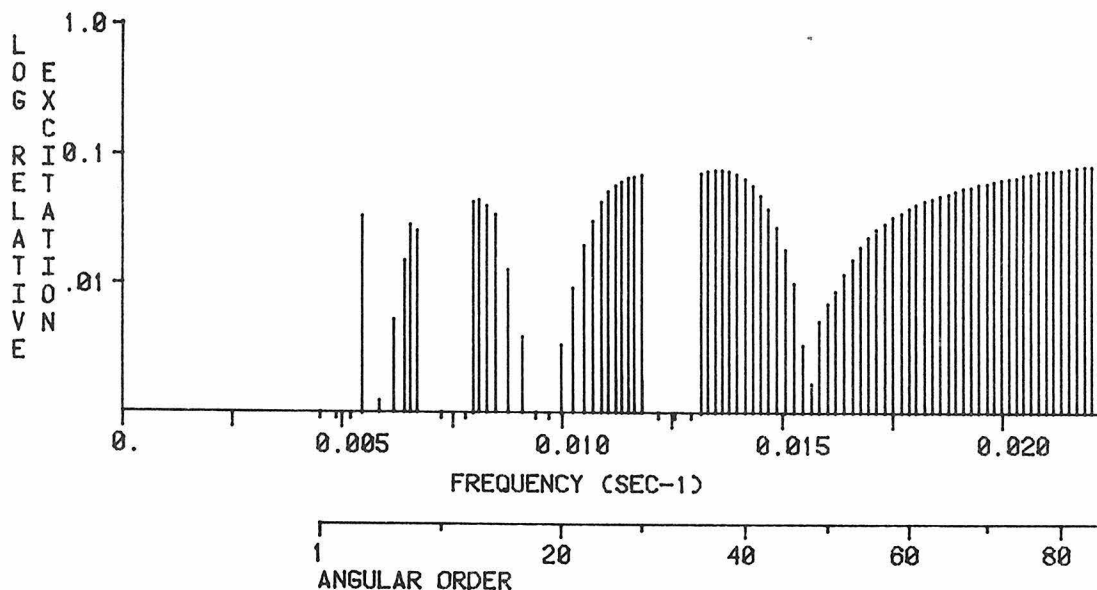
VERTICAL COMPONENT; RADIAL ORDER 13



MAXIMUM EXCITATION = 0.838620E -4 CM-SEC ; (13 S 44; T= 67.28 SEC)

EXCITATION NORMALIZED TO 0 S 150 (VERT. COMP.) ; 0.16027000E -2

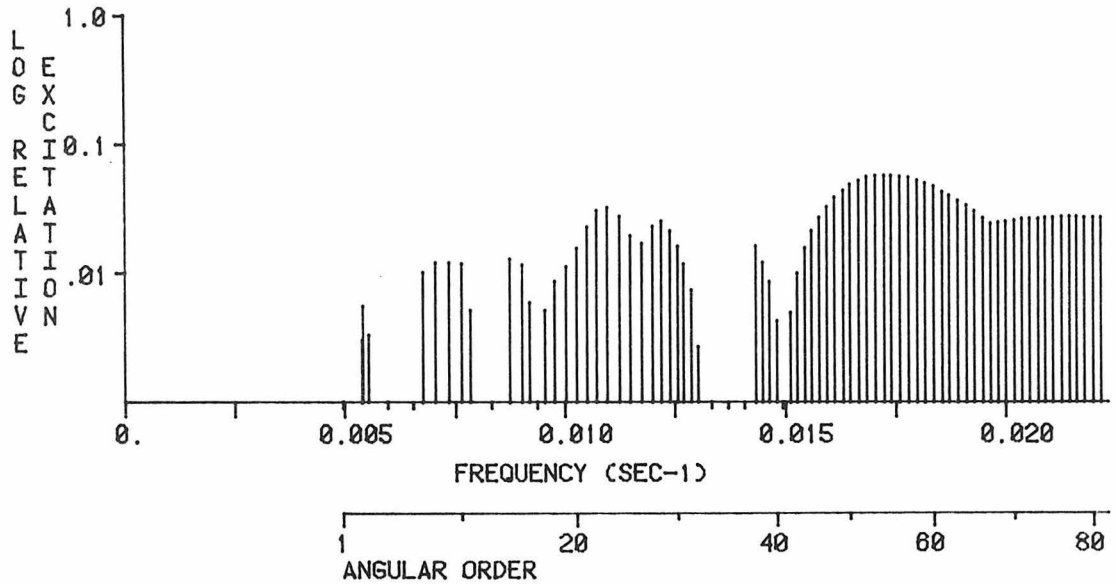
RADIAL COMPONENT; RADIAL ORDER 13



MAXIMUM EXCITATION = 0.125597E -3 CM-SEC ; (13 S 85; T= 45.13 SEC)

EXCITATION NORMALIZED TO 0 S 150 (RAD. COMP.) ; 0.14734600E -2

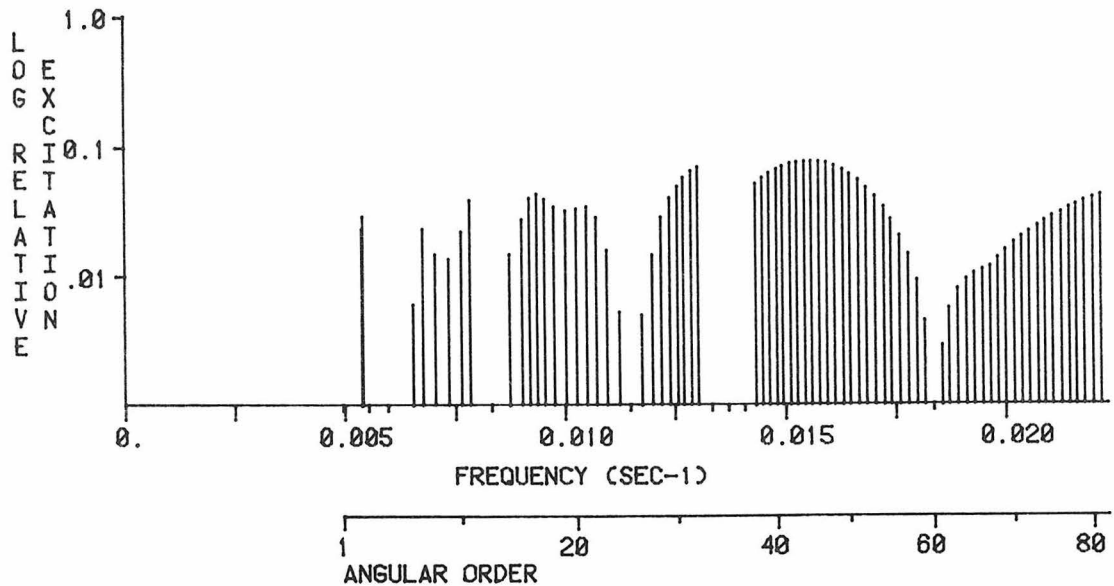
VERTICAL COMPONENT; RADIAL ORDER 14



MAXIMUM EXCITATION = 0.947090E -4 CM-SEC ; (14 S 54; T= 58.14 SEC)

EXCITATION NORMALIZED TO 0 S 150 (VERT. COMP.) ; 0.16027000E -2

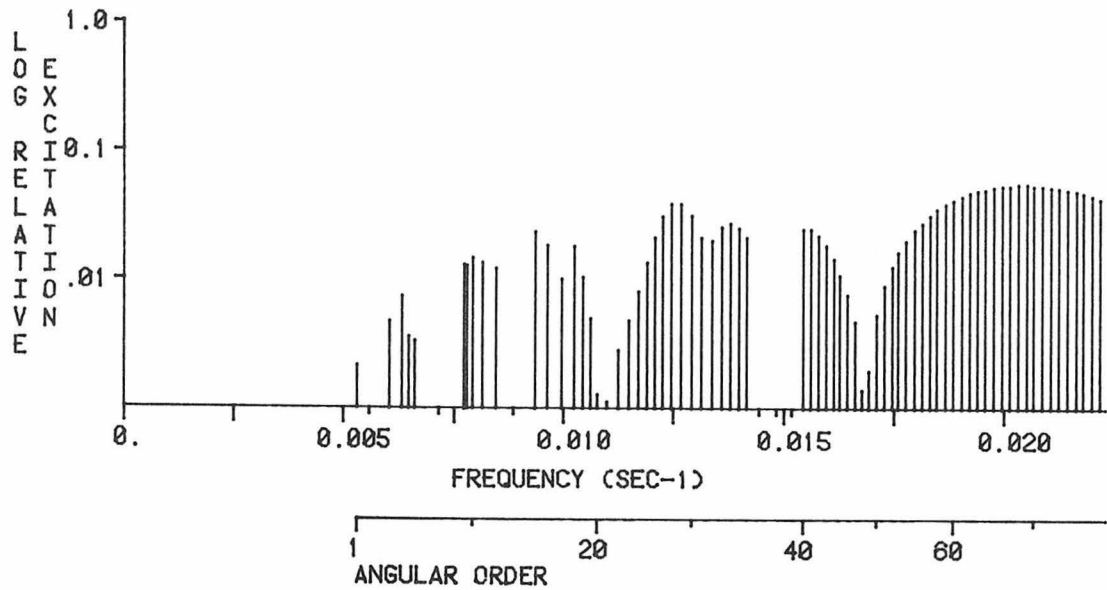
RADIAL COMPONENT; RADIAL ORDER 14



MAXIMUM EXCITATION = 0.115374E -3 CM-SEC ; (14 S 45; T= 64.16 SEC)

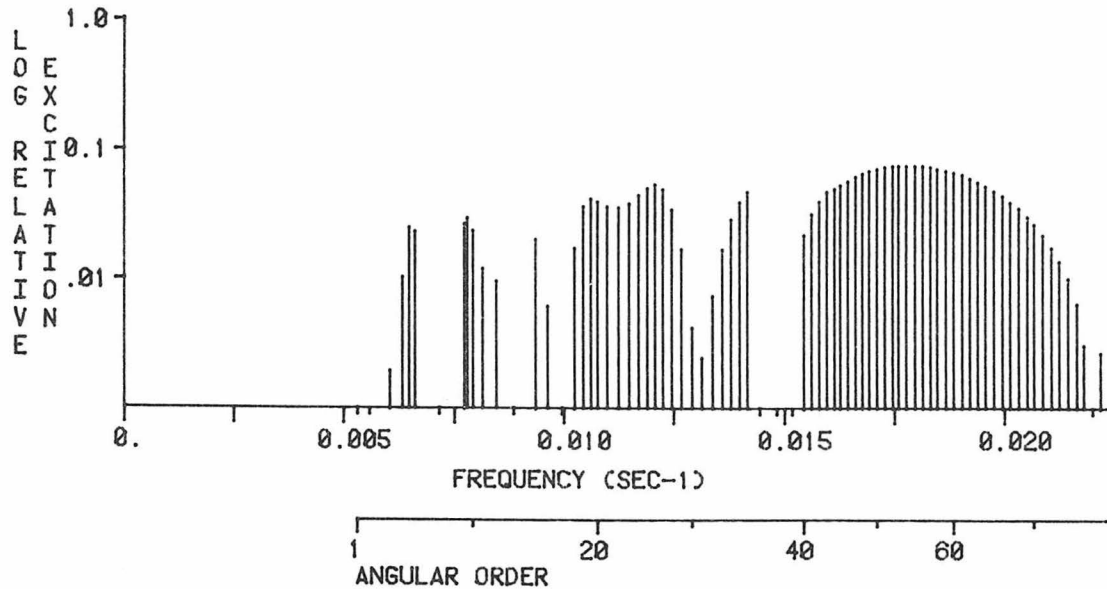
EXCITATION NORMALIZED TO 0 S 150 (RAD. COMP.) ; 0.14734600E -2

VERTICAL COMPONENT; RADIAL ORDER 15



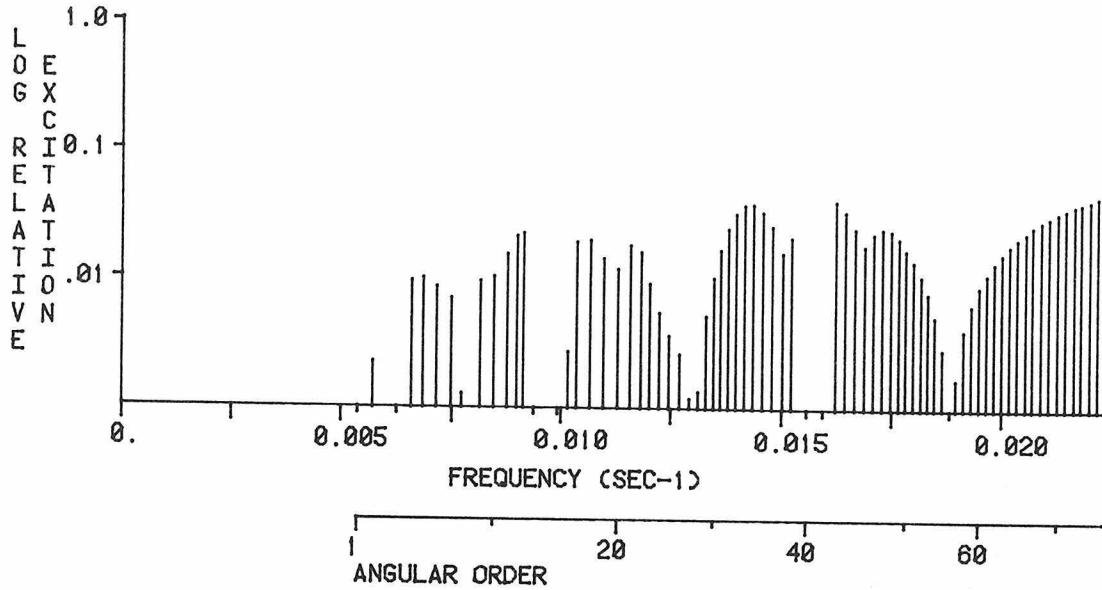
MAXIMUM EXCITATION = 0.887050E -4 CM-SEC ; (15 S 69; T= 48.86 SEC)
EXCITATION NORMALIZED TO 0 S 150 (VERT. COMP.) ; 0.16027000E -2

RADIAL COMPONENT; RADIAL ORDER 15



MAXIMUM EXCITATION = 0.113281E -3 CM-SEC ; (15 S 54; T= 56.33 SEC)
EXCITATION NORMALIZED TO 0 S 150 (RAD. COMP.) ; 0.14734600E -2

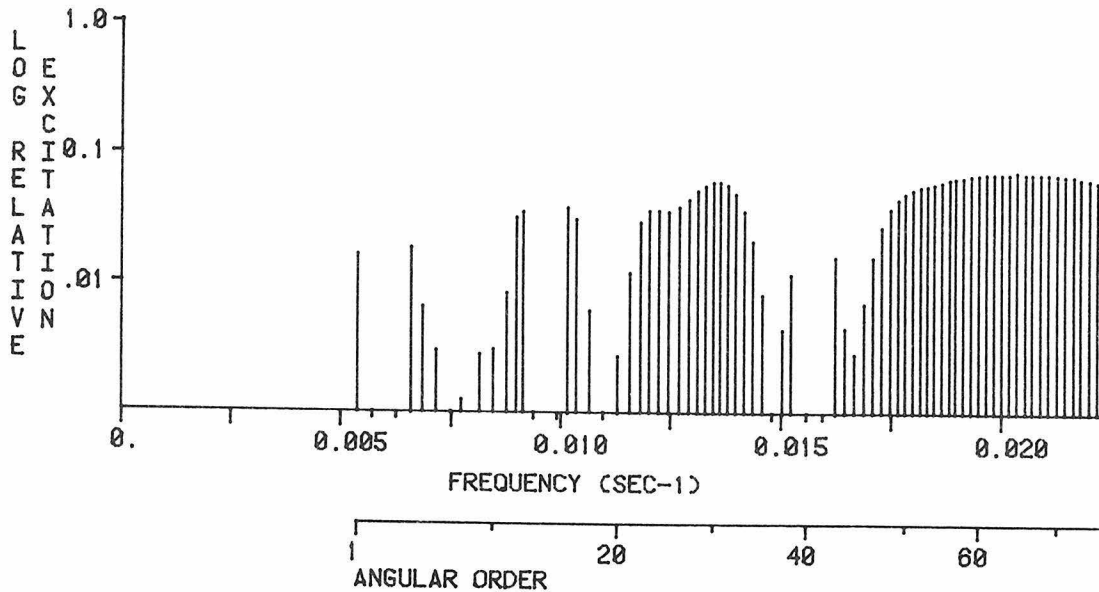
VERTICAL COMPONENT; RADIAL ORDER 16



MAXIMUM EXCITATION = 0.725360E -4 CM-SEC ; (16 S 75; T= 45.19 SEC)

EXCITATION NORMALIZED TO 0 S 150 (VERT. COMP.) ; 0.16027000E -2

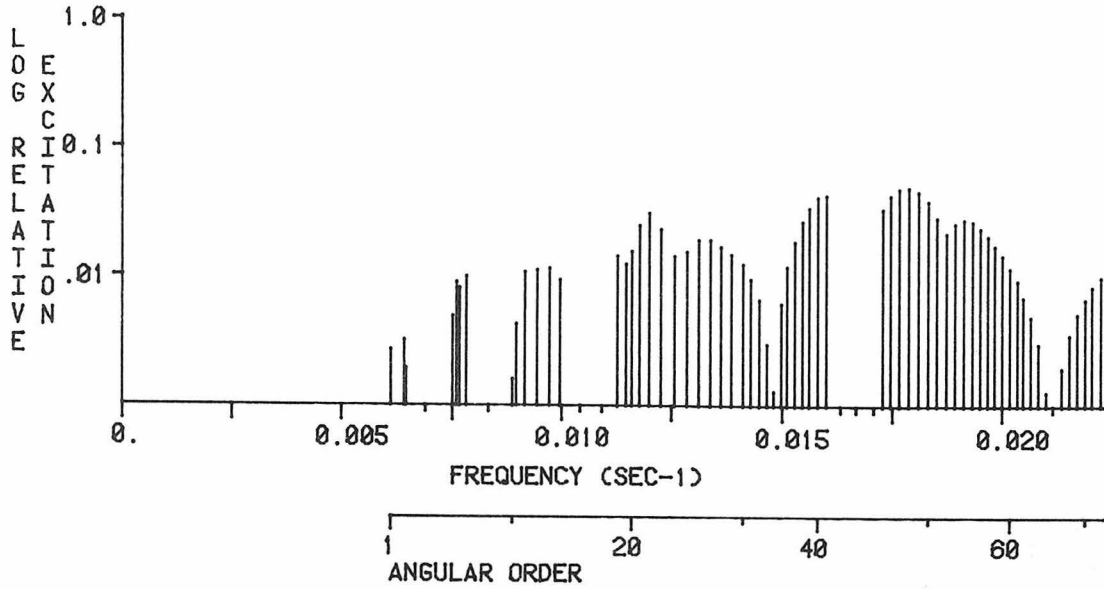
RADIAL COMPONENT; RADIAL ORDER 16



MAXIMUM EXCITATION = 0.108964E -3 CM-SEC ; (16 S 65; T= 49.22 SEC)

EXCITATION NORMALIZED TO 0 S 150 (RAD. COMP.) ; 0.14734600E -2

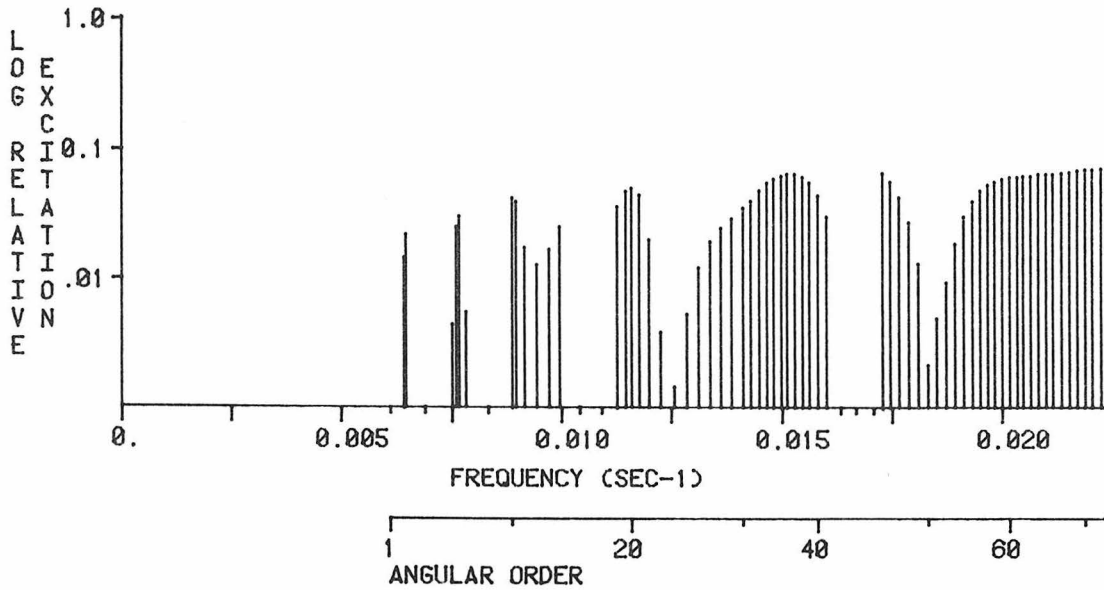
VERTICAL COMPONENT; RADIAL ORDER 17



MAXIMUM EXCITATION = 0.786520E -4 CM-SEC ; (17 S 48; T= 56.07 SEC)

EXCITATION NORMALIZED TO 0 S 150 (VERT. COMP.) ; 0.16027000E -2

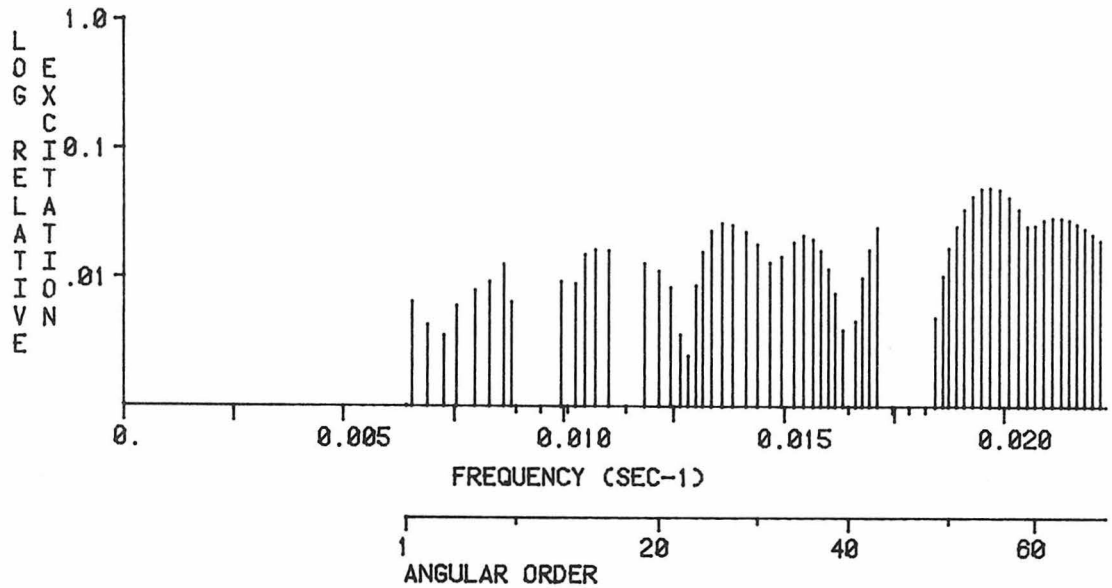
RADIAL COMPONENT; RADIAL ORDER 17



MAXIMUM EXCITATION = 0.108174E -3 CM-SEC ; (17 S 72; T= 45.06 SEC)

EXCITATION NORMALIZED TO 0 S 150 (RAD. COMP.) ; 0.14734600E -2

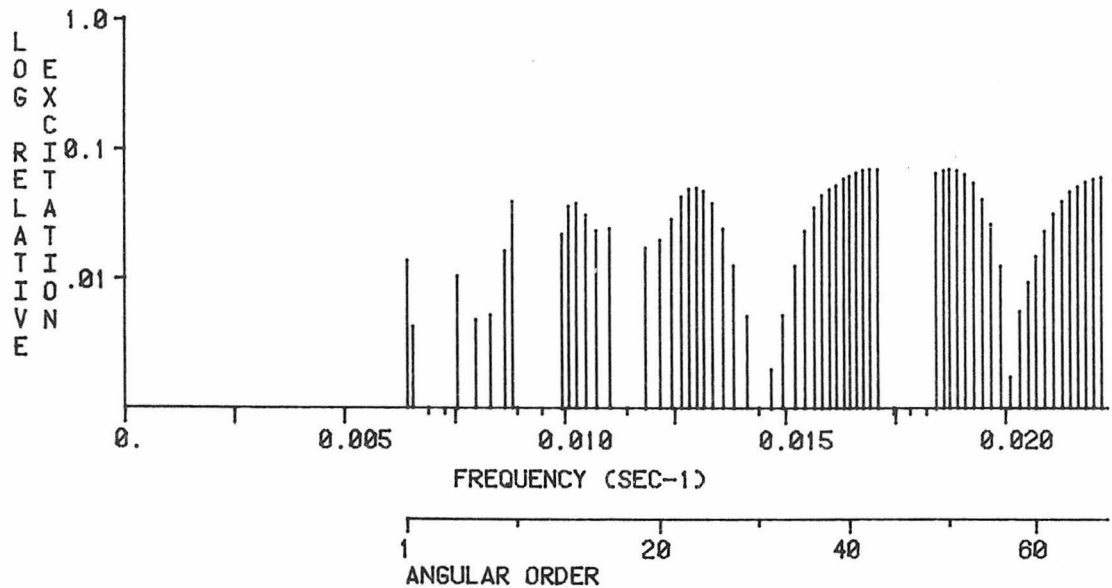
VERTICAL COMPONENT; RADIAL ORDER 18



MAXIMUM EXCITATION = 0.820090E -4 CM-SEC ; (18 S 55; T= 50.93 SEC)

EXCITATION NORMALIZED TO 0 S 150 (VERT. COMP.) ; 0.16027000E -2

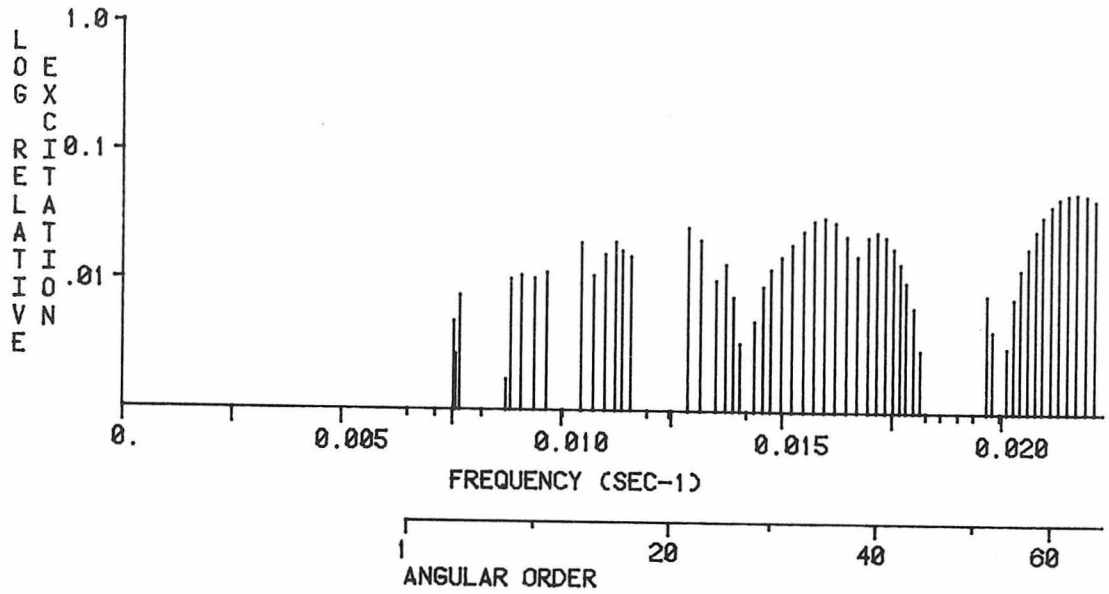
RADIAL COMPONENT; RADIAL ORDER 18



MAXIMUM EXCITATION = 0.105613E -3 CM-SEC ; (18 S 43; T= 59.12 SEC)

EXCITATION NORMALIZED TO 0 S 150 (RAD. COMP.) ; 0.14734600E -2

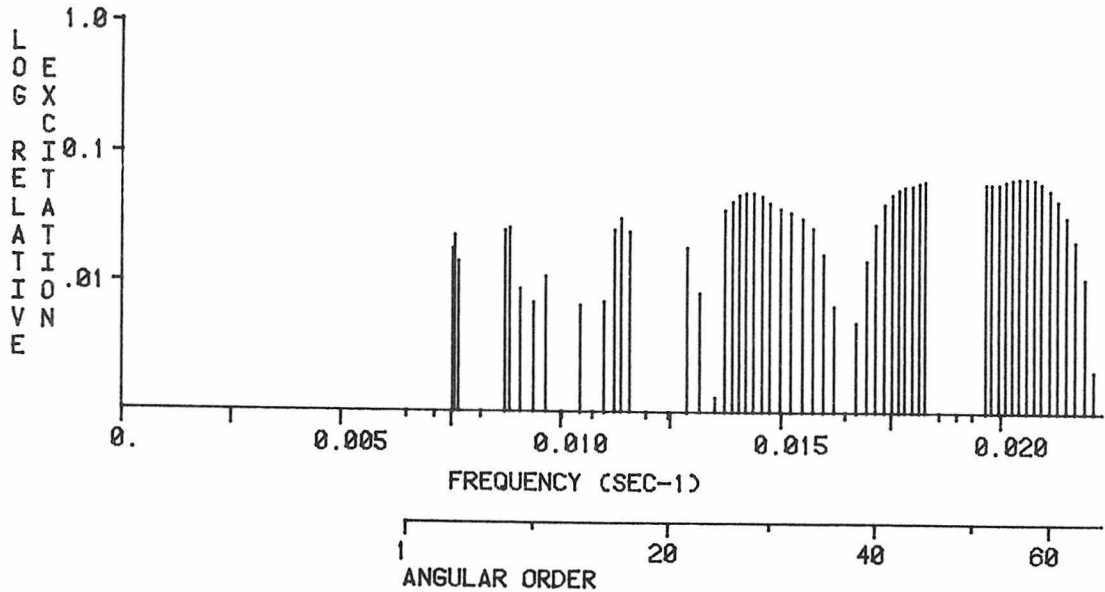
VERTICAL COMPONENT; RADIAL ORDER 19



MAXIMUM EXCITATION = 0.813940E -4 CM-SEC ; (19 S 63; T= 46.19 SEC)

EXCITATION NORMALIZED TO 0 S 150 (VERT. COMP.) ; 0.16027000E -2

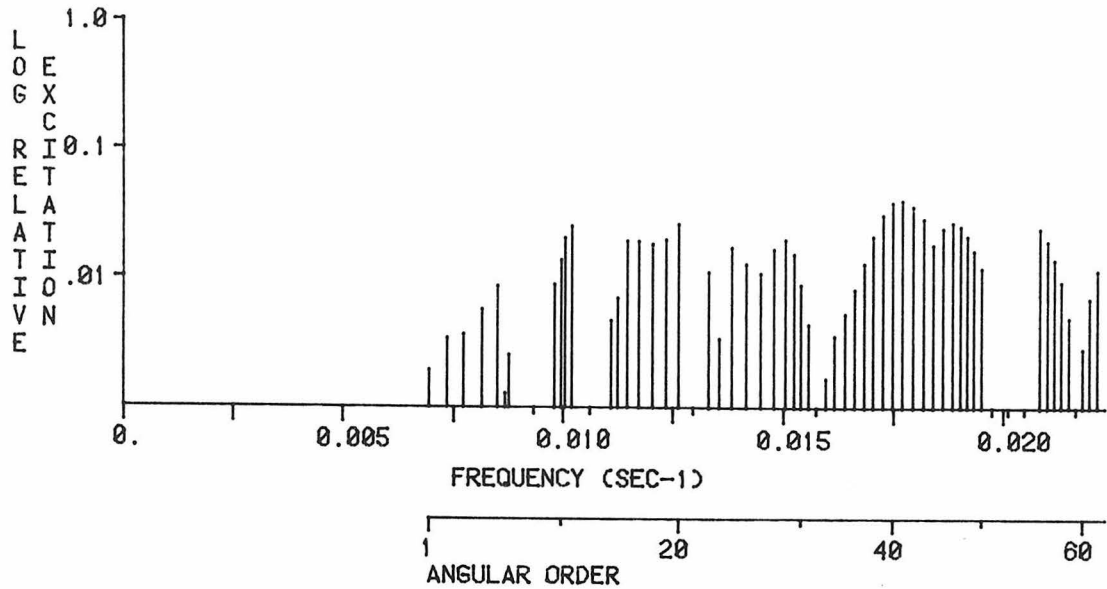
RADIAL COMPONENT; RADIAL ORDER 19



MAXIMUM EXCITATION = 0.992910E -4 CM-SEC ; (19 S 57; T= 48.66 SEC)

EXCITATION NORMALIZED TO 0 S 150 (RAD. COMP.) ; 0.14734600E -2

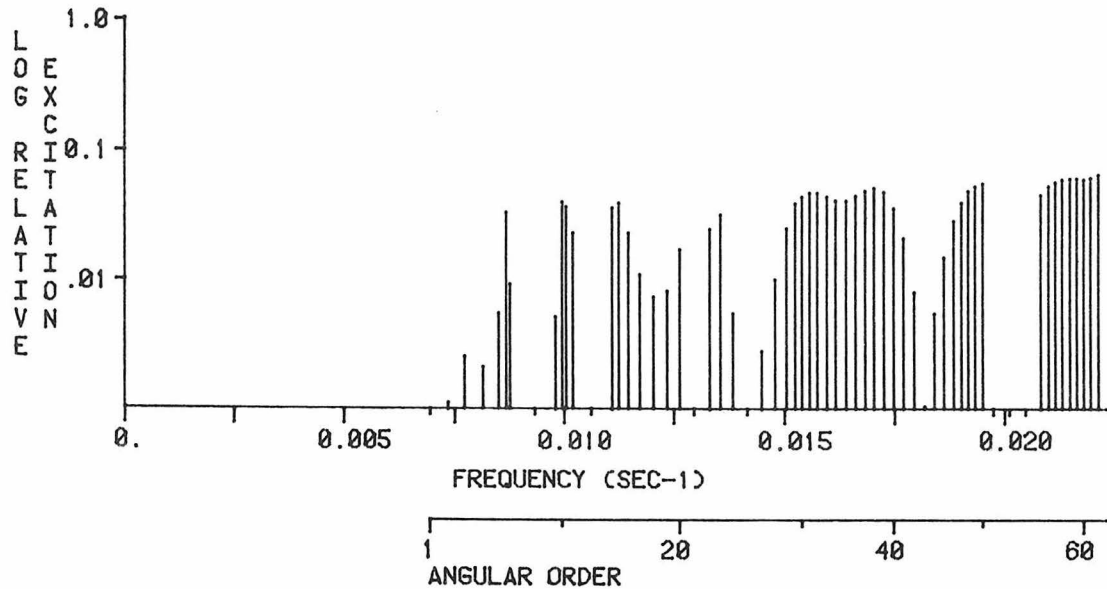
VERTICAL COMPONENT; RADIAL ORDER 20



MAXIMUM EXCITATION = 0.654770E -4 CM-SEC ; (20 S 41; T= 56.59 SEC)

EXCITATION NORMALIZED TO 0 S 150 (VERT. COMP.) ; 0.16027000E -2

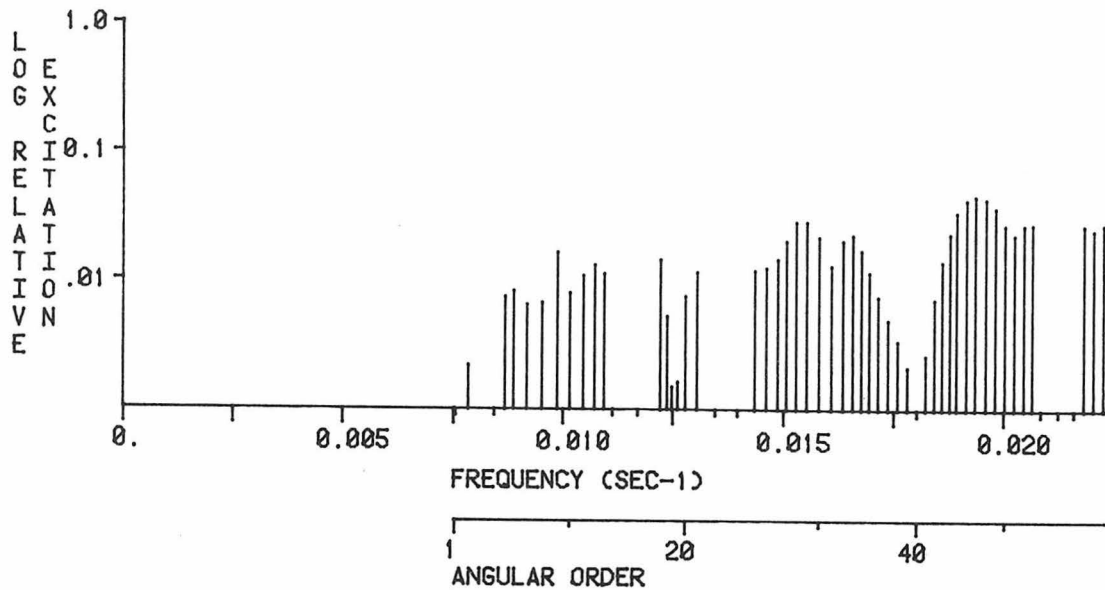
RADIAL COMPONENT; RADIAL ORDER 20



MAXIMUM EXCITATION = 0.974130E -4 CM-SEC ; (20 S 62; T= 45.30 SEC)

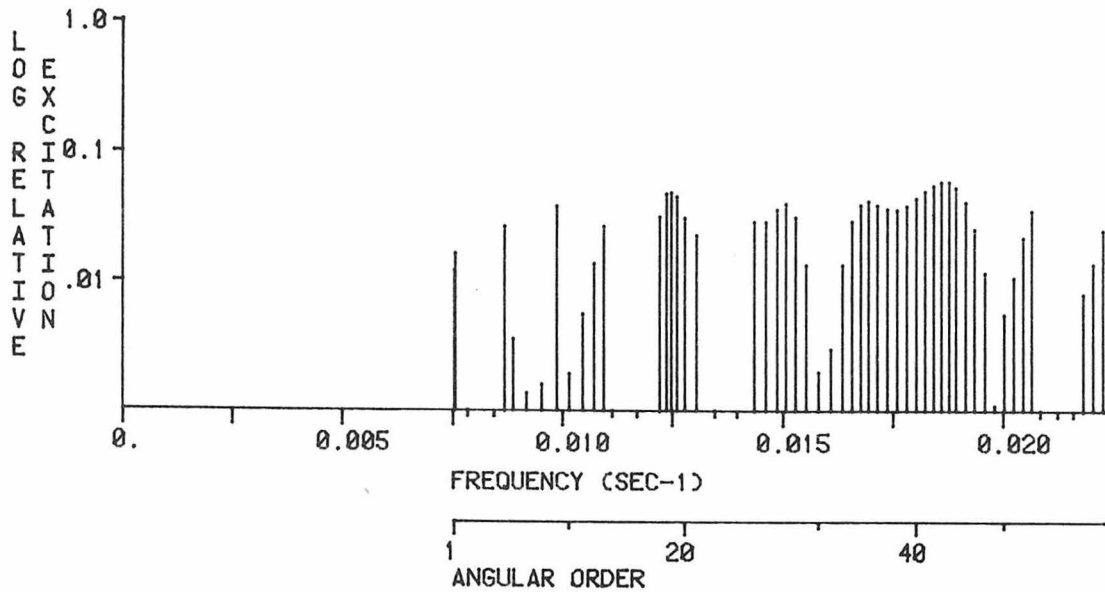
EXCITATION NORMALIZED TO 0 S 150 (RAD. COMP.) ; 0.14734600E -2

VERTICAL COMPONENT; RADIAL ORDER 21



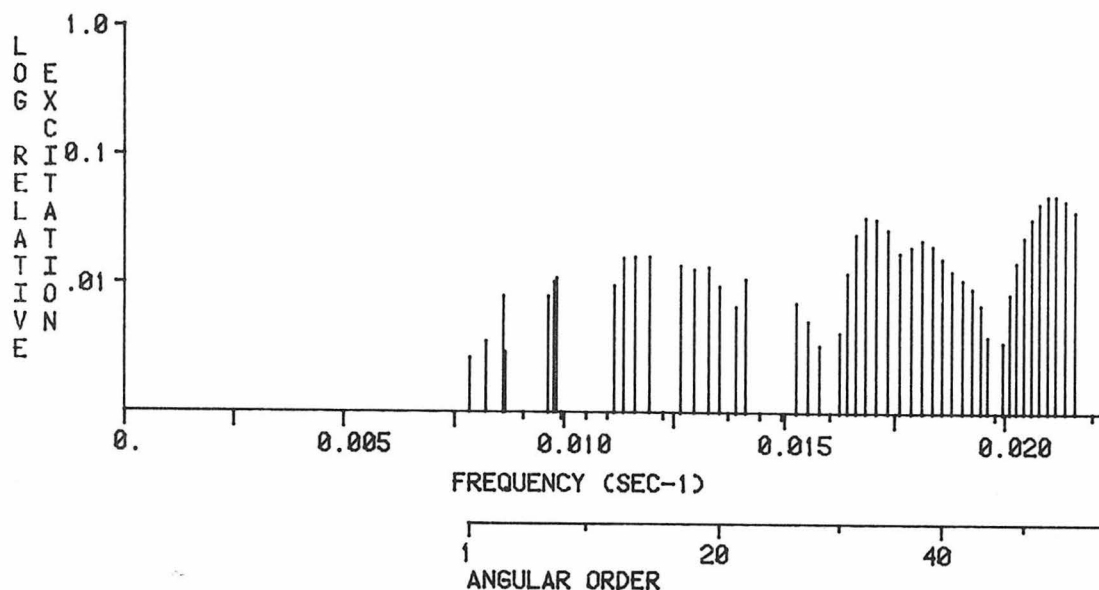
MAXIMUM EXCITATION = 0.740400E -4 CM-SEC ; (21 S 47; T= 51.75 SEC)
EXCITATION NORMALIZED TO 0 S 150 (VERT. COMP.) ; 0.16027000E -2

RADIAL COMPONENT; RADIAL ORDER 21



MAXIMUM EXCITATION = 0.886790E -4 CM-SEC ; (21 S 44; T= 53.39 SEC)
EXCITATION NORMALIZED TO 0 S 150 (RAD. COMP.) ; 0.14734600E -2

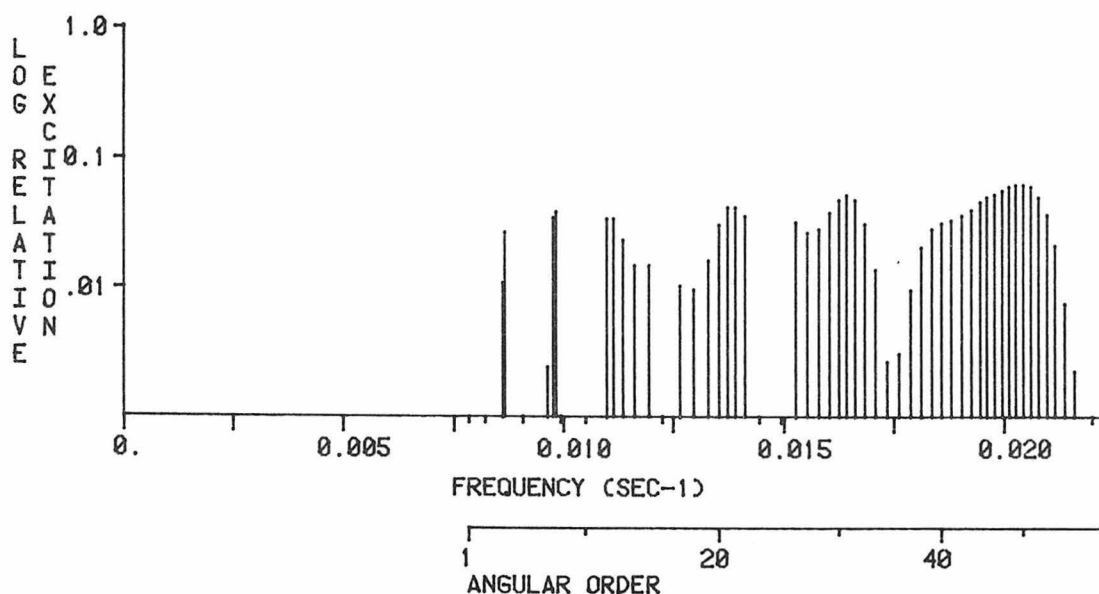
VERTICAL COMPONENT; RADIAL ORDER 22



MAXIMUM EXCITATION = 0.792430E -4 CM-SEC ; (22 S 54; T= 47.30 SEC)

EXCITATION NORMALIZED TO 0 S 150 (VERT. COMP.) ; 0.16027000E -2

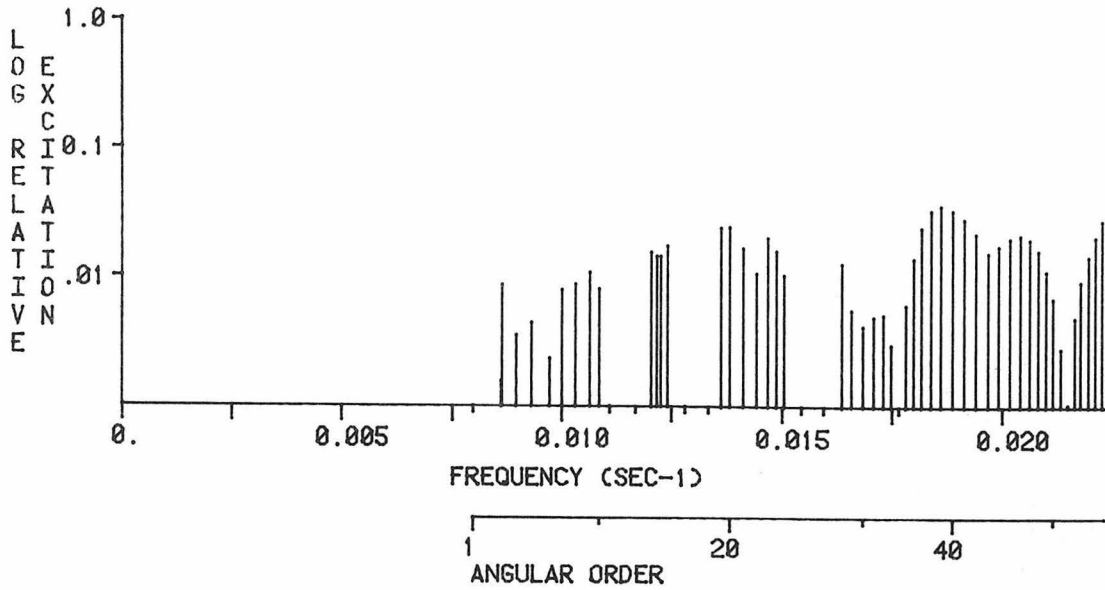
RADIAL COMPONENT; RADIAL ORDER 22



MAXIMUM EXCITATION = 0.947520E -4 CM-SEC ; (22 S 50; T= 49.03 SEC)

EXCITATION NORMALIZED TO 0 S 150 (RAD. COMP.) ; 0.14734600E -2

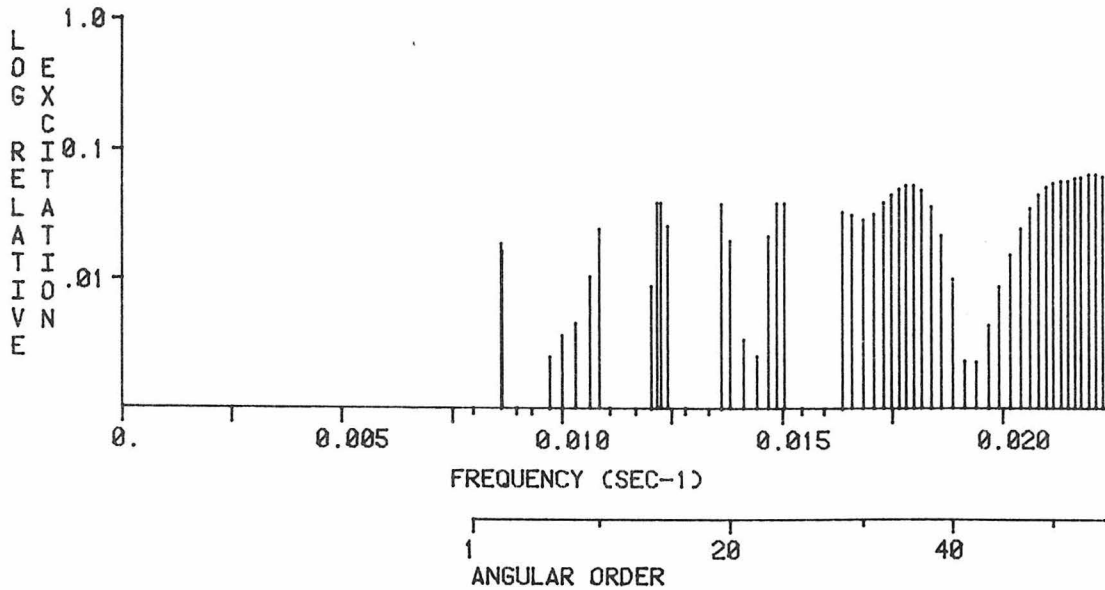
VERTICAL COMPONENT; RADIAL ORDER 23



MAXIMUM EXCITATION = 0.585315E -4 CM-SEC ; (23 S 39; T= 53.84 SEC)

EXCITATION NORMALIZED TO 0 S 150 (VERT. COMP.) ; 0.16027000E -2

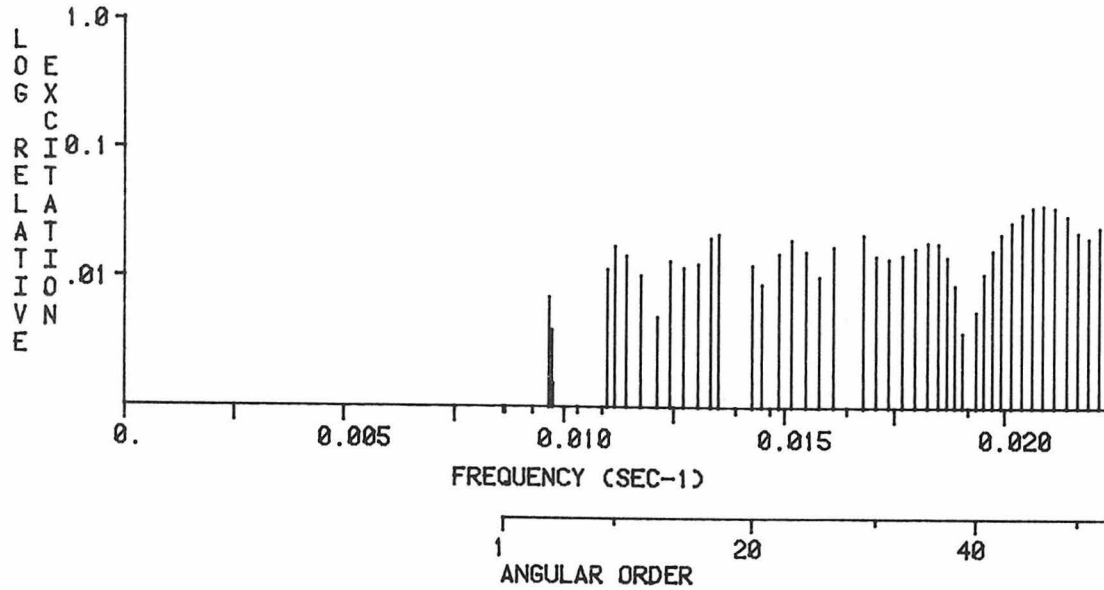
RADIAL COMPONENT; RADIAL ORDER 23



MAXIMUM EXCITATION = 0.962020E -4 CM-SEC ; (23 S 56; T= 45.34 SEC)

EXCITATION NORMALIZED TO 0 S 150 (RAD. COMP.) ; 0.14734600E -2

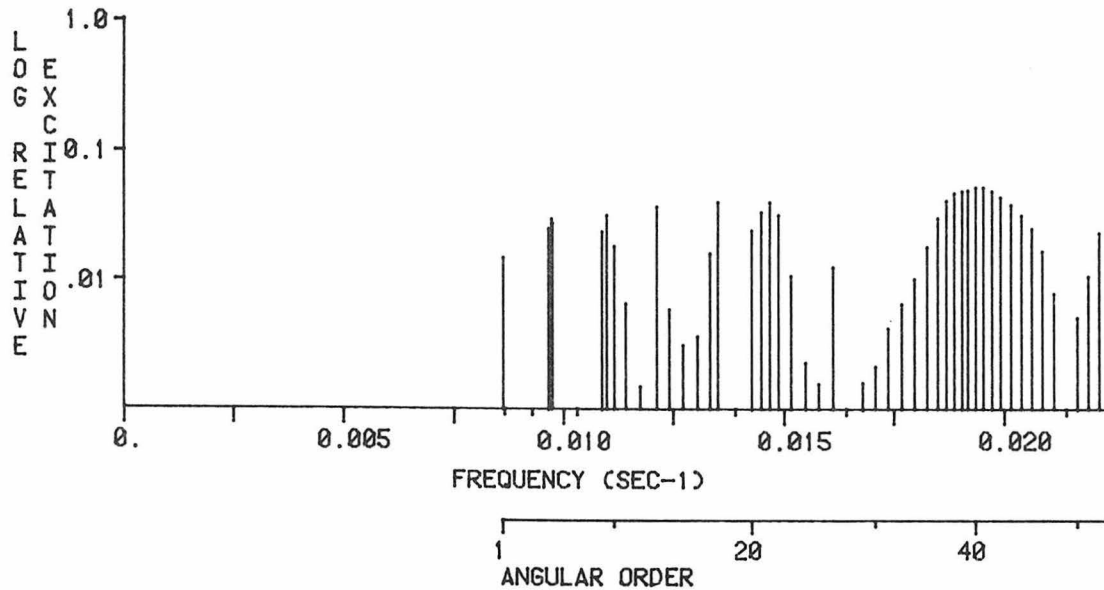
VERTICAL COMPONENT; RADIAL ORDER 24



MAXIMUM EXCITATION = 0.596450E -4 CM-SEC ; (24 S 47; T= 47.95 SEC)

EXCITATION NORMALIZED TO 0 S 150 (VERT. COMP.) ; 0.16027000E -2

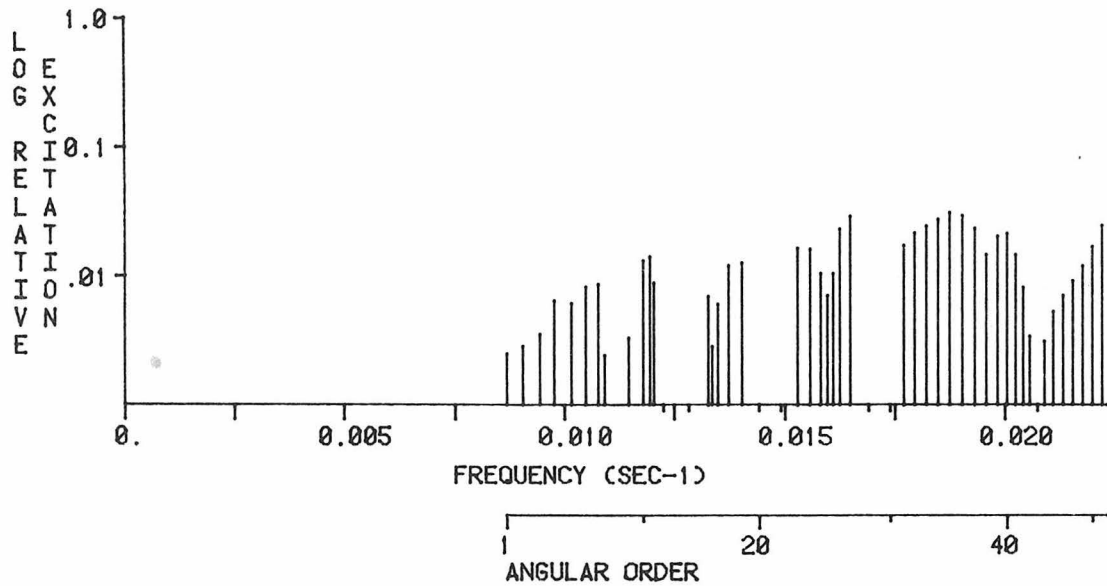
RADIAL COMPONENT; RADIAL ORDER 24



MAXIMUM EXCITATION = 0.788050E -4 CM-SEC ; (24 S 40; T= 51.77 SEC)

EXCITATION NORMALIZED TO 0 S 150 (RAD. COMP.) ; 0.14734600E -2

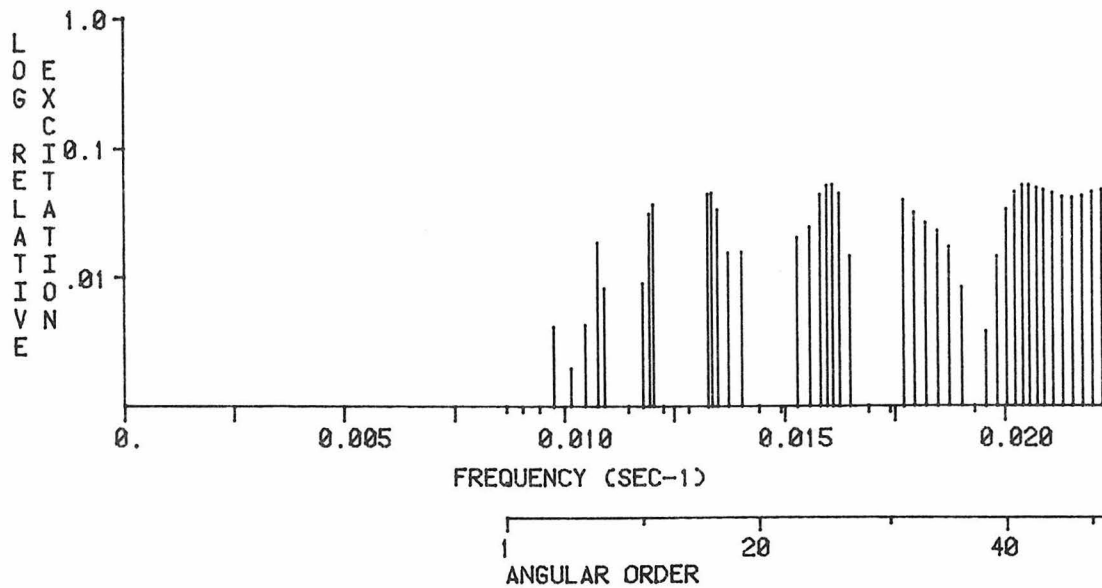
VERTICAL COMPONENT; RADIAL ORDER 25



MAXIMUM EXCITATION = 0.496596E -4 CM-SEC ; (25 S 35; T= 53.44 SEC)

EXCITATION NORMALIZED TO 0 S 150 (VERT. COMP.) ; 0.16027000E -2

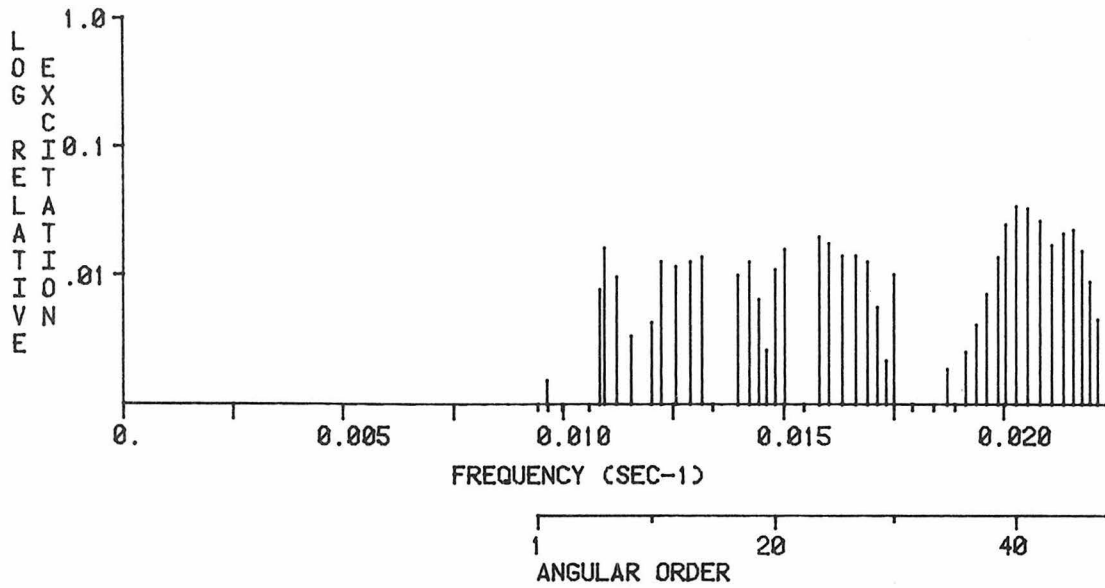
RADIAL COMPONENT; RADIAL ORDER 25



MAXIMUM EXCITATION = 0.784210E -4 CM-SEC ; (25 S 26; T= 62.21 SEC)

EXCITATION NORMALIZED TO 0 S 150 (RAD. COMP.) ; 0.14734600E -2

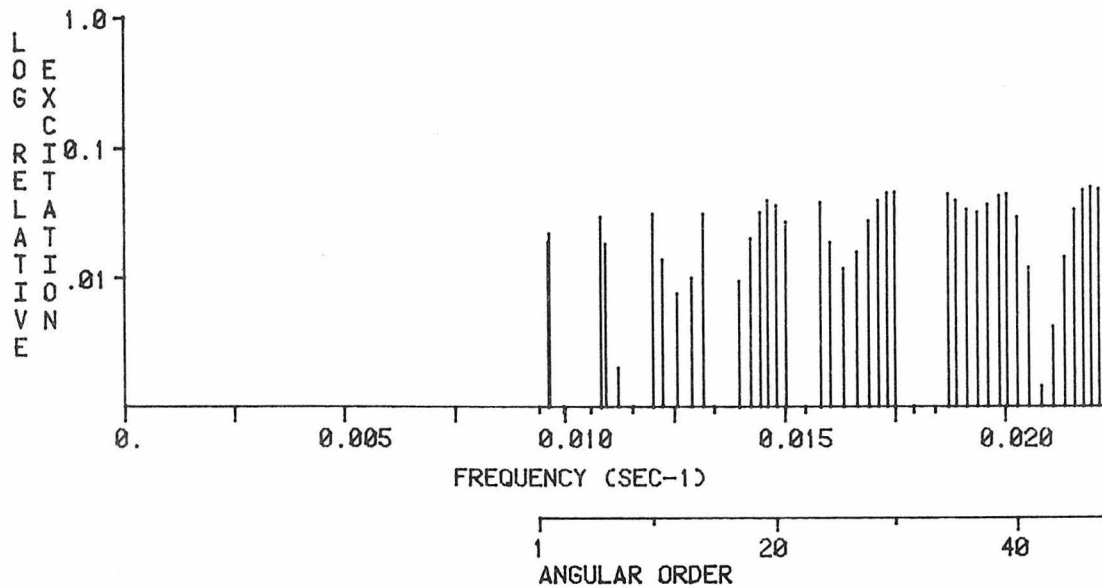
VERTICAL COMPONENT; RADIAL ORDER 26



MAXIMUM EXCITATION = 0.555833E -4 CM-SEC ; (26 S 40; T= 49.37 SEC)

EXCITATION NORMALIZED TO 0 S 150 (VERT. COMP.) ; 0.16027000E -2

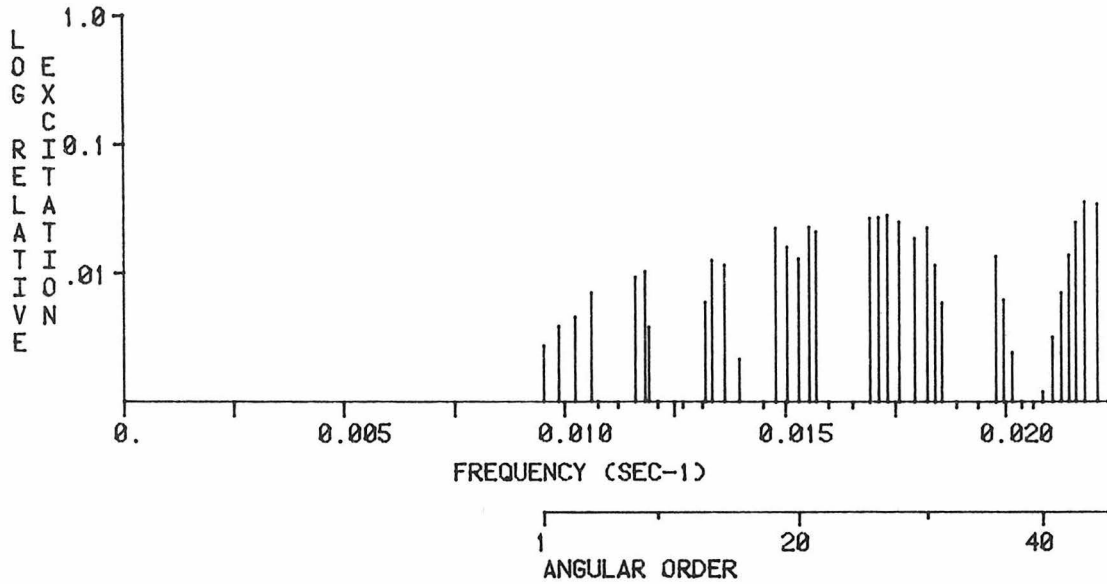
RADIAL COMPONENT; RADIAL ORDER 26



MAXIMUM EXCITATION = 0.747690E -4 CM-SEC ; (26 S 47; T= 45.64 SEC)

EXCITATION NORMALIZED TO 0 S 150 (RAD. COMP.) ; 0.14734600E -2

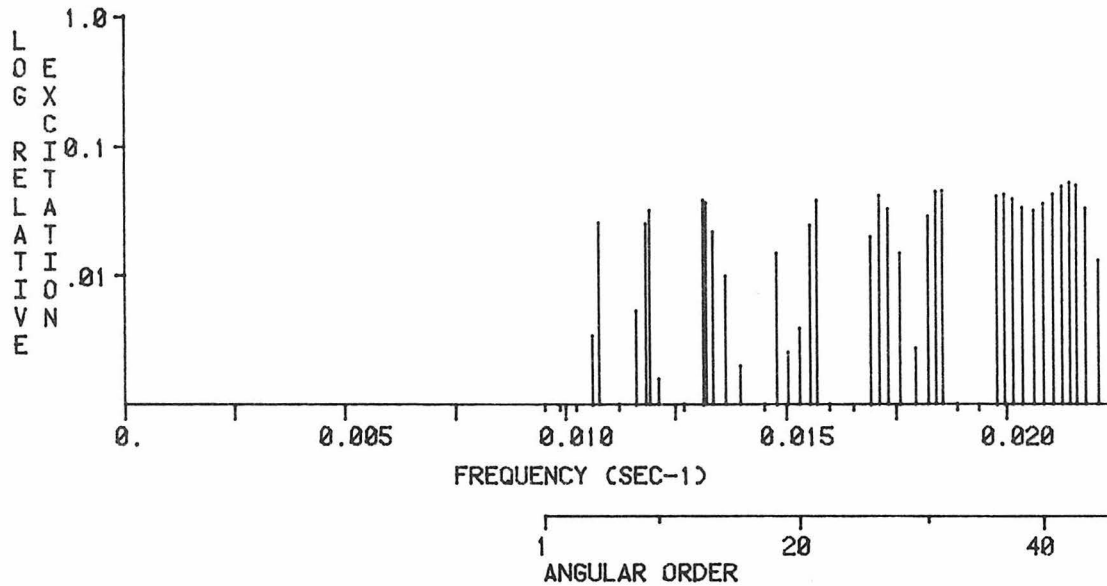
VERTICAL COMPONENT; RADIAL ORDER 27



MAXIMUM EXCITATION = 0.570595E -4 CM-SEC ; (27 S 45; T= 45.93 SEC)

EXCITATION NORMALIZED TO 0 S 150 (VERT. COMP.) ; 0.1602700E -2

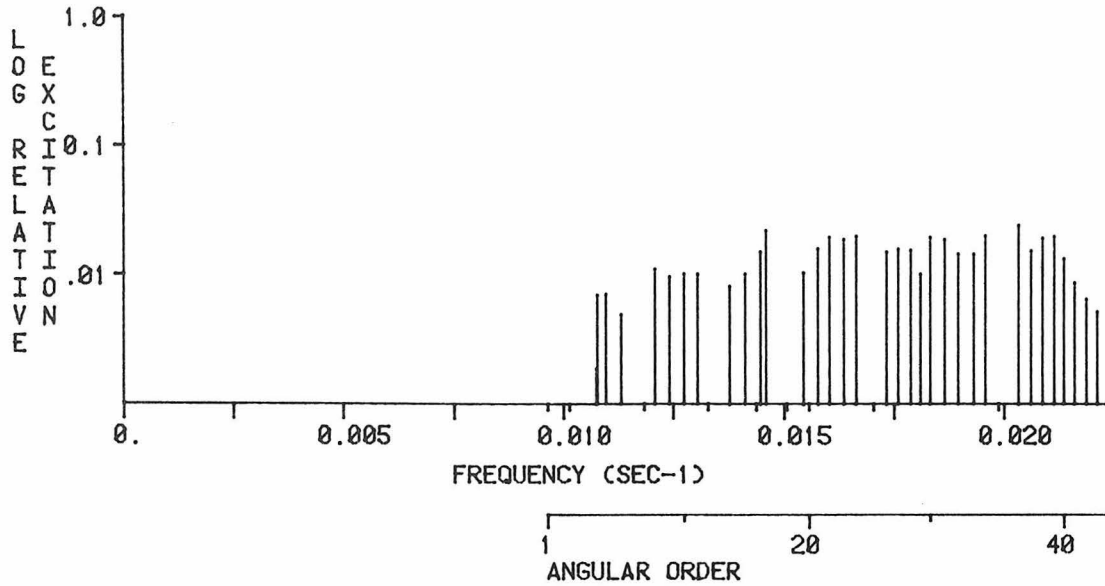
RADIAL COMPONENT; RADIAL ORDER 27



MAXIMUM EXCITATION = 0.792740E -4 CM-SEC ; (27 S 43; T= 46.75 SEC)

EXCITATION NORMALIZED TO 0 S 150 (RAD. COMP.) ; 0.1473460E -2

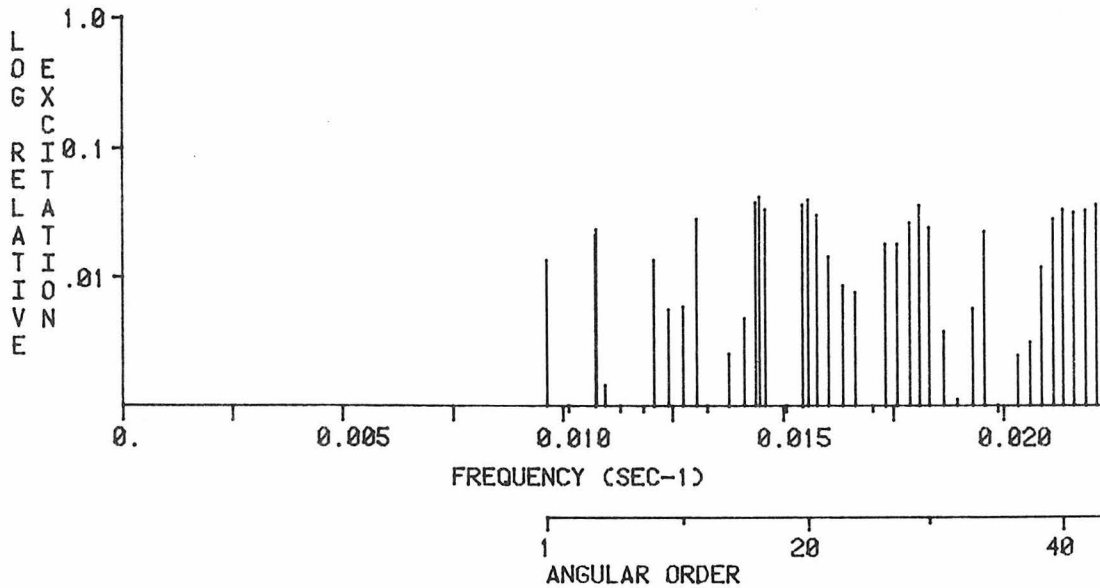
VERTICAL COMPONENT; RADIAL ORDER 28



MAXIMUM EXCITATION = 0.391189E -4 CM-SEC ; (28 S 36; T= 49.30 SEC)

EXCITATION NORMALIZED TO 0 S 150 (VERT. COMP.) ; 0.16027000E -2

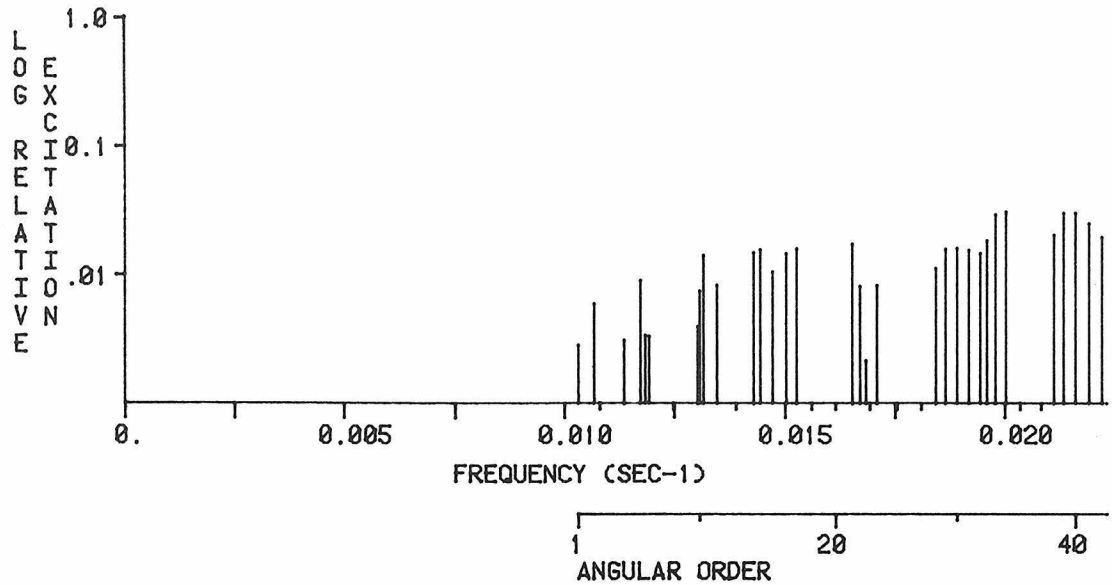
RADIAL COMPONENT; RADIAL ORDER 28



MAXIMUM EXCITATION = 0.632620E -4 CM-SEC ; (28 S 16; T= 69.24 SEC)

EXCITATION NORMALIZED TO 0 S 150 (RAD. COMP.) ; 0.14734600E -2

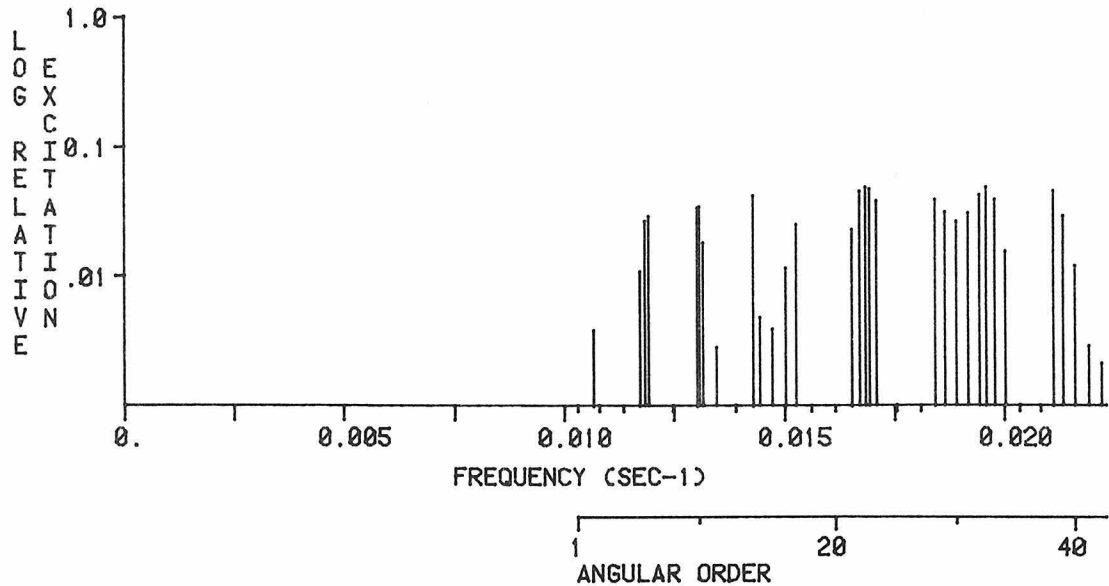
VERTICAL COMPONENT; RADIAL ORDER 29



MAXIMUM EXCITATION = 0.501729E -4 CM-SEC ; (29 S 35; T= 50.01 SEC)

EXCITATION NORMALIZED TO 0 S 150 (VERT. COMP.) ; 0.16027000E -2

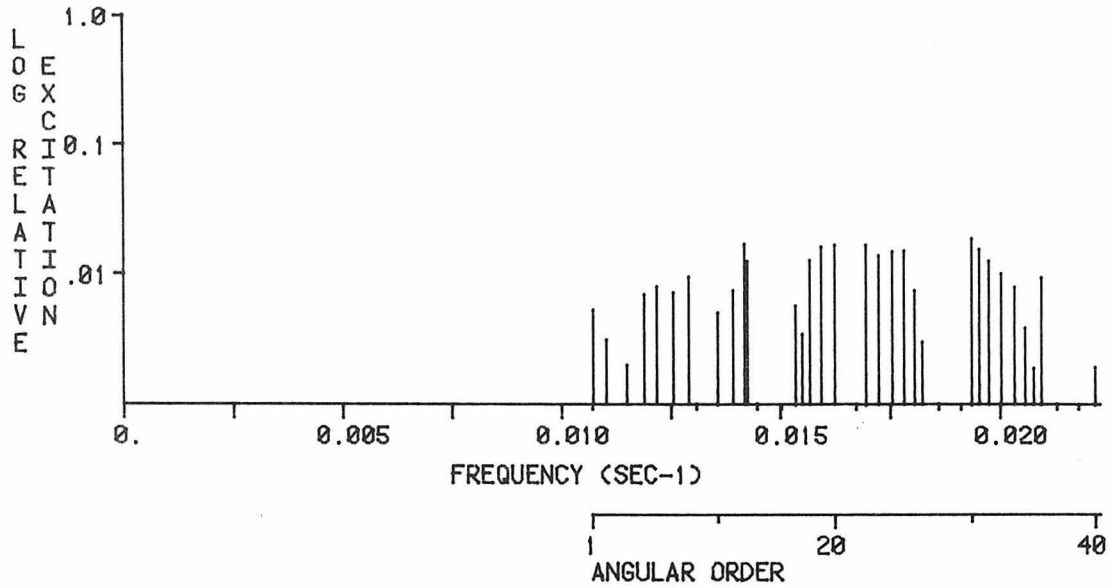
RADIAL COMPONENT; RADIAL ORDER 29



MAXIMUM EXCITATION = 0.733070E -4 CM-SEC ; (29 S 33; T= 51.13 SEC)

EXCITATION NORMALIZED TO 0 S 150 (RAD. COMP.) ; 0.14734600E -2

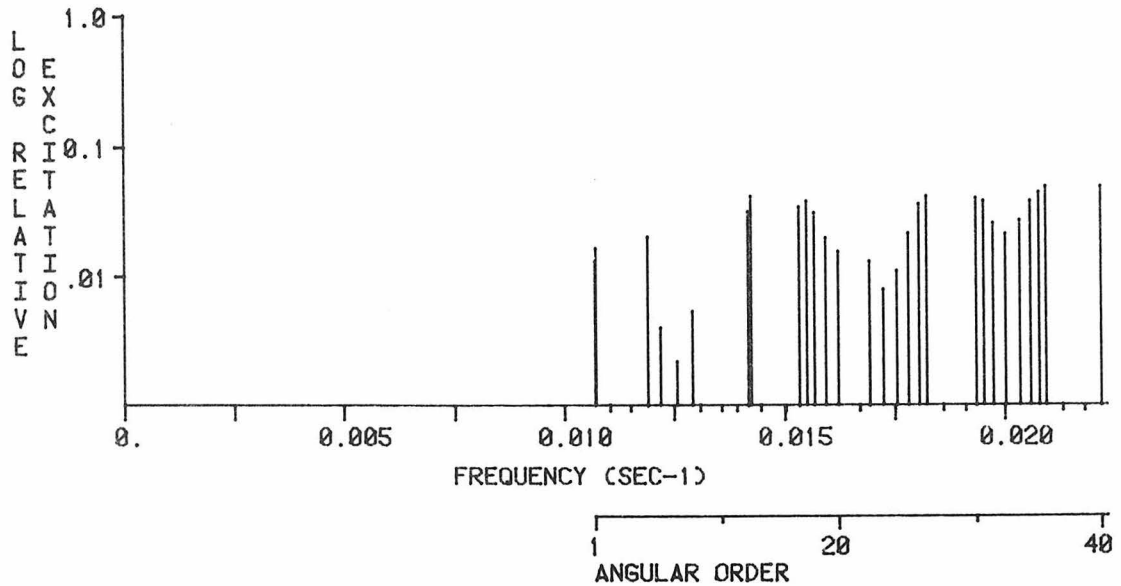
VERTICAL COMPONENT; RADIAL ORDER 30



MAXIMUM EXCITATION = 0.309811E -4 CM-SEC ; (30 S 30; T= 51.79 SEC)

EXCITATION NORMALIZED TO 0 S 150 (VERT. COMP.) ; 0.16027000E -2

RADIAL COMPONENT; RADIAL ORDER 30

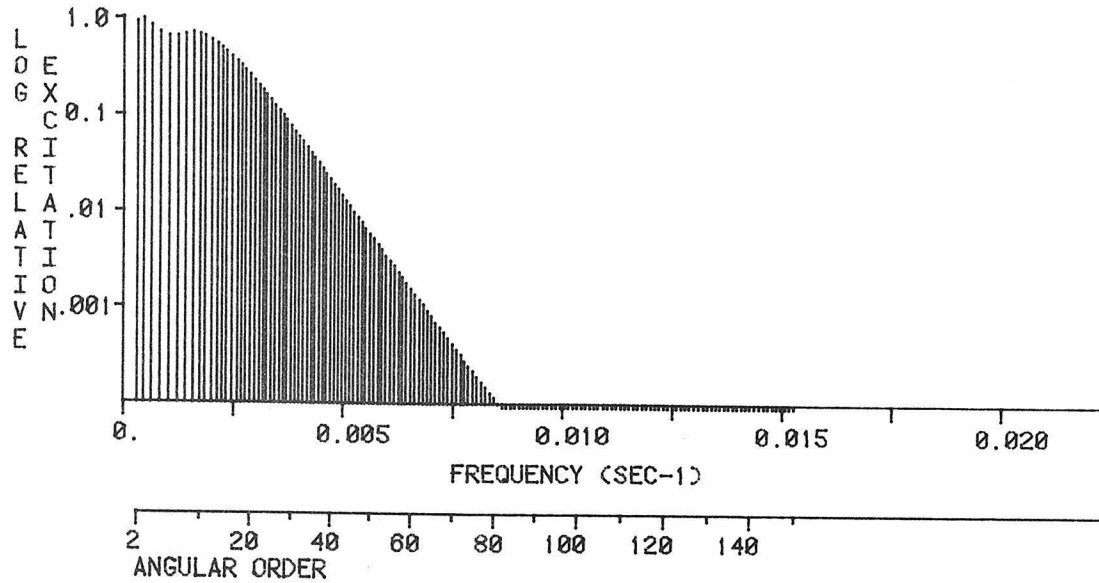


MAXIMUM EXCITATION = 0.737600E -4 CM-SEC ; (30 S 37; T= 47.84 SEC)

EXCITATION NORMALIZED TO 0 S 150 (RAD. COMP.) ; 0.14734600E -2

Figure A2.2 - The spheroidal excitation spectra for the 1964 Alaska earthquake with attenuation included. Both vertical and radial components of displacement are shown for the fundamental branch and first thirty overtone branches. The data window begins 12 hours after the origin time of the earthquake and has a duration of 20 hours. This corresponds to the average window in Dziewonski and Gilbert's (1972, 1973) studies of the Alaskan earthquake. All excitations are normalized to the maximum fundamental mode excitation and modes with an excitation more than 80 db below that maximum are plotted as small negative tick marks along the horizontal axis. This figure extends over the following 31 pages.

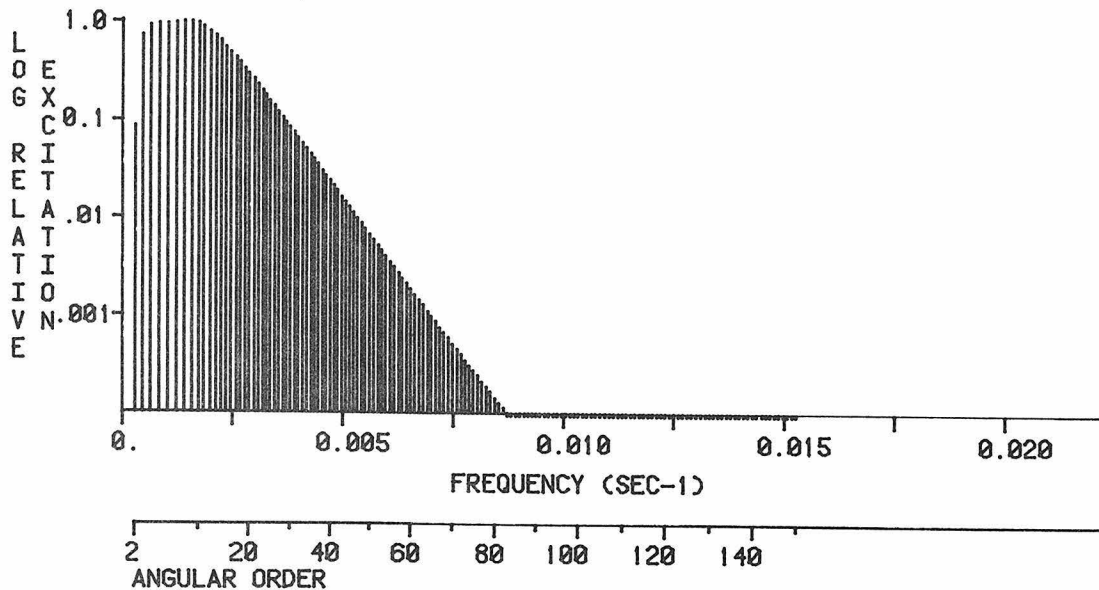
VERTICAL COMPONENT; RADIAL ORDER 0



MAXIMUM EXCITATION = 0.133859E -3 CM-SEC ; (0 S 3; T=2134.00 SEC)

ATTENUATION INCLUDED; RECORD STARTS AT 12.00 HRS.; LENGTH = 20.00 HRS.

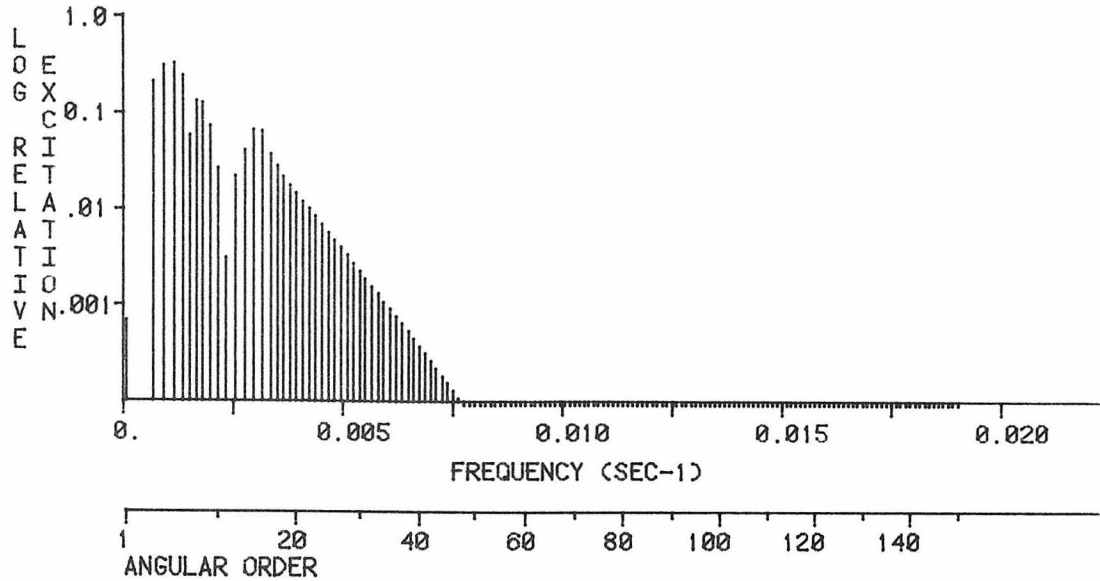
RADIAL COMPONENT; RADIAL ORDER 0



MAXIMUM EXCITATION = 0.844350E -4 CM-SEC ; (0 S 9; T= 633.95 SEC)

ATTENUATION INCLUDED; RECORD STARTS AT 12.00 HRS.; LENGTH = 20.00 HRS.

VERTICAL COMPONENT; RADIAL ORDER 1

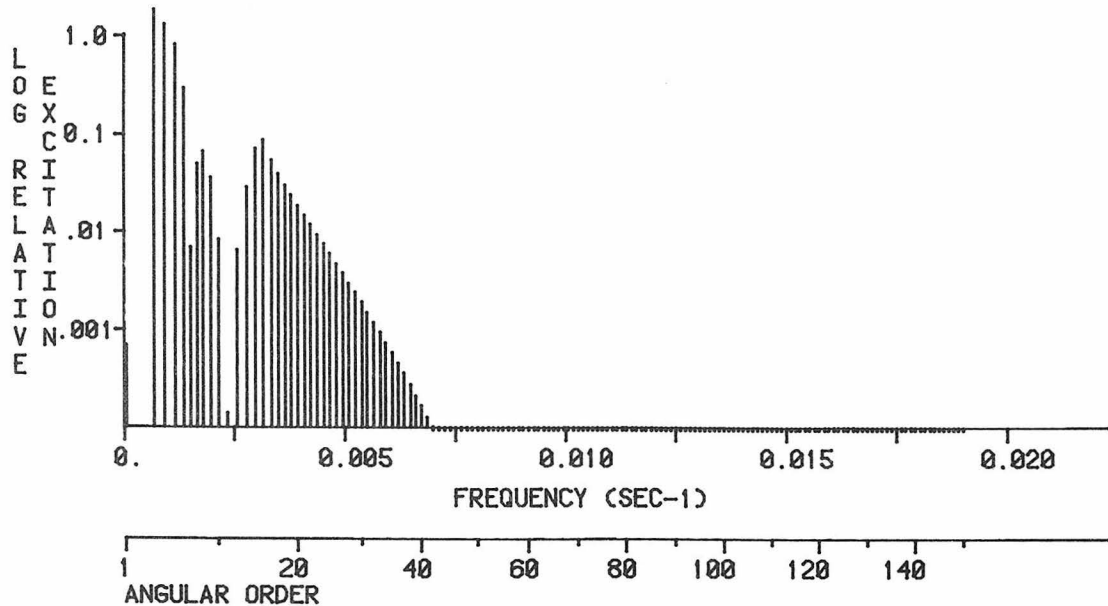


MAXIMUM EXCITATION = 0.431996E -4 CM-SEC ; (I S 4; T= 851.83 SEC)

EXCITATION NORMALIZED TO 0 S 3 (VERT. COMP.) ; 0.13385900E -3

ATTENUATION INCLUDED; RECORD STARTS AT 12.00 HRS.; LENGTH = 20.00 HRS.

RADIAL COMPONENT; RADIAL ORDER 1

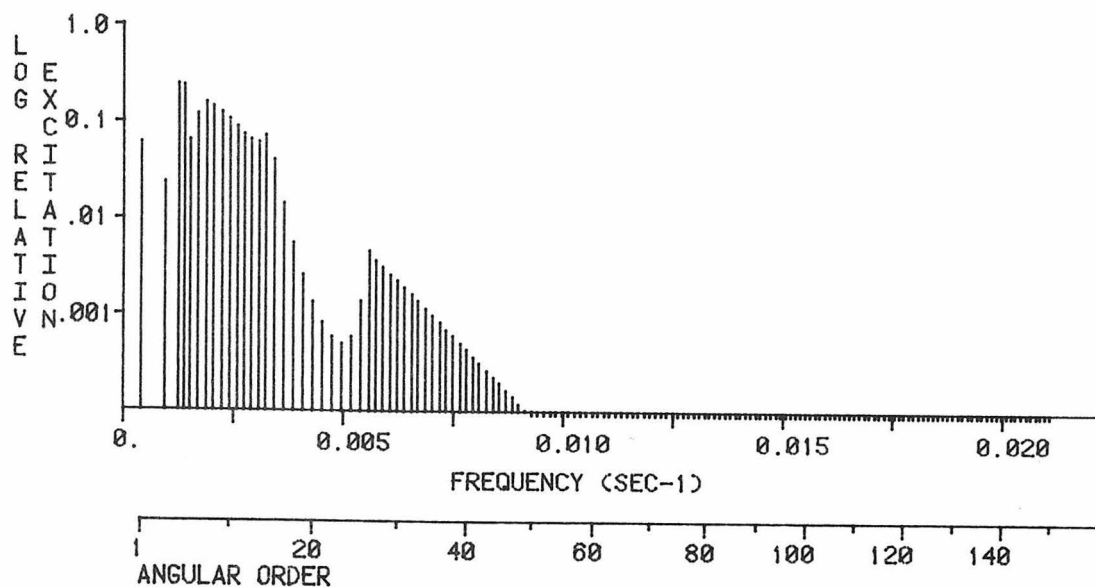


MAXIMUM EXCITATION = 0.152990E -3 CM-SEC ; (I S 2; T=1469.85 SEC)

EXCITATION NORMALIZED TO 0 S 9 (RAD. COMP.) ; 0.84435000E -4

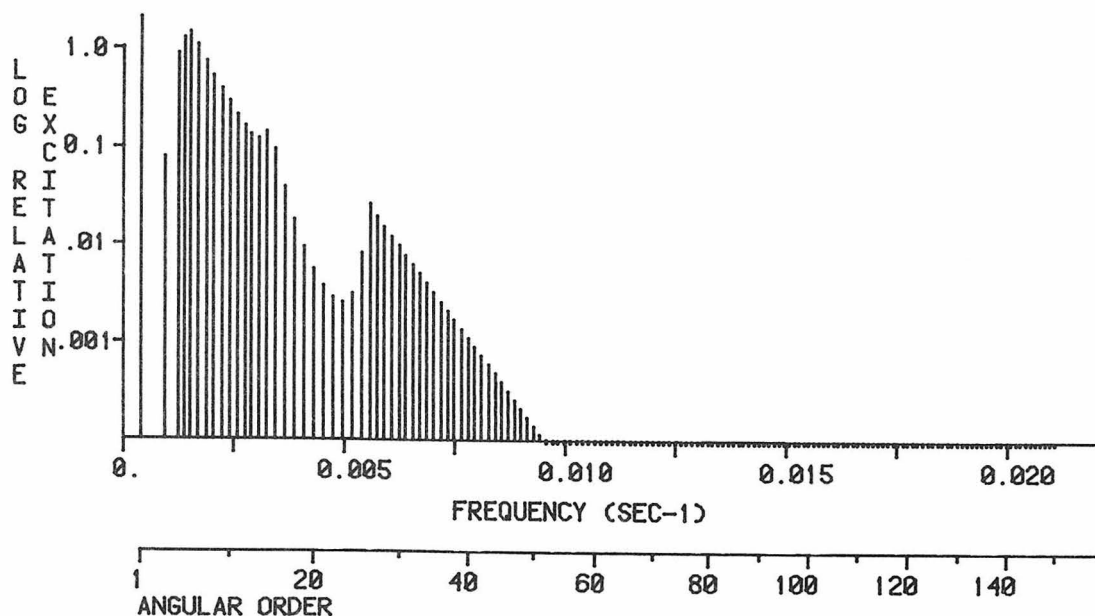
ATTENUATION INCLUDED; RECORD STARTS AT 12.00 HRS.; LENGTH = 20.00 HRS.

VERTICAL COMPONENT; RADIAL ORDER 2



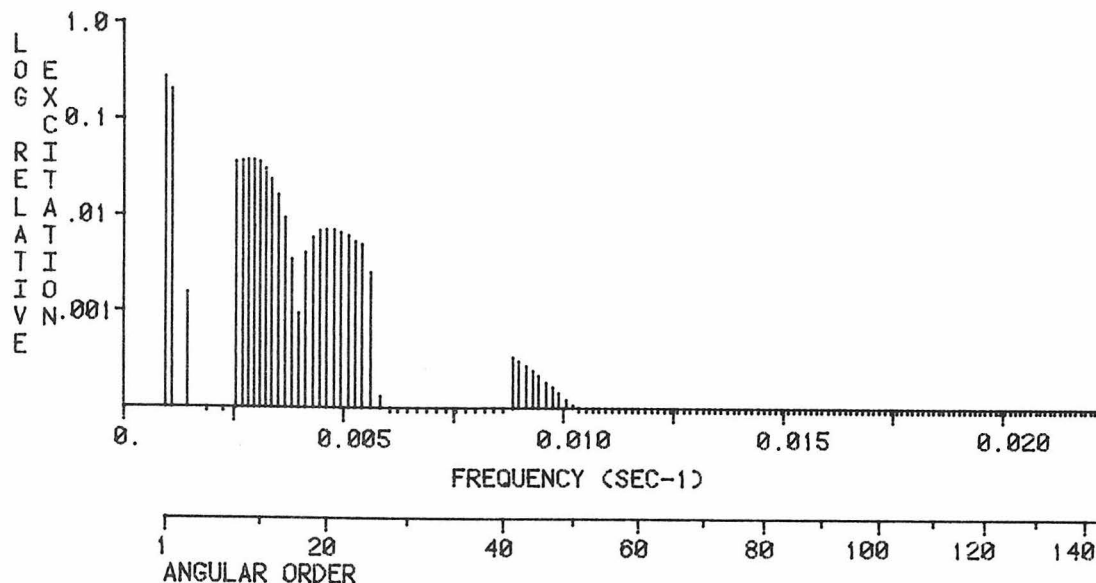
MAXIMUM EXCITATION = 0.329690E -4 CM-SEC ; (2 S 3; T= 805.58 SEC)
EXCITATION NORMALIZED TO 0 S 3 (VERT. COMP.) ; 0.13385900E -3
ATTENUATION INCLUDED; RECORD STARTS AT 12.00 HRS.; LENGTH = 20.00 HRS.

RADIAL COMPONENT; RADIAL ORDER 2



MAXIMUM EXCITATION = 0.171256E -3 CM-SEC ; (2 S 1; T=2476.08 SEC)
EXCITATION NORMALIZED TO 0 S 9 (RAD. COMP.) ; 0.84435000E -4
ATTENUATION INCLUDED; RECORD STARTS AT 12.00 HRS.; LENGTH = 20.00 HRS.

VERTICAL COMPONENT; RADIAL ORDER 3

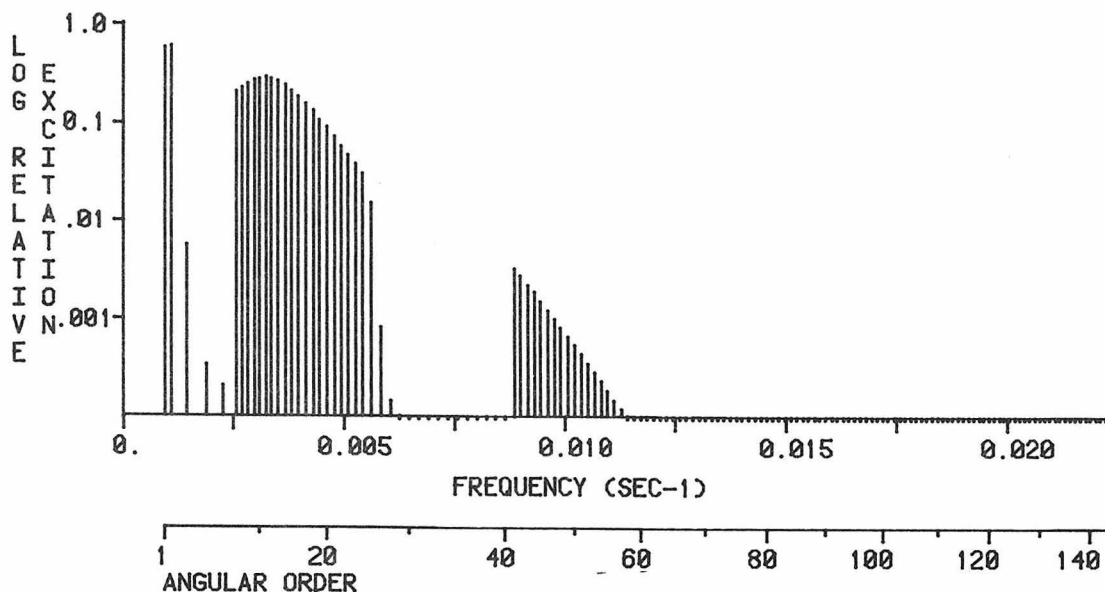


MAXIMUM EXCITATION = 0.363886E -4 CM-SEC ; (3 S 1; T=1060.82 SEC)

EXCITATION NORMALIZED TO 0 S 3 (VERT. COMP.) ; 0.13385900E -3

ATTENUATION INCLUDED; RECORD STARTS AT 12.00 HRS.; LENGTH = 20.00 HRS.

RADIAL COMPONENT; RADIAL ORDER 3

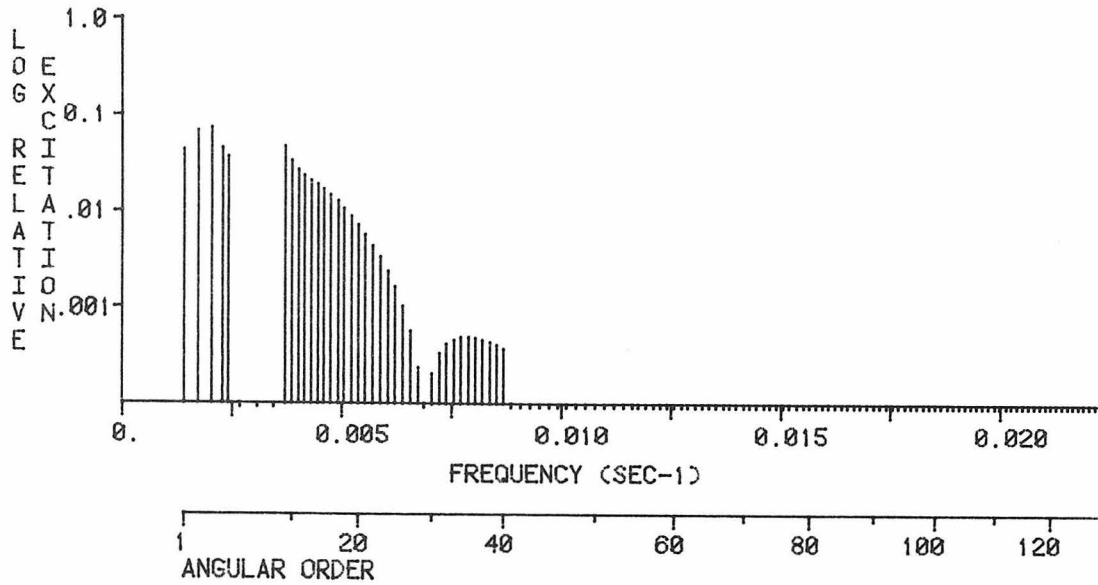


MAXIMUM EXCITATION = 0.500137E -4 CM-SEC ; (3 S 2; T= 903.15 SEC)

EXCITATION NORMALIZED TO 0 S 9 (RAD. COMP.) ; 0.84435000E -4

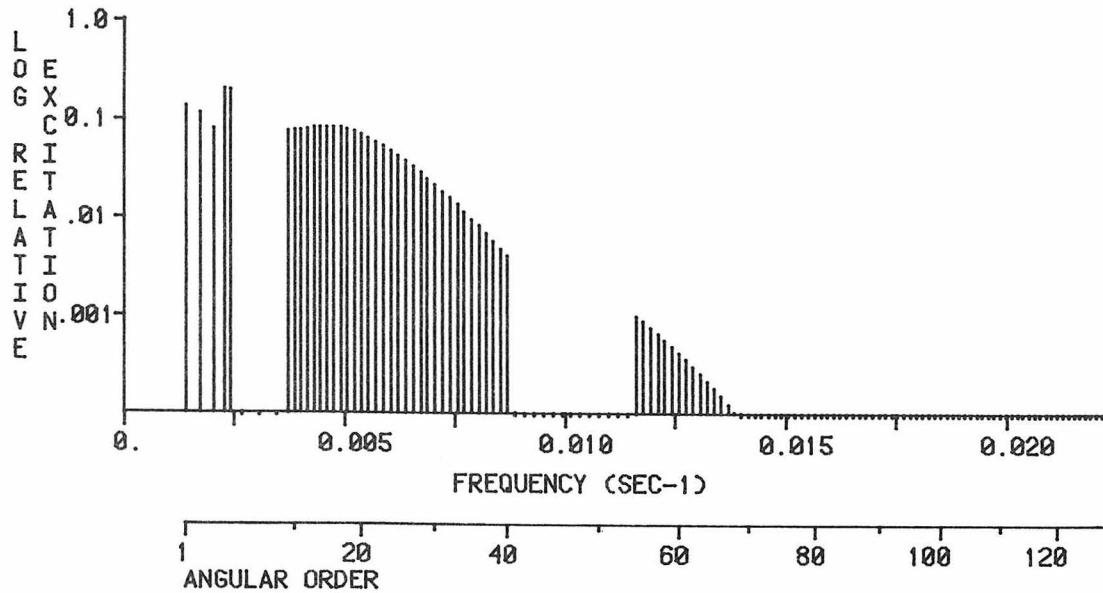
ATTENUATION INCLUDED; RECORD STARTS AT 12.00 HRS.; LENGTH = 20.00 HRS.

VERTICAL COMPONENT; RADIAL ORDER 4



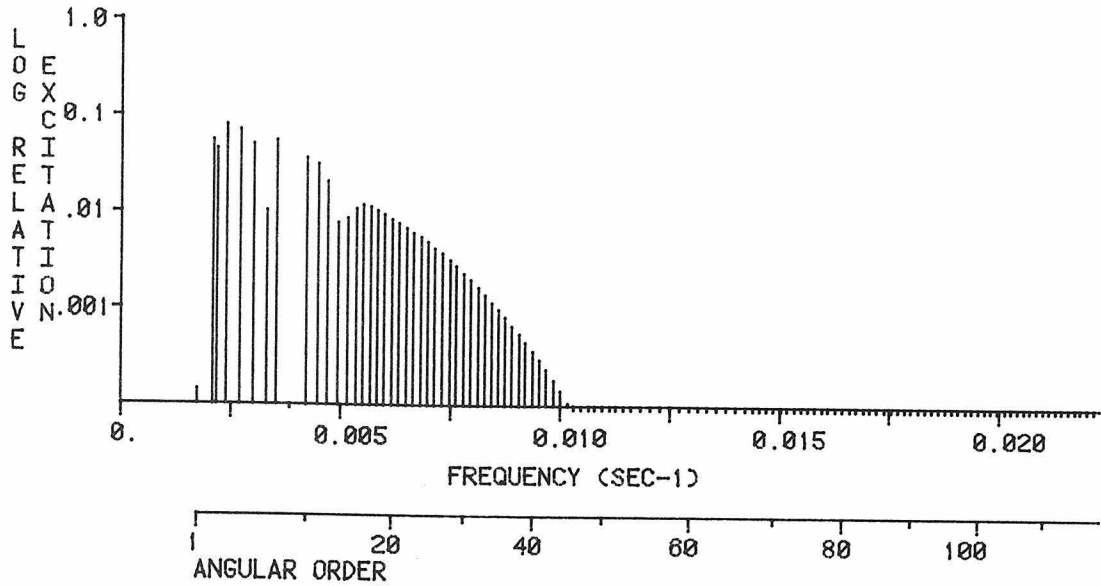
MAXIMUM EXCITATION = 0.973750E -5 CM-SEC ; (4 S 3; T= 488.38 SEC)
EXCITATION NORMALIZED TO 0 S 3 (VERT. COMP.) ; 0.13385900E -3
ATTENUATION INCLUDED; RECORD STARTS AT 12.00 HRS.; LENGTH = 20.00 HRS.

RADIAL COMPONENT; RADIAL ORDER 4



MAXIMUM EXCITATION = 0.165687E -4 CM-SEC ; (4 S 4; T= 438.61 SEC)
EXCITATION NORMALIZED TO 0 S 9 (RAD. COMP.) ; 0.84435000E -4
ATTENUATION INCLUDED; RECORD STARTS AT 12.00 HRS.; LENGTH = 20.00 HRS.

VERTICAL COMPONENT; RADIAL ORDER 5

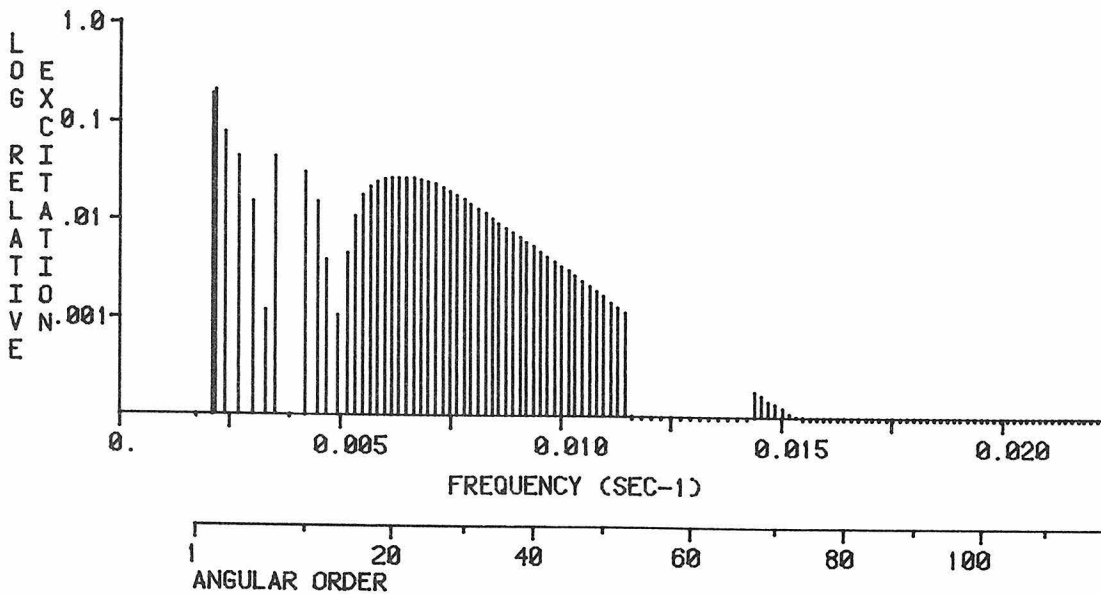


MAXIMUM EXCITATION = 0.105146E -4 CM-SEC ; (5 S 4; T= 420.50 SEC)

EXCITATION NORMALIZED TO 0 S 3 (VERT. COMP.) ; 0.13385900E -3

ATTENUATION INCLUDED; RECORD STARTS AT 12.00 HRS.; LENGTH = 20.00 HRS.

RADIAL COMPONENT; RADIAL ORDER 5

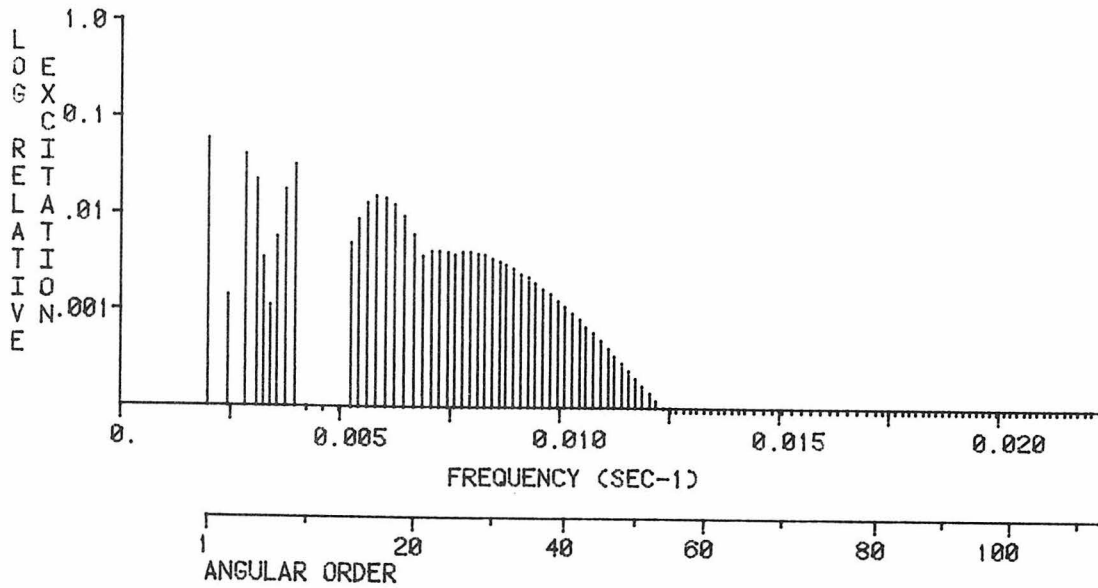


MAXIMUM EXCITATION = 0.170693E -4 CM-SEC ; (5 S 3; T= 460.70 SEC)

EXCITATION NORMALIZED TO 0 S 9 (RAD. COMP.) ; 0.84435000E -4

ATTENUATION INCLUDED; RECORD STARTS AT 12.00 HRS.; LENGTH = 20.00 HRS.

VERTICAL COMPONENT; RADIAL ORDER 6

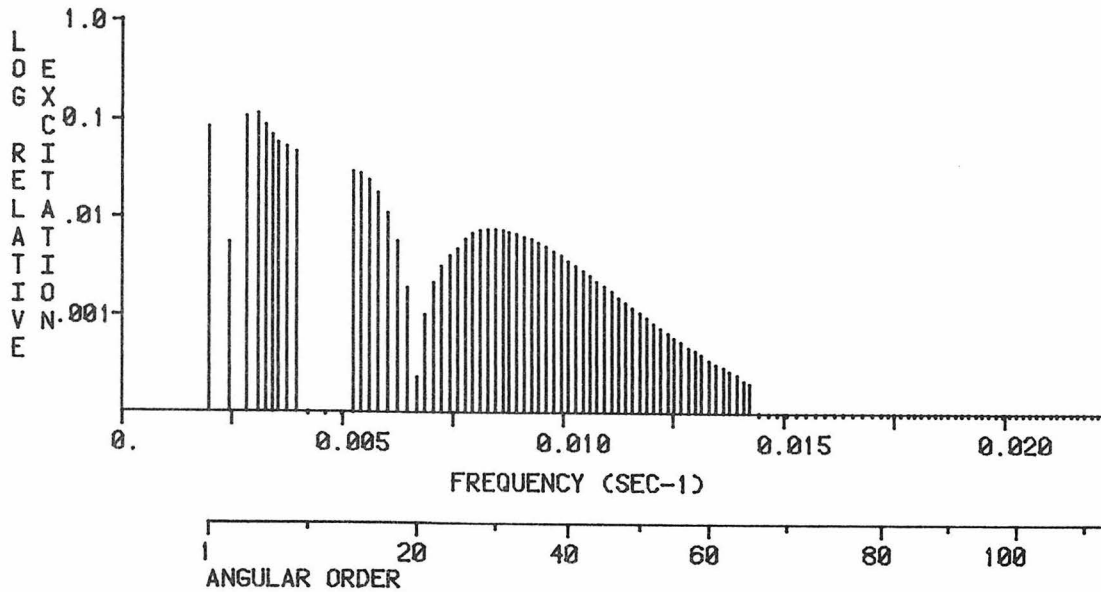


MAXIMUM EXCITATION = 0.784760E -5 CM-SEC ; (6 S 1; T= 505.47 SEC)

EXCITATION NORMALIZED TO 0 S 3 (VERT. COMP.) ; 0.13385900E -3

ATTENUATION INCLUDED; RECORD STARTS AT 12.00 HRS.; LENGTH = 20.00 HRS.

RADIAL COMPONENT; RADIAL ORDER 6

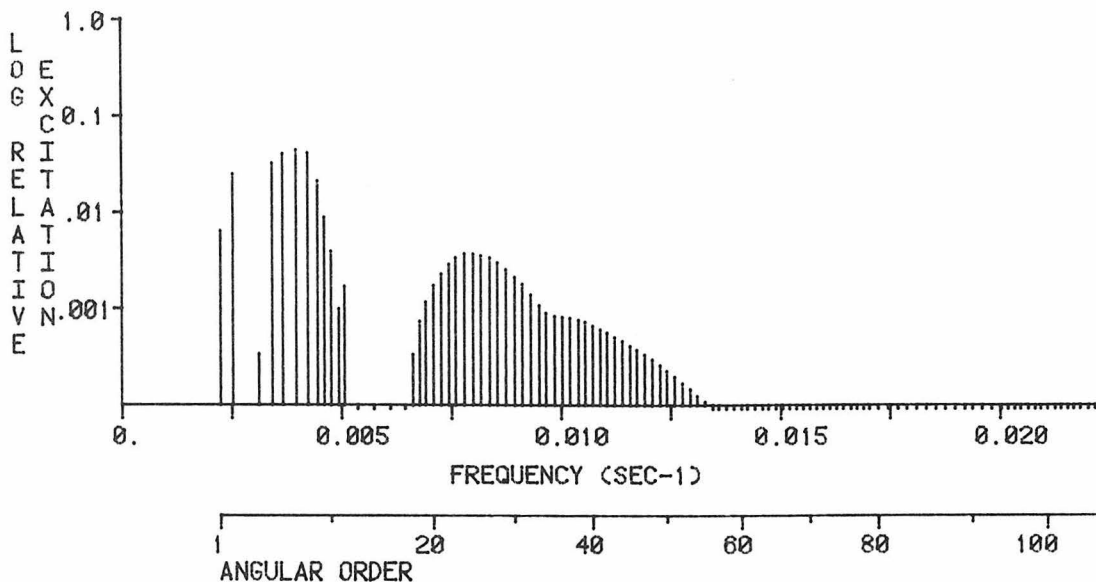


MAXIMUM EXCITATION = 0.967950E -5 CM-SEC ; (6 S 4; T= 323.58 SEC)

EXCITATION NORMALIZED TO 0 S 9 (RAD. COMP.) ; 0.84435000E -4

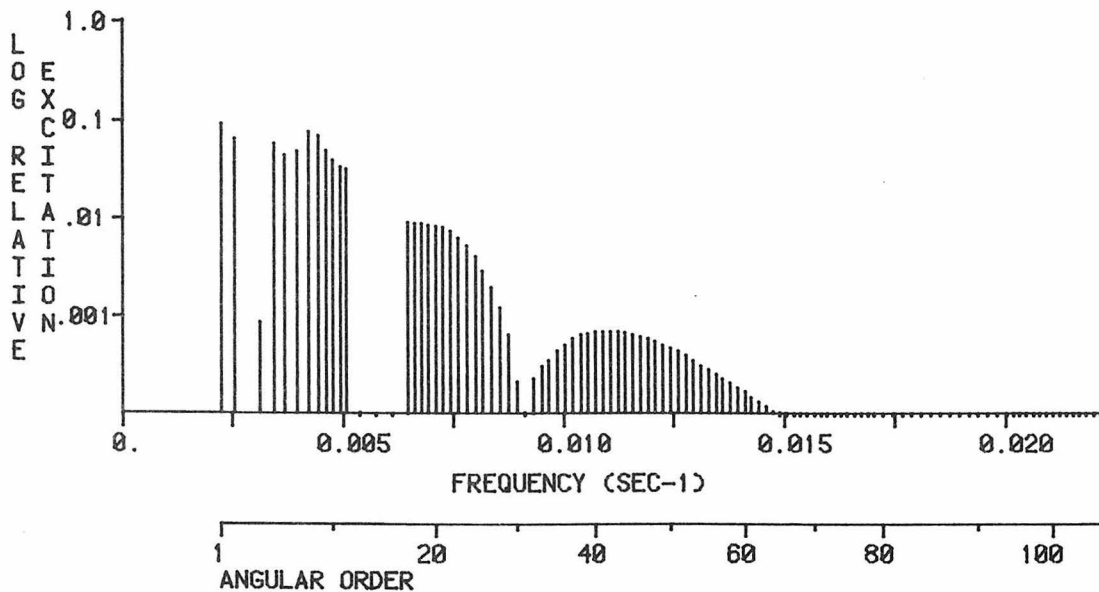
ATTENUATION INCLUDED; RECORD STARTS AT 12.00 HRS.; LENGTH = 20.00 HRS.

VERTICAL COMPONENT; RADIAL ORDER 7



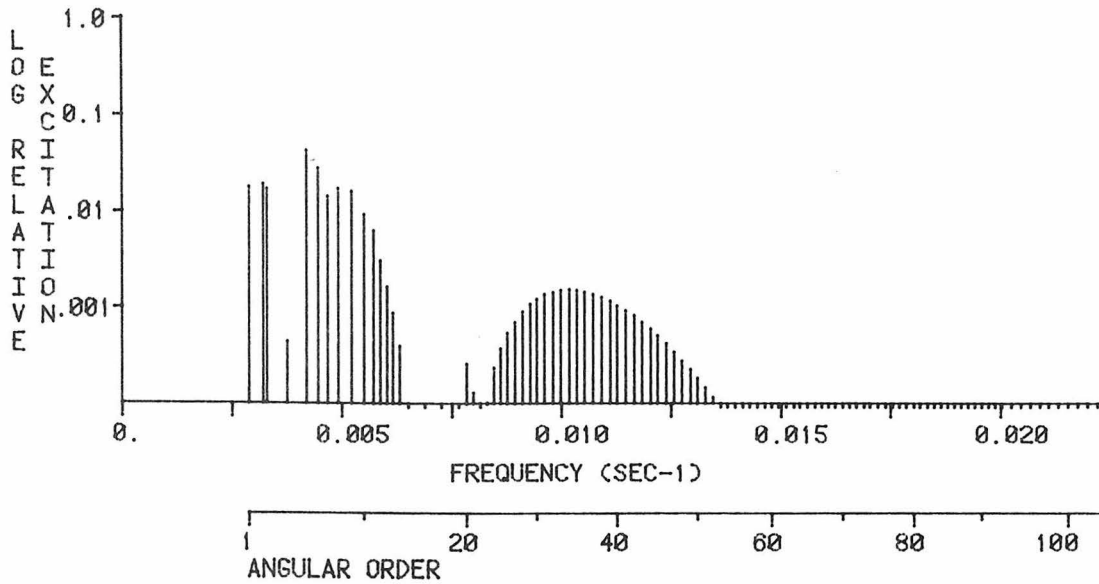
MAXIMUM EXCITATION = 0.578848E -5 CM-SEC ; (7 S 6; T= 252.79 SEC)
EXCITATION NORMALIZED TO 0 S 3 (VERT. COMP.) ; 0.13385900E -3
ATTENUATION INCLUDED; RECORD STARTS AT 12.00 HRS.; LENGTH = 20.00 HRS.

RADIAL COMPONENT; RADIAL ORDER 7



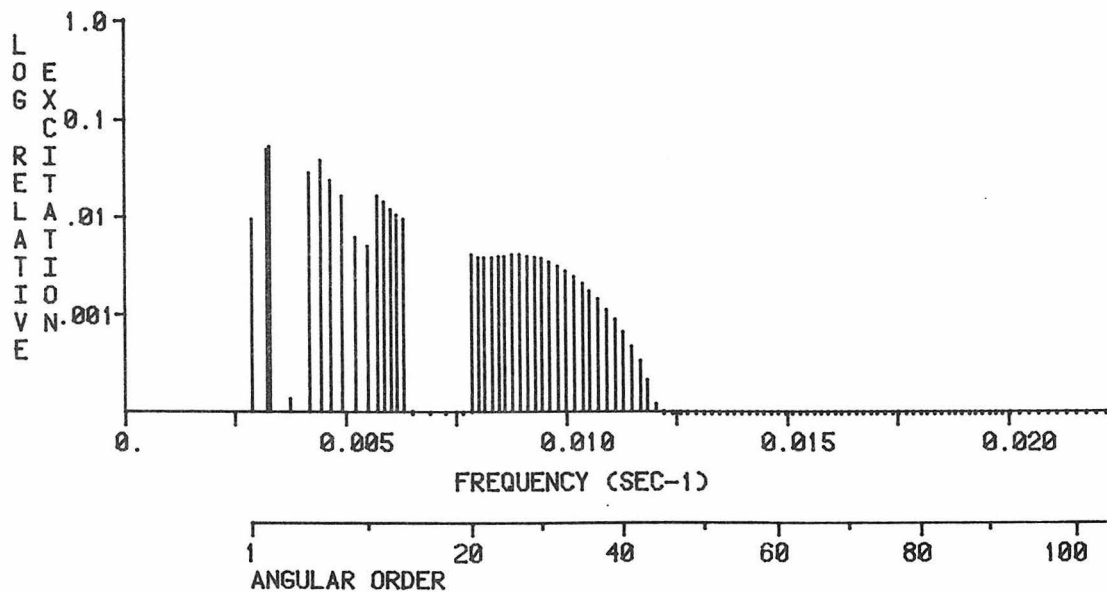
MAXIMUM EXCITATION = 0.748790E -5 CM-SEC ; (7 S 1; T= 449.22 SEC)
EXCITATION NORMALIZED TO 0 S 9 (RAD. COMP.) ; 0.84435000E -4
ATTENUATION INCLUDED; RECORD STARTS AT 12.00 HRS.; LENGTH = 20.00 HRS.

VERTICAL COMPONENT; RADIAL ORDER 8



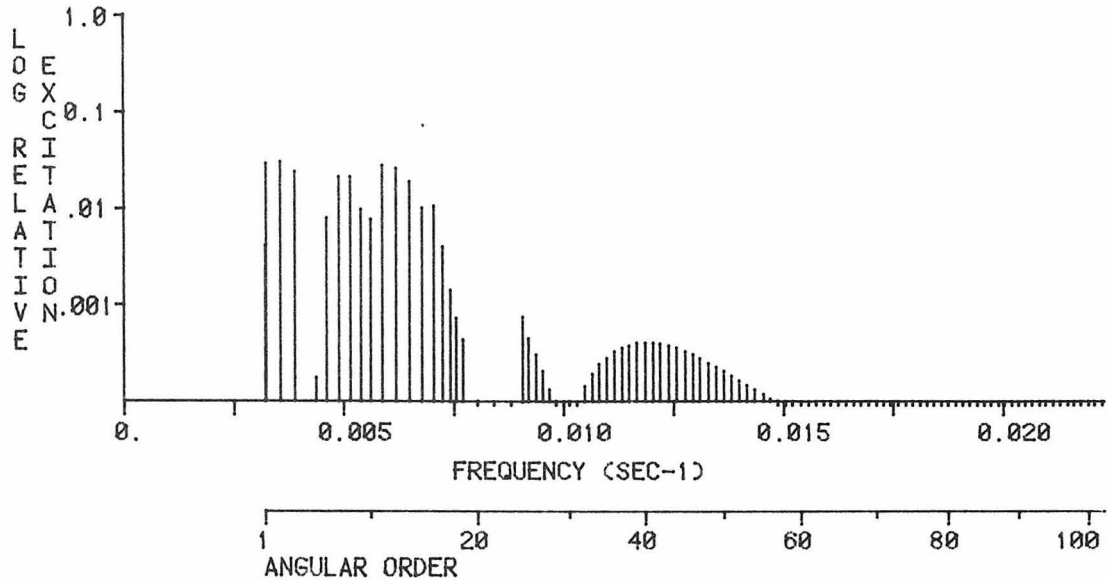
MAXIMUM EXCITATION = 0.560617E -5 CM-SEC ; (8 S 5; T= 240.07 SEC)
EXCITATION NORMALIZED TO 0 S 3 (VERT. COMP.) ; 0.13385900E -3
ATTENUATION INCLUDED; RECORD STARTS AT 12.00 HRS.; LENGTH = 20.00 HRS.

RADIAL COMPONENT; RADIAL ORDER 8



MAXIMUM EXCITATION = 0.444913E -5 CM-SEC ; (8 S 3; T= 304.26 SEC)
EXCITATION NORMALIZED TO 0 S 9 (RAD. COMP.) ; 0.84435000E -4
ATTENUATION INCLUDED; RECORD STARTS AT 12.00 HRS.; LENGTH = 20.00 HRS.

VERTICAL COMPONENT; RADIAL ORDER 9

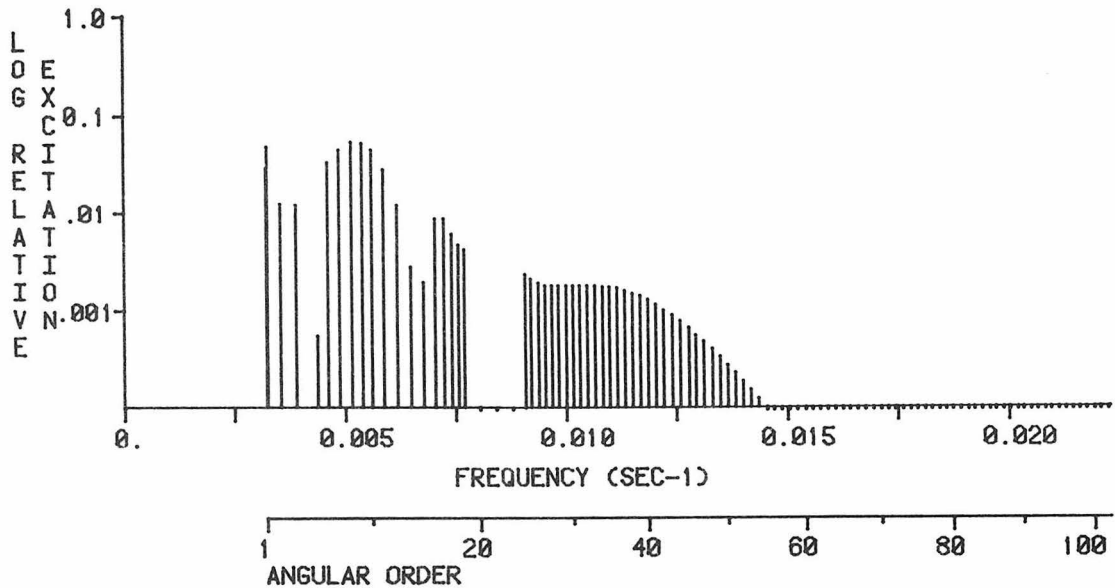


MAXIMUM EXCITATION = 0.406762E -5 CM-SEC ; (9 S 3; T= 281.35 SEC)

EXCITATION NORMALIZED TO 0 S 3 (VERT. COMP.) ; 0.13385900E -3

ATTENUATION INCLUDED; RECORD STARTS AT 12.00 HRS.; LENGTH = 20.00 HRS.

RADIAL COMPONENT; RADIAL ORDER 9

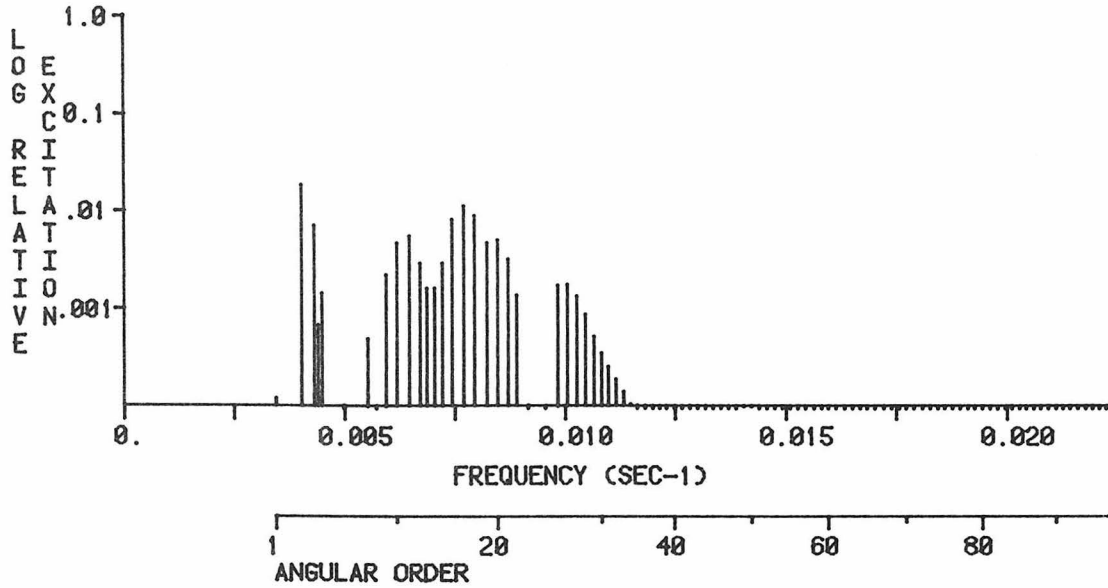


MAXIMUM EXCITATION = 0.456009E -5 CM-SEC ; (9 S 8; T= 194.45 SEC)

EXCITATION NORMALIZED TO 0 S 9 (RAD. COMP.) ; 0.84435000E -4

ATTENUATION INCLUDED; RECORD STARTS AT 12.00 HRS.; LENGTH = 20.00 HRS.

VERTICAL COMPONENT; RADIAL ORDER 10

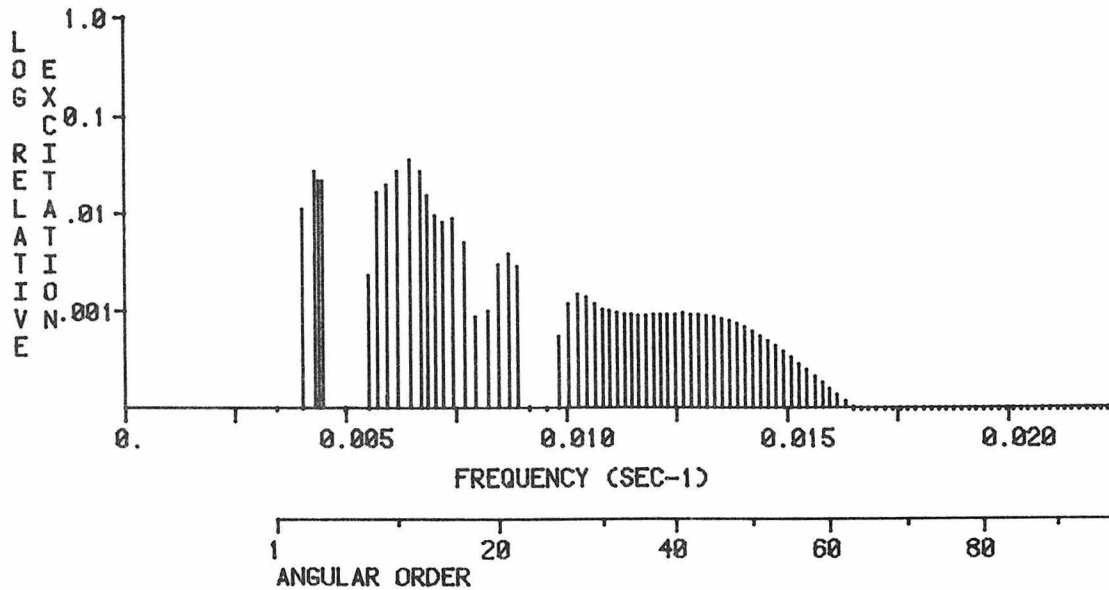


MAXIMUM EXCITATION = 0.246734E -5 CM-SEC ; (10 S 2; T= 247.85 SEC)

EXCITATION NORMALIZED TO 0 S 3 (VERT. COMP.) ; 0.13385900E -3

ATTENUATION INCLUDED; RECORD STARTS AT 12.00 HRS.; LENGTH = 20.00 HRS.

RADIAL COMPONENT; RADIAL ORDER 10

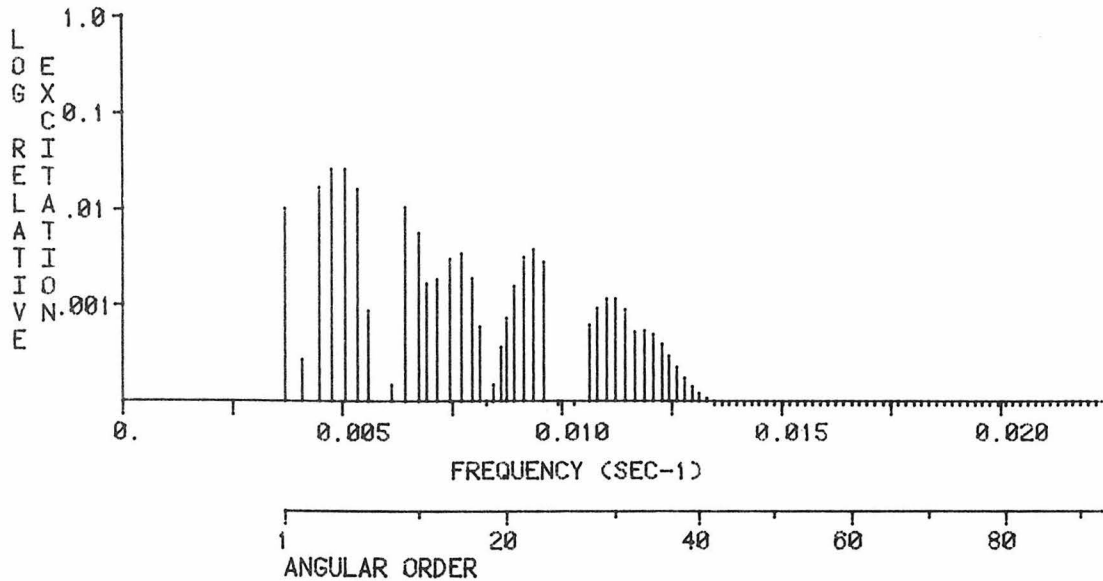


MAXIMUM EXCITATION = 0.295592E -5 CM-SEC ; (10 S 11; T= 155.03 SEC)

EXCITATION NORMALIZED TO 0 S 9 (RAD. COMP.) ; 0.84435000E -4

ATTENUATION INCLUDED; RECORD STARTS AT 12.00 HRS.; LENGTH = 20.00 HRS.

VERTICAL COMPONENT; RADIAL ORDER 11

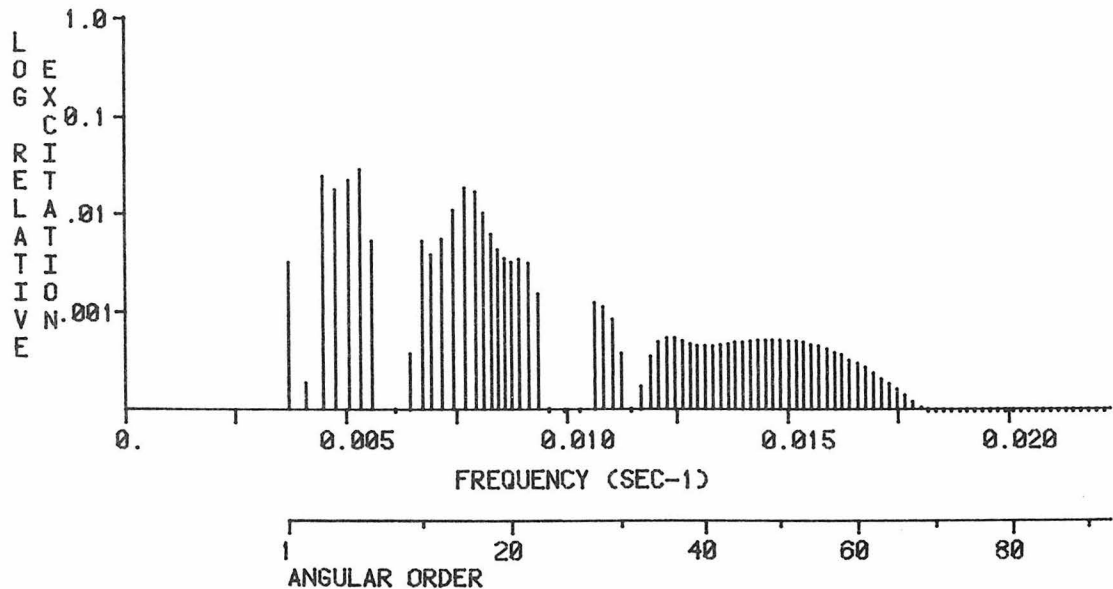


MAXIMUM EXCITATION = 0.350098E -5 CM-SEC ; (11 S 5; T= 197.13 SEC)

EXCITATION NORMALIZED TO 0 S 3 (VERT. COMP.) ; 0.13385900E -3

ATTENUATION INCLUDED; RECORD STARTS AT 12.00 HRS.; LENGTH = 20.00 HRS.

RADIAL COMPONENT; RADIAL ORDER 11

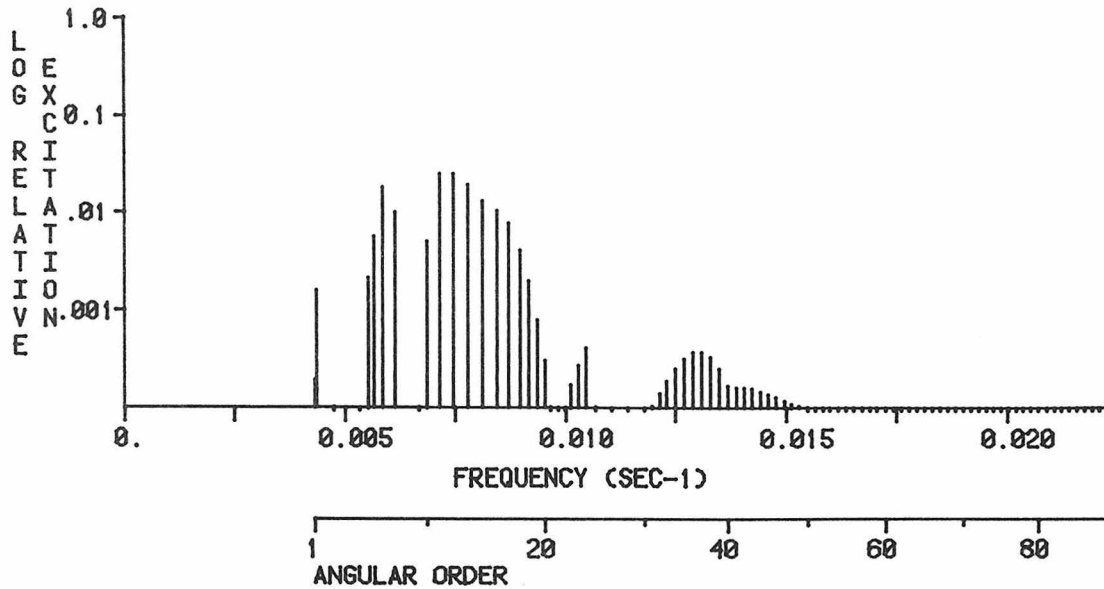


MAXIMUM EXCITATION = 0.235643E -5 CM-SEC ; (11 S 6; T= 186.94 SEC)

EXCITATION NORMALIZED TO 0 S 9 (RAD. COMP.) ; 0.84435000E -4

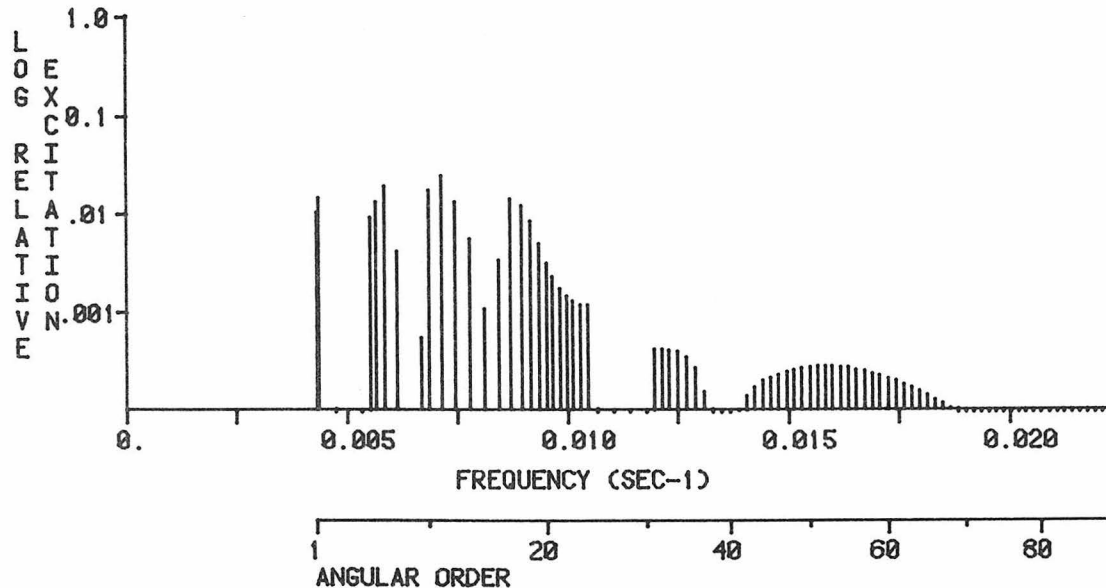
ATTENUATION INCLUDED; RECORD STARTS AT 12.00 HRS.; LENGTH = 20.00 HRS.

VERTICAL COMPONENT; RADIAL ORDER 12



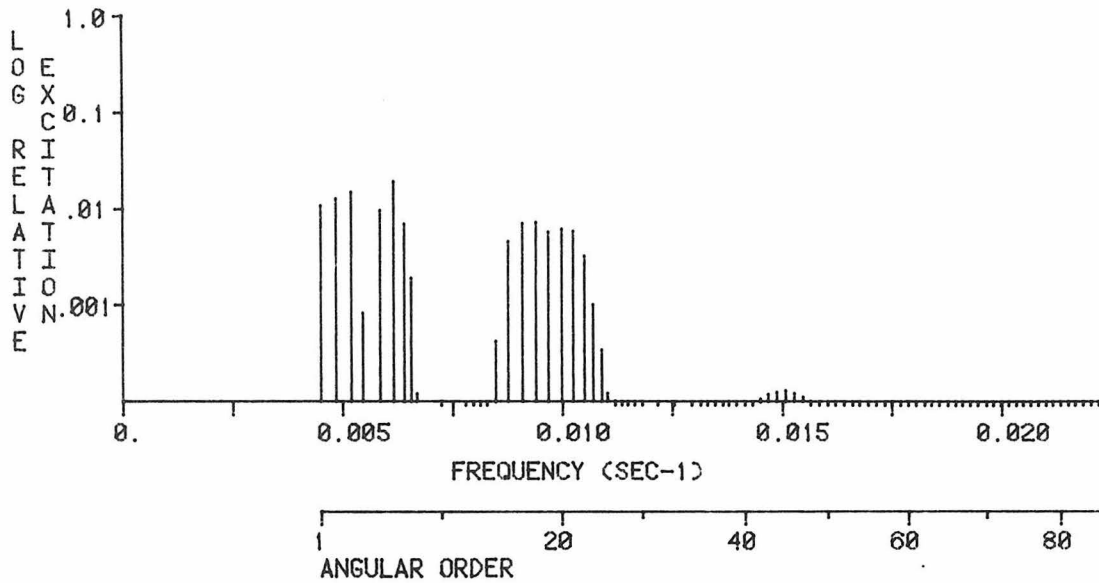
MAXIMUM EXCITATION = 0.332668E -5 CM-SEC ; (12 S 12; T= 134.26 SEC)
EXCITATION NORMALIZED TO 0 S 3 (VERT. COMP.) ; 0.13385900E -3
ATTENUATION INCLUDED; RECORD STARTS AT 12.00 HRS.; LENGTH = 20.00 HRS.

RADIAL COMPONENT; RADIAL ORDER 12



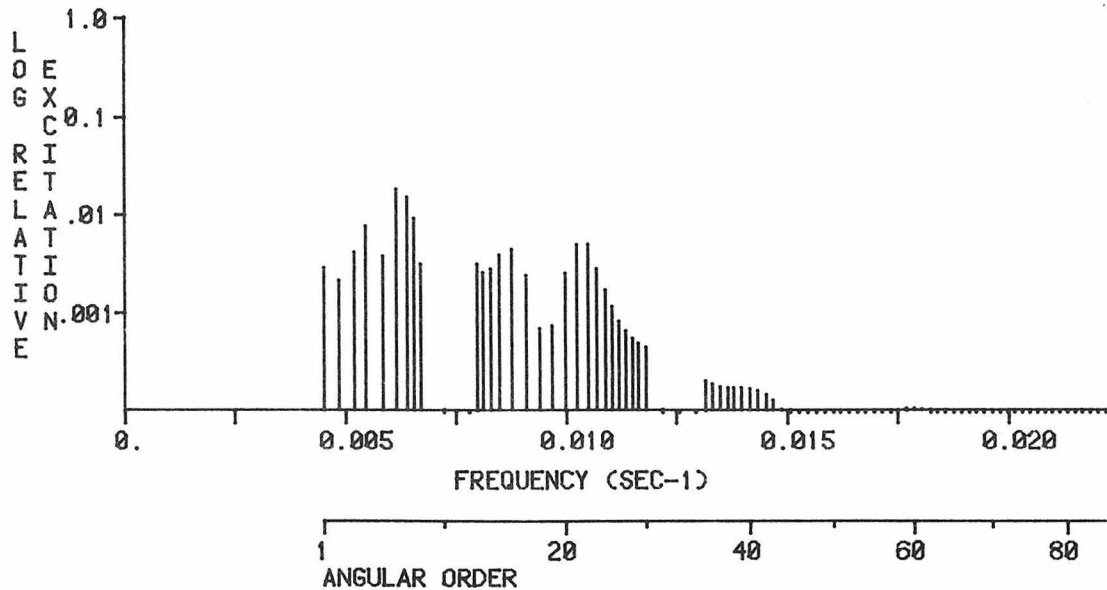
MAXIMUM EXCITATION = 0.207350E -5 CM-SEC ; (12 S 11; T= 140.20 SEC)
EXCITATION NORMALIZED TO 0 S 9 (RAD. COMP.) ; 0.84435000E -4
ATTENUATION INCLUDED; RECORD STARTS AT 12.00 HRS.; LENGTH = 20.00 HRS.

VERTICAL COMPONENT; RADIAL ORDER 13



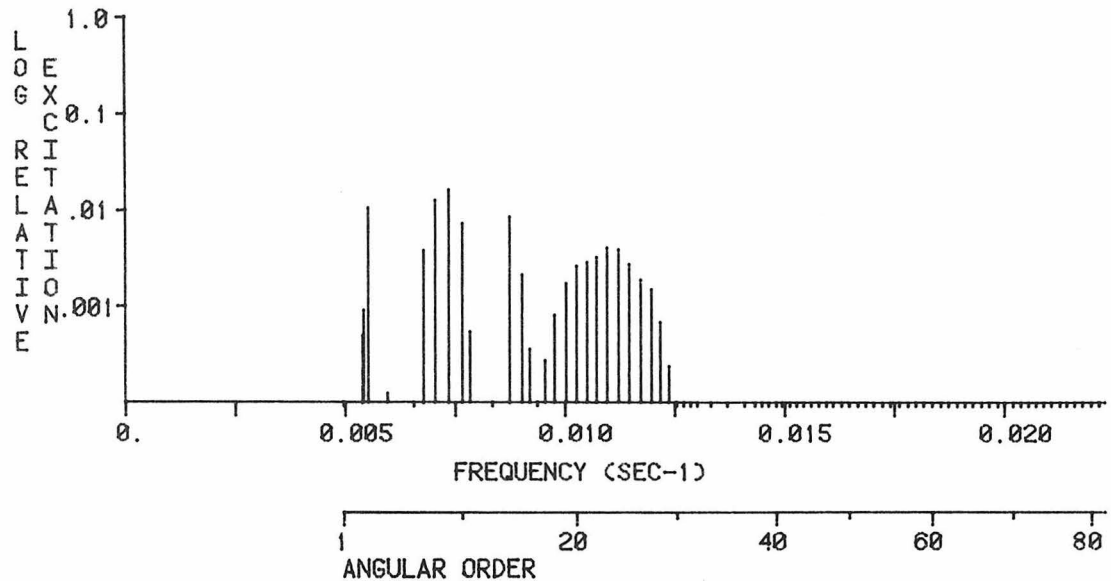
MAXIMUM EXCITATION = 0.253946E -5 CM-SEC ; (13 S 6; T= 162.40 SEC)
EXCITATION NORMALIZED TO 0 S 3 (VERT. COMP.) ; 0.13385900E -3
ATTENUATION INCLUDED; RECORD STARTS AT 12.00 HRS.; LENGTH = 20.00 HRS.

RADIAL COMPONENT; RADIAL ORDER 13



MAXIMUM EXCITATION = 0.155696E -5 CM-SEC ; (13 S 6; T= 162.40 SEC)
EXCITATION NORMALIZED TO 0 S 9 (RAD. COMP.) ; 0.84435000E -4
ATTENUATION INCLUDED; RECORD STARTS AT 12.00 HRS.; LENGTH = 20.00 HRS.

VERTICAL COMPONENT; RADIAL ORDER 14

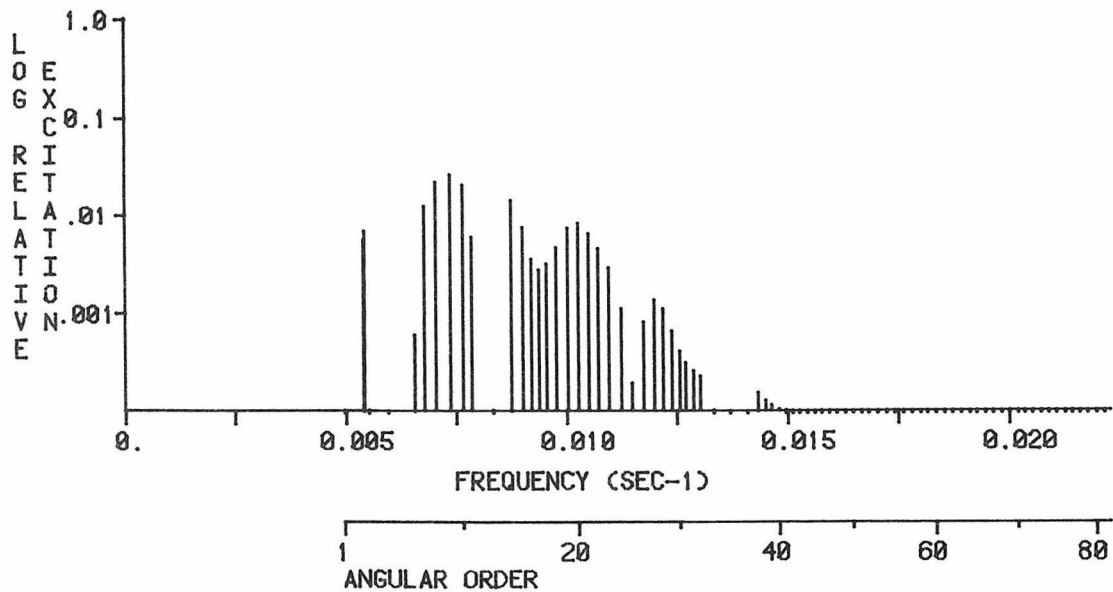


MAXIMUM EXCITATION = 0.220456E -5 CM-SEC ; (14 S 9; T= 136.10 SEC)

EXCITATION NORMALIZED TO 0 S 3 (VERT. COMP.) ; 0.13385900E -3

ATTENUATION INCLUDED; RECORD STARTS AT 12.00 HRS.; LENGTH = 20.00 HRS.

RADIAL COMPONENT; RADIAL ORDER 14

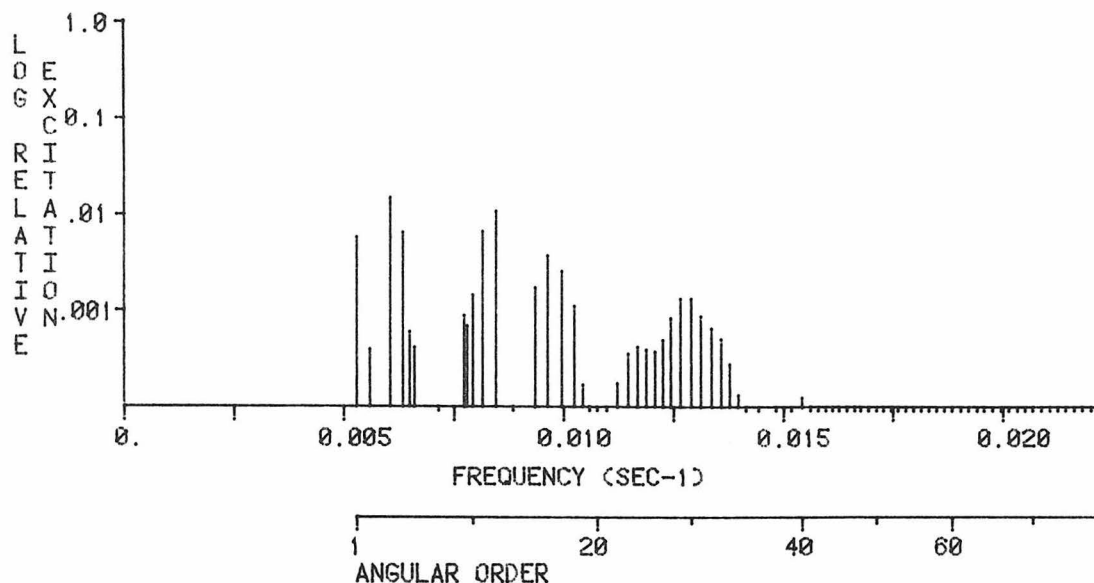


MAXIMUM EXCITATION = 0.224447E -5 CM-SEC ; (14 S 9; T= 136.10 SEC)

EXCITATION NORMALIZED TO 0 S 9 (RAD. COMP.) ; 0.84435000E -4

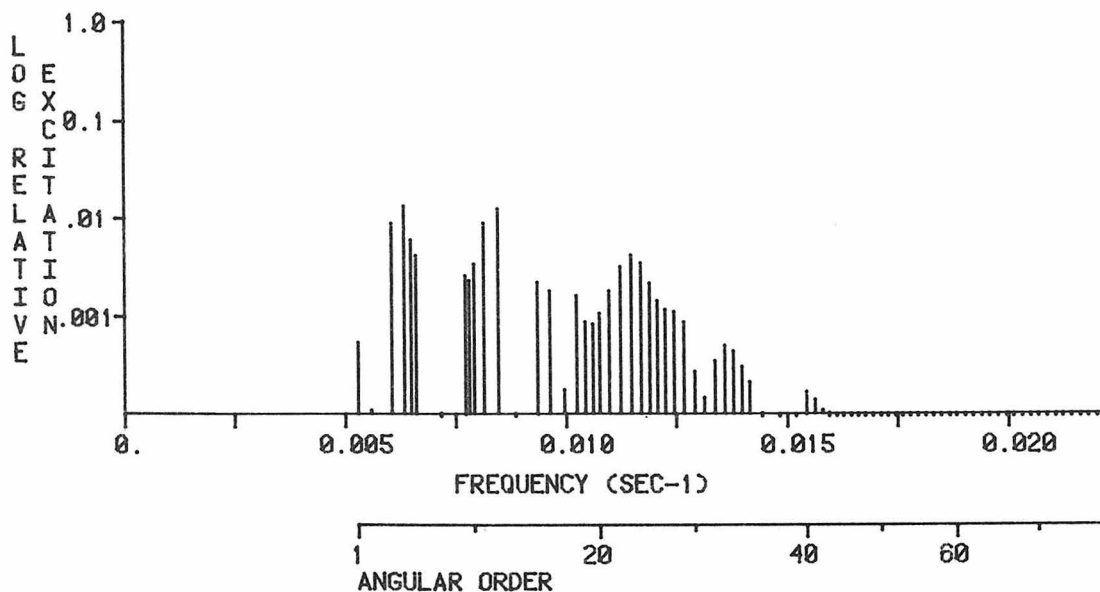
ATTENUATION INCLUDED; RECORD STARTS AT 12.00 HRS.; LENGTH = 20.00 HRS.

VERTICAL COMPONENT; RADIAL ORDER 15



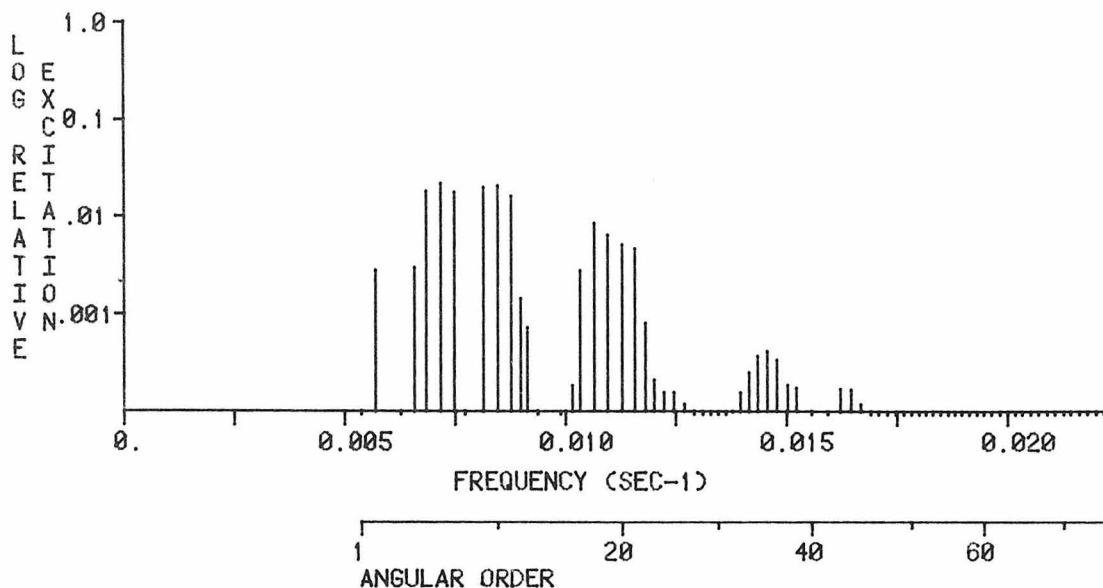
MAXIMUM EXCITATION = 0.198476E -5 CM-SEC ; (15 S 3; T= 165.87 SEC)
EXCITATION NORMALIZED TO 0 S 3 (VERT. COMP.) ; 0.13385900E -3
ATTENUATION INCLUDED; RECORD STARTS AT 12.00 HRS.; LENGTH = 20.00 HRS.

RADIAL COMPONENT; RADIAL ORDER 15



MAXIMUM EXCITATION = 0.111321E -5 CM-SEC ; (15 S 4; T= 158.01 SEC)
EXCITATION NORMALIZED TO 0 S 9 (RAD. COMP.) ; 0.84435000E -4
ATTENUATION INCLUDED; RECORD STARTS AT 12.00 HRS.; LENGTH = 20.00 HRS.

VERTICAL COMPONENT; RADIAL ORDER 16

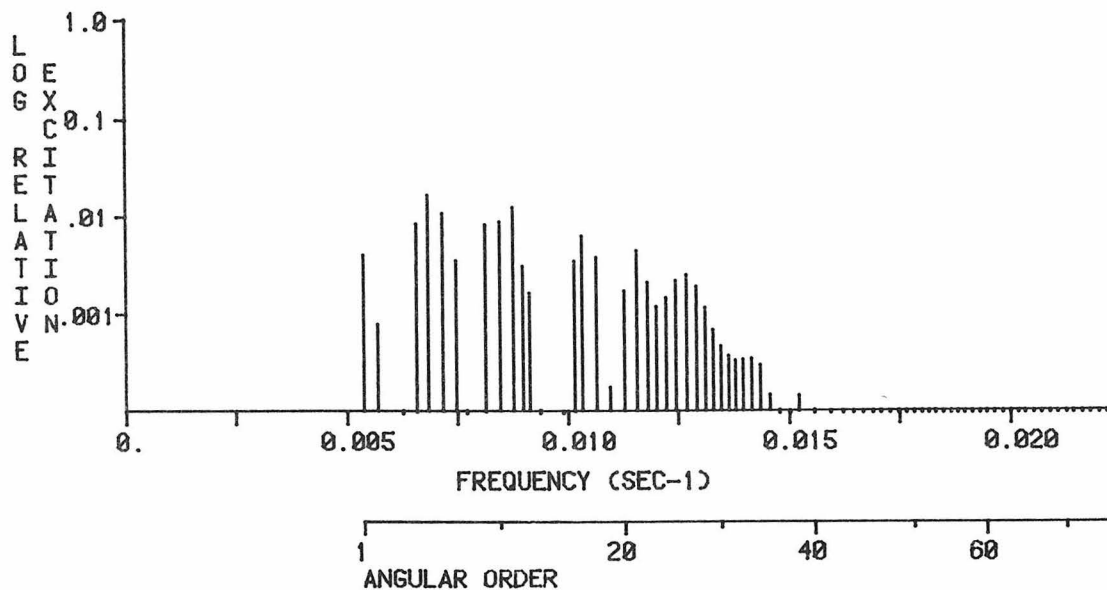


MAXIMUM EXCITATION = 0.287672E -5 CM-SEC ; (16 S 6; T= 139.86 SEC)

EXCITATION NORMALIZED TO 0 S 3 (VERT. COMP.) ; 0.13385900E -3

ATTENUATION INCLUDED; RECORD STARTS AT 12.00 HRS.; LENGTH = 20.00 HRS.

RADIAL COMPONENT; RADIAL ORDER 16

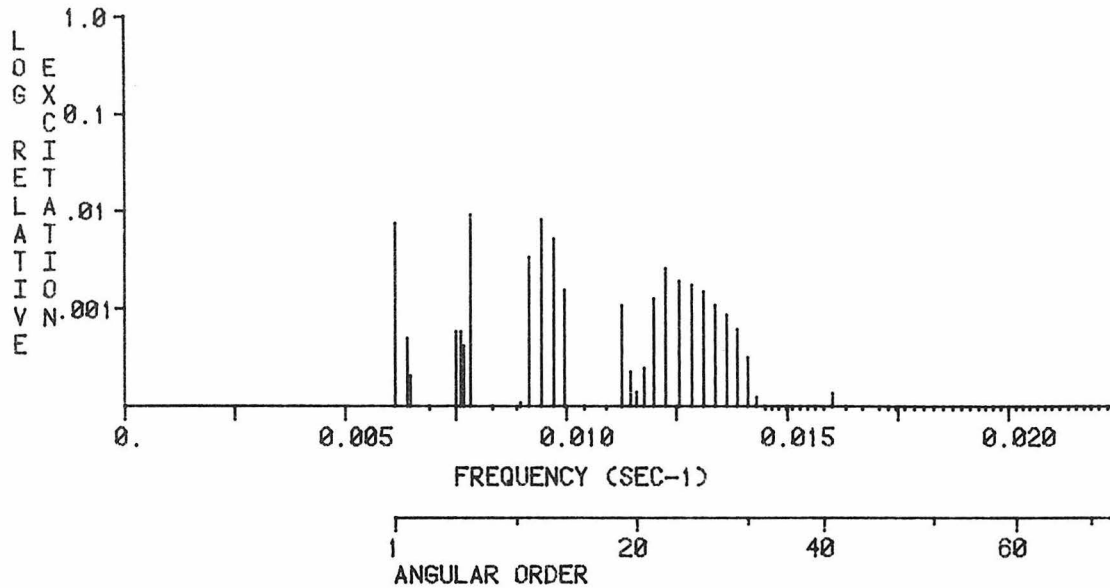


MAXIMUM EXCITATION = 0.141441E -5 CM-SEC ; (16 S 5; T= 146.39 SEC)

EXCITATION NORMALIZED TO 0 S 9 (RAD. COMP.) ; 0.84435000E -4

ATTENUATION INCLUDED; RECORD STARTS AT 12.00 HRS.; LENGTH = 20.00 HRS.

VERTICAL COMPONENT; RADIAL ORDER 17

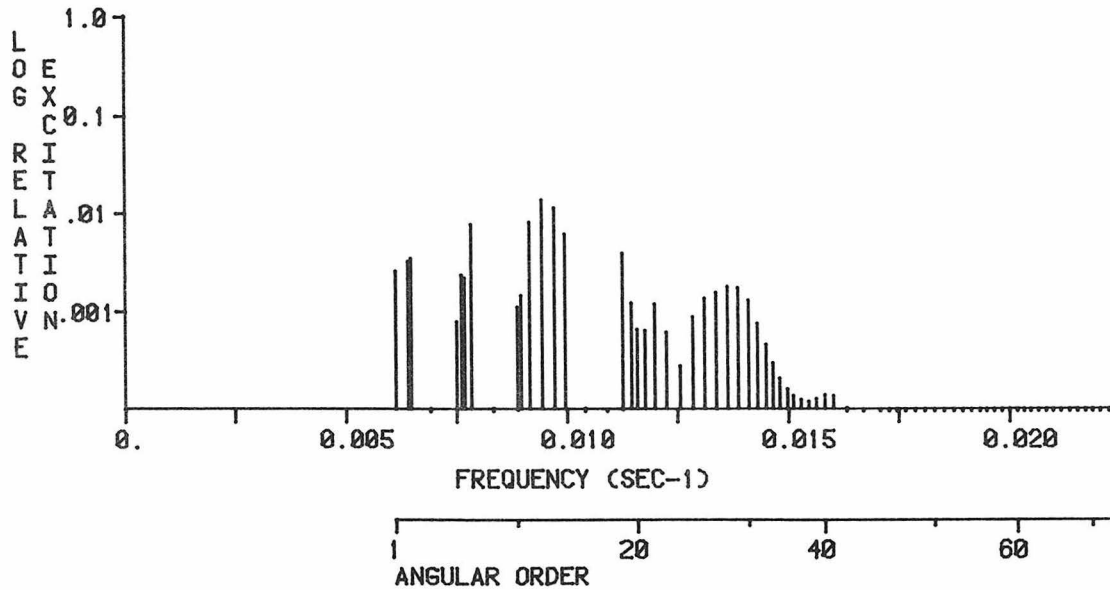


MAXIMUM EXCITATION = 0.125238E -5 CM-SEC ; (17 S 8; T= 128.03 SEC)

EXCITATION NORMALIZED TO 0 S 3 (VERT. COMP.) ; 0.13385900E -3

ATTENUATION INCLUDED; RECORD STARTS AT 12.00 HRS.; LENGTH = 20.00 HRS.

RADIAL COMPONENT; RADIAL ORDER 17

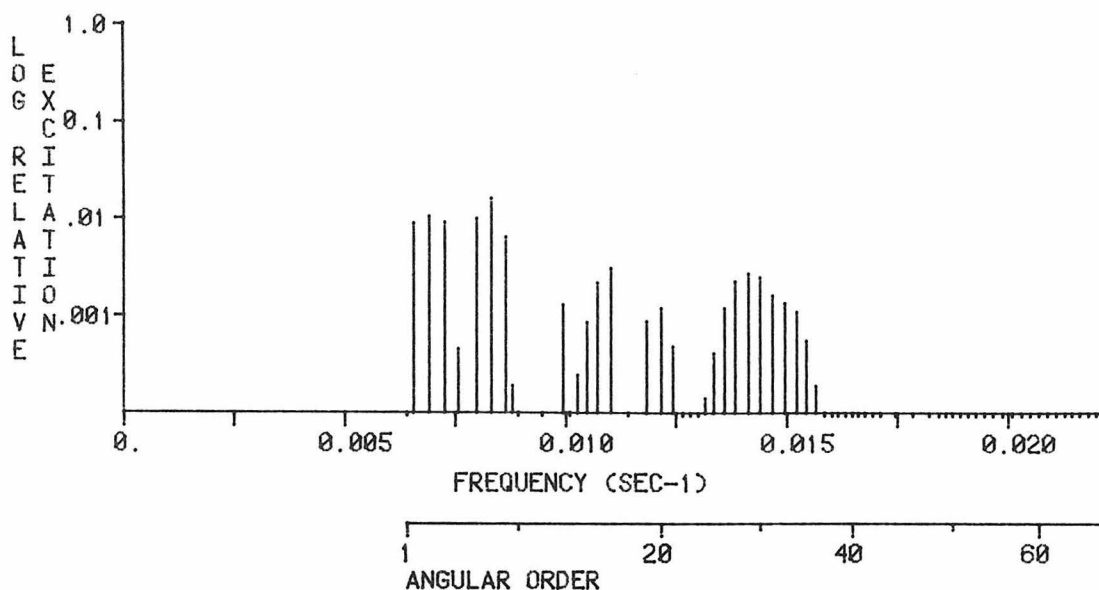


MAXIMUM EXCITATION = 0.114566E -5 CM-SEC ; (17 S 13; T= 106.01 SEC)

EXCITATION NORMALIZED TO 0 S 9 (RAD. COMP.) ; 0.84435000E -4

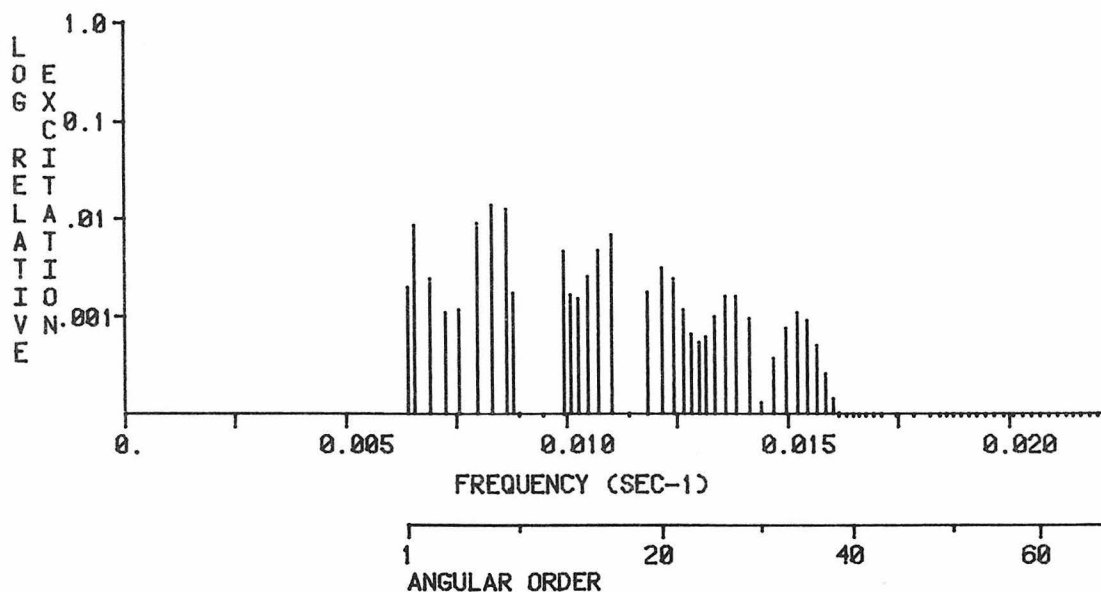
ATTENUATION INCLUDED; RECORD STARTS AT 12.00 HRS.; LENGTH = 20.00 HRS.

VERTICAL COMPONENT; RADIAL ORDER 18



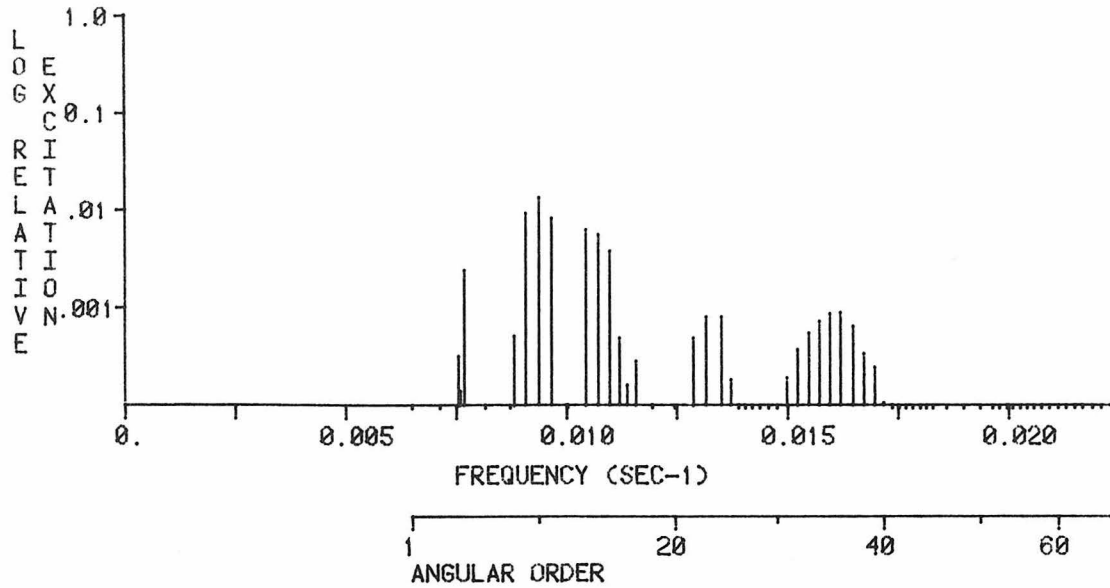
MAXIMUM EXCITATION = 0.215676E -5 CM-SEC ; (18 S 7; T= 120.41 SEC)
EXCITATION NORMALIZED TO 0 S 3 (VERT. COMP.) ; 0.13385900E -3
ATTENUATION INCLUDED; RECORD STARTS AT 12.00 HRS.; LENGTH = 20.00 HRS.

RADIAL COMPONENT; RADIAL ORDER 18



MAXIMUM EXCITATION = 0.113871E -5 CM-SEC ; (18 S 7; T= 120.41 SEC)
EXCITATION NORMALIZED TO 0 S 9 (RAD. COMP.) ; 0.84435000E -4
ATTENUATION INCLUDED; RECORD STARTS AT 12.00 HRS.; LENGTH = 20.00 HRS.

VERTICAL COMPONENT; RADIAL ORDER 19

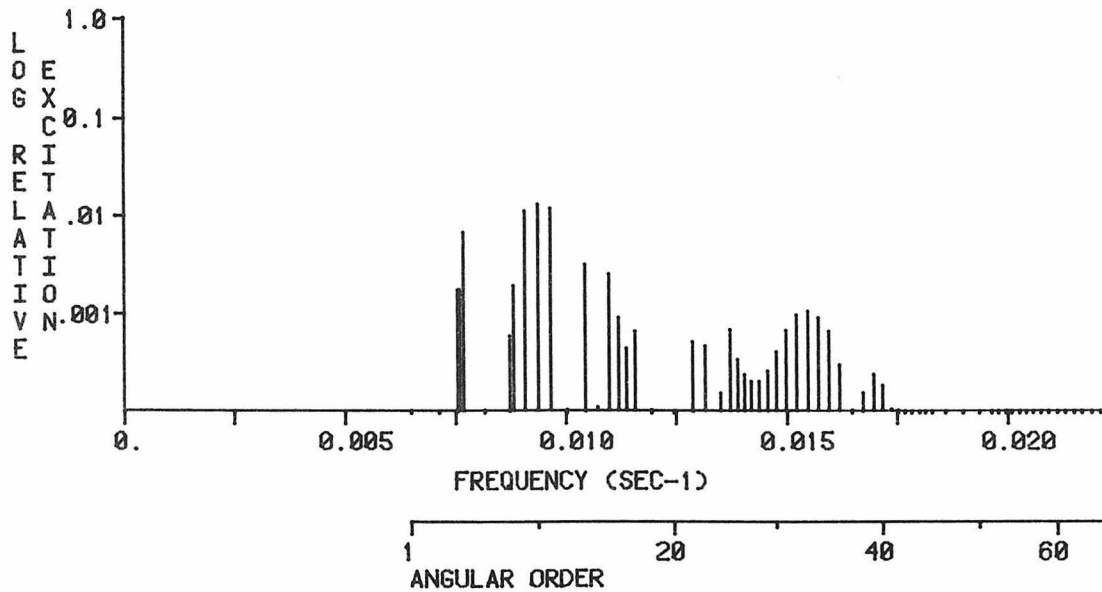


MAXIMUM EXCITATION = 0.175733E -5 CM-SEC ; (19 S 10; T= 106.89 SEC)

EXCITATION NORMALIZED TO 0 S 3 (VERT. COMP.) ; 0.13385900E -3

ATTENUATION INCLUDED; RECORD STARTS AT 12.00 HRS.; LENGTH = 20.00 HRS.

RADIAL COMPONENT; RADIAL ORDER 19

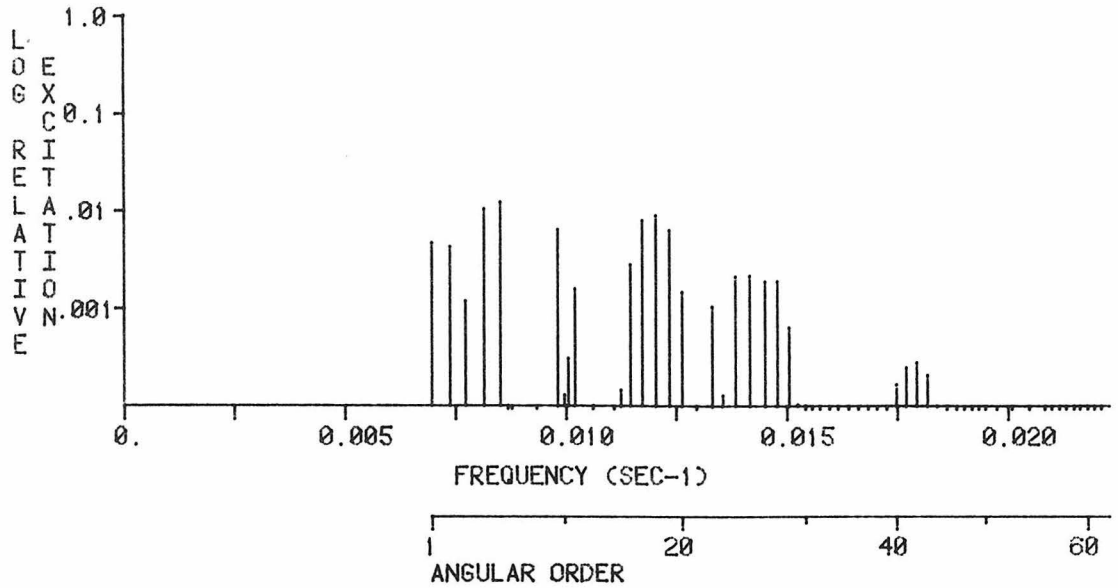


MAXIMUM EXCITATION = 0.109174E -5 CM-SEC ; (19 S 10; T= 106.89 SEC)

EXCITATION NORMALIZED TO 0 S 9 (RAD. COMP.) ; 0.84435000E -4

ATTENUATION INCLUDED; RECORD STARTS AT 12.00 HRS.; LENGTH = 20.00 HRS.

VERTICAL COMPONENT; RADIAL ORDER 20

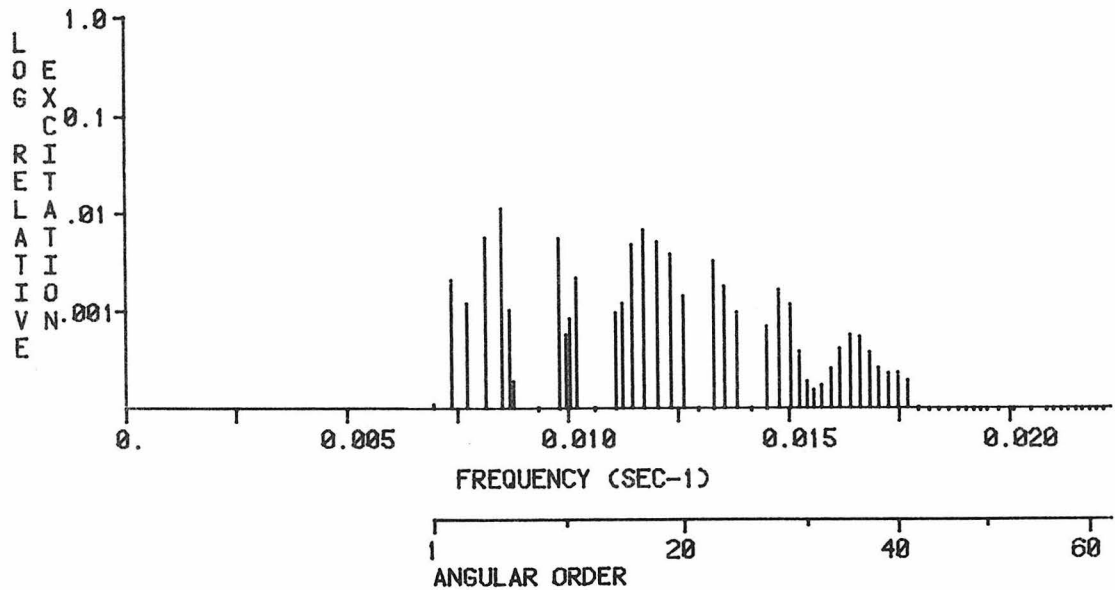


MAXIMUM EXCITATION = 0.161770E -5 CM-SEC ; (20 S 5; T= 117.98 SEC)

EXCITATION NORMALIZED TO 0 S 3 (VERT. COMP.) ; 0.13385900E -3

ATTENUATION INCLUDED; RECORD STARTS AT 12.00 HRS.; LENGTH = 20.00 HRS.

RADIAL COMPONENT; RADIAL ORDER 20

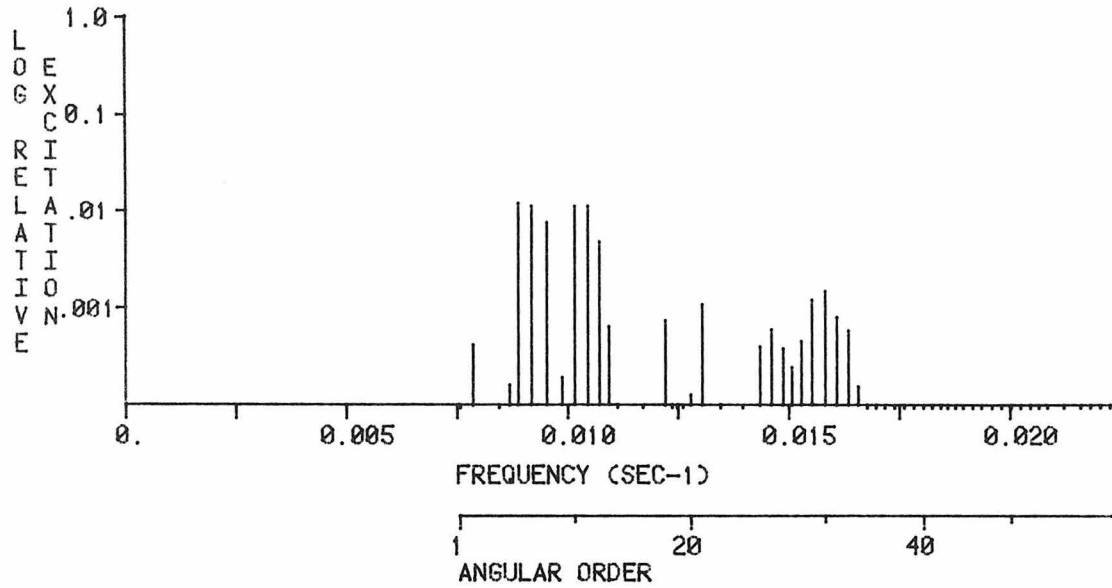


MAXIMUM EXCITATION = 0.950150E -6 CM-SEC ; (20 S 5; T= 117.98 SEC)

EXCITATION NORMALIZED TO 0 S 9 (RAD. COMP.) ; 0.84435000E -4

ATTENUATION INCLUDED; RECORD STARTS AT 12.00 HRS.; LENGTH = 20.00 HRS.

VERTICAL COMPONENT; RADIAL ORDER 21

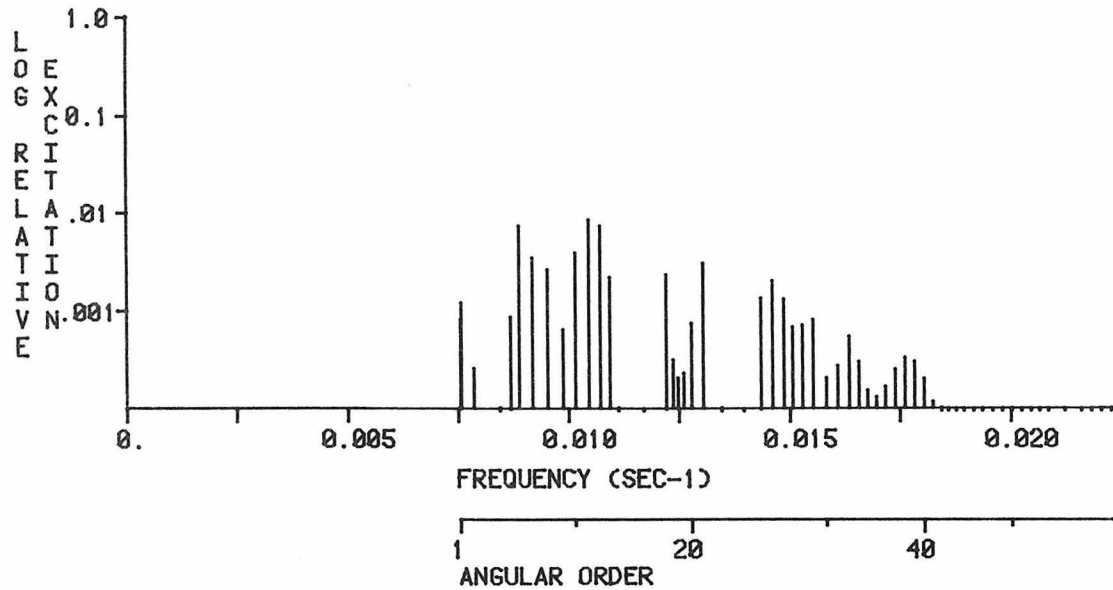


MAXIMUM EXCITATION = 0.157996E -5 CM-SEC ; (21 S 6; T= 112.97 SEC)

EXCITATION NORMALIZED TO 0 S 3 (VERT. COMP.) ; 0.13385900E -3

ATTENUATION INCLUDED; RECORD STARTS AT 12.00 HRS.; LENGTH = 20.00 HRS.

RADIAL COMPONENT; RADIAL ORDER 21

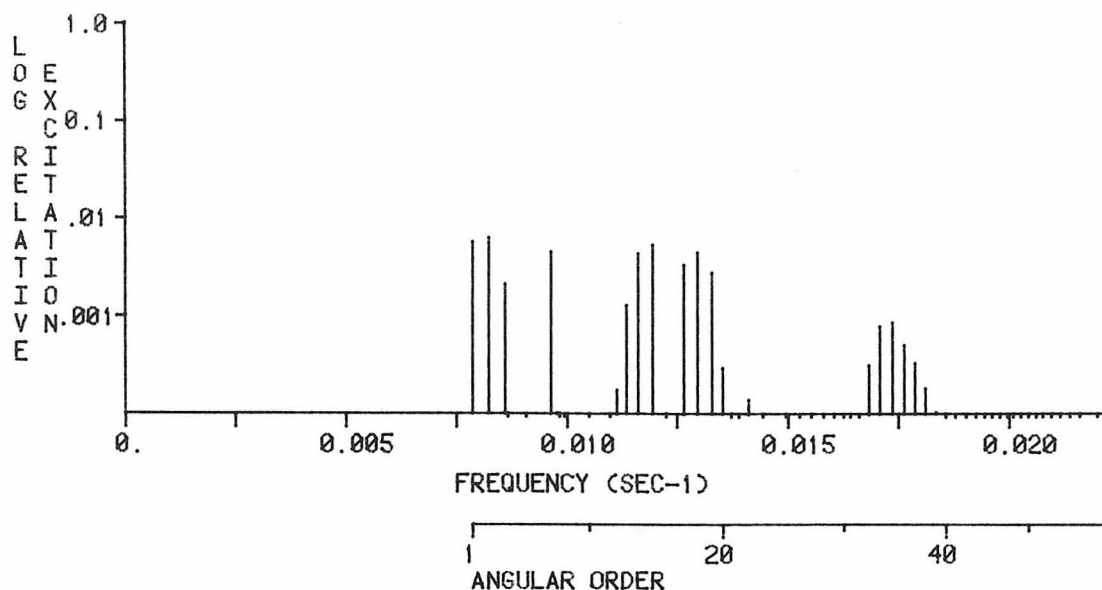


MAXIMUM EXCITATION = 0.708580E -6 CM-SEC ; (21 S 11; T= 95.81 SEC)

EXCITATION NORMALIZED TO 0 S 9 (RAD. COMP.) ; 0.84435000E -4

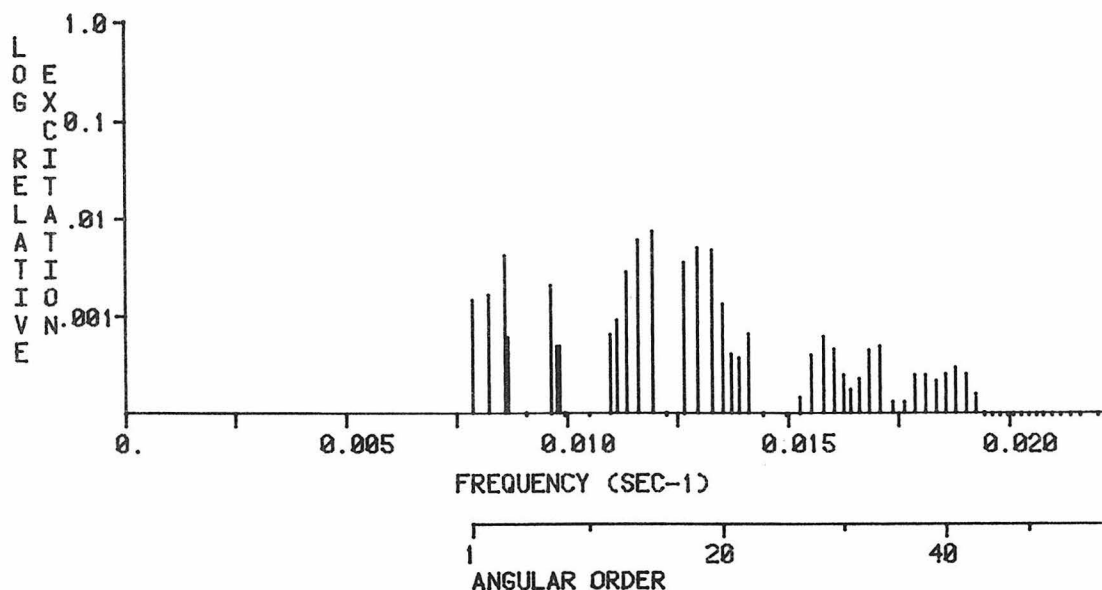
ATTENUATION INCLUDED; RECORD STARTS AT 12.00 HRS.; LENGTH = 20.00 HRS.

VERTICAL COMPONENT; RADIAL ORDER 22



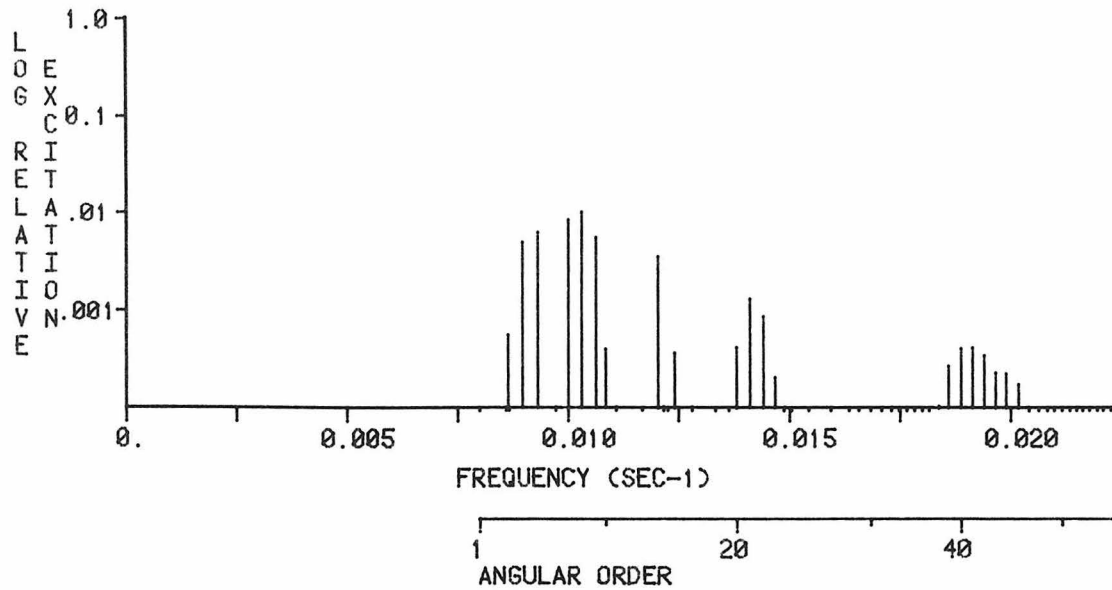
MAXIMUM EXCITATION = 0.840930E -6 CM-SEC ; (22 S 2; T= 121.87 SEC)
EXCITATION NORMALIZED TO 0 S 3 (VERT. COMP.) ; 0.13385900E -3
ATTENUATION INCLUDED; RECORD STARTS AT 12.00 HRS.; LENGTH = 20.00 HRS.

RADIAL COMPONENT; RADIAL ORDER 22



MAXIMUM EXCITATION = 0.620564E -6 CM-SEC ; (22 S 15; T= 83.92 SEC)
EXCITATION NORMALIZED TO 0 S 9 (RAD. COMP.) ; 0.84435000E -4
ATTENUATION INCLUDED; RECORD STARTS AT 12.00 HRS.; LENGTH = 20.00 HRS.

VERTICAL COMPONENT; RADIAL ORDER 23

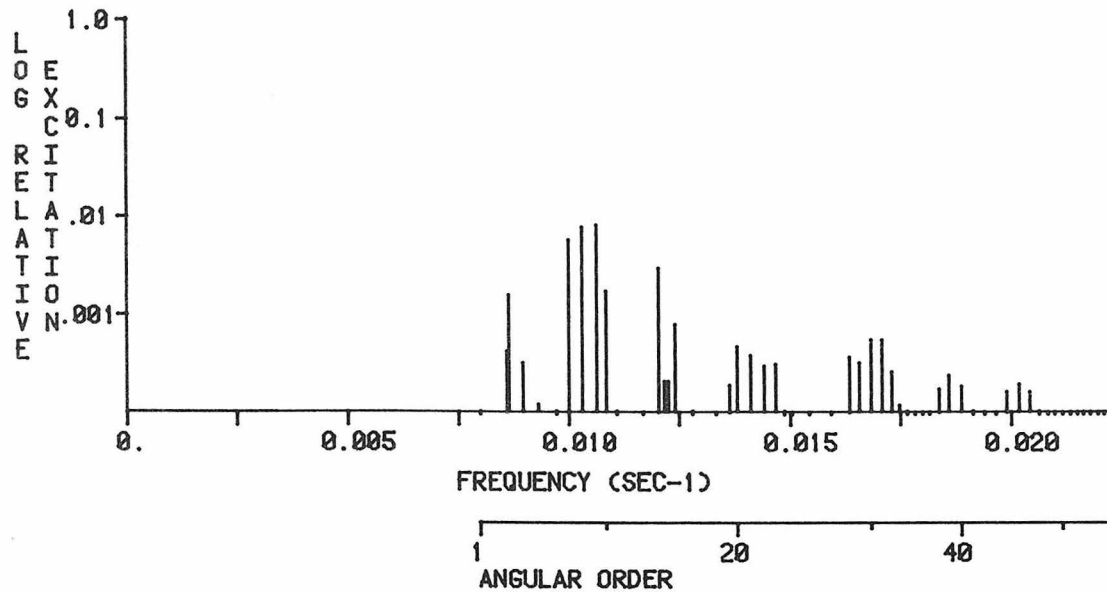


MAXIMUM EXCITATION = 0.135889E -5 CM-SEC ; (23 S 8; T= 96.98 SEC)

EXCITATION NORMALIZED TO 0 S 3 (VERT. COMP.) ; 0.13385900E -3

ATTENUATION INCLUDED; RECORD STARTS AT 12.00 HRS.; LENGTH = 20.00 HRS.

RADIAL COMPONENT; RADIAL ORDER 23

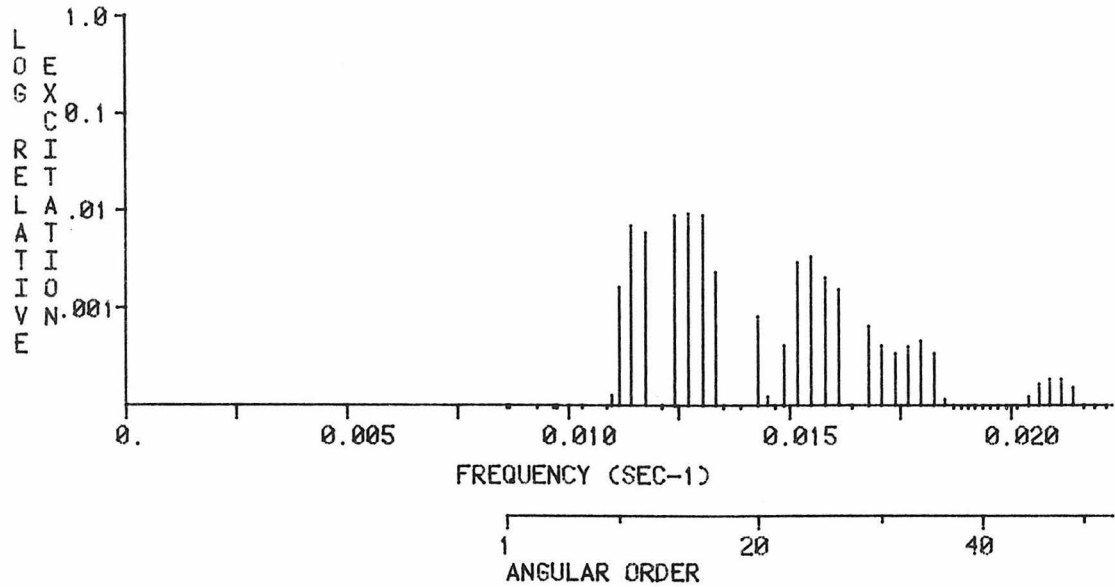


MAXIMUM EXCITATION = 0.676920E -6 CM-SEC ; (23 S 9; T= 94.22 SEC)

EXCITATION NORMALIZED TO 0 S 9 (RAD. COMP.) ; 0.84435000E -4

ATTENUATION INCLUDED; RECORD STARTS AT 12.00 HRS.; LENGTH = 20.00 HRS.

VERTICAL COMPONENT; RADIAL ORDER 24

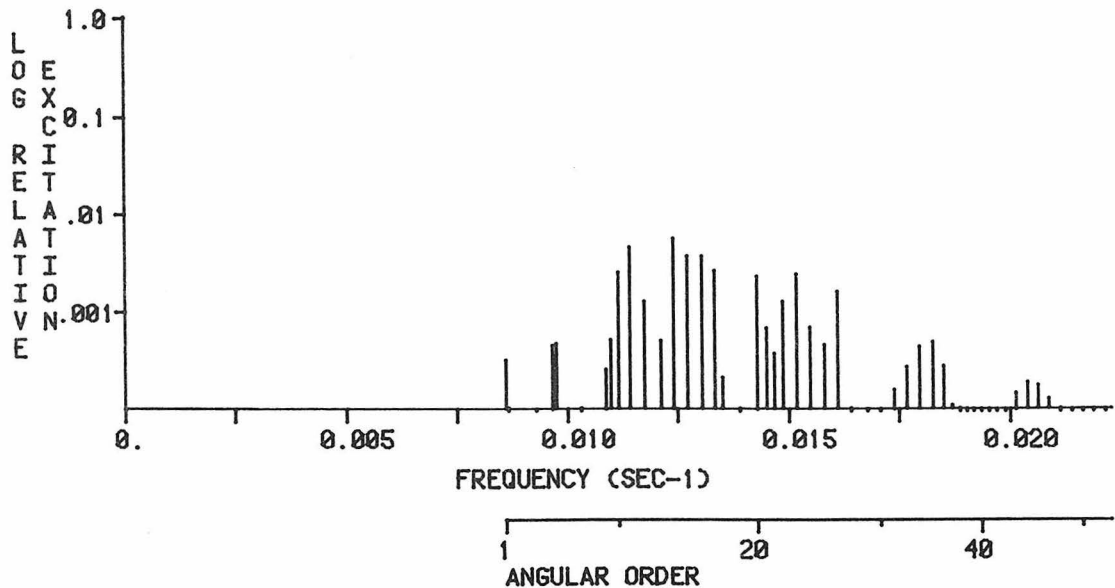


MAXIMUM EXCITATION = 0.128629E -5 CM-SEC ; (24 S 15; T= 78.77 SEC)

EXCITATION NORMALIZED TO 0 S 3 (VERT. COMP.) ; 0.13385900E -3

ATTENUATION INCLUDED; RECORD STARTS AT 12.00 HRS.; LENGTH = 20.00 HRS.

RADIAL COMPONENT; RADIAL ORDER 24

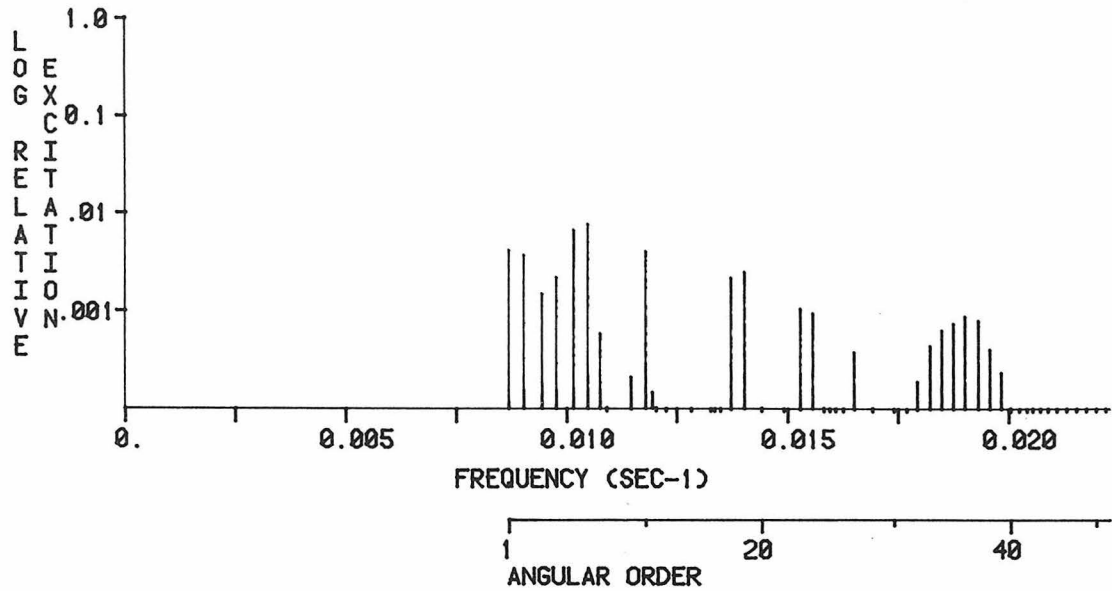


MAXIMUM EXCITATION = 0.480451E -6 CM-SEC ; (24 S 14; T= 80.80 SEC)

EXCITATION NORMALIZED TO 0 S 9 (RAD. COMP.) ; 0.84435000E -4

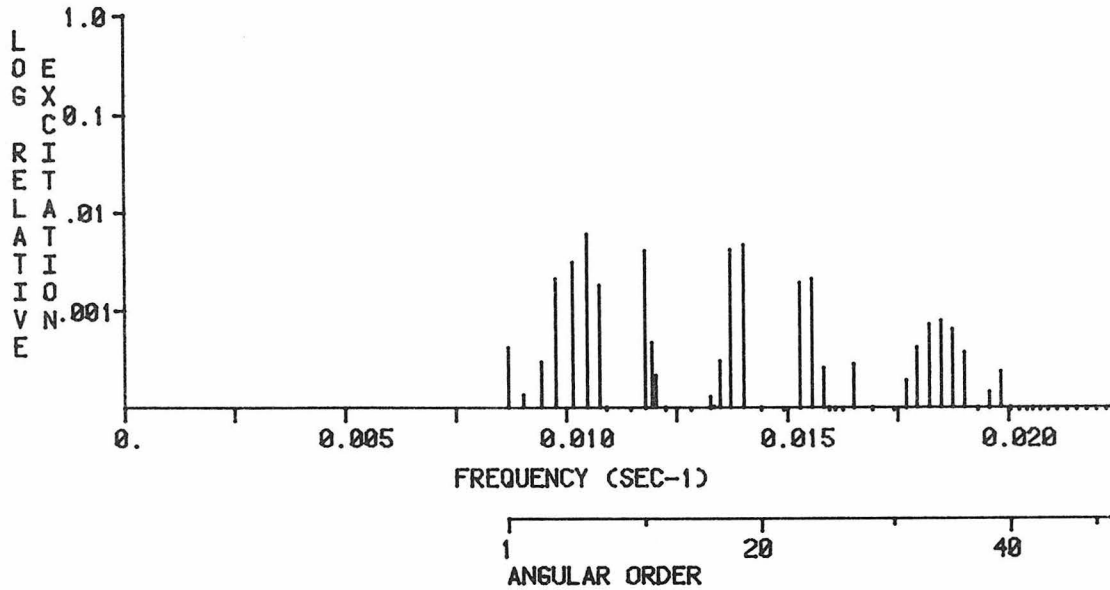
ATTENUATION INCLUDED; RECORD STARTS AT 12.00 HRS.; LENGTH = 20.00 HRS.

VERTICAL COMPONENT, RADIAL ORDER 25



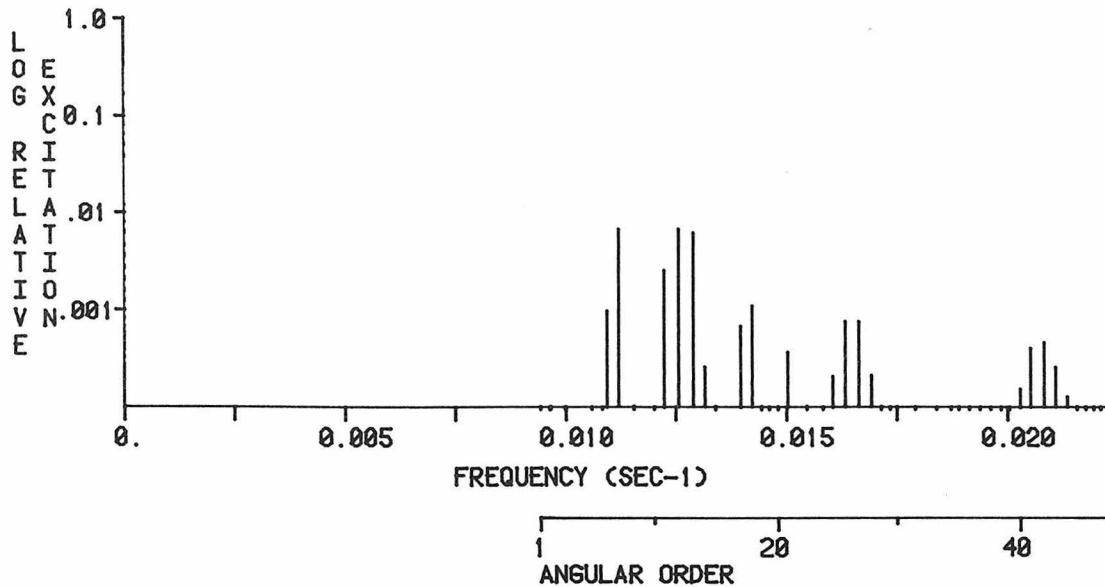
MAXIMUM EXCITATION = 0.104386E -5 CM-SEC ; (25 S 6; T= 95.48 SEC)
EXCITATION NORMALIZED TO 0 S 3 (VERT. COMP.) ; 0.13385900E -3
ATTENUATION INCLUDED; RECORD STARTS AT 12.00 HRS.; LENGTH = 20.00 HRS.

RADIAL COMPONENT, RADIAL ORDER 25



MAXIMUM EXCITATION = 0.496973E -6 CM-SEC ; (25 S 6; T= 95.48 SEC)
EXCITATION NORMALIZED TO 0 S 9 (RAD. COMP.) ; 0.84435000E -4
ATTENUATION INCLUDED; RECORD STARTS AT 12.00 HRS.; LENGTH = 20.00 HRS.

VERTICAL COMPONENT; RADIAL ORDER 26

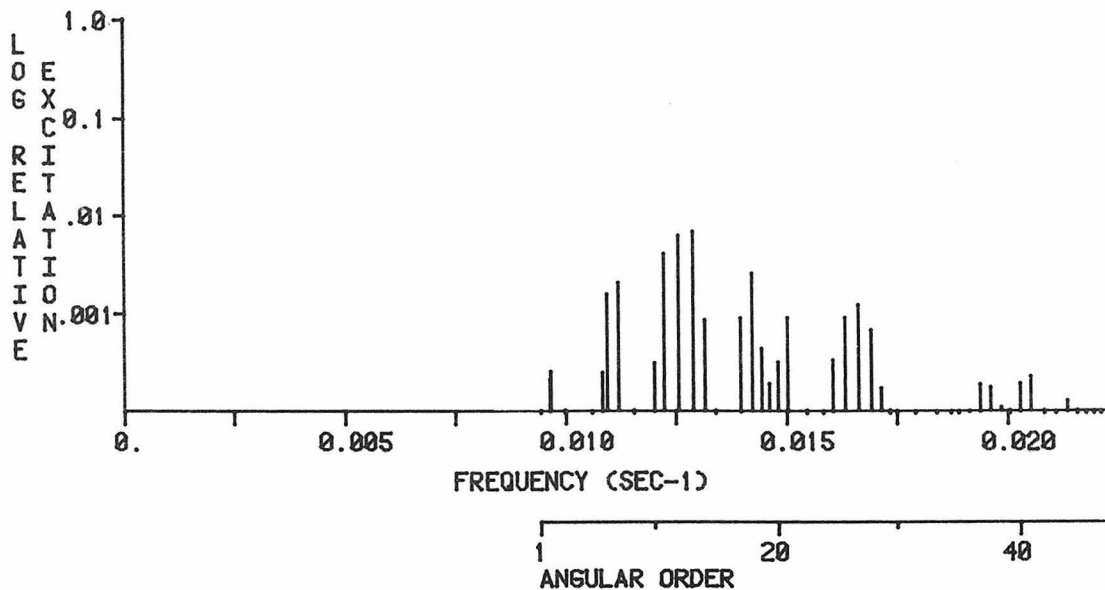


MAXIMUM EXCITATION = 0.910660E -6 CM-SEC ; (26 S 8; T= 89.34 SEC)

EXCITATION NORMALIZED TO 0 S 3 (VERT. COMP.) ; 0.13385900E -3

ATTENUATION INCLUDED; RECORD STARTS AT 12.00 HRS.; LENGTH = 20.00 HRS.

RADIAL COMPONENT; RADIAL ORDER 26

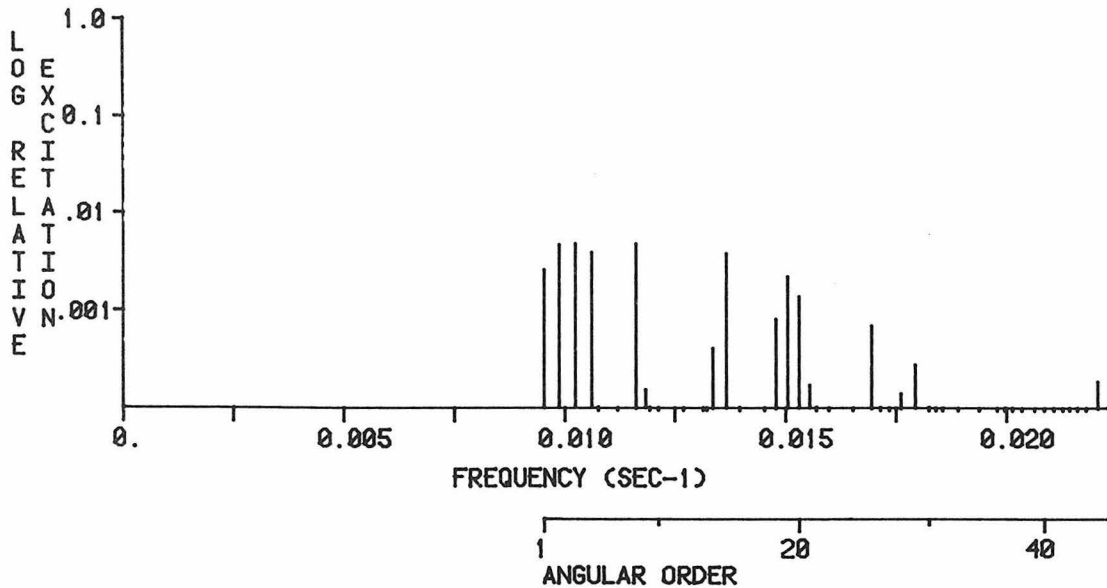


MAXIMUM EXCITATION = 0.581064E -6 CM-SEC ; (26 S 13; T= 77.71 SEC)

EXCITATION NORMALIZED TO 0 S 9 (RAD. COMP.) ; 0.84435000E -4

ATTENUATION INCLUDED; RECORD STARTS AT 12.00 HRS.; LENGTH = 20.00 HRS.

VERTICAL COMPONENT; RADIAL ORDER 27

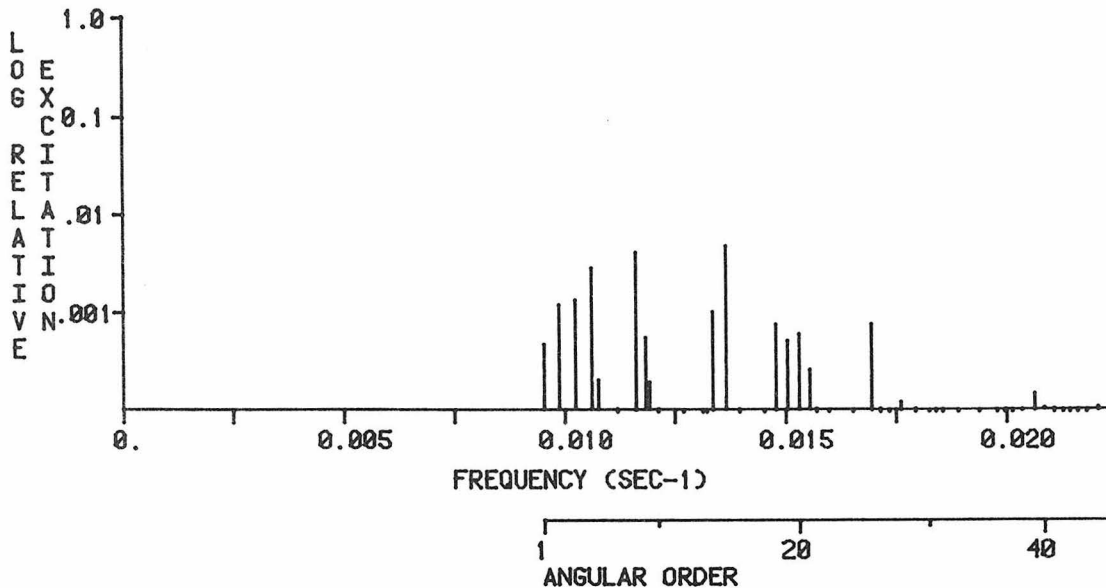


MAXIMUM EXCITATION = 0.642740E -6 CM-SEC ; (27 S 7; T= 86.11 SEC)

EXCITATION NORMALIZED TO 0 S 3 (VERT. COMP.) ; 0.13385900E -3

ATTENUATION INCLUDED; RECORD STARTS AT 12.00 HRS.; LENGTH = 20.00 HRS.

RADIAL COMPONENT; RADIAL ORDER 27

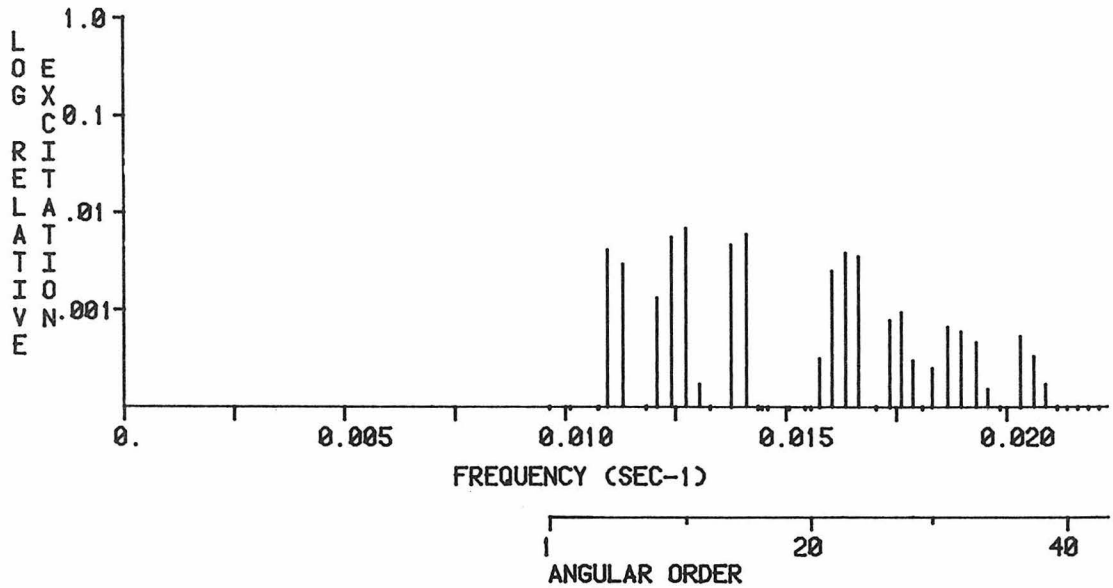


MAXIMUM EXCITATION = 0.406973E -6 CM-SEC ; (27 S 15; T= 73.43 SEC)

EXCITATION NORMALIZED TO 0 S 9 (RAD. COMP.) ; 0.84435000E -4

ATTENUATION INCLUDED; RECORD STARTS AT 12.00 HRS.; LENGTH = 20.00 HRS.

VERTICAL COMPONENT; RADIAL ORDER 28

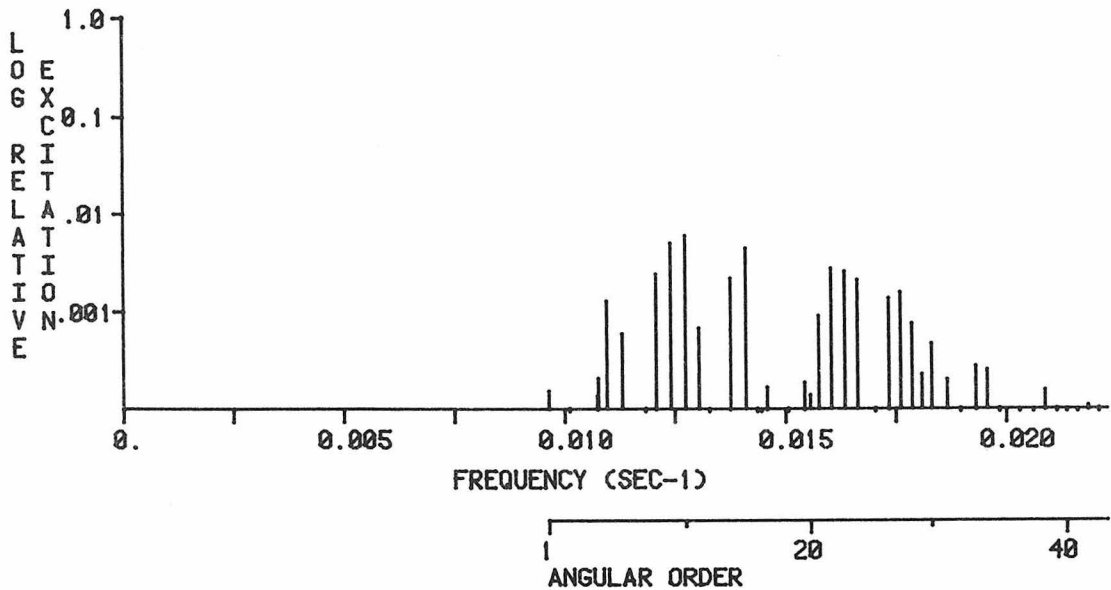


MAXIMUM EXCITATION = 0.954590E -6 CM-SEC ; (28 S 10; T= 78.54 SEC)

EXCITATION NORMALIZED TO 0 S 3 (VERT. COMP.) ; 0.13385900E -3

ATTENUATION INCLUDED; RECORD STARTS AT 12.00 HRS.; LENGTH = 20.00 HRS.

RADIAL COMPONENT; RADIAL ORDER 28

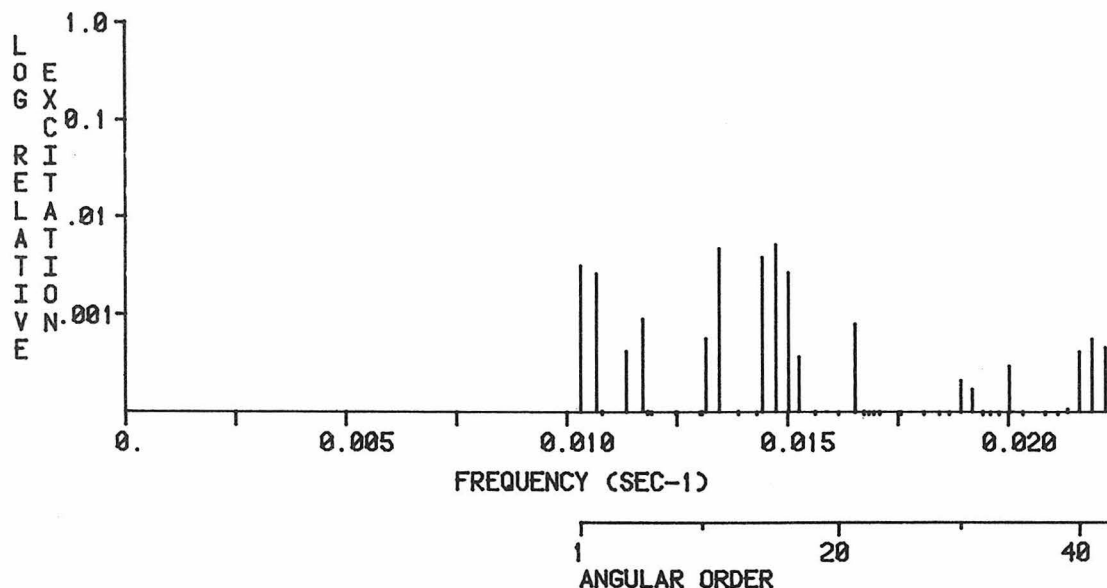


MAXIMUM EXCITATION = 0.508096E -6 CM-SEC ; (28 S 10; T= 78.54 SEC)

EXCITATION NORMALIZED TO 0 S 9 (RAD. COMP.) ; 0.84435000E -4

ATTENUATION INCLUDED; RECORD STARTS AT 12.00 HRS.; LENGTH = 20.00 HRS.

VERTICAL COMPONENT; RADIAL ORDER 29

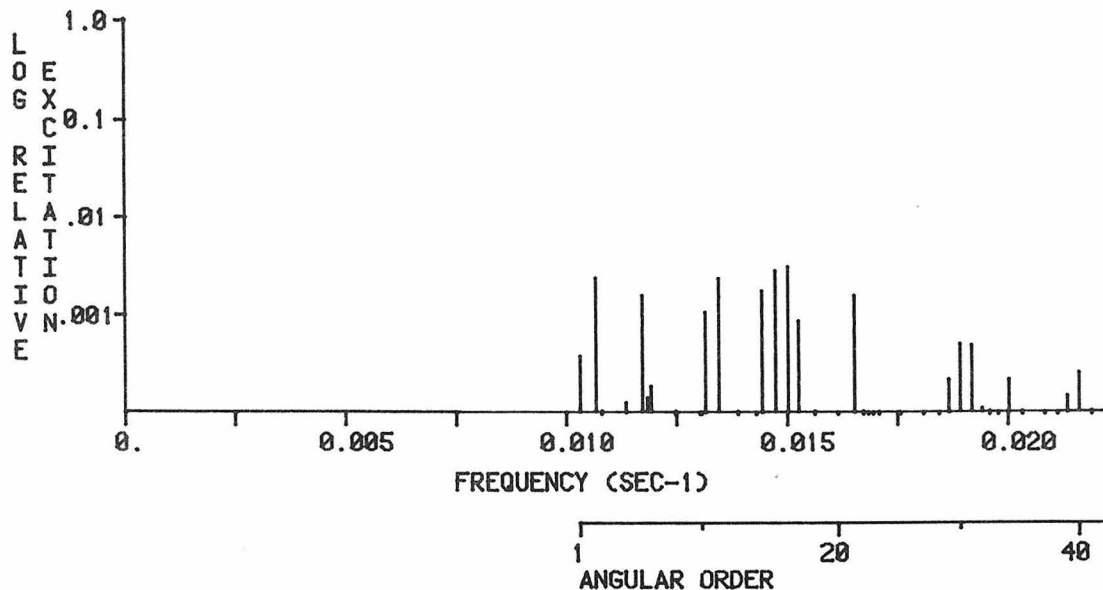


MAXIMUM EXCITATION = 0.689620E -6 CM-SEC ; (29 S 16; T= 67.96 SEC)

EXCITATION NORMALIZED TO 0 S 3 (VERT. COMP.) ; 0.13385900E -3

ATTENUATION INCLUDED; RECORD STARTS AT 12.00 HRS.; LENGTH = 20.00 HRS.

RADIAL COMPONENT; RADIAL ORDER 29

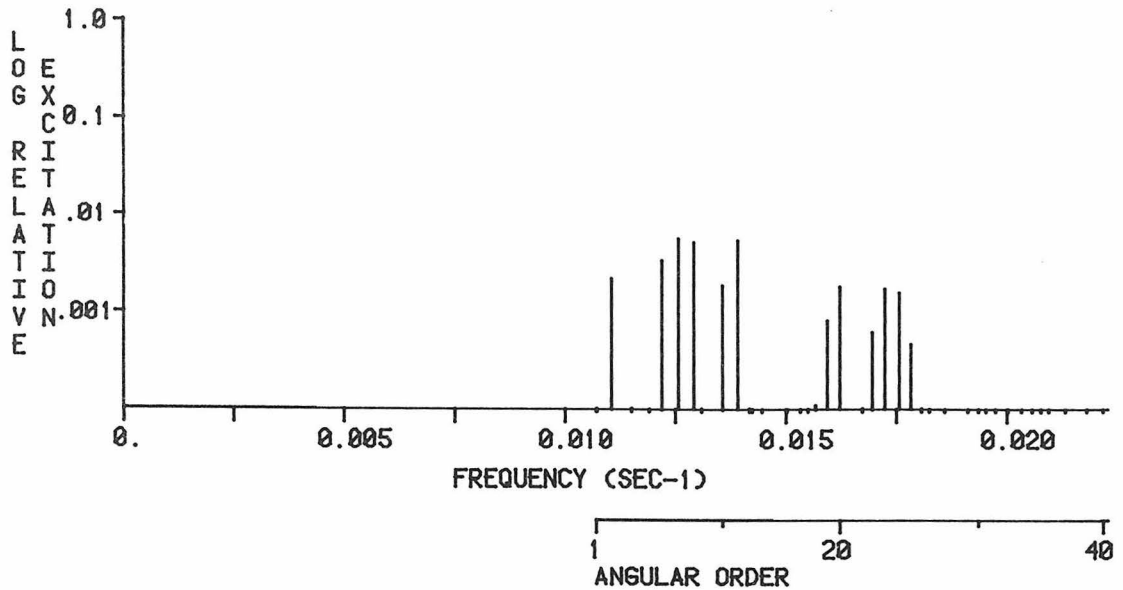


MAXIMUM EXCITATION = 0.261001E -6 CM-SEC ; (29 S 17; T= 66.63 SEC)

EXCITATION NORMALIZED TO 0 S 9 (RAD. COMP.) ; 0.84435000E -4

ATTENUATION INCLUDED; RECORD STARTS AT 12.00 HRS.; LENGTH = 20.00 HRS.

VERTICAL COMPONENT; RADIAL ORDER 30

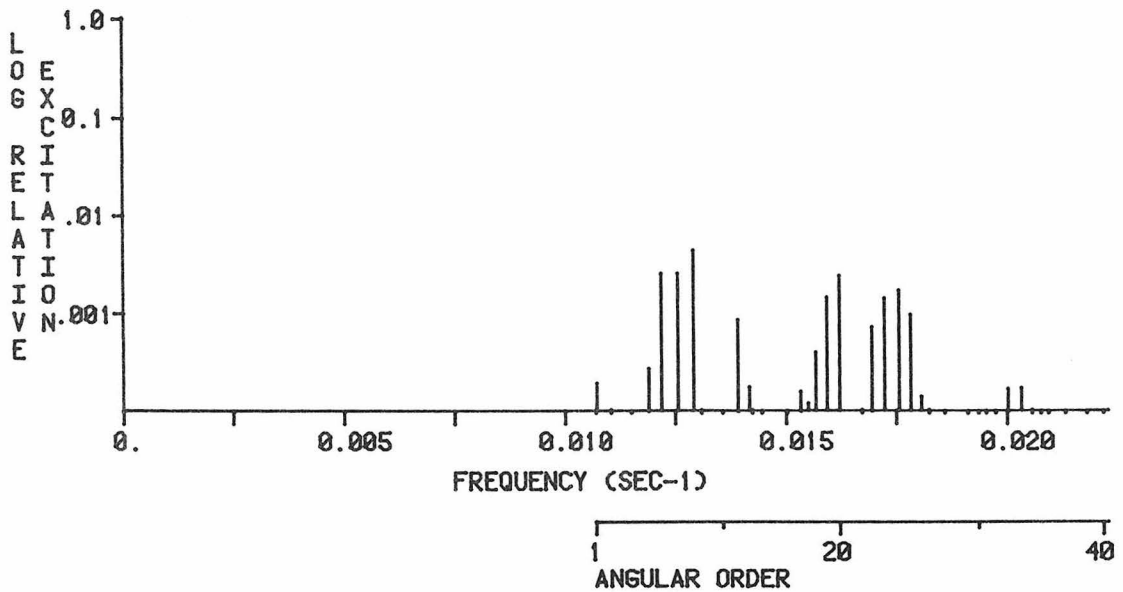


MAXIMUM EXCITATION = 0.773740E -6 CM-SEC ; (30 S 7; T= 79.76 SEC)

EXCITATION NORMALIZED TO 0 S 3 (VERT. COMP.) ; 0.13385900E -3

ATTENUATION INCLUDED; RECORD STARTS AT 12.00 HRS.; LENGTH = 20.00 HRS.

RADIAL COMPONENT; RADIAL ORDER 30



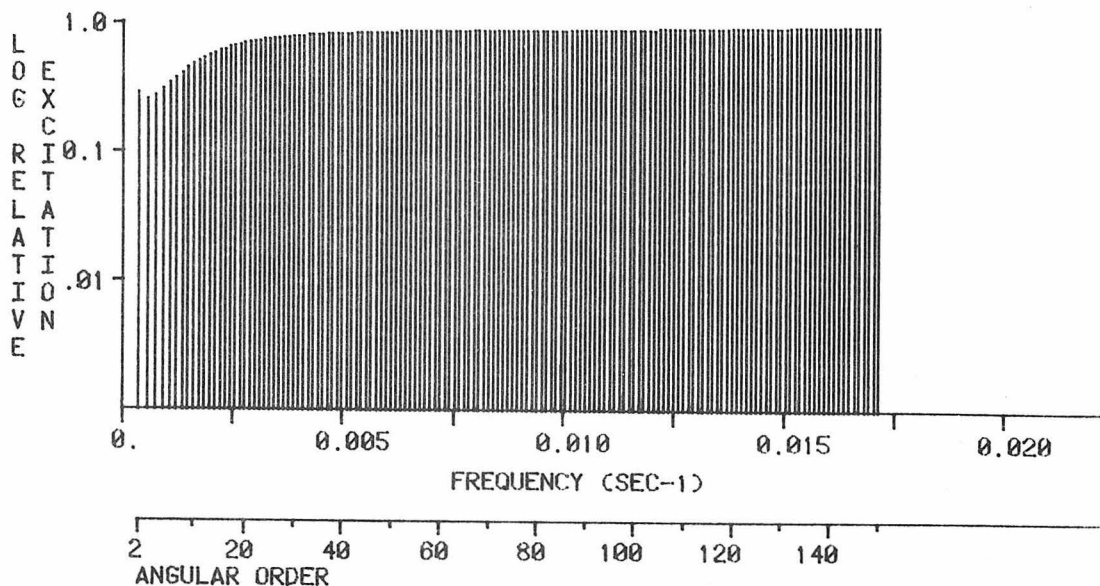
MAXIMUM EXCITATION = 0.369734E -6 CM-SEC ; (30 S 8; T= 77.59 SEC)

EXCITATION NORMALIZED TO 0 S 9 (RAD. COMP.) ; 0.84435000E -4

ATTENUATION INCLUDED; RECORD STARTS AT 12.00 HRS.; LENGTH = 20.00 HRS.

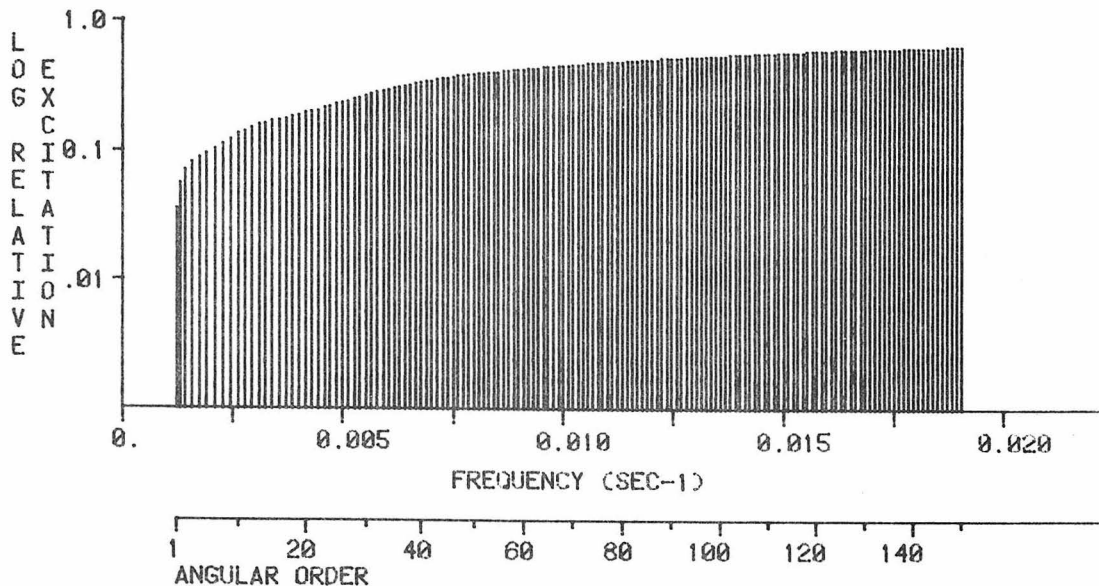
Figure A2.3 - The excitation spectra for the fundamental toroidal modes and the first seven toroidal overtone branches generated by the 1964 Alaska earthquake. All excitations are normalized to the maximum fundamental mode excitation. This figure extends over the following 4 pages.

TRANSVERSE COMPONENT; RADIAL ORDER 0



MAXIMUM EXCITATION = 0.842600E -3 CM-SEC ; (0 T 150; T= 58.41 SEC)

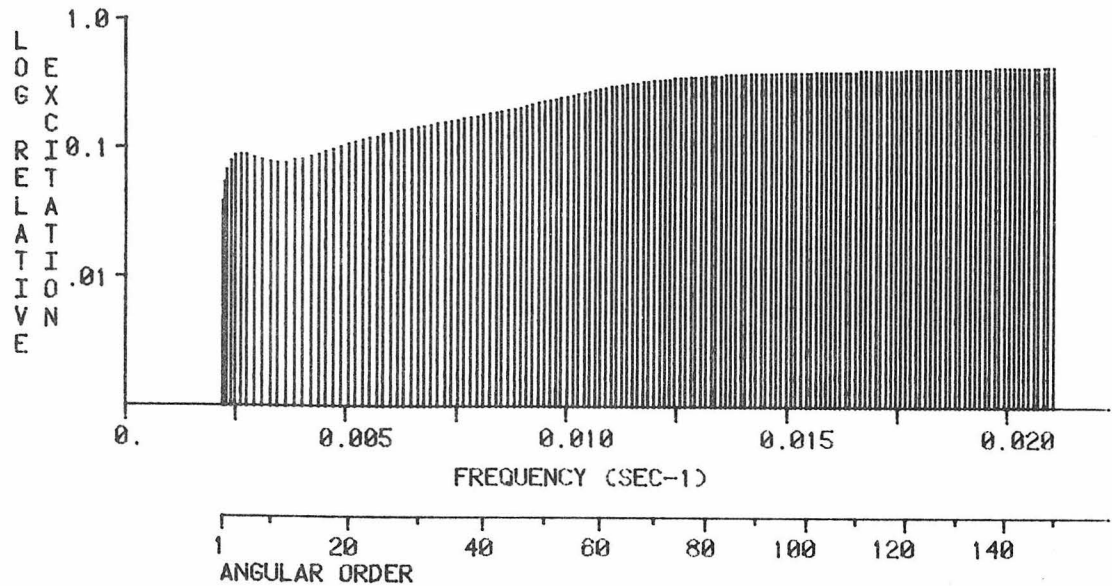
TRANSVERSE COMPONENT; RADIAL ORDER 1



MAXIMUM EXCITATION = 0.546276E -3 CM-SEC ; (1 T 150; T= 52.63 SEC)

EXCITATION NORMALIZED TO 0 T 150 ; 0.842600E -3

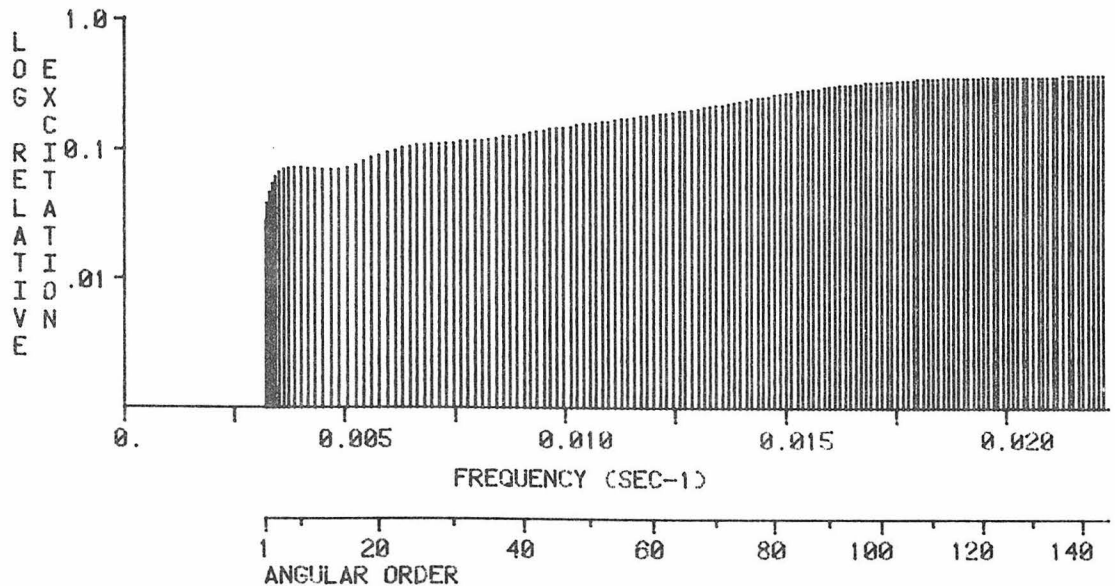
TRANSVERSE COMPONENT; RADIAL ORDER 2



MAXIMUM EXCITATION = 0.381689E -3 CM-SEC ; (2 T 150; T= 47.00 SEC)

EXCITATION NORMALIZED TO 0 T 150 ; 0.842600E -3

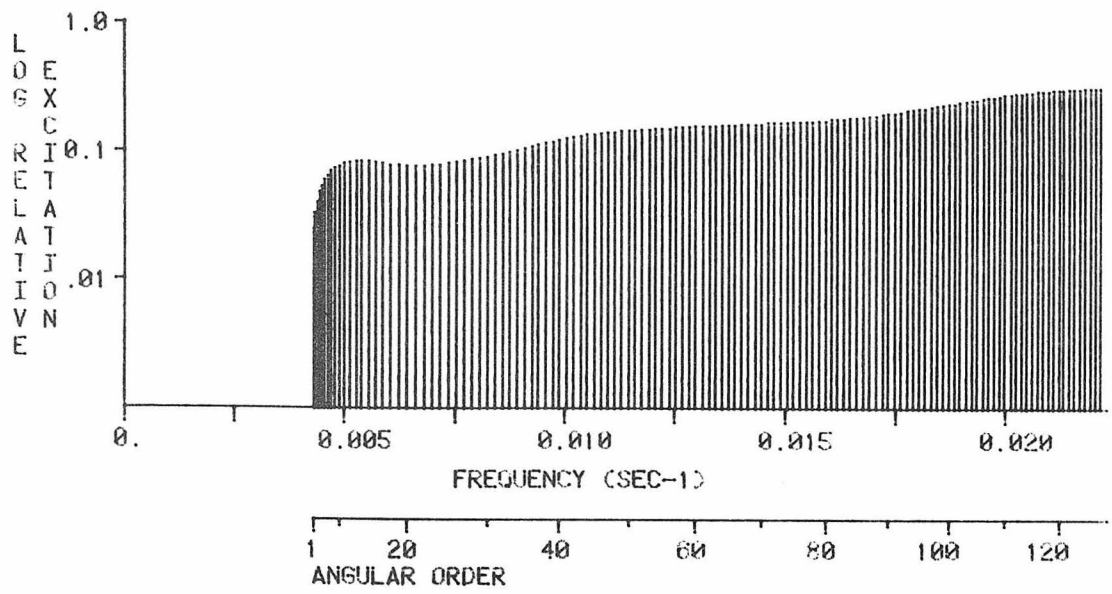
TRANSVERSE COMPONENT; RADIAL ORDER 3



MAXIMUM EXCITATION = 0.318506E -3 CM-SEC ; (3 T 144; T= 45.15 SEC)

EXCITATION NORMALIZED TO 0 T 150 ; 0.842600E -3

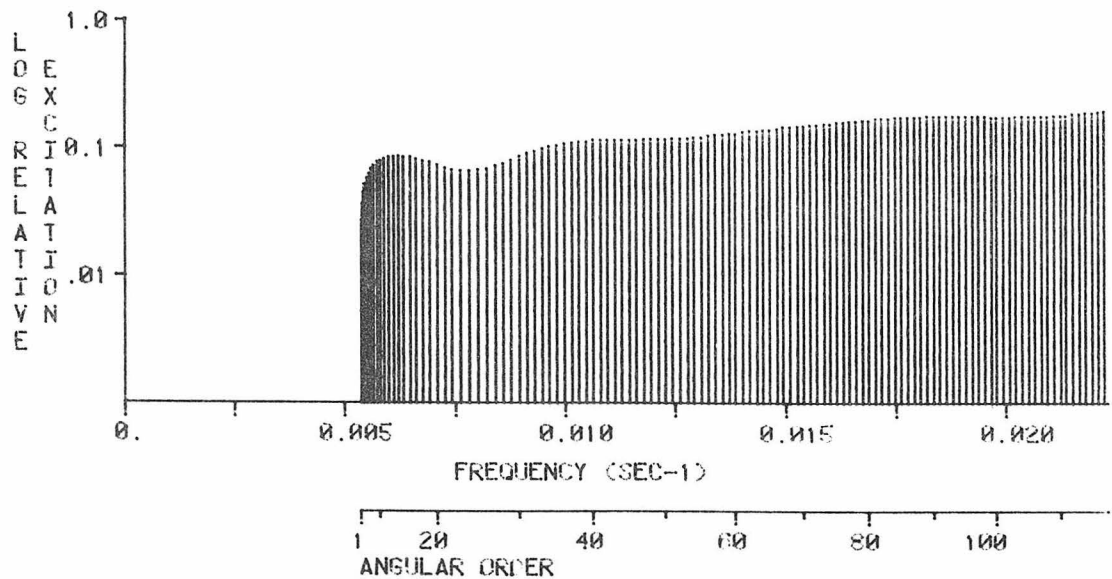
TRANSVERSE COMPONENT; RADIAL ORDER 4



MAXIMUM EXCITATION = 0.275809E -3 CM-SEC ; (4 T 128; T= 45.23 SEC)

EXCITATION NORMALIZED TO 0 T 150 ; 0.842600E -3

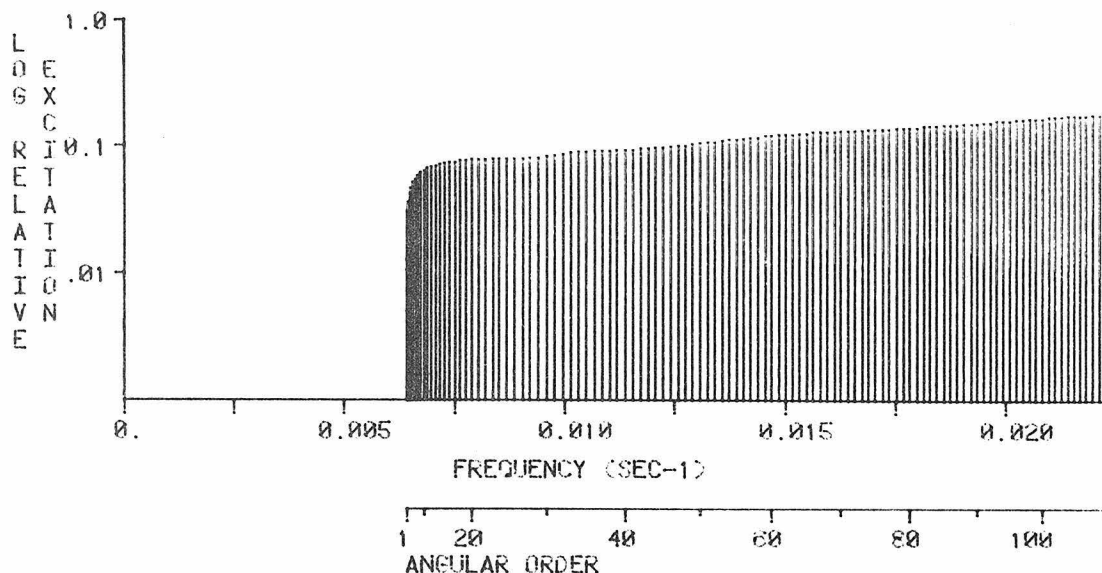
TRANSVERSE COMPONENT; RADIAL ORDER 5



MAXIMUM EXCITATION = 0.170400E -3 CM-SEC ; (5 T 117; T= 45.00 SEC)

EXCITATION NORMALIZED TO 0 T 150 ; 0.842600E -3

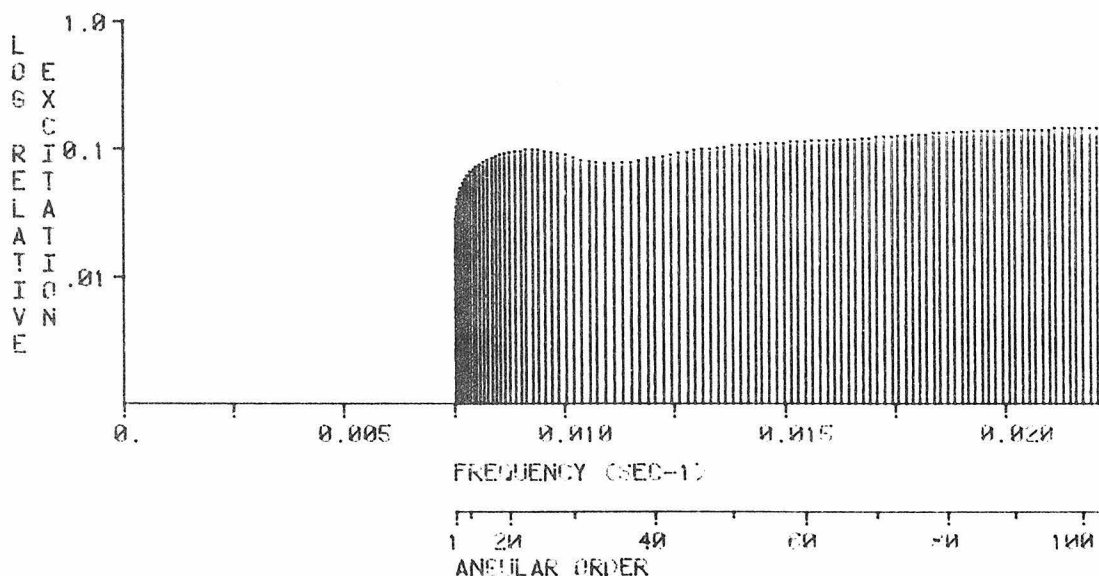
TRANSVERSE COMPONENT; RACIAL ORDER 6



MAXIMUM EXCITATION = 0.152977E -3 CM-SEC ; (6 T 110; T= 45.00 SEC)

EXCITATION NORMALIZED TO 0 T 150 ; 0.842000E -3

TRANSVERSE COMPONENT; RACIAL ORDER 7

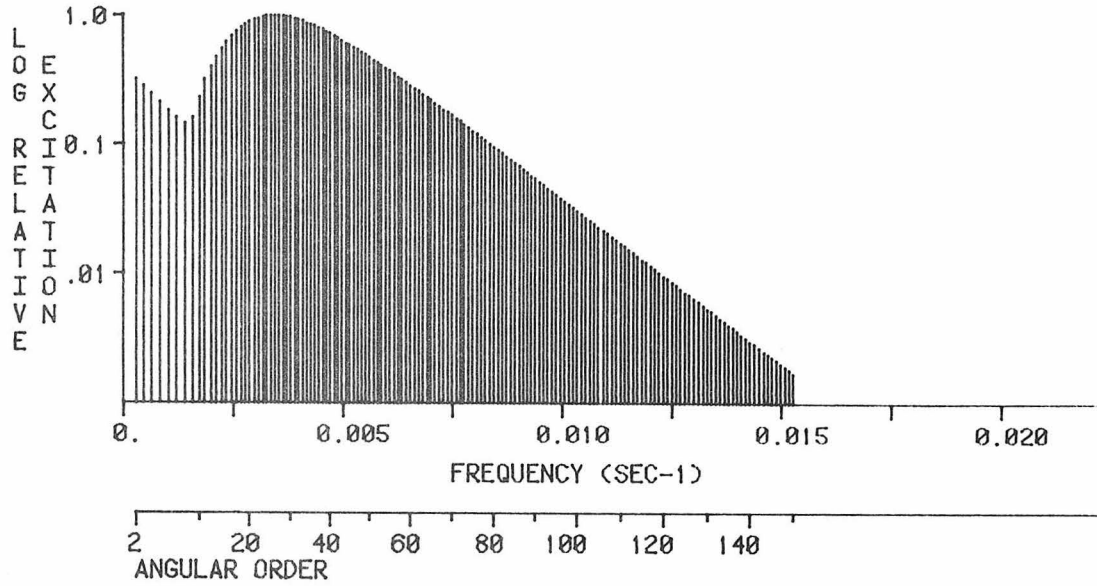


MAXIMUM EXCITATION = 0.127542E -3 CM-SEC ; (7 T 103; T= 45.10 SEC)

EXCITATION NORMALIZED TO 0 T 150 ; 0.842000E -3

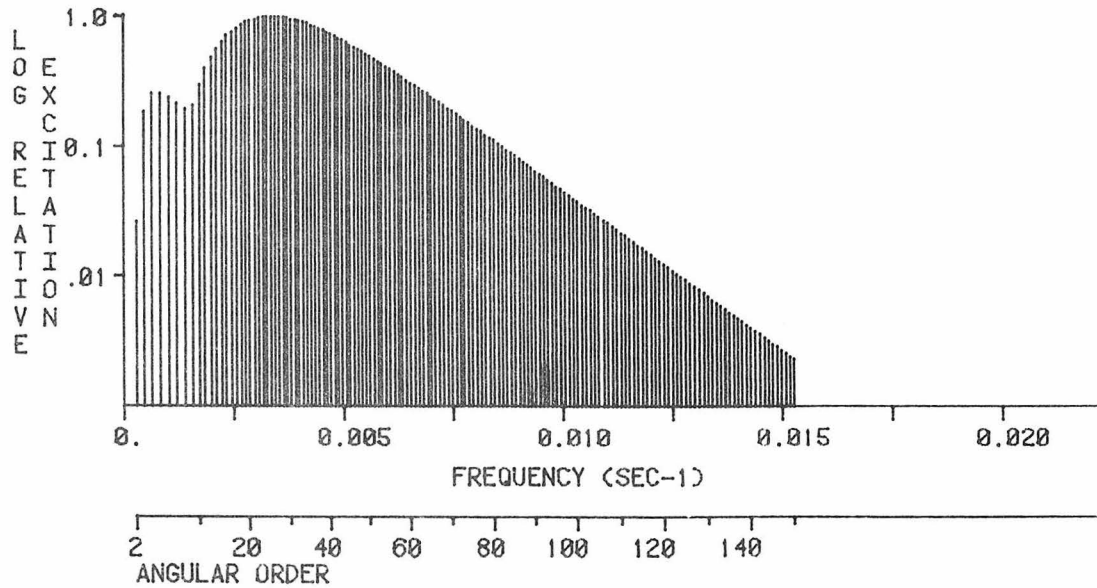
Figure A2.4 - The excitation spectra for the fundamental spheroidal branch and first thirty spheroidal overtone branches generated by the 1970 deep Columbia earthquake. Both the vertical and the radial components of displacement are shown. All excitations are normalized to the maximum fundamental mode excitation on the appropriate component. Modes with an excitation level more than 60 db below the maximum fundamental mode excitation are plotted as small negative tick marks along the horizontal axis. This figure extends over the following 31 pages.

VERTICAL COMPONENT; RADIAL ORDER 0



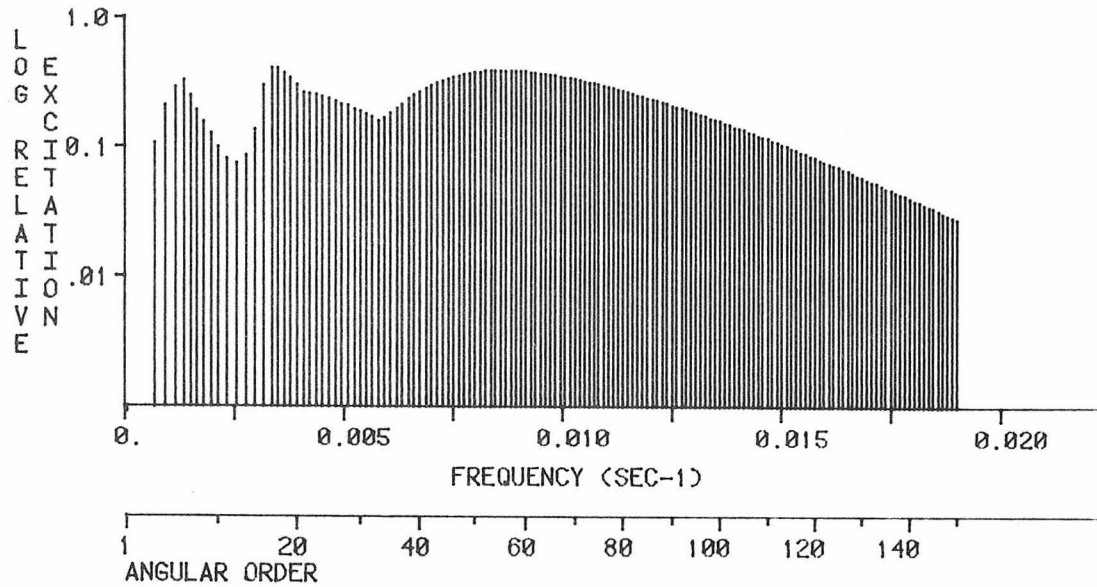
MAXIMUM EXCITATION = 0.686730E -3 CM-SEC ; (0 S 26; T= 289.78 SEC)

RADIAL COMPONENT; RADIAL ORDER 0



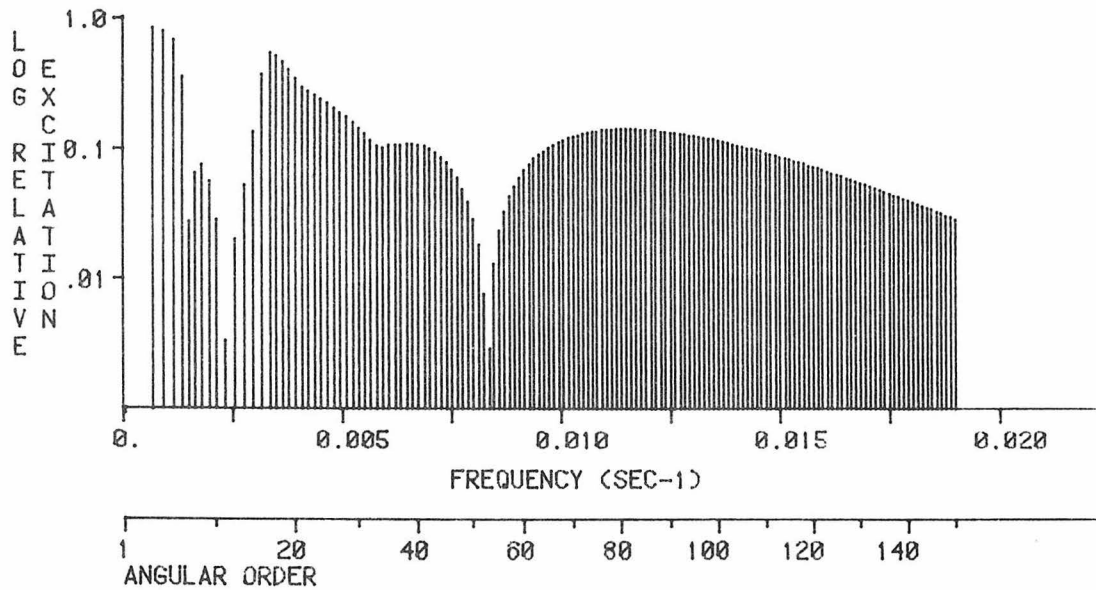
MAXIMUM EXCITATION = 0.468734E -3 CM-SEC ; (0 S 25; T= 297.75 SEC)

VERTICAL COMPONENT; RADIAL ORDER 1



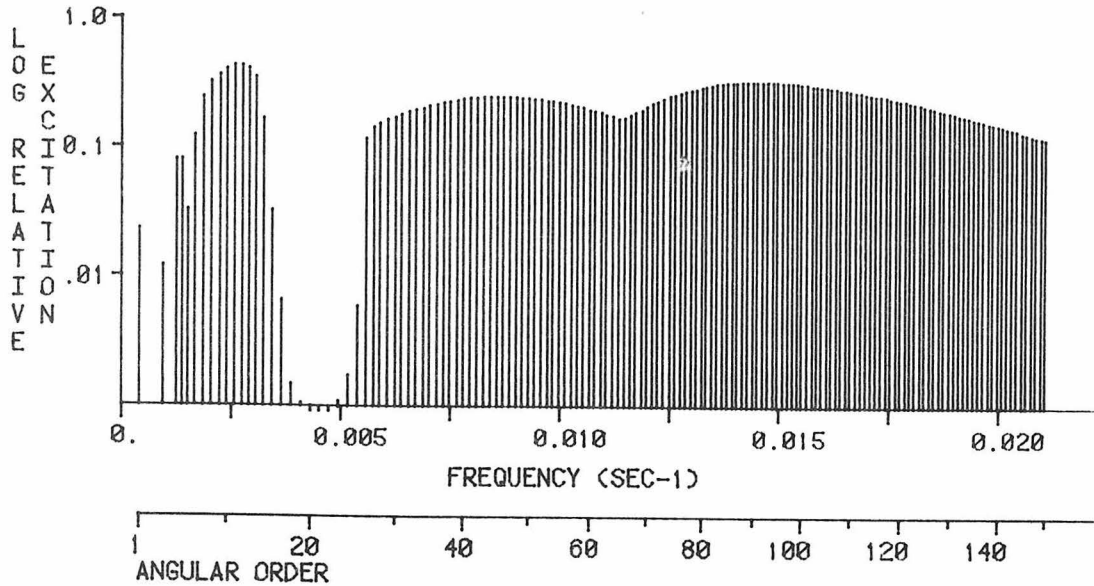
MAXIMUM EXCITATION = 0.279700E -3 CM-SEC ; (1 S 16; T= 299.39 SEC)
EXCITATION NORMALIZED TO 0 S 26 (VERT. COMP.) ; 0.68673000E -3

RADIAL COMPONENT; RADIAL ORDER 1



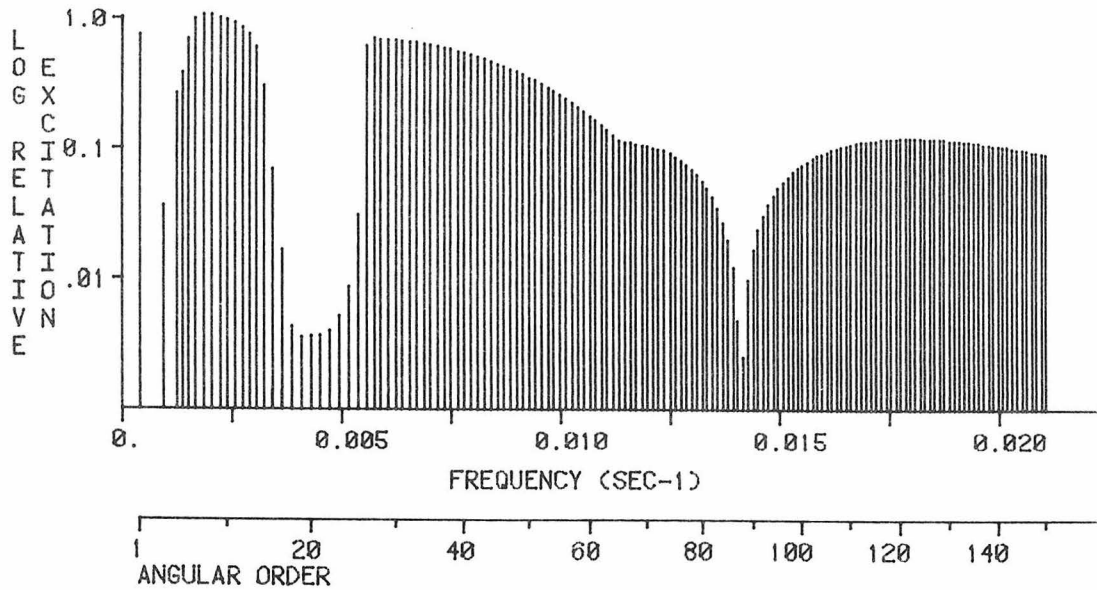
MAXIMUM EXCITATION = 0.392471E -3 CM-SEC ; (1 S 2; T=1469.85 SEC)
EXCITATION NORMALIZED TO 0 S 25 (RAD. COMP.) ; 0.46873400E -3

VERTICAL COMPONENT; RADIAL ORDER 2



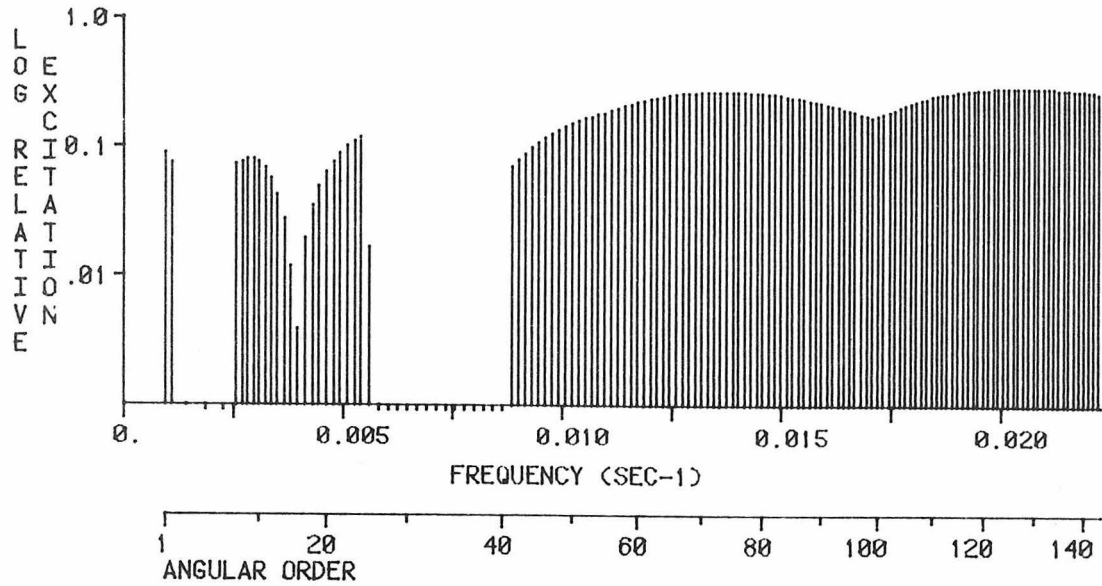
MAXIMUM EXCITATION = 0.293097E -3 CM-SEC ; (2 S 12; T= 365.15 SEC)
EXCITATION NORMALIZED TO 0 S 26 (VERT. COMP.) ; 0.68673000E -3

RADIAL COMPONENT; RADIAL ORDER 2



MAXIMUM EXCITATION = 0.496926E -3 CM-SEC ; (2 S 7; T= 536.17 SEC)
EXCITATION NORMALIZED TO 0 S 25 (RAD. COMP.) ; 0.46873400E -3

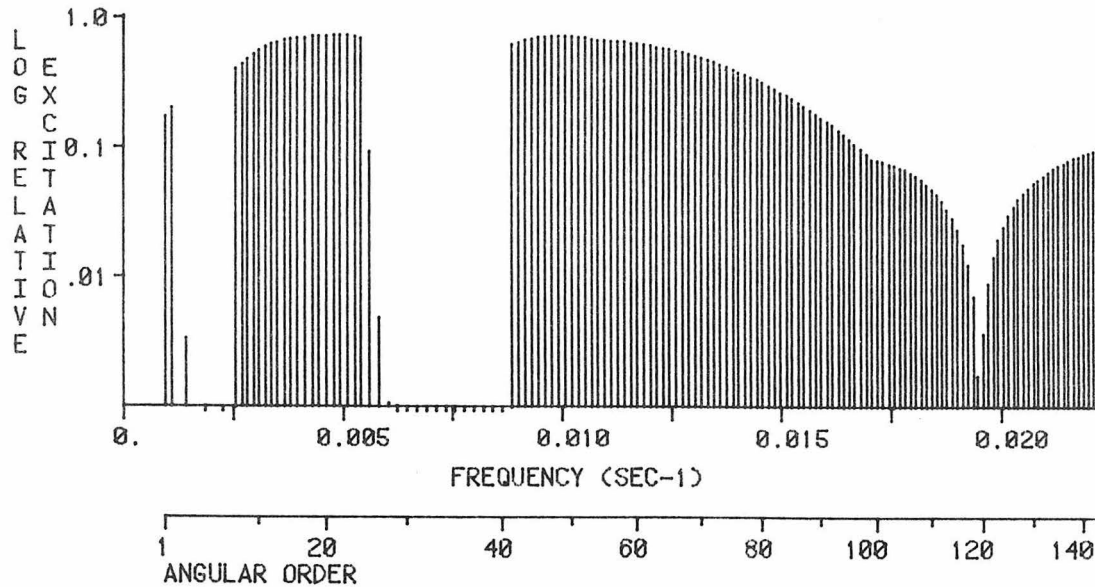
VERTICAL COMPONENT; RADIAL ORDER 3



MAXIMUM EXCITATION = 0.205974E -3 CM-SEC ; (3 S 127; T= 49.10 SEC)

EXCITATION NORMALIZED TO 0 S 26 (VERT. COMP.) ; 0.68673000E -3

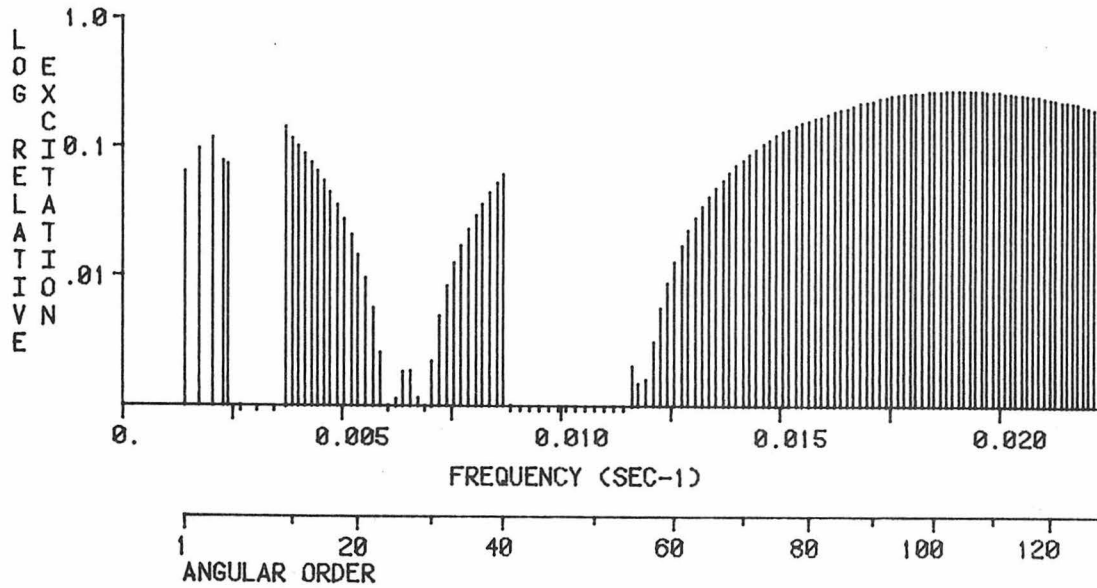
RADIAL COMPONENT; RADIAL ORDER 3



MAXIMUM EXCITATION = 0.341356E -3 CM-SEC ; (3 S 48; T= 100.98 SEC)

EXCITATION NORMALIZED TO 0 S 25 (RAD. COMP.) ; 0.46873400E -3

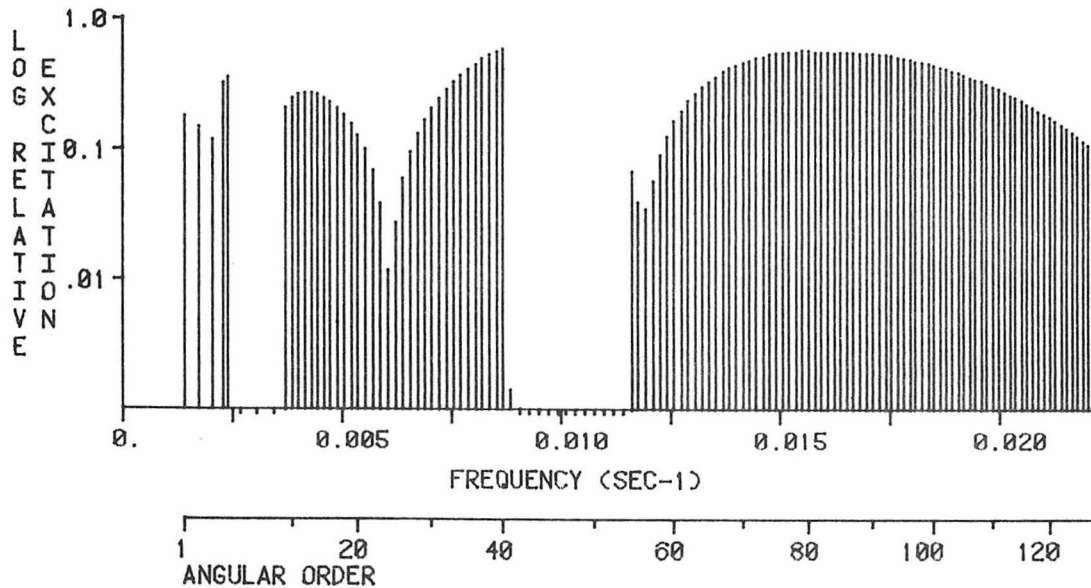
VERTICAL COMPONENT; RADIAL ORDER 4



MAXIMUM EXCITATION = 0.195391E -3 CM-SEC ; (4 S 105; T= 52.21 SEC)

EXCITATION NORMALIZED TO 0 S 26 (VERT. COMP.) ; 0.68673000E -3

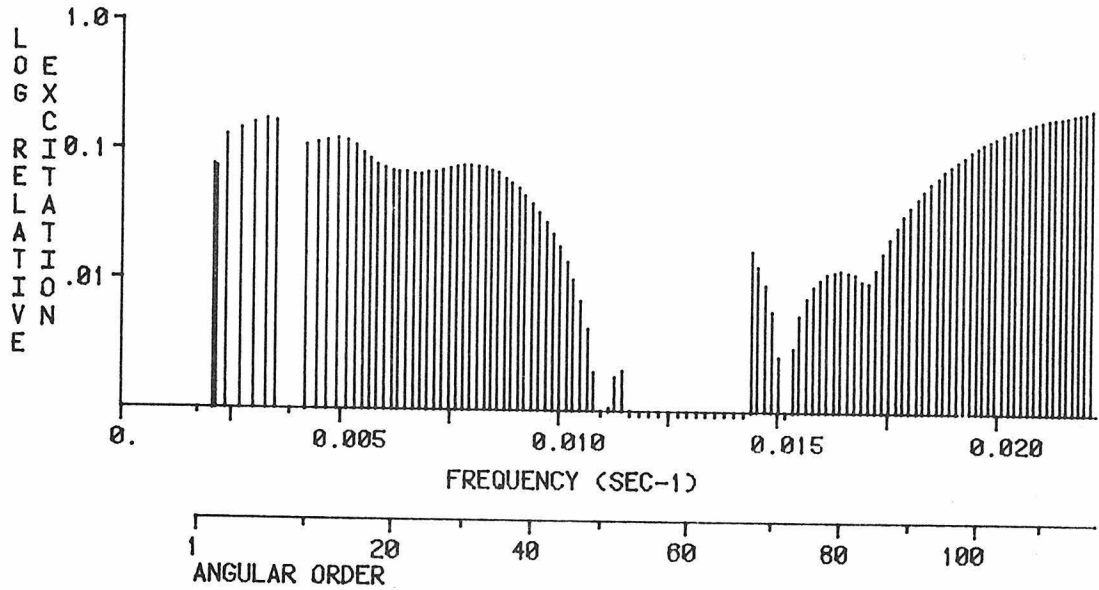
RADIAL COMPONENT; RADIAL ORDER 4



MAXIMUM EXCITATION = 0.280658E -3 CM-SEC ; (4 S 40; T= 115.46 SEC)

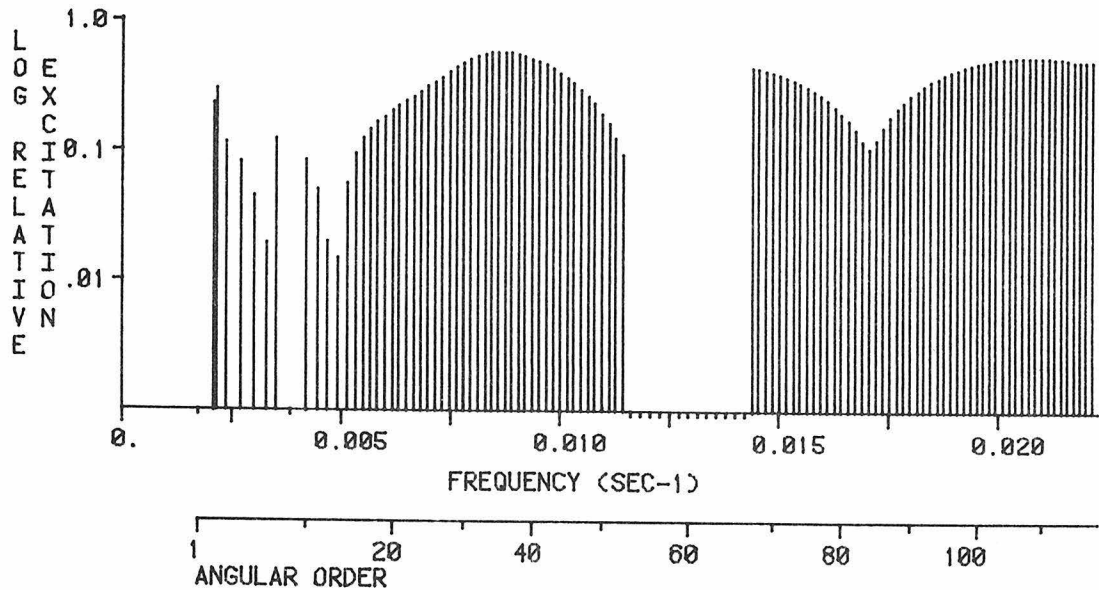
EXCITATION NORMALIZED TO 0 S 25 (RAD. COMP.) ; 0.46873400E -3

VERTICAL COMPONENT; RADIAL ORDER 5



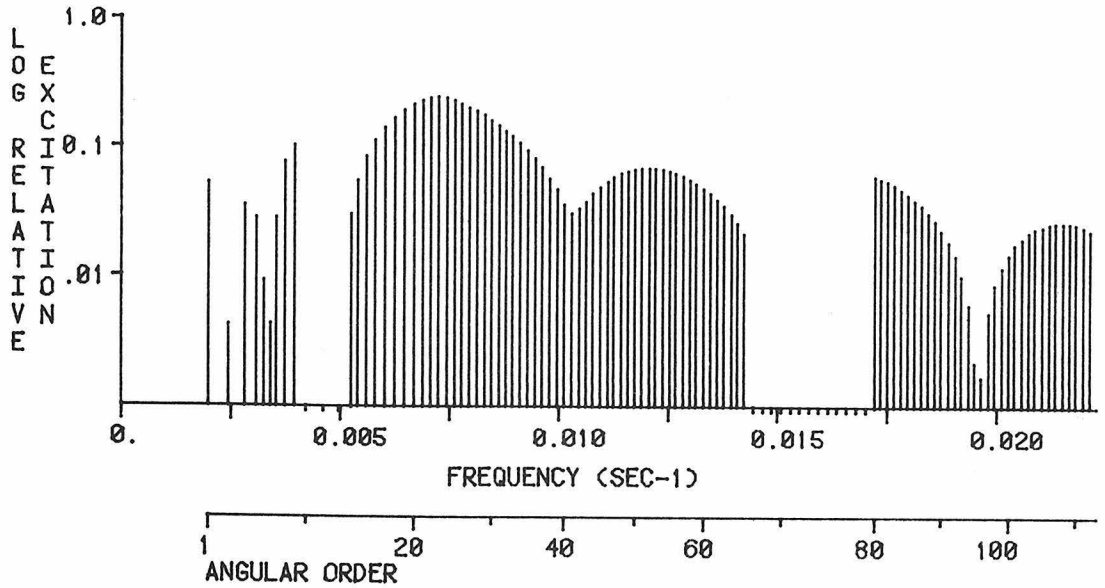
MAXIMUM EXCITATION = 0.155156E -3 CM-SEC ; (5 S 118; T= 45.24 SEC)
EXCITATION NORMALIZED TO 0 S 26 (VERT. COMP.) ; 0.68673000E -3

RADIAL COMPONENT; RADIAL ORDER 5



MAXIMUM EXCITATION = 0.274752E -3 CM-SEC ; (5 S 35; T= 116.68 SEC)
EXCITATION NORMALIZED TO 0 S 25 (RAD. COMP.) ; 0.46873400E -3

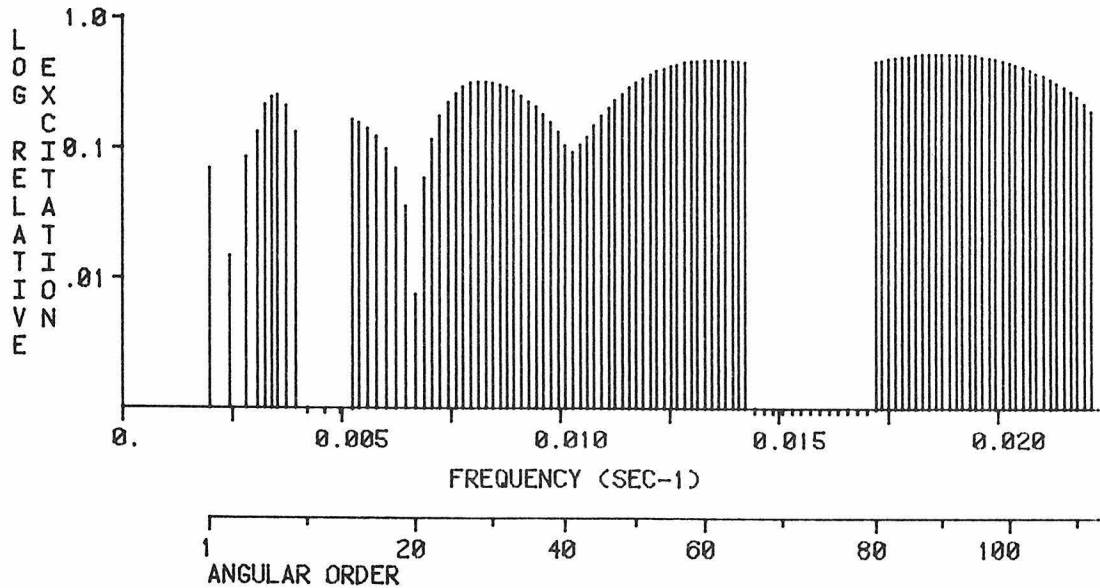
VERTICAL COMPONENT; RADIAL ORDER 6



MAXIMUM EXCITATION = 0.169576E -3 CM-SEC ; (6 S 23; T= 138.16 SEC)

EXCITATION NORMALIZED TO 0 S 26 (VERT. COMP.) ; 0.68673000E -3

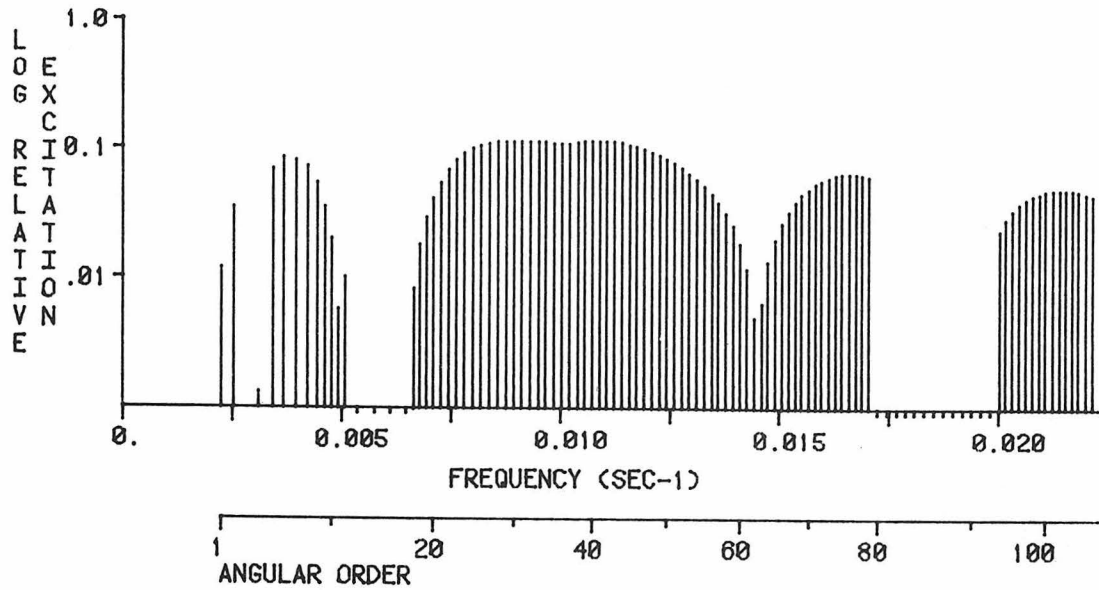
RADIAL COMPONENT; RADIAL ORDER 6



MAXIMUM EXCITATION = 0.257814E -3 CM-SEC ; (6 S 90; T= 53.49 SEC)

EXCITATION NORMALIZED TO 0 S 25 (RAD. COMP.) ; 0.46873400E -3

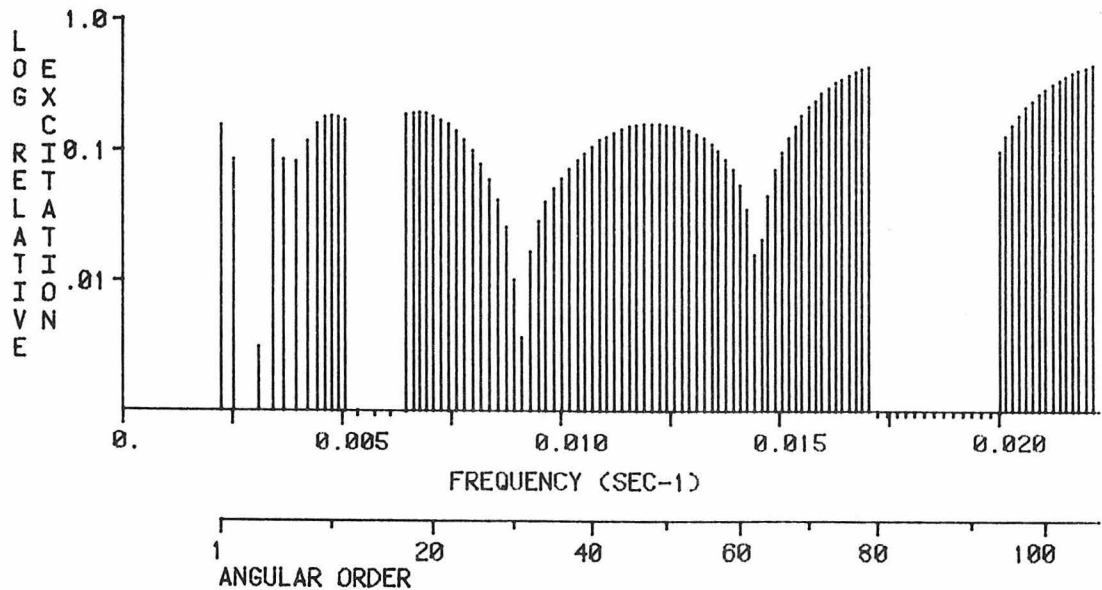
VERTICAL COMPONENT; RADIAL ORDER 7



MAXIMUM EXCITATION = 0.809100E -4 CM-SEC ; (7 S 41; T= 91.85 SEC)

EXCITATION NORMALIZED TO 0 S 26 (VERT. COMP.) ; 0.68673000E -3

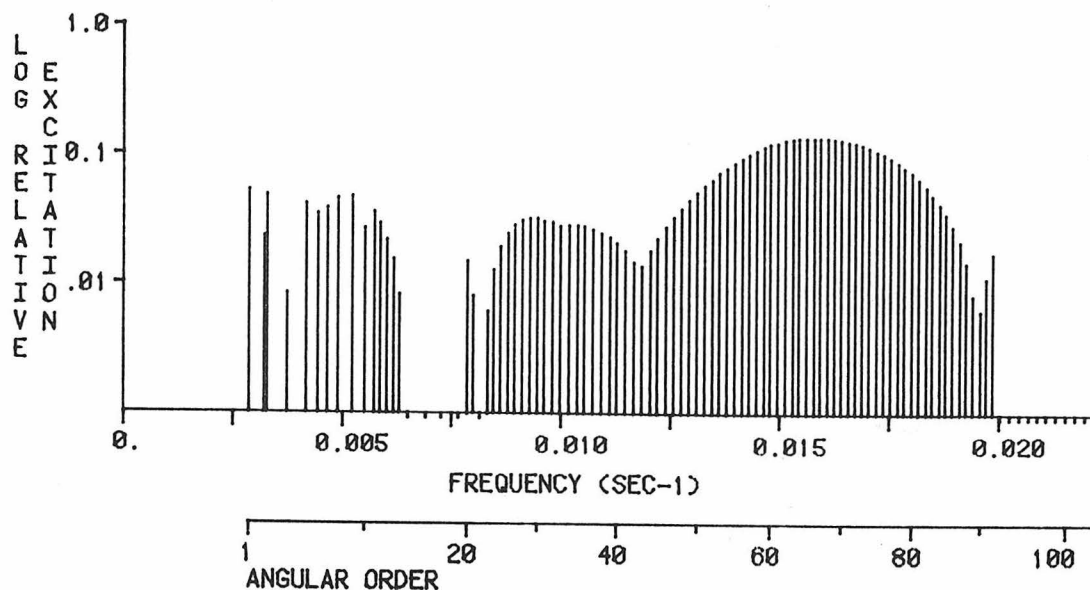
RADIAL COMPONENT; RADIAL ORDER 7



MAXIMUM EXCITATION = 0.216680E -3 CM-SEC ; (7 S 107; T= 45.26 SEC)

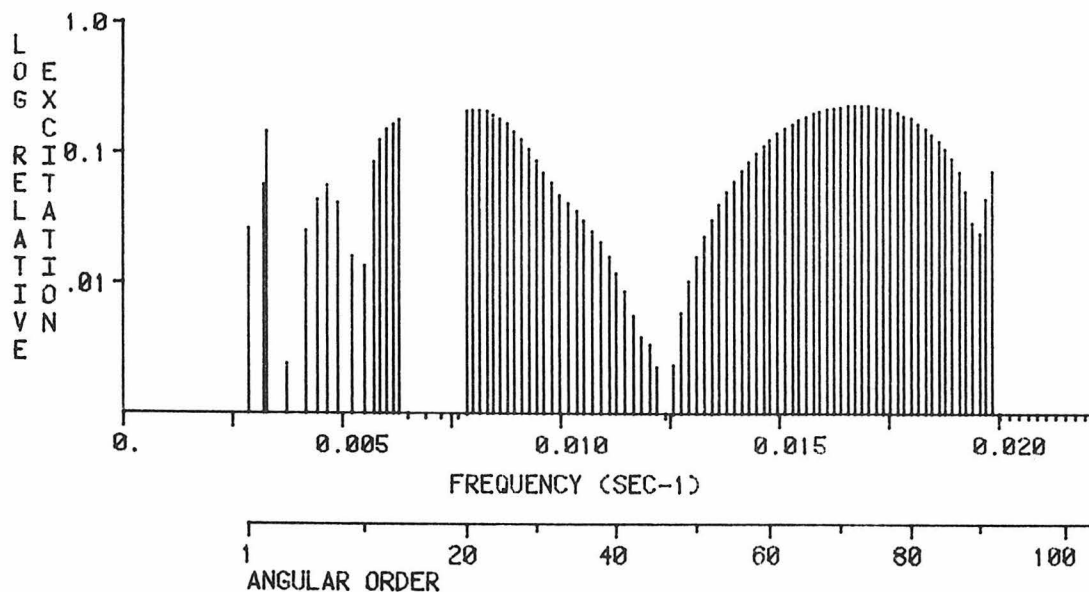
EXCITATION NORMALIZED TO 0 S 25 (RAD. COMP.) ; 0.46873400E -3

VERTICAL COMPONENT; RADIAL ORDER 8



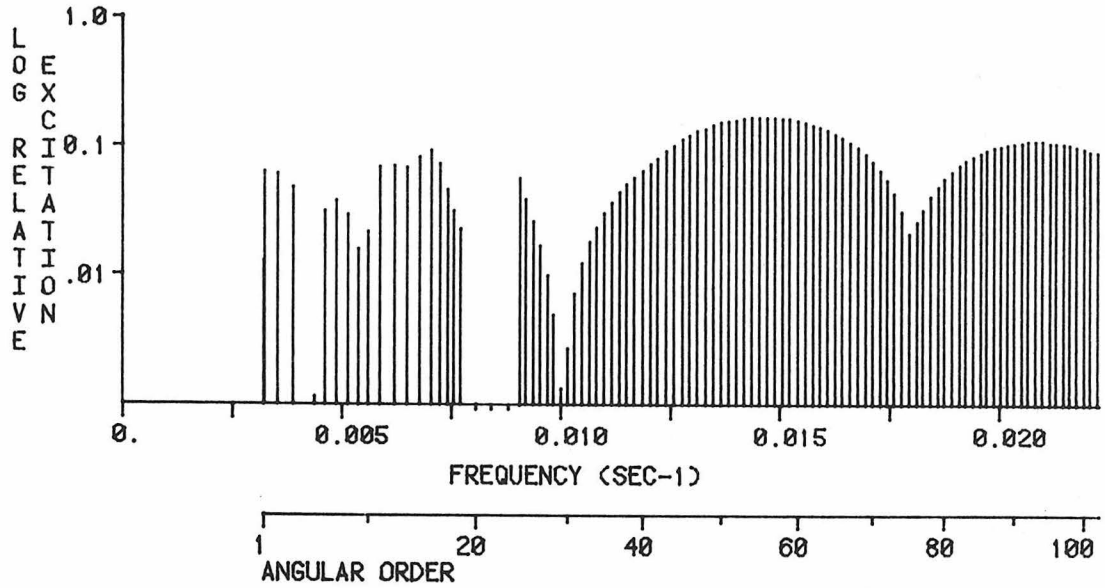
MAXIMUM EXCITATION = 0.968280E -4 CM-SEC ; (8 S 66; T= 63.52 SEC)
EXCITATION NORMALIZED TO 0 S 26 (VERT. COMP.) ; 0.68673000E -3

RADIAL COMPONENT; RADIAL ORDER 8



MAXIMUM EXCITATION = 0.112165E -3 CM-SEC ; (8 S 72; T= 59.86 SEC)
EXCITATION NORMALIZED TO 0 S 25 (RAD. COMP.) ; 0.46873400E -3

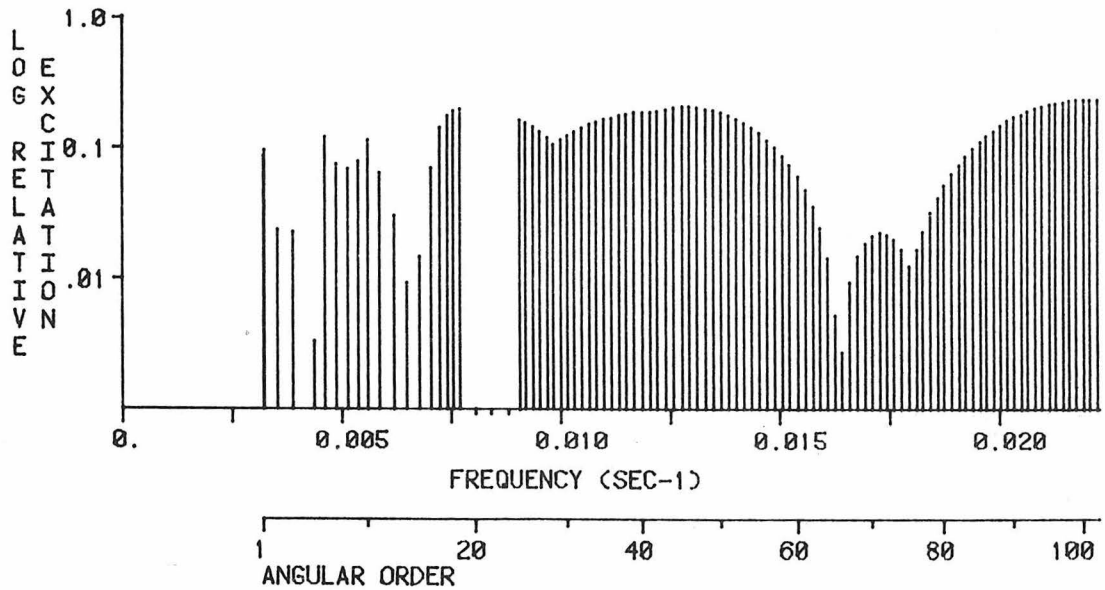
VERTICAL COMPONENT; RADIAL ORDER 9



MAXIMUM EXCITATION = 0.117841E -3 CM-SEC ; (9 S 56; T= 68.09 SEC)

EXCITATION NORMALIZED TO 0 S 26 (VERT. COMP.) ; 0.68673000E -3

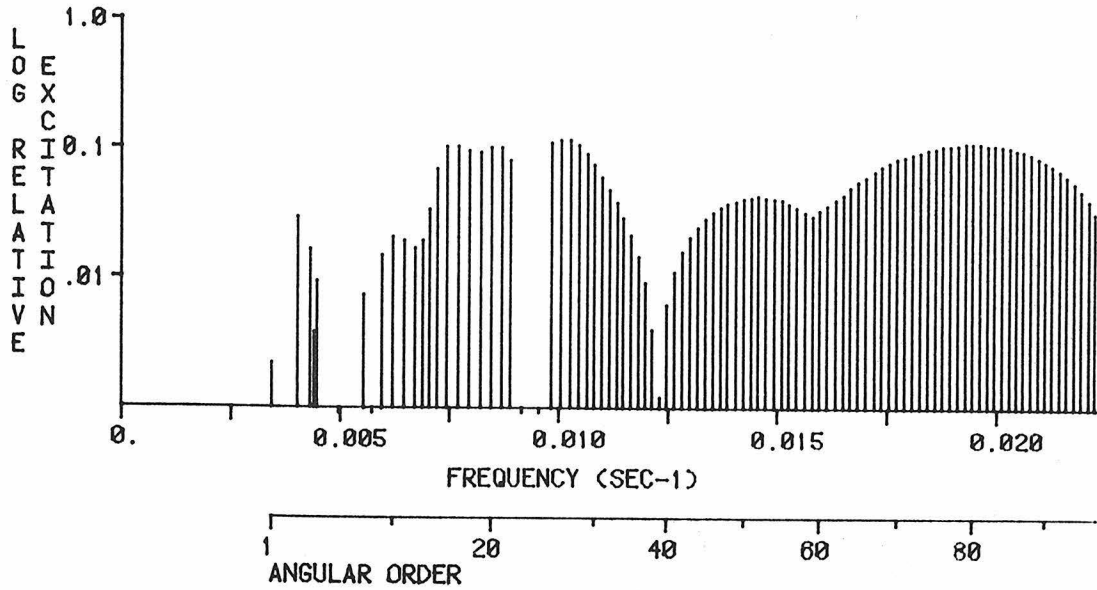
RADIAL COMPONENT; RADIAL ORDER 9



MAXIMUM EXCITATION = 0.113767E -3 CM-SEC ; (9 S 100; T= 45.70 SEC)

EXCITATION NORMALIZED TO 0 S 25 (RAD. COMP.) ; 0.46873400E -3

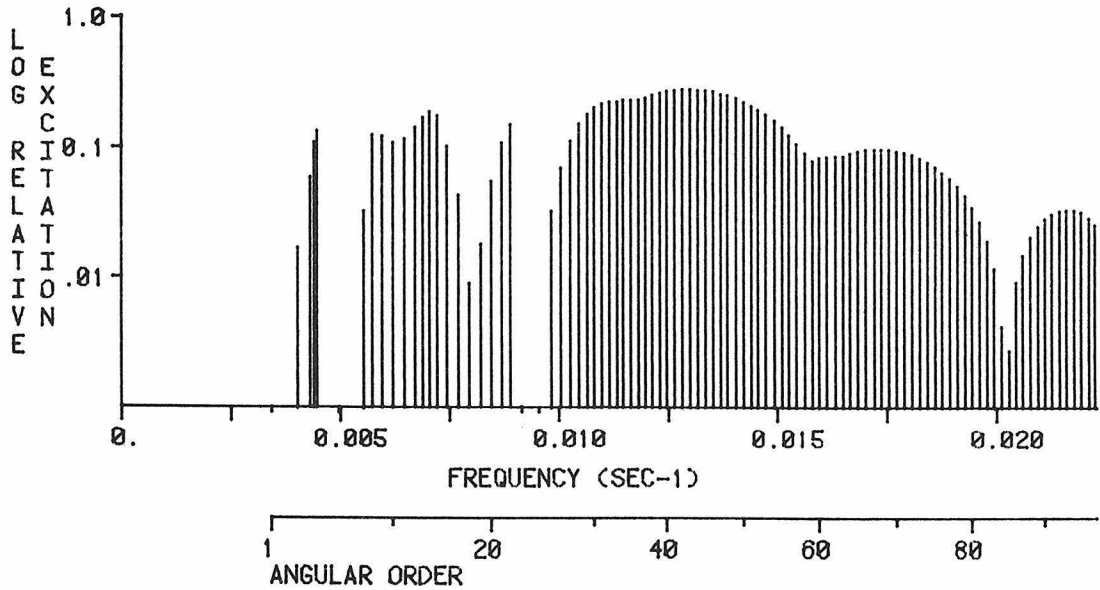
VERTICAL COMPONENT; RADIAL ORDER 10



MAXIMUM EXCITATION = 0.805200E -4 CM-SEC ; (10 S 26; T= 99.56 SEC)

EXCITATION NORMALIZED TO 0 S 26 (VERT. COMP.) ; 0.68673000E -3

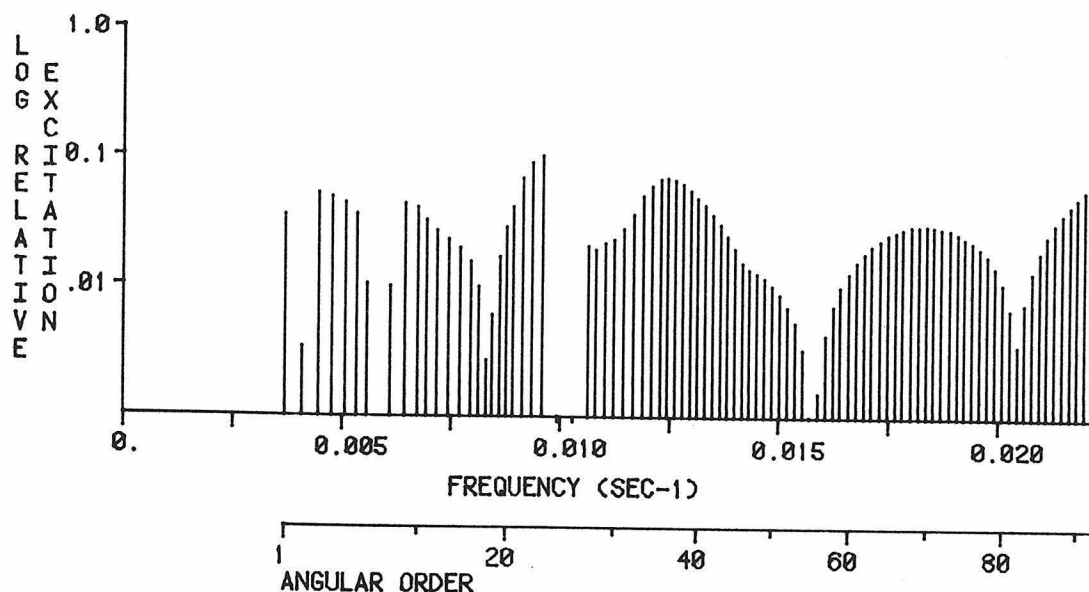
RADIAL COMPONENT; RADIAL ORDER 10



MAXIMUM EXCITATION = 0.135551E -3 CM-SEC ; (10 S 43; T= 77.05 SEC)

EXCITATION NORMALIZED TO 0 S 25 (RAD. COMP.) ; 0.46873400E -3

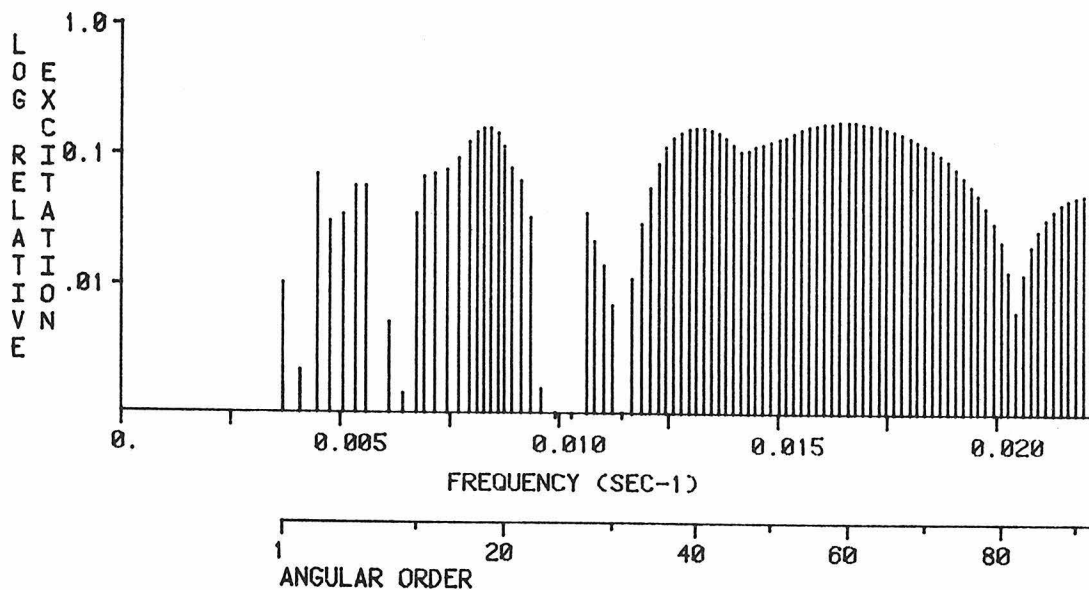
VERTICAL COMPONENT; RADIAL ORDER 11



MAXIMUM EXCITATION = 0.713970E -4 CM-SEC ; (11 S 24; T= 104.37 SEC)

EXCITATION NORMALIZED TO 0 S 26 (VERT. COMP.) ; 0.68673000E -3

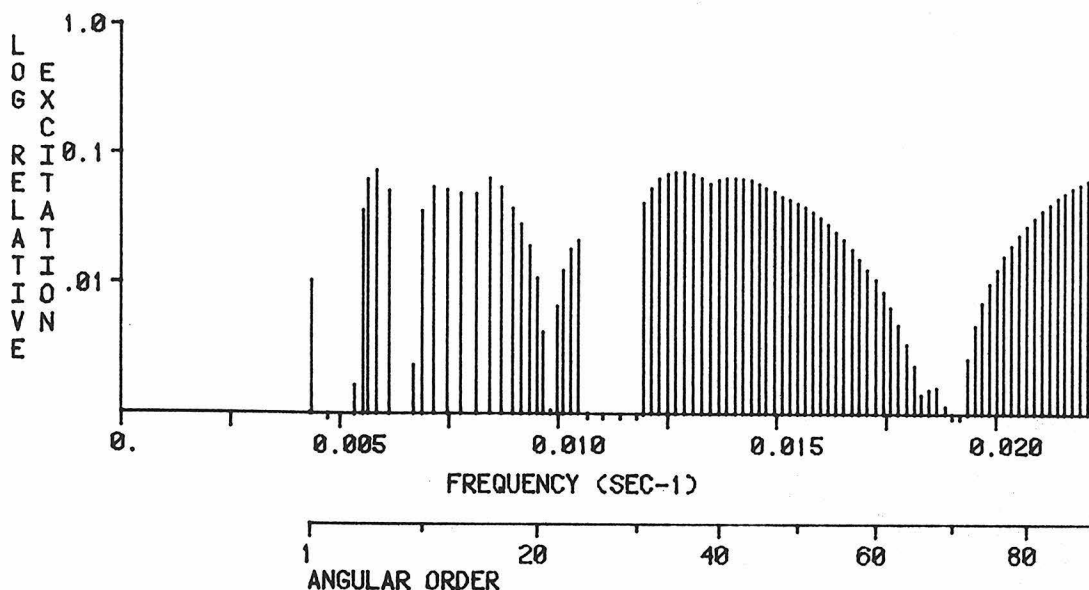
RADIAL COMPONENT; RADIAL ORDER 11



MAXIMUM EXCITATION = 0.870610E -4 CM-SEC ; (11 S 60; T= 60.35 SEC)

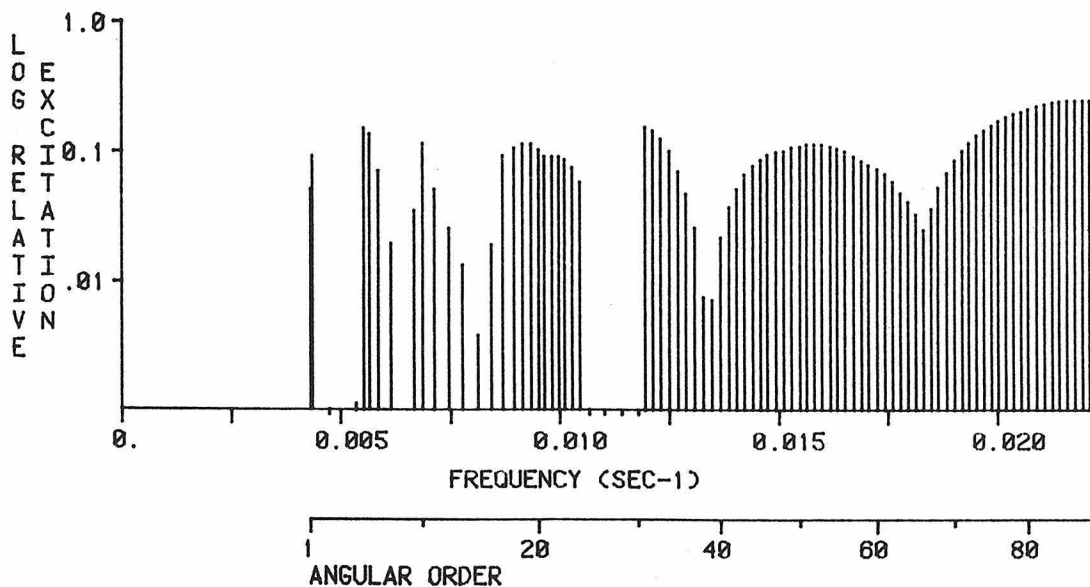
EXCITATION NORMALIZED TO 0 S 25 (RAD. COMP.) ; 0.46873400E -3

VERTICAL COMPONENT; RADIAL ORDER 12



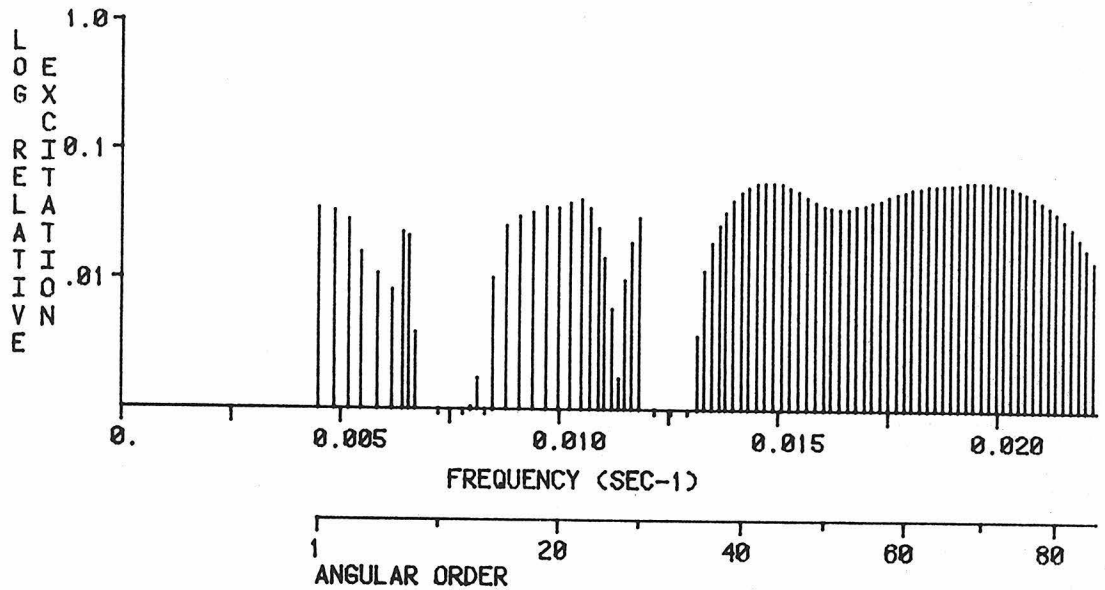
MAXIMUM EXCITATION = 0.516021E -4 CM-SEC ; (12 S 7; T= 170.70 SEC)
EXCITATION NORMALIZED TO 0 S 26 (VERT. COMP.) ; 0.68673000E -3

RADIAL COMPONENT; RADIAL ORDER 12



MAXIMUM EXCITATION = 0.123054E -3 CM-SEC ; (12 S 87; T= 45.71 SEC)
EXCITATION NORMALIZED TO 0 S 25 (RAD. COMP.) ; 0.46873400E -3

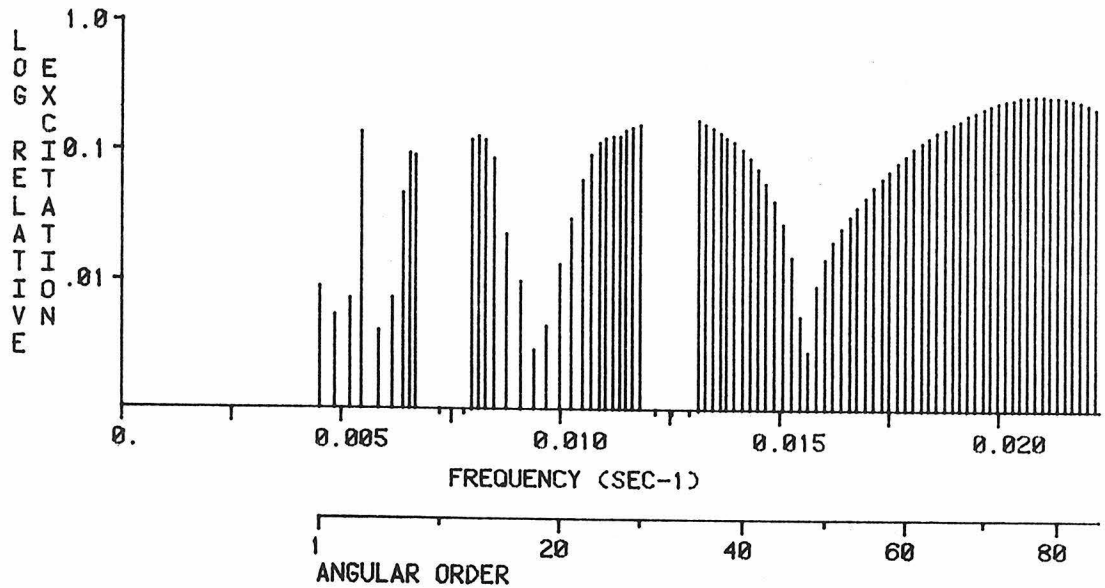
VERTICAL COMPONENT; RADIAL ORDER 13



MAXIMUM EXCITATION = 0.414125E -4 CM-SEC ; (13 S 70; T= 51.03 SEC)

EXCITATION NORMALIZED TO 0 S 26 (VERT. COMP.) ; 0.68673000E -3

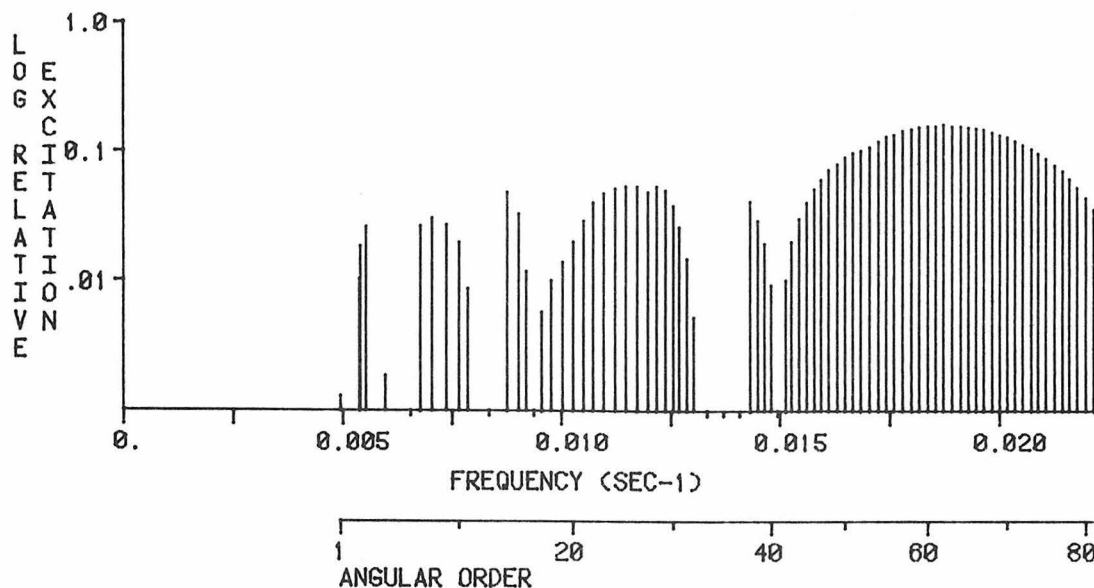
RADIAL COMPONENT; RADIAL ORDER 13



MAXIMUM EXCITATION = 0.132647E -3 CM-SEC ; (13 S 78; T= 47.69 SEC)

EXCITATION NORMALIZED TO 0 S 25 (RAD. COMP.) ; 0.46873400E -3

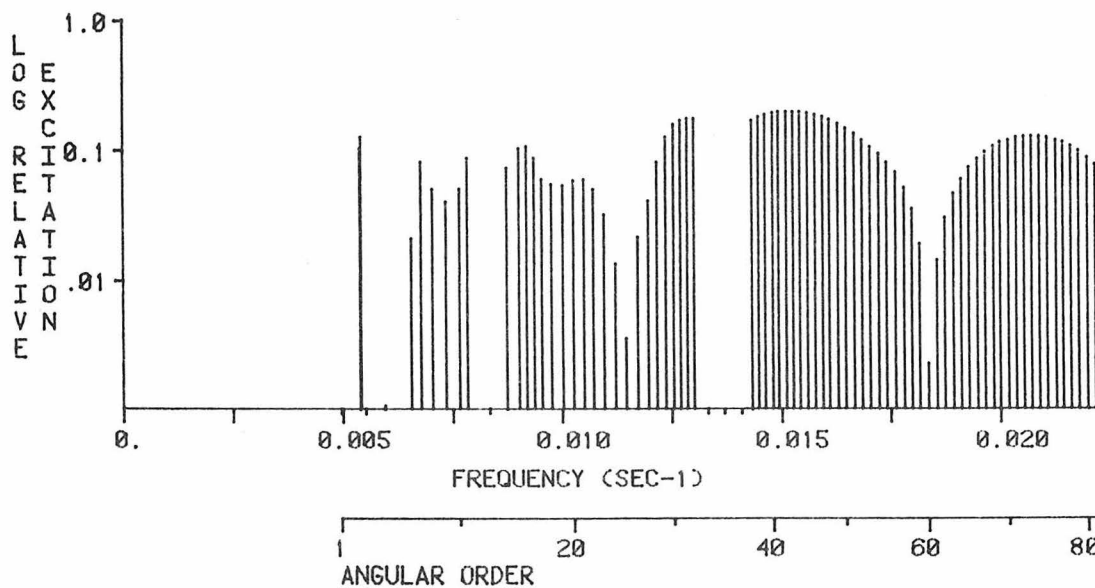
VERTICAL COMPONENT; RADIAL ORDER 14



MAXIMUM EXCITATION = 0.113380E -3 CM-SEC ; (14 S 62; T= 53.49 SEC)

EXCITATION NORMALIZED TO 0 S 26 (VERT. COMP.) ; 0.68673000E -3

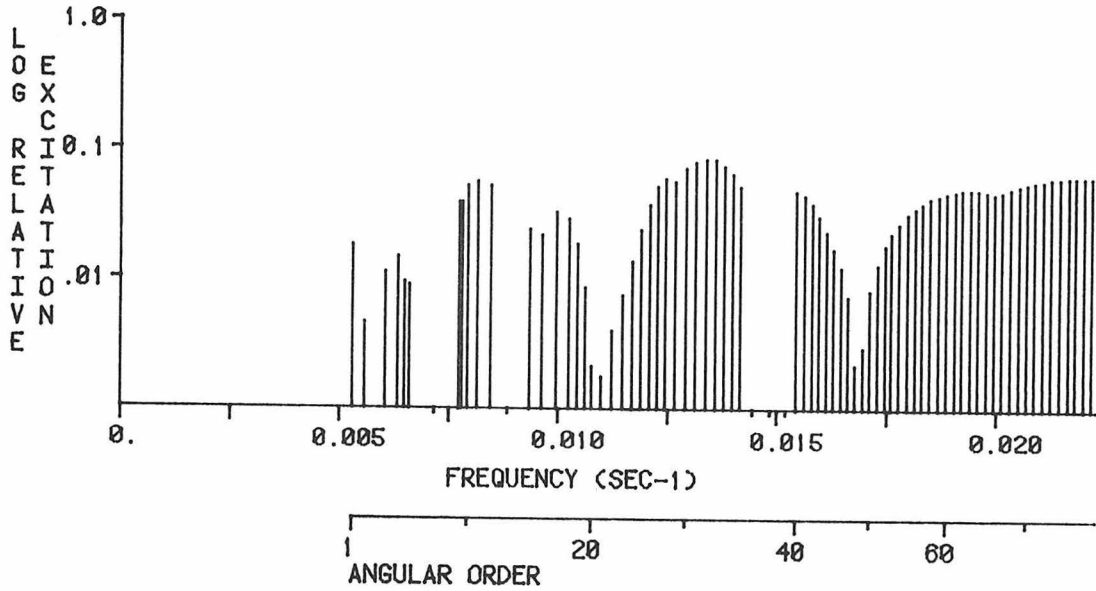
RADIAL COMPONENT; RADIAL ORDER 14



MAXIMUM EXCITATION = 0.961520E -4 CM-SEC ; (14 S 43; T= 65.55 SEC)

EXCITATION NORMALIZED TO 0 S 25 (RAD. COMP.) ; 0.46873400E -3

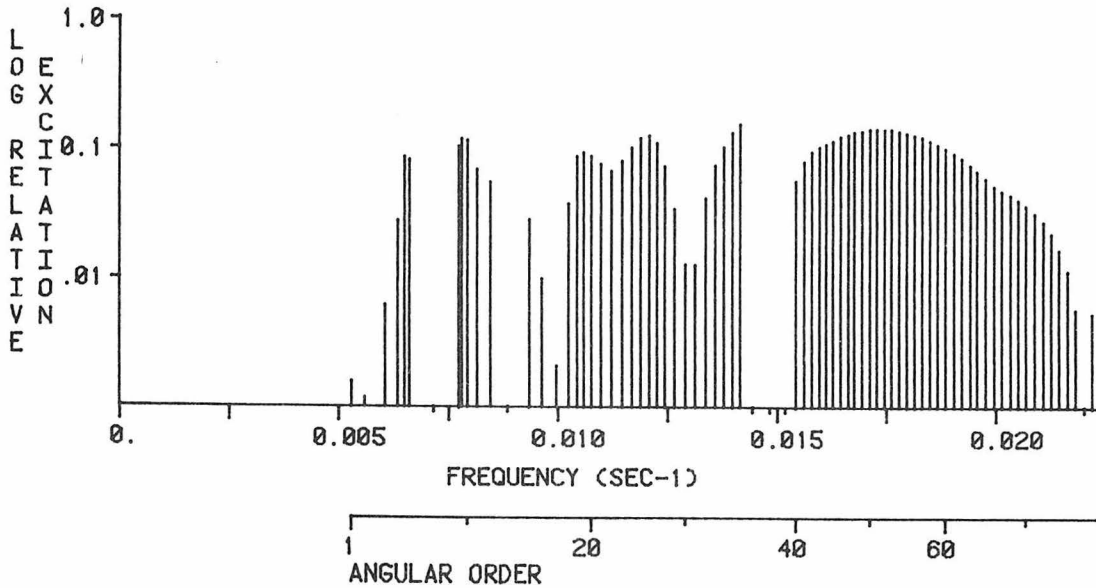
VERTICAL COMPONENT; RADIAL ORDER 15



MAXIMUM EXCITATION = 0.592024E -4 CM-SEC ; (15 S 32; T= 74.92 SEC)

EXCITATION NORMALIZED TO 0 S 26 (VERT. COMP.) ; 0.68673000E -3

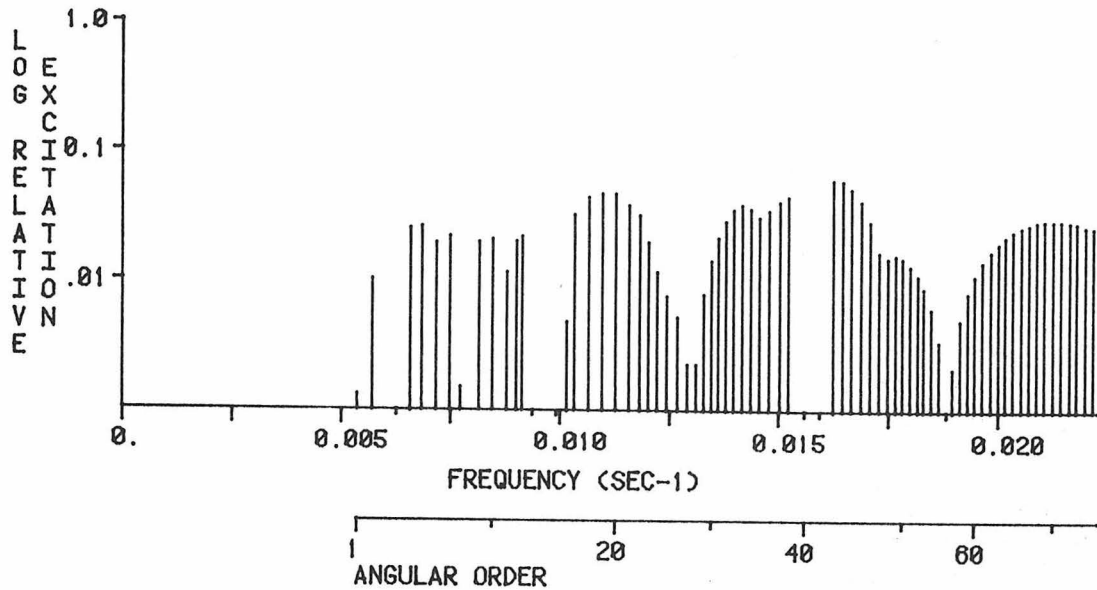
RADIAL COMPONENT; RADIAL ORDER 15



MAXIMUM EXCITATION = 0.750240E -4 CM-SEC ; (15 S 36; T= 70.76 SEC)

EXCITATION NORMALIZED TO 0 S 25 (RAD. COMP.) ; 0.46873400E -3

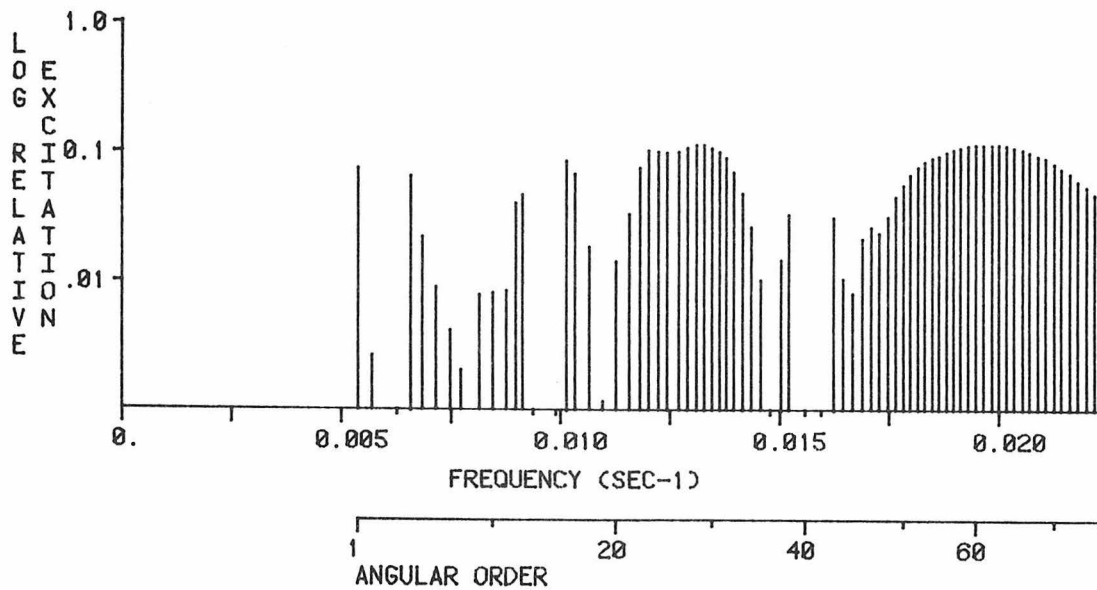
VERTICAL COMPONENT; RADIAL ORDER 16



MAXIMUM EXCITATION = 0.417350E -4 CM-SEC ; (16 S 42; T= 61.67 SEC)

EXCITATION NORMALIZED TO 0 S 26 (VERT. COMP.) ; 0.68673000E -3

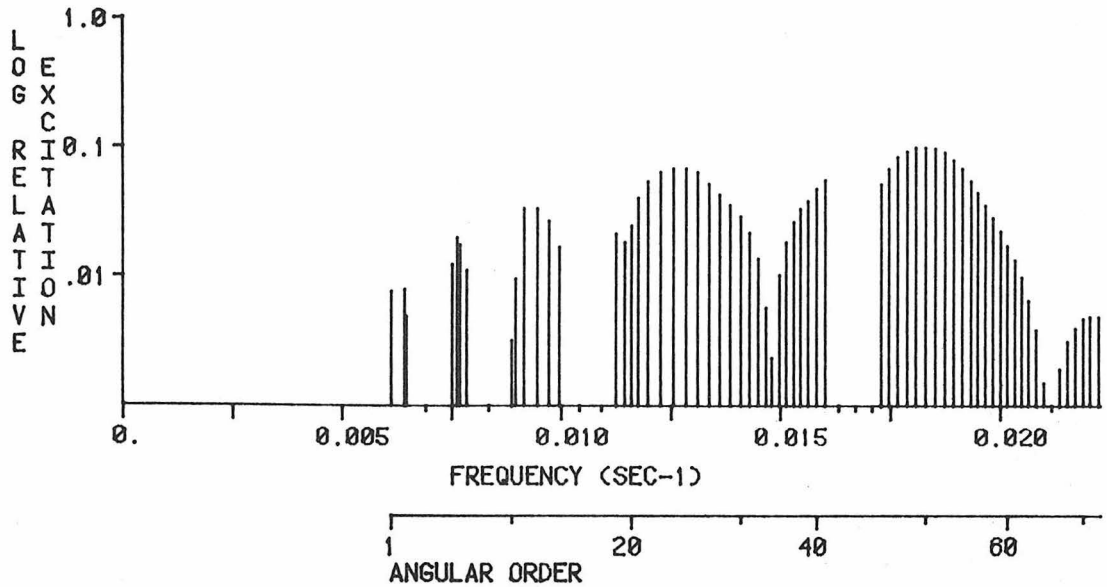
RADIAL COMPONENT; RADIAL ORDER 16



MAXIMUM EXCITATION = 0.561054E -4 CM-SEC ; (16 S 61; T= 50.98 SEC)

EXCITATION NORMALIZED TO 0 S 25 (RAD. COMP.) ; 0.46873400E -3

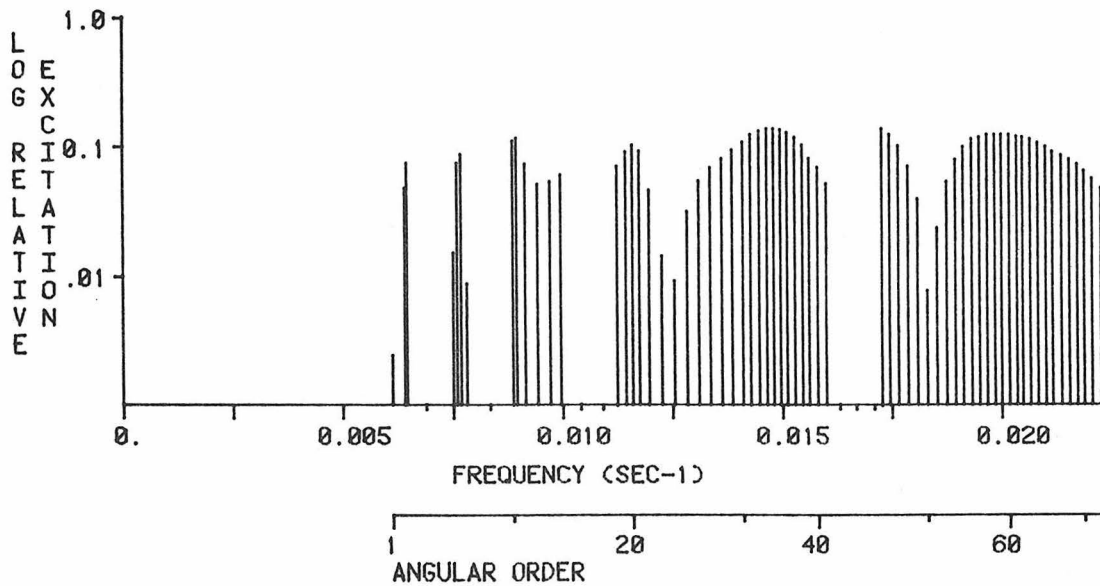
VERTICAL COMPONENT; RADIAL ORDER 17



MAXIMUM EXCITATION = 0.701240E -4 CM-SEC ; (17 S 50; T= 54.73 SEC)

EXCITATION NORMALIZED TO 0 S 26 (VERT. COMP.) ; 0.68673000E -3

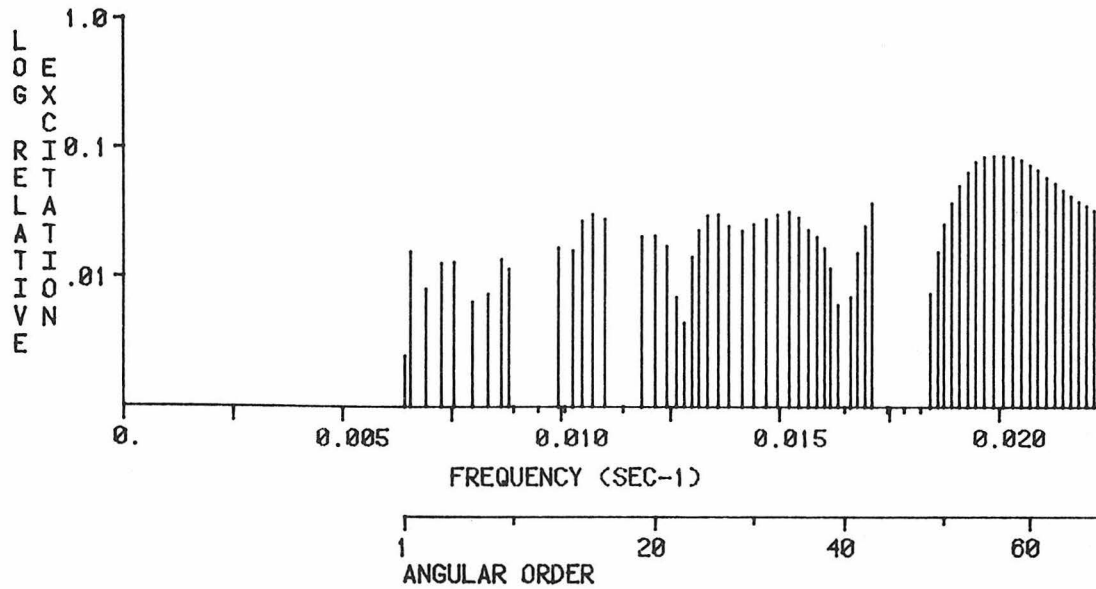
RADIAL COMPONENT; RADIAL ORDER 17



MAXIMUM EXCITATION = 0.673310E -4 CM-SEC ; (17 S 45; T= 57.98 SEC)

EXCITATION NORMALIZED TO 0 S 25 (RAD. COMP.) ; 0.46873400E -3

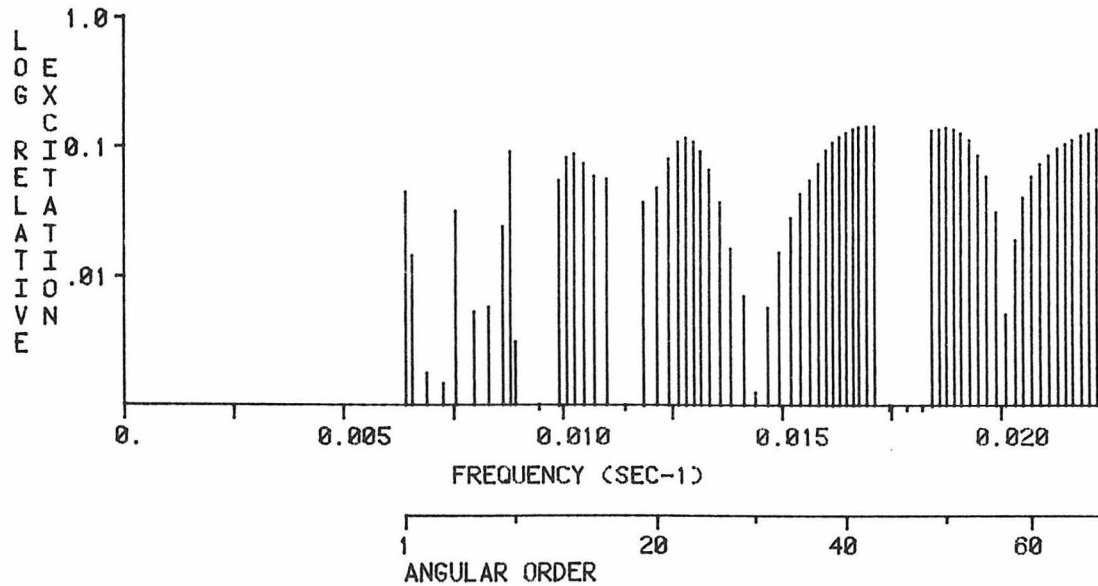
VERTICAL COMPONENT; RADIAL ORDER 18



MAXIMUM EXCITATION = 0.618718E -4 CM-SEC ; (18 S 57; T= 49.85 SEC)

EXCITATION NORMALIZED TO 0 S 26 (VERT. COMP.) ; 0.68673000E -3

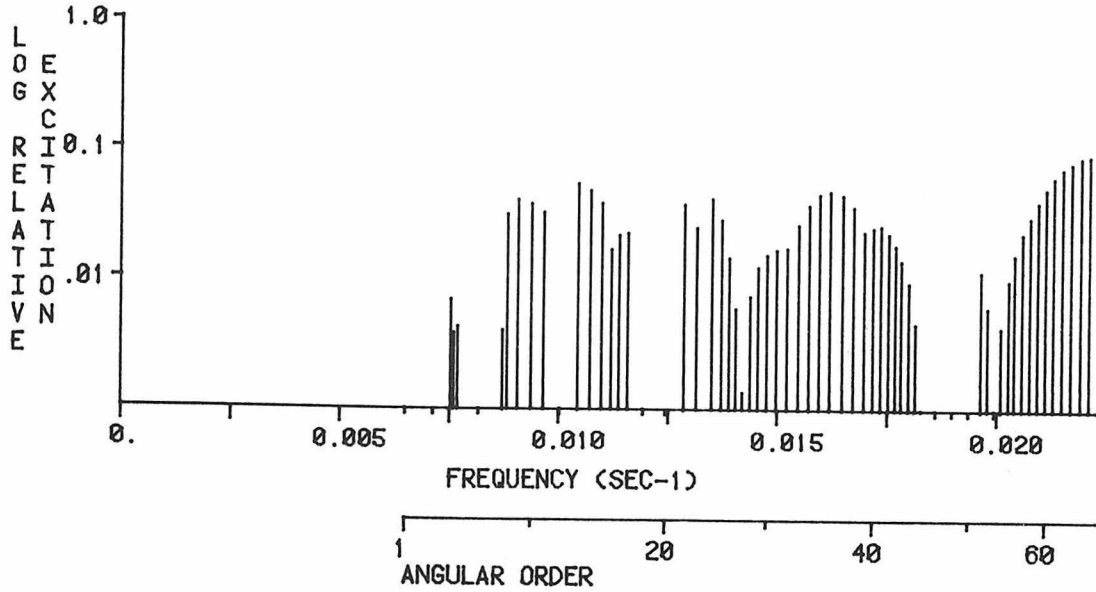
RADIAL COMPONENT; RADIAL ORDER 18



MAXIMUM EXCITATION = 0.701280E -4 CM-SEC ; (18 S 43; T= 59.12 SEC)

EXCITATION NORMALIZED TO 0 S 25 (RAD. COMP.) ; 0.46873400E -3

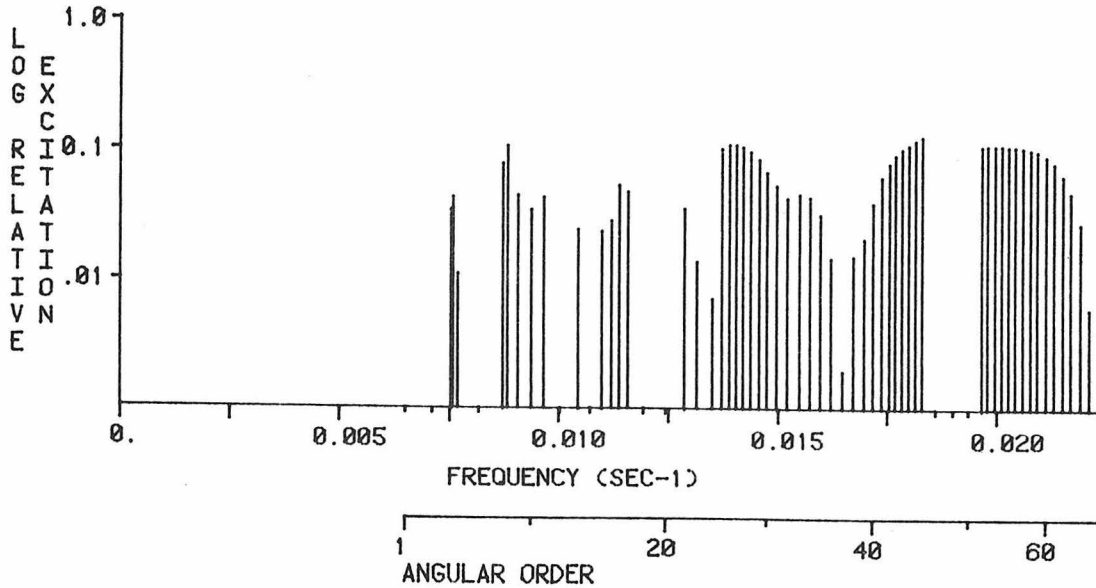
VERTICAL COMPONENT; RADIAL ORDER 19



MAXIMUM EXCITATION = 0.660190E -4 CM-SEC ; (19 S 65; T= 45.36 SEC)

EXCITATION NORMALIZED TO 0 S 26 (VERT. COMP.) ; 0.68673000E -3

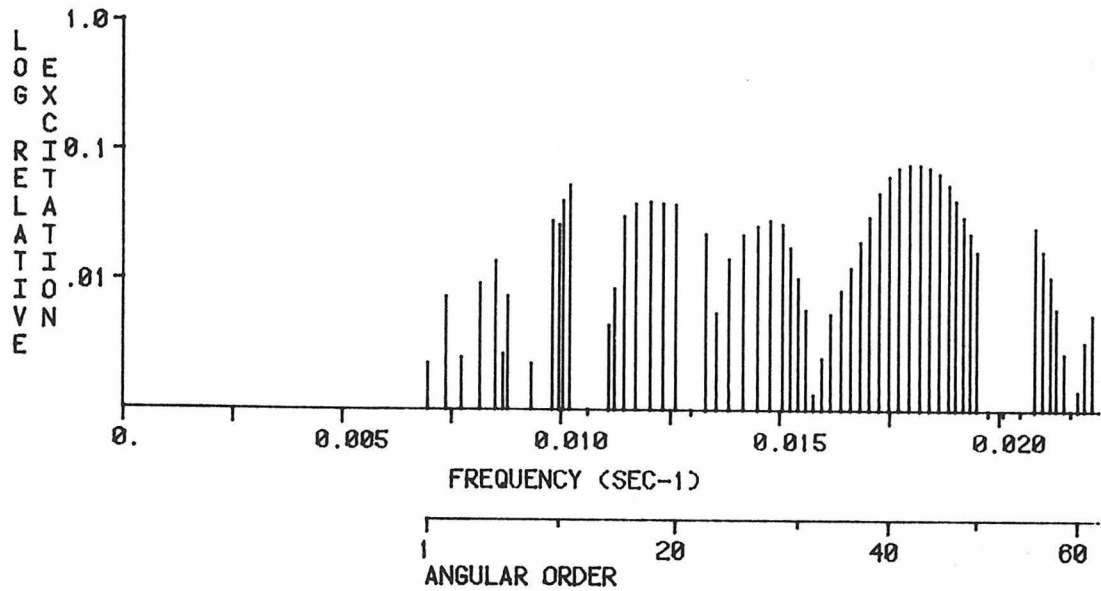
RADIAL COMPONENT; RADIAL ORDER 19



MAXIMUM EXCITATION = 0.620330E -4 CM-SEC ; (19 S 47; T= 54.80 SEC)

EXCITATION NORMALIZED TO 0 S 25 (RAD. COMP.) ; 0.46873400E -3

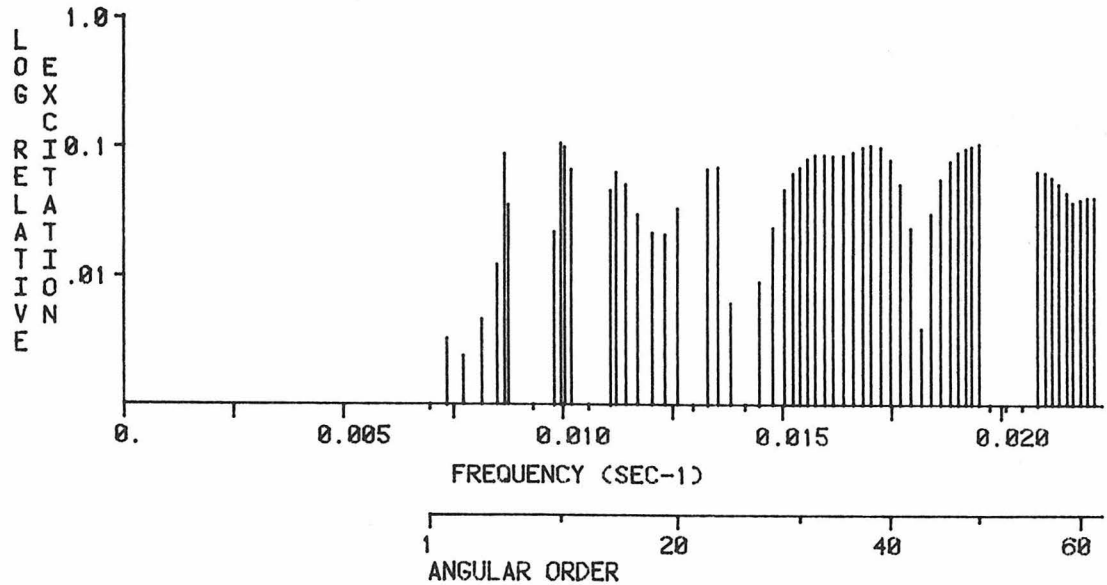
VERTICAL COMPONENT; RADIAL ORDER 20



MAXIMUM EXCITATION = 0.549190E -4 CM-SEC ; (20 S 43; T= 55.11 SEC)

EXCITATION NORMALIZED TO 0 S 26 (VERT. COMP.) ; 0.68673000E -3

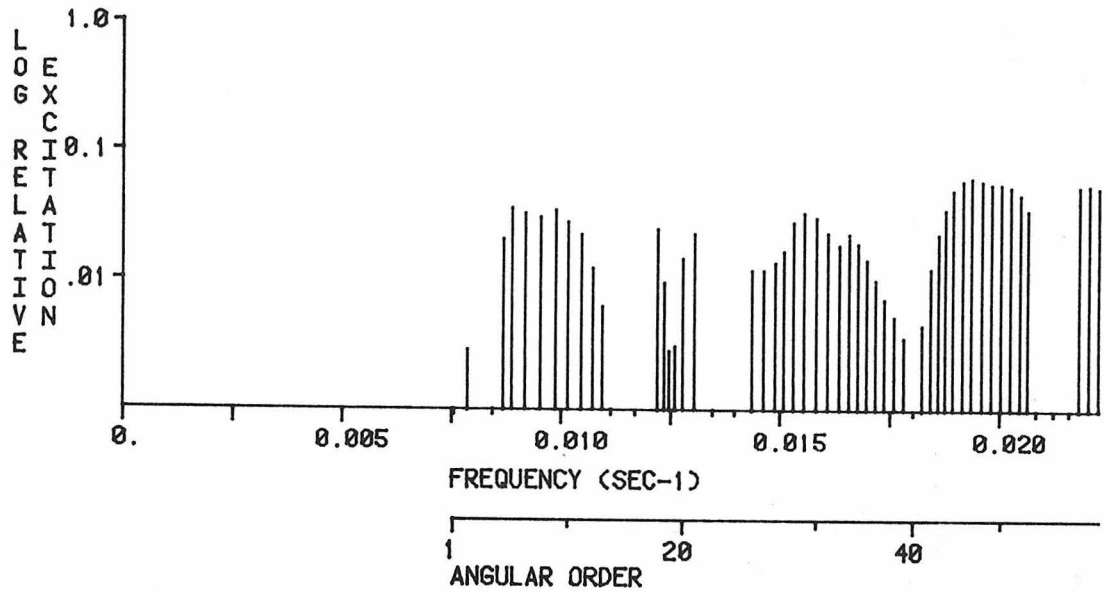
RADIAL COMPONENT; RADIAL ORDER 20



MAXIMUM EXCITATION = 0.508951E -4 CM-SEC ; (20 S 10; T= 100.62 SEC)

EXCITATION NORMALIZED TO 0 S 25 (RAD. COMP.) ; 0.46873400E -3

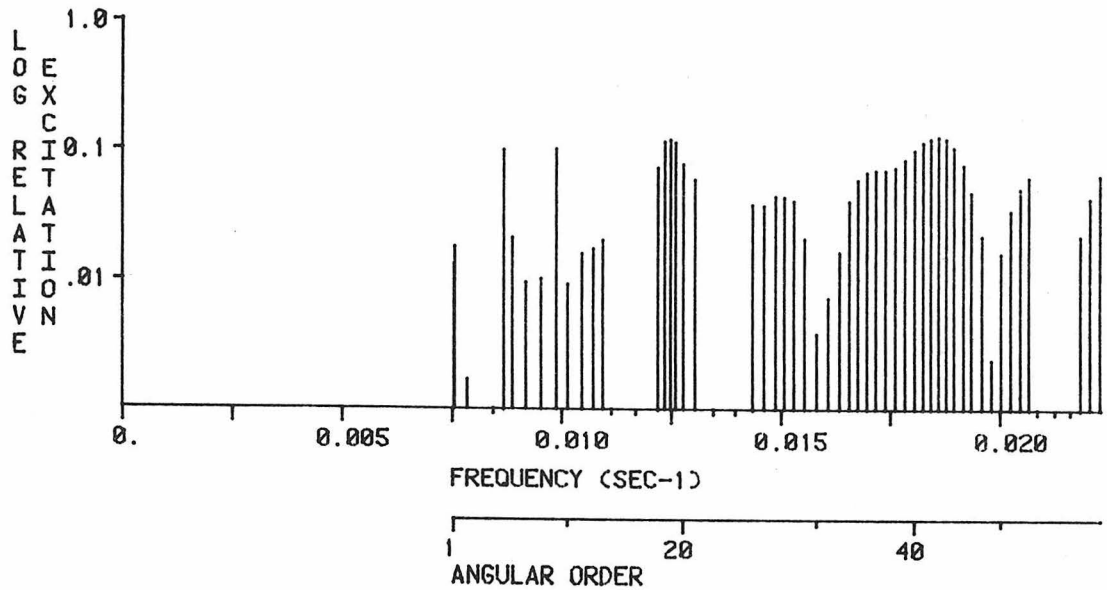
VERTICAL COMPONENT; RADIAL ORDER 21



MAXIMUM EXCITATION = 0.442594E -4 CM-SEC ; (21 S 47; T= 51.75 SEC)

EXCITATION NORMALIZED TO 0 S 26 (VERT. COMP.) ; 0.68673000E -3

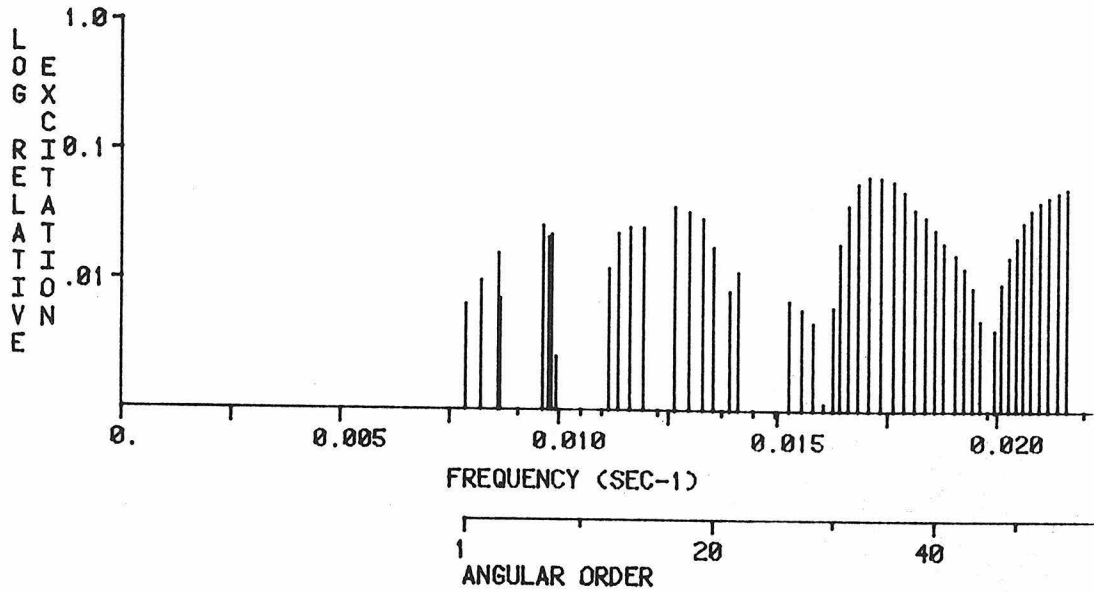
RADIAL COMPONENT; RADIAL ORDER 21



MAXIMUM EXCITATION = 0.619561E -4 CM-SEC ; (21 S 43; T= 53.89 SEC)

EXCITATION NORMALIZED TO 0 S 25 (RAD. COMP.) ; 0.46873400E -3

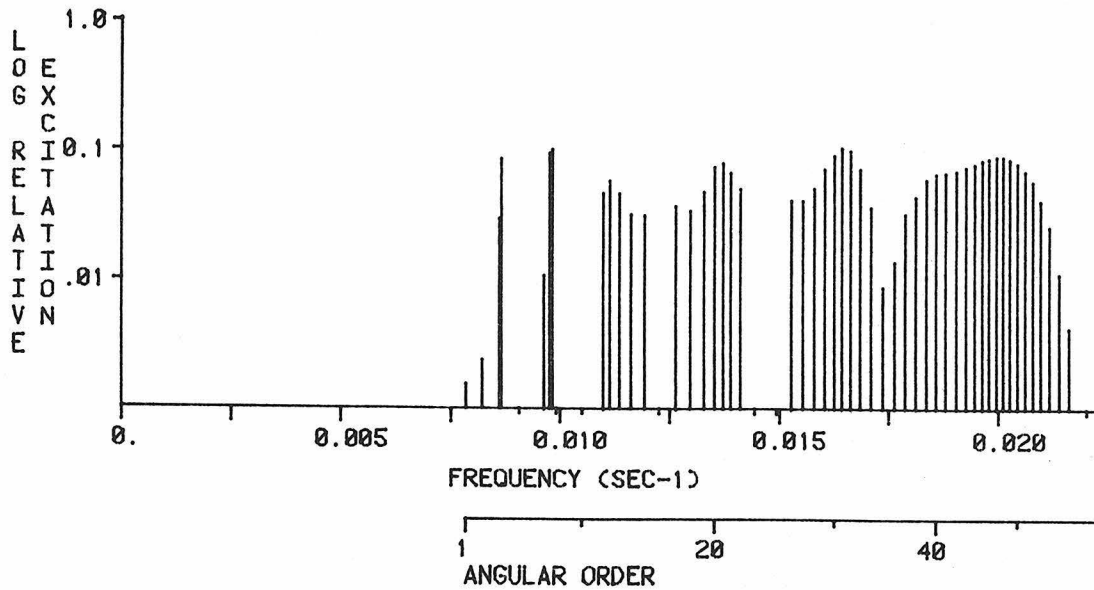
VERTICAL COMPONENT; RADIAL ORDER 22



MAXIMUM EXCITATION = 0.452571E -4 CM-SEC ; (22 S 34; T= 58.61 SEC)

EXCITATION NORMALIZED TO 0 S 26 (VERT. COMP.) ; 0.68673000E -3

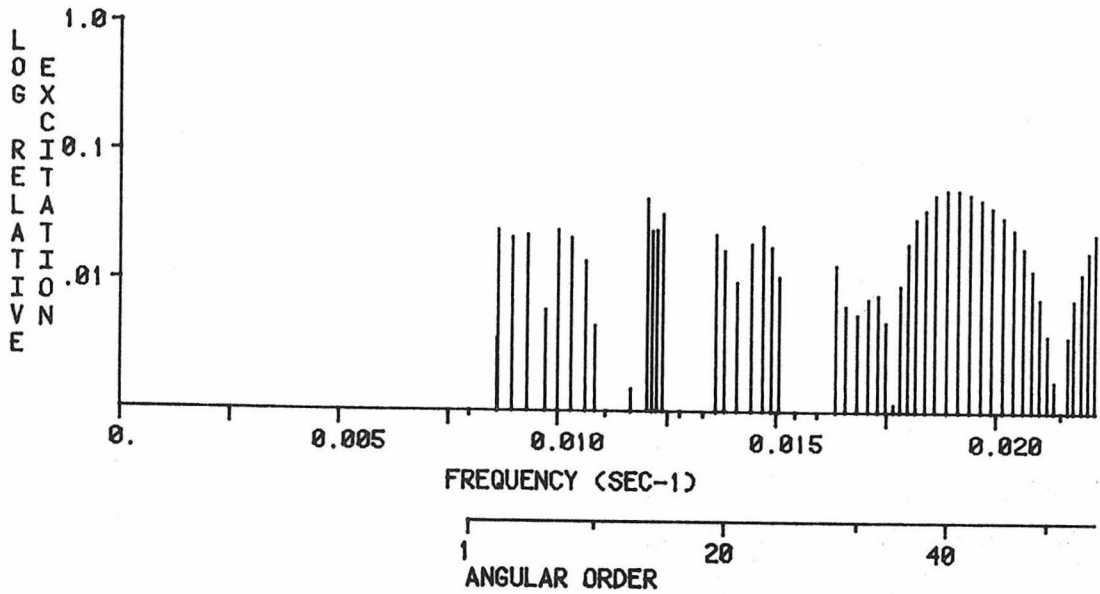
RADIAL COMPONENT; RADIAL ORDER 22



MAXIMUM EXCITATION = 0.508302E -4 CM-SEC ; (22 S 31; T= 60.92 SEC)

EXCITATION NORMALIZED TO 0 S 25 (RAD. COMP.) ; 0.46873400E -3

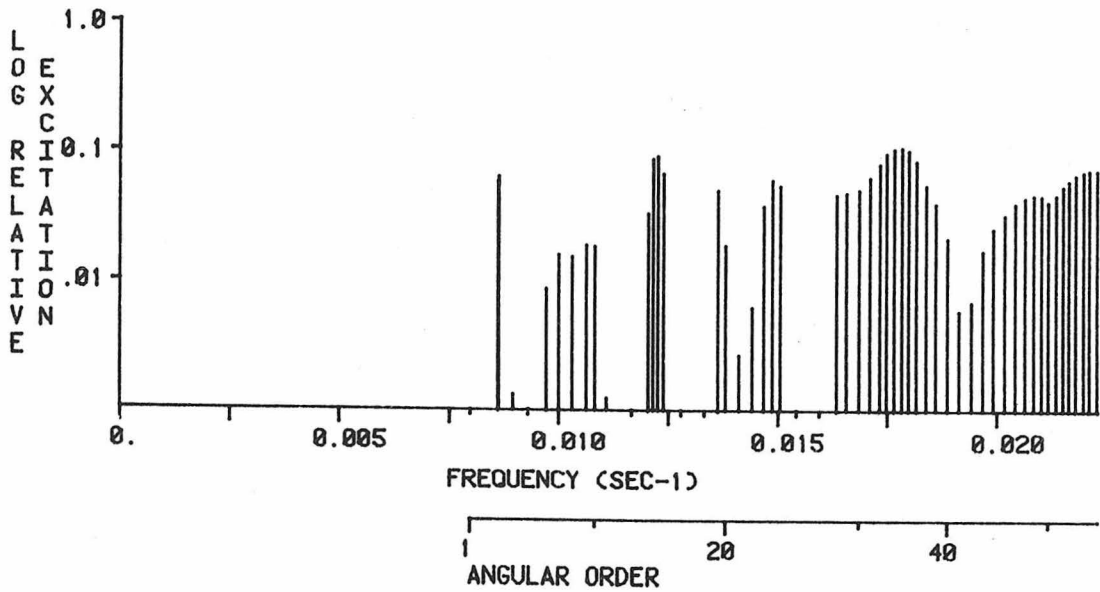
VERTICAL COMPONENT; RADIAL ORDER 23



MAXIMUM EXCITATION = 0.369229E -4 CM-SEC ; (23 S 40; T= 53.11 SEC)

EXCITATION NORMALIZED TO 0 S 26 (VERT. COMP.) ; 0.68673000E -3

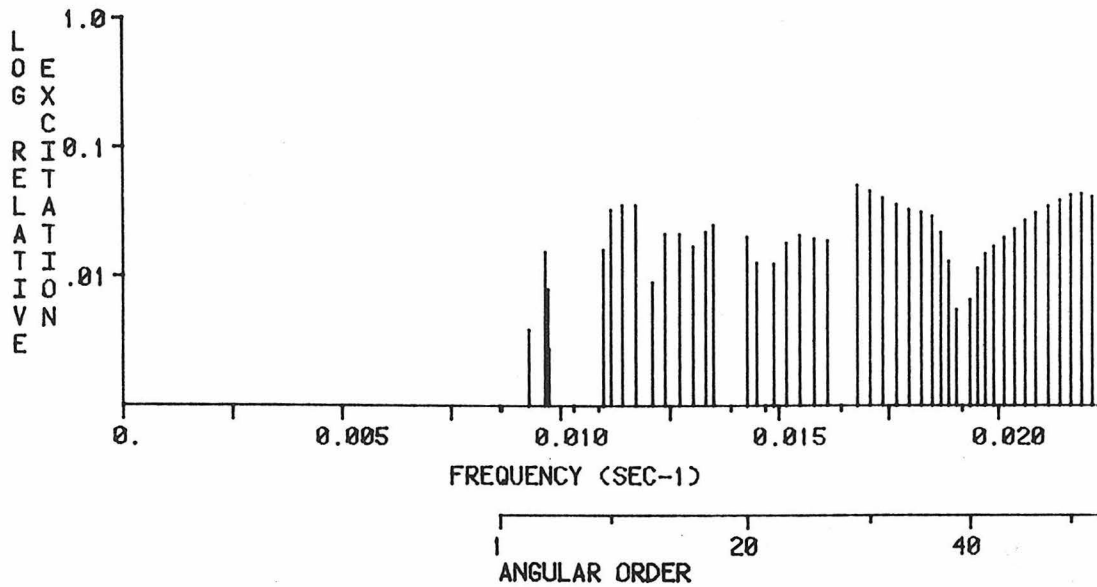
RADIAL COMPONENT; RADIAL ORDER 23



MAXIMUM EXCITATION = 0.528154E -4 CM-SEC ; (23 S 35; T= 56.23 SEC)

EXCITATION NORMALIZED TO 0 S 25 (RAD. COMP.) ; 0.46873400E -3

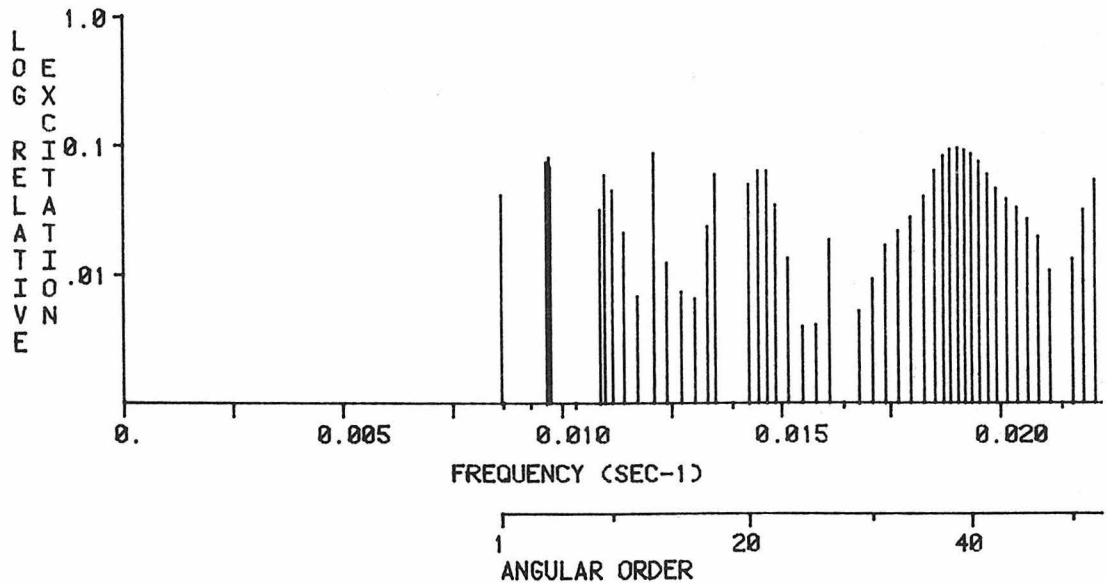
VERTICAL COMPONENT; RADIAL ORDER 24



MAXIMUM EXCITATION = 0.352460E -4 CM-SEC ; (24 S 29; T= 59.65 SEC)

EXCITATION NORMALIZED TO 0 S 26 (VERT. COMP.) ; 0.68673000E -3

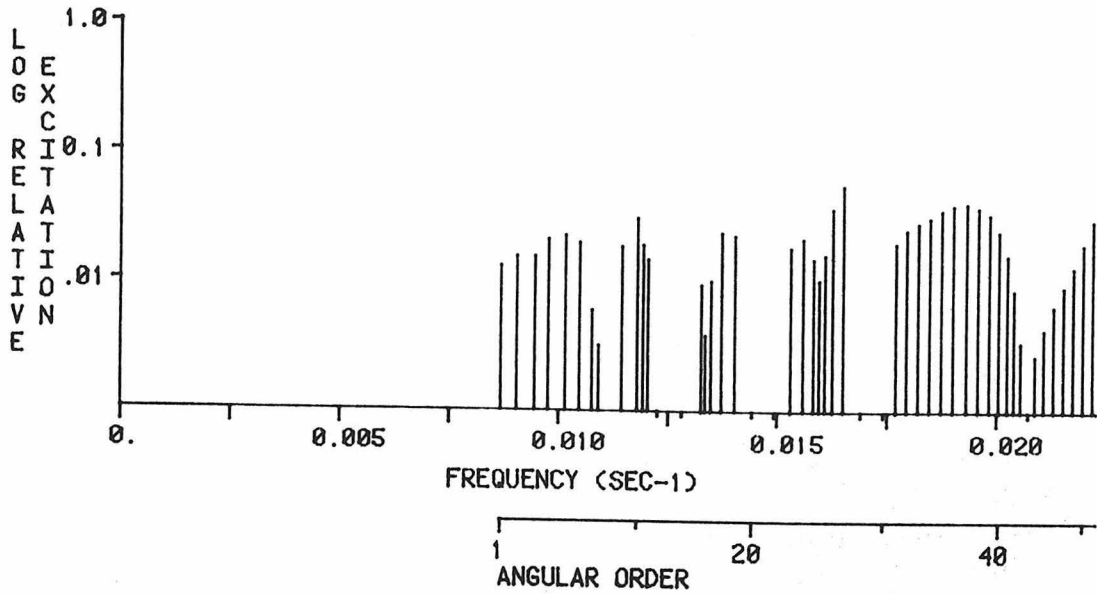
RADIAL COMPONENT; RADIAL ORDER 24



MAXIMUM EXCITATION = 0.458051E -4 CM-SEC ; (24 S 38; T= 52.63 SEC)

EXCITATION NORMALIZED TO 0 S 25 (RAD. COMP.) ; 0.46873400E -3

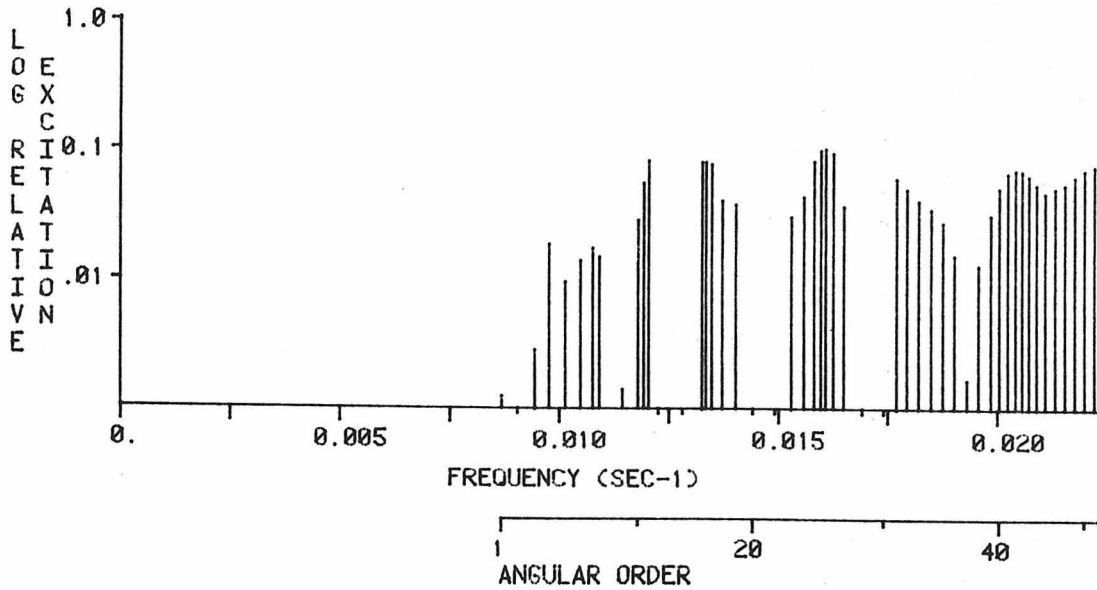
VERTICAL COMPONENT; RADIAL ORDER 25



MAXIMUM EXCITATION = 0.382176E -4 CM-SEC ; (25 S 28; T= 60.70 SEC)

EXCITATION NORMALIZED TO 0 S 26 (VERT. COMP.) ; 0.68673000E -3

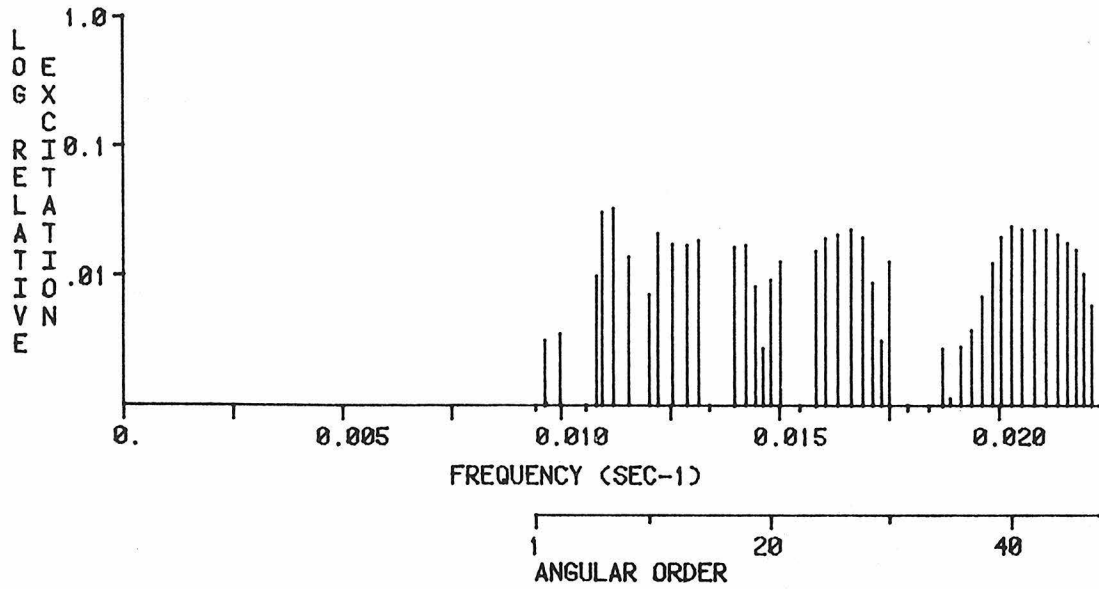
RADIAL COMPONENT; RADIAL ORDER 25



MAXIMUM EXCITATION = 0.504017E -4 CM-SEC ; (25 S 28; T= 62.21 SEC)

EXCITATION NORMALIZED TO 0 S 25 (RAD. COMP.) ; 0.46873400E -3

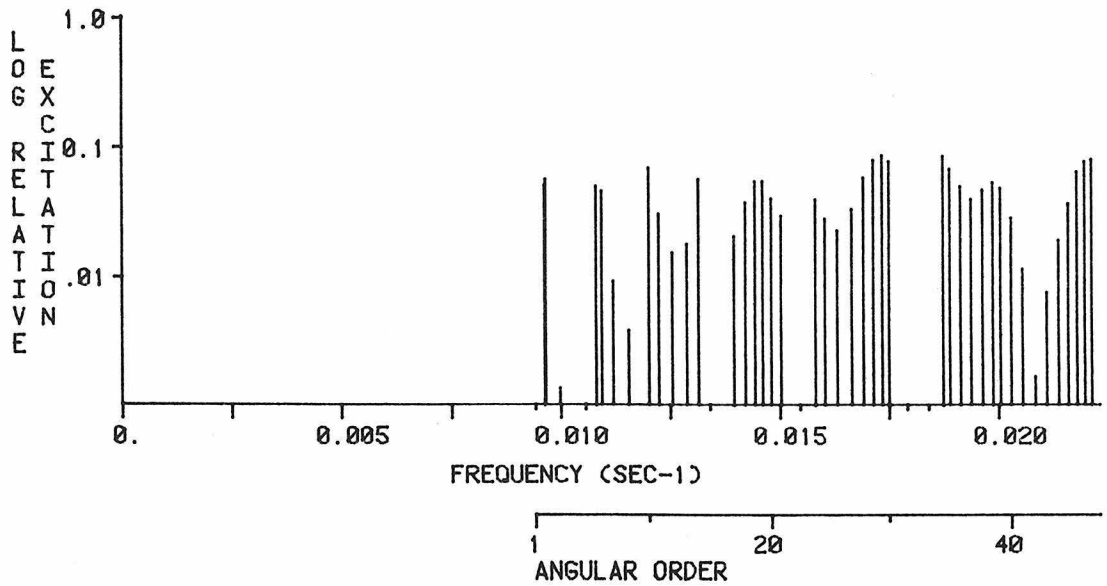
VERTICAL COMPONENT; RADIAL ORDER 26



MAXIMUM EXCITATION = 0.229718E -4 CM-SEC ; (26 S 8; T= 89.34 SEC)

EXCITATION NORMALIZED TO 0 S 26 (VERT. COMP.) ; 0.68673000E -3

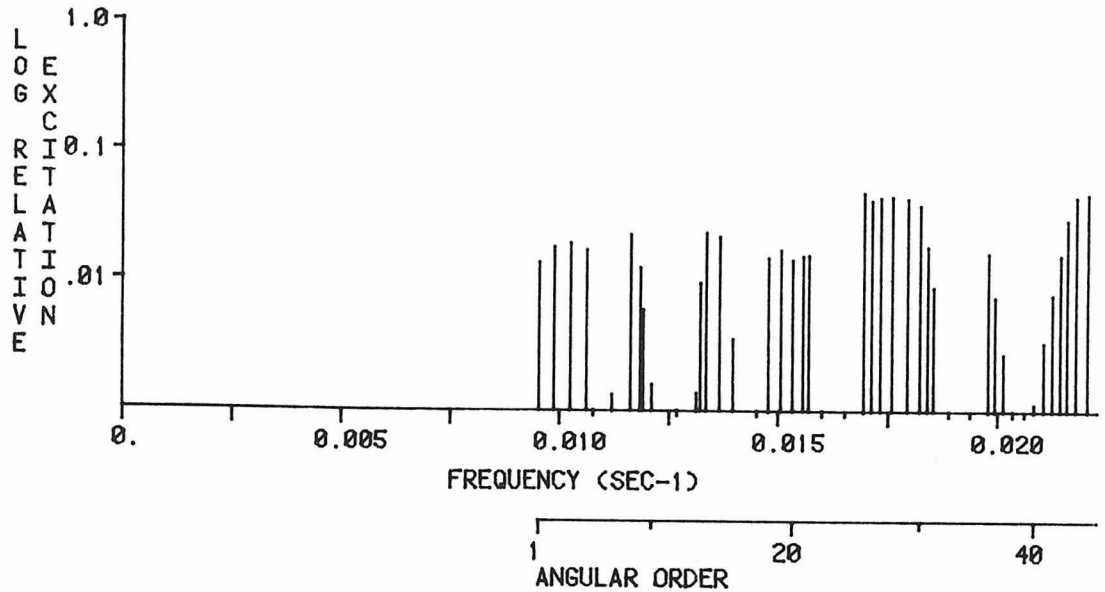
RADIAL COMPONENT; RADIAL ORDER 26



MAXIMUM EXCITATION = 0.415963E -4 CM-SEC ; (26 S 29; T= 57.81 SEC)

EXCITATION NORMALIZED TO 0 S 25 (RAD. COMP.) ; 0.46873400E -3

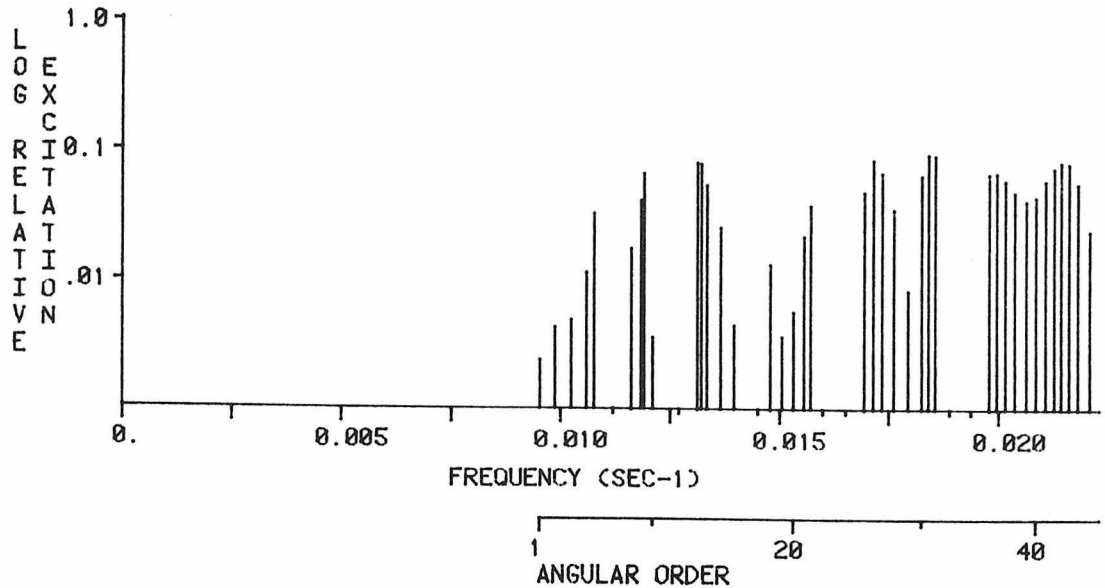
VERTICAL COMPONENT; RADIAL ORDER 27



MAXIMUM EXCITATION = 0.339237E -4 CM-SEC ; (27 S 46; T= 45.41 SEC)

EXCITATION NORMALIZED TO 0 S 26 (VERT. COMP.) ; 0.68673000E -3

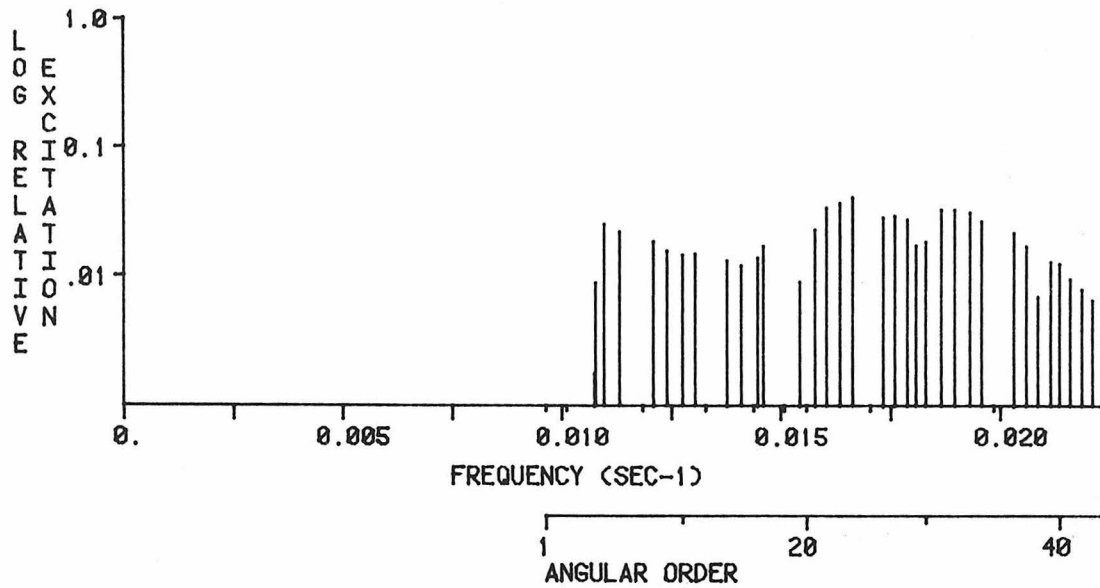
RADIAL COMPONENT; RADIAL ORDER 27



MAXIMUM EXCITATION = 0.462240E -4 CM-SEC ; (27 S 31; T= 54.45 SEC)

EXCITATION NORMALIZED TO 0 S 25 (RAD. COMP.) ; 0.46873400E -3

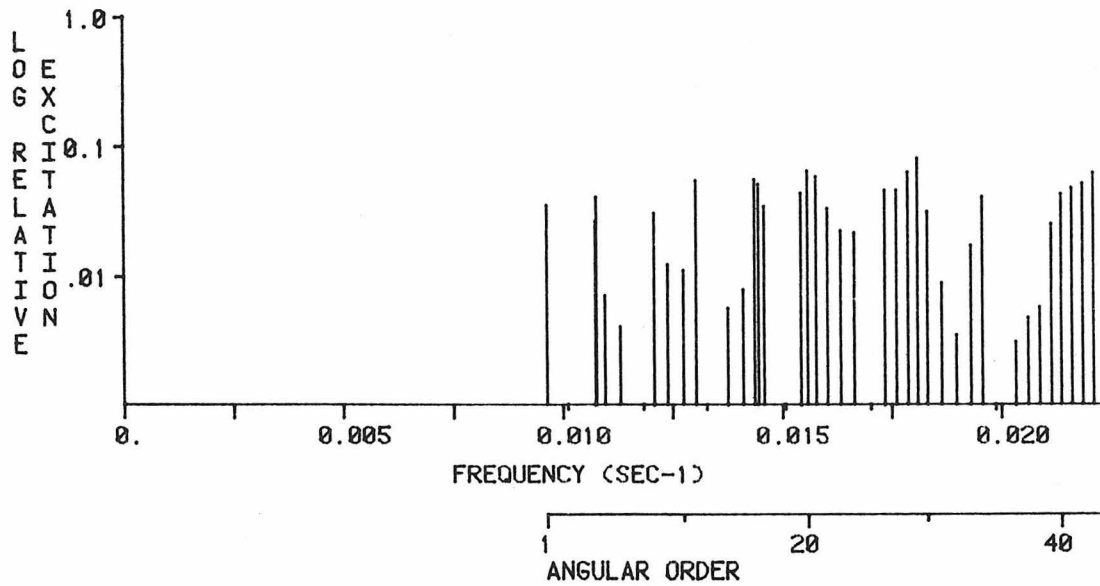
VERTICAL COMPONENT; RADIAL ORDER 28



MAXIMUM EXCITATION = 0.281031E -4 CM-SEC ; (28 S 24; T= 60.12 SEC)

EXCITATION NORMALIZED TO 0 S 26 (VERT. COMP.) ; 0.68673000E -3

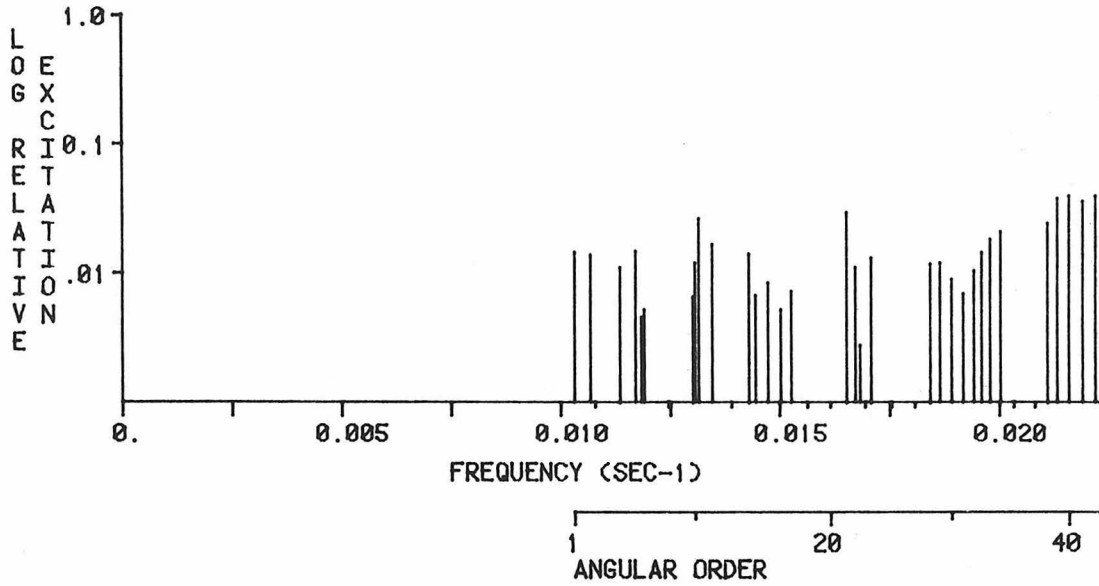
RADIAL COMPONENT; RADIAL ORDER 28



MAXIMUM EXCITATION = 0.395027E -4 CM-SEC ; (28 S 29; T= 55.40 SEC)

EXCITATION NORMALIZED TO 0 S 25 (RAD. COMP.) ; 0.46873400E -3

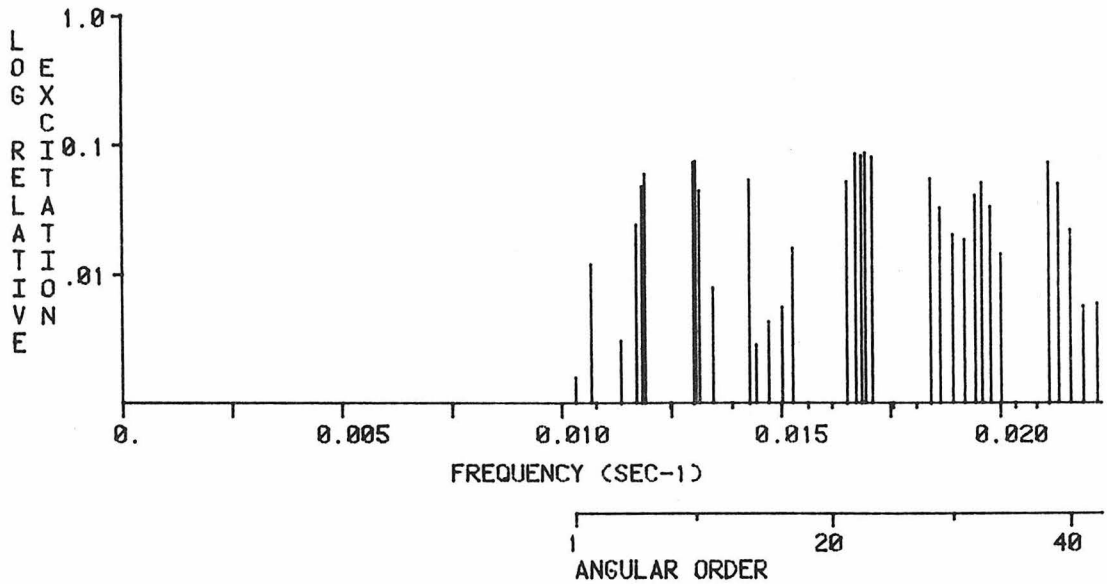
VERTICAL COMPONENT; RADIAL ORDER 29



MAXIMUM EXCITATION = 0.282950E -4 CM-SEC ; (29 S 40; T= 46.37 SEC)

EXCITATION NORMALIZED TO 0 S 26 (VERT. COMP.) ; 0.68673000E -3

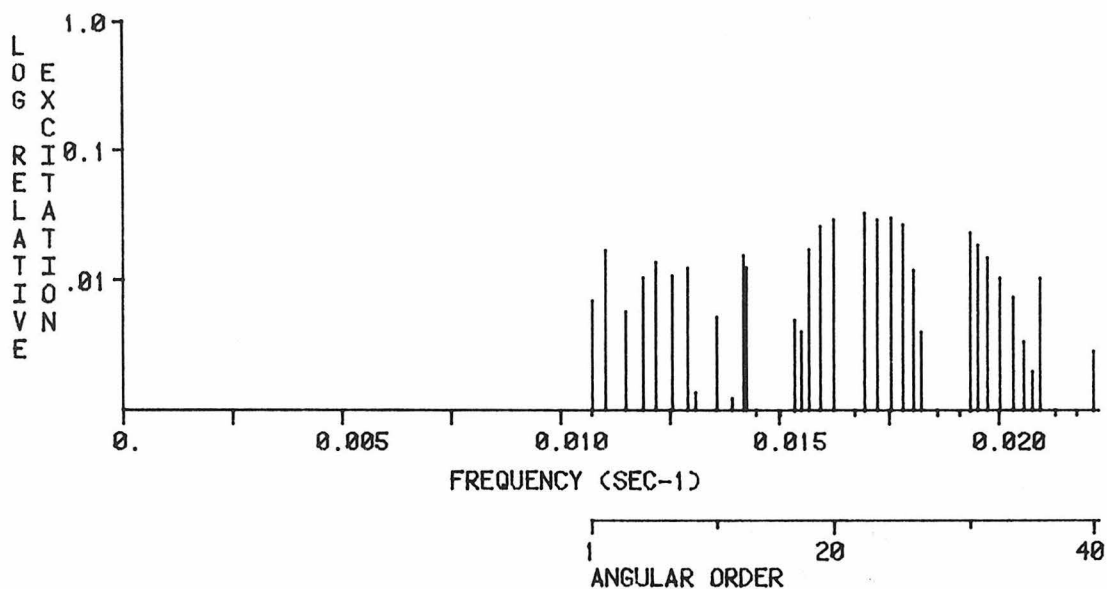
RADIAL COMPONENT; RADIAL ORDER 29



MAXIMUM EXCITATION = 0.421412E -4 CM-SEC ; (29 S 24; T= 59.10 SEC)

EXCITATION NORMALIZED TO 0 S 25 (RAD. COMP.) ; 0.46873400E -3

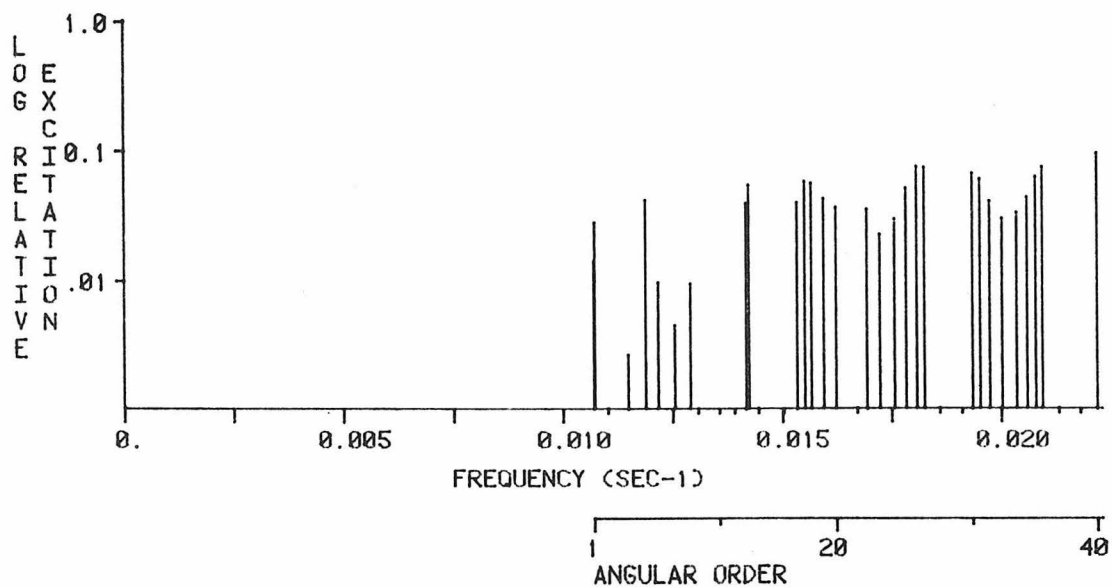
VERTICAL COMPONENT; RADIAL ORDER 30



MAXIMUM EXCITATION = 0.232363E -4 CM-SEC ; (30 S 22; T= 59.10 SEC)

EXCITATION NORMALIZED TO 0 S 26 (VERT. COMP.) ; 0.68673000E -3

RADIAL COMPONENT; RADIAL ORDER 30

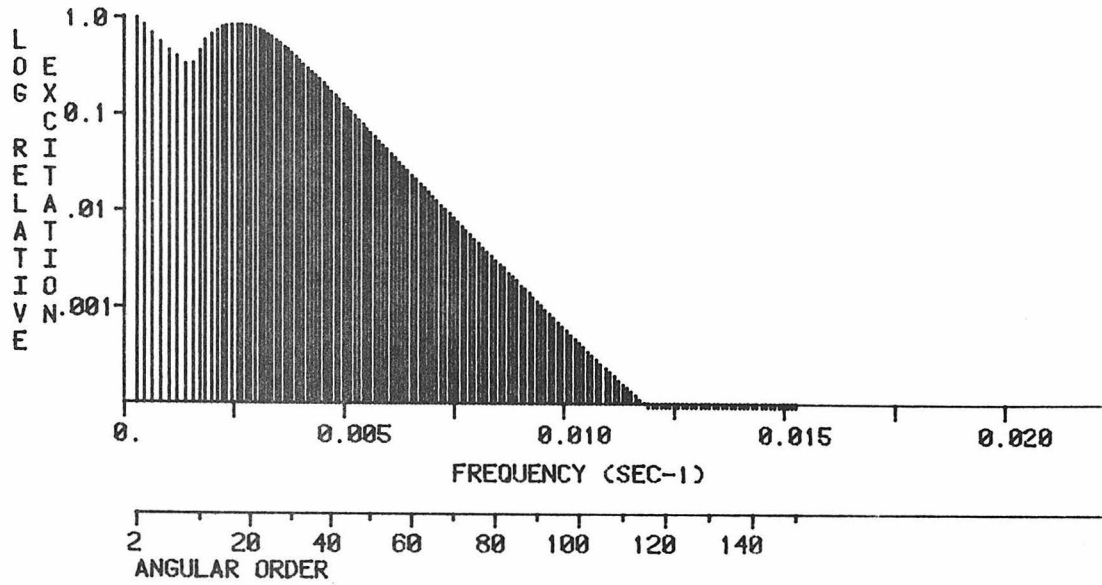


MAXIMUM EXCITATION = 0.454358E -4 CM-SEC ; (30 S 40; T= 45.18 SEC)

EXCITATION NORMALIZED TO 0 S 25 (RAD. COMP.) ; 0.46873400E -3

Figure A2.5 - The spheroidal excitation spectra for the 1970 deep Columbia earthquake with attenuation included. Both vertical and radial components of displacement are shown for the fundamental branch and first thirty overtone branches. The data window begins 3 hours after the origin time of the earthquake and has a duration of 18 hours. This corresponds to the average window in Gilbert and Dziewonski's (1975) study of the Columbia earthquake. All excitations are normalized to the maximum fundamental mode excitation and modes with an excitation more than 80 db below that maximum are plotted as small negative tick marks along the horizontal axis. This figure extends over the following 31 pages.

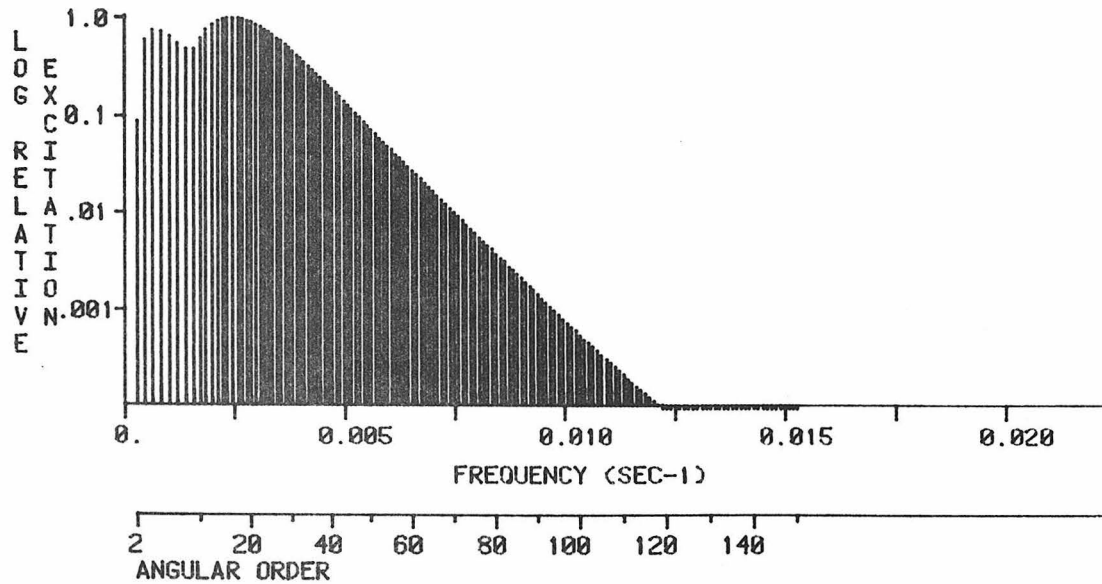
VERTICAL COMPONENT; RADIAL ORDER 0



MAXIMUM EXCITATION = 0.205163E -3 CM-SEC ; (0 S 2; T=3231.72 SEC)

ATTENUATION INCLUDED; RECORD STARTS AT 3.00 HRS.; LENGTH = 18.00 HRS.

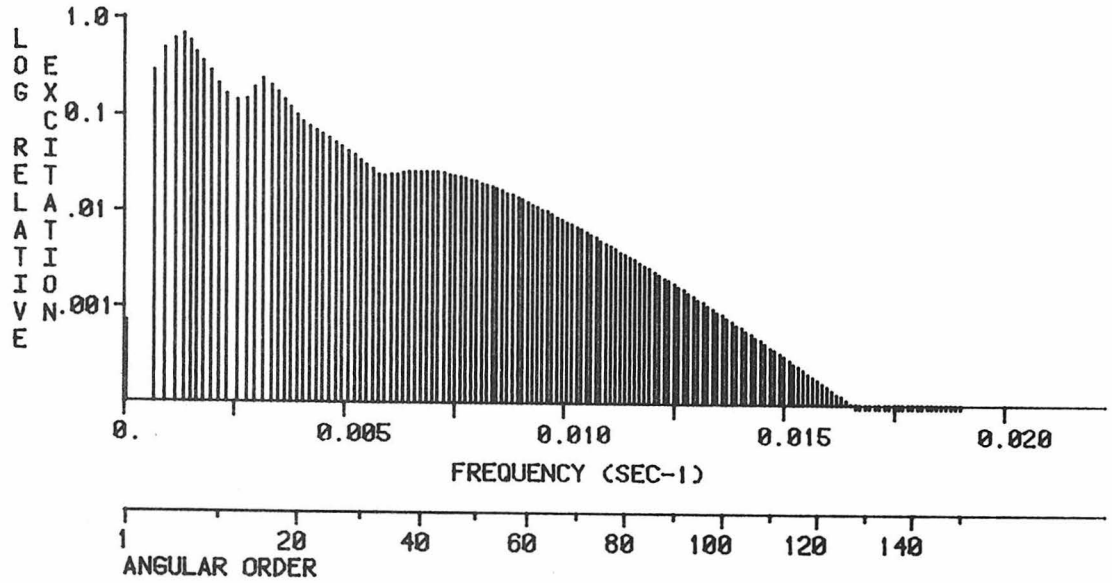
RADIAL COMPONENT; RADIAL ORDER 0



MAXIMUM EXCITATION = 0.131996E -3 CM-SEC ; (0 S 16; T= 406.98 SEC)

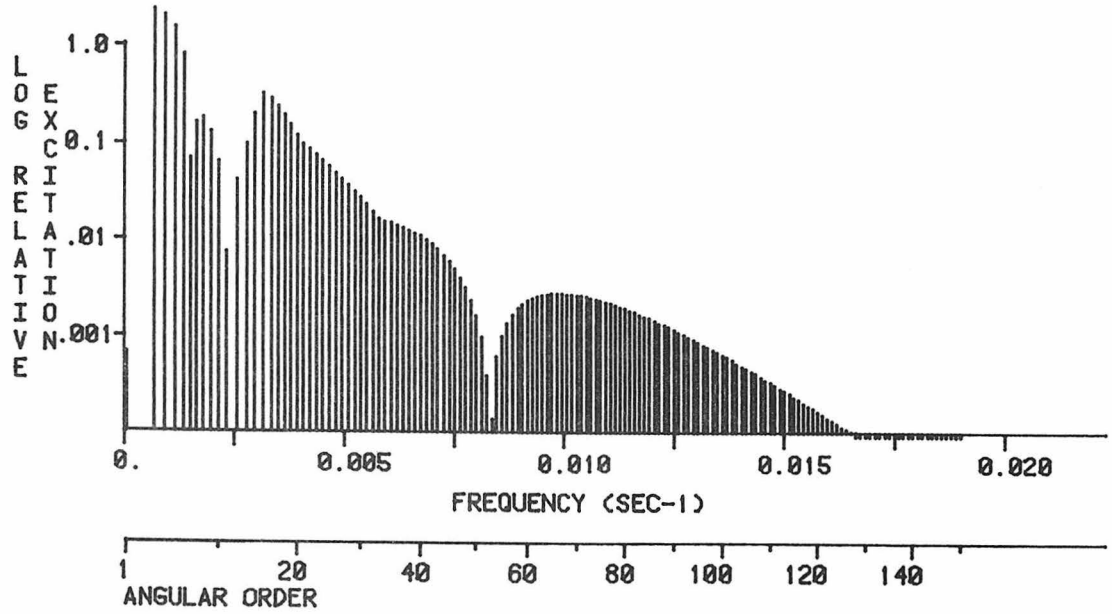
ATTENUATION INCLUDED; RECORD STARTS AT 3.00 HRS.; LENGTH = 18.00 HRS.

VERTICAL COMPONENT; RADIAL ORDER 1



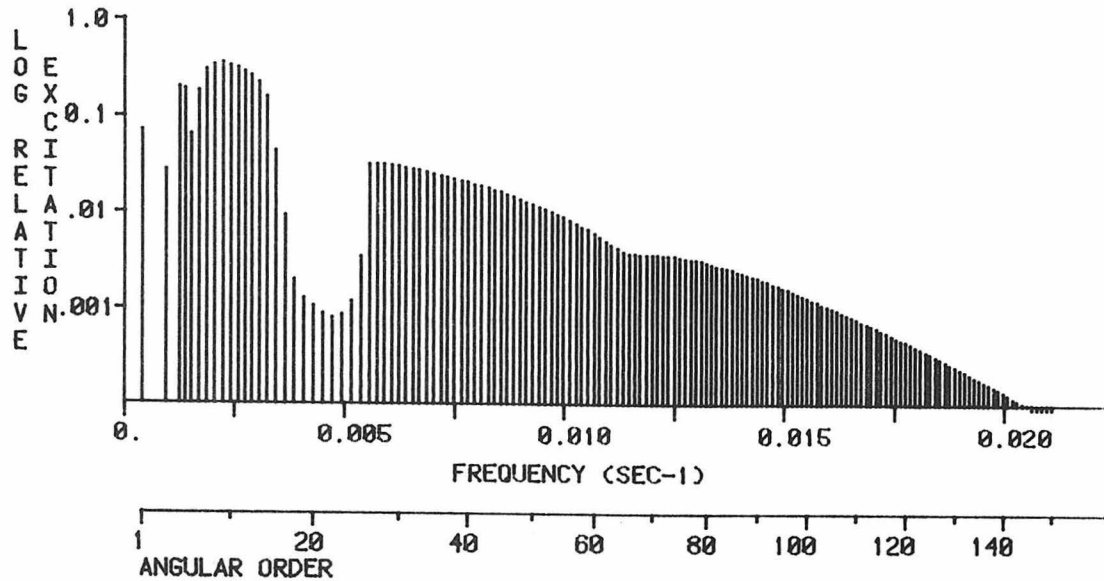
MAXIMUM EXCITATION = 0.142267E -3 CM-SEC ; (1 S 5; T= 729.19 SEC)
EXCITATION NORMALIZED TO 0 S 2 (VERT. COMP.) ; 0.20516300E -3
ATTENUATION INCLUDED; RECORD STARTS AT 3.00 HRS.; LENGTH = 18.00 HRS.

RADIAL COMPONENT; RADIAL ORDER 1



MAXIMUM EXCITATION = 0.311065E -3 CM-SEC ; (1 S 2; T=1489.85 SEC)
EXCITATION NORMALIZED TO 0 S 16 (RAD. COMP.) ; 0.13199600E -3
ATTENUATION INCLUDED; RECORD STARTS AT 3.00 HRS.; LENGTH = 18.00 HRS.

VERTICAL COMPONENT; RADIAL ORDER 2

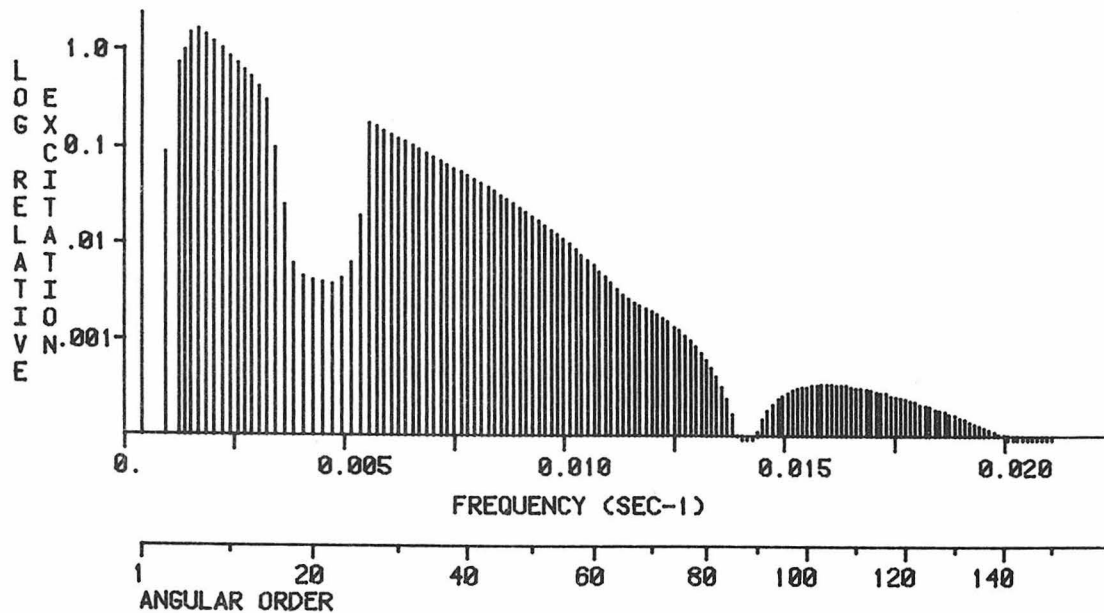


MAXIMUM EXCITATION = $0.708260E -4$ CM-SEC ; (2 S 9; T= 448.52 SEC)

EXCITATION NORMALIZED TO 0 S 2 (VERT. COMP.) ; $0.20516300E -3$

ATTENUATION INCLUDED; RECORD STARTS AT 3.00 HRS.; LENGTH = 18.00 HRS.

RADIAL COMPONENT; RADIAL ORDER 2

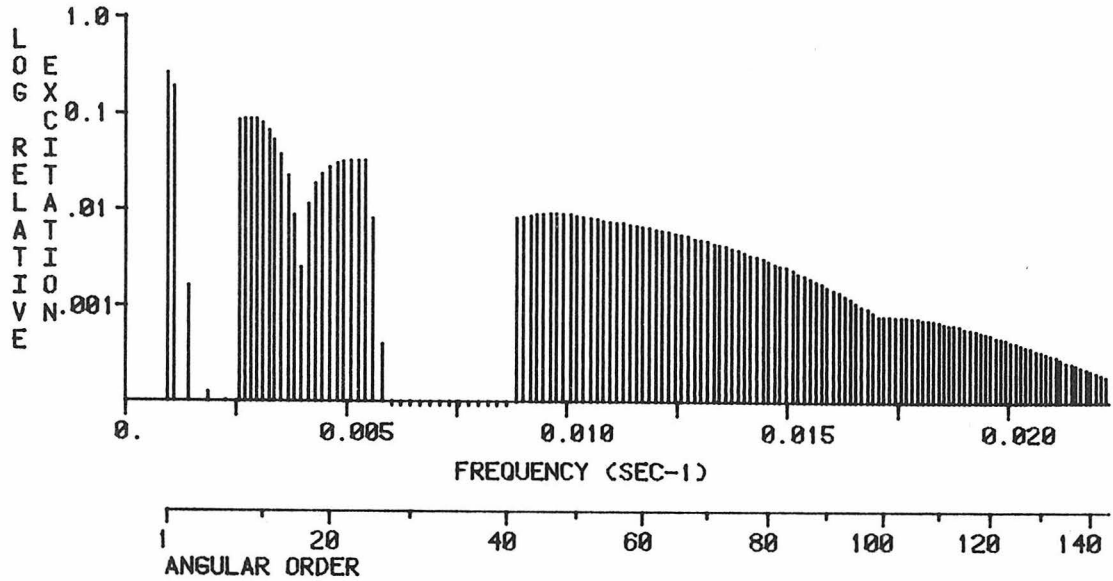


MAXIMUM EXCITATION = $0.309303E -3$ CM-SEC ; (2 S 1; T=2476.08 SEC)

EXCITATION NORMALIZED TO 0 S 16 (RAD. COMP.) ; $0.13199600E -3$

ATTENUATION INCLUDED; RECORD STARTS AT 3.00 HRS.; LENGTH = 18.00 HRS.

VERTICAL COMPONENT; RADIAL ORDER 3

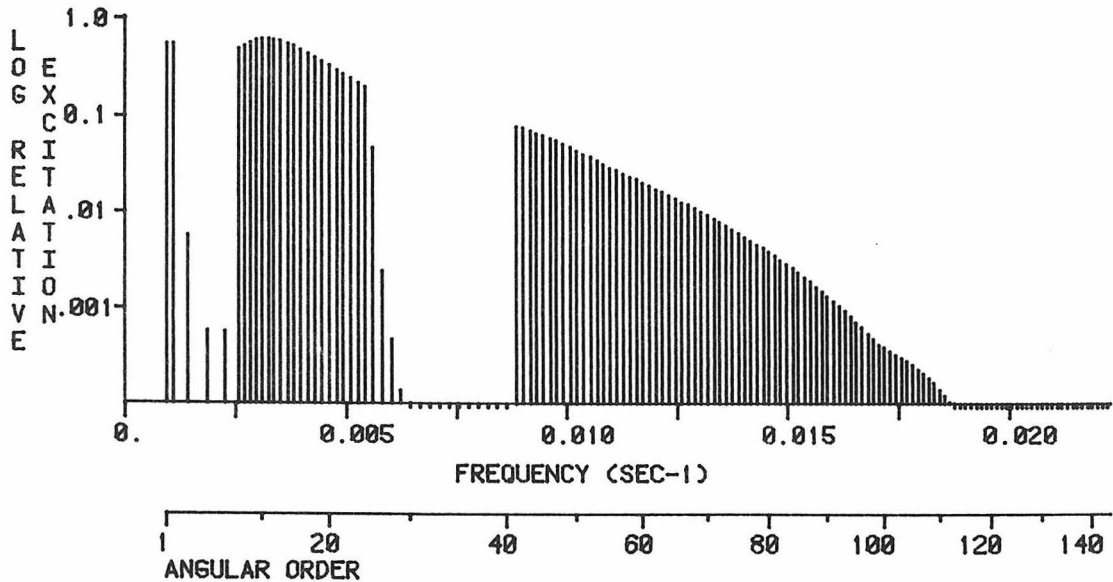


MAXIMUM EXCITATION = 0.540928E -4 CM-SEC ; (3 S 1; T=1060.82 SEC)

EXCITATION NORMALIZED TO 0 S 2 (VERT. COMP.) ; 0.20516300E -3

ATTENUATION INCLUDED; RECORD STARTS AT 3.00 HRS.; LENGTH = 18.00 HRS.

RADIAL COMPONENT; RADIAL ORDER 3

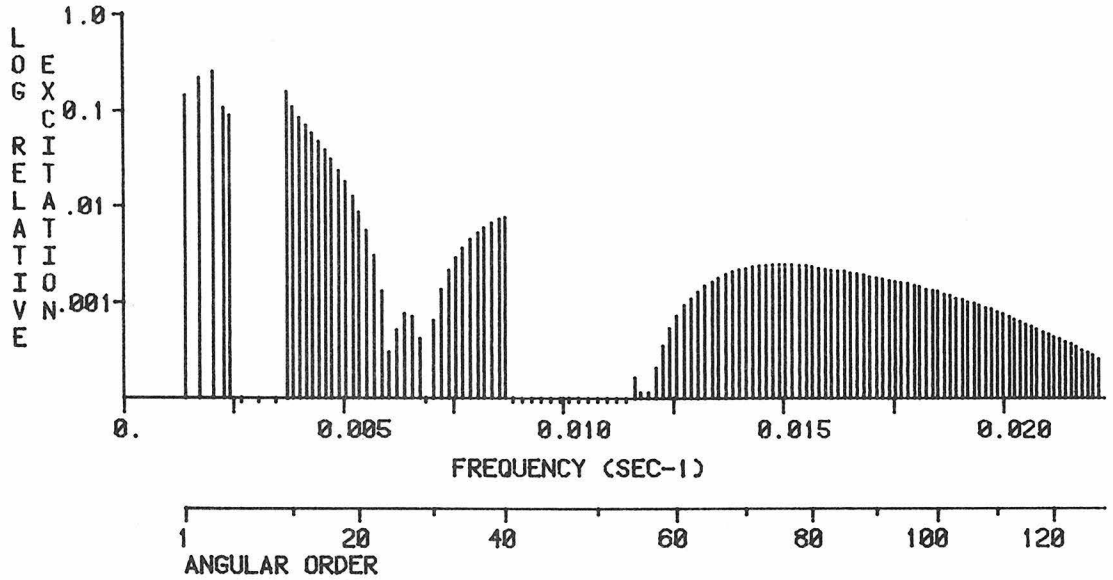


MAXIMUM EXCITATION = 0.811920E -4 CM-SEC ; (3 S 11; T= 310.32 SEC)

EXCITATION NORMALIZED TO 0 S 16 (RAD. COMP.) ; 0.13199600E -3

ATTENUATION INCLUDED; RECORD STARTS AT 3.00 HRS.; LENGTH = 18.00 HRS.

VERTICAL COMPONENT; RADIAL ORDER 4

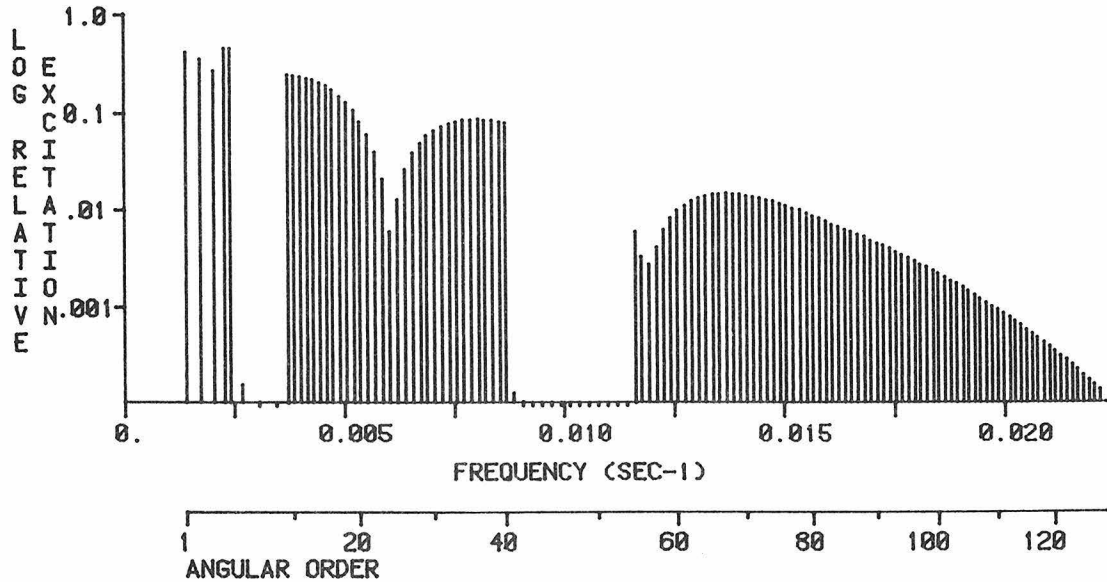


MAXIMUM EXCITATION = 0.513033E -4 CM-SEC ; (4 S 3; T= 488.38 SEC)

EXCITATION NORMALIZED TO 0 S 2 (VERT. COMP.) ; 0.20516300E -3

ATTENUATION INCLUDED; RECORD STARTS AT 3.00 HRS.; LENGTH = 18.00 HRS.

RADIAL COMPONENT; RADIAL ORDER 4

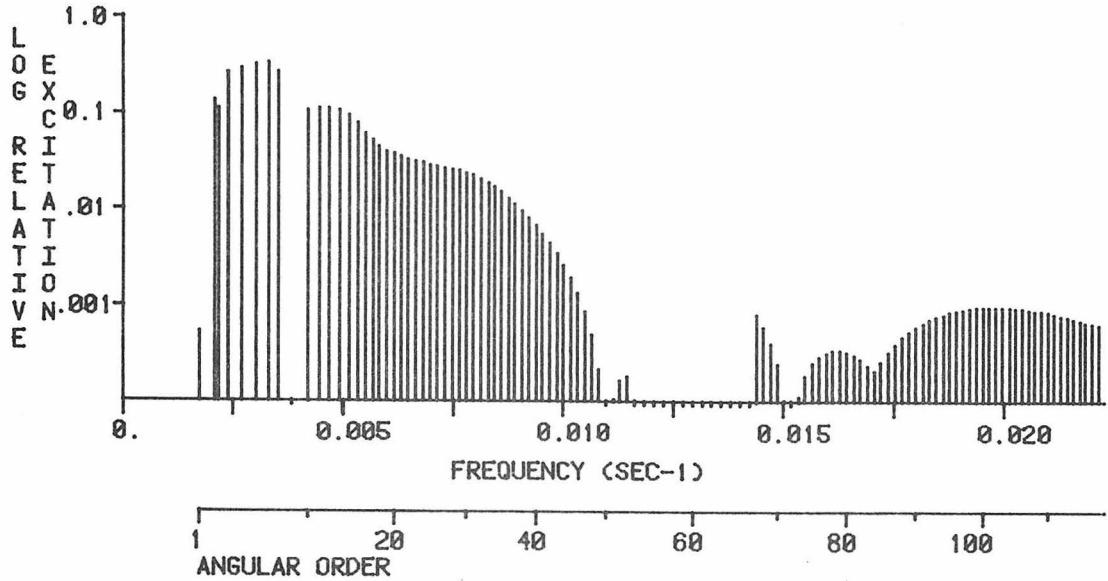


MAXIMUM EXCITATION = 0.613079E -4 CM-SEC ; (4 S 5; T= 414.66 SEC)

EXCITATION NORMALIZED TO 0 S 16 (RAD. COMP.) ; 0.13199600E -3

ATTENUATION INCLUDED; RECORD STARTS AT 3.00 HRS.; LENGTH = 18.00 HRS.

VERTICAL COMPONENT; RADIAL ORDER 5

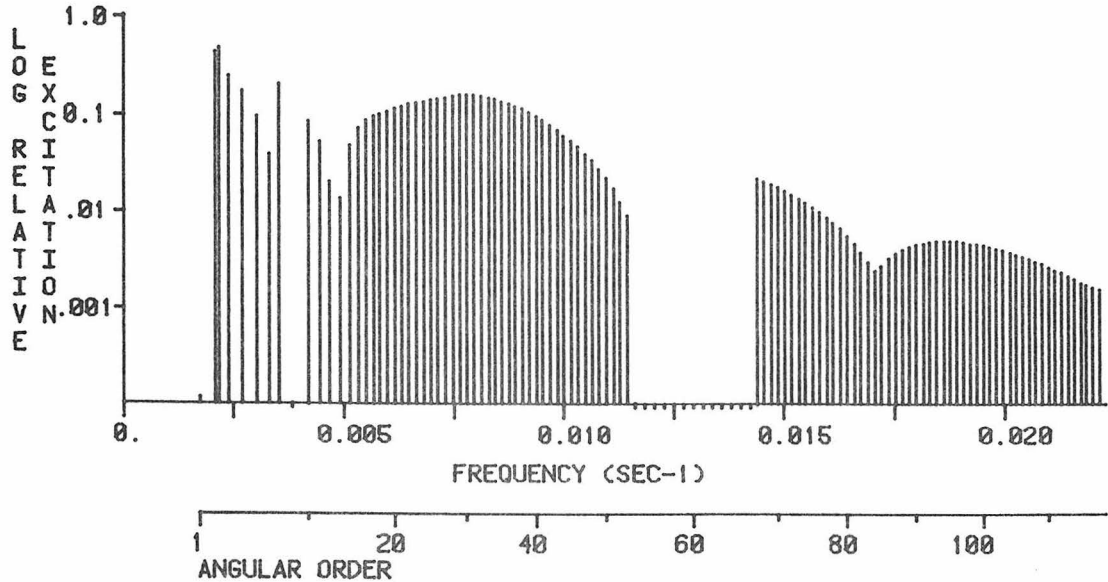


MAXIMUM EXCITATION = 0.672510E -4 CM-SEC ; (5 S 7; T= 303.76 SEC)

EXCITATION NORMALIZED TO 0 S 2 (VERT. COMP.) ; 0.20516300E -3

ATTENUATION INCLUDED; RECORD STARTS AT 3.00 HRS.; LENGTH = 18.00 HRS.

RADIAL COMPONENT; RADIAL ORDER 5

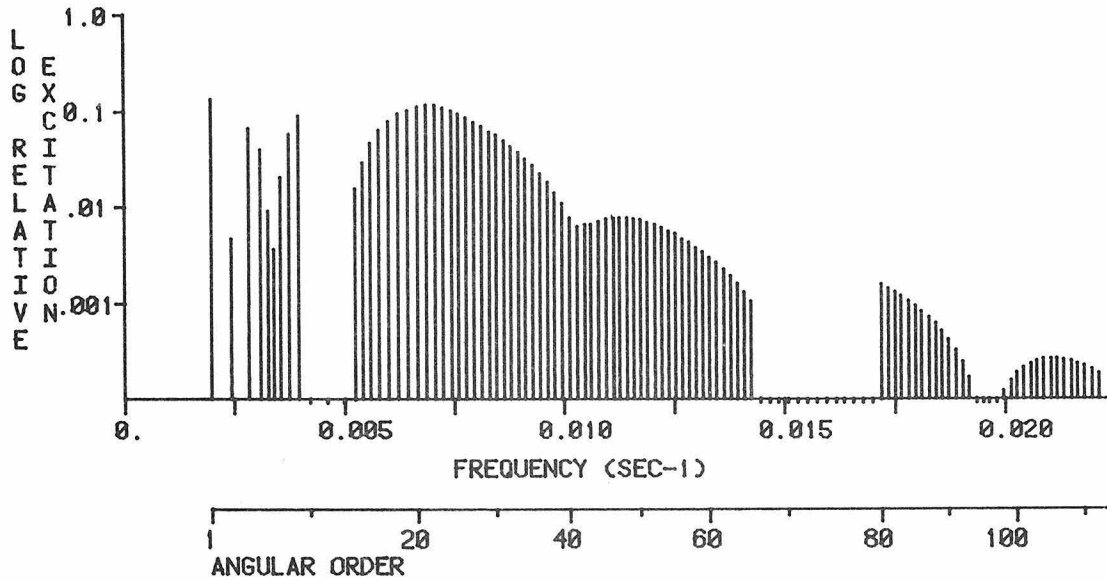


MAXIMUM EXCITATION = 0.624693E -4 CM-SEC ; (5 S 3; T= 460.70 SEC)

EXCITATION NORMALIZED TO 0 S 16 (RAD. COMP.) ; 0.13199600E -3

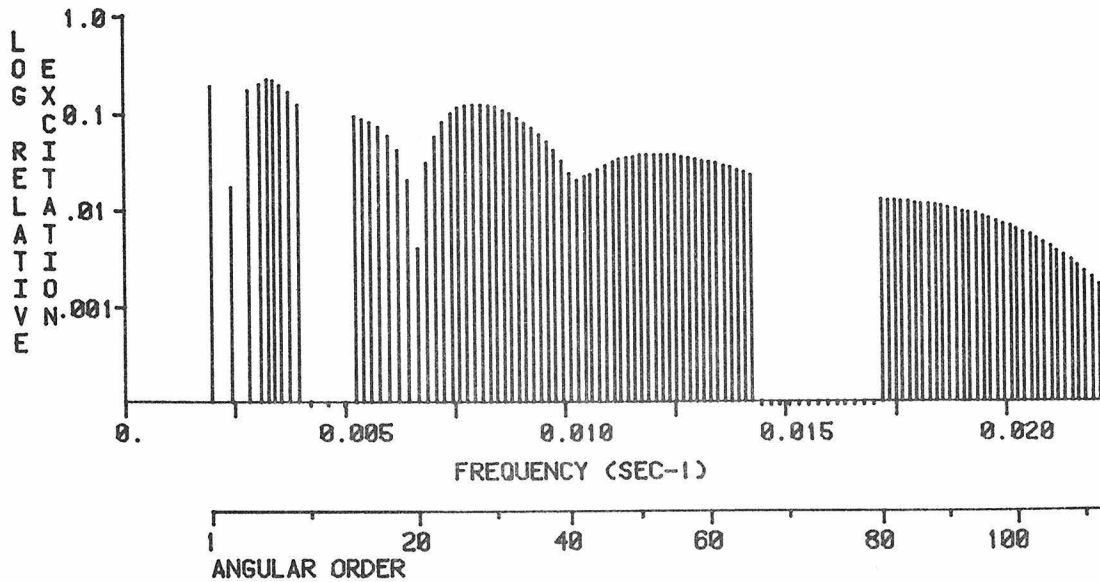
ATTENUATION INCLUDED; RECORD STARTS AT 3.00 HRS.; LENGTH = 18.00 HRS.

VERTICAL COMPONENT; RADIAL ORDER 6



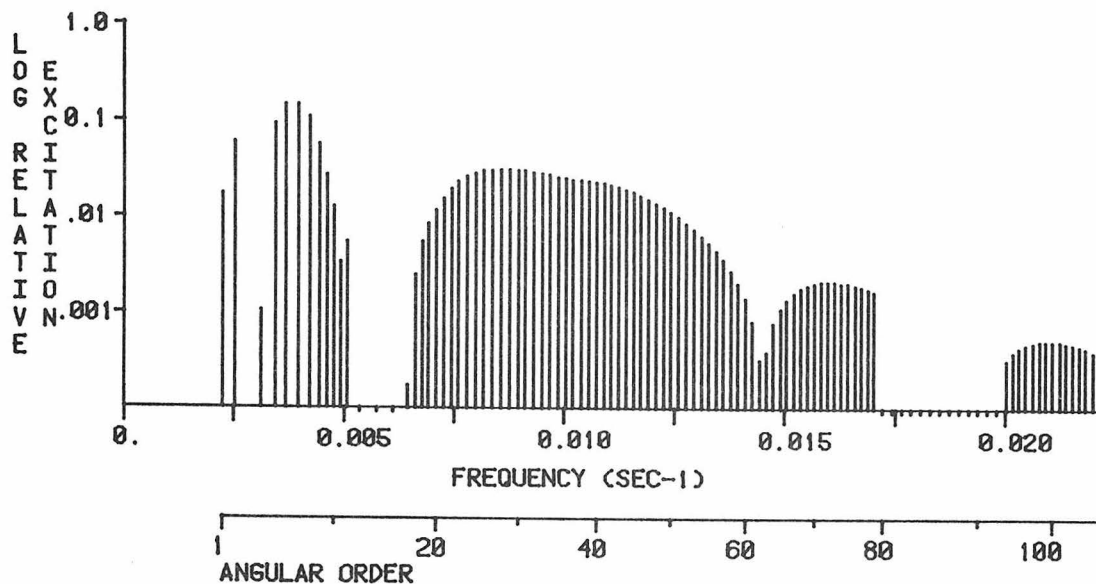
MAXIMUM EXCITATION = 0.281527E -4 CM-SEC ; (6 S 1; T= 505.47 SEC)
EXCITATION NORMALIZED TO 0 S 2 (VERT. COMP.) ; 0.20516300E -3
ATTENUATION INCLUDED; RECORD STARTS AT 3.00 HRS.; LENGTH = 18.00 HRS.

RADIAL COMPONENT; RADIAL ORDER 6



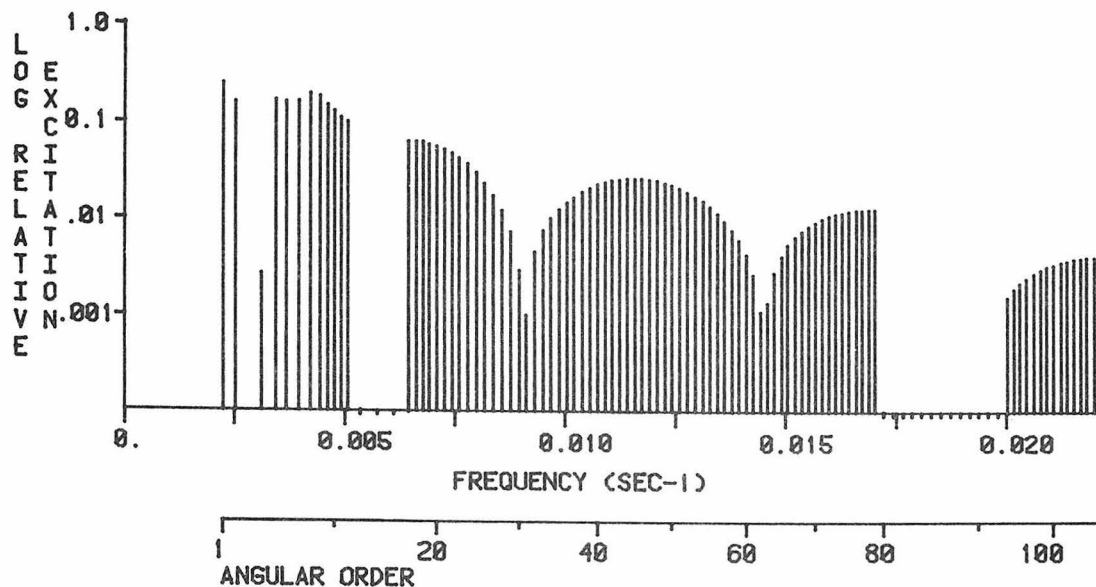
MAXIMUM EXCITATION = 0.297302E -4 CM-SEC ; (6 S 5; T= 306.22 SEC)
EXCITATION NORMALIZED TO 0 S 10 (RAD. COMP.) ; 0.13199600E -3
ATTENUATION INCLUDED; RECORD STARTS AT 3.00 HRS.; LENGTH = 18.00 HRS.

VERTICAL COMPONENT; RADIAL ORDER 7



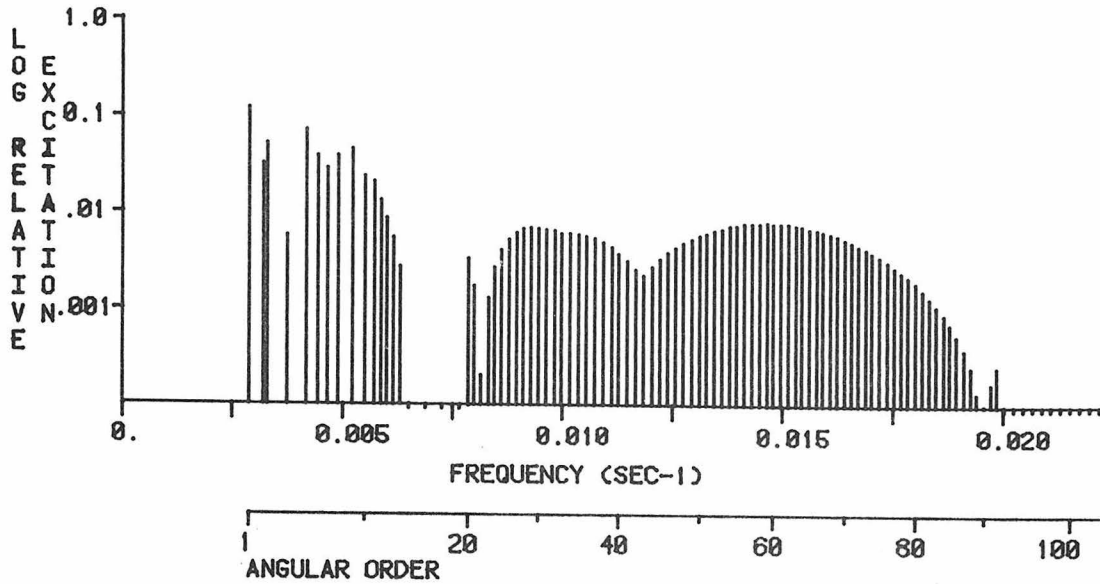
MAXIMUM EXCITATION = 0.302641E -4 CM-SEC ; (7 S 5; T= 273.37 SEC)
EXCITATION NORMALIZED TO 0 S 2 (VERT. COMP.) ; 0.20516300E -3
ATTENUATION INCLUDED; RECORD STARTS AT 3.00 HRS.; LENGTH = 18.00 HRS.

RADIAL COMPONENT; RADIAL ORDER 7



MAXIMUM EXCITATION = 0.323392E -4 CM-SEC ; (7 S 1; T= 449.22 SEC)
EXCITATION NORMALIZED TO 0 S 16 (RAD. COMP.) ; 0.13199600E -3
ATTENUATION INCLUDED; RECORD STARTS AT 3.00 HRS.; LENGTH = 18.00 HRS.

VERTICAL COMPONENT; RADIAL ORDER 8

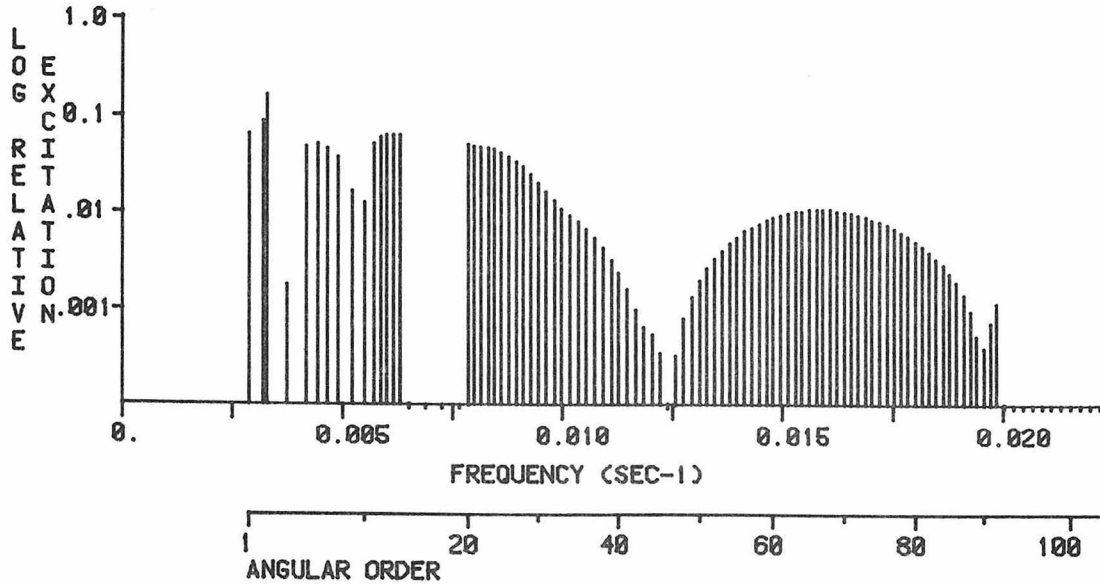


MAXIMUM EXCITATION = 0.255072E -4 CM-SEC ; (8 S 1; T= 348.31 SEC)

EXCITATION NORMALIZED TO 0 S 2 (VERT. COMP.) ; 0.20516300E -3

ATTENUATION INCLUDED; RECORD STARTS AT 3.00 HRS.; LENGTH = 18.00 HRS.

RADIAL COMPONENT; RADIAL ORDER 8

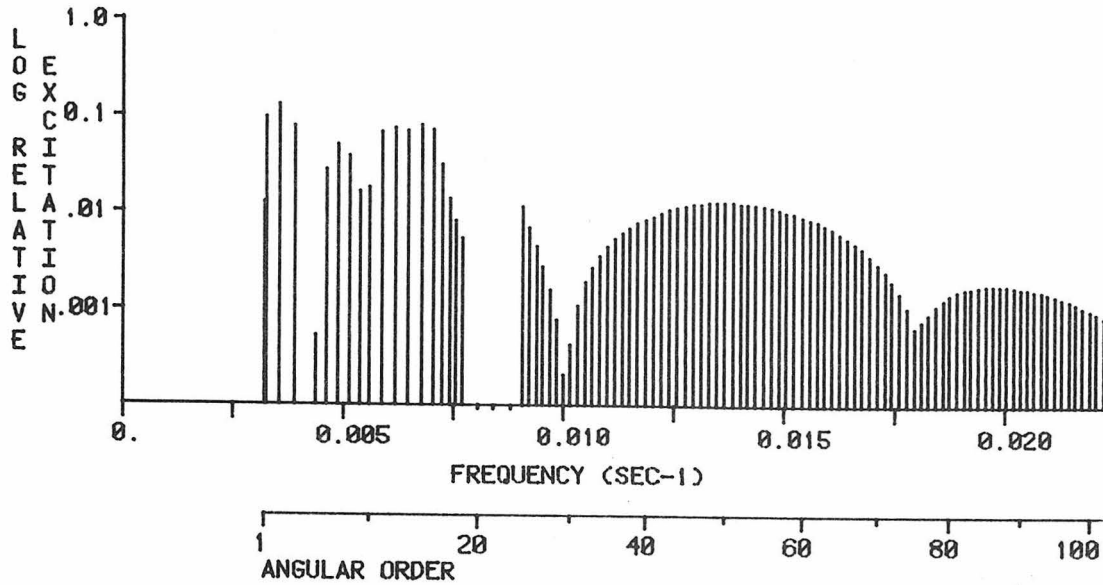


MAXIMUM EXCITATION = 0.212562E -4 CM-SEC ; (8 S 3; T= 304.26 SEC)

EXCITATION NORMALIZED TO 0 S 16 (RAD. COMP.) ; 0.13199600E -3

ATTENUATION INCLUDED; RECORD STARTS AT 3.00 HRS.; LENGTH = 18.00 HRS.

VERTICAL COMPONENT; RADIAL ORDER 9

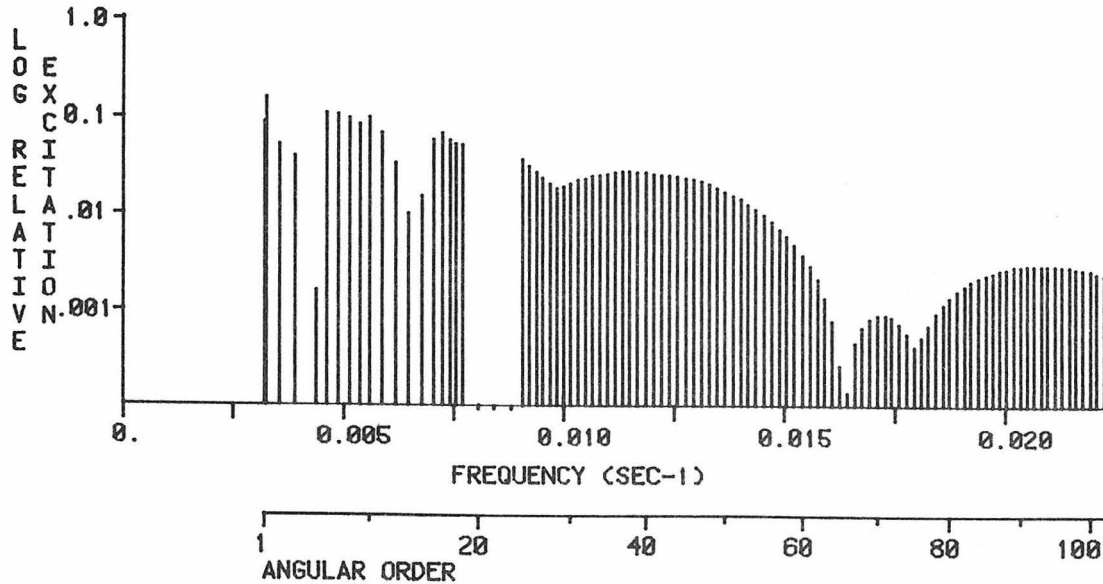


MAXIMUM EXCITATION = 0.266744E -4 CM-SEC ; (9 S 3; T= 281.35 SEC)

EXCITATION NORMALIZED TO 0 S 2 (VERT. COMP.) ; 0.20516300E -3

ATTENUATION INCLUDED; RECORD STARTS AT 3.00 HRS.; LENGTH = 18.00 HRS.

RADIAL COMPONENT; RADIAL ORDER 9

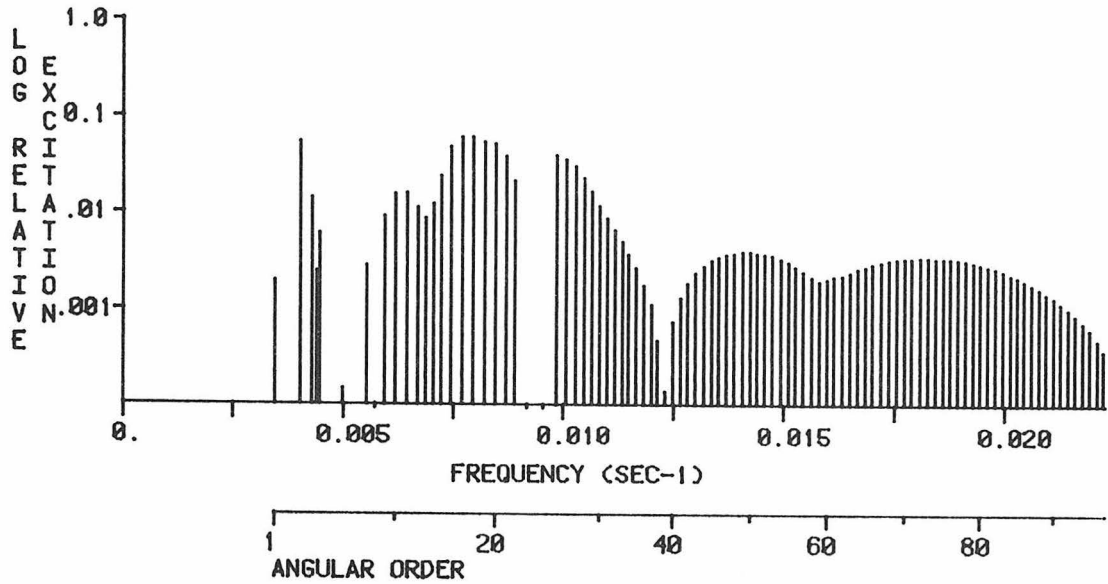


MAXIMUM EXCITATION = 0.204213E -4 CM-SEC ; (9 S 2; T= 309.18 SEC)

EXCITATION NORMALIZED TO 0 S 16 (RAD. COMP.) ; 0.13199600E -3

ATTENUATION INCLUDED; RECORD STARTS AT 3.00 HRS.; LENGTH = 18.00 HRS.

VERTICAL COMPONENT; RADIAL ORDER 10

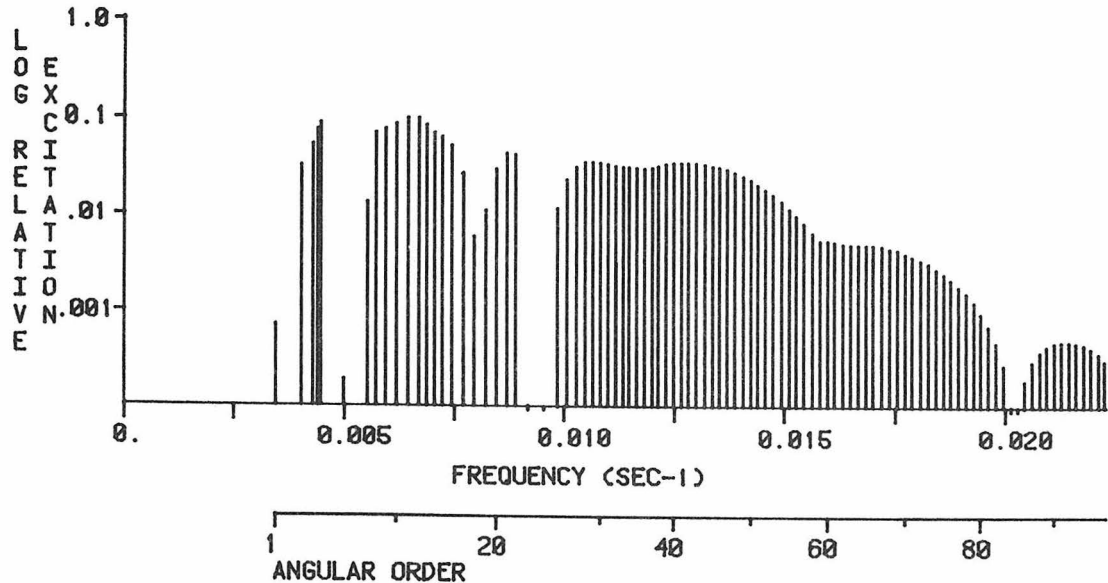


MAXIMUM EXCITATION = 0.123499E -4 CM-SEC ; (10 S 17; T= 130.24 SEC)

EXCITATION NORMALIZED TO 0 S 2 (VERT. COMP.) ; 0.20516300E -3

ATTENUATION INCLUDED; RECORD STARTS AT 3.00 HRS.; LENGTH = 18.00 HRS.

RADIAL COMPONENT; RADIAL ORDER 10

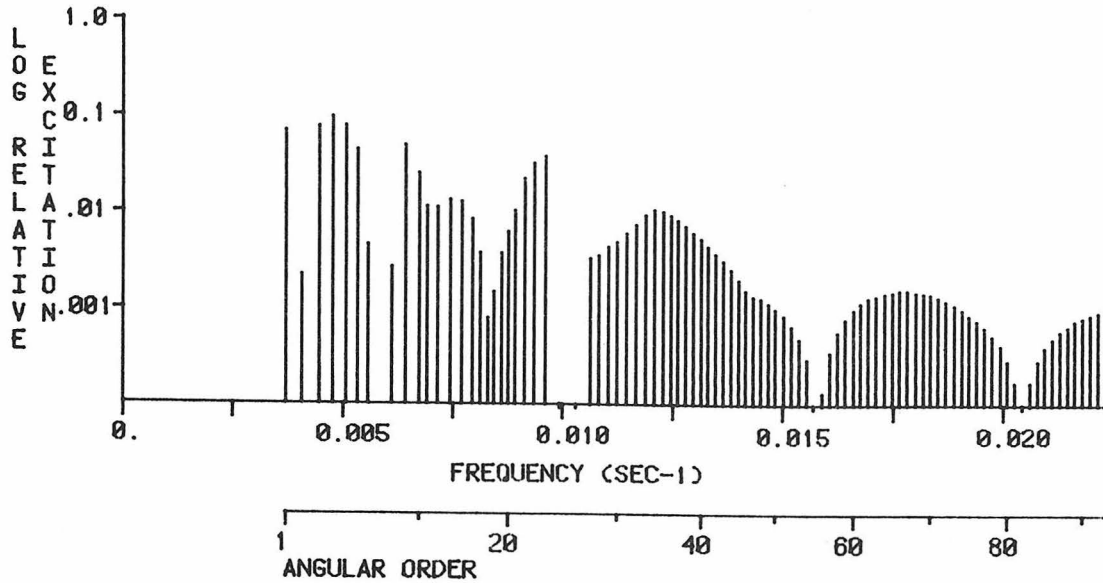


MAXIMUM EXCITATION = 0.133736E -4 CM-SEC ; (10 S 11; T= 155.03 SEC)

EXCITATION NORMALIZED TO 0 S 16 (RAD. COMP.) ; 0.13199600E -3

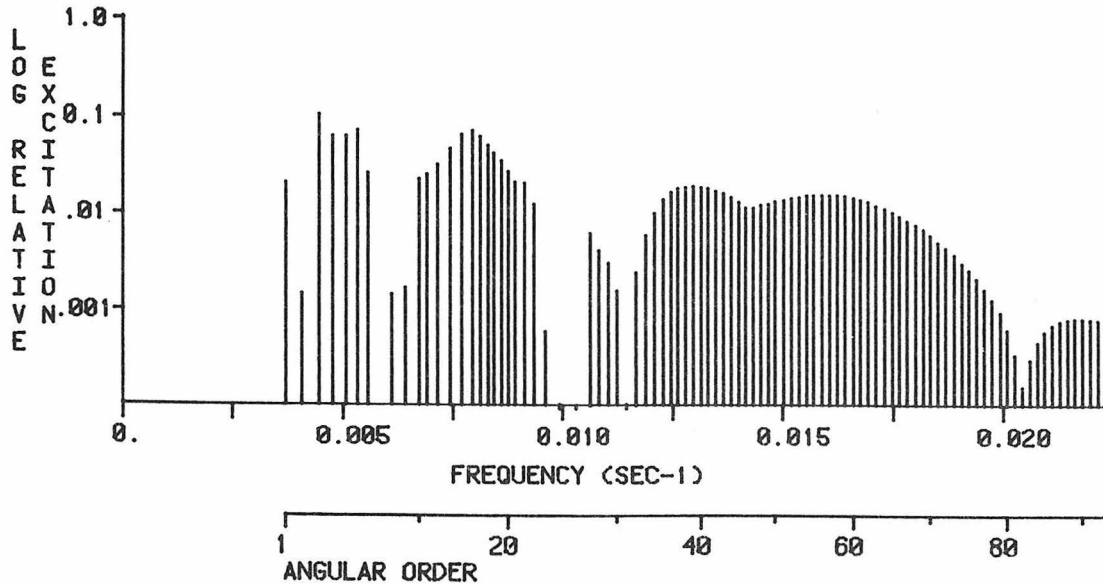
ATTENUATION INCLUDED; RECORD STARTS AT 3.00 HRS.; LENGTH = 18.00 HRS.

VERTICAL COMPONENT; RADIAL ORDER 11



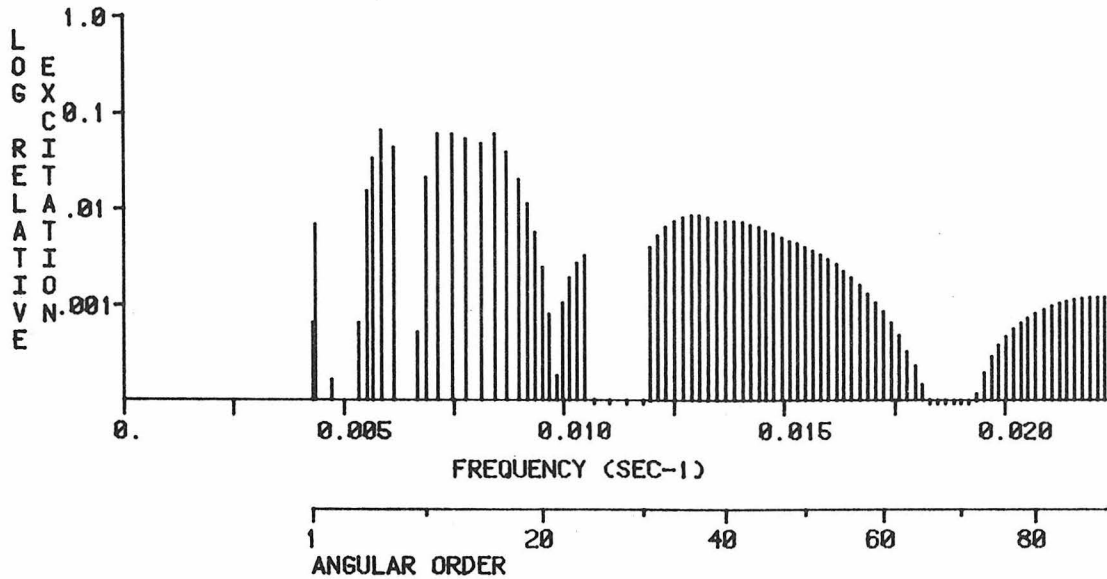
MAXIMUM EXCITATION = 0.193329E -4 CM-SEC ; (11 S 4; T= 209.81 SEC)
EXCITATION NORMALIZED TO 0 S 2 (VERT. COMP.) ; 0.20516300E -3
ATTENUATION INCLUDED; RECORD STARTS AT 3.00 HRS.; LENGTH = 18.00 HRS.

RADIAL COMPONENT; RADIAL ORDER 11



MAXIMUM EXCITATION = 0.136128E -4 CM-SEC ; (11 S 3; T= 224.05 SEC)
EXCITATION NORMALIZED TO 0 S 16 (RAD. COMP.) ; 0.13199600E -3
ATTENUATION INCLUDED; RECORD STARTS AT 3.00 HRS.; LENGTH = 18.00 HRS.

VERTICAL COMPONENT; RADIAL ORDER 12

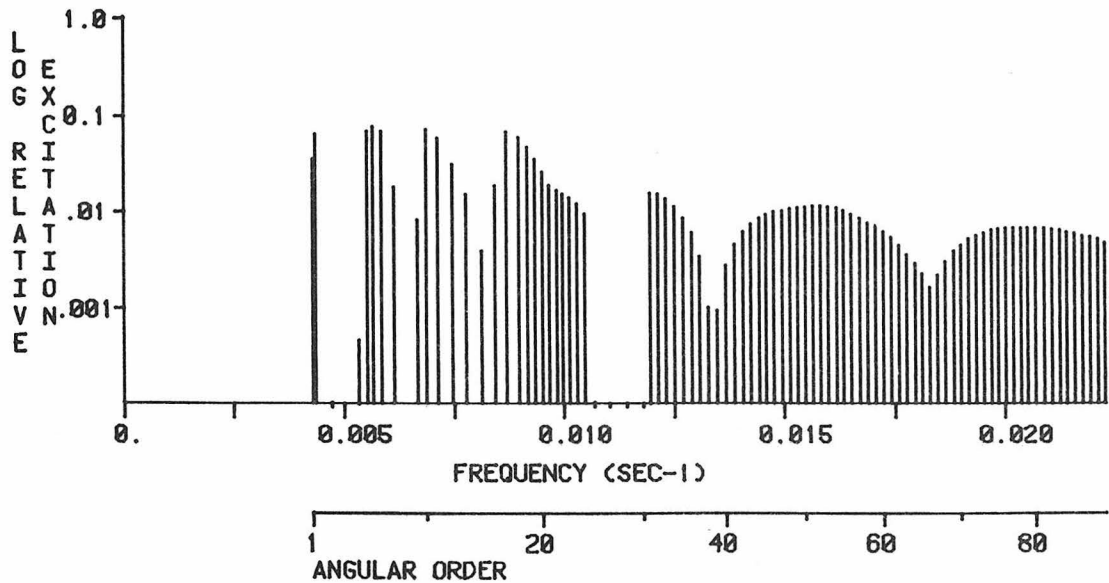


MAXIMUM EXCITATION = 0.134039E -4 CM-SEC ; (12 S 7; T= 170.70 SEC)

EXCITATION NORMALIZED TO 0 S 2 (VERT. COMP.) ; 0.20516300E -3

ATTENUATION INCLUDED; RECORD STARTS AT 3.00 HRS.; LENGTH = 18.00 HRS.

RADIAL COMPONENT; RADIAL ORDER 12

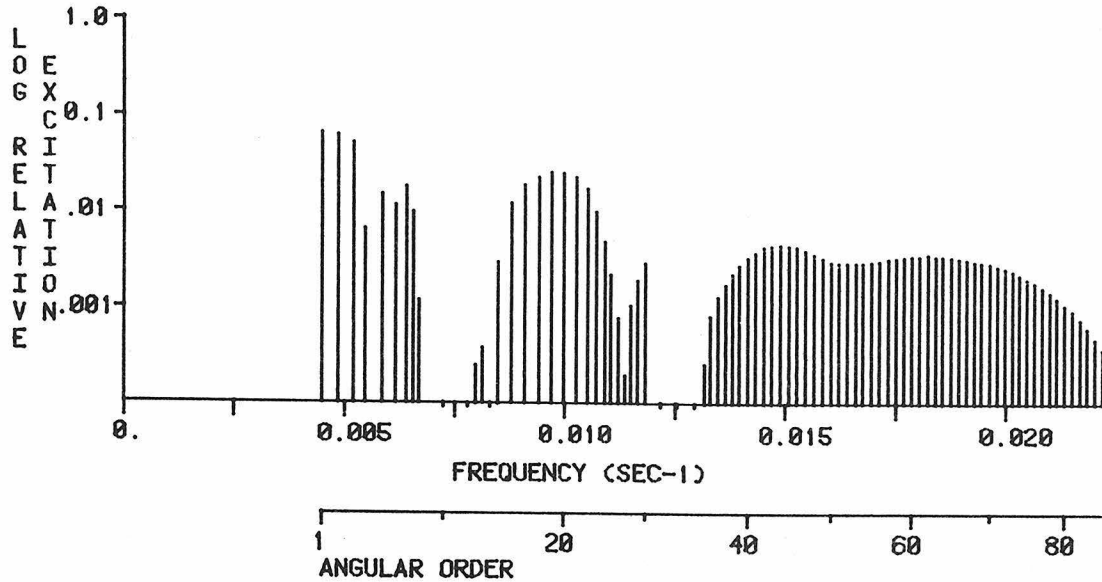


MAXIMUM EXCITATION = 0.100400E -4 CM-SEC ; (12 S 6; T= 176.96 SEC)

EXCITATION NORMALIZED TO 0 S 16 (RAD. COMP.) ; 0.13199600E -3

ATTENUATION INCLUDED; RECORD STARTS AT 3.00 HRS.; LENGTH = 18.00 HRS.

VERTICAL COMPONENT; RADIAL ORDER 13

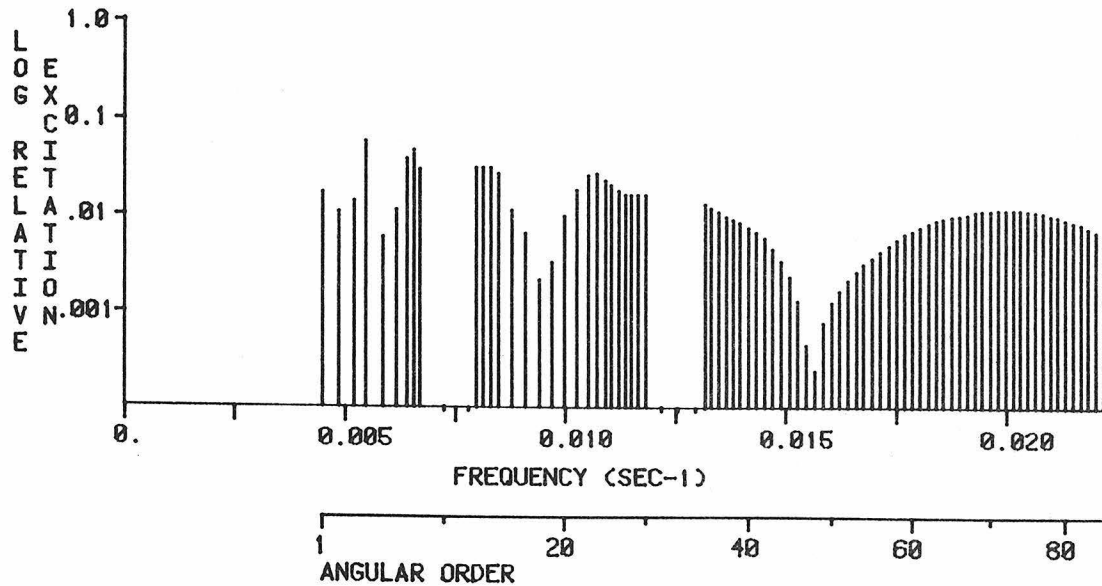


MAXIMUM EXCITATION = 0.134227E -4 CM-SEC ; (13 S 1; T= 222.48 SEC)

EXCITATION NORMALIZED TO 0 S 2 (VERT. COMP.) ; 0.20516300E -3

ATTENUATION INCLUDED; RECORD STARTS AT 3.00 HRS.; LENGTH = 18.00 HRS.

RADIAL COMPONENT; RADIAL ORDER 13

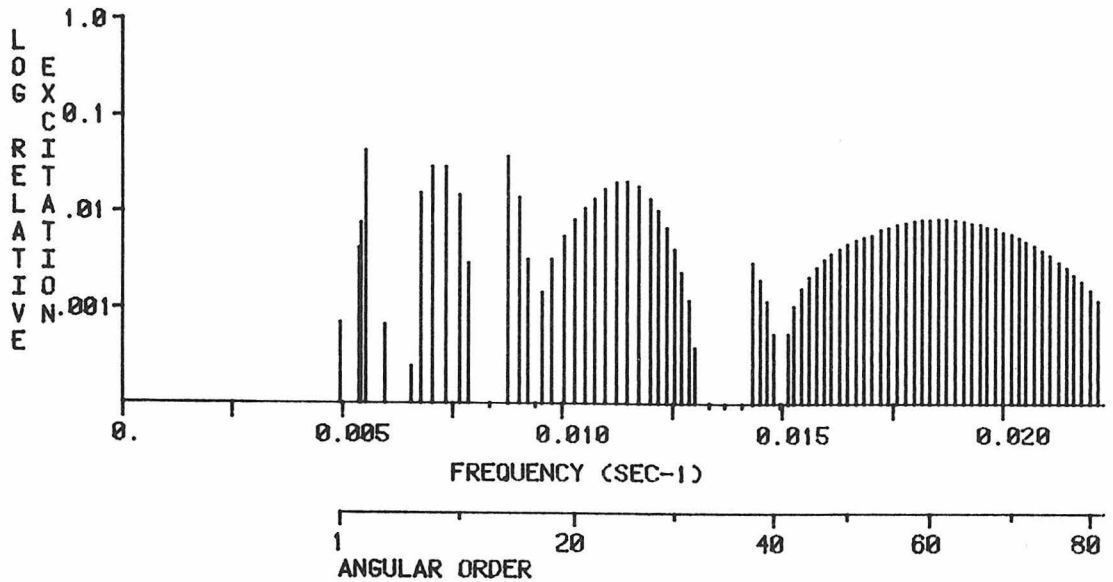


MAXIMUM EXCITATION = 0.781920E -5 CM-SEC ; (13 S 4; T= 183.17 SEC)

EXCITATION NORMALIZED TO 0 S 16 (RAD. COMP.) ; 0.13199600E -3

ATTENUATION INCLUDED; RECORD STARTS AT 3.00 HRS.; LENGTH = 18.00 HRS.

VERTICAL COMPONENT; RADIAL ORDER 14

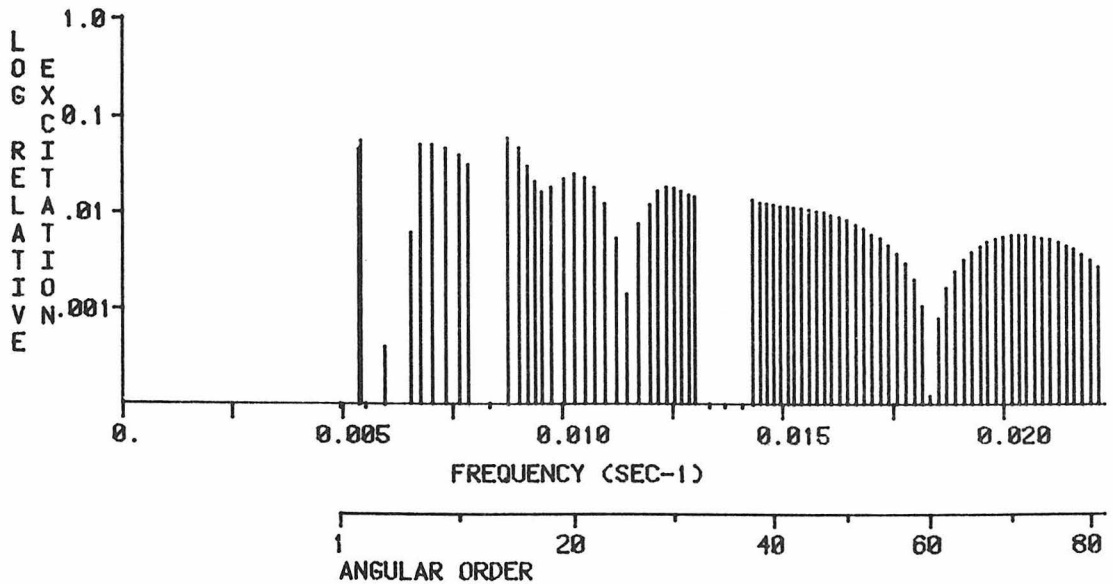


MAXIMUM EXCITATION = 0.881550E -5 CM-SEC ; (14 S 4; T= 180.46 SEC)

EXCITATION NORMALIZED TO 0 S 2 (VERT. COMP.) ; 0.20516300E -3

ATTENUATION INCLUDED; RECORD STARTS AT 3.00 HRS.; LENGTH = 18.00 HRS.

RADIAL COMPONENT; RADIAL ORDER 14

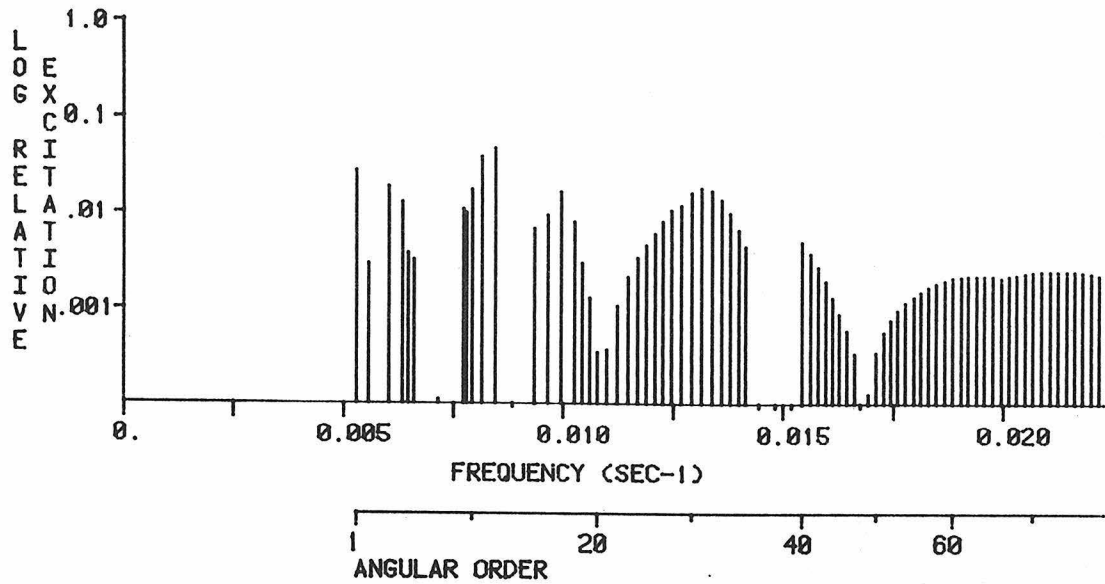


MAXIMUM EXCITATION = 0.790130E -5 CM-SEC ; (14 S 13; T= 114.46 SEC)

EXCITATION NORMALIZED TO 0 S 16 (RAD. COMP.) ; 0.13199600E -3

ATTENUATION INCLUDED; RECORD STARTS AT 3.00 HRS.; LENGTH = 18.00 HRS.

VERTICAL COMPONENT; RADIAL ORDER 15

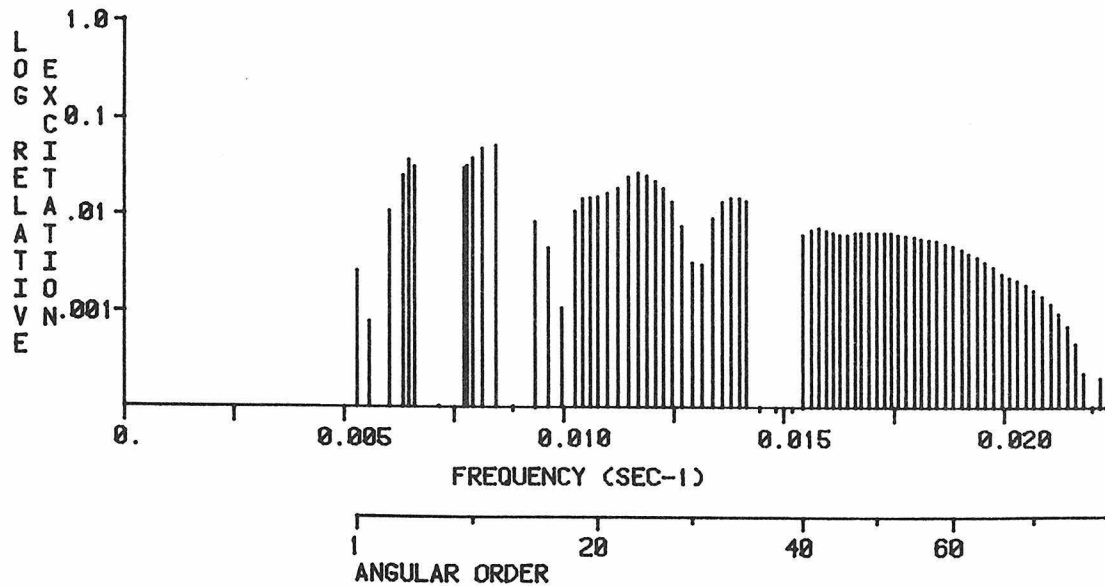


MAXIMUM EXCITATION = 0.940520E -5 CM-SEC ; (15 S 12; T= 118.56 SEC)

EXCITATION NORMALIZED TO 0 S 2 (VERT. COMP.) ; 0.20516300E -3

ATTENUATION INCLUDED; RECORD STARTS AT 3.00 HRS.; LENGTH = 18.00 HRS.

RADIAL COMPONENT; RADIAL ORDER 15

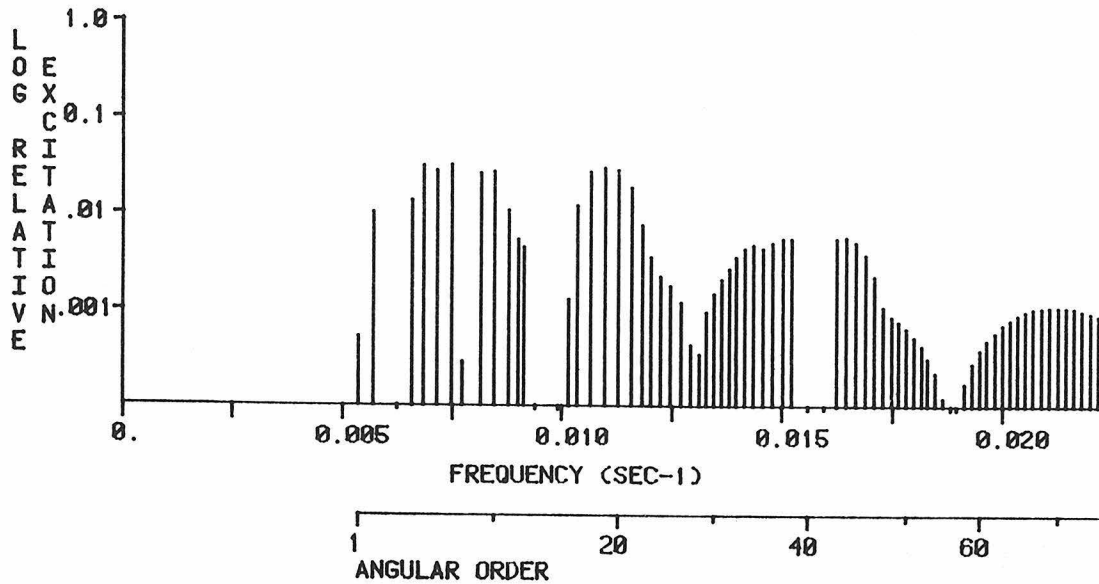


MAXIMUM EXCITATION = 0.683910E -5 CM-SEC ; (15 S 12; T= 118.56 SEC)

EXCITATION NORMALIZED TO 0 S 16 (RAD. COMP.) ; 0.13199600E -3

ATTENUATION INCLUDED; RECORD STARTS AT 3.00 HRS.; LENGTH = 18.00 HRS.

VERTICAL COMPONENT; RADIAL ORDER 16

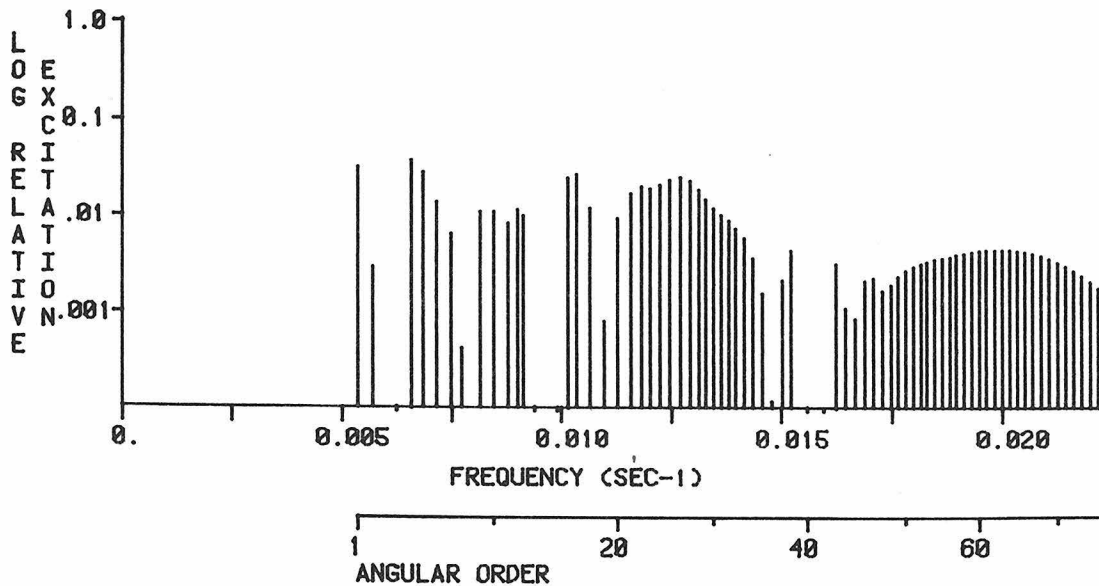


MAXIMUM EXCITATION = 0.659250E -5 CM-SEC ; (16 S 7; T= 133.78 SEC)

EXCITATION NORMALIZED TO 0 S 2 (VERT. COMP.) ; 0.20516300E -3

ATTENUATION INCLUDED; RECORD STARTS AT 3.00 HRS.; LENGTH = 18.00 HRS.

RADIAL COMPONENT; RADIAL ORDER 16

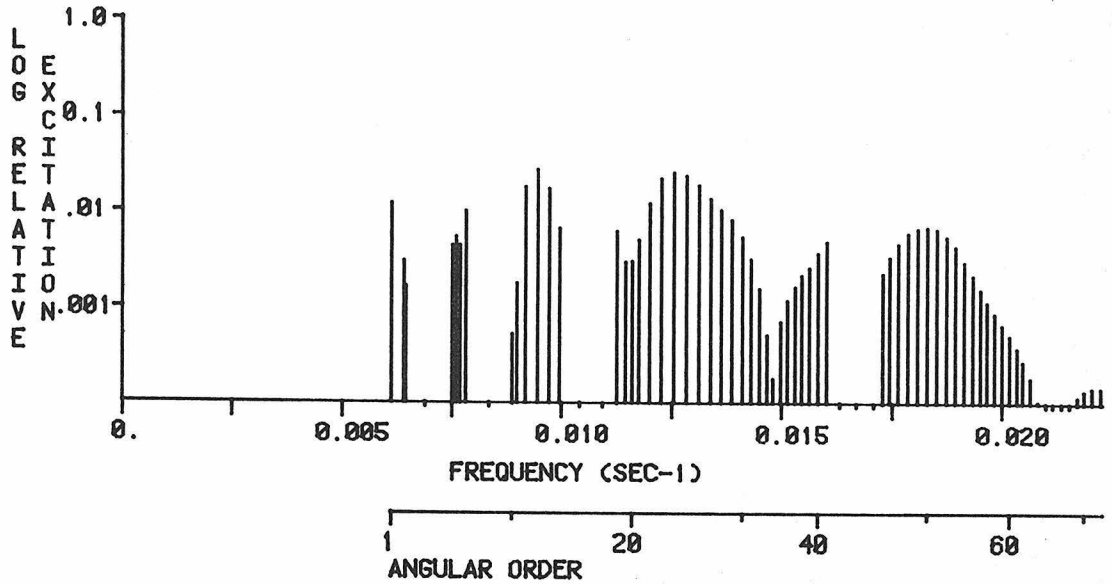


MAXIMUM EXCITATION = 0.496957E -5 CM-SEC ; (16 S 4; T= 152.29 SEC)

EXCITATION NORMALIZED TO 0 S 16 (RAD. COMP.) ; 0.13199600E -3

ATTENUATION INCLUDED; RECORD STARTS AT 3.00 HRS.; LENGTH = 18.00 HRS.

VERTICAL COMPONENT; RADIAL ORDER 17

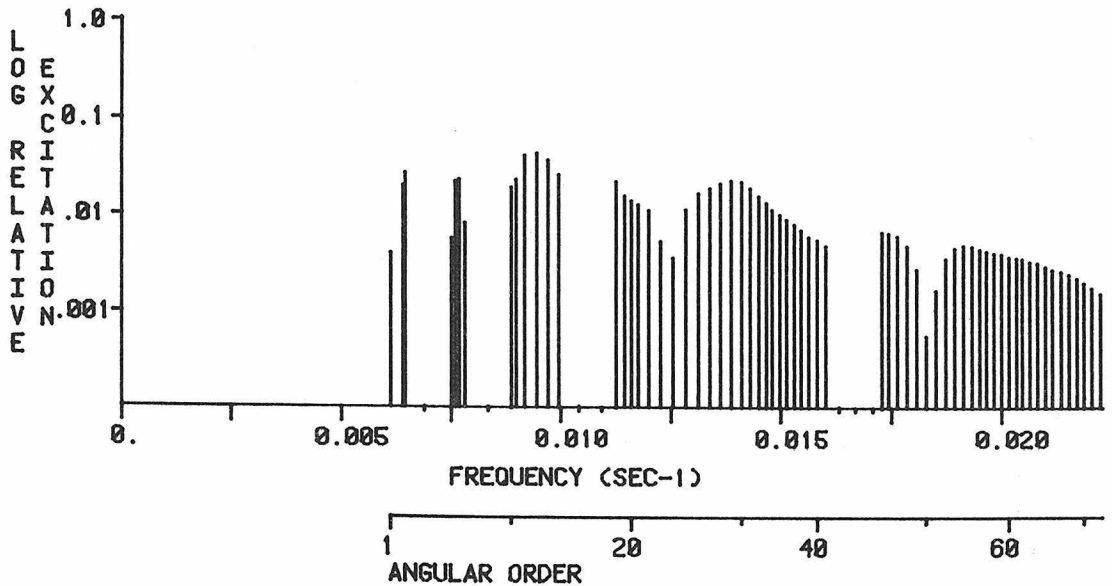


MAXIMUM EXCITATION = 0.550698E -5 CM-SEC ; (17 S 13; T= 106.01 SEC)

EXCITATION NORMALIZED TO 0 S 2 (VERT. COMP.) ; 0.20516300E -3

ATTENUATION INCLUDED; RECORD STARTS AT 3.00 HRS.; LENGTH = 18.00 HRS.

RADIAL COMPONENT; RADIAL ORDER 17

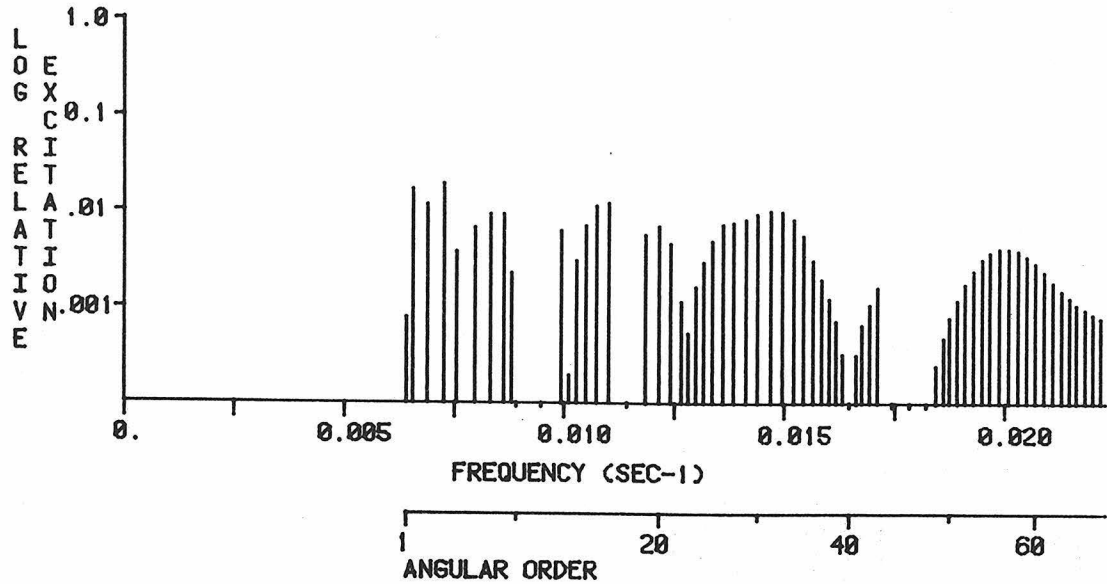


MAXIMUM EXCITATION = 0.574072E -5 CM-SEC ; (17 S 13; T= 106.01 SEC)

EXCITATION NORMALIZED TO 0 S 16 (RAD. COMP.) ; 0.13199600E -3

ATTENUATION INCLUDED; RECORD STARTS AT 3.00 HRS.; LENGTH = 18.00 HRS.

VERTICAL COMPONENT; RADIAL ORDER 18

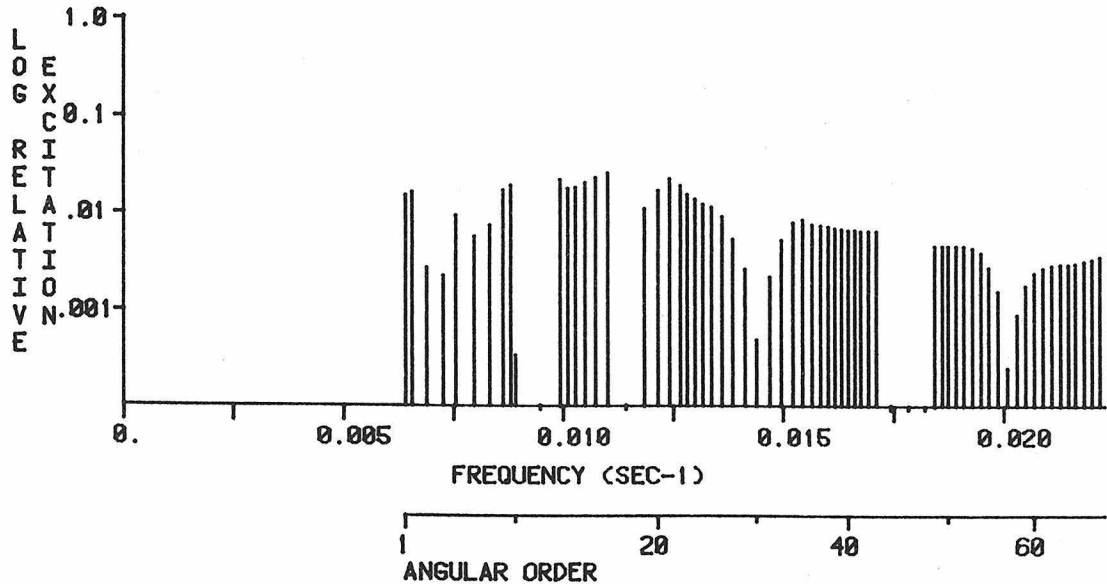


MAXIMUM EXCITATION = 0.397621E -5 CM-SEC ; (18 S 4; T= 138.13 SEC)

EXCITATION NORMALIZED TO 0 S 2 (VERT. COMP.) ; 0.20516300E -3

ATTENUATION INCLUDED; RECORD STARTS AT 3.00 HRS.; LENGTH = 18.00 HRS.

RADIAL COMPONENT; RADIAL ORDER 18

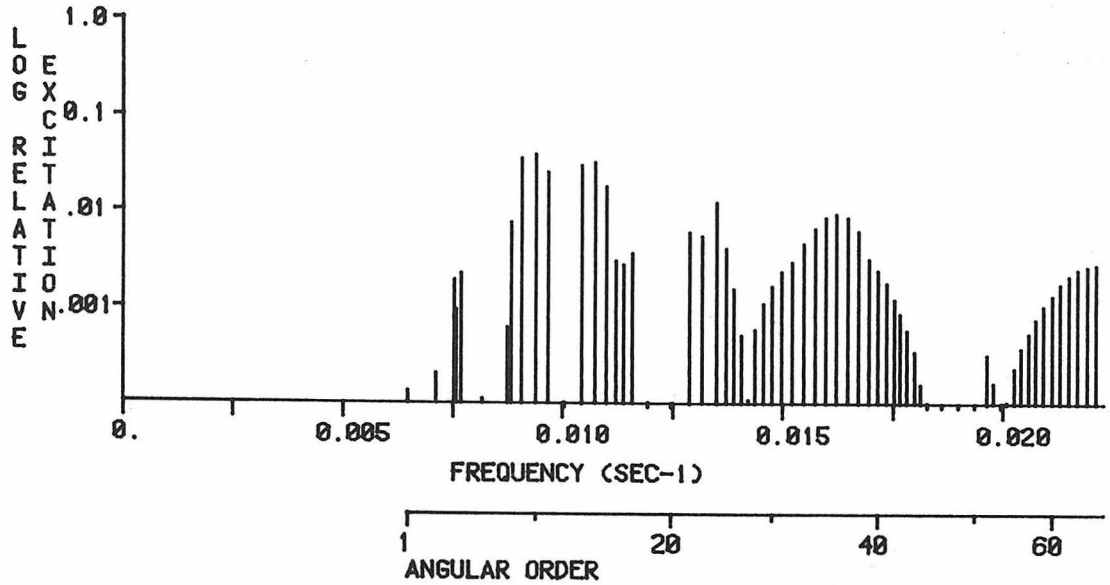


MAXIMUM EXCITATION = 0.348329E -5 CM-SEC ; (18 S 17; T= 90.90 SEC)

EXCITATION NORMALIZED TO 0 S 16 (RAD. COMP.) ; 0.13199600E -3

ATTENUATION INCLUDED; RECORD STARTS AT 3.00 HRS.; LENGTH = 18.00 HRS.

VERTICAL COMPONENT; RADIAL ORDER 19

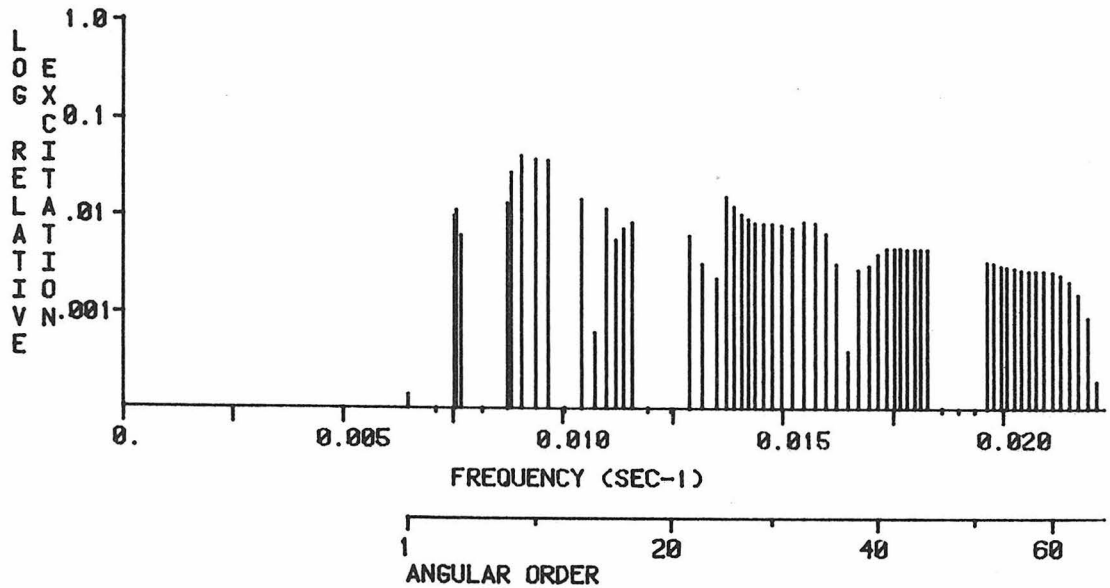


MAXIMUM EXCITATION = 0.799610E -5 CM-SEC ; (19 S 10; T= 106.89 SEC)

EXCITATION NORMALIZED TO 0 S 2 (VERT. COMP.) ; 0.20516300E -3

ATTENUATION INCLUDED; RECORD STARTS AT 3.00 HRS.; LENGTH = 18.00 HRS.

RADIAL COMPONENT; RADIAL ORDER 19

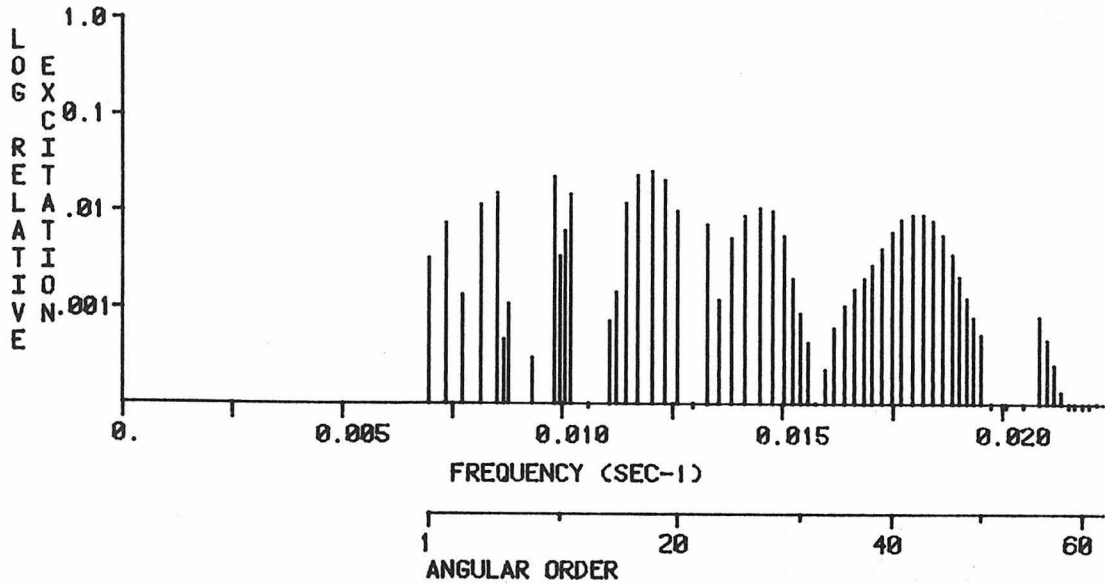


MAXIMUM EXCITATION = 0.539753E -5 CM-SEC ; (19 S 9; T= 110.53 SEC)

EXCITATION NORMALIZED TO 0 S 16 (RAD. COMP.) ; 0.13199600E -3

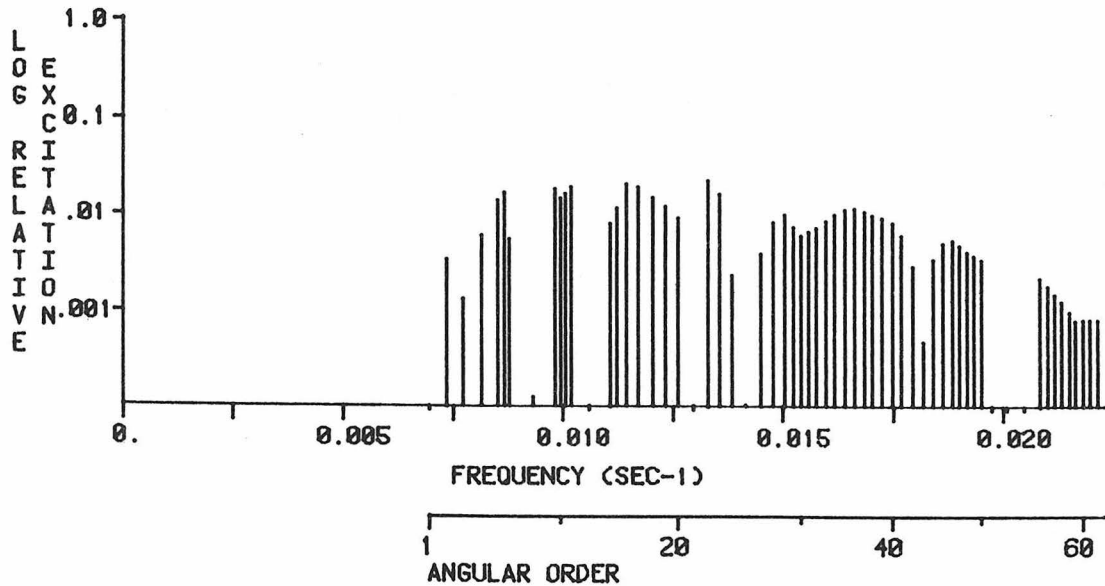
ATTENUATION INCLUDED; RECORD STARTS AT 3.00 HRS.; LENGTH = 18.00 HRS.

VERTICAL COMPONENT; RADIAL ORDER 20



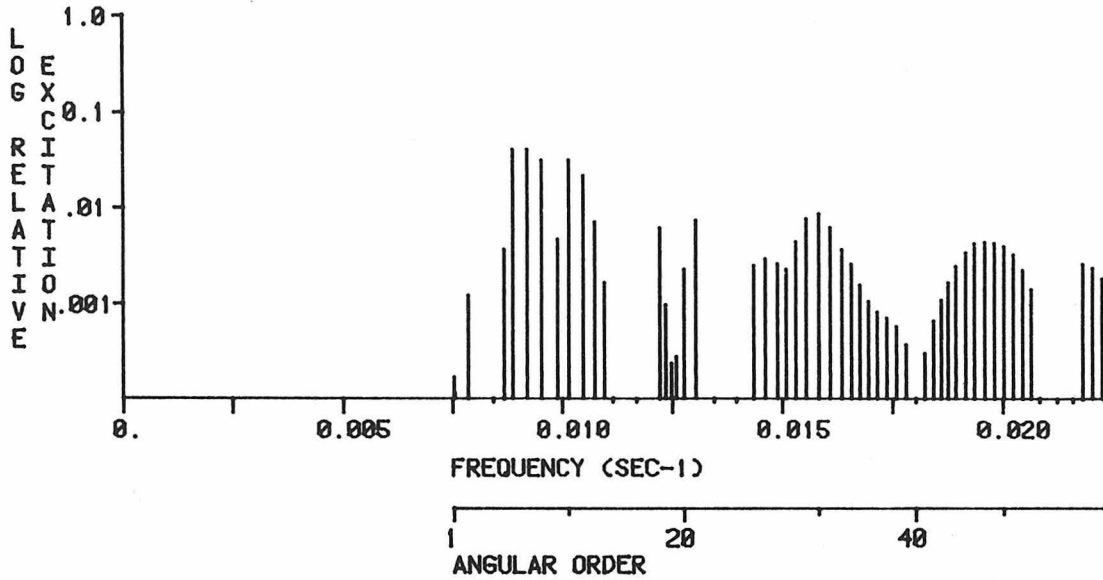
MAXIMUM EXCITATION = 0.540005E -5 CM-SEC ; (20 S 18; T= 83.19 SEC)
EXCITATION NORMALIZED TO 0 S 2 (VERT. COMP.) ; 0.20516300E -3
ATTENUATION INCLUDED; RECORD STARTS AT 3.00 HRS.; LENGTH = 18.00 HRS.

RADIAL COMPONENT; RADIAL ORDER 20



MAXIMUM EXCITATION = 0.297008E -5 CM-SEC ; (20 S 22; T= 75.35 SEC)
EXCITATION NORMALIZED TO 0 S 16 (RAD. COMP.) ; 0.13199600E -3
ATTENUATION INCLUDED; RECORD STARTS AT 3.00 HRS.; LENGTH = 18.00 HRS.

VERTICAL COMPONENT; RADIAL ORDER 21

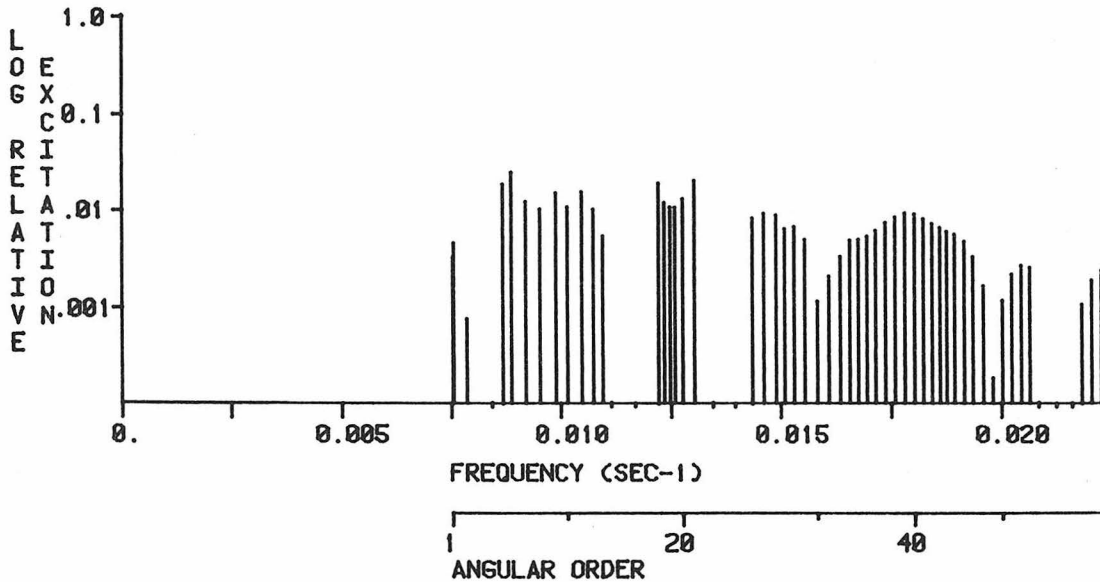


MAXIMUM EXCITATION = 0.822610E -5 CM-SEC ; (21 S 6; T= 112.97 SEC)

EXCITATION NORMALIZED TO 0 S 2 (VERT. COMP.) ; 0.20516300E -3

ATTENUATION INCLUDED; RECORD STARTS AT 3.00 HRS.; LENGTH = 18.00 HRS.

RADIAL COMPONENT; RADIAL ORDER 21

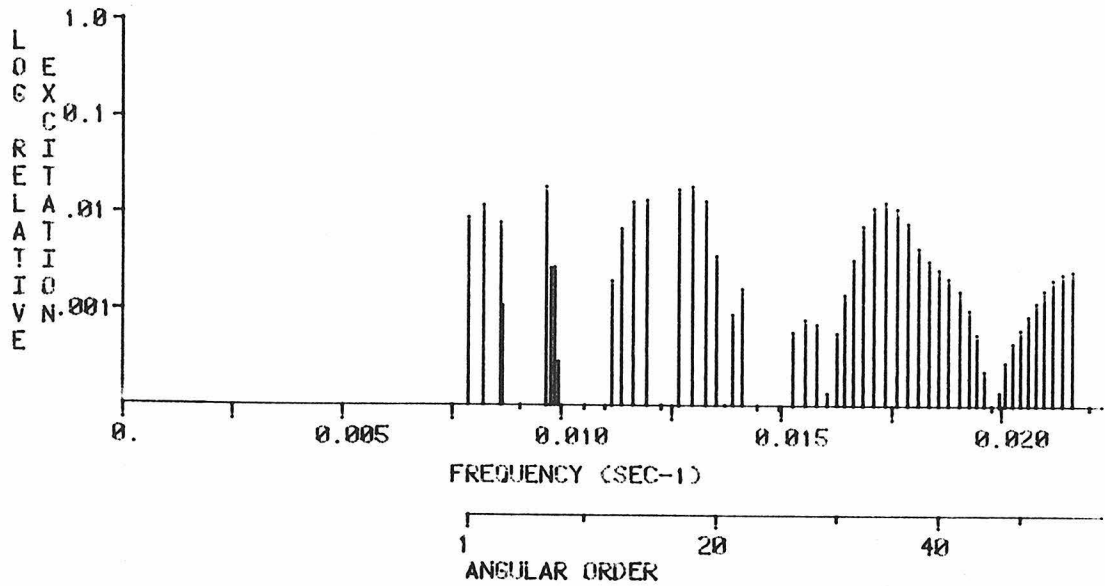


MAXIMUM EXCITATION = 0.326873E -5 CM-SEC ; (21 S 6; T= 112.97 SEC)

EXCITATION NORMALIZED TO 0 S 16 (RAD. COMP.) ; 0.13199600E -3

ATTENUATION INCLUDED; RECORD STARTS AT 3.00 HRS.; LENGTH = 18.00 HRS.

VERTICAL COMPONENT; RADIAL ORDER 22

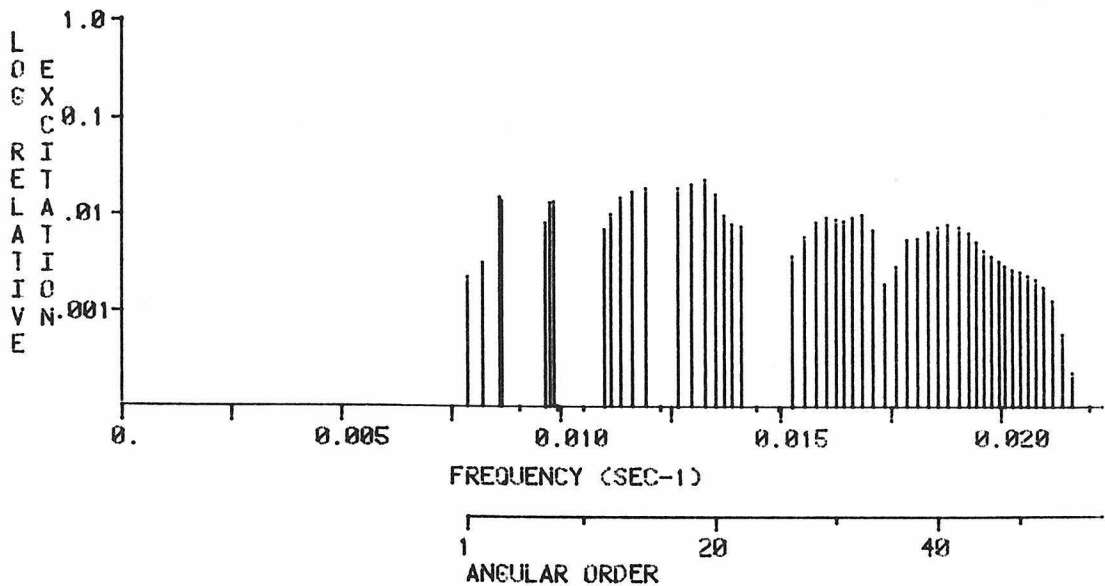


MAXIMUM EXCITATION = 0.405174E -5 CM-SEC ; (22 S 18; T= 77.23 SEC)

EXCITATION NORMALIZED TO 0 S 2 (VERT. COMP.) ; 0.20516300E -3

ATTENUATION INCLUDED; RECORD STARTS AT 3.00 HRS.; LENGTH = 18.00 HRS.

RADIAL COMPONENT; RADIAL ORDER 22

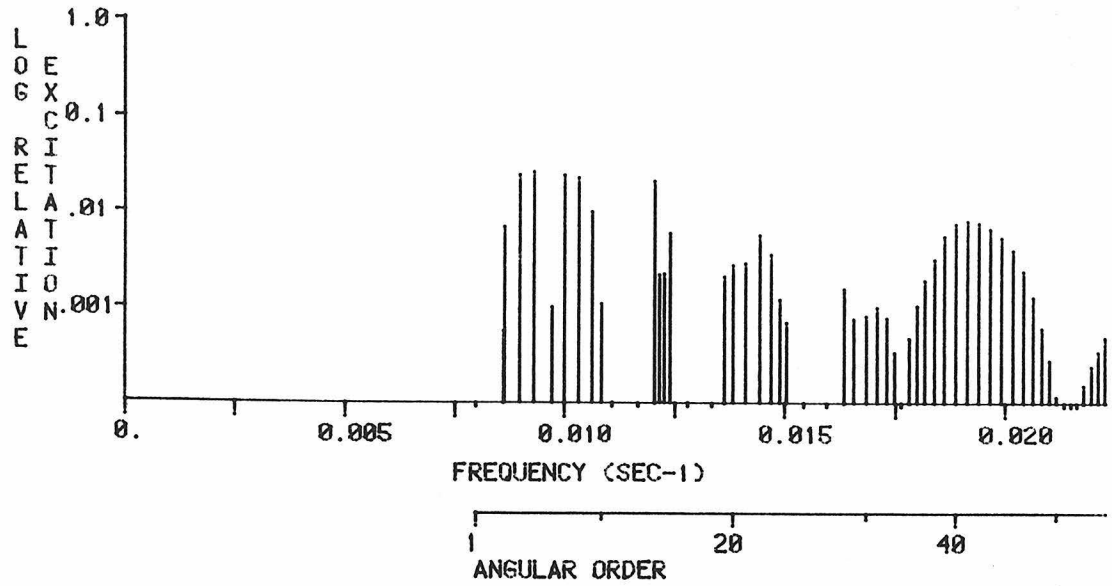


MAXIMUM EXCITATION = 0.308234E -5 CM-SEC ; (22 S 18; T= 75.45 SEC)

EXCITATION NORMALIZED TO 0 S 16 (RAD. COMP.) ; 0.13199600E -3

ATTENUATION INCLUDED; RECORD STARTS AT 3.00 HRS.; LENGTH = 18.00 HRS.

VERTICAL COMPONENT; RADIAL ORDER 23

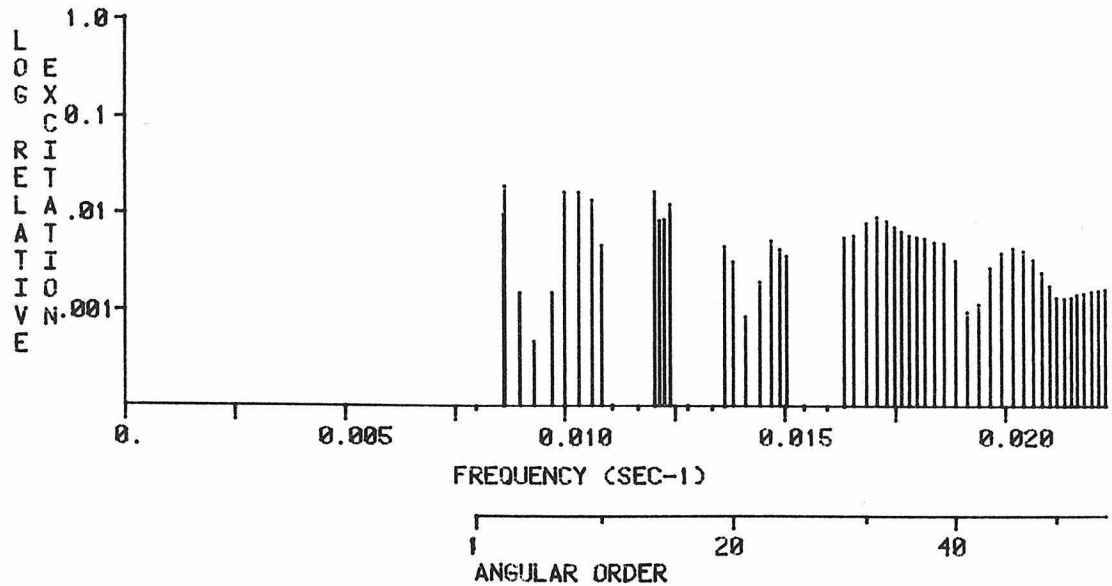


MAXIMUM EXCITATION = 0.524471E -5 CM-SEC ; (23 S 5; T= 107.61 SEC)

EXCITATION NORMALIZED TO 0 S 2 (VERT. COMP.) ; 0.20516300E -3

ATTENUATION INCLUDED; RECORD STARTS AT 3.00 HRS.; LENGTH = 18.00 HRS.

RADIAL COMPONENT; RADIAL ORDER 23

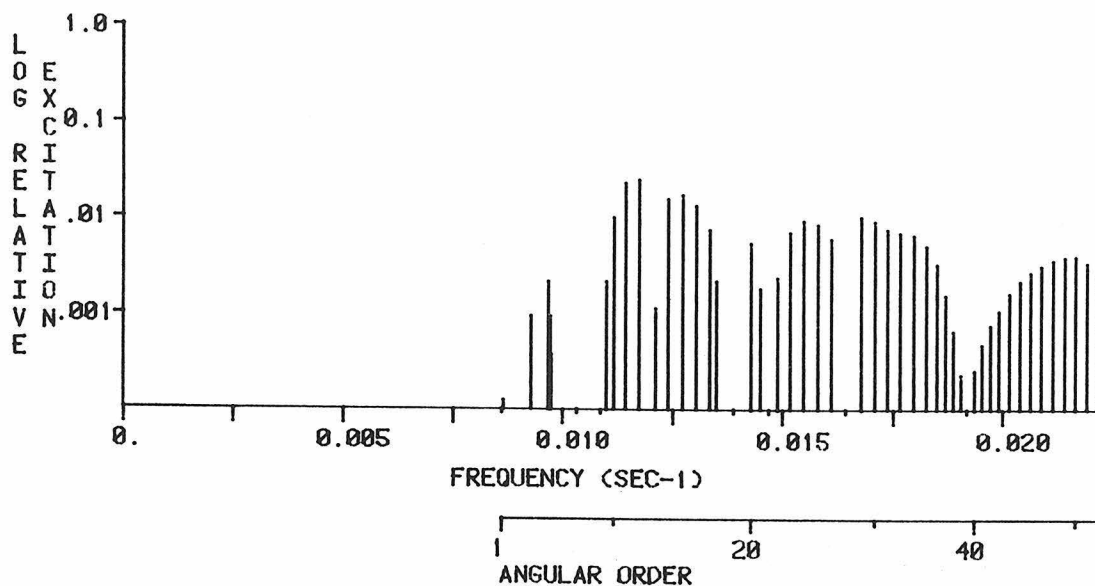


MAXIMUM EXCITATION = 0.248129E -5 CM-SEC ; (23 S 3; T= 116.09 SEC)

EXCITATION NORMALIZED TO 0 S 16 (RAD. COMP.) ; 0.13199600E -3

ATTENUATION INCLUDED; RECORD STARTS AT 3.00 HRS.; LENGTH = 18.00 HRS.

VERTICAL COMPONENT; RADIAL ORDER 24

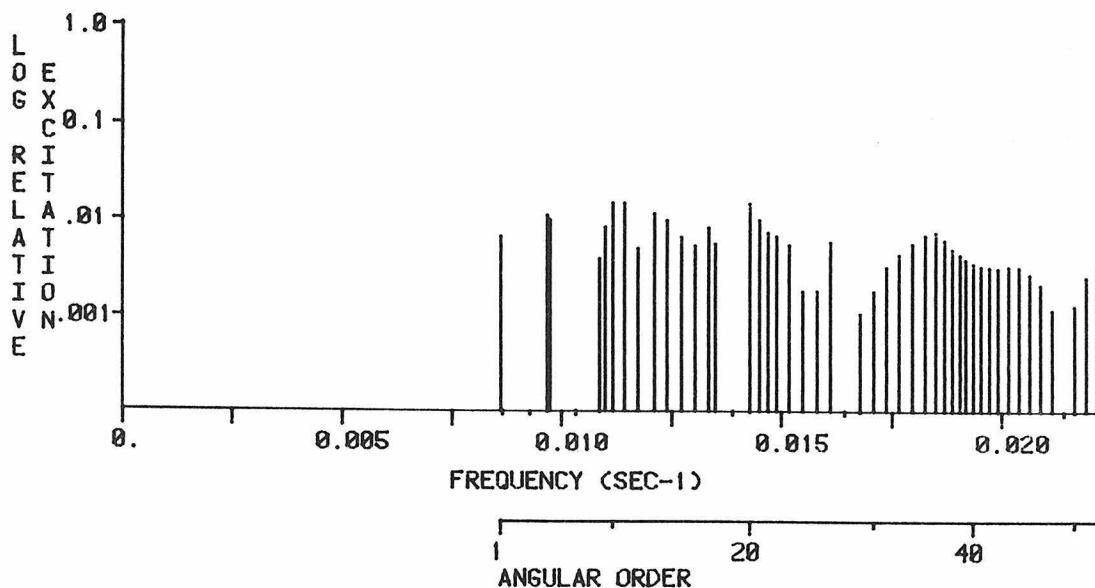


MAXIMUM EXCITATION = 0.509131E -5 CM-SEC ; (24 S 12; T= 85.22 SEC)

EXCITATION NORMALIZED TO 0 S 2 (VERT. COMP.) ; 0.20516300E -3

ATTENUATION INCLUDED; RECORD STARTS AT 3.00 HRS.; LENGTH = 18.00 HRS.

RADIAL COMPONENT; RADIAL ORDER 24

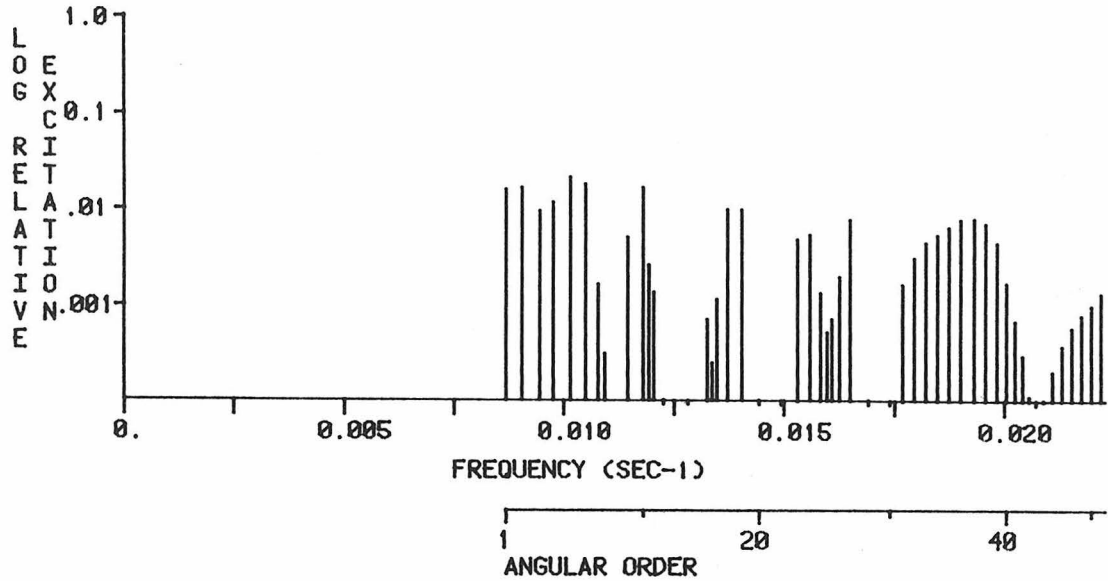


MAXIMUM EXCITATION = 0.200408E -5 CM-SEC ; (24 S 10; T= 89.67 SEC)

EXCITATION NORMALIZED TO 0 S 16 (RAD. COMP.) ; 0.13199600E -3

ATTENUATION INCLUDED; RECORD STARTS AT 3.00 HRS.; LENGTH = 18.00 HRS.

VERTICAL COMPONENT; RADIAL ORDER 25

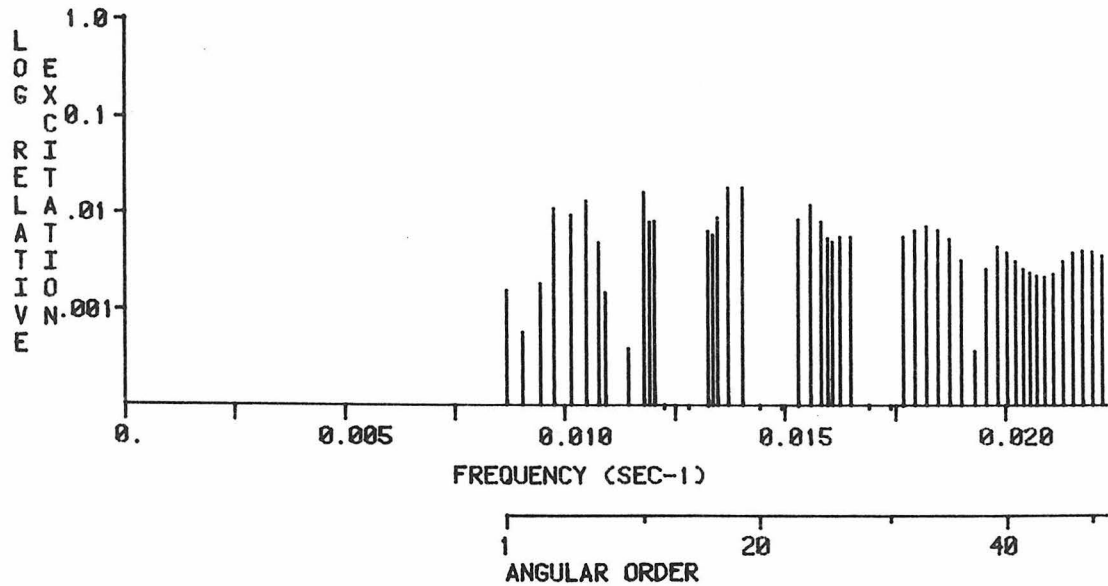


MAXIMUM EXCITATION = 0.441085E -5 CM-SEC ; (25 S 5; T= 98.74 SEC)

EXCITATION NORMALIZED TO 0 S 2 (VERT. COMP.) ; 0.20516300E -3

ATTENUATION INCLUDED; RECORD STARTS AT 3.00 HRS.; LENGTH = 18.00 HRS.

RADIAL COMPONENT; RADIAL ORDER 25

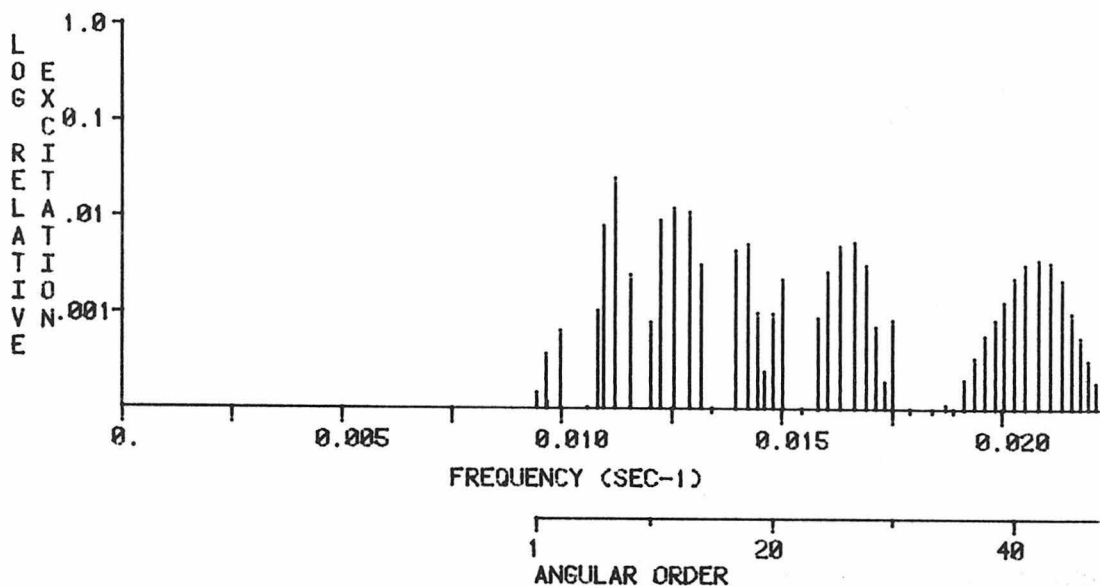


MAXIMUM EXCITATION = 0.245854E -5 CM-SEC ; (25 S 18; T= 72.97 SEC)

EXCITATION NORMALIZED TO 0 S 16 (RAD. COMP.) ; 0.13199600E -3

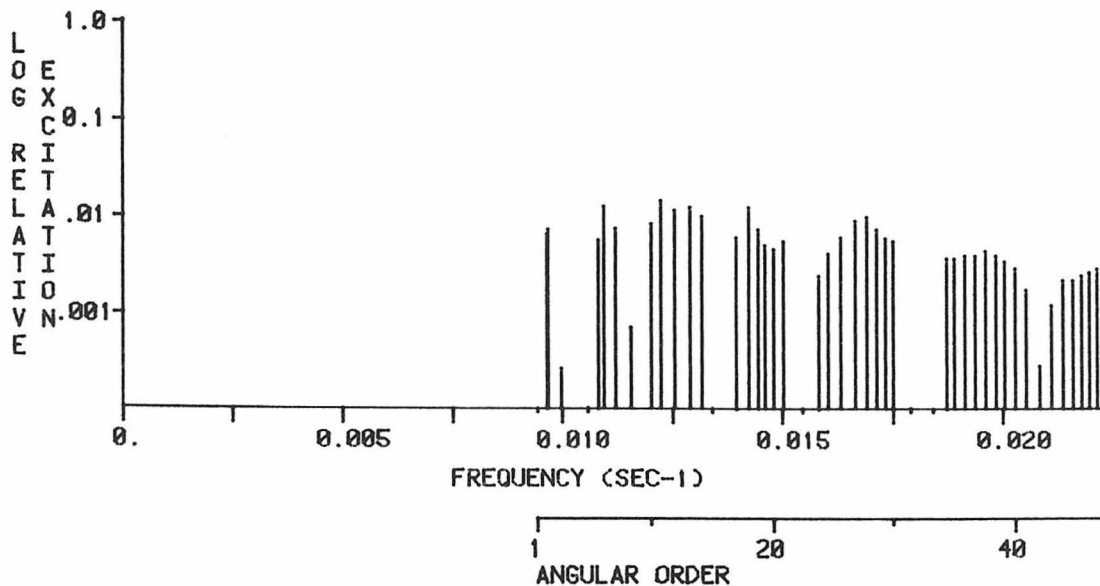
ATTENUATION INCLUDED; RECORD STARTS AT 3.00 HRS.; LENGTH = 18.00 HRS.

VERTICAL COMPONENT; RADIAL ORDER 26



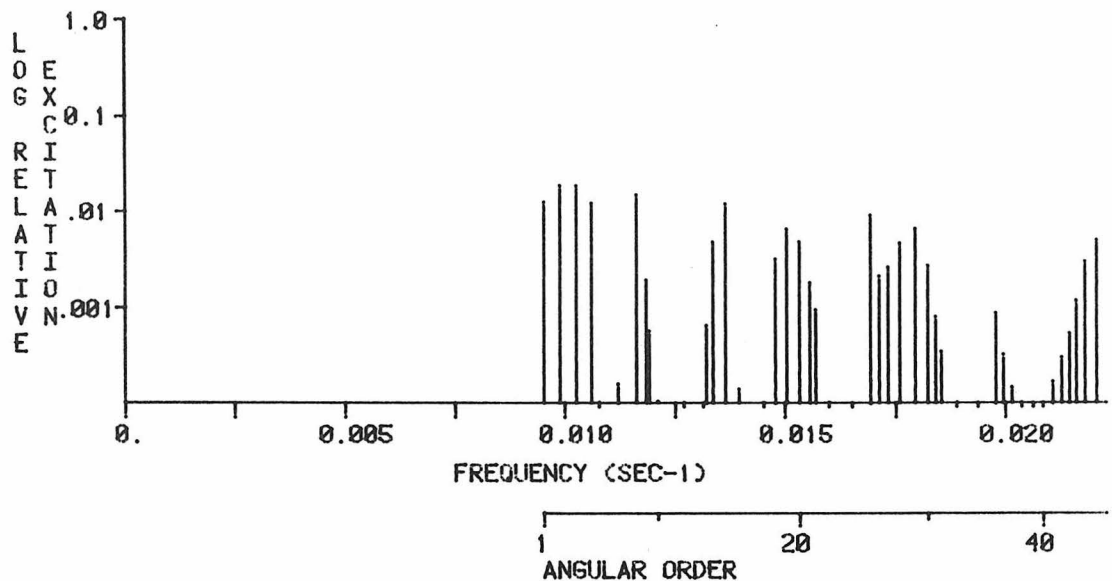
MAXIMUM EXCITATION = 0.528175E -5 CM-SEC ; (26 S 8; T= 89.34 SEC)
EXCITATION NORMALIZED TO 0 S 2 (VERT. COMP.) ; 0.20516300E -3
ATTENUATION INCLUDED; RECORD STARTS AT 3.00 HRS.; LENGTH = 18.00 HRS.

RADIAL COMPONENT; RADIAL ORDER 26



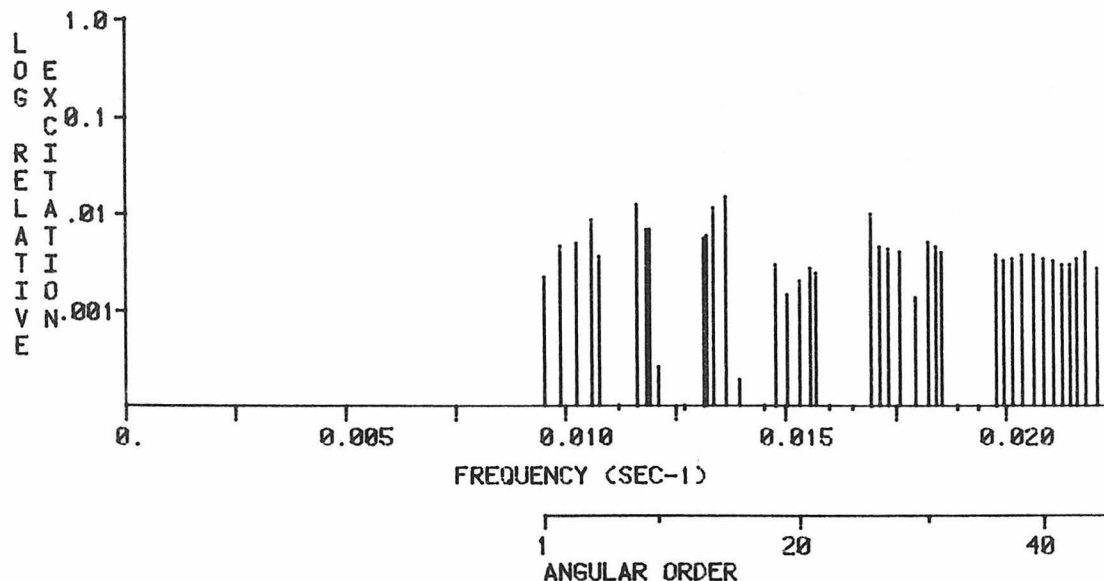
MAXIMUM EXCITATION = 0.191229E -5 CM-SEC ; (26 S 11; T= 81.81 SEC)
EXCITATION NORMALIZED TO 0 S 16 (RAD. COMP.) ; 0.13199600E -3
ATTENUATION INCLUDED; RECORD STARTS AT 3.00 HRS.; LENGTH = 18.00 HRS.

VERTICAL COMPONENT; RADIAL ORDER 27



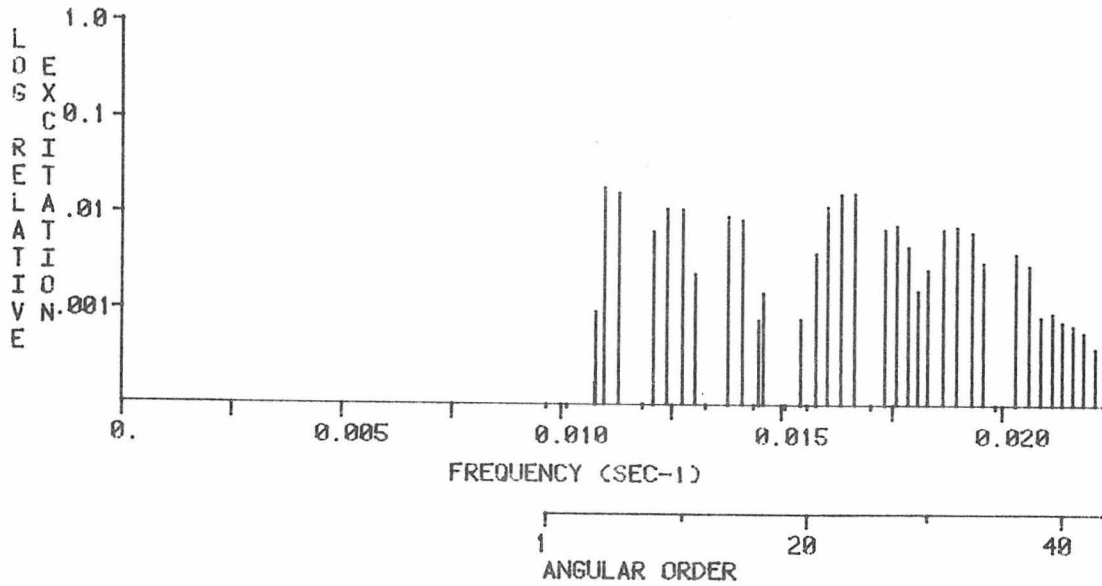
MAXIMUM EXCITATION = 0.381496E -5 CM-SEC ; (27 S 2; T= 101.39 SEC)
EXCITATION NORMALIZED TO 0 S 2 (VERT. COMP.) ; 0.20516300E -3
ATTENUATION INCLUDED; RECORD STARTS AT 3.00 HRS.; LENGTH = 18.00 HRS.

RADIAL COMPONENT; RADIAL ORDER 27



MAXIMUM EXCITATION = 0.198339E -5 CM-SEC ; (27 S 15; T= 73.43 SEC)
EXCITATION NORMALIZED TO 0 S 16 (RAD. COMP.) ; 0.13199600E -3
ATTENUATION INCLUDED; RECORD STARTS AT 3.00 HRS.; LENGTH = 18.00 HRS.

VERTICAL COMPONENT; RADIAL ORDER 28

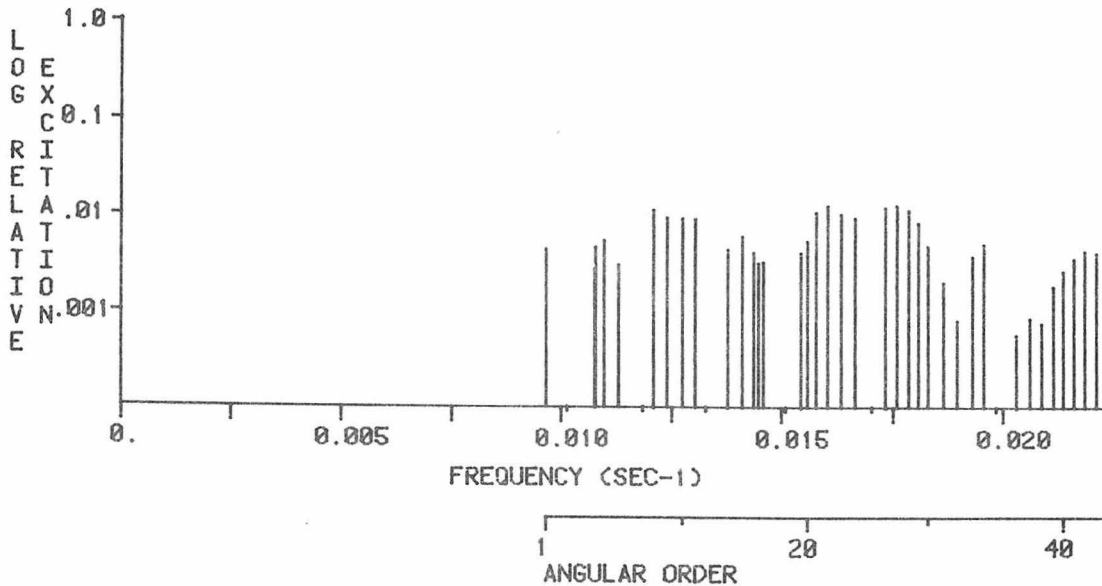


MAXIMUM EXCITATION = 0.377822E -5 CM-SEC ; (28 S 5; T= 91.30 SEC)

EXCITATION NORMALIZED TO 0 S 2 (VERT. COMP.) ; 0.20516300E -3

ATTENUATION INCLUDED; RECORD STARTS AT 3.00 HRS.; LENGTH = 18.00 HRS.

RADIAL COMPONENT; RADIAL ORDER 28

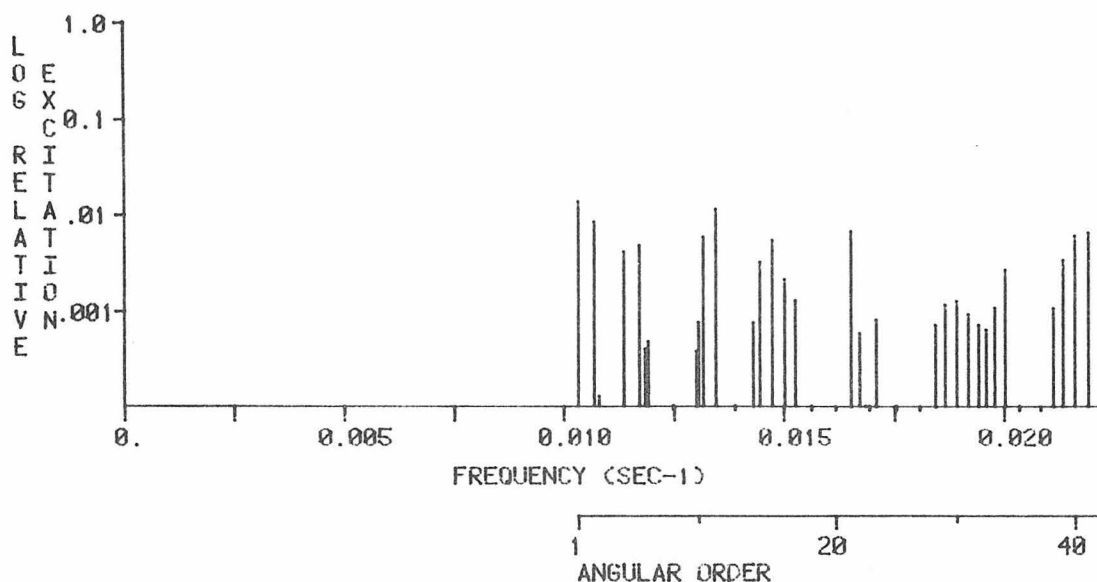


MAXIMUM EXCITATION = 0.171008E -5 CM-SEC ; (28 S 22; T= 62.41 SEC)

EXCITATION NORMALIZED TO 0 S 16 (RAD. COMP.) ; 0.13199600E -3

ATTENUATION INCLUDED; RECORD STARTS AT 3.00 HRS.; LENGTH = 18.00 HRS.

VERTICAL COMPONENT; RADIAL ORDER 29

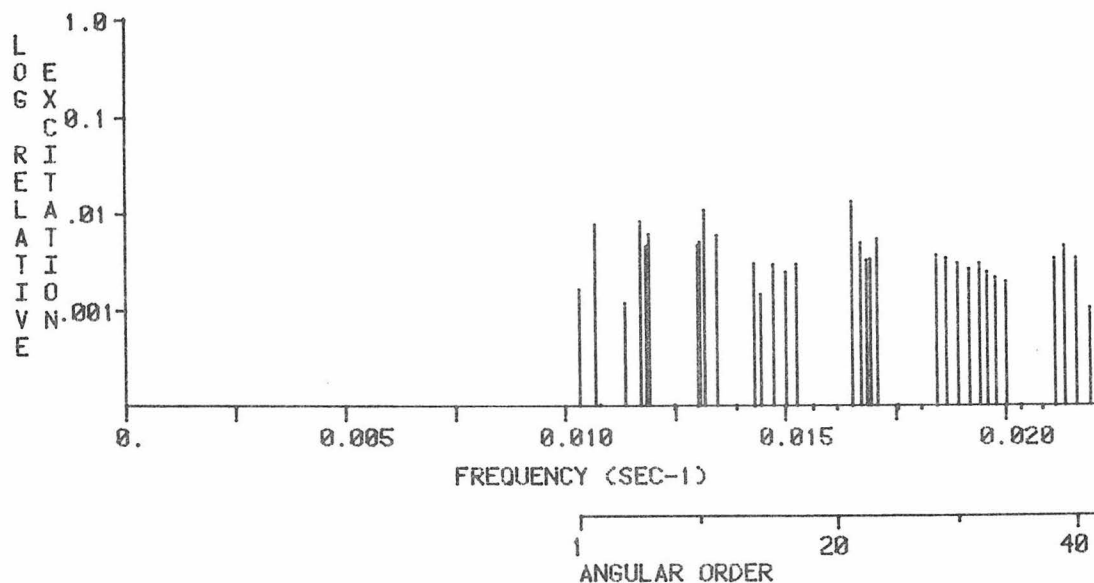


MAXIMUM EXCITATION = 0.284931E -5 CM-SEC ; (29 S 1; T= 37.89 SEC)

EXCITATION NORMALIZED TO 0 S 2 (VERT. COMP.) ; 0.20516300E -3

ATTENUATION INCLUDED; RECORD STARTS AT 3.00 HRS.; LENGTH = 18.00 HRS.

RADIAL COMPONENT; RADIAL ORDER 29

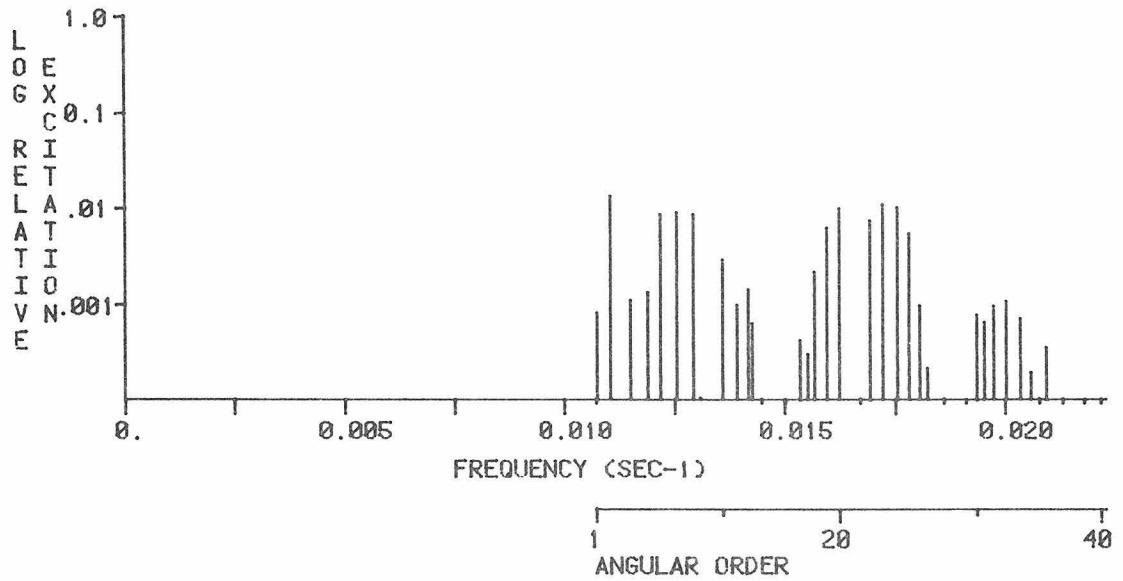


MAXIMUM EXCITATION = 0.176287E -5 CM-SEC ; (29 S 21; T= 60.57 SEC)

EXCITATION NORMALIZED TO 0 S 16 (RAD. COMP.) ; 0.13199600E -3

ATTENUATION INCLUDED; RECORD STARTS AT 3.00 HRS.; LENGTH = 18.00 HRS.

VERTICAL COMPONENT; RADIAL ORDER 30

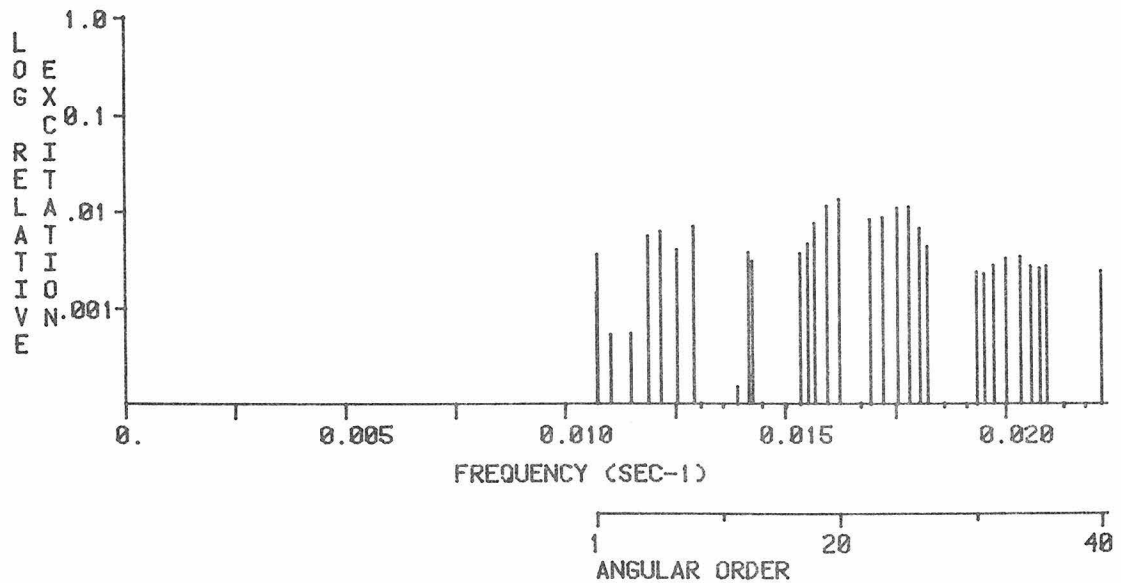


MAXIMUM EXCITATION = 0.272495E -5 CM-SEC ; (30 S 3; T= 90.65 SEC)

EXCITATION NORMALIZED TO 0 S 2 (VERT. COMP.) ; 0.20516300E -3

ATTENUATION INCLUDED; RECORD STARTS AT 3.00 HRS.; LENGTH = 18.00 HRS.

RADIAL COMPONENT; RADIAL ORDER 30



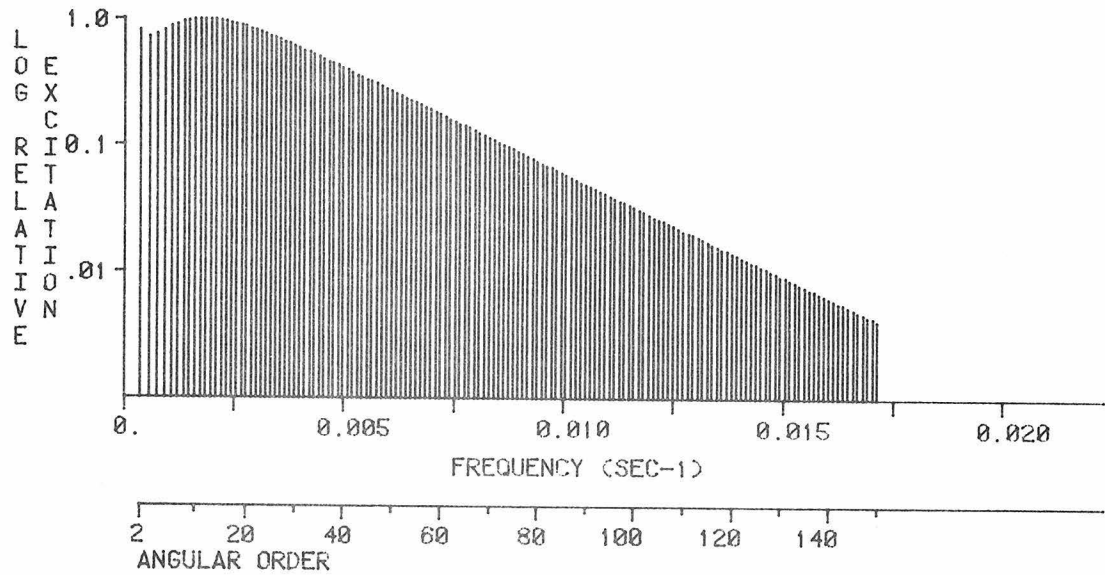
MAXIMUM EXCITATION = 0.175404E -5 CM-SEC ; (30 S 20; T= 61.66 SEC)

EXCITATION NORMALIZED TO 0 S 16 (RAD. COMP.) ; 0.13199600E -3

ATTENUATION INCLUDED; RECORD STARTS AT 3.00 HRS.; LENGTH = 18.00 HRS.

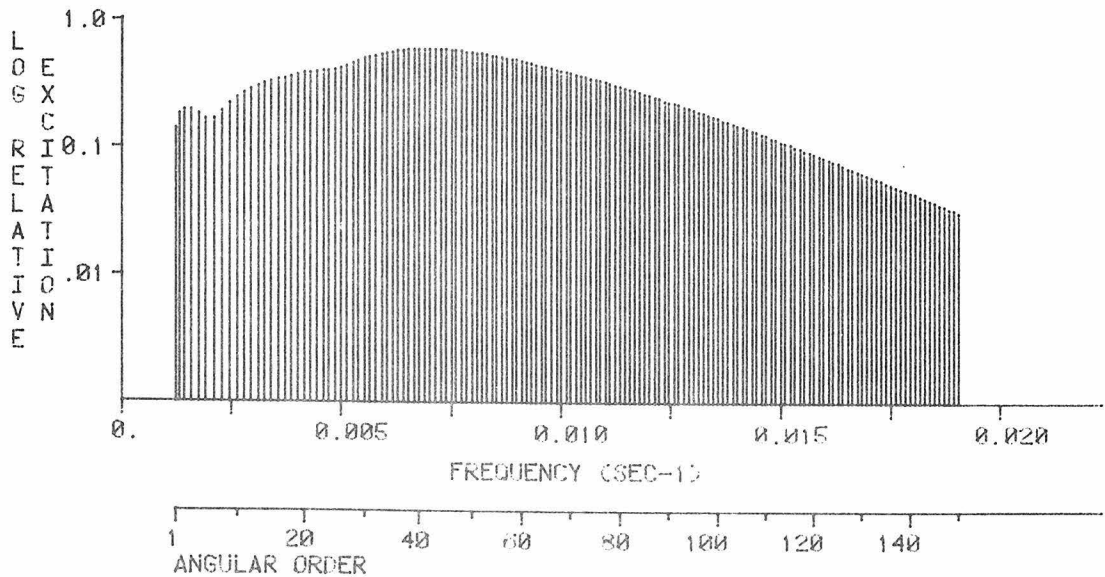
Figure A2.6 - The excitation spectra for the fundamental toroidal modes and the first seven toroidal overtone branches generated by the 1970 deep Columbia earthquake. All excitations are normalized to the maximum fundamental mode excitation. This figure extends over the following 4 pages.

TRANSVERSE COMPONENT; RADIAL ORDER 0



MAXIMUM EXCITATION = $0.480832E -3$ CM-SEC ; (0 T 12; T= 537.63 SEC)

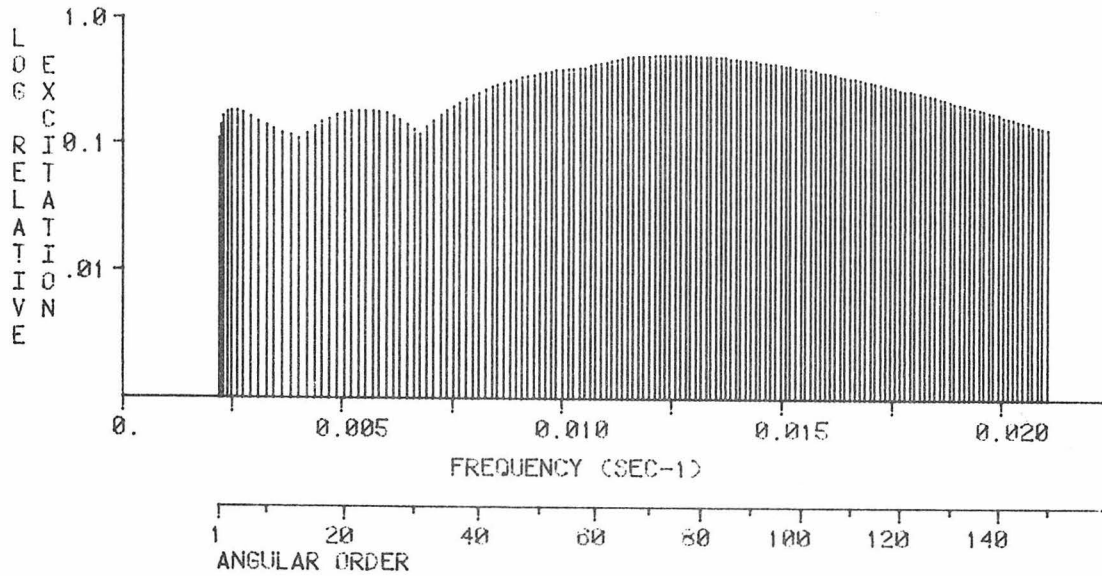
TRANSVERSE COMPONENT; RADIAL ORDER 1



MAXIMUM EXCITATION = $0.286542E -3$ CM-SEC ; (1 T 42; T= 142.59 SEC)

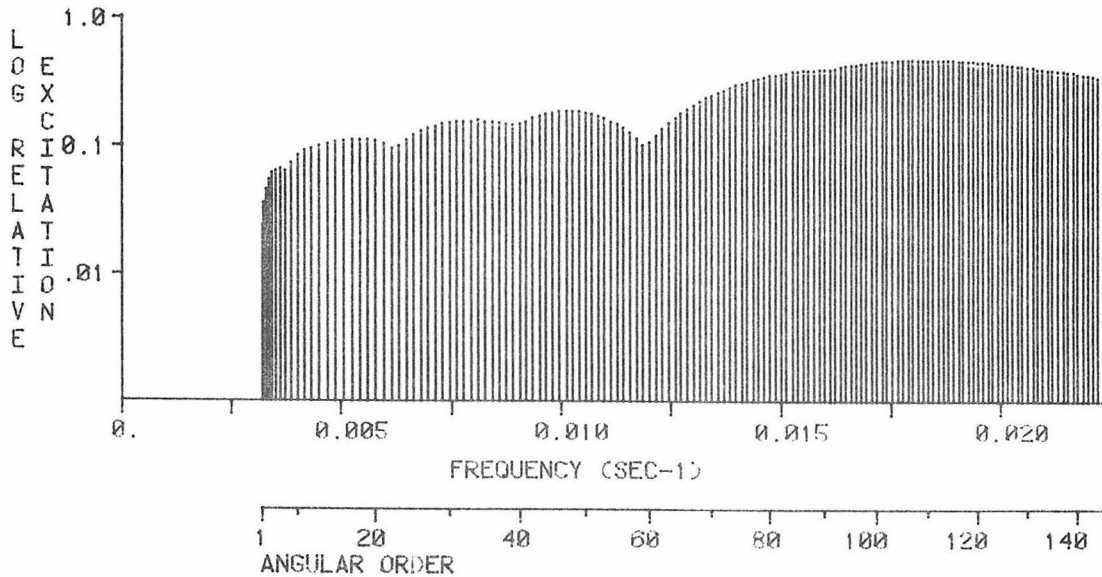
EXCITATION NORMALIZED TO 0 T 12 ; $0.480832E -3$

TRANSVERSE COMPONENT; RADIAL ORDER 2



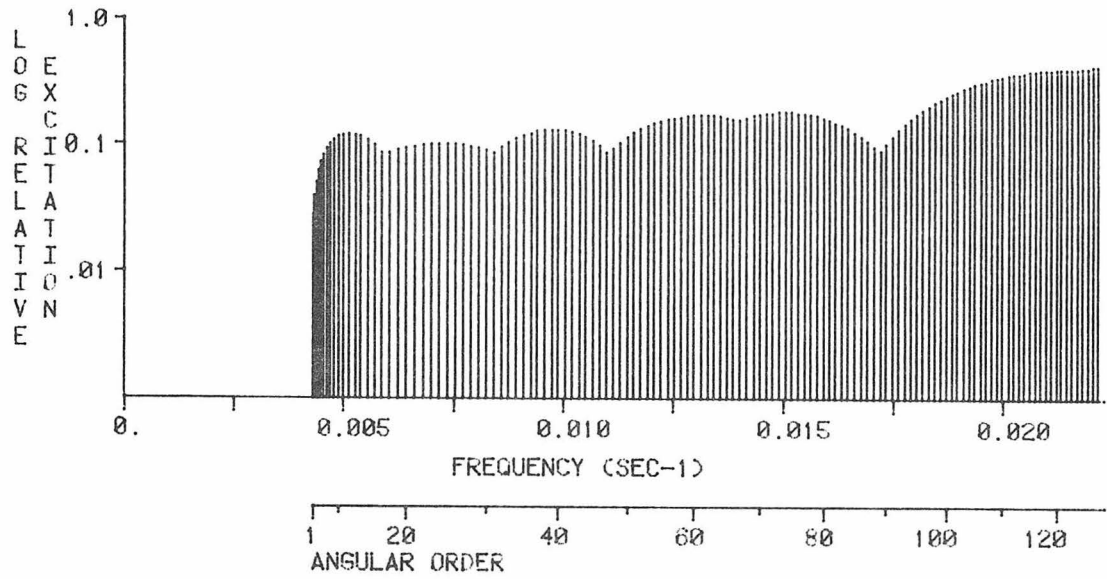
MAXIMUM EXCITATION = 0.249750E -3 CM-SEC ; (2 T 75; T= 79.64 SEC)
EXCITATION NORMALIZED TO 0 T 12 ; 0.480832E -3

TRANSVERSE COMPONENT; RADIAL ORDER 3



MAXIMUM EXCITATION = 0.234460E -3 CM-SEC ; (3 T 109; T= 54.96 SEC)
EXCITATION NORMALIZED TO 0 T 12 ; 0.480832E -3

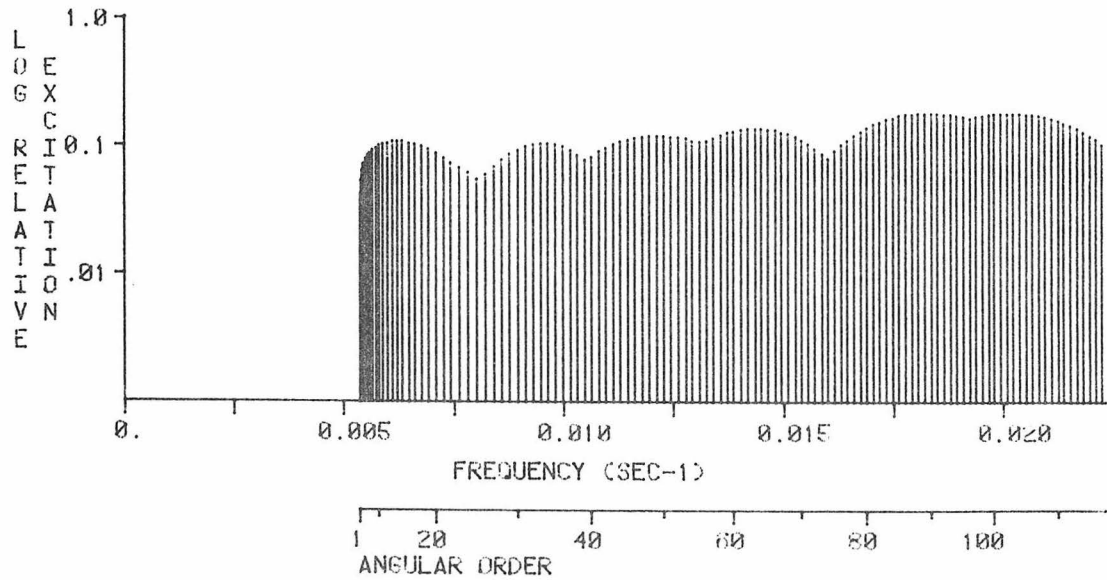
TRANSVERSE COMPONENT; RADIAL ORDER 4



MAXIMUM EXCITATION = 0.206299E -3 CM-SEC ; (4 T 128; T= 45.23 SEC)

EXCITATION NORMALIZED TO 0 T 12 ; 0.480832E -3

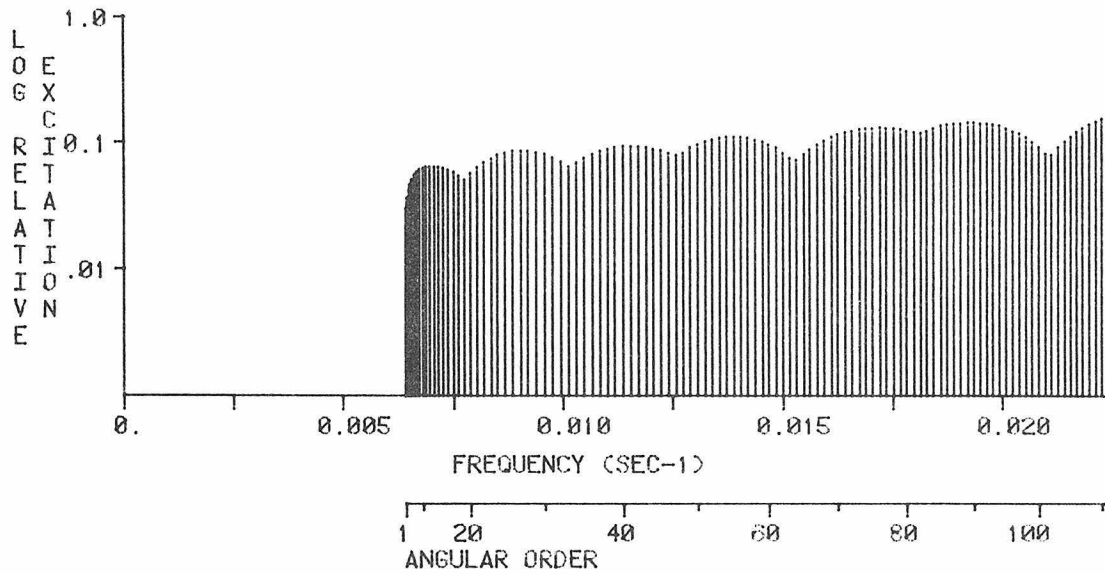
TRANSVERSE COMPONENT; RADIAL ORDER 5



MAXIMUM EXCITATION = 0.899080E -4 CM-SEC ; (5 T 102; T= 49.87 SEC)

EXCITATION NORMALIZED TO 0 T 12 ; 0.480832E -3

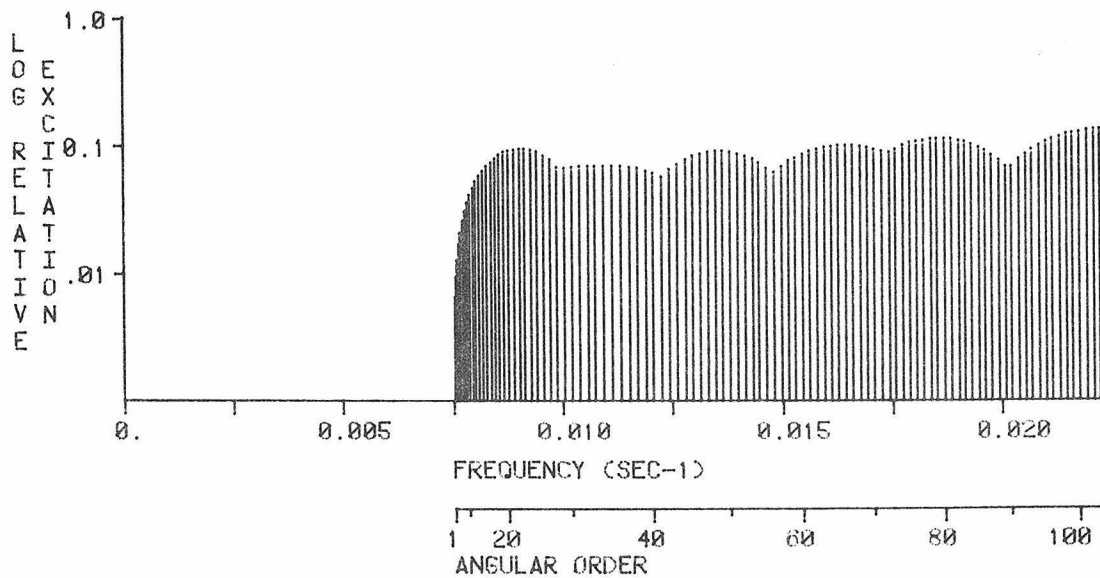
TRANSVERSE COMPONENT; RADIAL ORDER 6



MAXIMUM EXCITATION = 0.759030E -4 CM-SEC ; (6 T 110; T= 45.00 SEC)

EXCITATION NORMALIZED TO 0 T 12 ; 0.480832E -3

TRANSVERSE COMPONENT; RADIAL ORDER 7



MAXIMUM EXCITATION = 0.668620E -4 CM-SEC ; (7 T 103; T= 45.10 SEC)

EXCITATION NORMALIZED TO 0 T 12 ; 0.480832E -3